Mechanical Design Handbook for Elastomers

M. Darlow and E. Zorzi
Mechanical Technology Incorporated
Latham, New York

NASA

National Aeronautics
and Space Administration

**Scientific and Technical
Information Branch**

1981

TABLE OF CONTENTS

1.0   INTRODUCTION

It is the intent of this handbook to provide design engineers with a comprehensive guide in a convenient format for design of elastomer dampers for application in rotating machinery. Design data has been collected from an extensive group of references and, together with some recent information, assembled into a single volume. This handbook, which is intended to be a self-contained reference, includes some theoretical discussion where necessary to insure that the reader has an understanding of how and why dampers are used for rotating machines. A step-by-step procedure for the design of elastomer dampers is presented along with detailed examples of actual elastomer damper applications. In addition, numerous references are cited for the interested reader. The authors assume that the reader has a basic understanding of rotor dynamics and machinery vibration.

The design information presented is primarily intended for application in rotating machinery. Dampers of this type have been shown to be effective for controlling rotor vibrations; however, an historic lack of design data and designer experience with elastomer dampers has inhibited the expansion of their applications. A primary motivation for this handbook is to provide such data in a compact and convenient form and to encourage the use of elastomer dampers and elastomeric damping treatments.

A portion of the design data contained in this handbook is relevant to many mechanical design problems and applications of elastomers. For example, the elastomer dynamic property data may be utilized in the design of structural supports for shock and vibration isolation and insulation. Some basic information regarding the effect of structural damping is included in this work. However, specific information concerning the design of such structural members is beyond the scope of this handbook, but an extensive bibliography is provided at the conclusion of each chapter to aid the design engineer in finding a solution to the problem.

The term "elastomer" refers to a large variety of synthesized polymers as well as to natural rubber. These materials are capable of relatively large strains with essentially full recovery. This property of high elasticity (from which the term elastomer is derived) is the result of a particular type of molecular structure. As obtained from Reference 1.1, the principal attributes of this type of molecular structure are:

- The molecules must be very long and flexible, or to be more precise, there must be free rotation about most of the bonds joining together neighboring chain atoms;

- The molecules must be attached together here and there by either permanent chemical bonds or linkages, or by mechanical entanglements, either form of attachment being termed a cross-link;

- Apart from these cross-links, the molecules must be free to move readily past one another. This is to say, the intermolecular attractions which exist between all molecules must be small.

1

In addition to resiliency, elastomers provide energy dissipation which is the key to their ability to convert mechanical energy into heat energy, thereby damping.

Elastomers may be separated into the two general classifications of natural rubber and synthetic polymers. Particular synthetic polymers may be identified either by their generic type (such as fluorocarbon, chloroprene, etc.) or commonly used manufacturer trademarks [1.2]*. Specific compositions of particular synthetic polymers are further identified by surface hardness.®
This surface hardness, which is generally measured in durometer (or Shore® A hardness), is an indication of the static modulus of elasticity (or of the static shear modulus) of an elastomer. The specific elastomer types for which dynamic properties are presented in this handbook are polybutadiene, 70 and 90 durometer Viton (fluorocarbon elastomer), Buna-N, EPDM, and neoprene. Physical properties of these and many other types of elastomers are also presented in this handbook. These physical properties include all material properties (e.g., density and thermal conductivity) except for the dynamic moduli and dynamic shape factors which are referred to as dynamic properties. An extensive list of references are given from which additional material properties for a large variety of elastomer types may be obtained. Also, test methods are described in detail by which dynamic properties of additional elastomer materials may be determined.

A number of factors must be taken into consideration in elastomer material selection when designing elastomer dampers for rotating machines. The dynamic properties of an elastomer are a function of the strain, temperature, frequency, and preload to which the elastomer is subjected. In addition, many elastomer materials are sensitive to environmental factors, such as exposure to oil or other fluids, exposure to extreme temperatures, and aging. It is important for the designer to recognize that there are inherent variations in elastomer materials of the same type. In particular, there may be considerable variation among the same generic elastomer materials produced by different manufacturers. Even for a particular manufacturer, the batch-to-batch variation in elastomer material may be significant. These variations can have a significant effect on the dynamic properties of the elastomer.

In general, support flexibility and damping are provided in vibratory systems to reduce the transmission of shock and vibration. Of primary interest in this handbook is the reduction of vibrations through the addition of damping. The ultimate aim of vibration reduction is to reduce the potential of machinery failure and safety problems and to reduce the maintenance requirements of machinery. These goals are applicable to rotor vibration as well as structural vibration.

---

* Numbers in brackets refer to references in Section 1.1

® Registered Trademark, Shore Instruments and Manufacturing Co., Inc., Jamaica, N.Y.

2

The reduction of the transmission of shock or vibration may be referred to as either isolation or insulation. The term "isolation" is used when the object is to minimize the transmission of vibration from a machine to its environment. The term "insulation" is used when the object is to minimize the vibration transmitted from the environment to a machine. When referring to vibration isolation or insulation, as distinguished from vibration reduction, the primary concern is with the transmission media. That is, the object is not the dissipation of vibration energy but rather the reduction of vibration transmission. The purpose of vibration isolation or insulation is to reduce noise, general discomfort, machinery fatigue problems, associated safety problems and maintenance, and ultimately, to reduce operating costs.

The purpose of this handbook is to facilitate the use of elastomer dampers for applications on rotating machinery. To this end, a brief introductory discussion of elastomer dampers intended for those readers who are unfamiliar with elastomer dampers is presented. Currently, elastomer dampers enjoy broad use for control of unidirectional vibrations [1.3]. This is particularly true in the areas of vibration isolation and insulation. However, elastomer dampers have, unfortunately, seen very limited use in rotating machinery. As the necessary design information and new elastomers become more readily available, the use of elastomer dampers in rotating machinery should become much more common.

Elastomer dampers have a number of advantages over other types of dampers. They are easy to design, manufacture, assemble and maintain and have the general attribute of simplicity. They are also relatively inexpensive due to the requirement for less stringent tolerances and the inherent simplicity. Elastomer dampers are very durable and can easily handle shocks, rough handling, and an occasional moderate overload. If designed properly, maintenance is very simple and inexpensive. Elastomer dampers can tolerate substantial misalignment, which is of particular importance in rotor bearing applications. They also provide both support stiffness and damping and thus do not require parallel stiffness elements as conventional hydraulic mounts (squeeze-film dampers).

Elastomer dampers also have certain disadvantages which should be carefully considered during the design process. The inherent property of elastomer dampers of providing relatively low damping at high frequency is not always desirable. This is particularly true in rotating machines which operate at high frequencies. However, even when this condition exists, the level of damping provided by an elastomer damper may be sufficient to control rotor vibrations. Also, elastomer dampers tend to be somewhat sensitive to changes in ambient temperature (some materials more than others) and are generally useful only in a limited temperature range. Elastomers are also sensitive to other environmental factors, such as fluid compatibility. Environmental considerations can generally be handled successfully by an appropriate choice of elastomer material. One of the most formidable obstacles to designing consistent elastomer dampers is the variation that is generally found in the material composition of a single generic compound. This variation is not only observed between manufacturers, but also between batches from a single manufacturer. The designer should be aware that manufacturers may change the material composition of an elastomer between batches for cost or avail-

ability reasons. Such variations in the material composition can affect the dynamic properties.

It is useful to make several observations concerning the comparison of elastomer dampers with more conventional dampers (particularly squeeze-film dampers) for rotating machinery. Using proper design data, the predictions of stiffness and damping for elastomer dampers are just as good, or better, than those for squeeze-film dampers. Elastomer dampers are much less expensive and easier to manufacture and maintain than squeeze-film dampers. Elastomer dampers also provide much more adjustment flexibility during assembly and test procedures than do squeeze-film dampers. In particular, an elastomer damper can be designed in a modular fashion so that the elastomer material or configuration can be easily modified in order to change the damper properties. This is especially useful for prototype machines.

This handbook provides dynamic properties of several types of elastomers particularly suitable for use in rotating machinery dampers. (These dynamic properties have been determined for a range of operating conditions which span most practical rotordynamic applications.) The specific steps required for the design of elastomer dampers are reviewed in detail and include the procedures and justifications for the selection of a particular elastomer material and a particular elastomer geometric configuration, as well as the details involved in the design of the actual damper hardware. In order to provide as complete a reference as possible, a full range of physical properties, such as density and thermal conductivity, are also provided for a large variety of elastomer compositions. A discussion of environmental considerations such as fluid, ozone, and adhesive compatibility is also presented along with specific compatibility data for several elastomer materials. For the designer who finds it necessary to determine the dynamic properties for a particular sample of elastomer material, or for an elastomer material for which the dynamic properties are not available, a thorough discussion of the most common dynamic property test methods is presented. This handbook includes a detailed description of the procedure for performing the base excitation resonant mass test, which, of the tests discussed, is the most versatile and least sensitive to instrumentation error. Specific detailed examples of existing elastomer dampers are discussed, along with the steps encountered in the design process, to provide the reader with a complete picture of the design procedure. The design engineer is encouraged to use these elastomer damper designs as a basis for his own damper design.

1.1 References

1.1 Payne, A. R., and Scott, J. R., Engineering Design with Rubber, Interscience Publishers, Inc., New York, 1960.

1.2 Elastomer Material, Desk-Top Data Book, The International Plastics Selector, Inc., San Diego, California, 1977.

1.3 Göbel, E. F., Rubber Springs Design, John Wiley & Sons, New York, 1974.

2.0 FUNDAMENTALS OF DAMPER DESIGN

An understanding of basic vibration theory is required for the proper design
and specification of machinery dampers. For reader convenience, a brief
introduction to vibration theory is presented in this chapter. To fully
appreciate rotor vibration, an understanding of linear vibration theory is
fundamental. Thus, the introduction includes discussions of both unidirec-
tional and rotor-bearing vibration theory. Of course the principal interest
here is rotor-bearing system vibrations. A theoretical and historical back-
ground is also presented concerning the use of linear damping models, with
particular emphasis on rotor-bearing systems. Included is a discussion of
currently used types of rotor dampers and a comparison with elastomer dampers.

2.1 Unidirectional Vibration Theory

This section is intended to provide no more than a brief introduction to
vibration theory. Many references, such as [2.1]* through [2.3], are avail-
able which are much more complete in this regard.

Most real vibratory systems are composed of a continuum with finite mass
energy-storage and energy-dissipation characteristics. An ideal vibratory
system may be considered to be composed of a number of individual elements,
each with the capability to either store potential or kinetic energy or to
dissipate energy. The vibration phenomenon is a manifestation of an alter-
nating transfer of kinetic and potential energy. Simple system representa-
tions use elements which possess only one of these capabilities. These
representations are referred to as lumped parameter models. The number of
these elements required to accurately represent a real vibratory system
depends on several factors, including the geometry system constraints, trac-
tion loads, and the anticipated excitation frequencies. For the purpose of
this work, these lumped parameter model elements are assumed to behave
linearly. This assumption is a reasonable approximation for most small vibra-
tory motions.

The three fundamental lumped parameter model elements are: the spring, for
storing potential energy; the mass, for storing kinetic energy; and the
damper, for dissipating energy.

The simplest possible vibratory system representation is a single-degree-of-
freedom model for free vibration with no damping as illustrated schematically
in Figure 1 where m represents mass and k represents stiffness (or spring
constant). The term "free vibration" indicates that the system is provided
with a set of initial conditions and then allowed to vibrate freely with no
external influences. For the model in Figure 1, a mass is attached to a
rigid support by a linear spring which exerts a force proportional to its
change in length. This ideal (lumped parameter) spring is assumed massless**
so that the forces at the ends of the spring are equal in magnitude and

---

* Numbers in brackets indicate references found in Section 2.6.

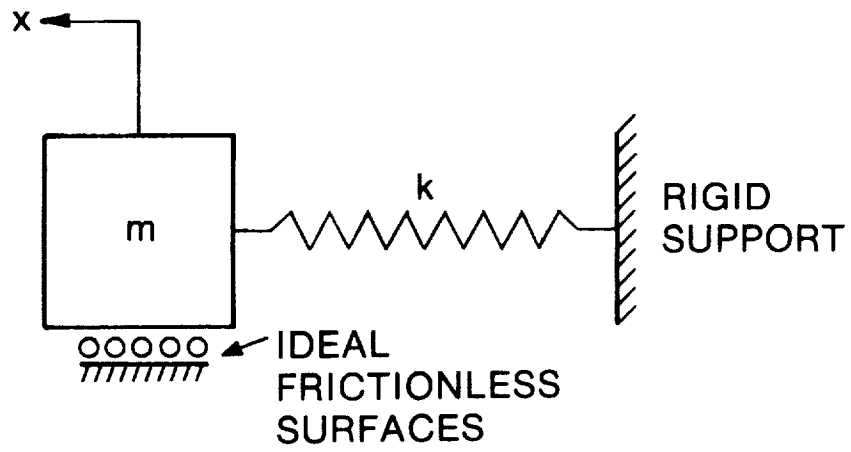** See [2.4] for details on the effect of spring mass on vibratory motion.

Fig. 1   Single-Degree-of-Freedom Free Vibrational Model With No Damping

opposite in direction. The force exerted by the mass is proprotional to acceleration. The motion of the mass is unidirectional with displacement x, where x is a function of time. The differential governing equation for this system may be obtained through the use of Newton's second law of motion, which may be stated as: the rate of change of momentum $\frac{d}{dt}$ $(m\dot{x})$* is equal to the vector sum of forces exerted on the body and takes place in the direction in which the force (vector sum) acts. If the mass is constant, the rate of change of momentum is equal to the mass times its acceleration $(m\ddot{x})$.

Since the system being considered is unidirectional, this law reduces to

$$m\ddot{x} = \Sigma \text{ (forces in the x-direction)} = -kx \qquad (2-1)$$

The negative sign indicates that the spring force is a restoring force (resists applied motion). The form of the restoring force indicates that the static equilibrium position is assumed to be at x equals zero.

Rearrangement of equation (2-1) results in the more familiar form of the governing equation given by

$$m\ddot{x} + kx = 0 \qquad (2-2)$$

The solution to this differential equation is

$$x = A\sin\omega_n t + B\cos\omega_n t \qquad (2-3)$$

where the constants A and B are determined from the initial conditions of the system and where ω_n, known as the undamped natural frequency or resonance, is given by:

$$\omega_n = \sqrt{k/m} \qquad (2-4)$$

The units of ω_n are radians per second.

Equation (2-3) may be rewritten in the form

$$X = C\sin(\omega_n t + \theta) \qquad (2-5)$$

where C is the amplitude of vibration given by:

$$C = \sqrt{A^2 + B^2} \qquad (2-6)$$

and θ is the phase angle of vibration given by

$$\theta = \arctan(B/A) \qquad (2-7)$$

The term "phase angle" can have slightly different meanings when used in different contexts. This form of vibration is referred to as simple harmonic motion due to the harmonic (cyclic) form of equations (2-3) and (2-5).

---

* Dots over the x represent derivatives with respect to time, i.e., $\dot{x} = \frac{dx}{dt}$

The vibratory system of Figure 1 is made slightly more complicated by the addition of a viscous damping element (the most commonly used model for an energy dissipation element) as shown in Figure 2 where b represents the viscous damping coefficient. The force exerted by a viscous damper is proportional to the relative velocity between the ends of the damper. The ideal damper, like the ideal spring, is assumed massless. Again considering only free vibration, the differential governing equation can be derived from Newton's second law to give

$$m\ddot{x} + b\dot{x} + kx = 0 \qquad (2-8)$$

The form of the solution to this differential equation depends on the value of b relative to the values of m and k (assuming all are positive). The criteria for the selection of the appropriate solution are dependent upon the value of the damping coefficient, b, relative to that of the critical damping value, b_c, which is defined by

$$b_c = 2\sqrt{km} = 2\, m\omega_n \qquad (2-9)$$

where ω_n is defined in equation (2-4). The ratio of the damping coefficient to the critical damping is referred to as the damping ratio, ζ, such that

$$\zeta = \frac{b}{b_c} \qquad (2-10)$$

- For the case in which the damping is less than critical (or underdamped) ($\zeta < 1$), the solution to equation (2-8) is of the form

$$x = e^{-bt/2m} (A\sin\omega_d t + B\cos\omega_d t) = Ce^{-bt/2m} \sin (\omega_d t + \theta) \qquad (2-11)$$

where A, B, C and θ are constants which depend on the initial conditions, and C and θ are related to A and B by equations (2-6) and (2-7). ω_d is called the damped natural frequency and is given by

$$\omega_d = \sqrt{k/m}\, (1 - \zeta^2)^{1/2} = \omega_n\, (1 - \zeta^2)^{1/2} \qquad (2-12)$$

and is given in units of radians per second. Note that for unidirectional vibration, the damped natural frequency, ω_d, is less than the undamped natural frequency, ω_n. The vibratory response represented by equation (2-11) is referred to as a transient damped oscillation. A plot of a typical damped oscillation response is presented in Figure 3.

- For the case in which the damping is exactly critical (or critically damped) ($\zeta=1$), the solution to equation (2-8) is of the form

$$x = (A = Bt)e^{-bt/2m} = (A + Bt)e^{-\omega_n t} \qquad (2-13)$$

where A and B are constants which depend on the initial conditions. For this case, a typical response plot is presented in Figure 4.

- For the case in which the damping is greater than critical (or overdamped) ($\zeta > 1$), the solution to equation (2-8) is of the form
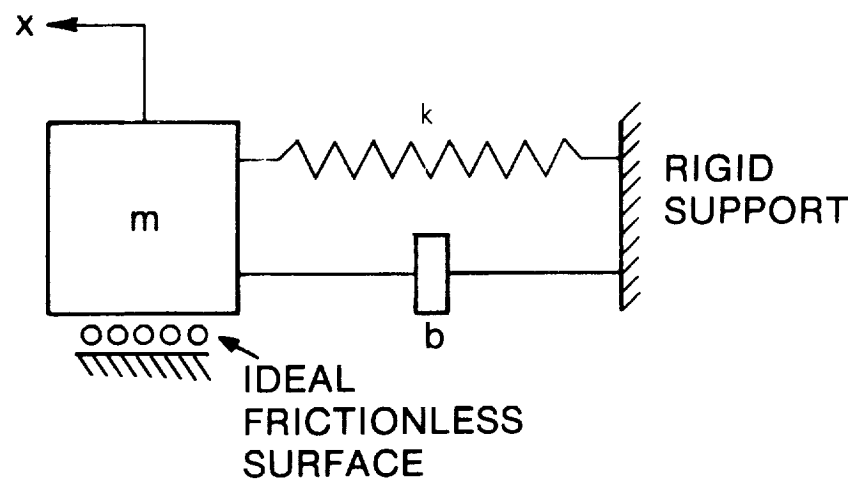
8

Fig. 2 Single-Degree-of-Freedom Free Vibrational Model With Viscous Damping

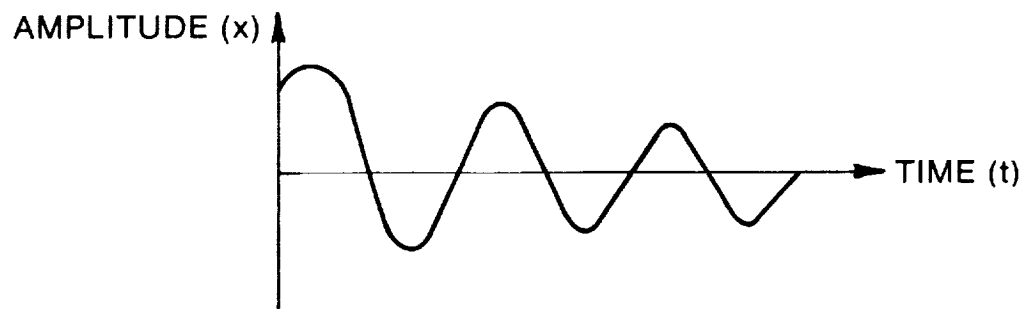**Fig. 3 Typical Damped Oscillation Response for a Single-Degree-of-Freedom Free Vibration System With Viscous Damping; $\rho < 1$ (Undamped)**
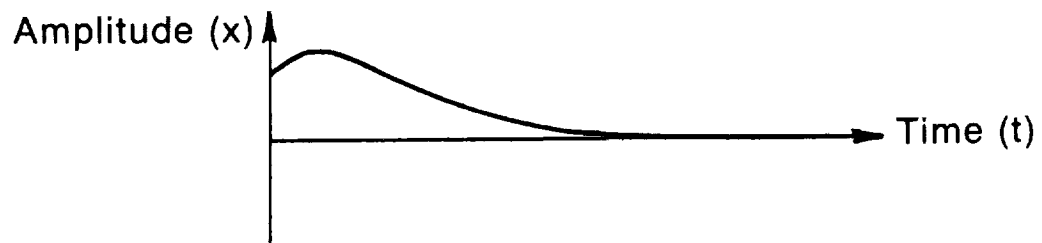
Fig. 4 Typical Response for Single-Degree-of-Freedom Free Vibration System With Viscous Damping; $\rho = 1$ (Critically Damped)

$$x = e^{-bt/2m} (Ae^{\omega_n\sqrt{\zeta^2-1}\,t} + Be^{-\omega_n\sqrt{\zeta^2-1}\,t}) \qquad (2-14)$$

where A and B, as before, are constants which depend on the initial conditions. For this case, a typical response plot is presented in Figure 5.

Most real vibratory systems are underdamped ($\zeta < 1$). This is generally true even with the addition of external damping supplied by specially configured dampers. On occasion, the addition of external damping may convert an underdamped system into a critically damped or overdamped system. However, this is a special case. Consequently, it is necessary to have methods for empirically evaluating damper effectiveness for underdamped systems, in order to determine the need for damping and to compare the effectiveness of various damper designs.

Several measures of damping effectiveness are in common use. Each of these measures has its own physical significance and is interrelated. One of these measures is damping ratio, ζ, which has been discussed above. Another is logarithmic decrement, δ, which is defined as the natural logarithm of the ratio of successive cycles of damped free vibration. That is,

$$\delta = \frac{1}{N} \ln\left(\frac{x_1}{x_n}\right) \qquad (2-15)$$

where x_1 is the amplitude of the first of the cycles, x_n is the amplitude of the Nth, and N is the number of consecutive cycles. Using equation (2-11), logarithmic decrement is found to be related to damping ratio by

$$\delta = 2\pi\zeta/(1 - \zeta^2)^{1/2} \qquad (2-16)$$

For small values of the damping ratio, this relationship reduces to

$$\delta \simeq 2\pi\zeta \text{ for } \zeta << 1 \qquad (2-17)$$

Positive values of log decrement indicate stability since $x_2 < x_1$ and the amplitude decreases with time. Conversely, negative values of log decrement indicate instability. A log decrement value of zero indicates a limit cycle, where the amplitude of vibration remains constant with time. For most practical dynamic systems, the attainment of a non-negative log decrement is not a sufficient stability criterion for two reasons. First, to insure safe and efficient operation of most machines, vibrations must not only be damped out, but damped out rapidly, as briefly sustained vibrations may be troublesome. Second, the log decrement is usually determined analytically for predicting system behavior. A safety margin is generally advisable whenever an analytical model is used to represent a real dynamic system.

Loss factor or loss coefficient (η), which represents the ratio of damping energy to strain energy [2.1], is also used as a measure of damping effectiveness. For light damping ($\zeta < 0.1$), the loss factor for a homogeneous element (not a system) is approximately equal to twice the damping ratio. A classification of damping units [2.5] is presented in Table 1, and the interrelationships [2.1] are presented in Table 2. When applied to elastomer elements or damper assemblies, the loss coefficient is defined as
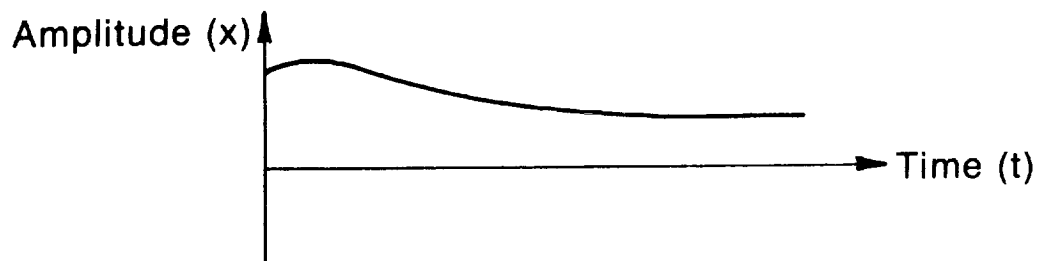
12

Amplitude (x)

Time (t)

Fig. 5 Typical Response for Single-Degree-of-Freedom Free Vibration System With Viscous Damping; $\rho > 1$ (Over Damped)

Table 1

DAMPING CLASSIFICATION*

I. PROPERTIES OF MATERIALS AND SPECIMENS

(1) Classification of type of damping units	(2) Preferred names	(3) Other names used	(4) Symbols and units — Material	(4) Symbols and units — Members	(5) Definition	Relation between specimen properties and system response
(A) ABSOLUTE ENERGY UNITS Stored or dissipated per cycle of stress.						$\eta_n = \dfrac{D_s}{2\pi U_s} = \dfrac{K_s''}{K_s'} = \dfrac{1}{Q_s} = \dfrac{1}{A_r} = B_n = B_w$
Material properties U and D give unit values.	Unit elastic Strain energy	Elastic energy strain energy	U in-lb/in³-cycle		Area under σ-ε curve from 0 to ε_{max}	$\tan \lambda = \dfrac{A_r}{\pi} = \dfrac{2\pi v_r}{\pi \omega} = \dfrac{T_r}{5.35\,\omega}$
	Total elastic strain energy			$U_s = U V_s \beta$ in-lb/cycle	Area under P_{res}-X curve from 0 to P_{max}	
Specimen properties U_s and D_s give total values for specimen S.	Unit damping energy	Specific damping Spec. hysteresis	D in-lb/in³-cycle		Area within σ-ε hysteresis loop	$\dfrac{b A_r}{\pi} = \dfrac{b \lambda v_r}{\pi} = \dfrac{b \lambda T_r}{27.3}$
	Total damping energy			$D_s = D V_s \beta$ in-lb/cycle	Area within P-X hysteresis loop	$-2\varepsilon B = \dfrac{v_r}{2\pi} = \dfrac{50}{\pi} = D_{rel} = \dfrac{\alpha}{\beta} \eta_r$
(B) COMPLEX MODULUS NOTATION Appropriate for linear materials.	Complex modulus		E^*, G^*, K^*, M^* lb/in²	K_s^* lb/in	$E^* = \|E^*\| e^{i\theta}$ $= E'(1 + i\eta)$	
Material properties: $E^* = E' + iE''$ Same for G^*, K^*, M^*.	Absolute modulus		$\|E^*\|, \|G^*\|$ $\|K^*\|, \|M^*\|$	$\|K_s^*\|$	$\|E^*\| = [E'^2 + E''^2]^{1/2}$	Note: For linear materials $a \sqrt{\beta} - 1$
Properties of Specimen, member, or total parts S. $K_s^* = K_s' + iK_s''$	Storage modulus	Elastic modulus Real modulus	E', G', K', M' lb/in²	K_s' lb/in	$E' = \|E^*\| \cos \delta$	Relations among unit properties of uniform materials
	Loss modulus	Dissipation modulus	E'', G'', K'', M'' lb/in²	K_s'' lb/in	$E'' = \|E^*\| \sin \delta$	$\eta_n \sim \eta_r$ $Q_n \sim Q$
(C) RELATIVE ENERGY UNITS Dimensionless ratios of damping energy D and strain energy U.	Loss coefficient	Loss factor Damping factor	η (eta)	$\eta_s = \eta \dfrac{\alpha}{\beta}$	$\eta = \dfrac{D}{2\pi U}$ $\eta_s = \dfrac{D_s}{2\pi U_s}$	$E' = \dfrac{2U}{\varepsilon^2}$ $\eta = \dfrac{E''}{E'}$
	Quality factor	Storage coef. Q factor	Q	$Q_s = Q \dfrac{\beta}{\alpha}$	$Q \sim \dfrac{2\pi U}{D}$ $Q_s = \dfrac{2\pi U_s}{D_s}$	$E'' = \dfrac{D}{\pi \varepsilon^2}$ $\eta = \dfrac{D}{2\pi U}$ $Q \sim \dfrac{2\pi U}{D}$ $Q = \dfrac{1}{E''} \dfrac{E'}{\eta}$

II. PROPERTIES OF COMPOSITES, STRUCTURES, ETC.

These properties are not covered in this monograph. Nomenclature and units under study by a ASA Committee initiated in 1965.

III. RESPONSE OF SYSTEMS UNDER EXCITATION

	Measured quantities or prop. of systems	How measured	Relations between system properties and specimens properties
(D) TEMPORAL DECAY of free vibrations in members. $X_x(t) = X_x(0) e^{-v_r t}$ $v_r = \left(\dfrac{1}{t}\right) \ln \left[\dfrac{X_x(0)}{X_x(t)}\right]$	Logarithmic decrement Δ_r (DELTA)	$X_x(n+1) = X_x(n) e^{-\Delta_r}$ $\Delta_r = \ln \dfrac{X_x(n)}{X_x(n+1)}$	$A_r = \dfrac{D_s}{2\pi U_s}$ $\Delta_r = \pi \dfrac{K_s''}{K_s'}$ $A_r = \pi \eta_s$ $A_r = \dfrac{\pi}{Q_s}$
Decay constant $v_r = \dfrac{20}{t} \log \dfrac{X_x(0)}{X_x(t)} = \dfrac{20}{t} \log \dfrac{X_x(0)}{X_x(t)}$ $v_r = \dfrac{(db)}{t}$ $\dfrac{20}{t} \log e^{v_r t} = 8.68 v_r$	Decay constant v_r (UPSILON) (in./in.) per sec	$v_r = -\dfrac{1}{t} \ln \dfrac{X_x(t)}{X_x(0)}$	$v_r = \dfrac{\omega D_s}{4\pi U_s}$ $v_r = \dfrac{\omega}{2} \dfrac{K_s''}{K_s'}$ $v_r = \dfrac{\omega}{2} \eta_s$ $v_r = \dfrac{\omega}{2Q_s}$
$\dfrac{20}{t} \log e^{v_r t} = 8.68 v_r$	T_r (UPSILON) (db) per sec	$T_r = 8.68 v_r$	$T_r = 0.69 \omega \dfrac{D_s}{U_s}$ $T_r = 4.35 v_r$ $T_r = 4.35 \omega \eta_s$ $T_r = \dfrac{4.35\,\omega}{Q_s}$
(E) SPATIAL ATTENUATION of waves in slender rods, beams, etc., having distributed parameters. $X_x(x) = X_x(0) e^{-v_y x}$ $v_y = \left(\dfrac{1}{y}\right) \ln \dfrac{X_x(0)}{X_x(y)}$	Logarithmic attenuation A_y	$X_x(l) = X_x(0) e^{-A_y}$ $A_y = \ln \dfrac{X_x(0)}{X_x(\lambda)}$	$A_y = \dfrac{1}{2b} \dfrac{D_s}{U_s}$ $A_y = \dfrac{\pi}{b} \dfrac{K_s''}{K_s'}$ $A_y = \dfrac{\pi}{b} \eta_s$ $A_y = \dfrac{\pi}{b} \dfrac{1}{Q_s}$
$v_y = \dfrac{(db)}{y}$ $\dfrac{20}{y} \log \dfrac{X_x(0)}{X_x(y)}$	Attenuation constant v_y (UPSILON) (in./in.) per in.	$v_y = -\dfrac{1}{y} \ln \dfrac{X_x(0)}{X_x(y)}$	$v_y = \dfrac{1}{2b\lambda} \dfrac{D_s}{U_s}$ $v_y = \dfrac{\pi}{b\lambda} \dfrac{K_s''}{K_s'}$ $v_y = \dfrac{\pi}{b\lambda} \eta_s$ $v_y = \dfrac{\pi}{b\lambda} \dfrac{1}{Q_s}$
$\dfrac{20}{y} \log e^{v_y y} = 8.68 v_y$	T_y (UPSILON) (db) per in.	$T_y = 8.68 v_y$	$T_y = \dfrac{4.35}{b\lambda} \dfrac{D_s}{U_s}$ $T_y = \dfrac{27.3}{b\lambda} \dfrac{K_s''}{K_s'}$ $T_y = \dfrac{27.3}{b\lambda} \eta_s$ $T_y = \dfrac{27.3}{b\lambda} \dfrac{1}{Q_s}$

(F) RESPONSE UNDER SINUSOIDAL LOADING; single-degree-of-freedom system (linear member-mass system). Vibration phase angle = φ. If exciting frequency is much smaller than resonance, then $\varphi = \lambda$. Resonance amplification factor = $A_r = Q_r$. Transmissibility T_r, res. curve bluntness = $B_n = B_w$.

$b = 1$ For longitudinal, shear, tension, compressive non-dispersive waves
$b = 2$ For simple bending waves

Classification of recommended damping units, their interrelations, and their relations to the measured quantities of damping testing systems.

14

Table 2

INTERRELATIONS AMONG COMMON DAMPING QUANTITIES IDEALIZED FOR
LUMPED-PARAMETER SYSTEMS OF ONE DEGREE-OF-FREEDOM*

$$\alpha = 20 \log e = 8.68 \qquad \omega_R = 2\pi f_R \qquad \omega_N^2 = \omega_R^2 - \kappa^2$$

	b/b_c	η	κ	Δ	D	Δf	Q	ψ
b/b_c	b/b_c	$2b/b_c$ $b \ll b_c$	$\omega_R b/b_c$	$2\pi b/b_c$ $b \ll b_c$	$a\omega_R b/b_c$	$\omega_R b/\pi b_c$	$b_c/2b$	$4\pi b/b_c$ $b \ll b_c$
η	$\eta/2$ $\eta \ll 1$	η	$\omega_R \eta/2$ $\eta \ll 1$	$\pi \eta$ $\eta \ll 1$	$a\omega_R \eta/2$ $\eta \ll 1$	$\omega_R \eta/2\pi$ $\eta \ll 1$	$1/\eta$ $\eta \ll 1$	$2\pi\eta$ $\eta \ll 1$
κ	κ/ω_R	$2\kappa/\omega_R$ $\kappa \ll \omega_R$	κ	$2\pi\kappa/\omega_N$	$a\kappa$	κ/π	$\omega_R/2\kappa$ $\kappa \ll \omega_R$	$4\pi\kappa/\omega_R$ $\kappa \ll \omega_R$
Δ	$\Delta/2\pi$ $\Delta \ll 2\pi$	Δ/π $\Delta \ll 2\pi$	$\omega_N \Delta/2\pi$	Δ	$a\omega_N \Delta/2\pi$	$\omega_N \Delta/2\pi^2$	$\pi/(\Delta - \Delta^2)$ $\Delta \ll 1$	$2(\Delta - \Delta^2)$ $\Delta \ll 1$
D	$D/a\omega_R$	$2D/a\omega_R$ $D \ll a\omega_R$	D/a	$2\pi D/a\omega_N$	D	$D/a\pi$	$a\omega_R/2D$ $D \ll a\omega_R$	$4\pi D/a\omega_R$ $D \ll a\omega_R$
Δf	$\pi \Delta f/\omega_R$ $\Delta f \ll \omega_R/\pi$	$2\pi \Delta f/\omega_R$ $\Delta f \ll \omega_R/\pi$	$\pi \Delta f$	$2\pi^2 \Delta f/\omega_N$	$a\pi \Delta f$	Δf	$\omega_R/2\pi \Delta f$ $\Delta f \ll \omega_R/\pi$	$4\pi^2 \Delta f/\omega_R$ $\Delta f \ll \omega_R/\pi$
Q	$1/2Q$ $2Q \gg 1$	$1/Q$ $2Q \gg 1$	$\omega_R/2Q$ $2Q \gg 1$	π/Q $2Q \gg 1$	$a\omega_R/2Q$ $2Q \gg 1$	$\omega_R/2\pi Q$ $2Q \gg 1$	Q	$2\pi/Q$
ψ	$\psi/4\pi$ $\psi \ll 4\pi$	$\psi/2\pi$ $\psi \ll 4\pi$	$\omega_R\psi/4\pi$ $\psi \ll 4\pi$	$\psi/2$ $\psi \ll 4\pi$	$a\omega_R\psi/4\pi$ $\psi \ll 4\pi$	$\omega_R\psi/4\pi^2$ $\psi \ll 4\pi$	$2\pi/\psi$	ψ

b/b_c = fraction of critical damping for viscous or equivalent-viscous damping, where c is the damping constant of the dashpot acting on the mass m in parallel to the spring stiffness k and c_c is the critical damping constant as given by Eq. (2.12)

η = loss factor of spring with complex stiffness given by $k(1 + j\eta)$

κ = decay constant of system in free vibration given in terms of viscous damping by $\kappa = c/2m$

Δ = logarithmic decrement of free vibration of system defined in terms of successive peak displacements during decay

D = decay rate of free vibrations expressed in decibels per second during exponential decay of amplitude

Δf = bandwidth of steady-state resonance of system as related at the half-power points

Q = quality factor of steady-state resonance of system as related to the resonant amplification factor, A_R

ψ = specific damping capacity of system in terms of ratio between energy dissipated per cycle and elastic energy-storage capacity of the system

* Reference 2.30

   With permission of McGraw Hill Book Co.

15

$$\eta = k_2/k_1 \tag{2-18}$$

where k_1 and k_2 are the real and imaginary parts of the complex stiffness, $k*$,

$$k* = k_1 + ik_2 \tag{2-19}$$

This is discussed in more detail in the next chapter. In terms of a viscous damping coefficient, the loss coefficient may be represented by

$$\eta = \omega b/k \tag{2-20}$$

Damping in elastomers is generally represented by hysteretic damping which is equivalent to the imaginary component of the complex stiffness given in equation (2-19). Hysteretic damping results in a dissipation force proportional to displacement (as compared to viscous damping which is proportional to velocity), but ninety degrees out of phase with displacement.

The review of forced vibration begins with a single-degree-of-freedom, undamped system, as illustrated in Figure 6. The forcing function is assumed to be sinusoidal and may be realized as a force applied to the mass, shown in Figure 6(a). The response of the system is defined by the force or motion transmissibility, depending on the form of the forcing function. The force transmissibility is defined as the ratio of the force transmitted to the foundation to the force applied to the mass. The motion transmissibility is defined as the ratio of the motion of the mass to the applied motion of the foundation [2.1].

For the case in which a sinusoidal forcing function is applied to the mass, the governing equation becomes:

$$m\ddot{x} + kx = F_o \sin\omega t \tag{2-21}$$

where $F_o \sin\omega t$ is the forcing function. Equation (2-21) is not homogeneous; thus it has both a general and particular solution which together are given by

$$x = A\sin\omega_{nt} + B\cos\omega_{nt} + \frac{F_o/k}{1-\omega^2/\omega_n^2} \sin\omega t \tag{2-22}$$

and where A and B are constants that depend on the initial conditions. The first two terms on the right side of equation (2-22) form the general solution to equation (2-21). This is identical to the solution for the analogous free vibration case given by equation (2-3). In virtually all practical systems, there is some damping present which causes the general solution terms (also known as the transient solution) to disappear, or to become negligible, with time. However, the particular, or steady-state, solution, given by the last term in equation (2-22), does not diminish with time and is, therefore, of primary interest here.

Considering only the steady-state solution, the force transmissibility, T_F, is given by

16
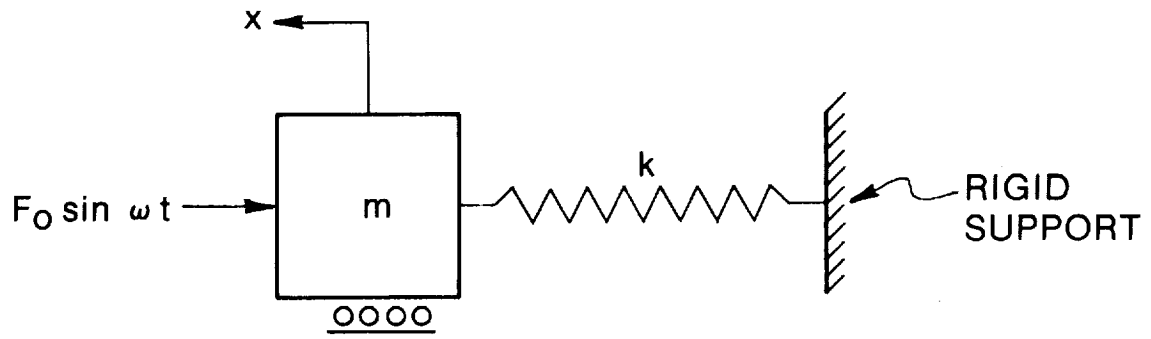
(a) FORCE APPLIED TO MASS
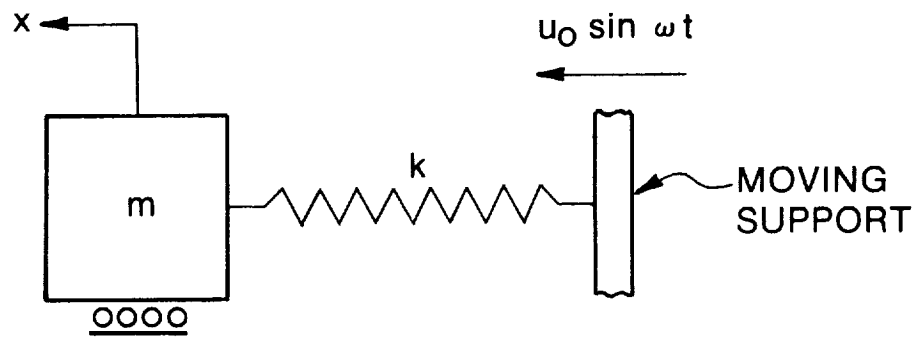
(b) PRESCRIBED MOTION OF FOUNDATION

Fig. 6   Undamped Single-Degree-of-Freedom Forced Vibration Models

$$T_F = (1 - \frac{\omega^2}{\omega_n^2})^{-1} \qquad (2\text{-}23)$$

where T_F is unbounded when the forcing frequency, ω, equals ω_n, the natural frequency. A plot of T_F as a function of the frequency ratio, ω/ω_n, is presented in Figure 7.

For the case in which the foundation has a prescribed sinusoidal motion, the governing equation becomes

$$m\ddot{x} + kx = kU_o \sin\omega t \qquad (2\text{-}24)$$

where $(U_o \sin\omega t)$ is the prescribed motion of the support. Equation (2-24) is very similar to equation (2-21) and, thus, has a similar solution given by

$$X = A\sin\omega_n t + B\cos\omega_n t + \frac{U_o}{1-\omega^2/\omega_n^2} \sin\omega t \qquad (2\text{-}25)$$

As for equation (2-22), the first two terms on the right side of equation (2-25) form the transient solution, while the last term represents the steady-state solution.

Again considering only the steady-state solution, the motion transmissibility, T_M, is given by

$$T_M = (1-\omega^2/\omega_n^2)^{-1} \qquad (2\text{-}26)$$

where T_M is unbounded for a frequency ratio of unity. Note that, for this model, the force and motion transmissibilities are identical. Thus, the plot in Figure 7 applies to motion transmissibility as well as to force transmissibility.

A viscous damping element is now added to the forced vibration models of Figure 6, resulting in a single-degree-of-freedom system with viscous damping as illustrated by the models of Figure 8. The forcing function, as before, can be represented as either a force applied to the mass (Figure 8a) or a prescribed motion of the foundation (Figure 8b).

For the case in which a sinusoidal forcing function is applied to the mass, the governing equation becomes

$$m\ddot{x} + b\dot{x} + kx = F_o\sin\omega t \qquad (2\text{-}27)$$

where $F_o\sin\omega t$ is the applied force. For reasons given above, only the steady-state solution of equation (2-27) is considered. For positive values of b (in general, b is not negative, although it may be zero), a phase angle exists between the forcing function, $F_o\sin\omega t$, and the steady-state response x.

This response is given by

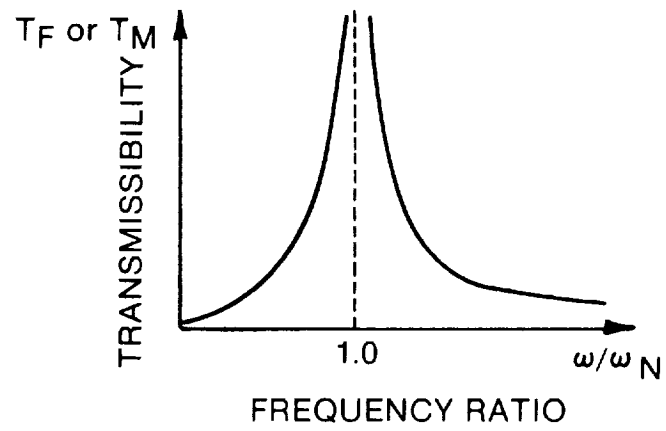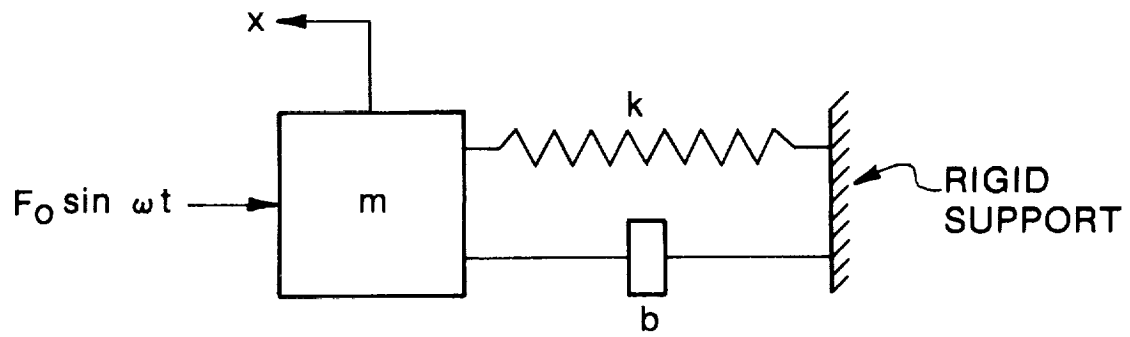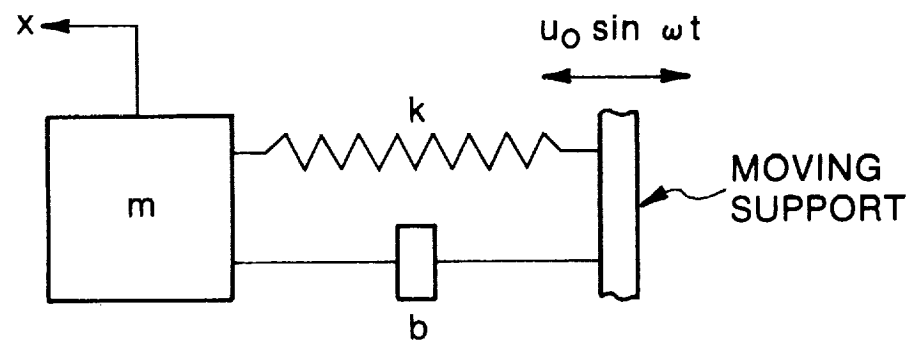$$x = R\sin(\omega t - \theta) \qquad (2\text{-}28)$$

18

Fig. 7 Transmissibility of a Single-Degree-of-Freedom Forced Vibration System With No Damping as a Function of the Frequency Ratio

a) FORCE APPLIED TO MASS

b) PRESCRIBED MOTION OF FOUNDATION

Fig. 8   Single-Degree-of-Freedom Forced Vibration Model With Viscous Damping

where

$$R = \frac{F_o}{k} \left[(1-\omega^2/\omega_n^2)^2 + (2\zeta\omega/\omega_n)^2\right]^{-1/2} \tag{2-29}$$

and

$$\theta = \arctan\left[(2\zeta\omega/\omega_n)/(1-\omega^2/\omega_n^2)\right] \tag{2-30}$$

ζ and ω_n are as defined in equations (2-10) and (2-4), respectively.

The relationship between the force transmitted to the foundation and the applied force is more complex than for the undamped system presented above. For the damped system, both the spring and damper transmit force to the foundation. The total force transmitted to the foundation, F_T, is given by

$$F_T = b\dot{x} + kx \tag{2-31}$$

where the two terms on the right are ninety degrees out of phase with each other. The ratio of the transmitted force, F_T, to the magnitude of the applied force, F_o, becomes*

$$\frac{F_T}{F_o} = T \sin(\omega t - \Psi) \tag{2-32}$$

where

$$T = \sqrt{\frac{1 + (2\zeta\omega/\omega_n)^2}{(1-\omega^2/\omega_n^2)^2 + (2\zeta\omega/\omega_n)^2}} \tag{2-33}$$

$$\Psi = \text{Arctan}\left[\frac{2\zeta(\omega/\omega_n)^3}{1 - (\omega^2/\omega_n^2) + (4\zeta^2\omega^2/\omega_n^2)}\right] \tag{2-34}$$

and T and Ψ are referred to as the transmissibility and the phase angle, respectively. Note that, for positive values of ζ, T is bounded for all values of ω. Thus, the presence of damping is necessary to control vibration at a system resonance when comparing equation (2-33) to equation (2-23). Plots of transmissibility, T, and phase angle, Ψ, are presented as functions of the frequency ratio for several values of ζ in Figures 9 and 10, respectively.

The maximum value of the displacement, x, from equation (2-28), occurs for a forcing frequency equal to $\left[\omega_n (1-2\zeta^2)^{1/2}\right]$. Note that, for positive ζ, the maximum steady-state response (in terms of displacement) always occurs for forcing frequencies less than the undamped natural frequency. This is generally true for unidirectional vibratory systems. As will be seen in the next section, this is not true for lateral vibration of rotating machines.

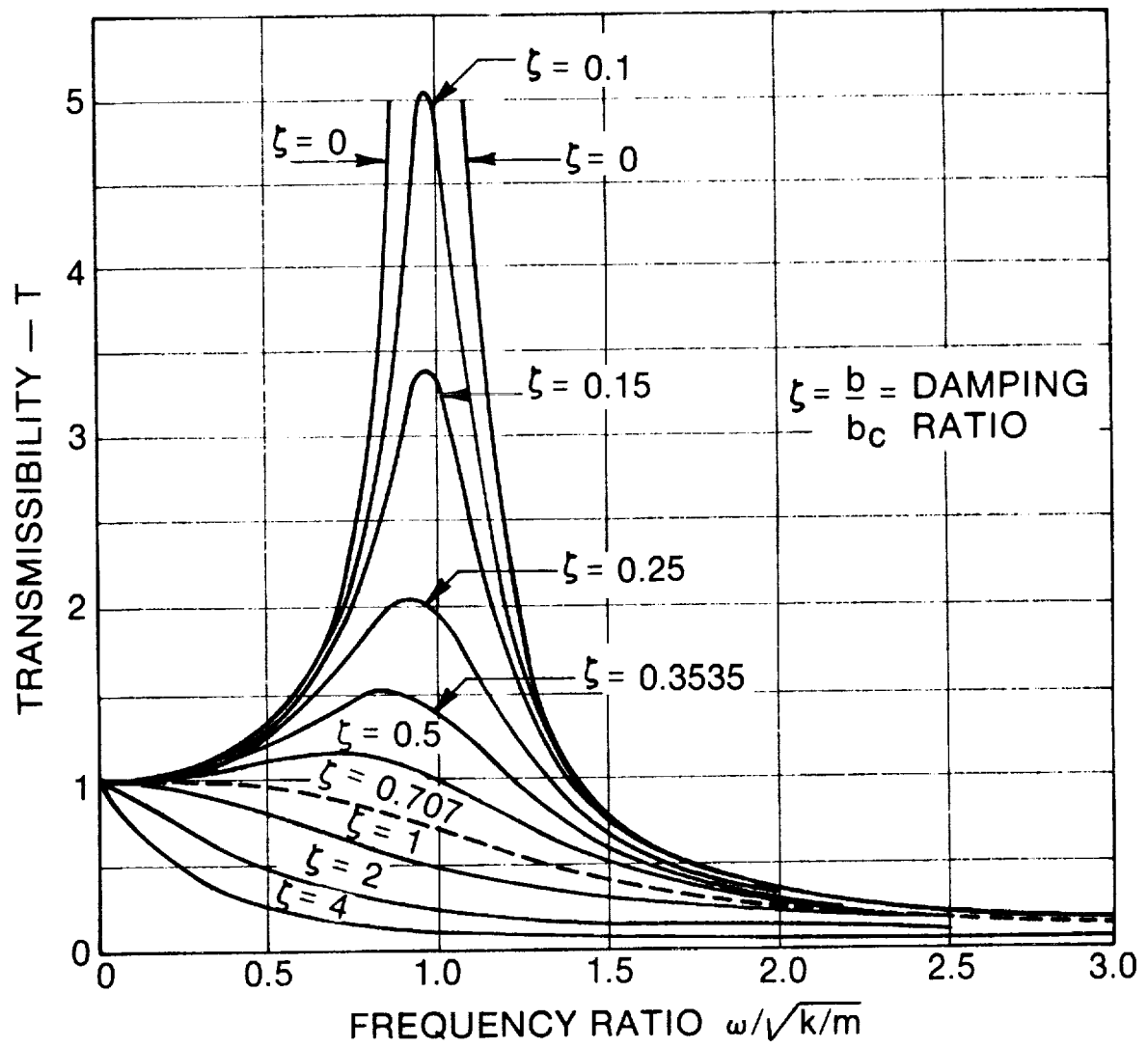* Equations (2-32) through (2-34) are from Reference 2.1.

21

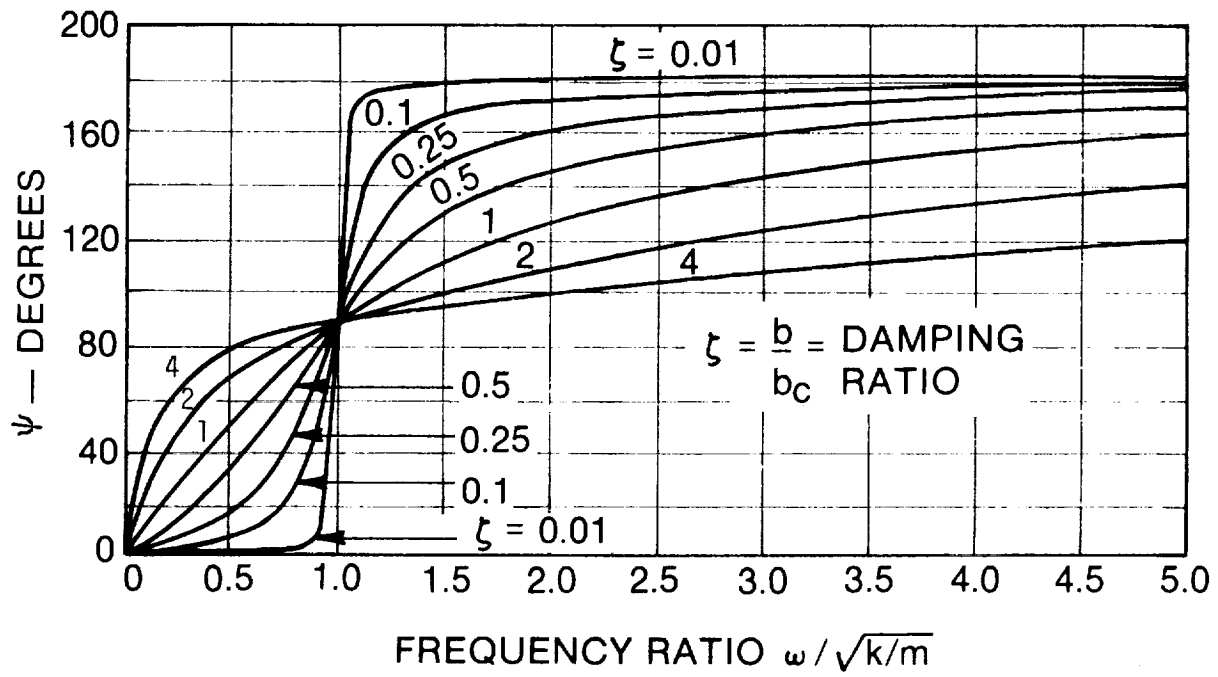Fig. 9 Transmissibility versus Frequency Ratio

Fig. 10 Phase Angle versus Frequency Ratio

23

For the case in which the foundation has a prescribed sinusoidal motion (Figure 8b), the governing equation becomes

$$m\ddot{x} + b\dot{x} + kx = bu_o\omega\cos\omega t + ku_o\sin\omega t \qquad (2\text{-}35)$$

where $u_o\sin\omega t$ is the prescribed displacement of the foundation and, thus, $u_o\omega\cos\omega t$ is the related prescribed velocity of the foundation (the velocity is the time derivative of the displacement). Again, considering only the steady-state solution to equation (2-35), the response is given by

$$x = Tu_o \sin(\omega t - \Psi) \qquad (2\text{-}36)$$

where T and Ψ are defined by equations (2-33) and (2-34), respectively. Analogous to equation (2-32), the motion transmissibility and phase angle are defined by

$$\frac{x}{u_o} = T \sin(\omega t - \Psi) \qquad (2\text{-}37)$$

from equation (2-36). Thus, the force transmissibility and phase angle are identical to the motion transmissibility and phase angle for the corresponding forms of the forced vibration. Consequently, Figures 9 and 10 apply to both damped forced vibration cases.

In general, practical vibratory systems have more than one degree of freedom. Practical systems can usually be represented with reasonable accuracy by a finite number of spring, mass, and damper elements, connected together in some fashion. This is often referred to as a lumped parameter representation. Real systems may exhibit free or forced vibration or a combination of both. Damping is often added to systems intentionally to aid in vibration reduction. In such cases, one end of the damper is generally attached to a rigid support. Reduced support stiffness (by the installation of soft members) is sometimes used to isolate (or insulate) vibration. Dynamic absorbers, which themselves have two or more degrees of freedom, are also used occassionally to isolate (or insulate) vibration. For a more complete discussion of multiple-degree-of-freedom systems, the reader is referred to Reference 2.1 through 2.4.

2.2 Vibrations in Rotating Machinery

Section 2.2 is intended to provide an introduction to the theory of rotor bearing vibrations. A few references, [2.6] through [2.9], are available which provide a fairly complete treatment of rotor bearing vibration.

Any machines which have rotating components are classified as rotating machines. This classification includes machinery in a broad range of sizes. Some typical small rotating machines are gyroscopes, electric motors for household appliances, and turbochargers. Medium-size rotating machines include aircraft gas turbine engines, small industrial compressors, electric motors, and internal combustion engines. Some large rotating machines are steam turbine/generator sets, ground-based gas turbine/generator sets, large industrial compressors, large diesel engines, and power transmission equipment. Vibrations of rotating machines can lead to serious problems, parti-

ularly in the areas of noise pollution, operator (and consumer) safety, and machinery operating expenses. For example, unscheduled downtime and repair costs resulting from unexpected machinery failure can have a devastating impact on operating expenses. Consequently, areas which have seen intensive developmental effort in the past several years (with a high level of continued effort in the foreseeable future) are vibration monitoring, vibration diagnostics, and vibration suppression; the latter includes the development of elastomer dampers for rotating machinery. Suppression of vibration in rotating machinery is generally accomplished either by removing the sources of vibration or by the dissipation of vibrational energy through damping (or, most frequently, by a combination of the two).

Rotor vibration is generally classified according to the direction and frequency of the vibratory motion. The three directions of motion illustrated in Figure 11 are lateral, axial, and torsional. Lateral motion involves a displacement and/or rotation of the rotor centerline. In this context, rotation is about an axis intersecting and normal to the rotor centerline. Axial motion occurs parallel to the rotor centerline. Torsional vibration involves a rotation (or twisting) of the rotor about its centerline relative to a frame of reference fixed at some point in the rotor. Vibrations which occur at the frequency of rotation of the rotor are referred to as synchronous vibrations. Those which occur at other frequencies are known as nonsynchronous vibrations. In geared systems, where two or more rotors are operating at different speeds, a different synchronous frequency is associated with each rotor.

Elastomer dampers have been used to control torsional as well as lateral vibration. Further discussion of rotor vibration in this handbook will address only lateral vibrations. Both synchronous and nonsynchronous vibrations can be controlled by elastomer dampers. Synchronous rotor (lateral) vibration is usually due to mass unbalance in the rotor, although other synchronous forcing functions are occasionally present. Rotor mass unbalance results from an eccentricity of the centroidal axis of the rotor C_G relative to its geometric center. In practice, this unbalance is generally a result of unavoidable imperfections in rotor manufacture and assembly. Synchronous vibration is usually stable; although, if large motions are sustained, it can often lead to rapid machinery failure.

Synchronous vibration due to unbalance is most often controlled through a combination of rotor balancing and external (or support) damping, particularly when the rotor operates above one or more critical speeds* (or synchronous resonances). Rotor balancing refers to any of a number of procedures used for applying intentional unbalance to a rotor in order to compensate for existing unbalance and thereby reduce synchronous rotor vibration [2.6, 2.9]. Since a rotor can never be "perfectly" balanced, some damping is required to control vibrations at rotor critical speeds (although bearing damping is sometimes sufficient). Very often, rotor balancing by itself is not sufficient to adequately control synchronous rotor

---

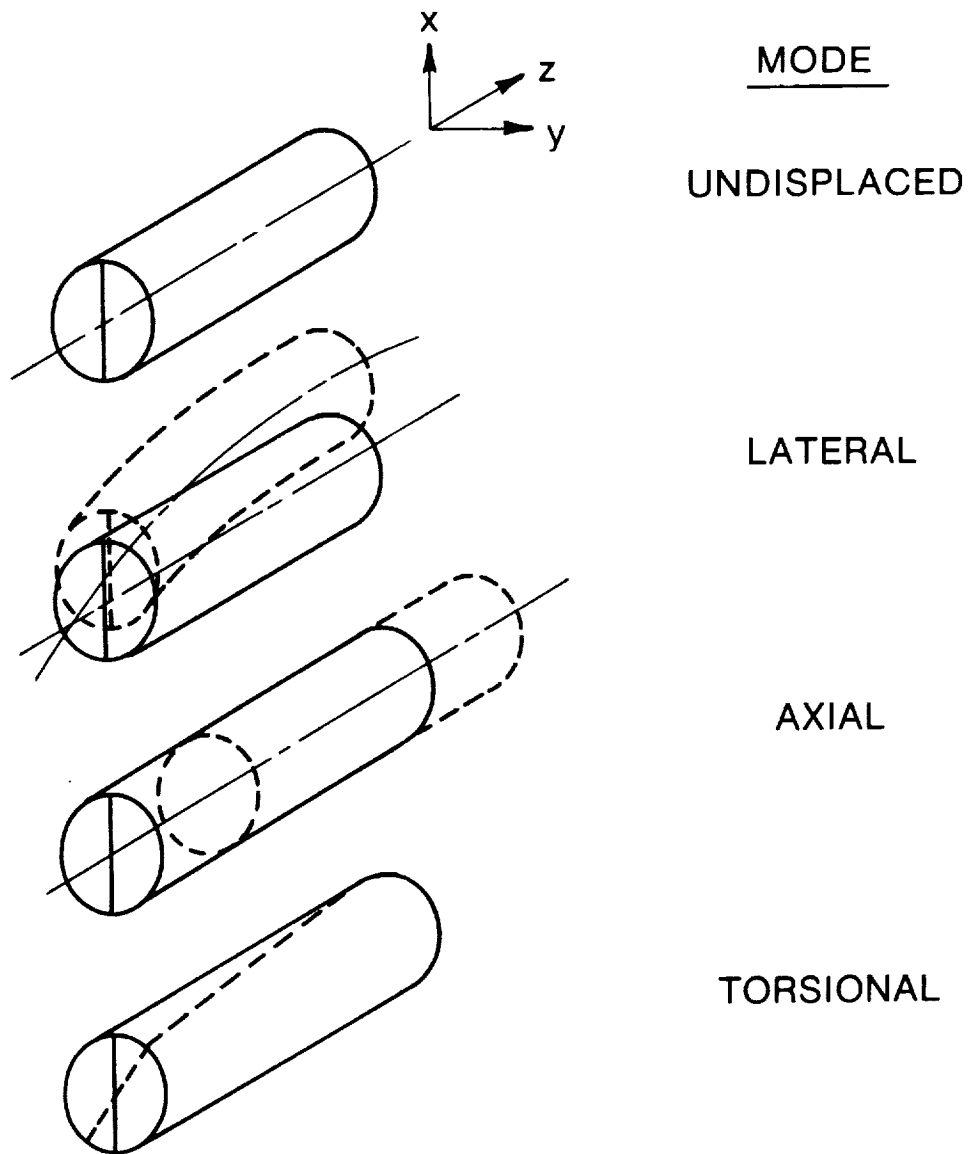* which operate at speeds above critical speeds are often termed "high speed" rotors

Fig. 11 Rotor Vibration Modes

26

vibration. Thus, the use of external damping is often required in addition to rotor balancing. Also, the addition of external damping generally permits the reduction of balancing tolerances, which can result in a substantial reduction in rotor manufacturing and assembly costs.

In 1919, H. H. Jeffcott [2.10] presented an analysis of a simple, concentrated-mass, flexible rotor which included the effect of external damping. Although the model is very simple, the analysis demonstrated the shifting of phase of the center of gravity of the rotor as a critical speed is traversed. The analysis has been proved experimentally and has subsequently formed the basis of later analyses of synchronous vibration in damped rotors, using more realistic rotor models. Jeffcott's analysis is based on the rotor model illustrated in Figure 12. This model consists of a longitudinally and laterally symmetric rotor with a single concentrated mass in the center supported by a flexible, massless shaft, which is, in turn, mounted on simple supports. This analysis also applies to the rotor model presented in Figure 13, as long as the values of the model parameters (mass, stiffness, damping and eccentricity) are the same for both models. The analysis assumes small deflections, linear and symmetric stiffness, and viscous damping with no gyroscopic effect. An end view of the rotor model is presented in Figure 14, where the origin of the stationary (nonrotating) coordinate system "XY" is located at the undeflected centerline of the rotor. For a vertical rotor, the undeflected centerline is coincident with the line of bearing centers. For a horizontal rotor, these two lines differ by the static gravity sag of the rotor. The point E represents the deflected centerline of the rotor, while the point M represents the location of the center of mass of the rotor. Since the coordinate system is not rotating, the sketch in Figure 14 represents an instant of time when the line EM is at an angle ωt from the X axis. Rotating of the rotor is counter-clockwise. The coordinates of the point E at that instant in time are x and y. The coordinates of the point M at the same instant in time are x´ and y´, related to x and y by

$$x´ = x + a \cos\omega t \qquad (2\text{-}38)$$

$$y´ = y + a \sin\omega t \qquad (2\text{-}39)$$

where a is the fixed distance between points E and M. This fixed distance is known as the mass eccentricity of the rotor. The differential equations of motion for the rotor are

$$m\ddot{x}´ + b\dot{x} + kx = 0 \qquad (2\text{-}40)$$

$$m\ddot{y}´ + b\dot{y} + ky = 0 \qquad (2\text{-}41)$$

where m is the mass of the rotor and b and k are the external viscous damping and stiffness coefficients, respectively. In the X-direction, the inertial term, mx´, is proportional to the acceleration in the X-direction of the point M. However, the damping and stiffness act at the point E and, therefore, result in forces proportional to $\dot{x}$ and x, respectively. The forces in the Y-direction act in a similar fashion. Substituting equations (2-38) and (2-39) into equations (2-40) and (2-41), eliminating x´ and y´, and rearranging terms gives equations (2-42) and (2-43), which are valid for a constant value of rotational speed, ω.
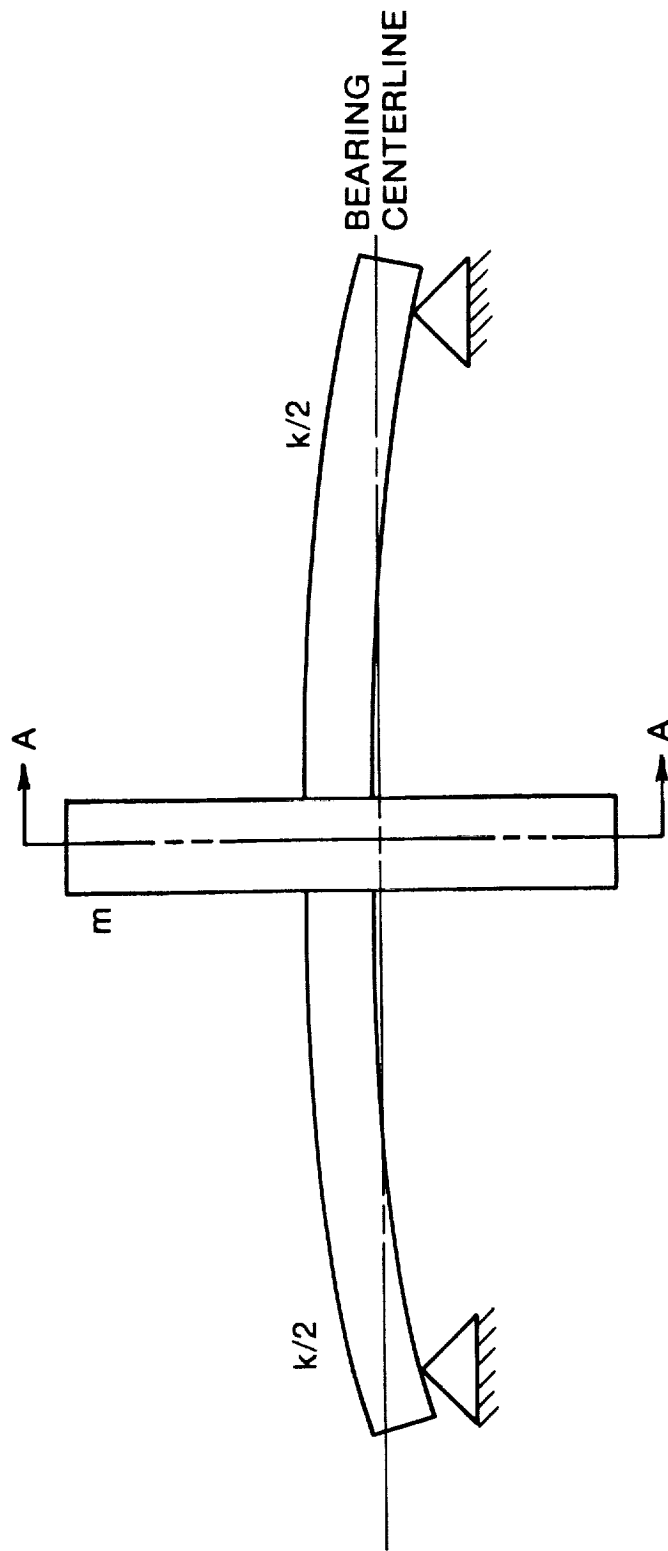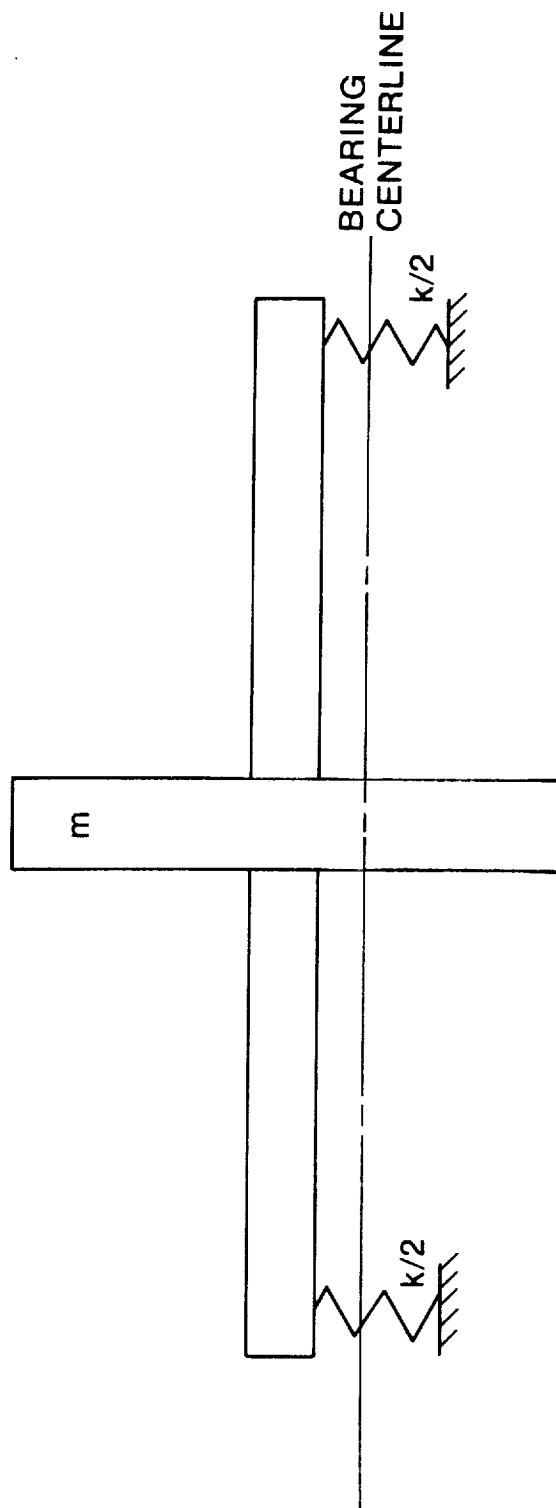
27

Fig. 12 Rotor Model Used for Original Jeffcott Analysis

Fig. 13 Analogous Rotor Motor for Original Jeffcott Analysis

Fig. 14 Cross-Sectional View of Jeffcott Rotor Model (Section "A-A" of Fig. 12)

30

$$\ddot{mx} + b\dot{x} + kx = ma\omega^2\cos\omega t \qquad\qquad (2-42)$$

$$\ddot{my} + b\dot{y} + ky = ma\omega^2\sin\omega t \qquad\qquad (2-43)$$

Note that the rotor system is assumed to be symmetric with respect to the XY coordinate system. That is, the system parameters (damping and stiffness) are assumed to have equal values in the X and Y directions. (Further, gyroscopic or bearing cross coupling terms have not been included.)

Equations (2-42) and (2-43) may be easily solved by substituting an assumed solution into the differential equations and solving for the constants, since the form of the solution is obvious from Figure 14. Jeffcott solved these equations for both the transient (general) and steady-state (particular) solutions. Only the steady-state (synchronous) solutions are of interest here. From Figure 14, it is clear that

$$x = A\cos(\omega t-\beta) \qquad\qquad (2-44)$$

and

$$y = A\sin(\omega t-\beta) \qquad\qquad (2-45)$$

where A is the distance from 0 to E and β is known as the phase angle.

Substituting equations (2-44) and (2-45) and their derivatives into equations (2-42) and (2-43) and solving for the constants A and β gives:

$$A = \frac{ma\omega^2}{\sqrt{(k-m\omega^2)^2 + b^2\omega^2}} \qquad\qquad (2-46)$$

$$\beta = \arctan\frac{b\omega}{k-m\omega^2} \qquad \text{where } 0 \le \beta \le \pi \qquad (2-47)$$

The critical speed of the rotor is defined as the speed at which the value of A is a maximum. The equation for the critical speed, ω_{CR}, may be derived by differentiating equation (2-46) with respect to ω, setting it equal to zero, and solving for ω, resulting in

$$\omega_{CR} = \frac{2k}{\sqrt{4mk-2b^2}} \qquad\qquad (2-48)$$

It is apparent from equation (2-48) that the effect of increasing the damping is to increase the critical speed.

The phase, β, increases from zero to 180 degrees (0 to π radians) as the speed is increased and has a value greater than or equal to 90 degrees (0.5 π radians) at the critical speed. By comparison, the phase angle at resonance for a unidirectional vibratory system is less than or equal to 90 degrees.

31

The amplitude of rotor precession for any rotational speed, given by equation (2-46), is directly proportional to rotor mass eccentricity, a. Thus, it is also proportional to the rotor mass unbalance represented by the term (ma). The rotor transmissibility, T_r, is defined as the ratio of the amplitude, A, to the mass eccentricity, a, and is given by

$$T_r = \frac{A}{a} = \frac{m\omega^2}{\sqrt{(k-m\omega^2)^2 + b^2\omega^2}} = \frac{(\omega/\omega_n)^2}{\sqrt{[1 - (\omega/\omega_n)^2]^2 + 4\zeta^2(\omega/\omega_n)^2}} \qquad (2-49)$$

where ω_n and ζ are given by equations (2-4) and (2-10), respectively. Equation (2-49) is clearly analogous to the equation for transmissibility of a unidirectional vibratory system, given by equation (2-33). If the damping of a rotordynamic system is reduced to zero, ω_{CR} becomes equal to ω_n and the amplitude becomes unbounded at the critical speed for any value of rotor mass unbalance. Thus, for operation at a critical speed, rotor amplitude is limited only by the existence of damping.

Nonsynchronous vibrations, unlike synchronous vibrations, are often unstable. These unstable vibrations are generally characterized by an onset speed or load. Below this onset, this vibration is stable and generally not apparent. Above the onset, this vibration may be unstable and is often destructive. The addition of external damping generally raises the speed or load at which the onset of instability occurs. If the onset is raised beyond the operating conditions of the rotor, this vibration is considered to be acceptable.

There are many possible sources of nonsynchronous vibration. Several of these are listed below. References are provided for the interested reader.

1. Oil whip in fluid-film bearings [2.11, 2.12]

2. Ball-pass excitation in rolling-element bearings

3. Alford's tip clearance forces [2.13]

4. Propeller flutter [2.14]

5. Torque whirl [2.15]

6. Internal damping from material hysteresis, shrink fits, spline friction and coupling friction [2.16, 2.17]

7. Gear mesh excitation

8. External sources of vibration such as the firing of reciprocating machines, and floor vibrations and fluid and pipe vibration from other machines

9. Rotor/stator rubs [2.18]

10. Anisotrophy in rotor, e.g., nonsymmetric shaft stiffness [2.19, 2.20]

Additional information on general nonsynchronous rotor vibrations may be found in References 2.21, 2.22, and 2.23.

2.3 External Damping in Rotating Machinery

The use of external damping to control vibrations in rotating machinery is not only desirable but is often necessary to insure safe machinery operation. External damping, which is generally stabilizing, is defined as damping acting on motion relative to a stationary frame of reference. External damping is most often provided in bearings or bearing supports. Internal damping, as distinguished from external damping, is defined as damping which acts on motion relative to a rotating reference frame. In general, internal (shaft) damping has a destabilizing effect on high-speed rotor operation.

External damping is often used in conjunction with rotor balancing for controlling synchronous vibration by reducing vibration amplitude. The use of external damping in this context generally permits balancing tolerances to be relaxed and increases the tolerance of a rotor to long-term balance degradation. The existence of external damping also increases rotor system tolerance to sudden changes in unbalance which may be due, for example, to blade loss in a gas turbine engine. The external damping helps to control the transient as well as the steady-state response resulting from such a sudden change in unbalance. Occasionally, the application of external damping actually eliminates the need for balancing and is a very reliable method of controlling nonsynchronous vibrations. Thus, external damping is often used for reduction of vibration amplitude as well as for control of potential instabilities from nonsynchronous vibration. In many cases the application of external damping is the only means of vibration control, short of redesigning the rotor system or changing the operating specifications (e.g., reducing design speed or load).

External damping may be provided in several ways. In some cases the external damping is coincidental in the design of the rotor system and not specified. In such cases it is very difficult or, in fact, impossible to either predict or control the level of the external damping. The most common sources of coincidental external damping are bearings and structure. Fluid-film bearings often provide substantial damping to the rotor system. On the other hand, rolling-element bearings generally provide very little external damping. Consequently, rolling-element bearings must often be designed to operate in series with some type of mechanical damper.

Mechanical dampers can provide a source of external damping. In such cases the level of damping is relatively controllable and predictable depending upon the type of damper used. Mechanical dampers are most often designed to operate in series with bearings as integral parts of the bearing supports. Several types of mechanical dampers are in current use. Currently, the most commonly used mechanical damper in rotating machinery is the squeeze-film damper (hydraulic mount). This type of damper is, essentially, a nonrotating fluid-film bearing. The damper is composed of concentric nonrotating journals, and the space between the journals is filled with a fluid, usually oil. Squeeze-film dampers have a number of advantages of which the most important is their acceptance by designers based upon years of experience. If properly designed, they are capable of providing high levels of damping. In general, the operating temperature of squeeze-film dampers is limited only by the entrapped fluid.

33

There are a number of disadvantages to the use of squeeze-film dampers, particularly in comparison to elastomer dampers. Squeeze-film dampers generally require some sealing or scavenging of fluid, or both, and often require a filtered oil supply and/or cooling hardware. This results in an increase in the cost and complexity of the hardware. The higher cost of squeeze-film dampers is due to the complexity of design, the large number of parts required, and the tight tolerances that are generally necessary. Squeeze-film dampers may also require a parallel support stiffness component which represents yet more hardware and higher cost. For the interested reader, additional information on squeeze-film dampers is available from References 2.24 through 2.27.
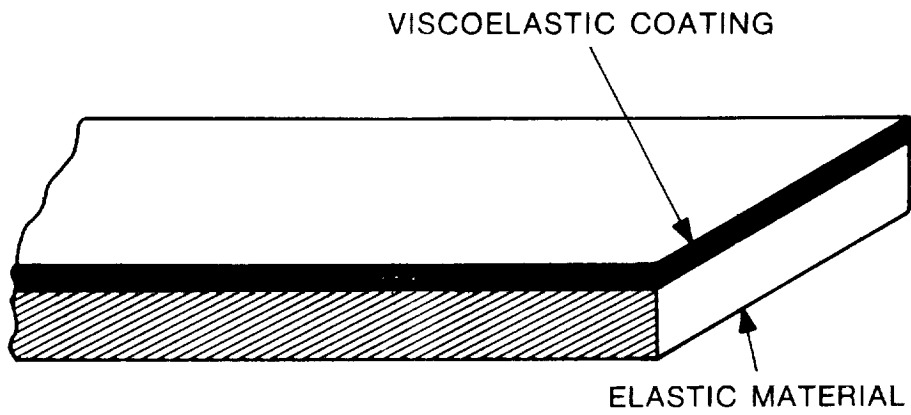
Another type of mechanical damper which is in relatively common use in rotating machinery is the coulomb damper. This type of damper provides a dissipative force which is independent of position or velocity and always acts in a direction which opposes the relative velocity across the damper. Coulomb damping is usually provided by dry friction between two solid surfaces. Coulomb dampers have the advantages of relative simplicity and low cost. However, they also have a number of disadvantages which tend to limit their application. It is extremely difficult to predict or design for the level of damping in a coulomb damper. A threshold force exists below which the coulomb damper does not participate in the dynamics of the rotor system and does not provide any energy dissipation. Coulomb dampers often exhibit substantial inconsistency in operation. Specifically, they are generally sensitive to small changes in preload force, operating temperature, and mating surface wear, all of which tend to change with time during operation. In general, coulomb dampers are not considered to be very reliable and, thus, are generally not used for most critical rotor applications. They also do not lend themselves to compact designs, a requirement for many applications. Additional information on coulomb dampers is available from References 2.28 and 2.29.

Elastomers are beginning to see use as mechanical dampers for rotating machinery, and are occasionally used in the form of O-rings for sealing squeeze-film dampers. In this application the elastomers provide an additional level of damping. Dampers which employ elastomers as the sole source of damping are not currently in common use. This is primarily due to the general lack of demonstrated reliability and lack of available design data for elastomer dampers.
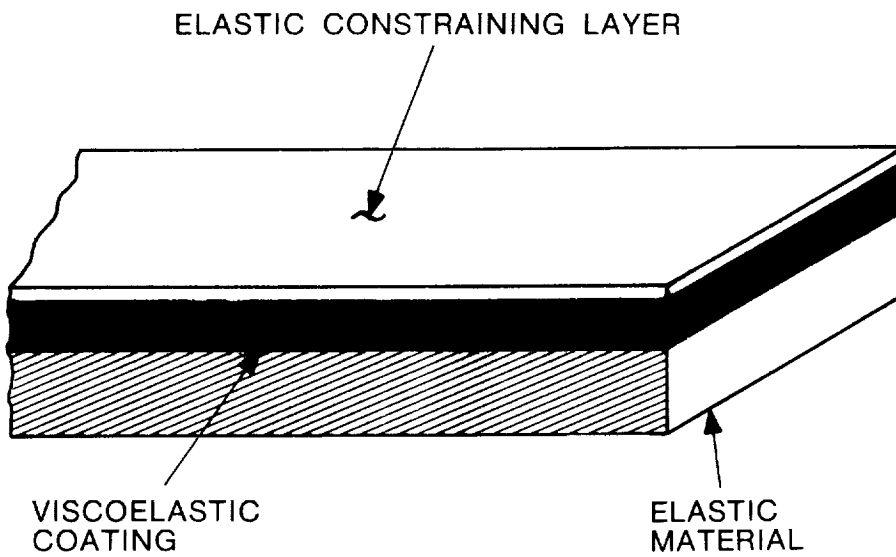
For completeness in this discussion of damping, a brief description of visco-elastic damping in structural (constrained layer) applications follows, although it is not the main theme of this handbook.

2.4 Viscoelastic Structural Damping

The application of energy-dissipative material to structural elements for achieving a reduction in unwanted vibrations is certainly not new. A method often employed in the automotive industry is to spray a panel with a protective coating which not only protects the panel from environmental attack but also provides a mechanism for the reduction in noise level. This under-coating technique is often referred to as unconstrained extensional* damping, since the energy loss mechanism is provided by the coating when the base material experiences tensile or compressive deformations (Figure 15a). The aircraft industry also uses this technique by applying a damping layer in

34

VISCOELASTIC COATING

ELASTIC MATERIAL

(a) UNCONSTRAINED DAMPING TREATMENT

ELASTIC CONSTRAINING LAYER

VISCOELASTIC
COATING

ELASTIC
MATERIAL

(b) CONSTRAINED DAMPING TREATMENT

Fig. 15 Viscoelastic Layer Damping Treatment

35

the form of damping tape over the base structure. Shear* damping is another
popular form of damping treatment which is characterized by the sandwiching
of an energy dissipative layer between two layers of more rigid materials.
Deformation of this constrained sandwiched structure (Figure 15b) provides
shear loading in the damping layer which may reduce vibrations.

One of the first works in this area was published by Oberst who studied the
bending vibrational effects of an elastic plate coated on one side with a
layer of viscoelastic material [2.32]. Oberst found that not only is the
damping of the composite structure dependent upon the loss factor of the
viscoelastic material, but that damping is also dependent on the stiffness
and thickness of the viscoelastic material.

Another pioneer in this field was Kerwin who is generally acknowledged as
being first to provide an analysis of the shear damping mechanism of a
constrained viscoelastic layer (constrained between the thin elastic con-
straining layer and the basic elastic structure). Kerwin [2.33] establishes
a complex stiffness relationship, demonstrates that the neutral axis of the
composite system is frequency dependent, and also demonstrates that the
normal force in the viscoelastic layer may be neglected, since the magnitude
of the modulus for the viscoelastic material is generally at least an order
of magnitude smaller than the modulus of the elastic layers.

Kerwin's work, although limited to an infinitely long or simply supported
beam which is subject to bending, has been extended by Di Taranto and
Blasingame [2.34, 2.35] to a more generalized form. Reference 2.34 develops
a sixth-order, complex, homogeneous partial differential equation which
describes the axial displacement of a viscoelastic layer which is constrained
between the two elastic layers of the beam. Mead and Markus [2.36] have
extended the work of Di Taranto et al by developing a sixth-order partial
differential equation for the transverse vibrations of the same beam con-
figuration. Both the work of Di Taranto and Blasingame [2.34, 2.35] and
Mead and Markus' publication [2.36] are restricted to a free beam which is
not subjected to axial loading.

Many other authors have extended the state of analytical and experimental
investigation to multilayered and other variations of the basic three-
layered configuration. For example, Derby, Ruzicka, Schubert and Pepi
[2.37, 2.38] have presented comprehensive experimental data relating to
the viscoelastic shear damped characteristics of composite structures.
Reference 2.37 provides a review of the design equations including the govern-
ing design parameters for various shear damped configurations. Derby et al
[2.37] also provides extensive experimental results for L-shaped, T-shaped,
circular, tubular, and rectangular composite material cross-section beams.
The iterative scheme for design implementation presented in [2.37] was
improved upon by the latter publication [2.38] to provide a more direct
utilization of design data.

Grootenhuis, Agbasiere and Nakra [2.39, 2.40, 2.41], along with Frohrib
[2.42], Nashif and Nicholas [2.43, 2.44], Plass [2.46] and Schwarzl [2.47]
have published extensive literature on multiple-layered rectangular beam

---

* See Ross, Ungar and Kerwin [2.31] for a review of both types of damping
   treatments.

treatments as well as on viscoelastic composite structures. Investigations such as those published by Parfitt [2.48] and Plunkett and Lee [2.49] have analyzed the sandwiched viscoelastic-elastic structure for various cut lengths of the constraining layer. Reference 2.49 provides a thorough discussion of this system as well as an optimization of the length of the constraining layers for single and multiple-laywered laminated structures. An excellent review of the state of the art in viscoelastic structual damping is contained in the work of Nakra [2.50]. Recent applications are provided in papers presented at a conference on viscoelastic damping [2.51].

2.5 Summary

An understanding of basic linear vibration theory is required for effective design of machinery dampers. A dynamic system may be represented as a series of masses, springs and dampers. Several measures of damping effectiveness, as a primary mechanism for vibration control, are in common use, including damping ratio, logarithmic decrement and loss coefficient. Dynamic systems may be subjected to free or forced vibration. Free vibration exists when a dynamic system is given a set of perturbations and then allowed to vibrate freely, without an external influence. When a dynamic system vibrates under the influence of an external forcing function, usually harmonic, the system is said to undergo forced vibration. Although real vibratory systems possess an infinite number of degrees of freedom, they can generally be represented reasonably well by models with a finite number of degrees of freedom.

Rotordynamic systems may be subjected to synchronous and nonsynchronous vibrations. Synchronous vibrations have a frequency equal to the speed of rotation of the rotor. Nonsynchronous vibrations occur at frequencies other than synchronous. Synchronous vibrations are most often due to rotor mass unbalance. Nonsynchronous vibrations, which are frequently unstable, may result from any of a number of sources, several of which are listed above. Both synchronous and nonsynchronous vibrations, if not controlled, are potentially destructive. Damping is one of the most practical means a designer has to control synchronous as well as nonsynchronous vibrations.

The use of external damping to control the vibration of rotating machines has been discussed. Reference has been made to the use of dampers in bearing supports, and particularly to squeeze-film and coulomb dampers which are currently the most popular types of mechanical dampers. Elastomer dampers are not currently in common use for rotating machines. However, they have an excellent potential in this area. Their primary disadvantage is a lack of available design data. This handbook seeks to fill this need by providing design data for expanding the use of elastomer dampers.

The material in this chapter was intended only as introductory background information and was not in any way intended to be exhaustive. For more detail, numerous references have been cited and are listed below.

2.6 References

2.1   Harris, C.M., and Crede, C., editors, Shock and Vibration Handbook, Second Edition, McGraw-Hill, New York, 1976.

2.2   Den Hartog, J.P., Mechanical Vibrations, Fourth Edition, McGraw-Hill Book Company, Inc., New York, New York, 1956.

2.3   Timoshenko, S., *Vibration Problems in Engineering*, D. Van Nostrand Co., Inc., Princeton, New Jersey, Third Edition, 1955.

2.4   Thomson, W.T., *Vibration Theory and Application*, Prentice Hall, Inc., Englewood Cliffs, N.J., 1965.

2.5   Lazan, B.J., *Damping of Materials and Members in Structural Mechanics*, Pergamon Press, New York, 1968.

2.6   Dimentberg, F.M., *Vibrations of Rotating Shafts*, Butterworth and Co., Ltd., London, 1961.

2.7   Tondl, A., *Some Problems in Rotordynamics*, Publishing House Czechoslovakian Academy of Sciences, Prague, 1965.

2.8   Loewy, R.G., and Piarulli, V.J., *Dynamics of Rotating Shafts*, Shock and Vibration Monograph, No. 4, Naval Research Laboratory, Washington, D.C., 1969.

2.9   Rieger, N.F., and Crofoot, J.F., *Vibrations of Rotating Machinery*, *Part I: Rotor-Bearing Dynamics*, The Vibration Institute, Claredon Hills, Illinois, 1977.

2.10 Jeffcott, H.H., "The Lateral Vibration of Loaded Shafts in the Neighborhood of a Whirling Speed--The Effect of want of Balance", *Phil.Mag.*, Series 6, Vol. 37, p. 304, 1919.

2.11 Hon, Y., "A Theory of Oil Whip", *J. of Appl. Mech*, Trans. ASME, pp. 189-198, June 1959.

2.12 Poritsky, H., "Contribution to the Theory of Oil Whip", Trans. ASME, Vol. 75, pp. 1153-1161, August 1953.

2.13 Alford, J.R., "Protecting Turbomachinery from Self-Excited Rotor Whirl", *Journal of Engineering for Power*, Trans. ASME, Series A, No. 4, pp. 333-344, October 1965.

2.14 Erich, F.F., "An Aeroelastic Whirl Phenomenon in Turbomachinery Rotors", ASME Transactions, *Journal of Engineering for Industry*, ASME Paper No. 73-DET-97, September 1973.

2.15 Vance, J.M., "Torque Whirl - A Theory to Explain Nonsynchronous Whirling Failures of Rotors with High Load Torque", ASME Paper No. 76-DE-29, Design Engineering Conference, Chicago, Illinois, April 5-8, 1976.

2.16 Robertson, D.L., "Hysteretic Influences on the Whirling of Rotors", *Proc. Inst. Mech. Engrs.*, London, Vol. 131, p. 513, 1935.

2.17 Marmol, R.A., Smalley, A.J., and Tecza, J.A., "Spline Coupling Induced Nonsynchronous Rotor Vibrations", *Journal of Mechanical Design*, Trans. ASME, Paper No. 79-DET-60.

2.18 Ehrich, F.F., "The Dynamic Stability of Rotor/Stator Radial Hubs in Rotating Machinery", ASME Trans., *J. of Eng. Ind.*, November 1969, pp. 1025-1028.

2.19 Yamamoto, T., and Hiroshi, O., "On the Unstable Vibrations of a Shaft Carrying an Unsymmetric Rotor", J. of Appl. Mech., Trans. ASME, Paper No. 64-APM-32, 1964.

2.20 Smalley, A.J., Tessarzik, J.M., and Badgley, R.H., "The Stability of an Asymmetric Rotor in Damped Supports", ASME Paper No. 78-GT-172, presented at the 1978 ASME Gas Turbine Conference, April 1978.

2.21 Pontsky, H., "Rotor Stability", Proceedings of the Fifth U.S. National Congress of Applied Mechanics, ASME, pp. 37-61, 1966.

2.22 Gunter, E.J., Dynamic Stability of Rotor-Bearing Systems, NASA SP-113, Office of Technical Utilization, U.S. Government Printing Office, Washington, D.C., 1966.

2.23 Lund, J.W., "Some Unstable Whirl Phenomena in Rotating Machinery", The Shock and Vibration Digest, Volume 7, No. 6, June 1975.

2.24 Thomsen, K.K., and Anderson, H., "Experimental Investigation of a Simple Squeeze-Film Damper", ASME Paper No. 73-DET-101.

2.25 Vance, J.M., and Kirton, A.J., "Experimental Measurement of the Dynamic Force Response of a Squeeze-Film Bearing Damper", Journal of Engineering for Industry, Trans. ASME, Series B, Vol. 97, No. 4.

2.26 Sharma, R.K., and Botman, M., "An Experimental Study of the Steady-State Response of Oil-Film Dampers", ASME Paper No. 77-DET-33.

2.27 Marmol, R.A., and Vance, J.M., "Squeeze-Film Damper Characteristics for Gas Turbine Engines", ASME Paper No. 77-DET-18.

2.28 Nestondes, E.J., A Handbook on Torsional Vibration, The University Press, Cambridge, England, 1958, p. 587.

2.29 Darlow, M.S., and Smalley, A.J., "Design and Application of a Scale Model Test Rig for Supercritical Power Transmission Shafting", MTI Report 79TR44, June 1978.

2.30 Harris, C.M. and Crede, C.E., editors, Shock and Vibration Handbook, Vol. 2, Data Analysis, Testing, and Methods of Control, McGraw-Hill Book Company, New York, 1961.

2.31 Ross, D., Ungar, E.E. and Kerwin, E.M., Jr., "Damping of Plate Flexural Vibrations by Means of Viscoelastic Laminae", Structural Damping Colloquium, ASME Meeting, Atlantic City, New Jersey, p. 49, December 1969.

2.32 Oberst, V.H., "Uber Die Dampfung Der Biegeschwingungen Dunner Bleche Durch Fest Haftende Belage", Acustica, Heft 4, p. 181, 1952.

2.33 Kerwin, E.M., Jr., "Damping of Flexural Waves by a Constrained Visco-elastic Layer", Journal of the Acoustical Society of America, Vol. 31, No. 7, p. 952, July 1968.

2.34   Di Taranto, R.A., "Theory of Vibratory Bending for Elastic and Visco-
       elastic Layered Finite-Length Beams", Journal of Applied Mechanics,
       p. 881, December 1965.

2.35   Di Taranto, R.A. and Blasingame, W., "Composite Damping of Vibrating
       Sandwich Beams", Journal of Engineering for Industry, p. 633, November
       1967.

2.36   Mead, D.J. and Markus, S., "The Forced Vibration of a Three-Layered,
       Damped Sandwich Beam with Arbitrary Boundary Conditions", Sound
       Vibration, Vol. 10 (2), p. 163, 1969.

2.37   Derby, T.F., Ruzicka, J.E., Schubert, D.W. and Pepi, J.S., "Damping of
       Structural Composites with Viscoelastic Shear-Damping Mechanisms",
       NASA Contractor Report, NASA CR-742, March 1967.

2.38   Derby, T.F. and Ruzicka, J.E., "Loss Factor and Resonant Frequency of
       Viscoelastic Shear-Damped Structural Composites", NASA Contractor
       Report, NASA CR-1269, February 1969.

2.39   Grootenhuis, P. and Agbasiere, J.A., "Flexural Vibration of Symmetrical
       Multilayered Beams with Viscoelastic Damping", Journal of Mechanical
       Engineering Science, Vol. 10, No. 3, 1968.

2.40   Grootenhuis, P., "The Control of Vibrations with Viscoelastic Materials",
       Journal of Sound and Vibration, Vol. 11, p. 421, 1970.

2.41   Grootenhuis, P. and Nakra, B.C., "Structural Damping Using a Four Layer
       Sandwich", ASME Paper No. 71-Vibr-20, 1971.

2.42   Frohrib, D., "The Optimum Design of Five-Ply Viscoelastic Isolation
       Flexures for Point-Inertial Loading", Shock and Vibration Bulletin,
       No. 38, Part 3, p. 37, November 1968.

2.43   Nashif, A.D. and Nicholas, T., "Vibration Control by a Multiple-Layered
       Damping Treatment", The Shock and Vibration Bulletin, No. 41, Part 2,
       p. 121, December 1971.

2.44   Nashif, A.D. and Nicholas, T., "Attenuation of Vibrational Amplitudes
       Through the Use of Multiple-Layered Damping Treatments", ASME Paper
       No. 71-Vibr-40, 1971

2.45   Nicholas, T., "The Effects of Rotary Inertia and Shear Deformation on
       the Flexural Vibrations of a Two-Layered Viscoelastic Beam", Shock and
       Vibration Bulletin, No. 38, Part 3, p. 13, November 1968.

2.46   Plass, H.T., Jr., "Damping of Vibrations in Elastic Rods and Sandwich
       Structures by Incorporation of Additional Viscoelastic Material",
       III Midwest Conference on Solid Mechanics, 1957.

2.47   Schwarzl, F., "Forced Bending and Extensional Vibrations of a Two-Layered
       Compound Linear Viscoelastic Beam", Acoustica, Vol. 8, p. 21, August 1962.

2.48   Parfitt, G.G., "The Effect of Cuts in Damping Tapes", Int. Cong.
       Acoust., 4th Copenhagen, P. 21, August 1962.

2.49   Plunkett, R. and Lee, C.T., "Length Optimization for Constrained
       Viscoelastic Layer Damping", Journal of Acoustical Society of America,
       Vol. 48, No. 1, Part 2, p. 150, 1970.

2.50   Nakra, B.C., "Vibration Control with Viscoelastic Materials", Shock
       and Vibration Digest, Vol. 8(6), 1975.

2.51   Rogers, L. (ed), "Conference on Aerospace Polymeric Viscoelastic
       Damping Technology for the 1980's", AFFDL-TM-78-78-FBA, Feb. 1978.

3.0 REVIEW OF LITERATURE ON ELASTOMERS AND ELASTOMER DAMPERS

There is substantial literature concerning elastomer materials, most of which has appeared since the development of synthetic polymers in the 1940s. A survey of this literature is presented in this chapter with emphasis upon the dynamic properties and applications of elastomers. Most of this literature concerns theoretical and analytical work conducted in the areas of viscoelastic theory and elastomer chemistry. A significant quantity of experimental work with elastomers has also been reported, but much of this is in the form of laboratory experiments. Relatively little has been published describing practical applications of elastomers to vibration problems. The material that does exist is almost entirely in the area of unidirectional loading. Few publications are available concerning practical applications of elastomer dampers for rotating machines.

The literature has been divided into four broad categories consisting of:

- Theory and Elastomer Chemistry

- Experimental Determination of Elastomer Properties

- Material Properties

- Application

Obviously, each category may contain information which spans a number of these classifications. Accordingly, each is categorized according to its main emphasis and the author's intent.

3.1 Theory and Elastomer Chemistry

Three of the more well-known texts [3.1, 3.2, 3.3]* present a detailed development of viscoelastic theory. Bland's presentation [3.1] is highly analytical while those of Flügge [3.2] and Ferry [3.3] are oriented more toward physical interpretation. Ferry's discussion of elastomers is general, including a review of elastomer chemistry and the determination of dynamic properties. Treatments of viscoelasticity are also presented in other referenced texts. For example, Argonne et al, [3.4], presented a brief treatment of viscoelasticity, along with a discussion of elastomer chemistry. An extensive bibliography (as of 1966) was also included. Lazan [3.5] included a section on viscoelasticity with particular emphasis on material damping. Smalley and Tessarzik [3.6] included a section on thermo-viscoelasticity in which they considered the effect of temperature on viscoelastic behavior. Additional references on viscoelasticity include Alfrey [3.7], Eirick [3.8], Stuart [3.9], and Tobolsky [3.10]. Some of these references include discussions on elastomer chemistry as well as viscoelasticity.

---

* Numbers in brackets indicate references found in Section 3.6.

Several authors have extended the theory of viscoelasticity to consider numerical simulation of elastomer mechanical behavior. Herrmann [3.11] developed a general numerical approach, based on variational methods, for calculating mechanical properties of incompressible and nearly incompressible materials, including elastomers. Korites and Nelson [3.12] developed an analysis to consider the heating effect on the loss factor of an elastomer element mounted in a constrained layer and have also provided some experimental correlation. Ting and Tuan [3.13] investigated the temperature distribution in a viscoelastic cylinder resulting from cyclic internal pressure.

The molecular composition and chemical structure of polymers is discussed in many works. Materials Handbook [3.14] includes a cursory discussion of the chemical structure of a number of generic elastomer materials. Corrosion [3.15] includes a discussion on polymer chains and the effect of various chain configurations on the "environmental properties" of elastomers. (The term "environmental properties" refers to the capability of an elastomer to resist degradation from various environmental sources such as chemical solvents and surface abrasion.) Moore and Geyer [3.16] presented a theoretical evaluation of the adhesion properties of elastomers. (In this context, the term "adhesion properties" refers to the surface friction existing between an elastomer material and other solid surfaces, such as glass.) Additional references on elastomer chemistry include Billmeyer 3.17, Flory 3.18, Noller [3.19], and Schmidt and Marlies 3.20.

3.2 Experimental Determination of Elastomer Properties

The properties referred to here include both the general physical and dynamic properties of elastomers. In this context, general physical properties refers to nonmechanical properties (such as density and thermal conductivity), as well as static mechanical properties. Dynamic properties refer to the dynamic mechanical properties, such as shear modulus and Poisson's ratio. The test methods used for determination of these properties and the results of these tests are of significance.

There are numerous references dealing with the determination of the general physical properties of elastomers (including the effects of environmental conditions). For example, Adkins and Gent [3.21] investigated the static stiffness of natural rubber cylindrical bushings for various directions of loading. Beerbower et al [3.22] investigated elastomer-fluid compatibility for hydraulic systems and have developed a method by which this compatibility can be predicted for various elastomer-fluid combinations. The American Society for Testing and Materials (ASTM) has published standards for many general physical property tests for elastomers [3.23].

Numerous works provide information on elastomer properties. Substantial testing has been conducted to determine the dynamic properties of various elastomer materials. Payne [3.24, 3.25, 3.26] described test procedures for measuring shape factor and determining the form of stress-strain relationships of elastomers. He also provided experimental and theoretical comparisons. Although primarily concerned with the static loading of elastomers, he also considered the effect of dynamic loading on the mechanical properties. Baltrukonis et al [3.27] described a test method for determining the dynamic

43

properties of elastomers using torsional deflection. Rightmire [3.28] described a method for measuring Poisson's ratio of elastomers. Rightmire notes that small variations in Poisson's ratio (less than 1%) can result in substantial differences in the load capacity of elastomers. Cannon et al [3.29] described a resonant mass test method for elastomer compression specimens for which data could be taken at resonance only. Accordingly, phase angle measurement was not required for this test procedure, but the frequency range of data acquisition was extremely limited.

In 1973, a symposium on the measurement of dynamic properties of elastomers and elastomeric mounts was presented at the Society of Automotive Engineers, Automotive Engineering Conference. Fourteen papers were presented at the symposium and subsequently published in a proceedings. Although the primary interest was with elastomer mounts for automobile suspensions, these papers provided a great deal of valuable insight into the general area of dynamic property measurement for elastomers. These papers cover a broad range of subjects including polymer development, test procedures, and product design.

Those papers concerned with test procedures were almost unanimous in support of the transmitted force testing technique over the resonant beam method. Miller [3.30] presented a history of dynamic testing of elastomers whereas Leonard [3.31] described the mechanical fundamentals involved in elastomer testing. Nachtigal [3.32] presented the fundamentals of instrumentation and computation for elastomer tests. Brouwer [3.33] presented a review of the resonant beam test method, with emphasis on its inherent problems. Owens [3.34] and Wilson [3.35] described the transmitted force method. Hillberry et al [3.36] described an instrument used for performing transmitted force testing with direct analog readout. Danko and Svarovsky [3.37] discussed the use of minicomputers for the determination of nonlinear damping coefficients. Nemec [3.38] and Paul and Hillberry [3.39] discussed an error analysis and correlation of several existing resonant beam test machines. Anderson [3.40] described a parameterization of elastomers to relate test results to product design. Sommer and Meyer [3.41] discussed the effect of composition, processing and test conditions on the dynamic properties measured. Puydak [3.42] and Koons [3.43] discussed dynamic testing and quality control in polymer development.

In 1973, a symposium on recent advances and developments in testing rubber and related materials was presented by the American Society for Testing and Materials. Twelve papers were presented at this symposium and subsequently published in a proceedings [3.44]. Most of the papers in this volume were primarily concerned with elastomer chemistry or static testing of elastomers. However, two of these papers related directly to dynamic testing of elastomers. Warner [3.45] presented a detailed analytical background for the dynamic testing of elastomers and Hillberry [3.46] presented a review of current (1973) test equipment.

At about the same time, another method for dynamic testing of elastomers, referred to as the Base Excitation Resonant Mass (BERM) technique, was being developed. In a series of test programs extending over several years, Chiang and Tessarzik [3.47], Gupta et al [3.48], and Smalley and Tessarzik [3.49] developed the BERM technique and generated a substantial quantity of test data, primarily for polybutadiene. Subsequently, Darlow and Smalley [3.50]

adapted this technique for use with a rotating load test machine to provide a correlation between unidirectional load elastomer test results and rotating load applications. A reasonable correlation was found that verified the applicability of unidirectional testing to the design of dampers for rotating machinery. Smalley et al [3.51] presented a review of several test methods for elastomer testing, including the BERM method, as well as a discussion of instrumentation, testing philosophy and a brief analytical background for elastomer testing.

Many authors have presented the results of elastomer tests (both static and dynamic) for a variety of elastomer materials. Painter [3.52] presented the results of a series of tests with a broad temperature range (BTR) elastomer using an analog, nonresonant mass test system. These results showed that the effect of temperature for this elastomer material was less than the corresponding effect for natural rubber of Buna-N. Gent and Lindley [3.53] presented experimental results derived from static tests for various shapes of elastomers, along with theoretical correlations. Hirsch and Boyce [3.54] described the result of a series of tests from which they determined the dynamic properties of an ethylene/acrylic elastomer. Maza [3.55] presented test results which related the dynamic properties of several elastomer materials, for frequencies above a kilohertz. Extensive test results for polybutadiene elastomers, using the BERM method, have been reported by Gupta et al [3.48], Smalley and Tessarzik [3.49], Tecza et al [3.56], and Darlow and Smalley [3.57].

Results have also been reported which relate the effect of various test parameters to the dynamic and static properties of elastomers. The test parameters most often of interest are temperature, frequency, strain, preload, and elastomer geometry. Ferry et al [3.58] and Williams et al [3.59] introduced the use of a single reduced variable to include the effects of both temperature and frequency on the dynamic properties of elastomers. This method of parameterization, referred to as the Williams-Landel-Ferry (WLF) method, permits accurate predictions to be made for operating conditions which are beyond the range of possible test conditions. This is done by varying frequency in such a way as to represent a particular variation in the temperature, or vice versa. Jones [3.60] successfully used the WLF method for several elastomer materials to determine temperature sensitivity. Moghe and Neff [3.61] presented the results of static tests in which the addition of fillers was found to increase the stiffness and reduce the Poisson's ratio of elastomers. This had a subsequent effect on the static shape factor. Sircar and Lamond [3.62, 3.63] described the strain dependence of the dynamic properties of various elastomer materials and different compositional blends. Holownia [3.64] described an experimental method for accurately measuring the static Poisson's ratio of elastomer materials and presented test results relating Poisson's ratio to the quantity of carbon black in the elastomer blend. Gupta et al [3.48] and others [3.49, 3.50, 3.56, 3.57, 3.65] reported the effect of temperature, heat dissipation and preload on the dynamic properties of polybutadiene elastomer. They also investigated the effect of strain and found this to be a more significant and consistent parameter than heat dissipation on the dynamic properties. Smalley et al [3.66, 3.67] reported the results of a series of tests using the BERM method for determining the dynamic properties of elastomer O-rings. The effects of temperature, strain, preload (in terms of squeeze and stretch)

45

and elastomer material on the dynamic properties were investigated. Smalley 3.68 presented a review of results obtained with polybutadiene and other elastomer materials as a function of several test parameters and for a variety of test hardware configurations.

The American Society of Testing and Materials has published testing standards for elastomers for a large variety of static and general property tests 3.23 . These include ASTM-G-395 for compression set, ASTM-D-695 for compressive properties and ASTM-C-177 for thermal conductivity. ASTM has also published a standard for dynamic property elastomer tests using a Yerzly mechanical oscillograph (ASTM-D-945). This apparatus is a free vibration device which is strictly mechanical and operates on the principle of a horizontal rocking lever arm. A sample may be tested in either compression or shear. Norrington 3.69 noted that this apparatus was only suitable for comparative measurements due to the nonlinearity introduced by the continually changing amplitude of oscillation. In addition, the measurements can generally be made over only a very limited frequency range which is determined by the geometry of the apparatus and the stiffness of the elastomer sample. Condensations of many of the ASTM test standards for elastomers are given in Elastomeric Materials 3.70 , which is a general handbook of elastomer material and properties.

3.3 Material Properties

Numerous references are available which provide collections of general physical properties for elastomers. However, very little data is available for dynamic properties of elastomers. Most of the elastomer dynamic properties which are available from the open literature are found in reports of test programs, such as those cited in the previous section. Data regarding the general physical properties of elastomers may also be found in published test results. In addition, a number of handbooks have collections of these properties in a format which is more compatible for design applications. Several handbooks are available which are devoted entirely to elastomers. One of the most comprehensive of these is Elastomeric Materials 3.70 . This handbook provides a large amount of data for a great variety of elastomer materials which are classified by both generic type and common tradenames. Payne and Scott 3.71 provided a modest tabulation of elastomer properties in the Appendix to their book on the application of elastomers. Other handbooks, which are devoted entirely to elastomers and contain useful property information, include those by McCann 3.72 , Manufacturing Chemists' Association 3.73 , Nielsen 3.74 , and Simonds 3.75 .

General mechanical handbooks may also be found which provide useful elastomer property data. Mechanical Behavior of Materials 3.4 provides general physical properties including the static modulus of elasticity for a number of common polymers. Mechanical Design and Systems Handbook 3.76 provides some dynamic properties for several elastomer materials. However, this data is provided for particular test frequencies, which are generally above one kilohertz and, thus, is somewhat limited for use in rotordynamic applications. Mark's Handbook for Mechanical Engineers 3.77 provides a list of environmental properties for several types of elastomers. Additional handbooks which provide information on elastomer properties include Vibration and Acoustics Measurement Handbook 3.78 and Materials and Design Engineering: Materials Selector Issue 3.79 .

3.4 Applications

The static and unidirectional dynamic applications of elastomers are discussed in a substantial quantity of literature. However, limited information is available on rotordynamic applications. Applications-oriented literature can be considered to include test results and property reference literature, such as that cited above. Application of this data, particularly the dynamic data, may not be straightforward.

Payne and Scott 3.71 discussed a number of geometric considerations for unidirectional loading, such as a compression specimen shape factor. They also provided a general design guide for elastomeric mounts. Göbel 3.80 provides considerable detail useful for the design of elastomer structures for unidirectional and torsional loading (e.g., shaft couplings). This discussion includes calculation methods, principles of construction and numerous examples. McGuire 3.81 and Weller 3.82 described helicopter rotor lead-lag dampers with elastomer elements. Nashif and Halvorsen 3.83 discussed the design of layered viscoelastic damping treatments for structural damping. Jones and Henderson 3.84 described the design of elastomer elements for guide vane support in gas turbine engines. Hertz 3.85 discussed the design of O-ring seals, taking into consideration the modulus of elasticity of the elastomer materials. Foster 3.86 discussed vibration isolation using elastomers and described the design of an elastomer support for spinning frames in textile mills. The Shock and Vibration Handbook 3.87 provides some general design information concerning the use of elastomers for vibration isolation. In a series of articles, Nagel discussed various aspects of elastomer component design including some specific applications 3.88 through 3.97 . Some design information is also available from various elastomer manufacturers' catalogs, such as that by the Minor Rubber Company 3.92 .

The design information available for elastomer dampers for rotating machinery is extremely limited. Most of the information that is available is empirical. However, analytical correlations are provided in some of the test result literature cited above. Finney and Gupta 3.93 applied a finite element analysis for elastomer application. However, in general, these analytical design tools are expensive to use.

There are apparently no complete design guides available for elastomer dampers for rotating machines. A few references are available which include detailed descriptions of actual elastomer dampers, and a number of patents have been obtained for elastomer dampers (including References 3.94 through 3.96) in 1972. In general, the patent disclosures describe the geometric design of the damper only and no elastomer specification is given. Potter 3.97 provided a general discussion of elastomer damper applications with specific reference to lead-lag rotary wing dampers. He stated that these dampers typically have a maintenance free service life of 1500 to 2000 flight hours and an operating temperature range of from -54° C $(-65^\circ$ F) to 93° C $(200^\circ$F). Anwar and Kramberger 3.98 discussed the use of elastomer mounts for fluid-film bearings and described the results of a series of unidirectional load tests. Fischer et al 3.99 described the design of a compliant surface spherical bearing for a gyroscope which utilized elastomer elements. In a series of references, Tecza and others 3.56, 3.100, 3.101 and 3.102 described in

detail the damper design and results of a series of tests utilizing an elastomer damper for a gas turbine rotor simulator. Smalley [3.68] provided a review of this effort in relation to its historical background. Zorzi et al [3.103] described a similar elastomer damper design used for a super-critical power transmission shaft. Details of these and other elastomer damper designs for rotating machines are presented in Section 8.0 of this handbook.

3.5 Summary

A review of the literature concerning elastomer materials and properties and the design of elastomer dampers has been presented in this section. Particular areas which have been discussed include viscoelastic theory, elastomer chemistry, experimental determination of properties, material property references, and applications-oriented literature. While the applications-oriented literature is the most pertinent to the practical design of elastomer dampers, it is also the most scarce. A number of the topics touched on in this section are covered in more detail in later sections of this handbook.

3.6 References

3.1   Bland, D.R., The Theory of Linear Viscoelasticity, Pergamon Press, New York, 1960.

3.2   Flugge, Wilhelm, Viscoelasticity, Blaisdell Publishing Company, Waltham, Massachusetts, 1967.

3.3   Ferry, J.D., Viscoelastic Properties of Polymers, J. Wiley and Sons, 1970.

3.4   McClintock, Frank A., and Argon, Ali S. (ed.), Mechanical Behavior of Materials, Addison-Wesley Publishing Company, Inc., Reading, Massachusetts, 1966.

3.5   Lazan, B.J., Damping of Materials and Members in Structural Mechanics, Pergamon Press, New York, 1968.

3.6   Smalley, A.J., and Tessarzik, J.M., "Development of Procedures for Calculating Stiffness and Damping Properties of Elastomers in Engineering Applications, Part III: The Effects of Temperature, Dissipation Level and Geometry", NASA Report CR-134939, Nov. 1975.

3.7   Alfrey, T., Jr., Mechanical Behavior of High Polymers, Interscience, New York, 1948.

3.8   Eirich, F.R. (ed.), Rheology: Theory and Applications, Vol. II, Academic Press, New York, 1958.

3.9   Stookey, S.D. and Stuart, H.A. (ed.), "Glass-Ceramics", Mech. Eng.
       82, 65-68, 1960. <u>Die Physik der Hochpolymeren</u>, Vol. 4, Springer,
       Berlin, 1956.

3.10   Tobolsky, A.V., <u>Properties and Structure of Polymers</u>, Wiley,
       New York, 1960.

3.11   Herrmann, Leonard R., "Elasticity Equations for Incompressible and
       Nearly Incompressible Materials by a Variational Theorem", <u>AIAA</u>
       <u>Journal</u>, Vol. 3, No. 10, pp. 1896-1900.

3.12   Korites, B.J., and Nelson, F.C., "The Influence of Dissipative
       Heating on the Loss Factor of a Viscoelasticity Damped Beam,"
       ASME Transactions, <u>Journal of Engineering for Industry</u>, November
       1969, pp. 975-980.

3.13   Ting, E.C., and Tuan, J.L., "Effect of Cyclic Internal Pressure on
       the Temperature Distribution in a Viscoelastic Cylinder", May 1973.

3.14   Brady, G.S., and Clauser, H.R. (ed.), <u>Materials Handbook</u>, eleventh
       edition, McGraw-Hill, 1977.

3.15   Shreir, L.L. (ed.), <u>Corrosion</u>, Vol. 2, Butterworths, London, 1978.

3.16   Moore, D.F., and Geyer, W., "A Review of Adhesion Theories for
       Elastomers", Wear, Vol. 22, 1972, pp. 113-141.

3.17   Billmeyer, F.W., Jr., <u>Textbook of Polymer Science</u>, Interscience
       New York, 1962.

3.18   Flory, P.J., <u>Principles of Polymer Chemistry</u>, Cornell University
       Press, Ithaca, New York, 1953.

3.19   Noller, C.R., Chemistry of Organic Compounds, 2nd ed., Saunders,
       Philadelphia, 1957.

3.20   Schmidt, A.X., and Marlies, C.A., <u>Principles of High-Polymer Theory</u>
       <u>and Practice</u>, McGraw-Hill, New York, 1948.

3.21   Adkins, J.E., and Gent, A.N., "Load-Deflection Relations of Rubber
       Bush Mountings", <u>British Journal of Applied Physics</u>, Vol. 5,
       October 1954, pp. 354-358.

3.22   Beerbower, A., Pattison, D.A., and Staffin, G.D., "Predicting
       Elastomer-Fluid Compatibility for Hydraulic Systems", <u>ASLE Trans-</u>
       <u>actions</u>, Vol. 6, 1963, pp. 80-88.

3.23   American Society for Testing and Materials, <u>1978 Annual Book of</u>
       <u>ASTM Standards</u>, Parts 37 and 38, ASTM, 1978.

3.24   Payne, A.R., "Dynamic Properties of Vulcanized Rubbers: 5 - Shape
       Factors and Functions in Rubber Engineering", Research Report No.
       84, Research Assoc. of British Rubber Manufacturers, January 1975.

3.25   Payne, A.R., "Shape Factors and Functions in Rubber Engineering, No. 1," The Engineer, February 27, 1959, p. 328.

3.26   Payne, A.R., "Shape Factors and Functions in Rubber Engineering, No. 2", The Engineer, March 6, 1959, p. 368.

3.27   Balktrukonis, J.H., Blomquist, D.S., Magrab, E.B., "Measurement of The Complex Shear Modulus of a Linear Viscoelastic Material", Technical Report No. 5 to NASA, under Research Grant No. NsG-125-61 (Suppl. 3), Catholic University of America, May 1964.

3.28   Rightmire, G.K., "An Experimental Method for Determining Poisson's Ratio of Elastomers", J Lub Tech, July 1930, pp. 281-388.

3.29   Cannon, C.M., Nashif, A.D. and Jones, D.I.G., "Damping Measurements on Soft Viscoelastic Materials Using a Tuned Damper Technique", Shock and Vibration Bulletin No. 38, Naval Research Laboratory, Washington, D.C., Part 3, November 1968, pp. 151-163.

3.30   Miller, H.E., "Dynamic Property Measurement of Elastomers and Elastomeric Mounts - Past, Present and Future", SAE Paper No. 730256, SAE/ASTM Symposium, Detroit, Michigan, Jan. 1973.

3.31   Leonard, R.G., "Fundamentals of Dynamic Properties Measurement of Elastomers: Part I - Measurement and Identification Principles", SAE Paper No. 730257, SAE/ASTM Symposium, Detroit, Michigan, Jan. 1973.

3.32   Nachtigal, C.L., "Fundamentals of Dynamic Properties Measurement of Elastomers: Part II - Instrumentation, Computation, and Compensation", SAE Paper No. 730258, SAE/ASTM Symposium, Detroit, Michigan, Jan. 1973.

3.33   Brouwer, F., "Resonant Beam System Development - Past to Present", SAE Paper No. 730259, SAE/ASTM Symposium, Detroit, Michigan, Jan. 1973.

3.34   Owens, J.H., "Application of Electrohydraulic Test Machines to Dynamic Testing of Elastomers", SAE Paper No. 730260, SAE/ASTM Symposium, Detroit, Michigan, Jan. 1973.

3.35   Wilson, W.J., "Evolution and Uses of Transmitted Force Measurement", SAE Paper No. 730261, SAE/ASTM Symposium, Detroit, Michigan, Jan. 1973.

3.36   Hillberry, B.M., Goodson, R.E., and Nachtigal, C.L., "Computation and Direct, Readout of Dynamic Properties: The Identifier", SAE Paper No. 73062, SAE/ASTM Symposium, Detroit, Michigan, Jan. 1973.

3.37   Danko, D.M. and Svarovsky, J.E., "An Application of Minicomputers for the Determination of Elastomeric Damping Coefficients and Other Properties", SAE Paper No. 730263, SAE/ASTM Symposium, Detroit, Michigan, Jan. 1973.

3.38   Nemec, J.E., "Correlation of Dynamic Properties Test Equipment",
        SAE Paper No. 730264, SAE/ASTM Symposium, Detroit, Michigan, Jan.
        1973.

3.39   Paul, A.S., Hillberry, B.M., "Error Analysis of the Resonant Beam
        Rubber Testing Machine", SAE Paper No. 730256, SAE/ASTM Symposium,
        Detroit, Michigan, Jan. 1973.

3.40   Anderson, A.D., "Testing and Parameterization of Elastomers for
        Modeling of Linear Vibration Systems", SAE Paper No. 730266, SAE/
        ASTM Symposium, Detroit, Michigan, Jan. 1973.

3.41   Sommer, J.G., and Meyer, D.A., "Factors Controlling the Dynamic
        Properties of Elastomeric Products", SAE Paper No. 730267, SAE/ASTM
        Symposium, Detroit, Michigan, Jan. 1973.

3.42   Puydak, R.C., "The Effective Use of Dynamic Testing in Raw Materials
        Development Programs", SAE Paper No. 730268, SAE/ASTM Symposium,
        Detroit, Michigan, Jan. 1973.

3.43   Koons, R.R., "Production and Quality Control of Elastomer Mounts",
        SAE Paper No. 730269, SAE/ASTM Symposium, Detroit, Michigan, Jan.
        1973.

3.44   Rubber and Related Products: New Methods for Testing and Analyzing,
        ASTM STP 553, American Society for Testing and Materials, 1974.

3.45   Warner, W.C., "Measuring Dynamic Properties of Vulcanizates", ASTM
        STP 553, American Society for Testing and Materials, 1974, pp. 31-35.

3.46   Hillberry, B.M., "A Review of Recent Developments in Forced Vibration
        Dynamic Testing of Elastomers", ASTM STP 553, American Society for
        Testing and Materials, 1974, pp. 142-161.

3.47   Chiang, T., Tessarzik, J.M., and Badgley, R.H., "Development of
        Procedures for Calculating Stiffness and Damping Properties of
        Elastomers in Engineering Applications, Part I: Verification of
        Basic Methods", NASA Report CR120905, March 1972.

3.48   Gupta, P.K., Tessarzik, J.M., and Cziglenyi, L., "Development of
        Procedures for Calculating Stiffness and Damping Properties of
        Elastomers in Engineering Applications, Part II: Elastomer Charac-
        teristics of Constant Temperature", NASA Report CR-134704, April
        1974.

3.49   Darlow, M.S., and Smalley, A.J., "Development of Procedures for
        Calculating Stiffness and Damping Properties of Elastomers in
        Engineering Applications, Part IV: Testing of Elastomers Under a
        Rotating Load", NASA Report CR-135355, November 1977.

3.50   Smalley, A.J., "Dynamic Testing of O-ring Properties", Elastomer Notebook (duPont), No. 198, October 1977, pp. 576-578.

3.51   Smalley, A.J., Tessarzik, J.M., and Badgley, R.H., "Testing for Material Dynamic Properties", ASME Publication: Vibration Testing - Instrumentation and Data Analysis, AMD-Vol. 12, 1975, p. 117.

3.52   Painter, G.W., "Dynamic Properties of BTR Elastomer", paper presented at SAE National Aeronautic Meeting, Los Angeles, California, 1958.

3.53   Gent, A.N. and Lindley, P.B., "The Compression of Bonded Rubber Blocks", Proc. Inst. Mech. Engrs., Vol. 173, No. 3, L59, pp. 111-117.

3.54   Hirsch, A.E., and Boyce, R.J., "Dynamic Properties of Ethylene/ Acrylic Elastomer: A New Heat Resistant Rubber", Rubbercon '77, Paper No. 10.

3.55   Maza, Victor M., "An Experimental Determination of the Dynamic Young's Modulus of Selected Viscoelastic Materials," Master's Thesis, Pennsylvania State University, August 1977.

3.56   Tecza, J.A., Darlow, M.S., and Smalley, A.J., "Development of Procedures for Calculating Stiffness and Damping Properties of Elastomers in Engineering Applications, Part V: Elastomer Performance Limits and the Design and Test of an Elastomer", NASA Report CR-159552. February 1979.

3.57   Darlow, M.S., and Smalley, A.J., "The Effects of Strain and Temperature on the Dynamic Properties of Elastomers", ASME Transactions, Journal of Mechanical Design, ASME Paper No. 79-DET-57, September 1979.

3.58   Ferry, J.D., Fitzgerald, E.R., Grandiene, L.D. and Williams, M.L., "Temperature Dependence of Dynamic Properties of Elastomers' Relaxation Distributions", Ind Eng Chem, Vol. 44, No. 4, April 1952, pp. 703-706.

3.59   Williams, M.L., Landel, R.F. and Ferry, J.D., "The Temperature Dependence of Relaxation Mechanisms in Amorphous Polymers and Other Glass-Forming Liquids", J Amer Chem Soc, 77, 370, 1955.

3.60   Jones, D.I.G., "Temperature-Frequency Dependence of Dynamic Properties of Damping Materials", Journal of Sound and Vibration, Vol. 33, No. 4 1974, pp. 451-470.

3.61   Moghe, S.R., and Neff, H.R., "Dependence of Compression Modulus on Poisson's Ratio", Rubber Chem Technol, 1973, p. 207.

3.62   Sircar, A.K. and Lamond, T.G., "Strain Dependent Dynamic Properties of Carbon Black Reinforced Vulcanizates: I - Individual Elastomers", Rubber Chem Technol, March-April 1974, p. 71.

3.63   Sircar, A.K. and Lamond, T.G., "Strain Dependent Dynamic Properties of Carbon Black Reinforced Vulcanizates: II - Elastomer Blends", Rubber Chem Technol, March-April 1974, p. 89.

3.64   Holownia, B.P., "Effect of Carbon Black on Poisson's Ratio in Elastomers", Rubber Chem Technol, May-June 1975, pp. 245-253.

3.65   Darlow, M.S., and Smalley, A.J., "Dynamic Properties of Elastomer Cartridge Specimens Under a Rotating Load", Technical Paper Presented at the Fifth World Congress of the Theory of Machines and Mechanisms, Montreal, Canada, July 1979.

3.66   Smalley, A.J., Darlow, M.S., and Mehta, R.K., "Stiffness and Damping of Elastomeric O-Ring Bearing Mounts", NASA Report CR-135328, November 1977.

3.67   Smalley, A.J., Darlow, M.S. and Mehta, R.K., "The Dynamics Characteristics of O-Rings", ASME Trans., Journal of Mechanical Design, Vol. 100, No. 1, January 1978, pp. 132-138.

3.68   Smalley, A.J., "Property Measurement and Application of Elastomer Dampers", presented at the Conference on Aerospace Polymeric Viscoelastic Damping, Dayton, Ohio, February 1978.

3.69   Naunton, W.J.S., The Applied Science of Rubber, Edward Arnold, Ltd., London, 1961.

3.70   Elastomeric Materials, Desk-Top Data Bank, The International Plastics Selector, Inc., San Diego, California, 1977.

3.71   Payne, A.R. and Scott, J.R., Engineering Design with Rubber, Interscience Publications, New York 1960.

3.72   McCann, H. (ed.), Modern Plastics, Encyclopedia Issue, Breskin, Bristol, Conn., 1961.

3.73   Manufacturing Chemists' Assoc., Technical Data on Plastics, Manufacturing Chemists' Assoc., Washington, D.C., 1957.

3.74   Nielsen, L.F., Mechanical Properties of Polymers, Reinhold, New York, 1962.

3.75   Simonds, H.R., Source Book of the New Plastics, Vol. 1, Reinhold, New York, 1959. See also Vol. 2, 1961.

3.76   Rothbart, Harold A. (ed.), Mechanical Design and Systems Handbook, McGraw-Hill, New York, 1964.

3.77   Baumeister, Theodore and Marks, Lionel S. (ed.), _Standard Handbook for Mechanical Engineers_, Seventh Edition, McGraw-Hill, New York, 1967.

3.78   Blake, Michael P., and Mitchell, William S. (ed.), _Vibration and Acoustic Measurement Handbook_, Spartan Books, New York, 1972.

3.79   Clauser, H.R. (ed.), _Materials in Design Engineering_, Materials Selector Issue, Reinhold, New York, 1962.

3.80   Gobel, E.F., _Rubber Springs Design_, John Wiley and Sons, New York, 1974.

3.81   McGuire, D.P., "The Application of Elastomeric Lead-Lag Dampers to Helicopter Rotors", 46th Shock and Vibration Symposium, San Diego, California, October 1975.

3.82   Weller, William H., "Load and Stability Measurements on a Soft-Inplace Rotor System Incorporating Elastomeric Lead-Lag Dampers", NASA TN D-8437, July 1977.

3.83   Nashif, A.D., and Halvorsen, W.G., "Design Evaluation of Layered Viscoelastic Damping Treatments", _Sound and Vibrations_, Materials Reference Issue, July 1978, pp. 12-17.

3.84   Jones, D.I.G., and Henderson, J.P., "Damping Materials Provide Low-Cost Solutions to Vibration Problems", _Sound and Vibration_, August 1978, pp. 3-6.

3.85   Hertz, D.L., "O-rings for Low-Pressure Service", _Machine Design_, April 1979, pp. 94-98.

3.86   Foster, L.W., "One Stage and 2 Stage Vibration Isolators as Applied to High Speed Textile Spindles to Achieve Noise Reduction", ASME Transactions, _Journal of Mechanical Design_, June 1977, pp. 8-15.

3.87   Harris, C.M., and Crede, C. (ed.), _Shock and Vibration Handbook_, Second Edition, McGraw-Hill, New York, 1976.

3.88   Nagel, W.B., "Designing with Rubber: Part 1, The Design Surface", _Machine Design_, June 23, 1977, pp. 84-88.

3.89   Nagel, W.B., "Designing with Rubber: Part 2, Parts in Tension or Compression", _Machine Design_, July 7, 1977, pp. 78-81.

3.90   Nagel, W.B., "Designing with Rubber: Part 3, Parts in Shear or Torsion", _Machine Design_, July 21, 1977, pp. 100-105.

3.91   Nagel, W.B., "Designing with Rubber: Part 4, Some Real-Life Applications", _Machine Design_, August 11, 1977, pp. 101-106.

3.92   "An Engineers Guide to Elastomer Selection", Catalog Number 2778, Minor Rubber Co., Bloomfield, New Jersey, 1979.

3.93   Finney, R.H., and Gupta, Bhagwati, "Design of Elastomeric Components by Using the Finite Element Technique", Lord Kinematics, Erie, Pennsylvania.

3.94   Maas, Otto Robert, "Resilient Mounting Arrangement", U.S. Patent No. 3639015, February 1, 1972.

3.95   Leanart, Gunnar Oskar, "Bearing for Precision Apparatus", U.S. Patent No. 3698773, October 17, 1972.

3.96   Bando, Sigeru, "Bearing Adapter", U.S. Patent No. 3672734, June 27, 1972.

3.97   Potter, J.L., "Improving Reliability and Eliminating Maintenance with Elastomeric Dampers for Rotor Systems", J.Am. Helicopter Society, Vol. 18, No. 1, January 1973, pp. 23-28.

3.98   Anwar, I, and Kramberger, F., "Testing of Elastic Mounts for Application in Bearings", Franklin Inst. Research Lab Interim Report I-C2429, August, 1975.

3.99   Fischer, Wm. H., Gu, A.L., Gupta, P.K., and Walowit, J.A., "Design and Development of Compliant Bearing Materials for a Directional Control Gyroscope", MTI Report 74-TR12, January, 1974.

3.100   Tecza, J.A., Darlow, M.S., Jones, S.W., Smalley, A.J., and Cunningham, R.E., "Elastomer Mounted Rotors an Alternative for Smooth Running Turbomachinery", ASME paper 79GT149, presented at the Gas Turbine Conference and Exhibit and Solar Energy Conference in San Diego, Ca., March 12-15, 1979.

3.101   Tecza, J.A., Darlow, M.S., Smalley, A.J., and Cunningham, R.E., "Design of Elastomer Dampers for a High-Speed Flexible Rotor", ASME Paper No. 79-DET-88, presented at the 1979 ASME Vibrations Conference, St. Louis, Missouri, September 1979.

3.102   Smalley, A.J., "Elastomeric Damping Validated", Elastomer Notebook (duPont), No. 207, April 1979, pp. 665-669.

3.103   Zorzi, E.S., Burgess, G., and Cunningham, R., "Elastomer Damper Performance-A Comparison with a Squeeze Film for a Supercritical Power Transmission Shaft", ASME 80-GT-162, March 1980.

4.0 DYNAMIC BEHAVIOR OF VISCOELASTIC MATERIALS

Viscoelastic materials combine the properties of purely elastic materials with those of purely viscous materials. For elastic materials, a one-to-one relationship exists between stress and strain, and the stress is independent of the rate of strain. When an ideal elastic element is subjected to a cyclic deformation, the stress and strain remain in phase. For a linear elastic material stress is proportional to strain (i.e. Hooke's Law). An ideal viscous material is characterized by a relationship between stress and rate of strain and for a sinusoidal cyclic deformation, the stress leads the strain by ninety degrees. For a linear viscous element (represented by a viscous damper, described in Section 2.0), stress is directly proportional to the rate of strain, with the proportionality constant being the viscous damping coefficient.

Viscoelastic materials are characterized by creep and stress relaxation. Creep is the process whereby the deformation of a viscoelastic material under a sustained load increases with time to an asymptotic limit. Similarly, load relaxation is the process whereby the load required to maintain a constant strain decreases with time. Stress in a viscoelastic material is related to both strain and the rate of strain and, for cyclic deformation, is not in-phase with strain. Viscoelastic materials, like elastic materials, may be either linear or nonlinear. Warnaka [4.1]* has shown that several typical elastomer materials behave as nearly linear viscoelastic materials for frequencies in the range of 100 to 1000 Hertz and for dynamic strain levels up to 0.1. The elastic and viscous moduli for elastomers tend to be functions of frequency, temperature, strain, geometry and material composition. The effects of frequency and temperature are inversely related, as discussed below. The basic relationships and parametric influences of viscoelasticity are discussed in several references including References 4.2, 4.3 and 4.4.

4.1 Basic Relationships

If a load cycle is applied repeatedly to an elastomer element, the process of relaxation causes hysteresis - that is, a load deformation curve which depends on the sign of the rate of change of load as well as on the load's magnitude. Figure 16 presents a representative elliptical hysteresis loop. Implicit in such a load deflection curve or hysteresis loop is a loss of energy per cycle equal to the area of the hysteresis loop. Expressed in another way, elements with such a load-deflection curve provide energy dissipation or damping (in this case, hysteretic damping, as discussed in Section 2.0). As shown by Lazan [4.5], the material behavior for an elliptical hysteresis loop is linear, and the hysteretic damping, k_2, may be expressed as

$$k_2 = \frac{D_s}{\pi x_1^2} \qquad (4-1)$$

---

* Numbers in brackets indicate References found in Section 4.7
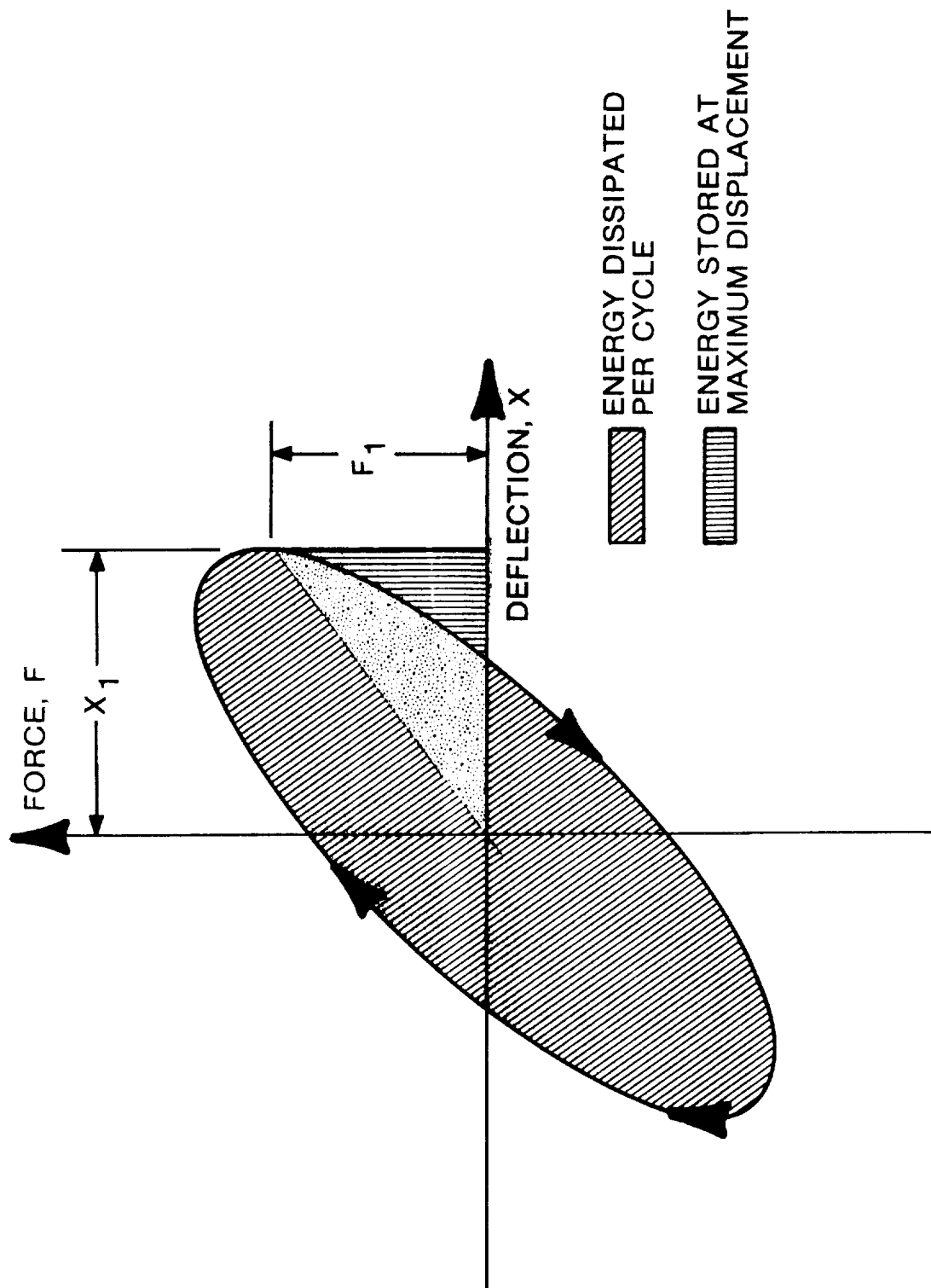
Fig. 16 Load-Deflection Curve for an Elastomer Showing Hysteresis as a Result of the Relaxation Process

ENERGY DISSIPATED PER CYCLE

ENERGY STORED AT MAXIMUM DISPLACEMENT

FORCE, F

DEFLECTION, X

X_1

F_1

where D_s is the area of the hysteresis loop and x_1 is the amplitude. It is also possible to define stiffness in terms of this loop as the ratio between force at maximum deflection and the value x_1 of maximum deflection.

$$k_1 = F_1/x_1 \qquad (4-2)$$

where F_1 and x_1 are defined in Figure 16.

A linear elastomer element undergoing a repeated deflection cycle defined by

$$x = x^* e^{i\omega t} \qquad (4-3)$$

gives rise to a cyclic force variation described by

$$F = F^* e^{i\omega t} \qquad (4-4)$$

where: ω is the frequency (rad/sec)

           x is the instantaneous displacement (m)

           F is the instantaneous force (N)

           t is time

         x^*, F^* are complex numbers defining the amplitude and phase of the displacement and force variations (and it is understood that only the real parts of equations (4-3) and (4-4) are used to establish values for x and F).

The force and displacement may be related by

$$F = k^* x \qquad (4-5)$$

where k^* is a complex number

$$k^* = k_1 + ik_2 \qquad (4-6)$$

and is generally a function of frequency, temperature, dynamic strain, and geometry, as well as material. The quantities k_1 and k_2 are generally referred to as the stiffness and damping of the elastomer element and are likewise functions of the parameters listed above. The damping ability of an elastomer element is sometimes expressed in terms of a loss coefficient (nondimensional) which relates damping to stiffness, or the energy dissipated per cycle (D_s) to the energy stored at maximum displacement (U_s)

$$\eta = \frac{k_2}{k_1} = \frac{D_s}{2\pi U_s} \qquad (4-7)$$

where $k^* = k_1(1 + i\eta)$

4.2 The Effects of Geometry

For a general elastomer element, the geometry can normally be characterized by a certain area of the element (A) which is stressed and a certain dimension of the element, (h), which is strained. Figure 17 shows two elastomer element geometries which have been tested often for dynamic stiffness and damping and which illustrate the effects of geometry. For the shear element, the stressed area, A, is its width times its length (b·ℓ), and the strained dimension is its thickness, h. For the compression element, the stressed area is the top area of the cylinder (π d^2/4), and its strained dimension is the height, h.

For the shear element, stiffness and damping can be related to effective moduli as follows:

$$\text{Stiffness:} \qquad k_1 = G'_{eff} \frac{A}{h} \qquad (4-8)$$

$$\text{Damping:} \qquad k_2 = G''_{eff} \frac{A}{h} \qquad (4-9)$$

where G'_{eff}, G''_{eff} are shear moduli, commonly referred to as the effective storage and loss moduli, respectively, such as

$$G* = G' + iG''$$

For the compression element, stiffness and damping can be related to the effective moduli as follows:

$$\text{Stiffness:} \qquad k_1 = 3 \, G'_{eff} \frac{A}{h} \qquad (4-10)$$

$$\text{Damping:} \qquad k_2 = 3 \, G''_{eff} \frac{A}{h} \qquad (4-11)$$

where the factor of 3 arises from the classical elasticity relationship $E = 2(1 + \nu)G$ and the fact that elastomer Poisson's ratios are typically in the range of 0.4945 to 0.4999 (Holowina [4.6]). Any errors in applying this classical elasticity relationship to dynamic behavior of a viscoelastic material are implicit in the statement that G'_{eff}, G''_{eff} are effective moduli. G'_{eff}, G''_{eff} are, generally, functions of the material, the frequency, the amplitude of loading, the temperature, the initial strain and the geometry. They are, therefore, component rather than material properties.

For static loading the effects of bending can be shown [4.2] to cause the following relationship between effective and true modulus for the shear element of Figure 17.

$$(G'_{eff})_o = G'_o \frac{1}{1 + h^2/3\ell^2} \qquad (4-12)$$

where ℓ is the dimension of the sheared area in the direction parallel to the loading, h is the thickness, and the subscript, o, implies static loading. In Figure 18, the stiffness correction factor (G'_{eff}/G'_o) is plotted as a function of h/ℓ for a rectangular shear element. Under static compression loading, the interaction of axial, radial and circumferential stresses was shown by Gent and Lindley [4.7], Hattori and Takei [4.8], and Payne [4.9] to

59

LOAD

WIDTH, b

LENGTH, ℓ

←THICKNESS, h

SHEAR ELEMENT

LOAD

HEIGHT, h

DIAMETER, d
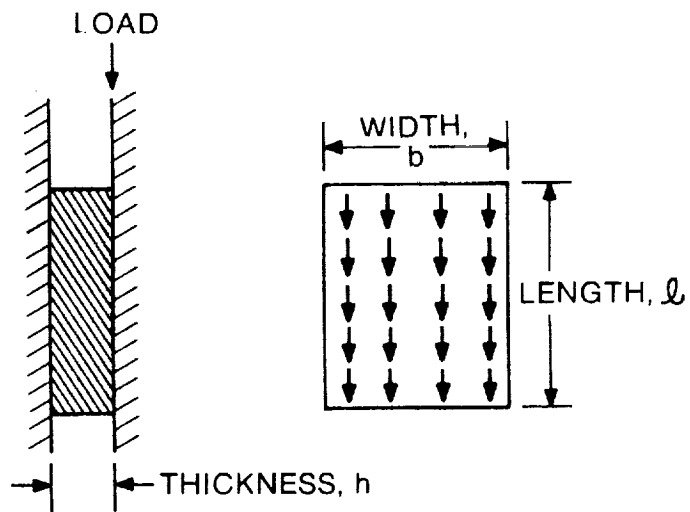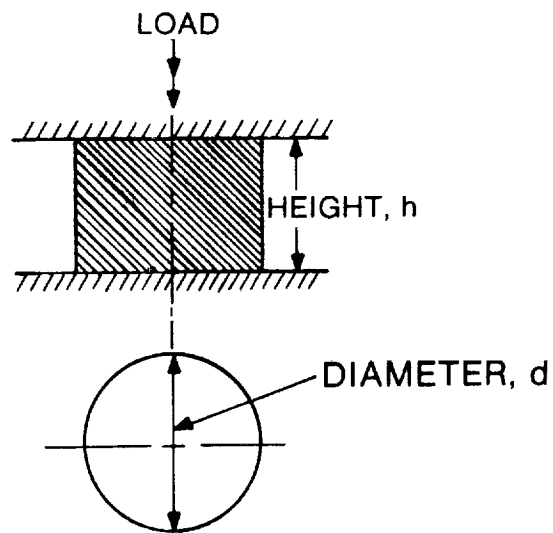
COMPRESSION ELEMENT

Fig. 17   Test Element for Shear and Compression Loading

60
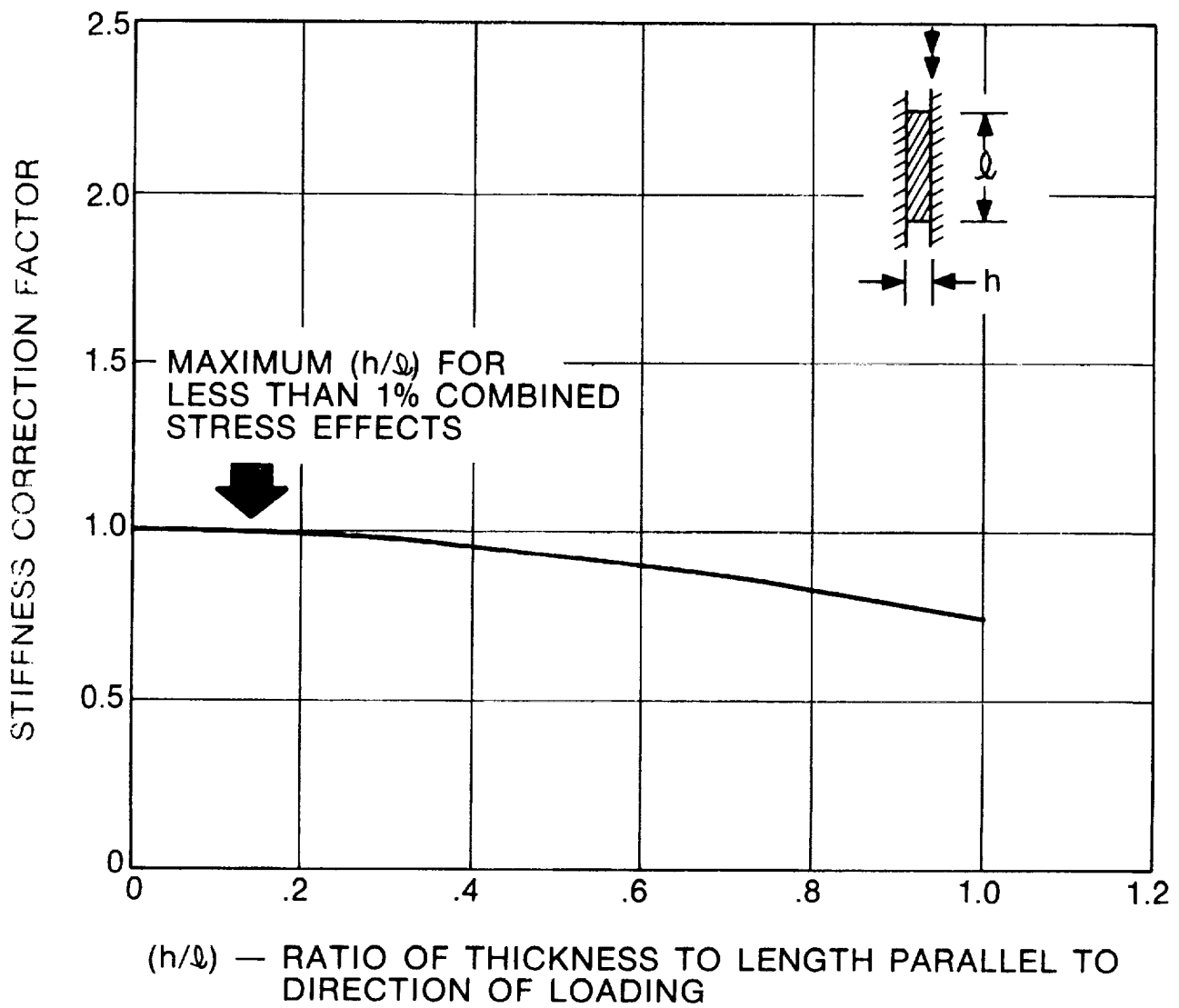
Fig. 18 Static Stiffness Correction Factor, Rectangular Shear Specimen.

61

give the following relationship between apparent, or effective, static modulus and actual, or true, static modulus:

$$(G'_{eff})_o = G'_o (1 + \beta S^2) \qquad (4\text{-}13)$$

where S is a shape factor defined as the ratio of the loaded area to the unloaded area (d/4h for a cylinder) and β is a coefficient, shown by Gent and Lindley [4.7] to be equal to 2.

A more complete expression based on the work of Gent and Lindley [4.7], which attempts to account for bulk compressibility effects, is given by:

$$\frac{G'_o}{(G'_{eff})_o} = (1 + \beta S^2)^{-1} + \frac{3\ G'_o}{B} \qquad (4\text{-}14)$$

where B is the bulk modulus for the material. However, this expression has been tested by Moghe and Neff [4.10] using classical elasticity solutions and shown to be incomplete for large values of S due to an additional dependence on Poisson's ratio. For values of S less than 10, however, neither the second term in equation (4-14) nor the inadequacies due to Poisson's ratio effects are significant.

In Figure 19, the static stiffness correction factor $((G'_{eff})_o/G'_o)$ is plotted against the ratio of diameter to height, as given by equation (4-13) with $\beta = 2$, for a compression loaded cylinder. The existence of such a square law dependence on shape factor has been verified experimentally by Payne [4.9]. He showed that, for natural rubbers, the shape coefficient, β, was close to 2 but, for harder materials the coefficient β could fall by as much as 50 percent. Under low-frequency dynamic loading (10 Hz) Payne also demonstrated that the effective storage modulus varied with shape factor according to a square law.

The analytical or experimental quantification of the effects of geometry (shape) at higher frequencies appears to be limited. Cannon, Nashif, and Jones [4.11] have demonstrated that shape has a pronounced influence on the effective storage modulus of cylindrical specimens, in the frequency range of 250 to 500 Hz. Smalley and Tessarzik [4.12] have evaluated the effect of frequency on shape factor for a particular elastomer material and geometry.

In practice, more complex elastomer geometries are sometimes used such that the elastomer elements are not subjected to pure shear or pure compression, but rather a combination of the two. A common example of such a practical elastomer configuration is a radially loaded ring cartridge. Figure 20 illustrates the geometry of typical elastomer ring cartridge. The elastomer material separates the inner diameter of one cylinder from the outer diameter of a second, smaller cylinder. The loading of interest is radial; that is, it tends to move one cylinder radially eccentric to the other.

Three methods of considering geometric effects are reviewed in this section:

- Beam-Column Method

- Method of Göbel [4.13]

62
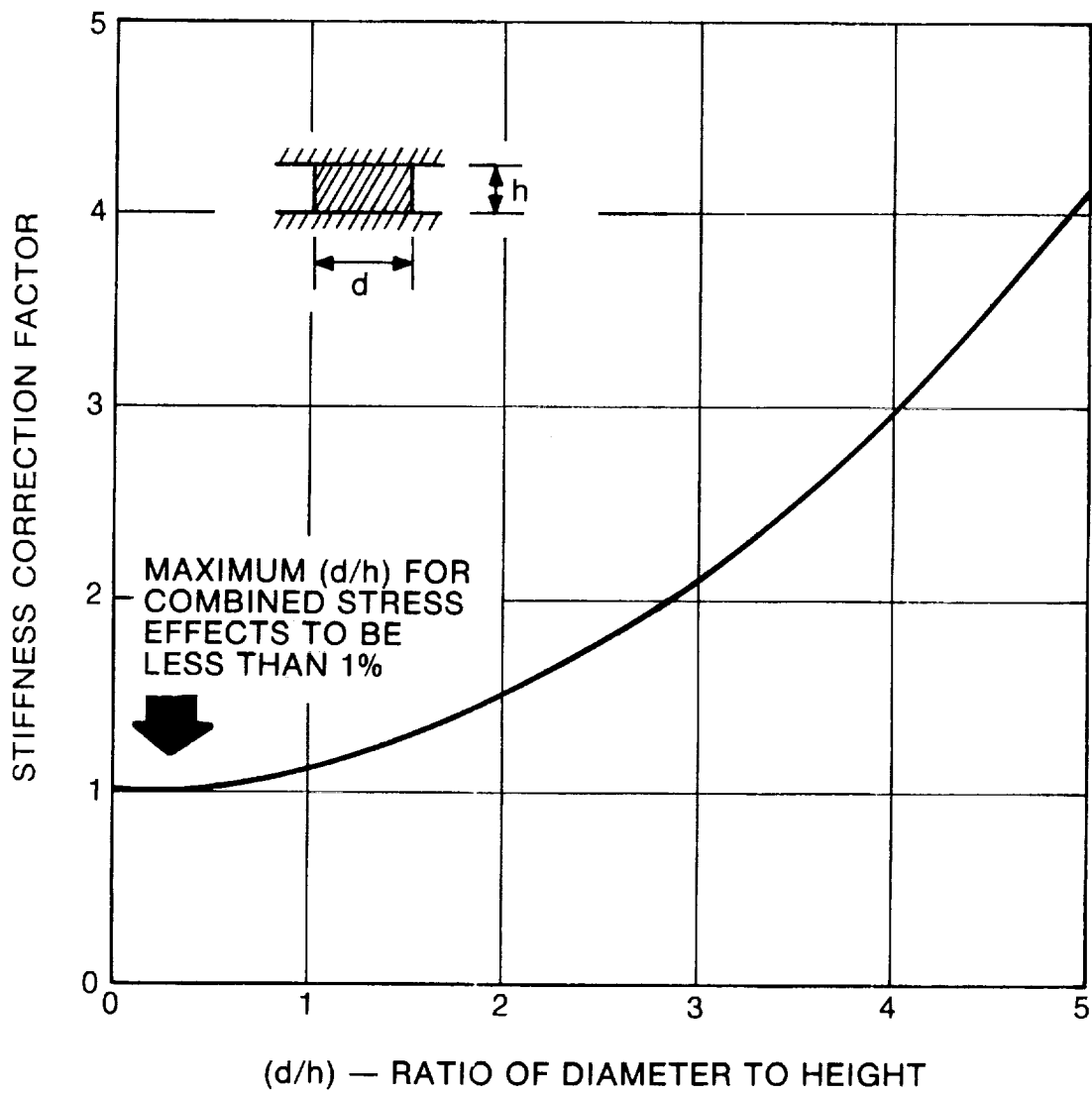
Fig. 19 Static Stiffness Correction Factor, Cylindrical Compression Element.

ELASTOMER
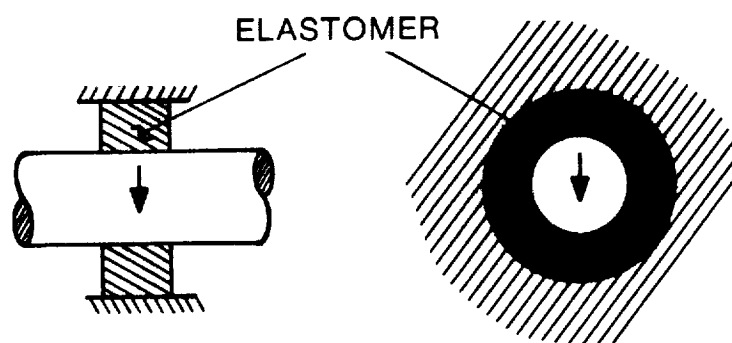
Fig. 20   Ring Cartridge Element

64

• Predictions Based Upon Plane Stress Analysis

Each of these is a 'static' analytical method; that is, it seeks a ratio of element stiffness to storage modulus (which is a function of the geometry only) and applies that ratio in the determination of dynamic stiffness and damping.

4.2.1 Beam-Column Method

In this development, the cartridge is assumed to be made up of a series of noninteracting, elemental column/beams, whose variation of thickness due to radius effects is small. Figure 21 illustrates the cartridge and the Beam-Column element, whose mean loaded area is

$$da = \bar{r} \, \ell d\theta \qquad (4\text{-}15)$$

where ℓ is the length of the cartridge

$\bar{r}$ is the mean radius $= (r_1 + r_2)/2$.

Consider the rigid inner member to be displaced radially by a small radial distance e, relative to the rigid outer member. The compression deflection of the element is (e cos θ), where θ is the angle the radial line to the element makes with the direction of displacement. The shear deflection of the element is (e sin θ). So, considering the element to act independently of adjacent elements, the elemental compression and shear forces, df_c, df_s are

$$df_c = e \cos \theta \; E \; \frac{\bar{r} \, \ell d\theta}{(r_2 - r_1)} \qquad (4\text{-}16)$$

$$df_s = e \sin \theta \; G \; \frac{\bar{r} \, \ell d\theta}{(r_2 - r_1)} \qquad (4\text{-}17)$$

and the total force exerted at the mean radius is

$$F = \int_0^{2\pi} \frac{e \, \bar{r} \, \ell}{(r_2 - r_1)} \; E \cos^2 \theta \; d\theta + G \sin^2 \theta \; d\theta = \frac{e \, \bar{r} \, \ell \, \pi}{(r_2 - r_1)} \; E + G \qquad (4\text{-}18)$$

so that, if we assume E = 3G (Poisson's ratio $\nu = 0.5$ implied), then,

$$k_r = \frac{F}{e} = 2\pi \; \frac{(r_2 + r_1)}{(r_2 - r_1)} \; G\ell \qquad \underline{\text{BEAM-COLUMN RESULT}} \qquad (4\text{-}19)$$

A slightly different result is obtained if the tapering of beams and columns due to radius effects is accounted for.

$$k_r = \frac{4\pi \; G\ell}{\ell n(r_2/r_1)} \qquad \underline{\text{ACCOUNTING FOR}} \atop \underline{\text{RADIUS EFFECTS}} \qquad (4\text{-}20)$$

65
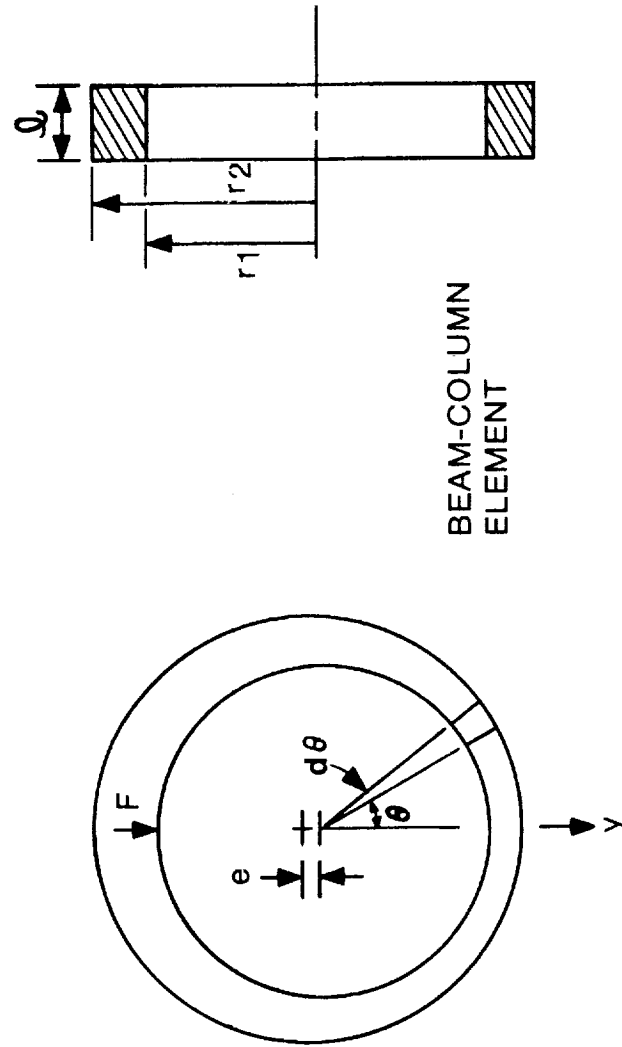
BEAM-COLUMN ELEMENT

Fig. 21 Cartridge Showing Beam-Column Element

66

But, as Table 3 shows, the reduction in stiffness due to radius effects is less than four percent for radius ratios up to a value of two. For most practical applications the radius ratio is much less than two.

Table 3

REDUCTION IN STIFFNESS DUE TO RADIUS EFFECTS
(Relative to Beam-Column Result)

r_2/r_1	Reduction
1.1	0.08%
1.5	1.35%
2.0	3.82%

4.2.2 Method of Göbel [4.13]

The method of Göbel initially follows a very similar development to the Beam-Column method accounting for radius effects, with an intermediate result:

$$k_r = \frac{\pi \ell}{\ln (r_2/r_1)} \ (G + E) \qquad (4-21)$$

However, Göbel then claims that, for $\frac{\ell}{(r_2 - r_1)} = 1$, the effective value of E given by

$$E_{eff} = 6.5 \ G \qquad (4-22)$$

and that, for other length to radius ratios, a correction factor, f_1, should be applied, so that

$$k_r = \frac{7.5 \ \pi \ell \ Gf_1}{\ln (r_2/r_1)} \qquad (4-23)$$

Göbel presents f_1 as a graphical function of $\ell/(r_2 - r_1)$. Payne and Scott [4.2] in their book ENGINEERING DESIGN WITH RUBBER present a cubic fit to Göbel's function:

$$f_1 = 1 + 0.0097 \ \ell^3/(r_2 - r_1)^3 \qquad (4-24)$$

which agrees closely with Göbel's graphical presentation. The basis for f_1, or for the statement $E_{eff} = 6.5 \ G$ is unclear from Göbel's work. These are not presented as empirical results, since no test data are given for this geometry. Göbel's method implies that $E_{eff} = 6.5 \ G$ is an asymptotic condition

for very short length cartridges. One set of static test data for the cartridge configuration (Adkins and Gent [4.11]) has been identified, and this data is compared with the prediction of the Beam-Column method and the method of Gobel in Figure 22 (after Reference 4.12). It shows good agreement at higher values of $\ell/(r_2 - r_1)$ between Göbel and test data, but at lower $\ell/(r_2 - r_1)$, the Beam-Column method appears to come closer due to a much sharper drop in stiffness of the test element. This comparison suggests that perhaps $E_{eff} = 6.5$ G is not a valid asymptotic condition for short cartridges.

4.2.3 Predictions Based Upon Plane Stress Analysis

The value of using a plane stress elastic analysis has also been investigated [4.12]. In this case, only a quarter of the cartridge was modeled and appropriate symmetry and antisymmetry boundary conditions were imposed. The quarter cartridge was embedded in a rectangular finite difference mesh and a finite displacement of the inner member relative to the outer member was imposed. A computer program was used to solve for the internal displacement field within the cartridge. Since it was not possible to employ a Poisson's ratio of 0.5 in this computer program, a value of 0.4983 was used together with a shear modulus value of 1.795×10^7 N/m^2. This combination of Poisson's ratio and shear modulus corresponds to a bulk modulus of 5.28×10^9 N/m^2, which is within the range of bulk moduli determined by Rightmire [4.15].

The stiffness was calculated by determining the component of shear and direct stress in the direction opposing the displacement, e, and integrating over the active cartridge surface to obtain the net force. The stiffness is, then, the ratio of net force to displacement.

Estimating Dynamic Values of Cartridge Stiffness and Damping. Each of these analytical methods described for the ring cartridge can be applied to a ring cartridge geometry. This has been done for a particular configuration (and two lengths) by Smalley and Tessarzik [4.12]. Their results are presented in Table 4 in nondimensional form; that is, the ratio of stiffness to the product of shear modulus and length is presented.

Table 4

NONDIMENSIONAL STIFFNESS FOR CARTRIDGES SELECTED
FOR TESTING (Inner and Outer Diameters: 1.905 and 2.858 cm)
(after Smalley and Tessarzik [4.12])

Method	k/Gℓ For ℓ = 0.476 cm	k/Gℓ For ℓ = 0.954 cm
Göbel	58.7	62.6
Plane Stress	35.1	35.1
Beam-Column	31.4	31.4
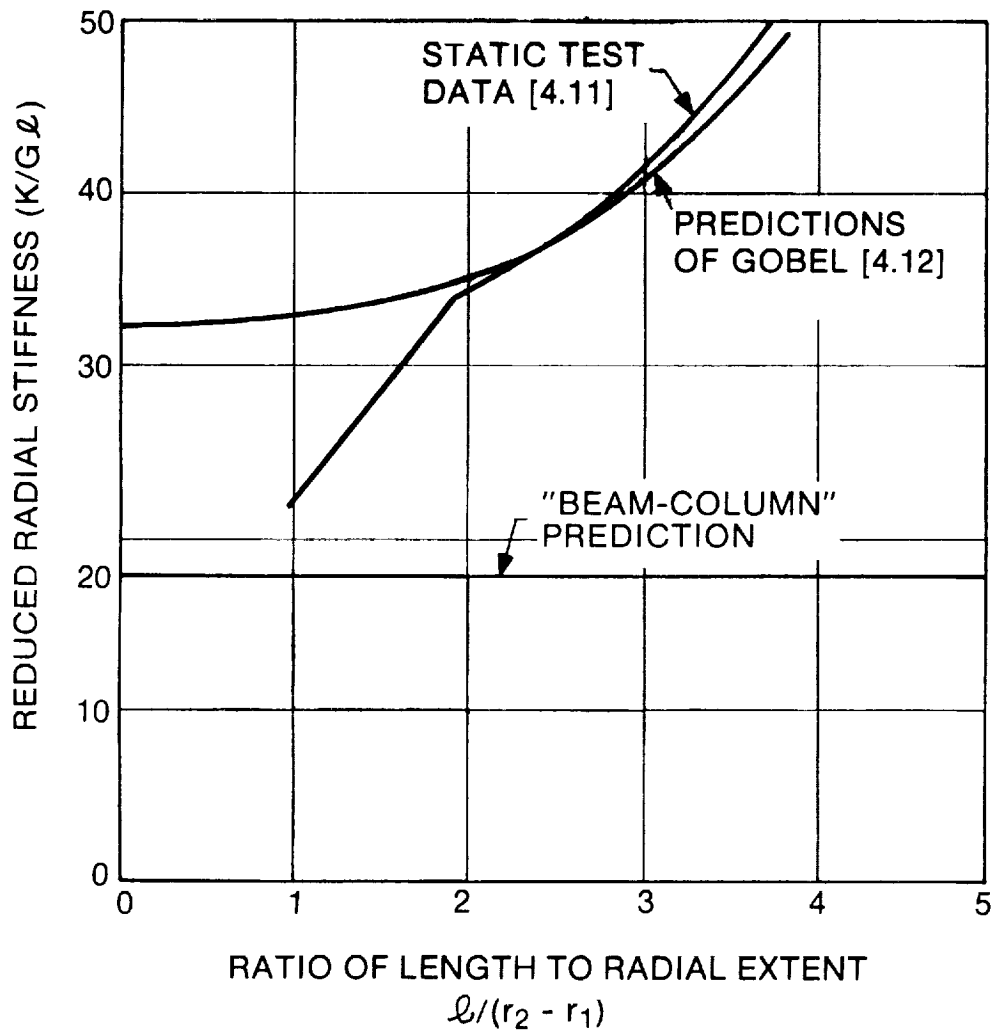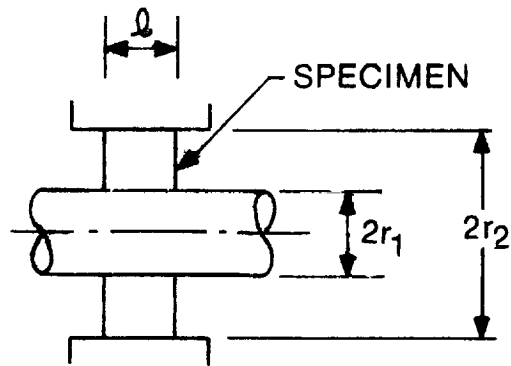
Fig. 22 Comparison of Prediction Methods for Cylindrical Cartridge
(After [4.12])

It is seen that only the Göbel Method reveals any dependence of this non-dimensional stiffness on length of the cartridge, and that the level of the Göbel predictions is substantially higher than that of the plane stress and Beam-Column predictions.

The assumption necessary to apply the Göbel and plane stress predictions in the determination of dynamic stiffness and damping is that:

$$\frac{k^*}{G^* \ell} = \frac{k_1}{G' \ell} \qquad (4-25)$$

where $k^* = k_1 + i k_2$ is the complex impedance of the cartridge, $G^* = G' + iG''$ is the complex modulus and ℓ is the length. That is, the relative distribution of stresses is independent of time under sinusoidal loading and displacement.

The simple Beam-Column method, without accounting for radius effects, may be developed directly using either G or G^*, as it assumes no interaction between elements. In other words, no further assumptions are necessary in applying it to dynamic stiffness and damping beyond the significant assumptions in its development already presented.

For a series of tests with two ring cartridge specimens, Smalley and Tessarzik [4.12] found that, using the Beam-Column analysis and the method of Göbel, stiffness and damping values were predicted which generally bracketed the test results. Neither of these methods appeared to provide consistently better correlations than the other.

4.3 The Effects of Frequency

As might be expected from a material whose behavior is governed by a time-dependent relaxation process, the slope and area of the hysteresis loop, together with the stiffness, damping, and loss coefficient, are functions of the frequency with which the load cycle is executed. It is generally observed that the dynamic stiffness is higher than the static value and that stiffness tends to increase with increasing frequency. Shown on a scale which may cover many decades of frequency, the general form of elastomer behavior variation has three distinct regions [4.16] which are illustrated in Figure 23:

- Rubbery

- Transition (leathery)

- Glassy

In the rubbery region, the behavior is, as implied, "rubbery". Elastomer elements are resilient and the damping is usually of the order of 10 to 30 percent of the stiffness. The hysteresis loop is a rather narrow ellipse. As the frequency increases, the transition region is encountered. Both stiffness and damping increase more rapidly in this region but the damping moves ahead of the stiffness and the hysteresis ellipse becomes broader. For a limited frequency range, damping (k_2) becomes higher than stiffness

70
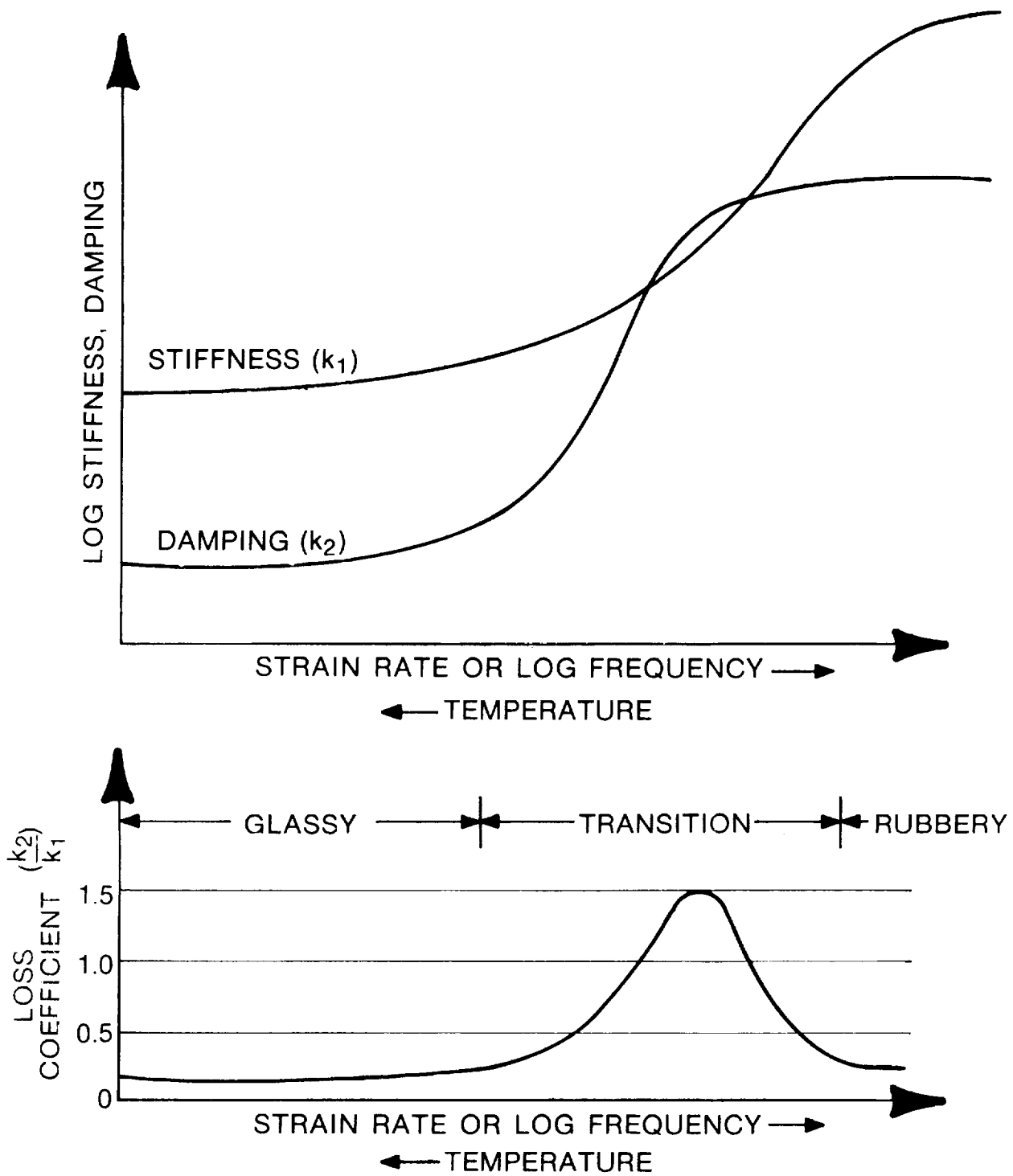
Fig. 23 Regimes of Elastomer Dynamic Behavior

(k_1) and the loss coefficient may become greater than 1.0. For further increases in frequency, the stiffness increases more than the damping, and in the glassy region both quantities level off. The rubbery and transition regions are those normally encountered in elastomers and offer the best opportunity for use in vibration control.

4.3.1 Representation of Frequency Dependence

Observed variation of stiffness and damping with frequency gives rise to discrete data points. For mathematical purposes it is convenient to seek, for an element, a continuous relationship between force and displacement (or stress and strain) which closely matches observed behavior. There are several possible approaches to this problem, with different levels of sophistication and convenience.

Generalized Viscoelastic Models. One approach in representing the frequency variation of stiffness and damping of an elastomer element is to replace the elastomer with a mechanical analog, consisting of a series of springs and viscous dashpots. The simplest models are the Maxwell and Voigt elements (Figure 24). Using these basic elements as building blocks, more complex systems of springs and dashpots may be developed, such as those shown in Figure 25.

The application of a triparameter model, shown in Figure 26, to elastomer specimen test data was demonstrated by Chiang, Tessarzik and Badgley [4.11]. For a selected general viscoelastic model, the methodology to determine the element values to best fit a particular variation of stiffness and damping with frequency was developed and demonstrated by Gupta, Tessarzik and Cziglenyi [4.18].

Generalized Force – Displacement Relationships. An alternative approach for representing the variation with frequency is to assume a general linear differential relationship between force and displacement:

$$a_o F + a_1 \frac{dF}{dt} + a_2 \frac{d^2F}{dt^2} + a_3 \frac{d^3F}{dt^3} + \ldots = c_o x + c_1 \frac{dx}{dt} + c_2 \frac{d^2x}{dt^2} + \ldots \quad (4-26)$$

and for sinusoidal loading and displacement:

$$F = F^* e^{i\omega t} \quad (4-27)$$

$$x = x^* e^{i\omega t} \quad (4-28)$$

So that equation (4-26) becomes:

$$(a_o + i\omega a_1 - \omega^2 a_2 - i\omega^3 a_3 + \ldots)F^* = (c_o + i\omega c_1 - \omega^2 c_2 - \ldots)x^* \quad (4-29)$$

and

$$\frac{F^*}{x^*} = \frac{c_o + i\omega c_1 - \omega^2 c_2 - i\omega^3 c_3 + \ldots}{a_o + i\omega a_1 - \omega^2 a_2 - i\omega^3 a_3 + \ldots} \quad (4-30)$$

72

a. MAXWELL ELEMENT
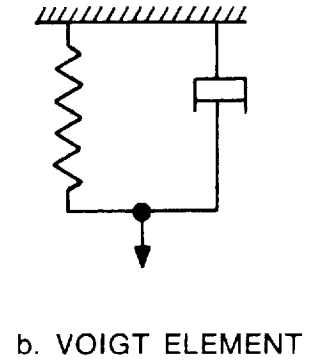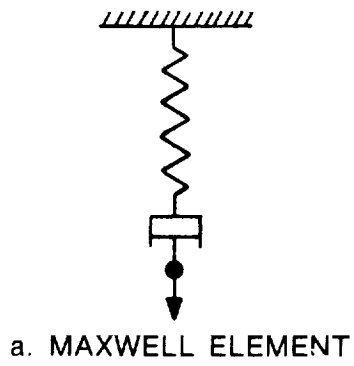
b. VOIGT ELEMENT

Fig. 24   Maxwell and Voigt Elements
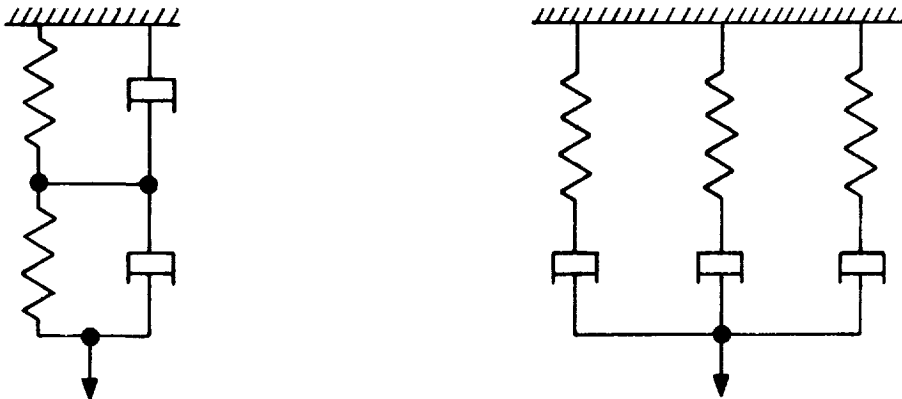
Fig. 25   Combination Systems
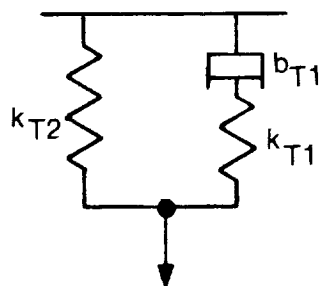
Fig. 26   Triparameter Model

73

A close connection exists between this generalized force displacement relationship and the generalized viscoelastic models since, for a given order of expansion on left- and right-hand sides of equation (4-26), there is a corresponding combination of springs and dashpots [4.16] which will give the same force-displacement relationship.

For example, the differential equation for the triparameter model (Figure 26) is

$$F + \frac{b_{T1}}{k_{T1}} \frac{dF}{dt} = k_{T2}y + \frac{b_{T1}}{k_{T1}} (k_{T2} = k_{T1}) \frac{dy}{dt} \qquad (4-31)$$

so that the nonzero coefficients of equation (4-26) for the triparameter model are

$$a_o = 1$$

$$a_1 = b_{T1}/k_{T1}$$

$$c_o = k_{T2} \qquad\qquad (4-32)$$

$$c_1 = b_{T1} (k_{T2} + k_{T1})/k_{T1}$$

Direct Fit of Mathematical Expression. A direct approach to this problem is to impose upon the data some correlation function and to seek those coefficients which give the best match between the function and the data. Polynomial, trigonometrical, or power-law relationships are some of the options available for this approach. It was found by Gupta et al [4.18] that the use of a power-law relationship was quite adequate to represent the behavior of elements of polybutadiene in the frequency range 100 to 1000 Hz. For engineering purposes, a known relationship between stiffness, damping, and the parameters discussed in this chapter for elastomer elements of different geometries is all that is required to use these elements in design for control of machinery vibrations. In essence, this approach may be considered as the use of a generalized Voigt element in which the storage and dissipative elements are a continuous function of frequency, temperature and strain.

Other methods which deal with the frequency dependence of viscoelastic materials have been developed. The reader is referred to recent publications such as [4.28] which deal with the constitutive behavior of viscoelastic media by application of generalized derivatives.

4.4 Influence of Temperature

In general, elastomer behavior is strongly influenced by temperature. Thus complete characterization of elastomer elements must provide their dynamic behavior over the frequency and temperature ranges of interest. In considering the effects of temperature, the following observations are often made:

- Temperature tends to be most influential where frequency is also strongly influential.

- Increasing temperature tends to produce the same results as decreasing frequency and vice versa.

Starting from these observations, a method of reducing the dynamic behavior of elastomers (and other polymers) covering a range of frequencies and temperatures to a single curve relating appropriate reduced properties was developed by Ferry, Fitzgerald, Grandine and Williams [4.19]. The method, sometimes referred to as the WLF law, is derived from a paper by Williams, Landell and Ferry [4.20] in which the mechanics of its implementation are described and demonstrated. The mathematical statement of this method is as follows:

$$(G_r)_{\omega,T} = (G_r)_{\alpha_\theta \omega, T_c} \tag{4-33}$$

$$Log_{10} \alpha_T = \frac{-8.86 \ (T - T_c)}{101.6 + (T - T_c)} \tag{4-34}$$

$$(G_r)_{\omega,T} = (G)_{\omega,\theta} \frac{T_c \rho}{T \rho_c} \tag{4-35}$$

where T_c is a characteristic temperature given by

$$T_c = T_t + (50 \pm 5)^\circ K \tag{4-36}$$

and T_t is the transition temperature between the rubbery and glassy states of the material.

G is the observed modulus at temperature θ and frequency ω.

G_r is the reduced modulus.

α_T is the coefficient by which test frequency is multiplied to obtain the corresponding reduced frequency at temperature θ_c.

ρ, ρ_c are the densities of the elastomer material at the specified temperature and the characteristic temperature, respectively.

By these relationships, knowledge of a modulus as a function of frequency at several temperatures may be interpreted as knowledge of reduced modulus over a wide frequency range at the characteristic temperature. This knowledge may be further interpreted to give the variation of modulus over a wide frequency range at any temperature between T_c and the maximum temperature tested.

The method has been demonstrated to be applicable to material properties of storage and loss moduli or to element properties of stiffness and damping. The additional information needed to implement and use the methods beyond

the elastomer dynamic data is the value of T_c. The transition temperature, T_t, may be measured independently or T_c may be inferred from a sufficiently large volume of dynamic data. With an assumption of constant density ($\rho = \rho_c$), equation (4-35) is often simplified to give

$$(G_r)_{\omega,T} = (G)_{\omega,T} \frac{T_c}{T} \qquad (4-37)$$

In cases where high filler loadings are present [4.21], equation (4-34) may not be an adequate representation of the relationship between temperature effect and frequency effect. In this case, it may be necessary to use the more general representation

$$Log_{10}\alpha_T = \frac{C_1(T - T_c)}{C_2 + (T - T_c)} \qquad (4-38)$$

where C_1 and C_2 (and if necessary T_c) are evaluated for best fit from test data by an iterative numerical procedure. Alternatively, T_c may be specified by equation (4-36) or chosen as some convenient temperature. The determination and use of $Log_{10}\alpha_T$ is discussed in more detail in the chapter on elastomer properties.

4.5 The Effect of Static and Dynamic Strain

Large values of static strain (preload) can have a significant effect on the dynamic properties of elastomer elements. However, for simple geometries (uniform strain and compression elements) the effect of modest preload levels (five percent or less) is generally not large. On the other hand, the effect of dynamic strain is generally quite pronounced [4.12, 4.22, 4.23, 4.24 and 4.25]. This effect has been shown to be mainly dependent on two factors: chemical and thermal [4.24, 4.25].

The chemical factor involves the way the bonding matrix is disrupted when strained. Two mechanisms are involved in this process. One, often referred to generally as strain softening, is substantially reversible in short times and involves the physical configurations of the particles in the moving matrix. Strain softening occurs in any elastomer sample but is most pronounced in materials with high carbon black loading. The other mechanism, referred to as structure, is substantially irreversible over periods of an hour or less and involves the weak chemical and physical interactions between the particles at rest. The division between these two mechanisms is not well defined and their effects have not been generally quantified.

The thermal factor, involving self-heating of the elastomer element, is most significant at high strains and relatively unimportant at low strains. This self-heating, due to thermal dissipation, has been analyzed and quantified [4.12] but has been shown not to account entirely for the effect of dynamic strain (which is reasonable, since strain softening was not considered) [4.26]. The effect of self-heating can be demonstrated with reasonable simplicity by an analysis of the thermal dissipation in an elastomer element under uniaxial stress [4.12].

A model intended to tie the effects of high dissipation to the change in

properties has been developed [4.12]. This model simply needs to have available values of G' and G'' as functions of frequency and temperature. The hypothesis of this model is that large amplitude vibrations, when imposed upon an elastomer element, give rise to dissipation of energy throughout the element. As a result, there is a tendency for the elastomer to heat up. The temperature distributions in the elastomer are governed by the equations of thermal conduction and appropriate boundary conditions. As a result of the distribution of temperature in the elastomer and the dependence of elastomer moduli on temperature, there is a distribution of material properties through the elastomer. Load equilibrium within the elastomer, accounting for this distribution of properties, governs the forces generated by the elastomer and its apparent stiffness and damping. The implementation of such a model in two or three dimensions could be very complicated. However, to typify the results given by such a model and to identify the major items of information needed while minimizing the complexity, a one-dimensional development has been undertaken [4.12]. An important assumption is that the time scale associated with the vibrational phenomena (less than 0.01 second) is short compared to the time scale associated with changes in the thermal condition of the material ($h^2 \rho C_p/k$, which is of the order of 40 seconds and higher).

4.5.1 One-Dimensional Model for Large Dissipation Effects [4.12]

This model is directed at either a shear or a compression element in which a uniaxial state of stress prevails. The temperature distribution is one-dimensional and the flow of heat is normal to the stressed area.

As a result of imposed conditions, an elastomer element in the form of a right circular cylinder is undergoing time varying changes in temperature, internal stress and displacement. The cylinder is as shown in Figure 27. It is assumed that stresses are uniaxial.

At any point

$$\sigma_z = \sigma(Z,t)e^{i\omega t} \tag{4-39}$$

$$U_z = U(Z,t)e^{i\omega t} \tag{4-40}$$

$$T_z = T(Z,t) \tag{4-41}$$

where σ_z is the normal axial stress

$\quad$ U_z is the axial displacement

$\quad$ T_z is temperature;

and it is understood that only the real parts of equations (4-39) and (4-40) apply. σ and U are complex numbers containing both amplitude and phase information. It is assumed that the amplitude functions σ, U are undergoing much slower changes with time than σ_z and U_z. In Reference [4.12], the governing
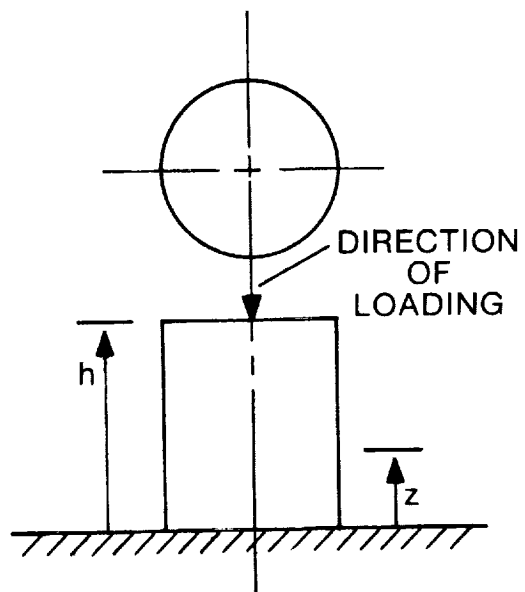
Fig. 27   Compression Loaded Cylinder

78

equations for this thermo-viscoelastic model for compression (Figure 27) and shear loading (Figure 28) are derived to give:

Energy equation:

$$\frac{\partial}{\partial Z}\left[K\,\frac{\partial T}{\partial Z}\right] - \rho\,C_p\,\frac{\partial T}{\partial t} = -\,\gamma G'' \left(\left|\frac{\partial U}{\partial Z}\right|\right)^2 \frac{\omega}{2} \qquad (4\text{-}42)$$

Equilibrium equation:

$$\left[\frac{\partial}{\partial Z}\right]\,G^*\,\frac{\partial U}{\partial Z} \qquad (4\text{-}43)$$

where $\gamma = 1$ for a shear element, and for a compression element, $\gamma = 3$.

The additional equations to be satisfied are:

Boundary conditions:

$$T = T_a \text{ at } Z = 0, h \qquad (4\text{-}44)$$

$$U = 0 \text{ at } Z = 0 \qquad (4\text{-}45)$$

For imposed displacement at top of element:

$$V = x^* \text{ at } Z = h \qquad (4\text{-}46)$$

For base excitation, equation of motion:

$$G^*\,\frac{\partial U}{\partial Z}\,A\,\mho - M\omega^2 U = M\omega^2 x_o^* \qquad (4\text{-}47)$$

where

x^* is the amplitude of displacement of top relative to base

x_o^* is base excitation amplitude (absolute)

M is the supported mass

ω is the base excitation frequency

A is the stressed area

T_o is the temperature at base and top

$\mho$ is defined above.

4.5.2 Solution of the Equations

As a result of the dependence of G* on temperature, the system of equations is nonlinear. While steady-state results are of most interest, solution in the time domain has been selected as more convenient to implement than an iterative solution. The solution method is a modification of the second-order

79
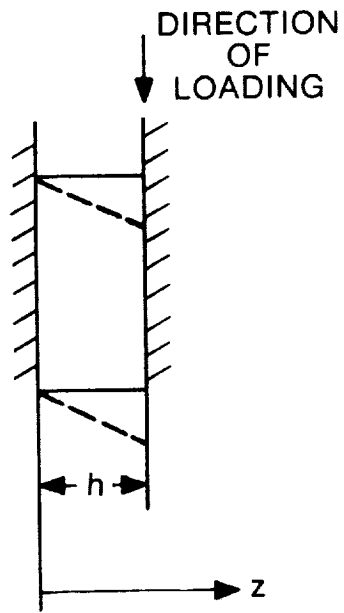
Fig. 28 Shear Element

Crank-Nicholson Method [4.25], in which nonlinear terms are evaluated by extrapolation forward one-half time-step.

The energy equation is written to apply at the time $t + \Delta t/2$.

$$1/2 \left\{ \frac{\partial}{\partial Z} \left[k \frac{\partial T}{\partial Z} \right] \right\}_t + 1/2 \left\{ \frac{\partial}{\partial Z} \left[k \frac{\partial T}{\partial Z} \right] \right\}_{t + \Delta t}$$

$$- \rho\, C_p\, \frac{(T_{t+\Delta t} - T_t)}{\Delta t}$$

$$= \left\{ - \gamma\, G'' \left| \frac{\partial U}{\partial Z} \right|^2 \frac{\omega}{2} \right\}_{t+\Delta t/2} = R_{t+\Delta t/2} \tag{4-48}$$

The left-hand side has a linear operator and consists of known quantities at time, t, and unknown quantities at time, $t + \Delta t$. The right-hand side is unknown since it is a function of temperature at time $t + \Delta t/2$, but can be approximated by the linear extrapolation from known quantities:

$$R_{t+\Delta/2} = (3/2)R_t - (1/2)R_{t-\Delta t} \tag{4-49}$$

The equation for U is solved at time $t + \Delta t$, once $T_{t+\Delta t}$ and the associated values of G^* are known.

The time integration solution is continued until results for successive time steps indicate that thermal equilibrium has been reached. The equilibrium distribution of temperature, material properties, and deflection will determine the steady-state behavior which will be observed once the initial thermal transients have died out.

An interesting feature of thermal transient behavior occurs when the base excitation boundary conditions apply. The frequency of excitation and supported mass can be such that the element causes subresonant vibrations when the element is cold but vibrates above resonance when the element gets hot due to self-heating. In this case, there is a wide swing in phase angle during the thermal transient and an inability to hold subresonant conditions for levels of dissipation higher than a certain limit. Observed stiffness and damping of the element at any time during the time integration, including equilibrium, are calculated as:

$$k_1 = \frac{\gamma A}{x^*} \, \mathrm{Re} \left\{ G^* \frac{\partial U}{\partial Z} \right\}_{Z=h} \tag{4-50}$$

$$k_2 = \frac{\gamma A}{x^*} \, \mathrm{Im} \left\{ G^* \frac{\partial U}{\partial Z} \right\}_{Z=h} \tag{4-51}$$

It is important to note that a number of material properties are needed to implement this analysis: in particular, density, specific heat and conductivity. In addition, if this analysis is to be applied with significance

to compression elements in which the stiffness correction factor (for geometry) is of order 1.5 and above, some account must be taken of the stiffness correction factor. An assumption may be made that the stiffness correction factors follow the functional dependence on frequency and geometry determined empirically for cylindrical elements and that the increase in effective modulus should take place on a local basis, and be reflected in the equilibrium equation:

$$\frac{\partial}{\partial Z} \left[G^*_{eff} \frac{\partial U}{\partial Z} \right] = 0 \tag{4-52}$$

In any case, to be truly representative, the results of this analysis must be modified to include the effects of strain softening and structure.

4.6 Summary

Elastomer materials are generally represented as linear viscoelastic materials with storage and loss moduli which are dependent upon frequency, temperature, strain, geometry and material composition. The dynamic properties of viscoelastic elements are characterized as complex stiffness, where the real part is the typical stiffness and the imaginary part is the hysteretic damping coefficient. The loss coefficient is defined as the ratio of the imaginary part of the stiffness to the real part. Similarly, the basic dynamic property of viscoelastic materials is the complex shear modulus. The real and imaginary parts of the shear modulus are the storage and loss moduli, respectively. Since elastomer materials are essentially incompressible, the Poisson's ratio is very nearly equal to 0.5, and the complex compressive modulus is very nearly equal to three times the complex shear modulus. The effects of geometry, frequency, temperature and strain on the dynamic properties of elastomers are very significant.

The effects of geometry have been considered for three basic loading configurations: pure shear, pure compression, and combined shear and compression in a ring cartridge. The effect of bending on a shear specimen with a length-to-thickness ratio of at least four has been shown to be negligible. The effect of end conditions on a compression specimen has been shown to be significant for diameter-to-thickness ratios greater than 0.5. Since it is generally not advisable to use compression specimens with smaller ratio's than this which may have the tendency towards column buckling, the effect of end conditions becomes important. Several analytical methods have been used to evaluate the effect of combined shear and bending in a ring cartridge. Some of these methods have been shown to give results which differ by as much as a factor of two. Experimental correlations have tended to fall in the range between the analytical prediction extremes, with none of the analytical methods giving consistently superior correlations.

Over many decades of frequency, elastomer behavior is characterized by three regions: rubbery, transition and glassy. Various modelling approaches have been used to represent the frequency dependence of elastomer dynamic properties including generalized viscoelastic models, generalized force-displacement relationships, and direct fit of mathematical expressions (particularly using power-law relationships).

The effect of temperature on the dynamic properties of elastomers has been

found to be opposite that of frequency. That is, increasing temperature tends to produce the same results as decreasing frequency and vice versa. A method of reduced variables, sometimes referred to as the WLF law, has been devised to combine the effects of temperature and frequency using a single reduced variable.

The effect of static strain (preload) on the dynamic properties of elastomers has been shown to be relatively insignificant for moderate values of preload. The effect of dynamic strain, which is extremely significant, can be attributed to two factors: a chemical factor (strain softening and structure) which is most significant at low to moderate strain values, and a thermal factor (self-heating) which is most significant at high strain values. While strain softening and structure are difficult to quantify, an analysis of self-heating is straightforward to a simple geometry and a uniaxial load. Using such an analysis, self-heating, as expected, has been shown to account for some, but not all, of the effects of dynamic strain.

4.7 References

4.1 Warnaka, G.E., "Dynamic Strain Effects in Elastomers", Rubber Chem. Technol, 1967, p. 407.

4.2 Payne, A.R. and Scott, J.R., Engineering Design with Rubber, Interscience Publications, New York, 1960.

4.3 Warner, W.C., "Measuring Dynamic Properties of Vulcanizates", Rubber and Related Products: New Methods for Testing and Analyzing, ASTM STP 553, American Society for Testing and Materials, 1974, pp. 31-55.

4.4 Smalley, A.J., Tessarzik, J.M., and Badgley, R.H., "Testing for Material Dynamic Properties", ASME Publication: Vibration Testing Instrumentation and Data Analysis, AMD Vol. 12, 1975, pp. 117-141.

4.5 Lazan, B.J., Damping of Materials and Members in Structural Mechanics, Pergamon Press, New York, 1968.

4.6 Holownia, B.P., "Effect of Carbon Black on Poisson's Ratio in Elastomers", Rubber Chem Technol, May-June 1975, pp. 245-253.

4.7 Gent, A.N. and Lindley, P.B., "The Compression of Bonded Rubber Blocks", Proc Inst Mech Engrs, Vol. 173, No. 3, L59, pp. 111-117.

4.8 Hattori, R. and Takei, K., J Soc Rubber Ind, Japan, Vol. 23, 1950, p. 194.

4.9 Payne, A.R., "Dynamic Properties of Vulcanized Rubbers: 5 - Shape Factors and Functions in Rubber Engineering", Research Report No. 84, Research Assoc of British Rubber Manufacturers, January 1975.

4.10 Moghe, S.R., and Neff, H.R., "Dependence of Compression Modulus on Poisson's Ratio", Rubber Chem Technol, 1973, p. 207.

4.11 Cannon, C.M., Nashif, A.D. and Jones, D.I.G., "Damping Measurements on Soft Viscoelastic Materials Using a Tuned Damper Technique", Shock and Vibration Bulletin No. 38, Naval Research Laboratory, Washington, D.C., Part 3, November 1968, pp. 151-163.

4.12 Smalley, A.J., and Tessarzik, J.M., "Development of Procedures for Calculating Stiffness and Damping Properties of Elastomers in Engineering Applications, Part III: The Effects of Temperature, Dissipation Level and Geometry", NASA Report CR-134939, November 1975.

4.13 Göbel, E.F., Berechnung and Gestaltung Von Gummifedern, Springer-Verbag, Berlin/Göttengen/Heidelberg, 1955.

4.14 Adkins, J.E., and Gent, A.N., "Load-Deflexion Relations of Rubber Bush Mountings", British Journal of Applied Physics, Vol. 5, October 1954, pp. 354-358.

4.15 Rightmire, G.K., "An Experimental Method for Determining Poisson's Ratio of Elastomers", J Lub Tech, July 1930, pp. 281-388.

4.16 Snowden, J.C., Vibration and Shock in Damped Mechanical Systems, J. Wiley and Sons, Inc., New York 1968.

4.17 Chiang, T., Tessarzik, J.M. and Badgley, R.H., "Development of Procedures for Calculating Stiffness and Damping Properties of Elastomers in Engineering Applications. Part I: Verification of Basic Methods", NASA Contractor Report No. CR-120965, March 1972.

4.18 Gupta, P.K., Tessarzik, J.M., and Cziglenyi, L., "Development of Procedures for Calculating Stiffness and Damping Properties of Elastomers in Engineering Applications. Part II: Elastomer Characteristics of Constant Temperature", NASA Contractor Report No. CR-134704, April 1974.

4.19 Ferry, J.D., Fitzgerald, E.R., Grandiene, L.D. and Williams, M.L., "Temperature Dependence of Dynamic Properties of Elastomers: Relaxation Distributions", Ind Eng Chem, Vol. 44, No. 4, April 1952, pp. 703-706.

4.20 Williams, M.L., Landel, R.F. and Ferry, J.D., "The Temperature Dependence of Relaxation Mechanisms in Amorphous Polymers and Other Glass-Forming Liquids", J Amer Chem Soc, 77, 370, 1955.

4.21 Howgate, P.G., "Properties of Polybutadiene Material Nicholls NEX 156G", Rubber and Plastics Research Association of Great Britain, Technical Report 3252, May 1977.

4.22 Sommer, J.G. and Meyer, D.A., "Factors Controlling the Dynamic Properties of Elastomeric Products", SAE Paper No. 720267, SAE/ASTM Sym, Detroit, Michigan, January 1973.

4.23 Sircar, A.K. and Lamond, T.G., "Strain Dependent Dynamic Properties of Carbon Black Reinforced Vulcanizates: I - Individual Elastomers", Rubber Chem Technol, March-April 1974, p. 71.

4.24 Howgate, P.G., "Report of Observations Made During the Visit of P.G. Howgate to MTI Latham", Rubber and Plastics Research Association of Great Britain, Technical Report 3558, October 1977.

4.25 Tecza, J.A., Darlow, M.S., and Smalley, A.J., "Development of Procedures for Calculating Stiffness and Damping Properties of Elastomers in Engineering Applications, Part V: Elastomer Performance Limits and the Design and Test of an Elastomer", NASA Report CR-159552, February 1979.

4.26 Darlow, M.S., and Smalley, A.J., "The Effects of Strain and Temperature on the Dynamic Properties of Elastomers", ASME Transactions, Journal of Mechanical Design, ASME Paper No. 79-DET-57, September 1979.

4.27 Carnahan, B., Luther, H.A. and Wilkes, J.O., Applied Numerical Methods, J. Wiley and Sons, Inc., New York 1969.

4.28 Badgley, R.L., "Applications of Generalized Derivatives to Viscoelasticity", AFML-TR-79-4103, November 1979.

5.0 MEASUREMENT OF DYNAMIC PROPERTIES OF ELASTOMERS

Various test methods have been used for determining the dynamic properties of elastomers. Experimental determination of these properties is necessary to correlate with, and supplement, the results of analytical procedures such as those discussed in Section 4.0. While providing important insight into the behavior of elastomers, analytical studies generally have been limited in their characterization of the effects of many significant parameters. Consequently, the emphasis has been on empirical determination of elastomer dynamic properties; this trend will probably continue into the near future.

In general, empirical relationships for elastomer dynamic properties involve the use of a Voight model (Section 4.0) where the damping is assumed to be hysteretic (Section 2.0) and is represented as the imaginary part of the complex stiffness, k*. Since it is not possible to measure k* directly, it is necessary to measure certain physical quantities (such as force and displacement) and compute k*. If general material properties (rather than test element properties) are desired, storage and loss moduli may be calculated from k* by considering the appropriate geometric relationships, as discussed in the previous section. The values of the storage and loss moduli for a given test element will be functions of frequency, temperature and strain. Empirical relations may be formulated to represent the effects of these parameters.

When designing an elastomer damper, it is desirable to use existing dynamic property data for elastomers (such as that provided in Section 6.0). However, this is not always possible. For example, if the design requires an elastomer material (or operating or environmental condition) for which the appropriate data is not available, it may be necessary to generate this data through a test program. This may also be desirable where special elastomer configurations are to be used or when critical applications require extremely accurate data and the elimination of variations due to minor compositional changes, which can influence the dynamic properties [5.1][†]. It has been shown that translational load test results are adequate for predictions of properties for rotating load dampers [5.2]. However, consideration of the effects of both compressive and shear deformation for appropriate geometries, such as radial buttons (Sections 6.0 and 8.0) is required.

Dynamic test systems may be considered to consist of two basic subsystems: 1) the mechanical hardware, with associated control electronics, that exercises the test specimen, and 2) the sensors and measurement electronics (generally referred to as instrumentation) which acquire the basic vibration data from which specimen properties are determined. Advances in electronics and, in particular, the improved capability of measuring phase angles between two signals have influenced a gradual shift towards simpler mechanical systems. These systems have fewer components of uncertain dynamic characteristics with more sophisticated electronics. Recently, the instrumentation subsystem has been expanded to include minicomputers for; test control, data acquisition and calculation of dynamic properties. Additional discussions on test instrumentation may be found in [5.3, 5.4 and 5.5].

---

† Numbers in brackets indicate References found in Section 5.7.

In this chapter, cursory descriptions are presented of a number of commonly
used test methods. These test methods may be separated into three categories:
forced resonant tests, free resonant tests and forced nonresonant tests.
Details of those and other test methods may be found in References 5.6
through 5.15.

Quick estimates of dynamic stiffness of elastomer specimens can be made from
static stiffness values. Static stiffness can either be measured directly
from static load tests or Shore ® (durometer) hardness, which can be measured
very easily using a durometer tester. The relationship between Shore ® A
hardness and static shear modulus is illustrated in Figure 29 5.16 . Dynamic
stiffness may then be estimated using frequency multipliers which are generally
in the range of 1.5 to 5 for low frequencies (larger for higher frequencies)
and low dynamic strain (smaller for high strain). These multipliers may be
deduced from static and dynamic properties of generic materials, although
they are generally functions of filler loading, as well as of elastomer
material. For example, a frequency multiplier of about four has been used
for a particular flourocarbon elastomer mix. However, for the engineer who
requires elastomers for their damping characteristics, a static measurement
offers no information on energy dissipation.

5.1 Forced Vibration Resonant Test Methods

These test methods employ resonant amplification of test specimen deformation.
Most of these test machines are essentially single-degree-of-freedom vibratory
systems, where the elastomer specimen provides most of the flexibility and
damping and the system inertia may be fixed or variable. For fixed-inertia
machines, the resonant frequency can be changed only by changing the elastomer
specimen material or geometry. Most of the early test machines fall into this
category due to the lack of availability of precision instrumentation (par-
ticularly for measuring phase angles). Most of the forced resonant methods
permit data to be taken only at resonance. The elastomer specimen stiffness
and damping are calculated from the resonant frequency and bandwidth and the
characteristics of the test machine, with no need for phase angle measurement.
With advances in instrumentation, newer methods evolved, such as the Base
Excitation Resonant Mass (BERM) method. The BERM method uses accurate phase
angle measurement to broaden the frequency range at which data can be taken
and reliable data may be acquired at off-resonance conditions.

Two forced resonant methods which use fixed inertias are the Tangorra Hystere-
simeter [5.17 and the vibrating reed [5.18, 5.19 . The Tangorra Hysteresimeter
is essentially a dynamic hardness tester (Figure 30). It consists of a vertical
rod made of nonmagnetic material and fitted with a Shore ® A hardness indentor
at the lower end. Attached to the rod are two permanent magnets, each of which
is surrounded by a coil. One magnet/coil combination is used to excite an
oscillatory vertical motion in the rod, and the other is used to measure the
motion. The frequency is varied around the system resonance, and the stiff-
ness and damping of the specimen are calculated at the resonant frequency. This
instrument has the advantages of low cost, fast operation, and insensitivity
to sample size or configuration; however, it is restricted to low strains and
a single frequency for a particular specimen.

® Registered Trademark, Shore Instrument and Manufacturing Co., Inc.
Jamaica, New York.
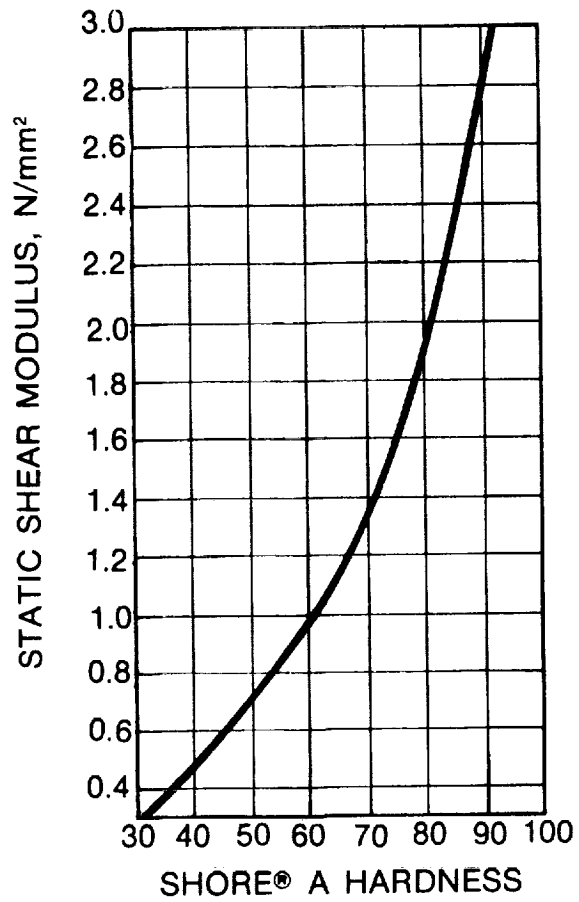
Fig. 29   Dependence of Static Shear Modulus on Hardness (After Reference [5.16])
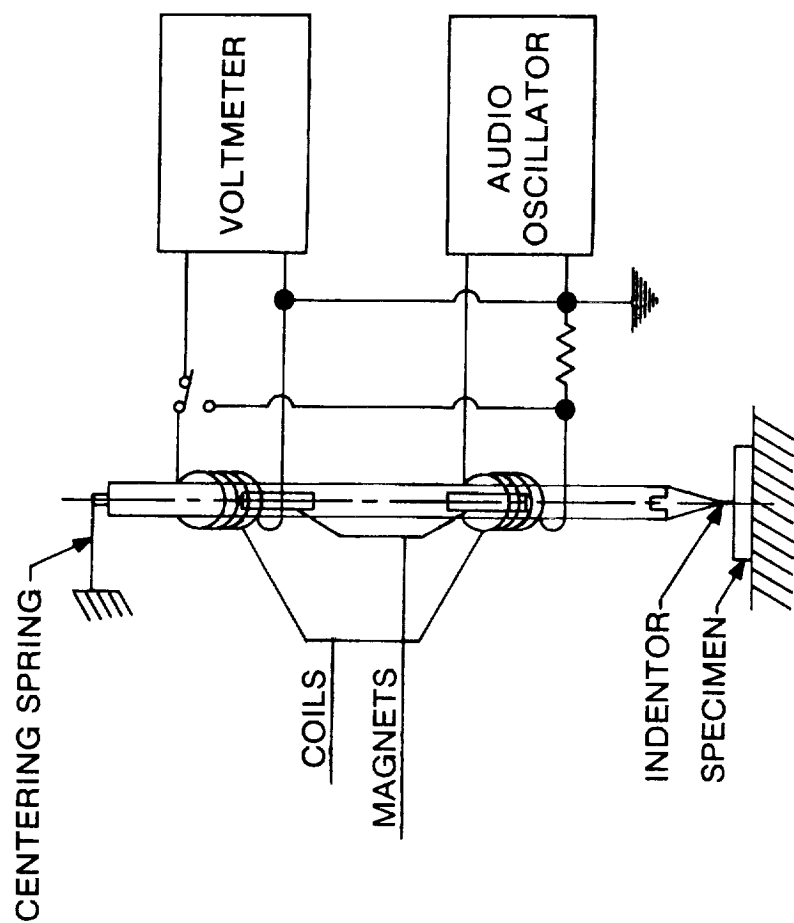
Fig. 30 Tangorra Hysteresimeter (After Reference [5.17])

89

A vibrating reed, shown schematically in Figure 31, is generally used for plastics or other "stiff" materials. However, by bonding an elastomer specimen to a metal strip or by adhering a small piece of metal at the bottom of an elastomer strip to respond to the exciting transformer, the vibrating reed may be used for elastomers. The storage and loss elastic moduli are calculated from the resonance frequency location, bandwidth, specimen dimensions and related machine constants. The vibrating reed has the advantages of being easily enclosed in an environmental chamber and suitable for high damping materials. However, it is limited to low strains and a single frequency for a particular specimen. Considerable operator skill is required for acquisition of accurate data.

Several forced resonant test methods have been used which provide for variable system inertia so that more than one frequency can be considered for a single test specimen. A machine described by Moyal and Fletcher [5.20] and shown in Figure 32 is a typical example of a forced resonance machine employing electrical vibrators for excitation. As seen in Figure 32, loudspeaker magnets (C) are used in conjunction with alternating current coils (B) on a steel bar (A) supported by springs (D) to produce a cyclic force to vibrate the elastomer sample. The frequency of the alternating current, and thus of the vibration, is varied to find the mechanical resonance of the system. The stiffness and damping of the test specimen are calculated from the amplitude and frequency of resonance and the driving current and mass of the system. Alternatively, the frequency can be left constant and the resonance found by varying the suspended mass (M).

Forced resonance test machines which take advantage of the properties of electro- and magneto-striction in metals for producing a cyclic deformation force, have been developed. These properties characterize the change in length of metals which occurs when it is subjected to an electric or magnetic field. In essence, resonance frequency and bandwidth of a metal rod undergoing electro- or magneto-striction are modified slightly by pressing an elastomer test piece against the end of the rod. The storage and loss moduli of the elastomer test piece are calculated from the changes in resonant frequency and bandwidth. There are restrictions on test piece size and frequency is not continuously variable. An example of a magneto-strictive method was presented by Nolle [5.21]; examples of electro-strictive methods were presented by Dietz et al [5.22] and Rhinehart [5.23].

In the middle 1950s, engineers at Chrysler Corporation developed the resonant beam tester for measurement of dynamic properties of elastomeric springs [5.24]. A simplified line drawing of the resonant beam tester is shown in Figure 33. The concept of the resonant beam tester took advantage of two facts: 1) through mechanical amplification by the beam (lever) ratio, the force required to exercise the specimen could be reduced and the velocity sensor sensitivity increased; and 2) by operating the system at resonance (with the test specimen acting as the system suspension and the beam acting as the mass), the magnitude of the excitation force could be greatly reduced. Best of all, the analytical relationships at resonance between test parameters and test specimen stiffness and damping were reduced to very simple forms which excluded difficult-to-measure phase relationships [5.14]. The three measured quantities were forced and displacement amplitudes and angular frequency. However, experience proved that repeatable results were difficult to obtain in spite
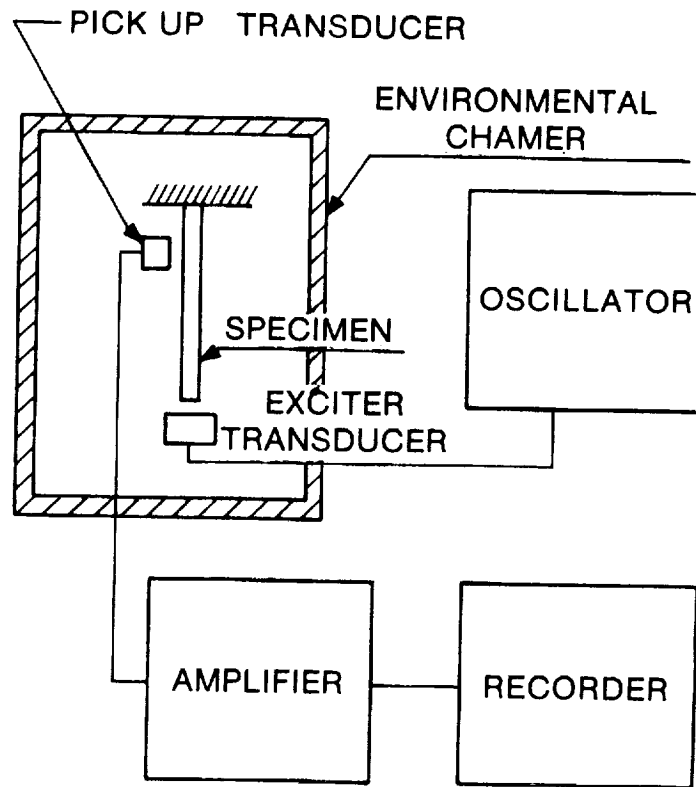
Fig. 31 Vibrating Reed (After Reference [5.8])
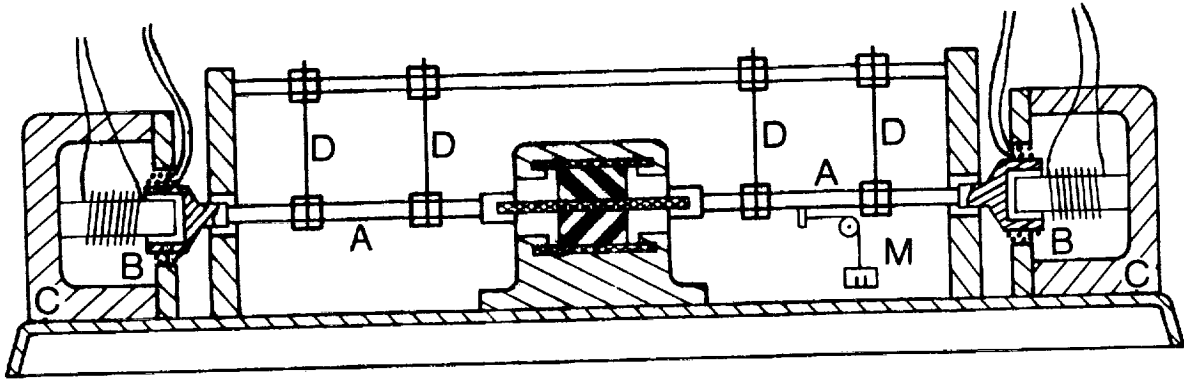
Fig. 32 Forced-Vibration Resonance Machine for Dynamic Tests (After Reference [5.20])
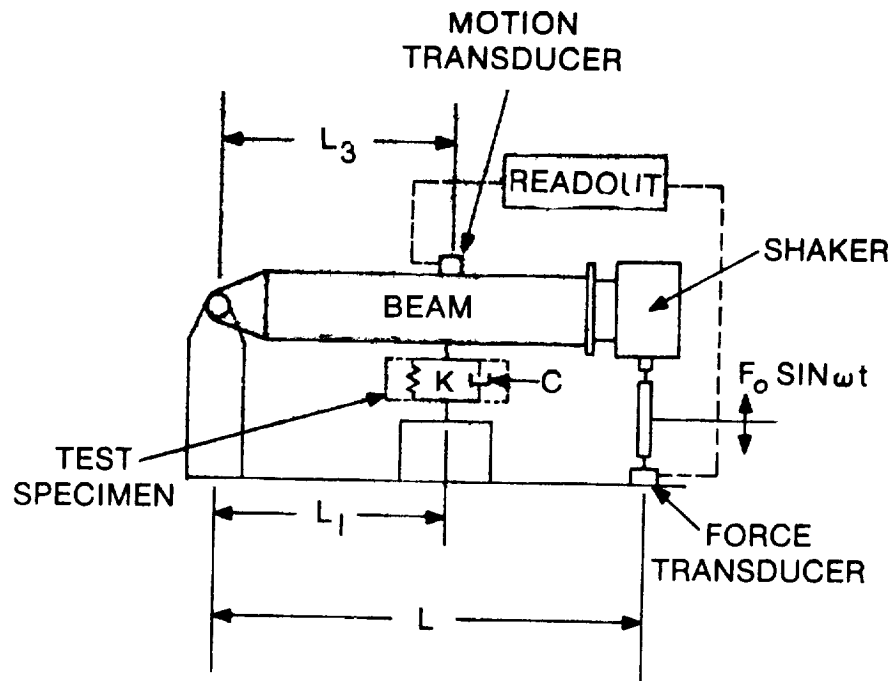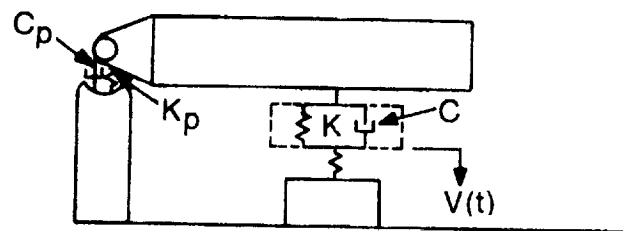
Fig. 33   Resonant Beam Testing Machine (After Reference [5.9])

of considerable refinement to the mechanical system. Inclusion of test specimen support stiffness and beam pivot stiffness and damping was shown to be necessary to eliminate significant errors (Figure 33) [5.14]. Correct determination of test specimen stiffness and damping with all system constants included requires an iterative solution, manageable only by a digital computer. Furthermore, operator error has shown to be significant in the use of an oscilloscope to determine the resonance condition [5.11].

Perhaps one of the earliest dynamic test machines, predating the resonant beam tester, was a test rig that incorporated many desirable features. This rig was, in many ways, the forerunner of today's advanced test machines. The schematic in Figure 34 shows a supporting frame that holds the test specimen in an in-line position with the axis of a shake table. The test specimen was loaded by a sizeable mass, and the stiffness and damping could be readily determined at the system resonance frequency.

By introducing the concept of variable mass so that the test frequency range may be covered by a number of resonant frequency points by replacing the velocity transducer by accelerometers mounted directly on either side of the elastomer, and by providing a displacement sensor for amplitude measurement across the elastomer, one can envision the evolution of advanced testing facilities.

There were at least two reported applications of the base excitation resonant techniques to elastomer material testing in the period between 1958 and 1968 [5.25, 5.26]. In both cases, electromagnetic shakers were used to excite an elastomer-supported mass system. Measured input-output accelerations were used for the calculation of material properties. In the earlier version, the mass was not varied in the vibrating system and a fairly complex, custom-made analog instrument was used for data reduction. In the second application, the mass was variable and test data was acquired only for the system resonance condition, thus making phase angle measurements unnecessary and simplifying the data reduction process. An interesting variant of the base excitation method was reported in Reference 5.27; a right circular cylinder was excited in torsion, and input-output measurements were made on both sides of the system resonance frequency.

Progress in the development of accurate digital phase meters and in the availability of phase-matched dual-channel tracking filters prepared the way for the development of the Base Excitation Resonant Mass (BERM) test method [5.28]. A schematic of the test rig, Figure 35, shows a unidirectional vibrating mass-spring system driven by an electromagnetic shaker. For either large test specimen preloads or very large masses (for low frequency testing), two radial guide bearings and two air cylinders are provided. These elements have small but finite stiffnesses and parasitic damping which must be independently measured and accounted for in the data reduction process. The full dynamic model of the test rig and the elastomer material test samples is shown in Figure 36. A significant feature of this test method is that data can be taken throughout a broad range of frequencies about the system resonance rather than only at resonant frequency. A detailed discussion of this test method is presented in a later subsection.

94
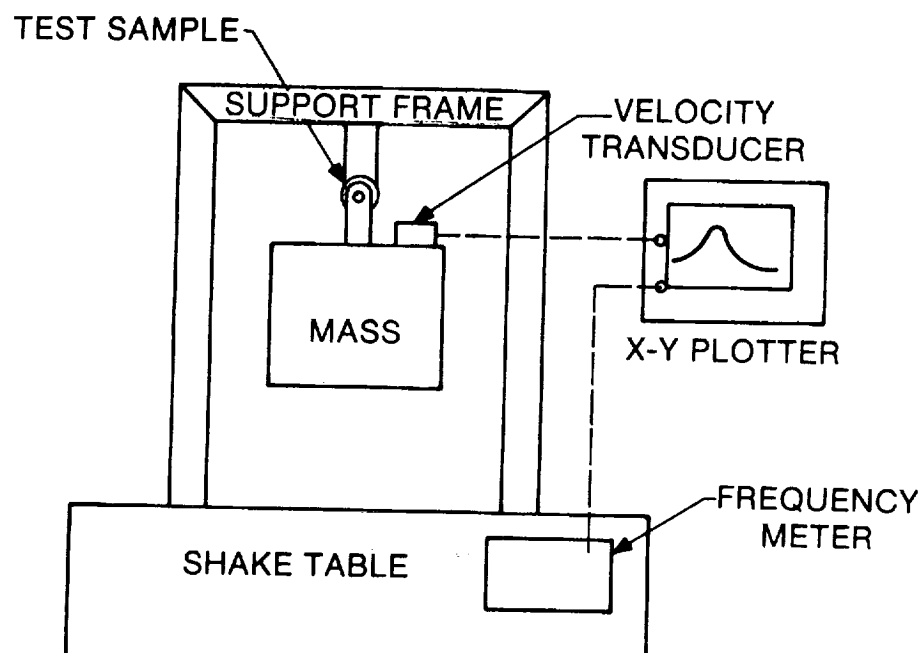
Fig. 34 Bootstrap Dynamic Rate Tester (After Reference [5.24])
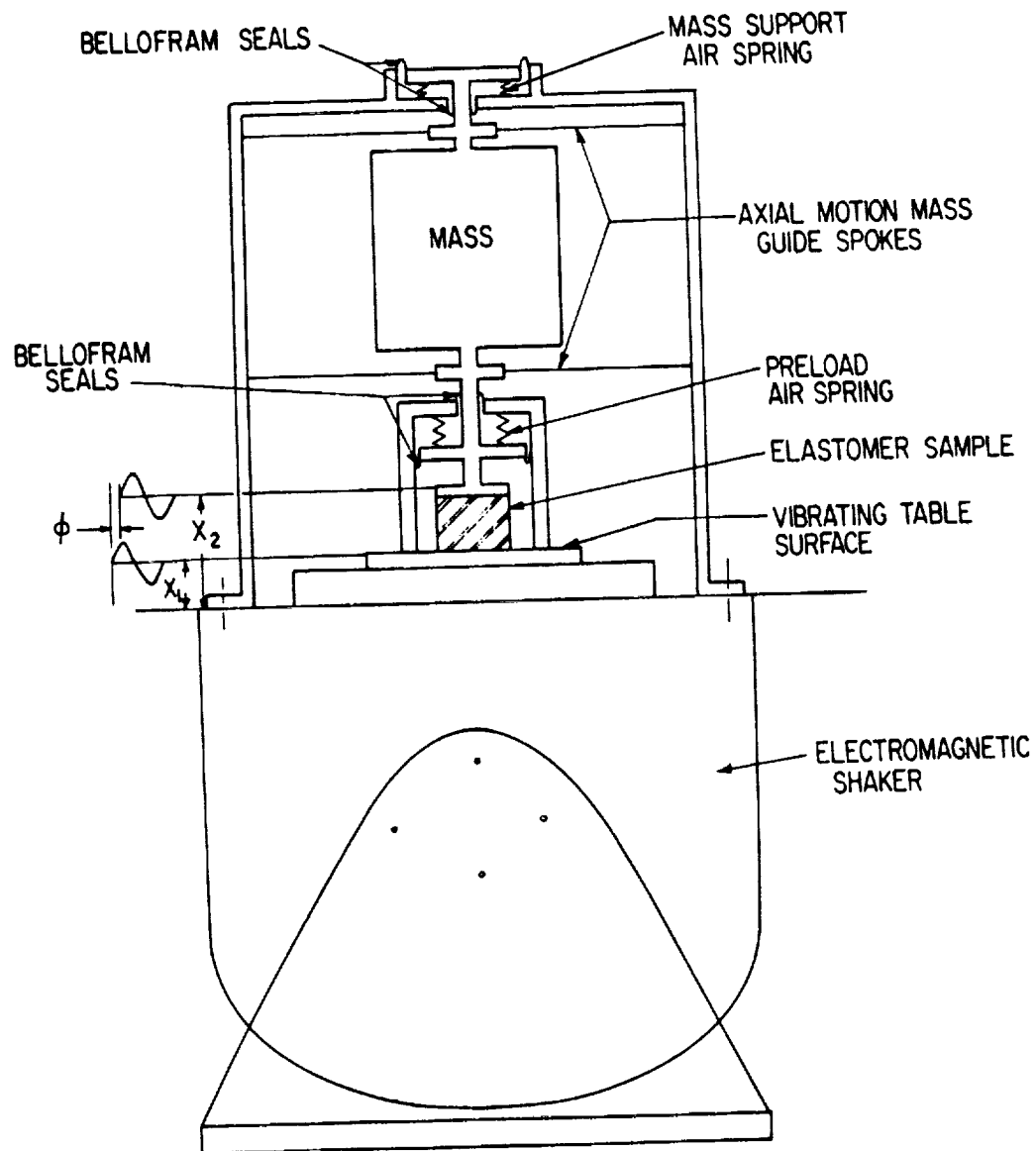
Fig. 35 Schematic of Base Excitation, Resonant Mass
Test Rig (After Reference [5.28])

96
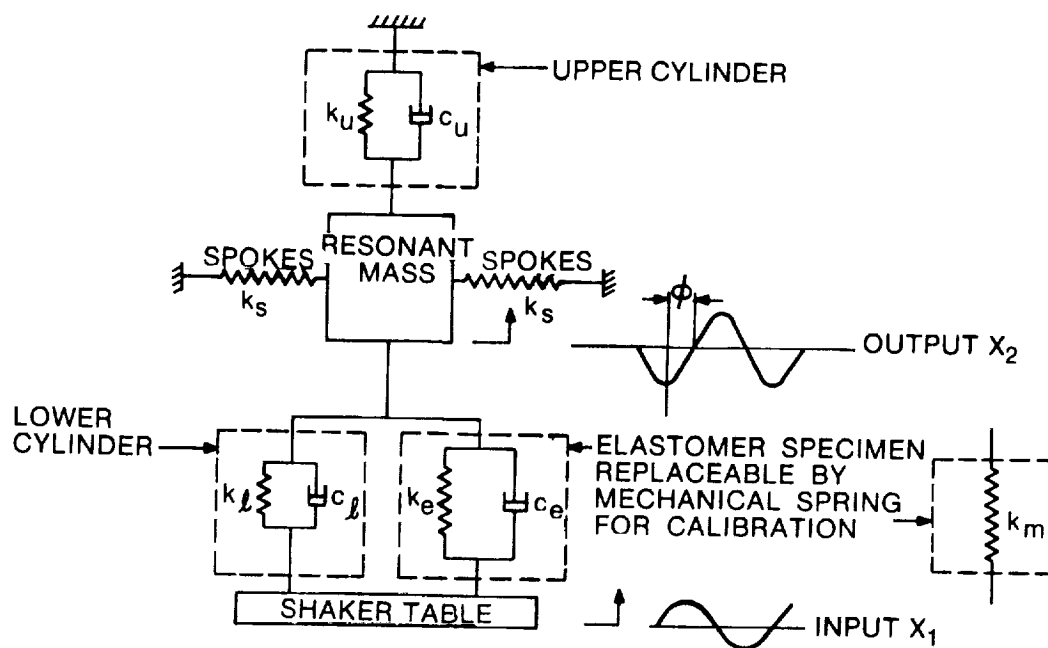
Fig. 36   Dynamic Model of Base Excitation, Resonant Mass Test Rig (After Reference [5.28])

5.2 Free Vibration Resonant Test Methods

These methods employ a rigid mass supported by a flexible elastomer specimen. The elastomer specimen is initially deformed and then released so that the mass is permitted to oscillate. These transient oscillations decay with time due to the damping in the elastomer. The elastomer properties are determined from the form of the damped oscillation. The frequency of the oscillation is used to calculate the elastomer stiffness, and the logarithmic decrement (Section 2.0) of the decaying waveform is used to calculate the damping. In general, these test methods have the advantages of simplicity, ease of application, and suitability for use in environmental chambers. The principal disadvantage is that, since the amplitude of oscillation (dynamic strain) is constantly changing, nonlinear elastomer behavior may not make it possible to account for effects of dynamic strain. These methods are also generally restricted to relatively low frequencies (less than 100 Hz).

The most commonly used test machine of this type is the Yerzley Oscillograph, shown in Figure 37. This device has been standardized by the American Society for Testing and Materials (D945-72) [5.29]. The Yerzley Oscillograph is strictly mechanical and operates on the principle of a horizontal rocking level arm. An elastomer specimen can be tested in either compression or shear. A pen attached to the end of the lever arm traces a damped sinusoidal curve on a rotating drum chart. This instrument can also be used for measuring the static stiffness of elastomer specimens.

A device even simpler than the Yerzley Oscillograph is the torsion pendulum [5.18], which is illustrated schematically in Figure 38. It consists of a suspended elastomer specimen which is clamped at the bottom to a moment of inertia bar. The pendulum is given an initial angular displacement and is released. A damped sinusoid is produced by measuring torque, linear displacement, angular displacement, or acceleration, and the dynamic properties of the elastomer are calculated from the natural frequency and logarithmic decrement. A more refined version of the torsion pendulum has been developed by the Research Association of British Rubber Manufacturers (RABRM) [5.15]. The operation of this device is essentially as described above, but it has been improved to provide increased horizontal stability and easily modified inertia.

5.3 Nonresonant Forced Vibration Test Methods

These methods involve the application of a sinusoidally varying force to an elastomer specimen under nonresonant conditions. In general, both stress and strain (force and deflection) are measured and used to calculate the dynamic properties of the elastomer specimen. These machines are generally restricted to low frequencies (less than 100 Hz). In general, within the limitations of these machines, frequency and strain are continuously variable.

With the earliest machines, the general procedure was to record the stress-strain hysteresis loop and calculate the elastomer dynamic properties from the dimensions of the ellipse (Section 4.0). These early machines include those described by Painter [5.30] (Figure 39), Roelig [5.31] (Figure 40), Lazan [5.32] (Figure 41), and Fletcher and Gent [5.33] (Figure 42). Somewhat
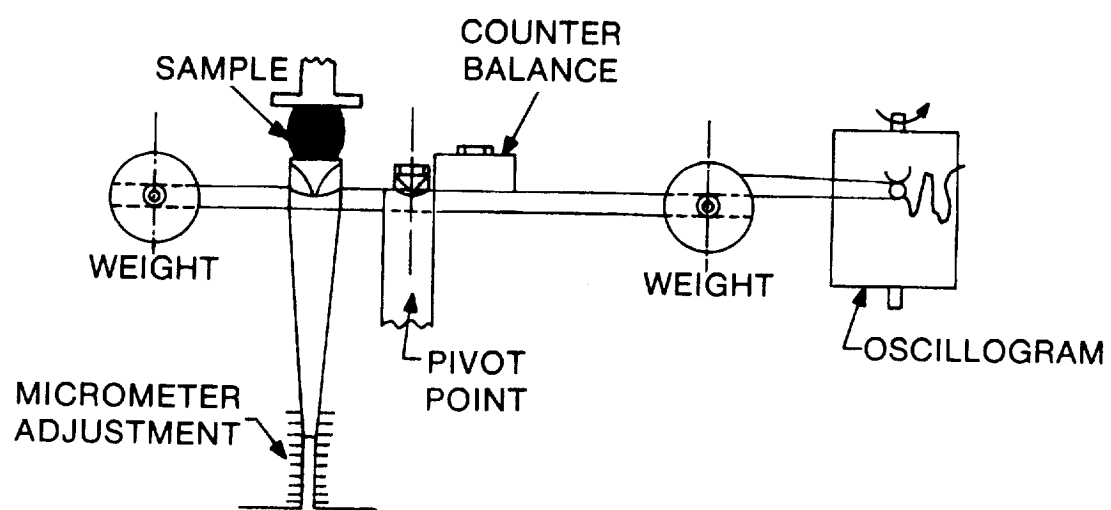
Fig. 37   Yerzley Oscillograph (After Reference [5.8])
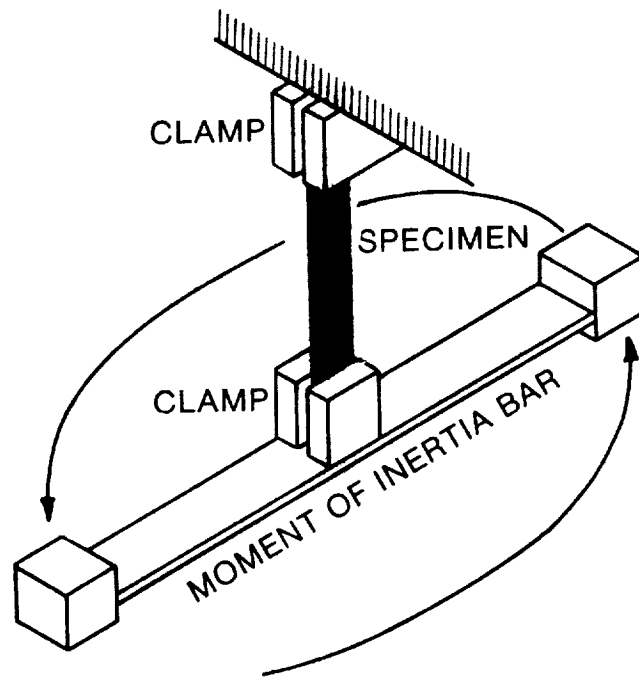
Fig. 38 Torsion Pendulum (After Reference [5.8])
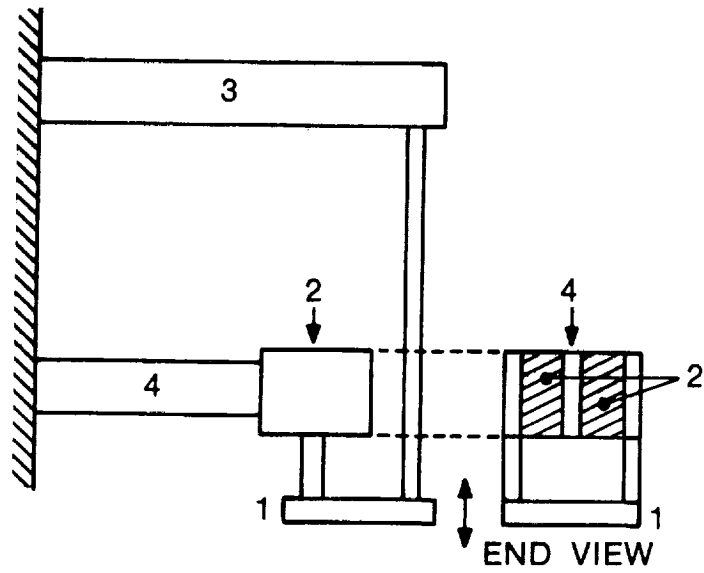
**Fig. 39 Forced-Vibration Nonresonant Test Machine
(After Reference [5.30])**

101
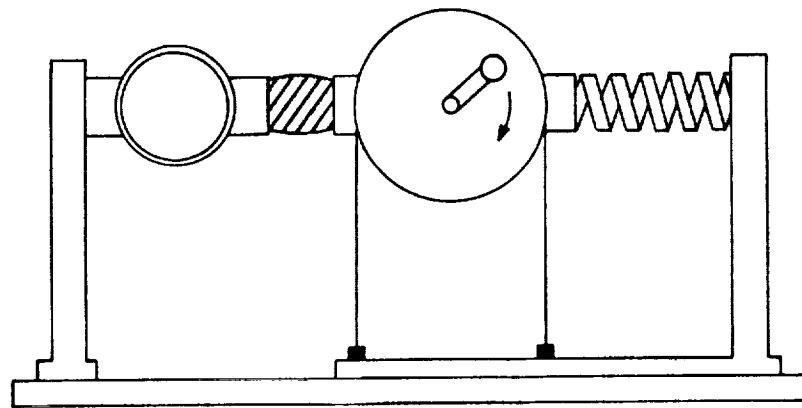
Fig. 40 Roeling Dynamic Test Machine, Forced-Vibration Nonresonant Type (After Reference [5.31])

END VIEW
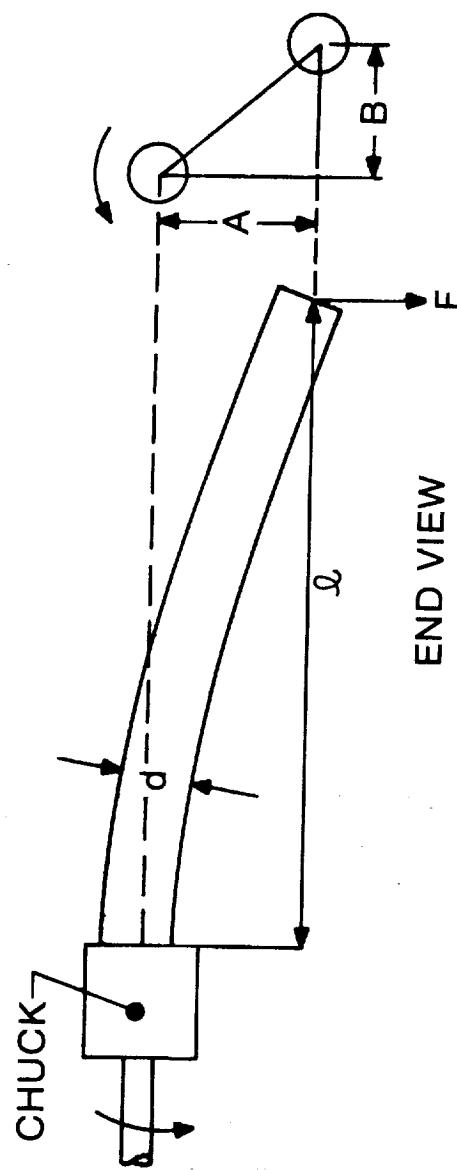
Fig. 41 Dynamic Test Apparatus, Forced-Vibration Nonresonant Type (After Reference [5.32])

OPTICAL SYSTEM

PHOTOCELLS
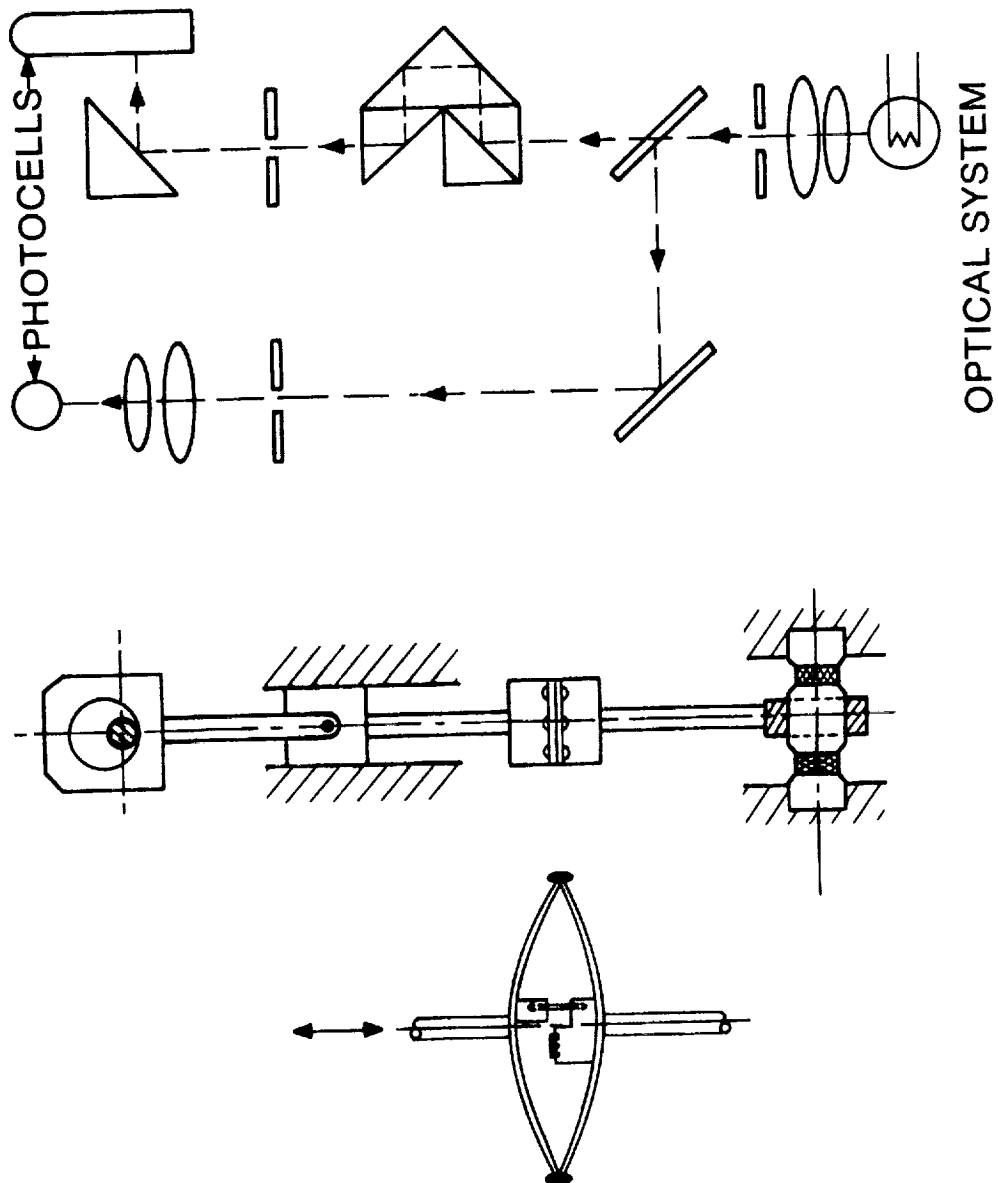
Fig. 42 Forced-Vibration Nonresonant Test Machine (After Reference [5.33])

more recently, a test machine was developed by Payne [5.34] (Figure 43) which has seen extensive use and is often referred to as the RABRM Sinusoidal-Strain Machine. This machine utilizes a rather elegant device for measuring the phase relationship between stress and strain. From the amplitudes of stress and strain (force and deflection) and their phase relationship, the dynamic properties of the elastomer specimen can be calculated directly. A rather specialized machine, referred to as a dynamic viscoelastometer, was designed by Takayanagi [5.35] (Figure 44) and is used for testing rubber-band-shaped elastomer specimens in tension.

Several test machines which have been developed within the past 15 years are grouped under the general classification of transmitted force machines (or methods). The transmitted force measurement method, as it is commonly used, has two main features: 1) the force and displacement measurements are made directly across the test specimen, thus eliminating all fixture compliances (which were significant for the resonant beam test rig described previously) and, 2) an electronic analog circuit that permits the calculation of specimen stiffness and damping at frequencies other than the system resonance. (It appears that adoption of the first feature alone to the resonant beam test rig would have been a significant improvement.) The development of the necessary electronics for the transmitted force measurement method was a lengthy and difficult process [5.13, 5.4]. This was primarily due to the need to handle very precisely and very small phase angles between measured quantities. This approach, once chosen, also affects the choice of instrumentation and sensors. For example, the use of accelerometers as sensors had to be rejected due to both the inherently low phase shift between force and deflection (for most elastomer applications) and the difficulty of matching two accelerometers and their associated signal conditioning equipment for such small angle measurements [5.3]. The consequences of this problem is demonstrated by the following:

> "Consider an elastomer having a stiffness of 1.75 x 10^7 N/m and a damping coefficient of 1.75 x 10^4 N-sec/m, that is excited at 5 Hz. If the phase error in the measurement is 0.1°, the computed value for the damping coefficient has an error of approximately 5%. Considering that it is not unusual to have a phase measurement error of at least 0.5°, this can be a serious problem." [5.36]

For reduction and improved accuracy in the electronic computation process, a minicomputer has been successfully employed with the transmitted force measurement method [5.5].

A typical example of a transmitted force machine is the closed-loop electrohydraulic test machine introduced in 1966 by MTS System Corporation. This machine was a logical pairing of the transmitted force measurement method with a mechanical test rig that used a hydraulic actuator and servovalve. This rig replaced the small electromagnetic shaker and the mechanical multiplier of the resonant beam test rig. A system schematic is shown in Figure 45. Unless the displacement sensor is mounted across the test specimen, the rigidity of the mechanical load bearing frame to avoid measurement errors has to be very high relative to the test specimen stiffness.
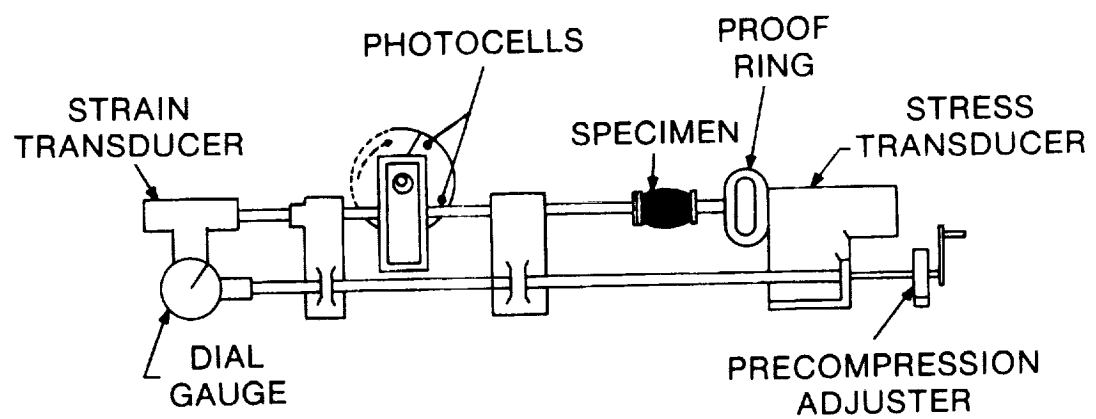
Fig. 43   Payne Dynamic Tester (After Reference [5.11])
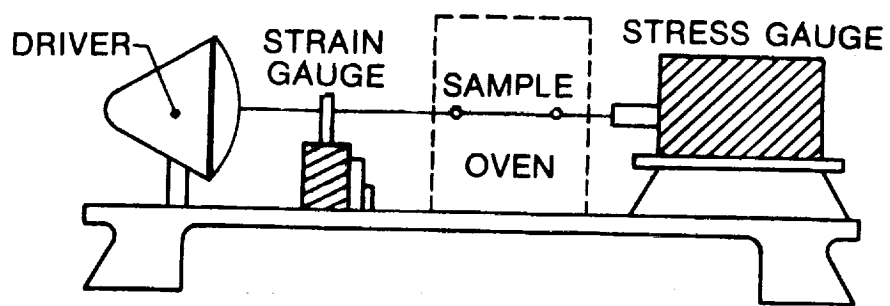
Fig. 44 Takayanagi Dynamic Viscoelastometer (After Reference [5.35])
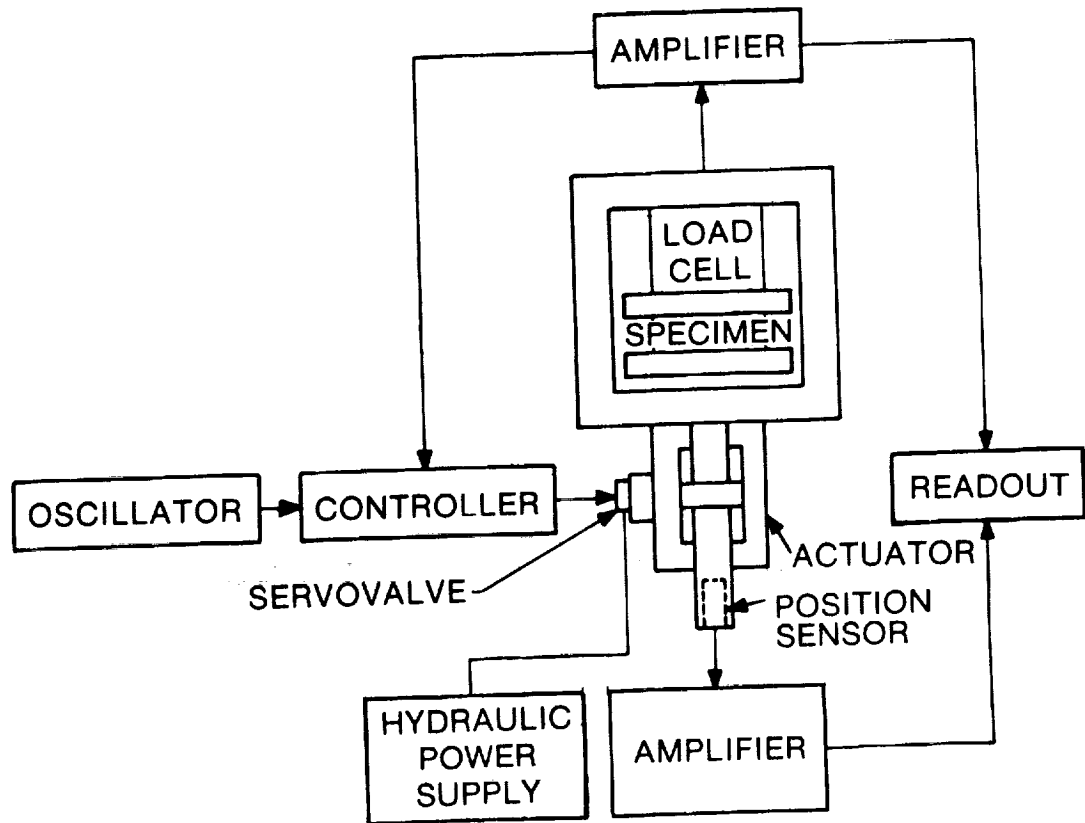
Fig. 45 System Schematic of Closed-Loop Electrohydraulic Test Machine (After Reference [5.12])

A similar machine, an electrodynamic tester, provides a more pure sinusoidal excitation than the electrohydraulic tester and was developed by Fort et al [5.37]. A sketch of the fixturing for this test machine is presented in Figure 46.

5.4 Other Test Methods

There are several additional test methods which do not fall into any of the classifications previously discussed. A number of these methods may be classified as wave propagation methods [5.15]. Wave propagation methods use the velocity and attenuation of waves travelling through an elastomer specimen to determine its dynamic properties. These methods are generally restricted to relatively high frequencies (above 500 Hz - which is relatively high by rotordynamics standards) and to materials with moderate levels of damping. With low damping materials, standing waves occur; with high damping materials, precise measurements are difficult. Several devices have been designed which use longitudinal waves. For example, an apparatus used by Witte et al [5.38] is shown in Figure 47, while one described by Morris et al [5.39] is shown in Figure 48. Transverse vibrations have also been used in a device described by Ballon and Silverman [5.40], shown in Figure 49. Some methods have used brief vibration pulses rather than continuous wave trains. Such methods have been found to be adequate for measuring bulk modulus, but not shear modulus.

Several test methods have been developed which utilize noncyclic displacements. The most common of these is the rebound resilience test which involves the measurement of the rebound of a mass falling on an elastomer specimen. Another is the rotary power loss machine (Figure 50), described by Bulgin and Hubbard [5.41], in which an elastomer specimen is subjected to periodic but isolated deformations while rotating against a rigid wheel.

There are also other classes of tests which are not strictly dynamic property tests but which relate, directly or indirectly, to dynamic properties. These include creep and stress relaxation tests, fatigue tests, vibration transmissibility tests, and tests on cushioning materials (shock tests). These test classes are described in detail and several examples are presented by Payne and Scott [5.15].

5.5 Base Excitation Resonant Mass Method

The Base Excitation Resonant Mass (BERM) test method has been shown to be an easy to use, effective means of measuring the dynamic properties of elastomer specimens [5.42]. The method provides for excellent control of the test conditions, while at the same time permitting maximum flexibility in the choice of these test conditions. Thus, with a sufficiently large shaker and a properly designed test fixture, tests can be conducted for a variety of elastomer geometries and a broad range of frequencies, temperatures and strains. With relatively simple fixturing, tests can be run for frequencies in the range of 100 to 1000 Hz. By using a specially designed test specimen, the testing of frequencies up to 2000 Hz should be achievable, and the use of support fixtures for large resonant masses should permit tests to be run for frequencies as low as 20 Hz [5.42]. Tests have been run for elastomer specimens subjected to pure compression and pure shear, as well as for ring cartridge specimens [5.6] and O-rings [5.43]. Tests have also been run for peak-to-peak dynamic

109
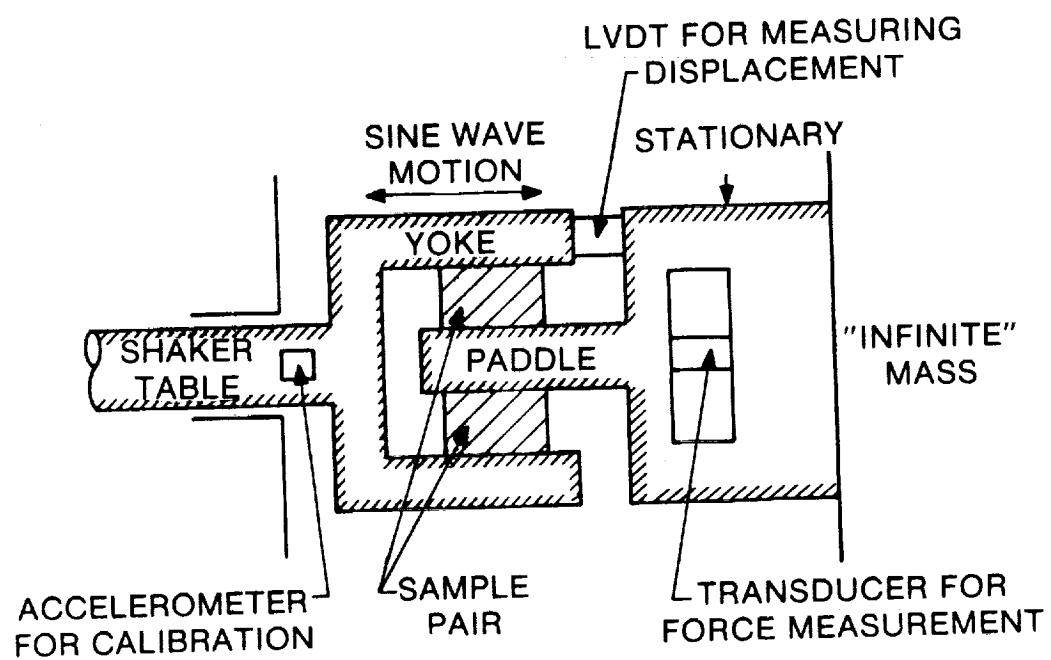
Fig. 46 Electrodynamic Tester (After Reference [5.8])

110
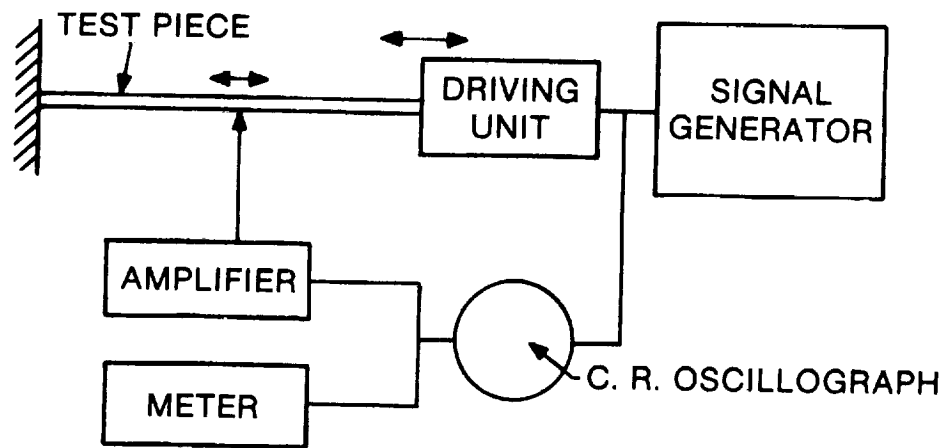
**Fig. 47   Dynamic Test Apparatus Using Logitudinal Wave Propagation
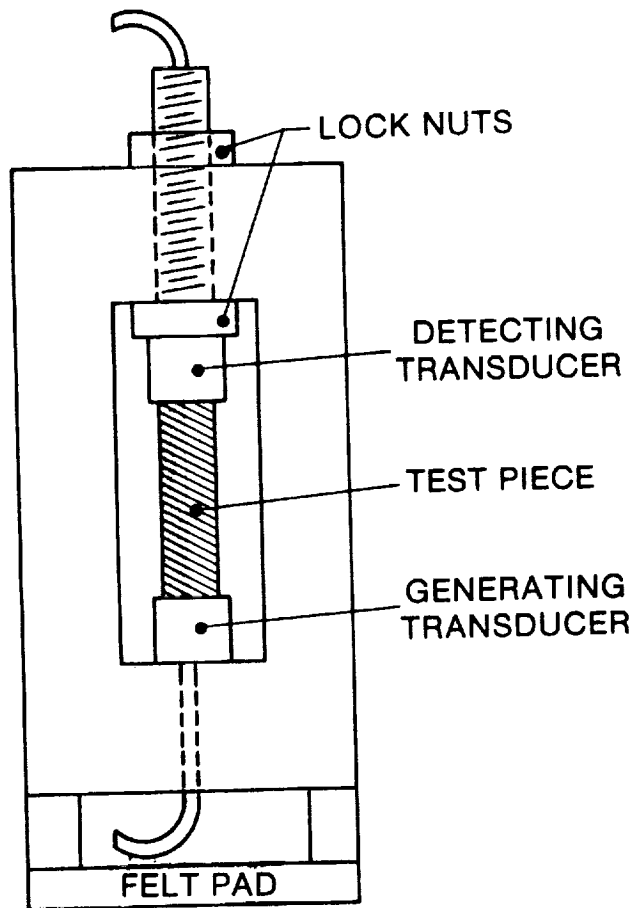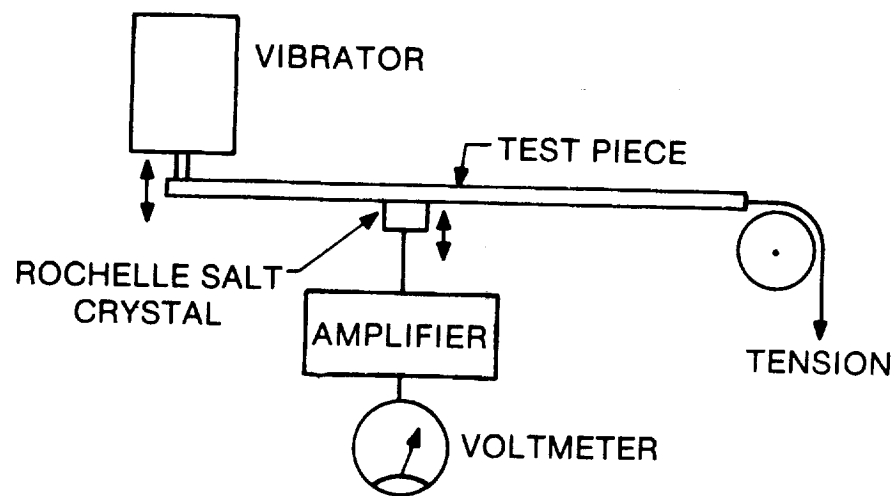(After Reference [5.38])**

Fig. 48 Dynamic Test Apparatus Using Longitudinal
Wave Propagation (After Reference [5.39])

**Fig. 49 Dynamic Test Apparatus Using Transverse Wave Propagation
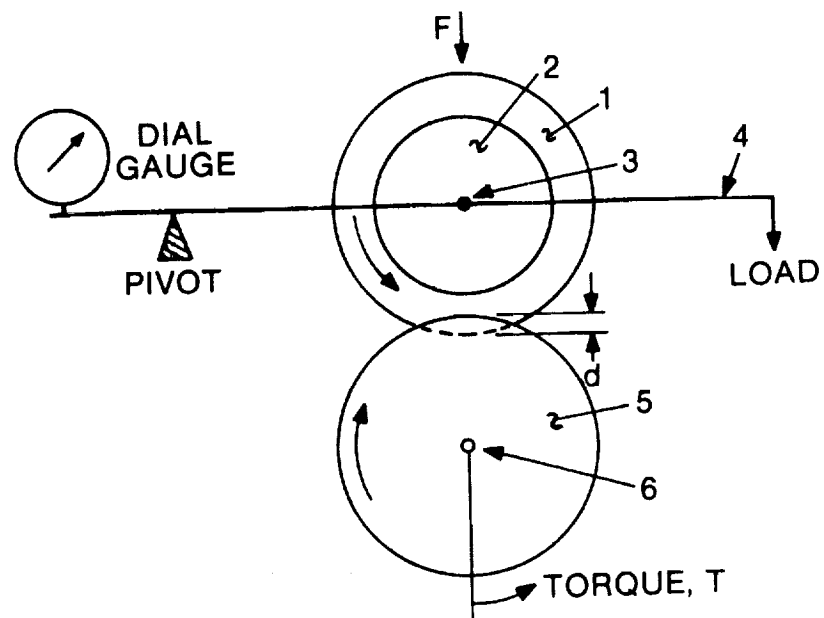(After Reference [5.40])**

Fig. 50 Rotary Power Loss Machine (After Reference [5.41])

114

strain in the range from 0.0005 to 0.08, and temperatures in the range of from 5-216°C (41-420°F). A description of a typical BERM test rig is presented, including the associated instrumentation and test procedures, in sufficient detail to be used as a guide in the performance of similar tests. Much of the design data presented in Chapter 6 is a result of BERM tests performed at MTI.

The basic features of this test rig were developed by Chiang and Tessarzik [5.44] and others [5.28, 5.6, and 5.42]. The test rig was designed to impose precisely measured uniaxial vibration amplitudes upon a selected elastomer sample at desired test frequencies and under selected force preloads. The rig is capable of testing elastomer samples of virtually any size and shape over a wide frequency range. (The test sample cavity used is a cylinder approximately 12.7 cm (5 in) high by 12.7 cm (5 in.) in diameter.) Selection of the resonant mass to match elastomer sample properties permits testing at very high amplitudes at resonance with correspondingly lower amplitudes at off-resonance conditions. Thus, maximum test amplitudes are limited by elastomer characteristics and shaker input power rather than by the test rig itself.

The vibration input to the test rig was obtained from a commercially available electromagnetic shaker system* capable of delivering 66,700 N (15,000 lb) force in the sinusoidal mode of vibration. The test fixture contained ambient temperature control facilities in the form of heating elements and cooling coils embedded in the sample base holder and flow paths for hot and cold air. Uncertainties due to temperature variations were minimized by accurately controlling the ambient temperature and by removing much of the heat generated in the specimen. Two different holding plate configurations provided shear and compression loading of the samples. A slight modification of the test rig permitted testing of ring cartridges, and a similar fixture was used for testing O-rings.

A schematic of the basic test rig can be seen in Figure 35 and a layout drawing of the same rig appears in Figure 51. Figure 52 shows the test rig mounted on the exciter table.

The test rig was designed to meet the following functional requirements:

1. Very low parasitic damping.

2. Inertia mass loading of the elastomer test sample with weights ranging from approximately 0.8 to 227 kg (1.8 to 500 lb).

3. Means for accurately controlling force preloading of the elastomer test sample.

4. Temperature control of the ambient air within the test specimen cavity.

---

* Ling Electronics, Model 335A Shaker with PP-35/70 VC Power Amplifier and SCO-100 Servo Control Center.
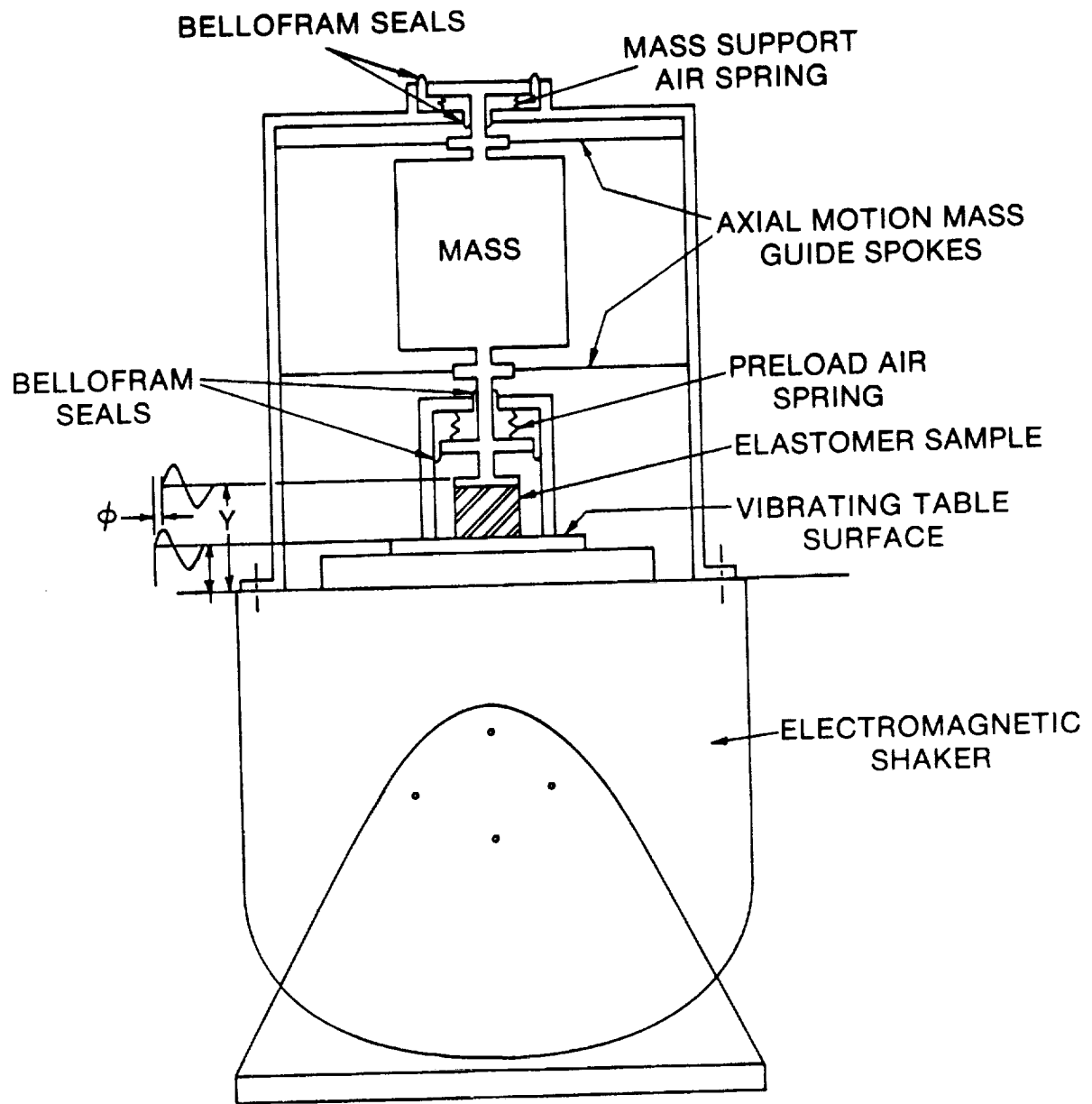
Fig. 51   BERM Test Rig Design

116
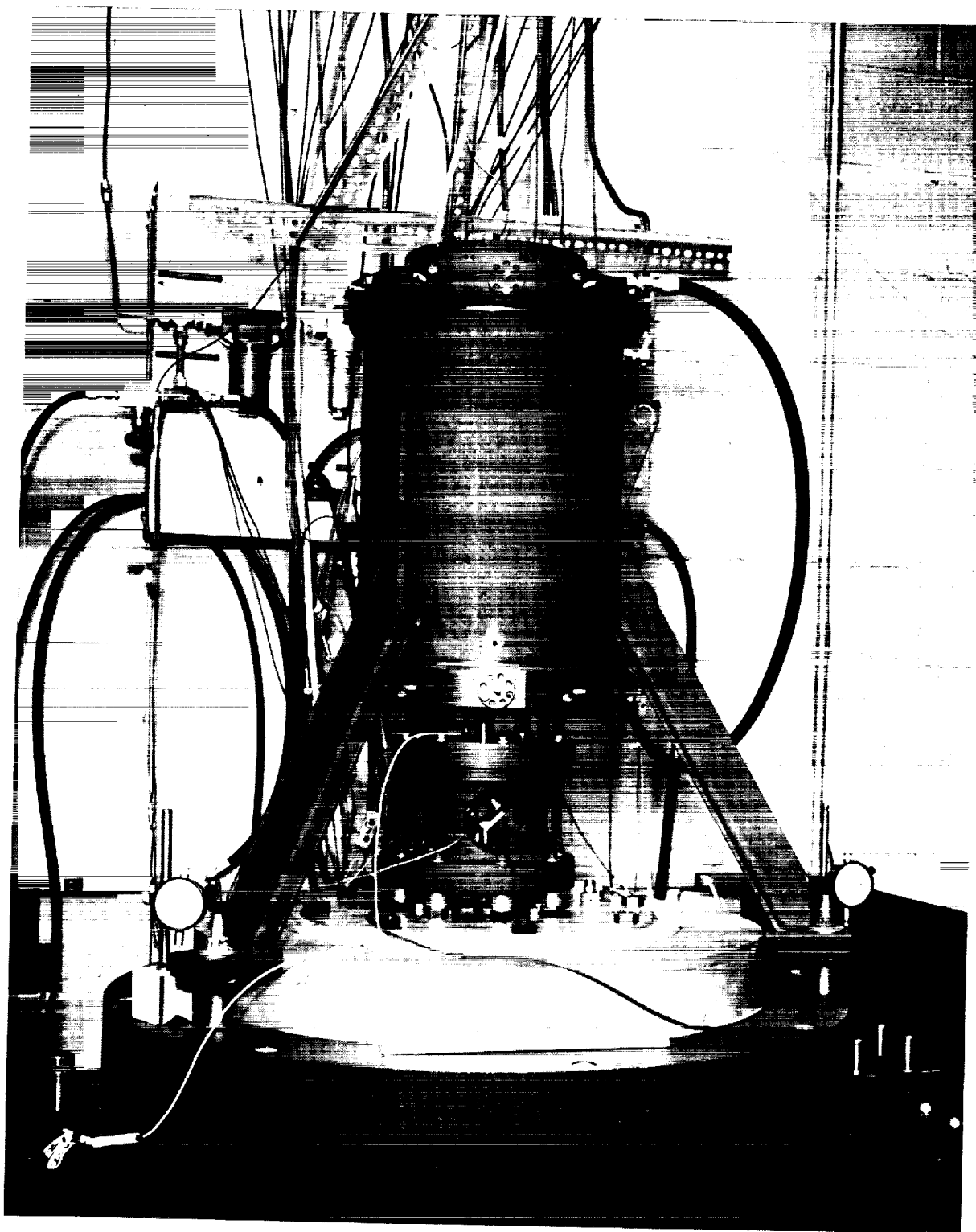
Fig. 52   Elastomer Test Rig Mounted on Vibration Table

117

The rig employs a unidirectional vibrating mass-spring system. In its simplest form, this concept might consist of an elastomer spring to which various amounts of inertia mass are bonded, and the system could be completely free of parasitic damping or stiffness contributions from test rig elements. However, the practical requirements of balancing rather large inertia masses - up to 227 kg (500 lbs) - on top of the elastomer spring and the desired mechanism to provide elastomer sample preloading at all test frequencies introduce additional elements which have finite stiffnesses and small amounts of parasitic damping. Two radial guide bearings for large inertia masses and two air cylinders are required for preloading the elastomer samples. The stiffness and damping properties of these elements have an influence on the test rig response, but these properties can be independently measured and accounted for to minimize these effects on reported data.

The resonant mass bonded to the top of the elastomer specimens consists of a number of elements. For high-frequency tests in which only a minimum of mass is required, the resonant mass can be reduced to the top plate of the specimen holder and the preload piston. The top plate is made of aluminum and the preload piston is made of titanium for minimum weight. Increased mass for medium- or low-frequency testing is provided by rigidly attaching a long rod to the top of the preload piston and by adding steel weights. The weights are centered by the rod and are axially restrained by spacers of various lengths and a lock nut near the upper end of the rod. The rod receives radial support from two "frictionless" guide bearings; Figure 53 shows one of the dismounted bearings. Each bearing consists of a hub and 12 steel spokes. The hub is fitted over the end of the rod and is axially clamped. This kind of bearing arrangement provides good radial stiffness for reasonably high spoke tension but provides only limited freedom for axial motion if overstressing of the spokes is to be avoided. Consequently, changes in preload on the test specimen must be accompanied by lowering or raising of the outer frame, to which the guide bearings are attached.

Preload of the elastomer test specimens is controlled by a pair of air cylinders. The lower cylinder is located directly above the test specimen. Its piston is attached to the specimen's upper holding-plate and exerts a downward force on the specimen. The upper cylinder is located at the top of the test rig and its piston exerts an upward force on the resonant mass. When the resonant mass is large, the desired preload is usually achieved by pressurizing the lower cylinder and exerting a downward force in addition to the weight of the mass. The upper and lower preload pistons are sealed in their cylinders by two rolling diaphragm seals (Bellofram 3C-600-37-FPT and 3-119-119-CBJ). The air cylinder inlet hole is 0.762 mm (0.030 in.) in diameter, making each cylinder essentially a closed cavity under vibration conditions. A constant preload force on the test specimen is maintained through regulation of air pressure in the cylinders.

The ambient temperature within the elastomer test specimen cavity is controlled through the combined effect of both electric heating cables and water-cooled tubes that are installed in the base plate below the test specimens; Figure 54 is a photograph of the installed heating-cooling elements. The grooves in which the heating cable and the tubing are embedded have a
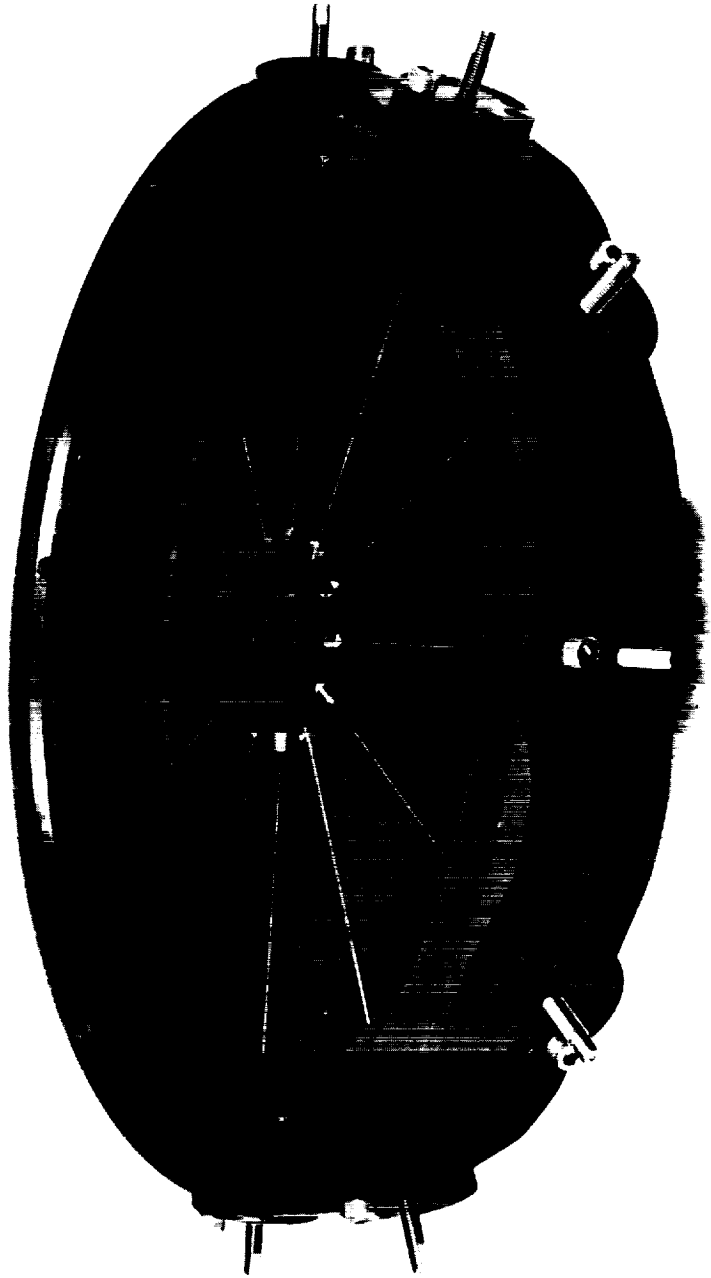
118
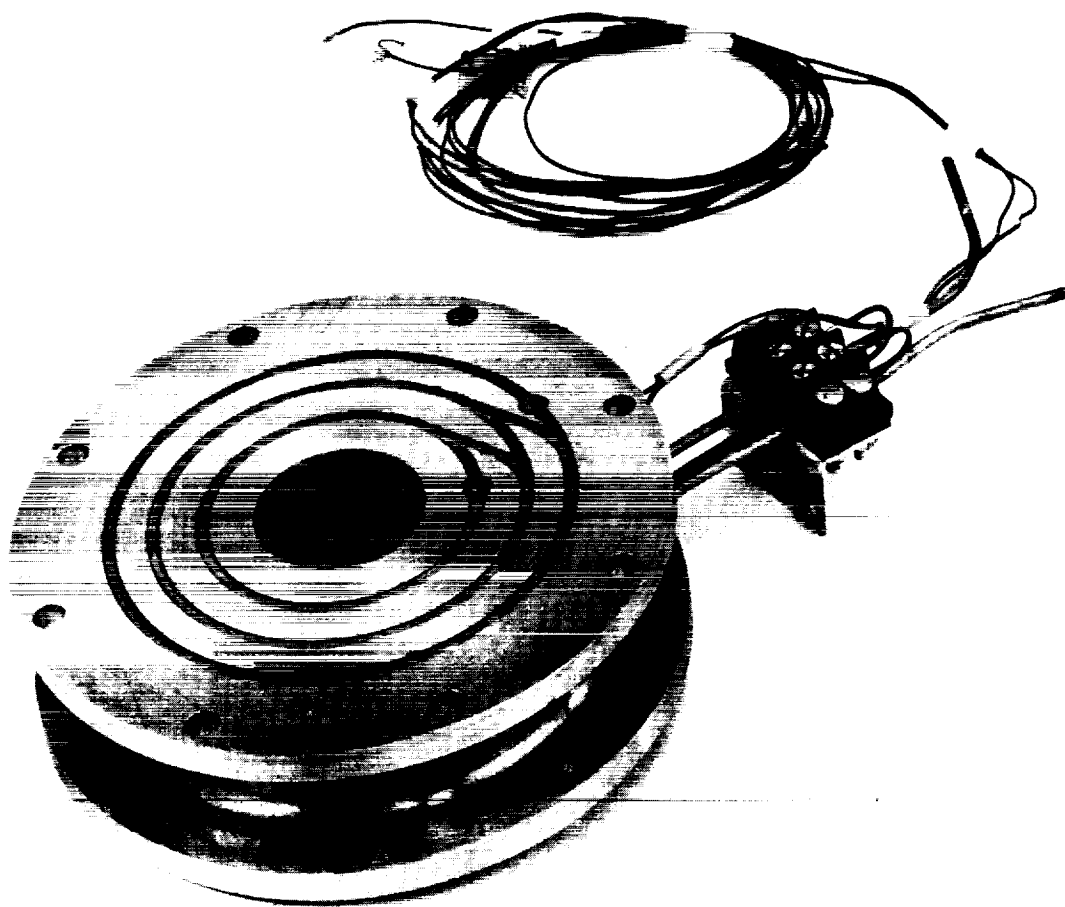
Fig. 53   Radial Guide Bearing

Fig. 54   Elastomer Test Sample Base with Installed Cooling Coils
and Heating Cables

120

reverse taper to insure secure and rattle-free operation in a vibration environment. The electric heater is automatically controlled by a temperature controller which obtains the necessary feedback from a thermocouple embedded in the metal of the base plate. Additional temperature control is obtained through the use of hot and cold air injected into the test rig cavity.

For certain test conditions, not all available features of the test rig are needed. In particular, for test frequencies above 100 Hz, neither the mass support air spring nor the guide spokes (guide bearings) are required. The simplified configuration consists of a shake-table-mounted base plate to which the elastomer samples are bonded and a second plate bonded to the free side of the elastomer samples. A piston with Bellofram seals and various amounts of deadweight attached to the second plate vibrate freely on the elastomer spring when the base plate is subjected to sinusoidal vibrations from the shake table.

The piston cavity is externally pressurized with air and serves to preload the elastomer sample in a static mode. An overall view of the simplified test rig preload cylinder is given in Figure 55, where a small mass is attached to the free end of the preload piston seen protruding from the cylinder. A certain amount of preload is needed to insure that the compression specimen is always in contact with the excited mass. Preload adjustment also permits the effect of preload on the dynamic characteristics of elastomer to be assessed. Preload is optional for shear, cartridge or O-ring configurations. For tests made without static preload required, removal of the seals and piston further simplifies the rig.

Four test configurations have been tested at MTI using the BERM setup:

- Shear-Type Samples

- Compression-Type Samples

- Cartridge-Type Samples

- O-rings.

The shear test sample was made from four individual elastomer strips, each measuring 25.4 mm high, 48.8 mm long and 3.2 mm thick (1.0 x 1.92 x 0.125 inch). Each individual strip was glued with its large face to the side of a square aluminum block and with the opposite face glued to one additional aluminum holding block; Ren* plastic TWA-1077 adhesive has been used with excellent success. An assembled test element is shown in Figure 56. In the assembly of the test fixture, the four holding blocks were bolted to the shake table while the elastomer-supported center block was attached to, and therefore became part of, the resonant mass.

The compression test sample consisted of 10 individual elastomer cylinders, each measuring 12.7 mm in diameter and 6.5 mm high (0.5 by 0.25 inch). These cylinders were arranged in a circular pattern and glued with their faces to

---

* Ren Plastics, Lansing, Michigan
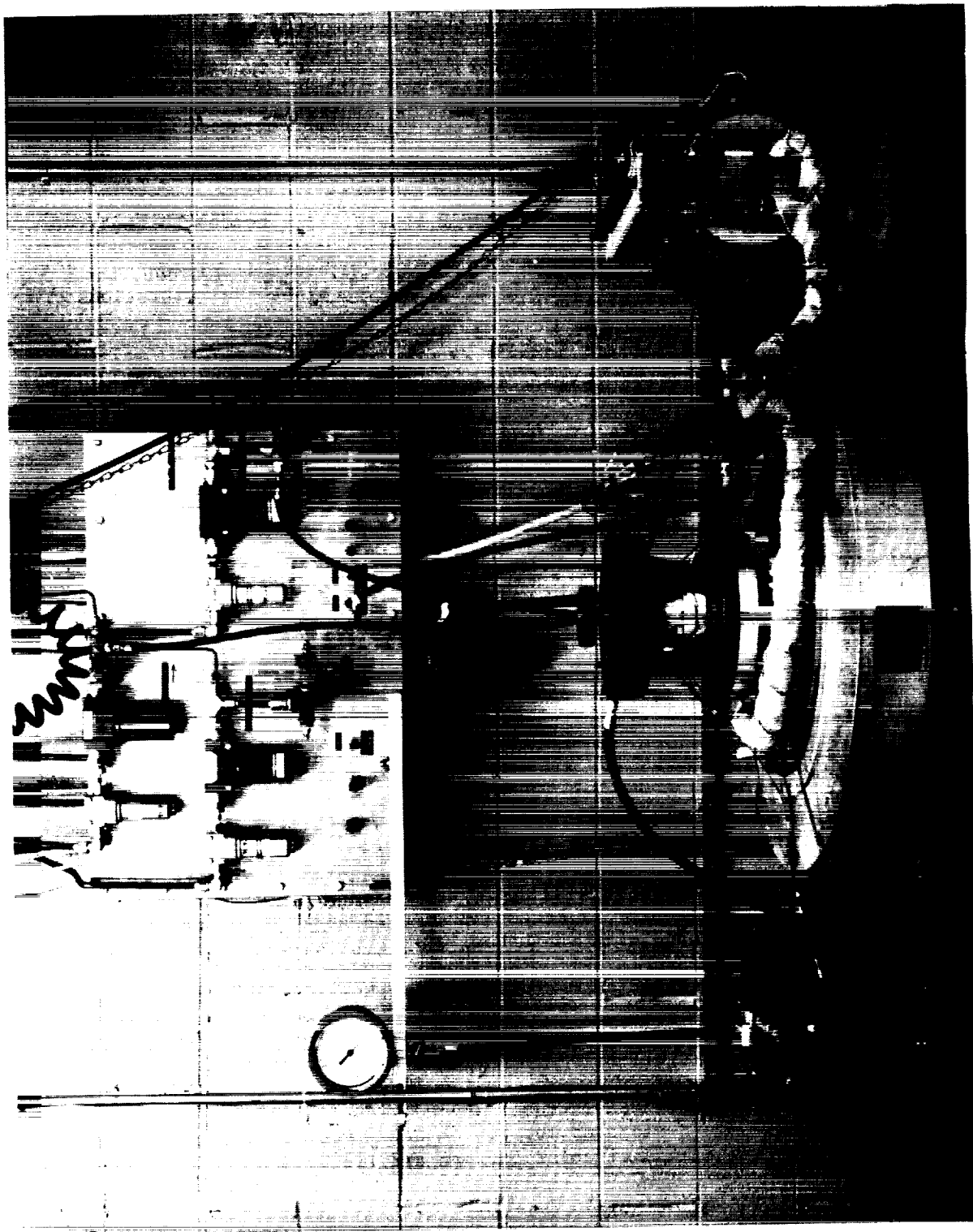
Fig. 55 View of Shake-Table-Mounted BERM Test Rig with Preload Cylinder and Small Mass
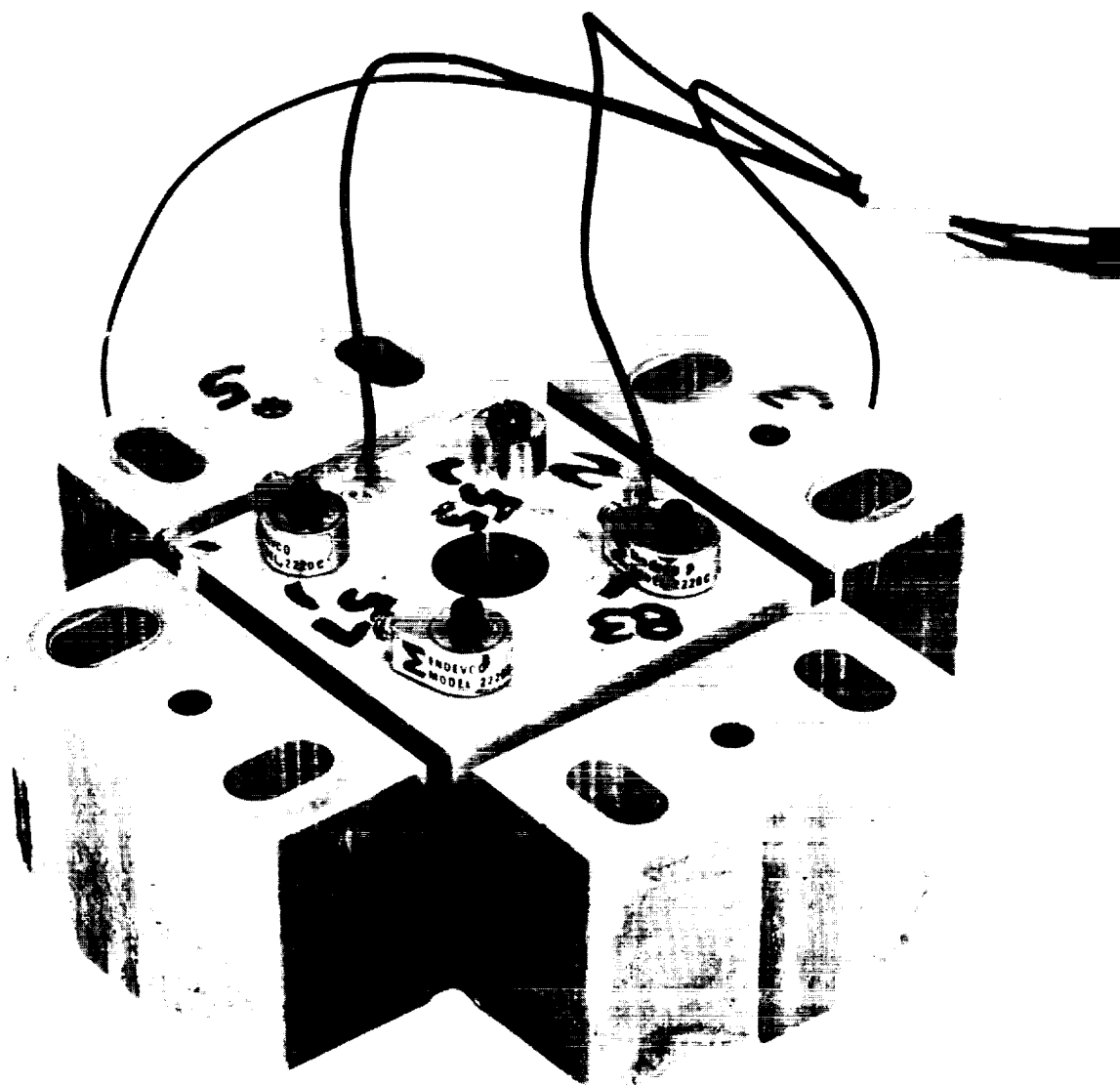
122

Fig. 56 Test Assembly of Four Elastomer Shear Specimens,
Each 2.54 cm (1.0 in.) High

123

two aluminum plates; see Figure 57. The bottom plate was anchored to the shake table, and the top plate was connected to the resonant mass.

Individual cartridge test specimens were made up of an annular elastomer body with rectangular cross section held between the cylindrical bore of a rectangular shell structure and a round shaft of smaller diameter. The elastomer ring was molded to the shaft and bonded to the surrounding shell, which was of split design to facilitate initial assembly and, later, to facilitate static preloading prior to testing. Figure 58 shows one cartridge specimen before and after assembly of the outer shell around the bonded elastomer ring on the shaft.

A manufacturing drawing of the cartridge elastomer specimens is shown in Figure 59. The manufacturing process of the cartridge elements evolved from discussions with the manufacturer. Since a split shell was desirable so that positive radial preload could be applied for testing, molding of the elastomer to both shaft and outer shell was not considered feasible because tensile stresses, set up in the elastomer due to material shrinkage, would not be circumferentially symmetrical. In the selected manufacturing process, the elastomer was first molded on the shaft and then ground on the outer diameter to the dimension of the circular hole in the assembled shell with a small interference tolerance. The outer shell was then clamped around the elastomer and the assembly heat cured. Bonding of the elastomer to the shell was facilitated by a special coating applied to the bore of the shell prior to assembly; this coating is clearly visible in Figure 58.

Prior to assembly into a complete test sample, all cartridge elements received a uniform preload of 5.3% of their uncompressed radial heights. Preloading was accomplished by replacing the shims, measuring 1.625 mm between the halves of the outer shell, with reduced-thickness shims, only 1.120 mm thick. The assembly of the individual elastomer cartridges into the complete test sample is depicted in Figure 60. A 4-cartridge assembly was the largest that could effectively be packaged within the existing size constraints of the test rig.

A similar test fixture was used for determining the dynamic properties of elastomer O-rings. This test fixture is shown in Figure 61. The ambient temperature was maintained by means of an insulated thermal cover and an insulated base to enclose the test specimen. Both high-temperature heating air and controllable cooling air were provided to accurately control the temperature.

The uncomplicated measurement requirements of the base excitation resonant mass testing method are one of its primary attributes. These measurement requirements are:

1. Displacement measurement of elastomer support plate attached to the vibration table, relative to ground

2. Displacement measurement of elastomer support plate attached to the resonant mass, relative to ground
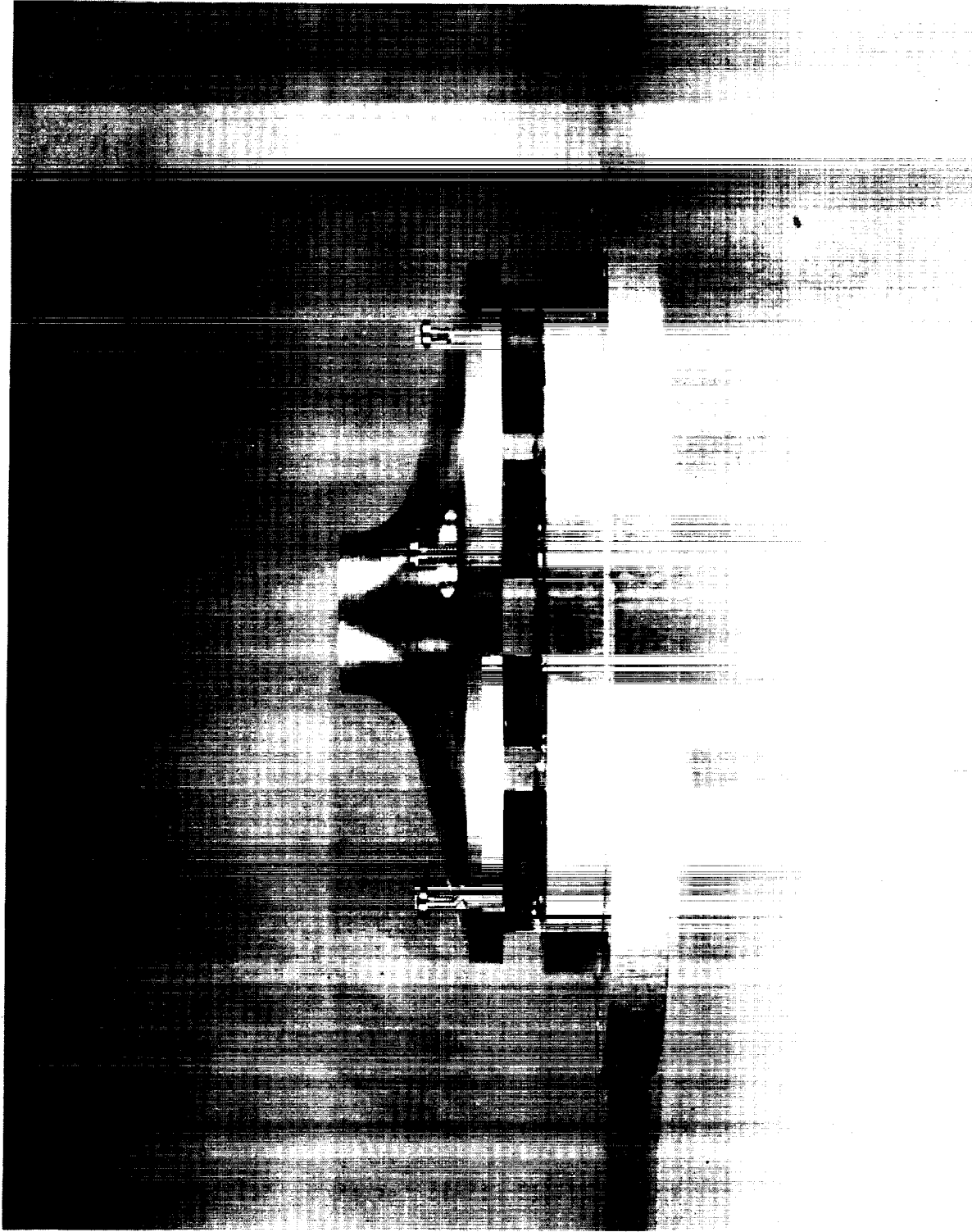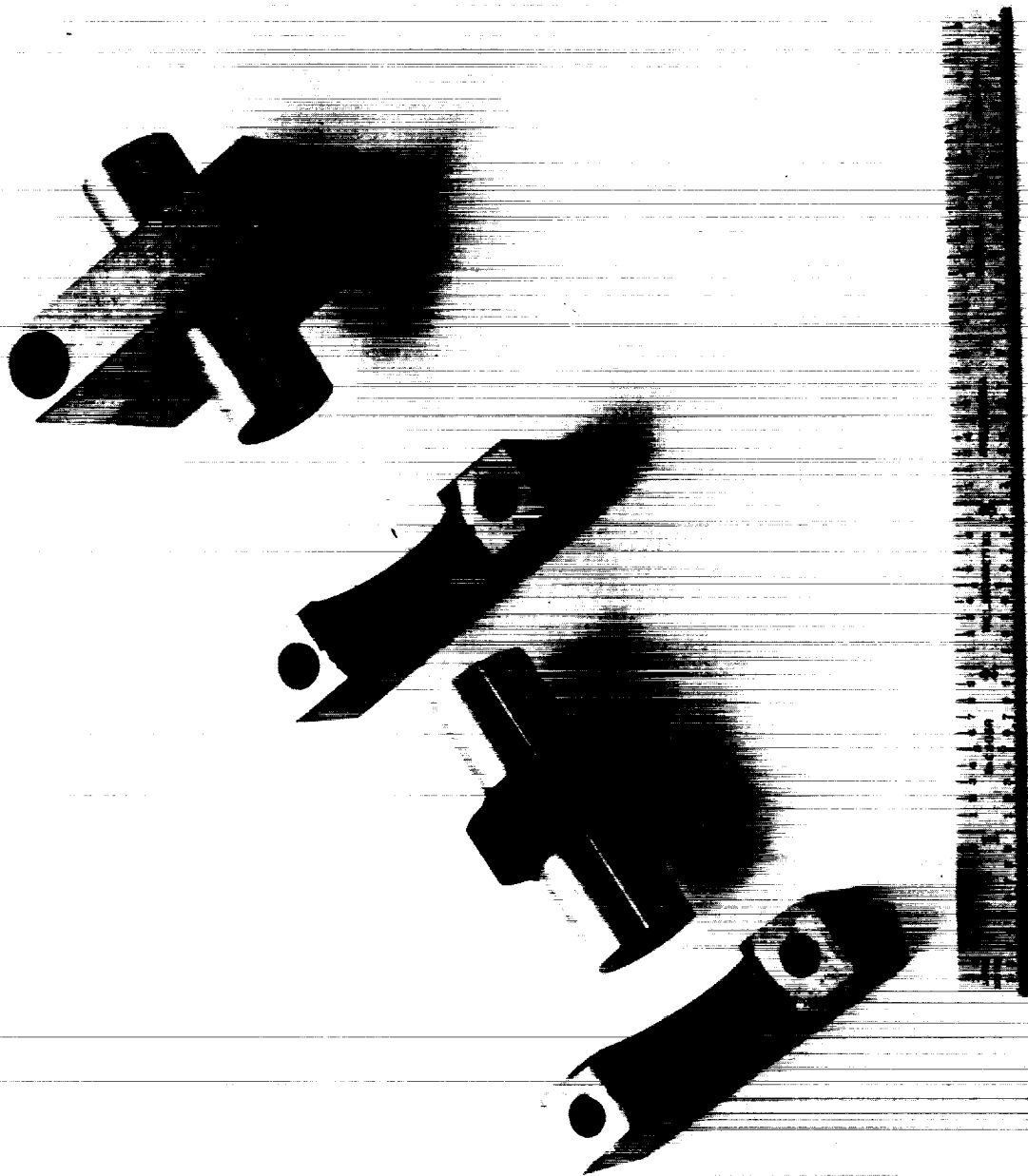
124

Fig. 57 Compression Test Sample

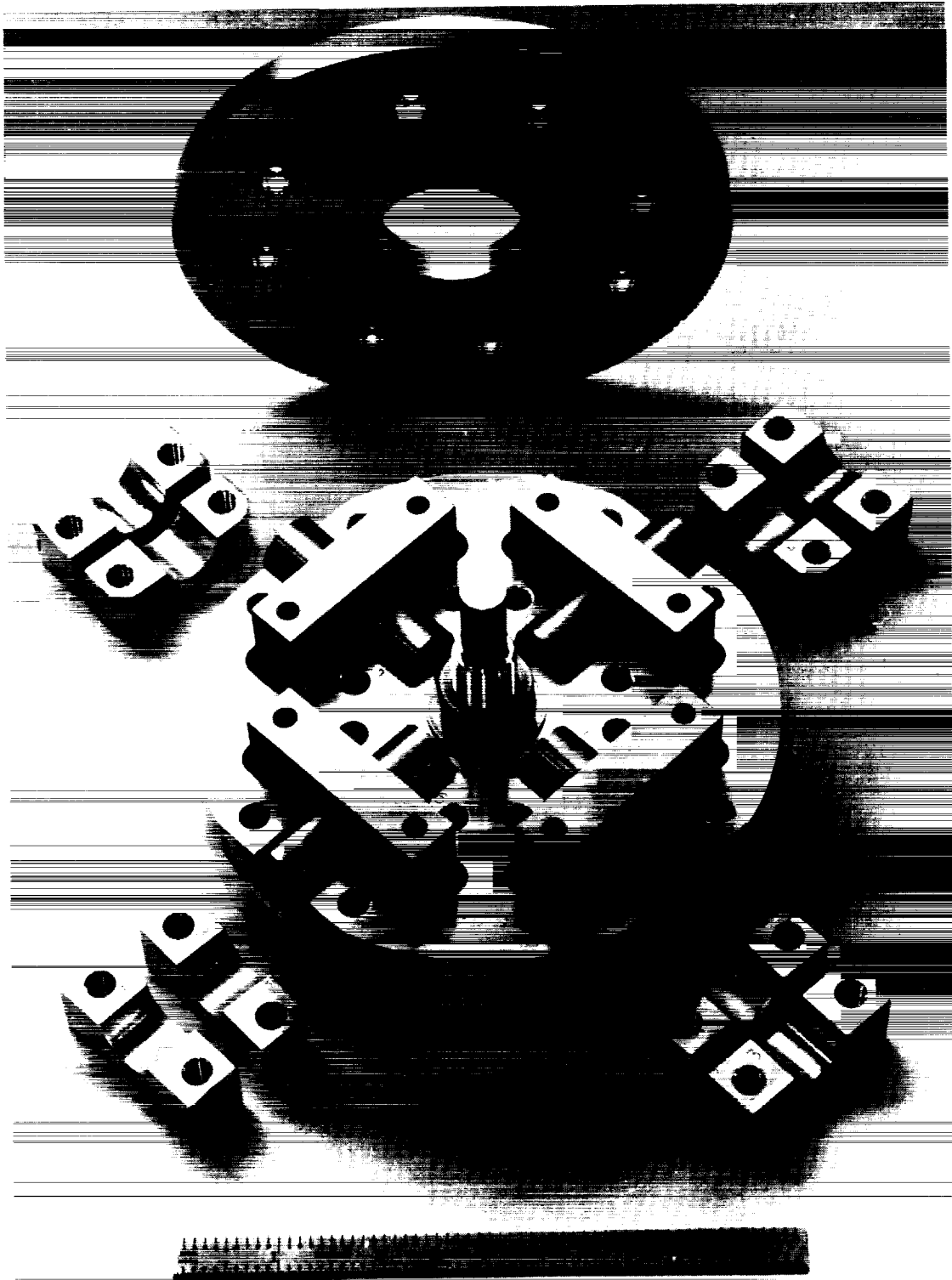Fig. 58 Elastomer Cartridge Specimen Before Bonding of Outer Shell (left) and with Outer Shell in Place (right)

Fig. 59   Elastomer Test Sample

NOTES:

1. MATERIAL: CARBON STEEL (EXCEPT ELASTOMER)

2. UNLESS OTHERWISE SPECIFIED CONCENTRICITY TO BE HELD WITHIN .010 TO -A-

3. ESTABLISHED DIMENSION MAY NOT VARY MORE THAN ±.001 FROM PART TO PART

P/N	"X"	"Y"
P1	.375	.09
P2	.187	.19

SECTION "A-A"

127

Fig. 60   Elastomer Cartridge Place in Top Plate (Inverted Position)

TEST SPECIMEN

HOT AIR

COLD AIR

SHAKER TABLE PLATEN
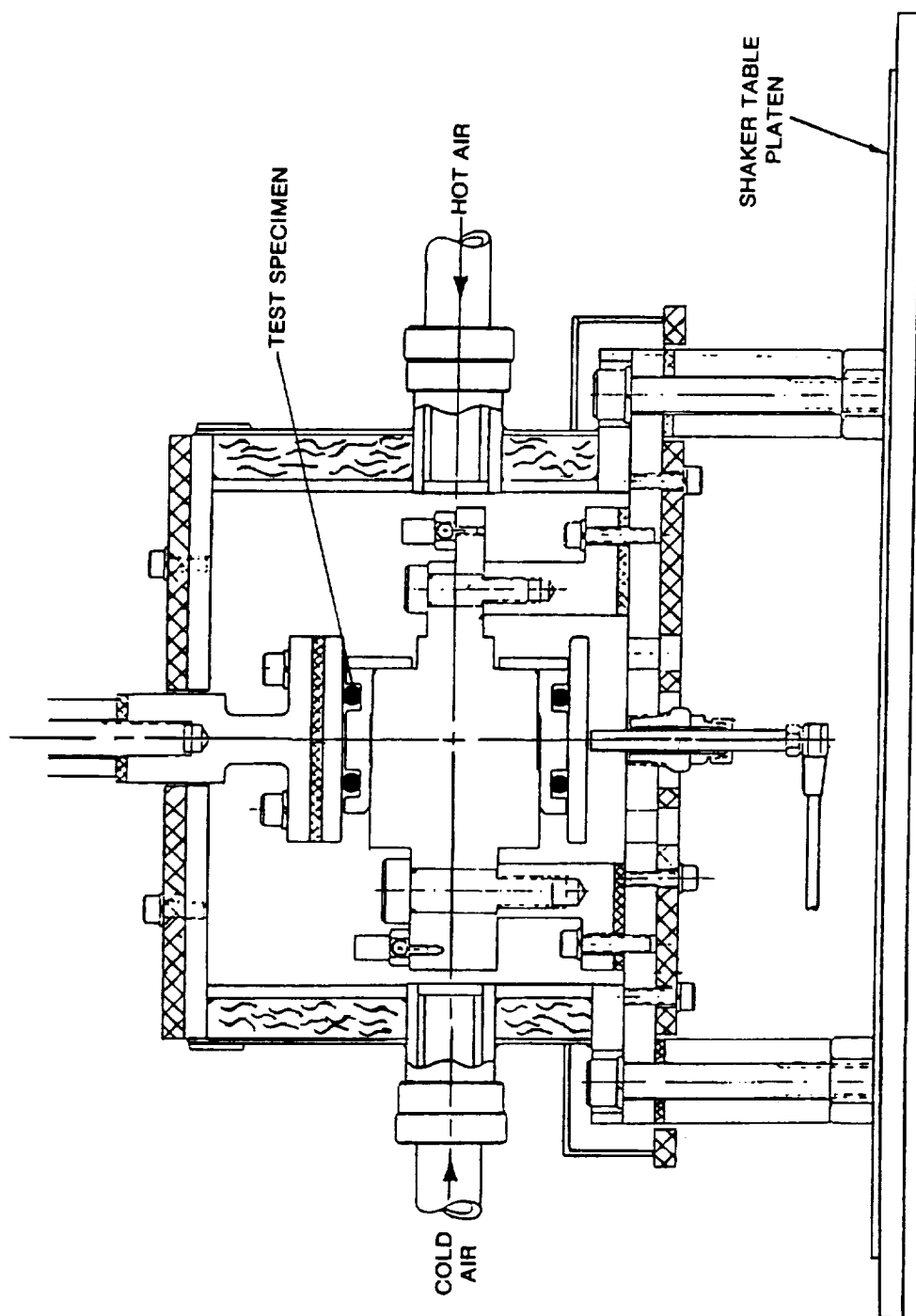
Fig. 61 Assembly Drawing: O-Ring Test Fixture

129

3. Phase angle measurement between displacement measurements (1) and (2) above

4. Displacement measurements between two elastomer support plates to insure the presence of required amplitude of elastomer motion

5. Vibration frequency

6. Temperature of elastomer support plates and ambient air temperature in test specimen cavity.

For convenience, acceleration was measured at points (1) and (2) above instead of displacement, but, since the motions were sinusoidal, the displacements are directly obtained from the accelerations. The very low level of motion of the shaker body (from which the shaker table is isolated by air springs) was also measured by accelerometers.

The input acceleration, point (1), was measured by an accelerometer located on the support base for the elastomer test samples. Output acceleration on the resonant mass, point (2), was determined from three accelerometers, mounted directly to the top plate attached to the elastomer specimens. The use of three accelerometers, spaced 90° apart with their output signals displayed on one oscilloscope screen, permitted immediate detection of nonaxial motions of the resonant mass. When nonaxial motions of the resonant mass occur, they manifest themselves either as amplitude or phase angle variations among the three signals or as a combination of both. (Testing experience revealed that noticeable nonaxial motions occurred only in a few instances at certain test frequencies. Test data was generally discarded when nonaxial motions were observed.) For the O-ring tests, two input and two output accelerometers were used. The displacement measurement, point (4), between the two elastomer support plates (relative amplitude across the elastomer) was accomplished with a noncontacting capacitance-type sensor.

Chromel-alumel-type thermocouples were used to measure the temperature in the metal directly adjacent to one or two elastomer specimens in each assembly at a distance of approximately 1.6 mm from the elastomer surfaces. In the shear sample, the thermocouples were embedded at the midface location. In the compression test samples, the thermocouples were directly above and below the center point of the flat surfaces of the cylindrical specimens. In the cartridge specimens, one thermocouple was located in the axis of the shaft at the midpoint of the elastomer, and two additional thermocouples were placed diametrically opposite in the metal of the outer shell, approximately 1.6 mm from the outer diameter of the elastomer ring and also at the axial midpoint location of the elastomer ring. In the O-ring fixture, the thermocouples were mounted in the inner and outer housings, immediately adjacent to each of the O-rings.

Displacement and acceleration data were displayed on oscilloscopes in real-time form and were, together with temperatures from individual thermocouples, displayed in digital form for monitoring purposes. Amplitude signals from the four accelerometers and the one displacement sensor were sequentially switched by a minicomputer-controlled analog scanner into a two-channel

130

tracking filter, which provided visual readout of vibration frequency and two filtered amplitude signals. One input accelerometer signal was fed at all times into one of the two tracking filter channels and from there into a phase meter, where it served as a reference signal for the measurement of the phase angle of the output acceleration signals and the displacement signal. The dc values proportional to phase angle and amplitude from the phase meter and tracking filter were then covered into digital form in digital voltmeters and read automatically by a PDP 11/34 minicomputer. The minicomputer acquired the data, performed some specified calculations, and printed the data and results of the calculations (including values for stiffness and damping) on a computer terminal used by the test rig operator. A schematic of the data acquisition system used at MTI* is presented in Figure 62.

One significant feature of the BERM method is the performance of the scheduled tests at near-resonance conditions. Since phase angle between base excitation and resonant mass response is an accurate indicator of the amount of damping in the region of resonance, measurements should preferably be made in the phase angle range of 15-165° [5.28]. This generally requires that the test frequency be approximately 0.9 to 1.5 times the critical frequency range of 100-1000 Hz with sufficient test points, therefore, necessitates changes in the size of the resonant mass. Typically, between five and seven different mass arrangements ranging from 0.5 to 15 kg were found sufficient to cover the desired test range. The smallest mass consisted of the elastomer test sample top plate only (with no additional weight attached). Increasingly larger mass combinations were obtained by attaching weights of up to 15 kg directly to the top plate. In the case of the compression sample which was tested with preload applied through the air piston cylinder arrangement, weights up to 10 kg were directly attached to the preload piston. For test frequencies in the range of 20 to 100 Hz, larger resonant masses were used with the support tripod (two to three different masses to cover the frequency range).

The following step-by-step process defines the procedure followed by the operator in executing the BERM tests for elastomer dynamic properties:

1. Select and install a resonant mass.

2. Statically preload the elastomer sample (for compression tests).

3. Enter information describing test conditions and resonant mass.

4. Enclose the elastomer test sample and allow the temperature control system time to adjust ambient temperature to the desired value.

---

* Mechanical Technology Incorporated, Latham, N.Y.
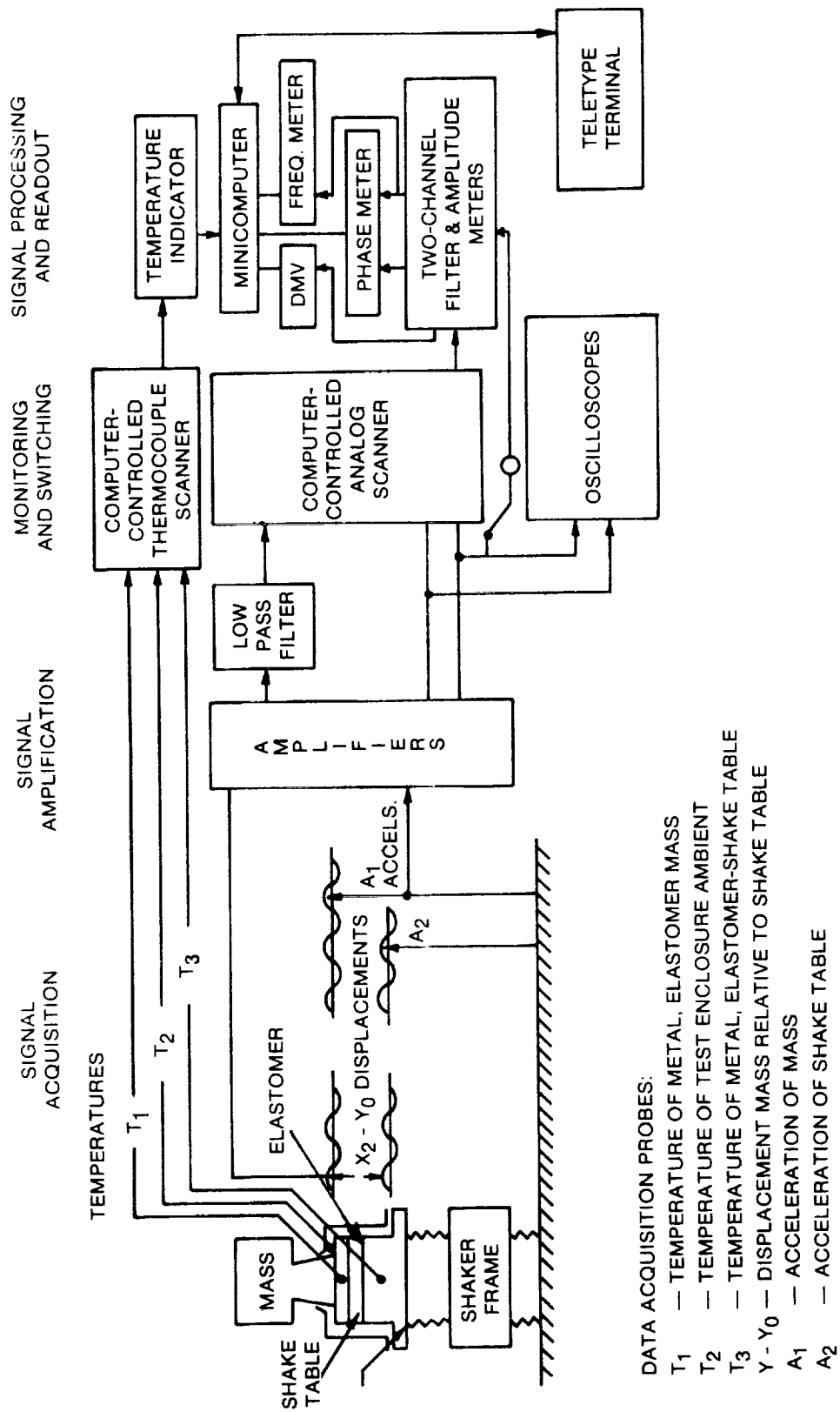
Fig. 62 Schematic of Data Acquisition for Measurement of Elastomer Dynamic Properties

DATA ACQUISITION PROBES:

T_1 — TEMPERATURE OF METAL, ELASTOMER MASS
T_2 — TEMPERATURE OF TEST ENCLOSURE AMBIENT
T_3 — TEMPERATURE OF METAL, ELASTOMER-SHAKE TABLE
$Y - Y_0$ — DISPLACEMENT MASS RELATIVE TO SHAKE TABLE
A_1 — ACCELERATION OF MASS
A_2 — ACCELERATION OF SHAKE TABLE

132

5. Conduct frequency scans with low vibration levels applied to the base of the elastomer holding fixture until the approximate resonant frequency of the system is found. It may be noted here that for a base-excited, single-degree of freedom spring-damper-mass system, resonance occurs at an angle smaller than 90°. The deviation from 90° is essentially determined by the amount of damping in the system.

6. Scrag the test specimen (run briefly at high amplitude) to eliminate the effect of structure (Section 4) and allow the specimen to reset for a few minutes before continuing.

7. Maintain predetermined strain in the elastomer test sample by adjustment of the shaker power input level, and adjust the vibration frequency to obtain the nearest specified test frequency. Provided none of the acceleration and displacement signals show signs of abnormalities (distortions, or indications of nonaxial motion of the resonant mass), instruct the computer to acquire data.

8. Instruct the computer to acquire data in the form of amplitude and phase for each sensor and temperature for each thermocouple. (The computer provides to the operator an immediate calculation of stiffness, damping and power dissipation per unit volume of elastomer along with the raw data from the sensors and thermocouples.)

9. Review these data and calculated results and indicate to the computer either that the data point is acceptable or not acceptable (normally it is acceptable).

10. If acceptable, store the data on a disk file; if not acceptable, discard the data point.

11. Change the vibration frequency to the next nearest test frequency (with the phase angle between 15 and 165°).

12. Repeat steps (5) through (10) for each specified value of strain.

13. Repeat tests, comprising steps (1) through (11), with each of the remaining masses in turn, each mass given a dynamic system with a different resonant frequency, permitting data to be taken at other test frequencies.

14. Adjust the ambient temperature in the test sample cavity to the next specified value.

15. Repeat steps (1) through (13) until data at all desired temperatures are obtained.

As mentioned, the test data is reduced by an on-line minicomputer. The primary objective of data reduction is to interpret these signals in terms of stiffness and damping. The structure of this data and the method of reduction can best be defined in relation to an analysis of a simple spring-mass-damper system subjected to base excitation, as shown in Figure 63.

The equation of motion for the mass is

$$m\ddot{x} + k_1(x_m - x_o) + b(\dot{x}_m - \dot{x}_o) = 0 \tag{5-1}$$

where x_m is displacement of mass

x_o is displacement of base.

It is reasonable to assume that the motions of the base and mass are harmonic so that

$$x_m = \text{Real} \left\{ x_m^* e^{i\omega t} \right\} \tag{5-2}$$

$$x_o = \text{Real} \left\{ x_o^* e^{i\omega t} \right\} \tag{5-3}$$

and the equation of motion may be rewritten

$$-\omega^2 m\, x_m^* e^{i\omega t} + k_1 (x_m^* - x_o^*)e^{i\omega t} + i\omega\, b(x_m^* - x_o^*)e^{i\omega t} = 0 \tag{5-4}$$

Dividing through by $e^{i\omega t}$, gives

$$(k_1 + ik_2) = \frac{\omega^2 m\, x_m^*}{x_m^* - x_o^*} \tag{5-5}$$

where $k_2 = \omega b$

Now, if ϕ is the phase angle between x_o and x_m, then

$$x_m^* = \left| x_m^* \right| \cos \phi - i \left| x_m^* \right| \sin \phi \tag{5-6}$$

$$x_o^* = \left| x_o^* \right| \tag{5-7}$$

and

$$(k_1 + ik_2) = \frac{\omega^2 m(\alpha \cos \phi - i\,\alpha \sin \phi)}{\alpha \cos \phi - i\,\alpha \sin \phi - 1} \tag{5-8}$$

where α is the transmissibility $\left| \dfrac{x_m^*}{x_o^*} \right|$. Thus,

134
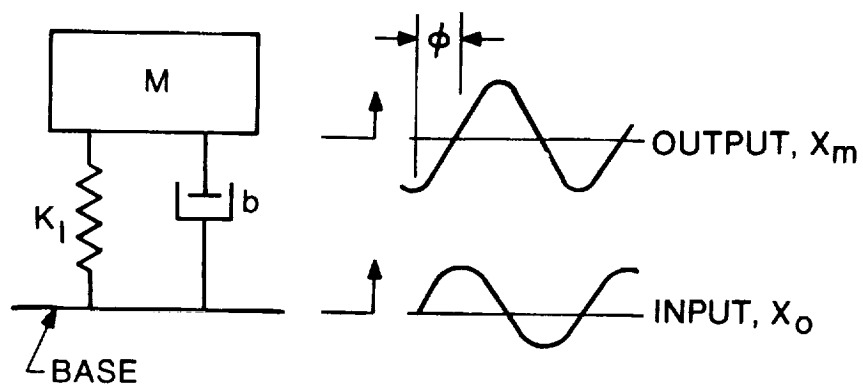
Fig. 63   Model of Base Excitation Resonant Mass System
for Data Reduction Analysis

$$k_1 + ik_2 = \frac{\omega^2 m (\alpha \cos \phi - i \alpha \sin \phi)(\alpha \cos \phi - 1 + i \alpha \sin \phi)}{(\alpha \cos \phi - 1)^2 + \alpha^2 \sin^2 \phi} \quad (5\text{-}9)$$

or

$$k_1 = \frac{\omega^2 m \alpha^2 - \alpha \cos \phi}{\alpha^2 - 2\alpha \cos \phi + 1} \quad (5\text{-}10)$$

and

$$k_2 = \frac{\omega^2 m \alpha \sin \phi}{\alpha^2 - 2\alpha \cos \phi + 1} \quad (5\text{-}11)$$

Thus, for known α, the transmissibility, or ratio of output amplitude $\left| x_m^* \right|$ to input amplitude x_o^*, and ϕ, the phase angle between input and output amplitudes, stiffness and damping (k_1 and k_2) can be evaluated directly; see equations 5-10 and 5-11.

These expressions based on the simplest one-degree-of-freedom model with no correction for tare damping or stiffness. This is in contrast to the expressions used in Reference 5.28 which make corrections for effects of damping in preload and load support pistons. The simplicity of the present treatment results from the simplicity and accuracy of the test procedure performed for the majority of the BERM tests, in which no external restraint of any kind was applied to the supporting mass. Only for the compression specimens is the preload piston employed. These expressions are, therefore, fully accurate for shear, cartridge, and O-ring specimens and are subject to some uncertainty only in the case of the compression specimens.

Statistical methods can be employed to develop empirical relations for test specimen or material dynamic properties as functions of the test parameters. Such empirical relations for several elastomer materials have been generated from BERM test results and are presented in Section 6.0.

5.6 Summary

Many test methods have been used for determining the dynamic properties of elastomers. These methods generally belong to one of three classifications: (1) forced vibration resonant test method, (2) free vibration resonant test method, and (3) forced vibration nonresonant test method. In general, the earliest methods which fall into the first classification were easy to use but suffered from the problem of severely limited test parameters. This limitation also applies to the methods which fall into the second classification.

The more recent forced resonant methods, particularly the Base Excitation Resonant Mass (BERM) method, have used advanced instrumentation, including on-line computers, to eliminate these disadvantages. The result is a test method which provides significant flexibility in the choice of test parameters, while requiring very straightforward operation and data reduction. The only major limitation of the BERM method is that it is not suitable for testing at very low frequencies (less than 20 Hz) due to the large resonant

136

masses required. However, for most rotordynamic applications, these frequencies are of minimal interest. (Fifty to 1000 Hz is generally of most interest and covers the operational characteristics of most high speed rotating equipment.)

Forced nonresonant methods have also matured with the advent of advanced instrumentation. These methods, however, are more sensitive to measurement error (particularly phase measurement error) than the BERM method and are restricted to low frequencies (less than 100 Hz) and low dynamic strain which makes them generally limited for rotordynamics applications.

Several other test methods have been used which do not fit into any of the three classifications. These include wave propagation methods and noncyclic displacement methods. Other classes of tests which are not strictly dynamic property tests, but relate, directly or indirectly, to dynamic properties include creep and stress relaxation tests, fatigue tests, vibration transmissibility tests, and shock tests.

5.7 References

5.1 Sommer, J.G. and Meyer, D.A., "Factors Controlling the Dynamic Properties of Elastomeric Products", SAE Paper No. 720267, SAE/ASTM Sym, Detroit, Michigan, January 1973.

5.2 Darlow, M.S., and Smalley, A.J., "Dynamic Properties of Elastomer Cartridge Specimens Under a Rotating Load", presented at the Fifth World Congress of the Theory of Machines and Mechanisms, Montreal, Canada, July 1979.

5.3 Nachtigal, C.L., "Fundamentals of Dynamic Properties Measurement of Elastomers: Part II - Instrumentation, Computation, and Compensation", SAE Paper No. 730258, SAE/ASTM Symposium, Detroit, Michigan, Jan 1973.

5.4 Hillberry, B.M., Goodson, R.E., and Nachtigal, C.L., "Computation and Direct Readout of Dynamic Properties: The Identifier", SAE Paper No. 73062, SAE/ASTM Symposium, Detroit, Michigan, Jan 1973.

5.5 Danko, D.M. and Svarovsky, J.E., "An Application of Minicomputers for the Determination of Elastomeric Damping Coefficients and Other Properties", SAE Paper No. 730263, SAE/ASTM Symposium, Detroit, Michigan, Jan 1973.

5.6 Smalley, A.J., and Tessarzik, J.M., "Development of Procedures for Calculating Stiffness and Damping Properties of Elastomers in Engineering Applications, Part III: The Effects of Temperature, Dissipation Level and Geometry", NASA Report CR-134939, Nov. 1975.

5.7 Tecza, J.A., Darlow, M.S., and Smalley, A.J., "Development of Procedures for Calculating Stiffness and Damping Properties of Elastomers in Engineering Applications, Part V: Elastomer Performance Limits and the Design and Test of an Elastomer", NASA Report CR-159552, February 1979.

5.8   Wasner, W.C., "Measuring Dynamic Properties of Vulcanizates", ASTM ETP 553, American Society for Testing and Materials, 1974, pp. 31-35.

5.9   Smalley, A.J., Tessarzik, J.M., and Badgley, R.H., "Testing for Material Dynamic Properties", Vibration Testing Instrumentation and Data Analysis, AMD Vol. 12, 1975, pp. 117-141.

5.10 Hillberry, B.M., "A Review of Recent Developments in Forced Vibration Dynamic Testing of Elastomers", ASTM STP 553, American Society for Testing and Materials, 1974, pp. 142-161.

5.11 Brouwer, F., "Resonant Beam System Development-Past to Present", SAE Paper No. 730259, SAE/ASTM Symposium, Detroit, Michigan, Jan. 1973.

5.12 Owens, J.H., "Application of Electrohydraulic Test Machines to Dynamic Testing of Elastomers", SAE Paper No. 730260, SAE/ASTM Symposium, Detroit, Michigan, Jan. 1973.

5.13 Wilson, W.J., "Evolution and Uses of Transmitted Force Measurement", SAE Paper No. 730261, SAE/ASTM Symposium, Detroit, Michigan, Jan. 1973.

5.14 Paul, A.S., Hillberry, B.M., "Error Analysis of the Resonant Beam Rubber Testing Machine", SAE Paper No. 730256, SAE/ASTM Symposium, Detroit, Michigan, Jan. 1973.

5.15 Payne, A.R. and Scott, J.R., Engineering Design with Rubber, Interscience Publications, New York 1960.

5.16 Gobel, E.F., Rubber Springs Design, John Wiley & Sons, New York, 1974.

5.17 Tangorra, G., Rubber Chemistry and Technology, Vol. 36, No. 4, 1963, pp. 1107-1118; Vol. 34, No. 1, 1961, pp. 347-356.

5.18 Nielson, L.E., Mechanical Properties of Polymers, Reinhold, 1962.

5.19 Ward, I.M., Mechanical Properties of Solid Polymers, Wiley-Interscience, 1971.

5.20 Moyal, J.E. and Fletcher, W.P. (1945), F. Sci. Instrum., 22, 167.

5.21 Nolle, A.W. (1948), F. Appl. Phys., 19, 753.

5.22 Dietz, A.G.H., Bockstruck, H.N. and Epstein, G. (1952). ASTM Preprint no. 134.

5.23 Rhinehart, J.S. (1941), F. Appl. Phys., 12, 811.

5.24 Miller, H.E., "Dynamic Property Measurement of Elastomers and Elastomeric Mounts - Past, Present, and Future", SAE Paper No. 730256, SAE/ASTM Symposium, Detroit, Michigan, Jan. 1973.

5.25 Painter, G.W., "Dynamic Properties of BTR Elastomers", SAE National Aeronautic Meeting, Los Angeles, California, 1958.

5.26 Cannon, C.M., Nashif, A.D. and Jones, D.I.G., "Damping Measurements on Soft Viscoelastic Materials Using a Tuned Damper Technique", Shock and Vibration Bulletin No. 38, Naval Research Laboratory, Washington, D.C., Part 3, November 1968, pp. 151-163.

5.27 Balktrukonis, J.H., Blomquist, D.S., and Magrab, E.B., "Measurement of the Complex Shear Modulus of a Linear Viscoelastic Material", Technical Report No. 5 to NASA, under Research Grant No. NaG-125-61 (Suppl. 3), Catholic University of America, May 1964.

5.28 Gupta, P.K., Tessarzik, J.M., and Cziglenyi, L., "Development of Procedures for Calculating Stiffness and Damping Properties of Elastomers in Engineering Applications. Part II: Elastomer Characteristics of Constant Temperature", NASA Contractor Report No. CR-134704, April 1974.

5.29 American Society for Testing and Materials, 1978 Annual Book of ASTM Standards, Part 37, ASTM, 1978.

5.30 Painter, G.W. (1954), Rubber Age, N.Y., 74, 701.

5.31 Roelig, H. (1938), Proc. Rubber Tech. Conf. Cambridge: Heffer. p. 821.

5.32 Lazan, B.J., (1950), Trans Amer. Soc. Metals, 4, 499.

5.33 Fletcher, W.P. and Gent, A.N. (1952), F. Sci. Instrum., 29, 186.

5.34 Davey, A.B. and Payne, A.R., Rubber in Engineering Practice, Maclaren and Sons, Ltd., London, 1964.

5.35 Takayanagi, M., Memoirs of the Faculty of Engineering, Kyushu University, Vol. 23, 1963, p. 41; Proceedings, Fourth International Congress on Rheology, Part 1, pp. 161-187.

5.36 Leonard, R.G., "Fundamentals of Dynamic Properties Measurement of Elastomers: Part I - Measurement and Identification Principles", SAE Paper No. 730257, SAE/ASTM Symposium, Detroit, Michigan, Jan. 1973.

5.37 Ford, B.W. and Warner, W.C., Rubber Chemistry and Technology, Vol. 44, No. 1, March 1971, pp. 249-257; Ford, B.W., Meyer, D.A., and Warner, W.C., U.S. Patent 3,699,808.

5.38 Witte, R.S., Mrowca, B.A. and Guth, E. (1949), F. Appl. Phys., 20, 481.

5.39 Morris, R.E., James, R.R. and Guyton, C.W. (1956), Rubber Age, N.Y., 78, 725.

5.40 Ballou, J.W. and Silverman, S.J. (1944), F. Acoust. Soc. Amer., 16, 113.

5.41 Bulgin, D. and Hubbard, G.D. (1958), Trans. Inst. Rubber Ind., 34, 201.

5.42 Smalley, A.J., "Property Measurement and Application of Elastomer Dampers", Presented at the Conference on Aerospace Polymeric Viscoelastic Damping, Dayton, Ohio, February 1978.

139

5.43 Smalley, A.J., Darlow, M.S., and Mehta, R.K., "The Dynamics Characteristics of O-Rings", ASME Trans., Journal of Mechanical Design, Vol. 100, No. 1, January 1978, pp. 132-138.

5.44 Chiang, T., Tessarzik, J.M., and Badgley, R.H., "Development of Procedures for Calculating Stiffness and Damping Properties of Elastomers in Engineering Applications, Part I: Verification of Basic Methods", NASA Report CR120905, March 1972.

6.0 ELASTOMER MATERIAL PROPERTIES

Access to reliable elastomer material properties is essential for the design of elastomer dampers. A collection of such properties for numerous elastomer materials is presented in this chapter. These material properties include both "general physical" properties and "dynamic" properties. The category of general physical properties includes properties such as density, environmentally related properties such as fluid compatibility, typical composition, static mechanical properties such as static shear modulus, and thermal, electrical and magnetic properties. Dynamic properties refer to the dynamic shear storage and loss moduli of the material and their variation with changes in operating conditions (e.g. frequency, strain, temperature, etc.).

The general physical properties data presented in this chapter have been collected from a number of references; the dynamic property data presented have been determined empirically from results of Base Excitation Resonant Mass (BERM) tests with several elastomer materials. (The BERM test method was discussed in Section 5.0.)

6.1 General Physical Properties

Values for many general physical properties are presented for a number of commonly used elastomer materials. This collection of data is intended to be a summary for reader convenience. A more complete collection of data would constitute a handbook in itself, as is illustrated by Reference 6.1, which is the source for much of the data presented in this section. The reader is encouraged to refer to Reference 6.1 for additional information and for materials not included herein. Also, while most of the data presented here is classified by generic elastomer type, Reference 6.1 also cross references many material properties to commercially available types (trade names).

Elastomer materials, including natural rubber, can be grouped into at least 20 general classes. A brief description of each of the generic classification of elastomers, which includes such information as chemical structure and compounding procedure is presented in Reference 6.1. A summary of the general properties for 18 generic classes of elastomers is presented in Table 5 [6.2]*.

Specific properties of several generic elastomer types are presented in Reference 6.3, some of which are reproduced here in Tables 6 through 12. Table 6 [6.2] provides a broad classification of desirable and undesirable characteristics of the seven elastomers listed. Some general properties, including resistance to a number of environmental conditions, is presented in Table 7. The hardness rating in Degrees British Standard (^{o}BS) is identical to the International Rubber Hardness (IRHD) and is essentially equivalent to the commonly used rating of durometer (or Shore Ⓡ A hardness). A direct relationship between elastomer hardness and static shear modulus has

---

* Numbers in brackets indicate references found in Section 6.5.

Ⓡ Registered Trademark, Shore Instruments and Manufacturing Co., Inc., Jamaica, N.Y.

Table 5

THE ELASTOMERS – DESIGNATIONS AND GENERAL PROPERTIES*

ASTM D 1418 Designation	Common Name or Representative Trade Name	Chemical Designation	General Properties
NR	Natural	Natural Polyisoprene	Excellent physical properties; good resistance to cutting, gouging, and abrasion; low heat, ozone, and oil resistance; poor resistance to petroleum-base fluids
IR	Polyisoprene	Synthetic Polyisoprene	Same properties as natural rubber; requires less mastication than natural rubber.
CR	Neoprene	Chloroprene	Excellent ozone, heat, and weathering resistance; good oil resistance; excellent flame resistance.
SBR	SBR	Styrene-Butadiene	Good physical properties; excellent abrasion resistance; not oil, ozone, or weather resistant.
NBR	Buna N	Acrylonitrile-Butadiene	Excellent resistance to vegetable, animal, and petroleum oils; poor low-temperature resistance.
IIR	Butyl	Isobutylene-Isoprene	Excellent weathering resistance; low permeability to gases; good resistance to ozone and aging; low tensile strength and resilience.
IIR	Chloro-Butyl	Chloro-Isobutylene-Isoprene	Same general properties as butyl.
BR	Butadiene	Polybutadiene	Excellent abrasion resistance and high resilience; used principally as a blend in other rubbers.
T	Thiokol	Polysulfide	Outstanding solvent resistance; other properties poor.
EPM	EPR	Ethylene Propylene	Good aging, abrasion, and heat resistance; not oil resistant.
EPDM	EPT	Ethyl Propylene Terpolymer	Good aging, abrasion, and heat resistance; not oil resistant.
CSM	Hypalon	Chlorosulfonated Polyethylene	Excellent ozone, weathering, and acid resistance; fair oil resistance; poor low-temperature resistance.
VMQ PVMQ FMQ	Silicone Silicone Fluorosilicone	Methyl-Vinyl Siloxane Phenyl-Methyl-Vinyl Siloxane Trifluoropropyl Siloxane	Excellent high and low temperature resistance; good mechanical properties at high temperature; low compression set; fair oil resistance. Fluorosilicone rubber has excellent oil resistance.
AU	Urethane	Polyurethane Diisocyanate	Exceptional abrasion, cut and tear resistance; high modulus and hardness; poor moist-heat resistance.
FPM	Viton	Fluorinated Hydrocarbon	Excellent high-temperature resistance, particularly in air and oil.
ACM	Acrylic	Polyacrylate	Excellent heat, oil and ozone resistance; poor water resistance.

* Reference 6.2

142

Table 6

SUMMARY OF ADVANTAGES AND DISADVANTAGES OF VARIOUS RUBBER TYPES*

Type	Useful Properties	Properties that Limit Usefulness
Natural	High resilience, tensile strength and elongation; wide hardness range; long flex life	Moderate to poor heat, oil, weather and ozone resistance
Butadiene-styrene	Better abrasion and general aging resistance than natural rubber	Moderate to poor oil, tear, weather and ozone resistance
Butyl	High weather, ozone, acid and alkali resistance; very low permeability to gases	Low tensile strength and resilience; high inflammability
Neoprene	High heat, aging, weather and flame resistance and flex life; moderate oil and chemical resistance	Only moderate in several important properties
Nitrile	Moderate to good heat and aging resistance; resistance to mineral oils, petroleum solvents, dilute acids and alkalis	Relatively poor cold resistance
Thiokol	Maximum oil and solvent resistance	High compression set; low tensile strength and elongation and heat resistance
Silicone	Maximum heat and cold resistance	Low strength properties; fairly high compression set; high cost

* Reference 6.3

143

Table 7

GENERAL PROPERTIES OF VULCANIZED RUBBERS*

	Natural	Butadiene-styrene (a)	Butyl	Neoprene	Nitrile (b)	Thiokol (c)	Silicone
Hardness range, °BS	30–100	35–100	35–85	40–90	40–100	40–90	40–85
Tensile strength (lb/in²):							
'pure gum'	>3000	VL	2000	3000	VL	VL	VL
technical (d)	800–4500	800–4000	800–2500	800–3000	800–2500	600–1500	400–1000
Elasticity (e)	H	H	FL	M	M	L	FL
tan δ: at 20°C	0·08	0·09–0·14	0·16	0·09	0·10–0·18	—	0·09
(f) at 70°C	0·06	0·08–0·10	0·08	0·08	0·09–0·11	—	0·08
Resistance to compression set	FH	FH	M	FH	M–FH	L	M
Tear strength	FH	M	M	H	M	L	L
Abrasion resistance	H	H	M	H	M	L	L
Resilience (rebound): cold	H	M	L	FH	M	L–M	H
hot	H	M	FH	FH	M	L–M	H
Heat resistance	FL	FL	M	FH	M–FH	L	VH
Cold resistance	H	H	H	FH	L–M	FH	VH
T_{10}, °C (g)	−55	−50	−50	−45	−20 to −30	−30 to −45	−60
Working temperature range, °C	−55 to +70	−45 to +100	−50 to +125	−20 to +120(k)	−20 to +120	−50 to +95	−90 to +250 (h)
Ageing resistance, general	M	M–FH	H	H	H	H	H
Resistance to sunlight	L	L	H	H	M	M	H
Resistance to ozone and corona	M	L–M	M–H	FH–H	L–M	H	H
Resistance to flame	L	L	L	H	L–M	L	H
Resistance to liquids:							
fuels (aliphatic)	L	L	L	M–H	H	H	L
fuels (aromatic)	L	L	L	L	M	H	L
Resistance to liquids:							
mineral lubricating oils	L	L	L	M	M–H	H	L
animal and vegetable oils	L–M	L–M	H	M–H	H	H	L–M
water	H	M–H	FH–H	M (j)	M	M	M
Electrical resistivity	H	H	H	M	M	M	H
Electrical power loss	L	L	L	M	FH	FH	L
Electrical breakdown strength	H	H	H	M	M	M	H
Adhesion to metals	H	H	M	H	H	L	M
Adhesion to fabrics	H	FH	FH	H	FH	L	M

Notes. The level of each property is denoted as follows: VH: very high   FH: fairly high   FL: fairly low
                                                                H: high   M: medium   L: low
                                                                                      VL: very low

(a) Usually known under the generic name GR-S or SBR.
(b) Copolymers of butadiene and acrylonitrile in various proportions; with increasing amount of the latter the resistance to fuels and oils increases but cold resistance deteriorates, i.e. T_{10} becomes higher.
(c) 'Thiokol' is a trade name applied to a variety of synthetic rubbers; most are thioplasts (i.e. polymers of organic sulphides), and the information tabulated refers to these.
(d) 'Pure gum' indicates a vulcanisate without fillers; 'technical' indicates the approximate range among the more usual technical compounds containing fillers.
(e) In the popular sense, i.e. ability to stretch and recover.
(f) For rubbers containing 45 parts (per 100 of polymer) carbon black (CK3), except the silicone rubber which contains a special filler; test frequency 16⅔ cps (Ecker, *Kaut. u. Gummi*, 1956, 9, WT2).
(g) The temperature at which elastic modulus is 10 times its value at 20°C.
(h) No *one* type covers this whole temperature range; individual types vary from −90/+150°C to −45/+250°C.
(j) Must be specially compounded to resist water absorption.
(k) Lower limit depends on type of neoprene, some types being more resistant than others to hardening by 'crystallisation.'

Although the following types of synthetic rubber are not likely to be used for general engineering purposes, high cost being often one adverse factor, it may be worth noting their special advantages:
  Fluorinated rubbers—excellent resistance to heat (operating range 0–250°C), fuels, oils and corrosive chemicals.
  Polyacrylate rubbers—good heat and oil resistance; hence useful where oil-resistance of silicone rubbers is inadequate.
  Polyurethane (or isocyanate) rubbers—very high tensile strength and resistance to abrasion and tearing.

144

* Reference 6.3

Table 8

SPECIFIC HEATS, THERMAL CONDUCTIVITIES, AND SPECIFIC GRAVITIES OF RUBBERS AND COMPOUNDING MATERIALS*

	Specific heat (c) cal/g °C	Conductivity cgs units (b)	Specific gravity
Rubbers, unvulcanised or soft 'pure gum' vulcanisates without filler:		$\times 10^{-5}$	
Natural rubber	0·45–0·50	32	0·92–0·98
Butadiene-styrene (GR-S, SBR) (a) .	0·44–0·48	60	0·94–1·00
Butadiene-acrylonitrile ('nitrile') (a).	0·47	60	0·94–1·10
Neoprene	0·52	45	1·25–1·30
Butyl	0·44–0·46	22	0·92–0·98
Barium sulphate (barytes) . .	0·11	80–250	4·3
China clay	0·21	60–145	2·6
Carbon black	0·20	35–67	1·8
Iron oxide (ferric oxide) . . .	0·16	185	5·0
Lithopone	0·115	90	3·6–4·2
Magnesium carbonate . . .	0·30	105	2·2
Whiting	0·20	70–85	2·7
Zinc oxide	0·12	140–165	5·6
Ebonite	0·33 (d)	38–44	1·2 (d)

Notes. (a) Properties depend on ratio of butadiene to other constituent; values given are therefore approximate.

(b) = cal/cm² sec °C/cm; to convert to BTU/sq ft hr °F/inch multiply by 2900.

(c) Specific heat for most rubbers increases with temperature by about 0·003–0·005 per °C; values quoted are for 20°–25°C.

(d) natural rubber ebonite without fillers.

Table 9

LINEAR COEFFICIENT OF THERMAL EXPANSION*

	Coefficient per °C
Rubbers, unvulcanised or soft 'pure gum' vulcanisates, i.e. without filler:	$\times 10^{-5}$
Natural rubber	22
Butadiene-styrene (GR-S, SBR)	22
Neoprene	20
Butyl	19
Silicone rubber	40
Ebonite	7
Mineral fillers (carbon black, whiting, zinc oxide) . .	c. 0·5 (i.e. negligible compared with rubbers)
Aluminium	2·5
Brass	2·0
Steel	1·2

* Reference 6.3

145

Table 10

VALUES OF THE 'CHARACTERISTIC TEMPERATURE' T_s and
GLASS-TRANSITION TEMPERATURE T_g FOR VARIOUS RUBBERS*

	T_s		T_g
	°K	°C	°C
Natural rubber:			
unvulcanised . . .	248	−25	−71
vulcanised (soft) . .	251 to 260 (a)	−22 to −13	−70 to −60
,, (ebonite) .	360	+87	—
,, (plasticised) (b)	240	−33	—
Butadiene-styrene rubbers (e):			
75:25	261 to 268	−12 to −5	−63 to −54
60:40	283	+10	—
55:45	293	+20	—
50:50	296	+23	— (e)
30:70	328	+55	—
75:25 (vulcanised) . .	276	+3	—
75:25 (vulcanised, plasti-			
cised) (d) . . .	257	−16	
Butadiene-acrylonitrile ('*nitrile*')			
rubbers, vulcanised (c):			
75:25	278	+5	−50 to −40
60:40	293	+20	−30 to −20
50:50	310	+37	−15 to +5
Neoprene GN, vulcanised .	272	−1	−46
Butyl rubber, unvulcanised .	—	—	−75 to −70
Silicone rubber . . .	—	—	−123

Notes. (a) Depends on the amount of combined sulphur; T_s approximately equals
the value for unvulcanised rubber plus 2·5°C for every 1% sulphur.
(b) 20 parts di-octyl sebacate per 100 rubber (Fletcher and Gent, *Brit. J.
Appl. Phys.*, 1957, **8**, 194).
(c) The numbers following are the ratios of butadiene to styrene (or acrylo-
nitrile) in the polymer; figures for butadiene-acrylonitrile rubbers have
been calculated indirectly and are therefore approximate.
(d) 40 parts ether plasticiser per 100 rubber (Fletcher and Gent, *loc. cit.*).
(e) Published data from various sources differ too much to give reliable
averages.

* Reference 6.3

146

Table 11

MECHANICAL PROPERTIES OF NATURAL RUBBER VULCANIZATES OF VARIOUS HARDNESS

Hardness, BS degrees	Young's Modulus (static), E*		Shear Modulus (static), G*		tan δ (a)		Ratio of Dynamic to Static Modulus (b)	
	lb/in²	10^4 N/m²	lb/in²	10^4 N/m²	(i)	(ii)	(i)	(ii)
30	120–160	83–110	40–50	28–35	0·03	–	–	
40	200–270	138–186	60–80	41–55	–	0·08	1·08–1·15	1·05–1·09
50	320–400	221–276	90–115	62–79	0·03–0·05	0·12	1·18	1·08
60	500–600	345–414	130–165	90–114	0·05–0·08	0·17	1·21–1·25	1·14–1·15
70	780–900	538–620	200–260	138–179	0·07–0·12	0·4	1·6 –1·9	1·31–1·37
75	1000±	690±	300±	207±	0·10–0·15	–	–	–
80	1300±	900±	400±	276±	0·13–0·18	–	–	–

Notes: (a) Column (i) refers to rubbers compounded with carbon black (HAF) only; column (ii) refers to commercial rubbers of unspecified composition (data from Firestone Industrial Products Co., Detroit). All figures refer to normal temperature and low frequency (2–20 cps).

(b) Determined by Yerzley Oscillograph at 2–5 cps and 20% deformation, in compression (i) or shear (ii); 'static' modulus is the tangent modulus, $d f/d e$.

Table 12

SUMMARY OF EFFECTS OF VULCANIZATION AND COMPOUNDING ON
DYNAMIC PROPERTIES*

Property	Region	Vulcanisation	Plasticizer	Filler
In-phase modulus (G' or E')	rubbery	Increase; 'plateau' lengthened	Decrease	Large increase; 'plateau' lengthened
	glassy	Little effect	Slight decrease	Increase
Out-of-phase modulus (G" or E")	rubbery	Increase	Increase	Increase
	glassy	Little effect	Increase	Increase
TAN δ = 1/Q approx.**	rubbery	Increase	Decrease	Increase
	glassy	Decrease	Decrease	Increase
	transition	Peak lowered and broadened	Peak lowered and broadened (at high plasticiser content peak may be raised again)	Peak lowered and broadened

* Reference 6.3

** Q is the peak (maximum) transmissibility, a quantity sometimes used by engineers in place of tan δ (see Section 2)

been demonstrated as shown in Figure 64 (from 6.4). Values of specific heat, thermal conductivity, specific gravity and linear coefficient of thermal expansion for several types of elastomers and compounding materials are presented in Tables 8 and 9. The characteristic and glass transition temperatures (as discussed in Section 4.0) for some typical mixes of several types of elastomers are presented in Table 10; static and low-frequency dynamic mechanical properties for natural rubber of various hardnesses are presented in Table 11; and the general effects of vulcanization and compounding are listed in Table 12. Specific lists of general properties for a large number of commercial compounds may be found in Reference 6.1 along with a listing of the relative resistance of twenty-two classes of elastomers to a number of classes of chemical agents. The resistance of a number of generic elastomer types to specific oils and solvents and to general environmental conditions are presented in Tables 13 and 14, respectively (from 6.2).

Due to an increased rate of oxidation, the use of elastomer materials at elevated temperatures has the effect of reducing the service life. This oxidation manifests itself as a decrease in tensile strength, elongation and resilience, and an increase in hardness. Eventually, cracks develop in the elastomer element and lead to failure. There is a threshold temperature below which the acceleration of aging is negligible. The high-temperature service limits for various elastomers are presented in the bar graph in Figure 65, 6.2. For a reasonable service life, the elastomer temperature generally should be maintained well below the high temperature limit indicated on Figure 65.

It has been shown 6.3 that the static compressive stress, f, is given by

$$f = -G \left[(1-\varepsilon) - (1-\varepsilon)^{-2} \right] s \qquad (6\text{-}1)$$

where G is the shear modulus, ε is the static compressive strain, and s is a shape function. For small ε, equation (6-1) reduces to

$$f \simeq 3G\varepsilon s \qquad (6\text{-}2)$$

and thus, the term 3Gs becomes the effective compression modulus. Since elastomers are nearly incompressible (Poisson's ratio is approximately 0.5), Young's modulus may be approximated as three times the shear modulus. Therefore, the effective compression modulus determined above differs from Young's modulus only by the factor of the shape function, s. The value of the shape function differs from unity because of the restriction of deformation perpendicular to the load at the bonded surfaces; see Figure 66. Static shape functions for several typical geometries, given in Reference 6.3 and reproduced in Table 15, has been extended to include frequency-dependent dynamic shape functions 6.5. This dynamic shape function (or factor) discussed in detail in Section 4.0, is also covered in Section 6.2.

Compatibility with adhesives is another important property of elastomer materials as related to damper design. This compatibility is particularly important when using elastomer elements that are subjected to shear loading since the adhesive must carry the entire shear load. In general, elastomer elements may be bonded to a structure (usually metal) either by including the structure in the vulcanization process or by introducing an adhesive

149
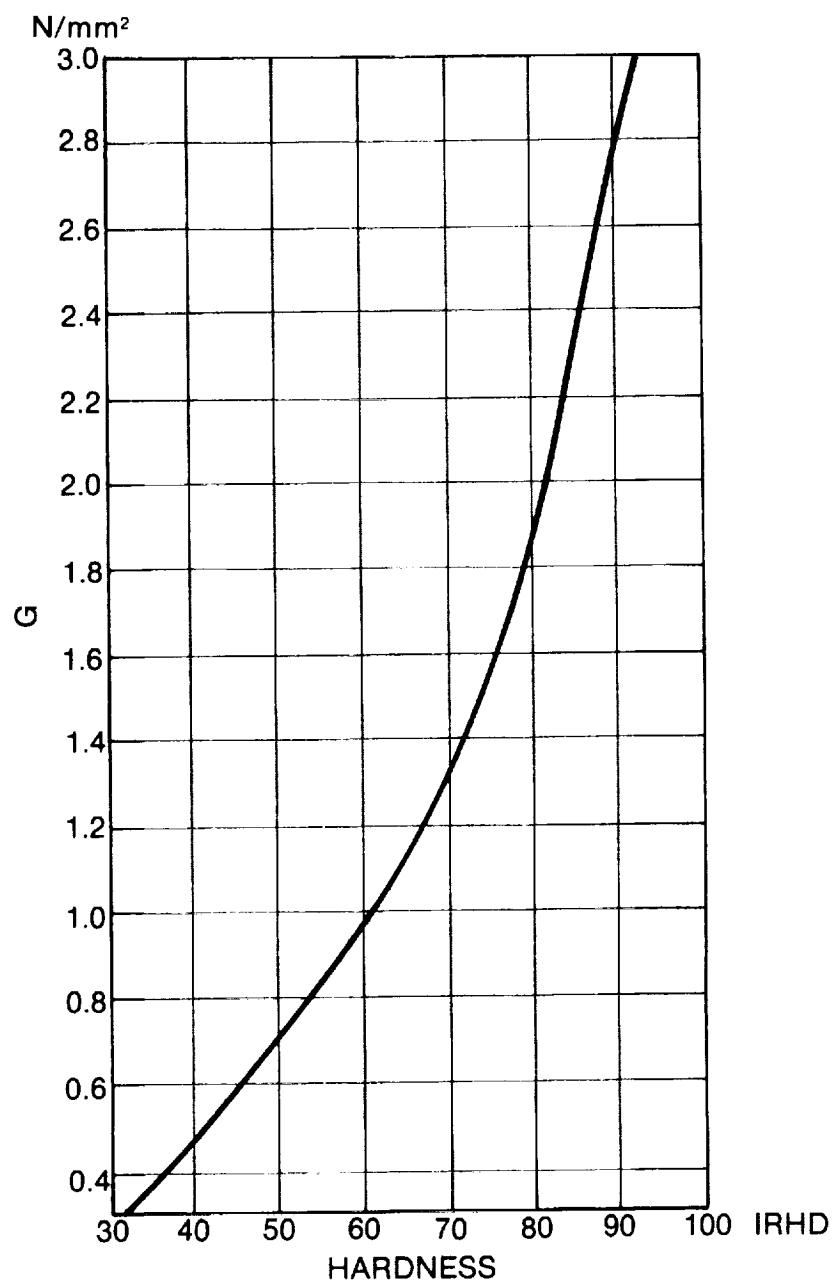
Fig. 64 Dependence of Shear Modulus on Hardness (After [6.4])

Table 13

OIL RESISTANCE OF ELASTOMERS*

Oil or Solvent	Elastomer								
	NR	SBR	CR	NBR	IIR	T	CSH	VHQ	FHQ
Animal Fats Milk, butter	C	C	B	A	A	X	A	A	A
Vegetable Oils Castor	A	A	A	A	A	X	A	A	A
Tung, corn, cotton seed, linseed, palm, soya bean	X	B-C	A-B	A	A	C	B	A	A
Aliphatic Hydrocarbons Gasoline, kerosene, crude petroleum lubricating oils	X	X	B	A	X	A	C-X	X	A
Aromatic Hydrocarbons Aniline, benzol, toluene, xylene cresols, creosotes	X	X	C-X	B-C	C-X	A-C	C-X	X	B
Asphalt, coal tar	X	X	B	A-B	X	A-C	B	C	A
Solvents Acetone	A	A	B	X	A	A	B	X	X
Carbon tetrachloride	X	X	X	C	X	C	X	X	B
Lacquer solvents	X	X	X	X	C	C	X	X	B
Methyl ethyl ketone	X	X	X	X	B	A	C	B	X
Nitrobenzene	X	X	X	X	X	X	X	X	C
Trichloroethylene	X	X	X	X	X	X	X	X	B

NR = Natural rubber
SBR = Styrene-butadiene
CR = Neoprene or chloroprene
NBR = Buna N or acrylonitrile-butadiene
IIR = Butyl or Isobutylene isoprene
T   = Polysulfide

CSM = Chlorosulfonated polyethylene
VHQ = Silicone   FHQ = Fluorosilicone

Key to Raitings
A=Good; B=Fair; C=Possible, but depends on conditions and specific compound; X=Unsuitable

* Reference 6.2

151

Table 14

ENVIRONMENTAL RESISTANCE OF ELASTOMERS*

Resistance To:	NR	IR	SBR	IIR	BR	EPM	CR	NBR	T	AU	VHQ	CSH	ACH	FPH
Flame	P	P	P	P	P	P	G	P	P	P		G	P	E
Impact	E	E	E	G	G	G	G	G	P	E	P	G	P	P
Abrasion	E	E	E	G	E	G	E	E	P	E	P	G	G	G
Tear	E	G	G	E	G	P	G	G	P	G	P	G	G	P
Cut Growth	E	E	G	E	G	G	G	G	P	G	G	G	G	P
Weather	G	G	G	E	G	E	E	G	E	E	E	E	E	E
Oxidation	G	E	G	E	E	G	E	P	E	E	E	E	E	E
Ozone	P	P	P	E	P	E	G	P	E	E	E	G	P	E
Radiation	G	G	G	P	P	P	P	P	G	G	G	G	G	G
Water	E	E	E	E	E	E	G	E	G	G	G	G	G	G
Acids	G	G	G	E	G	E	G	G	G	P	G	E	G	E
Alkalies	G	G	G	E	G	E	G	G	G	P	G	E	P	E
Gasoline, Kerosene	P	P	P	P	P	P	P	E	E	E	P	G	E	E
Benzol, Toluene	P	P	P	G	P	G	P	G	E	P	P	P	E	E
Degreaser Fluids	P	P	P	P	P	P	G	P	G	G	P	P	P	G
Alcohol	G	G	G	E	G	P	G	E	G	G	G	G	P	E
Synth Lubricants	P	P	P	G	P	P	P	G	G	P	P	P	G	G
Silicate Hydr Fluids	P	P	P	G	P	G	G	G	P	P	G	G	G	G
Phosphate-Hydr Fluids	P	P	P	G	P	E	P	P	P	P	G	P	P	P

E=Excellent; G=Good; P=Poor

Key:
NR = Natural rubber (natural polyisoprene)
IR = Synthetic rubber (synthetic polyisoprene)
SBR = Styrene-butadiene
IIR = Butyl (isobutylene isoprene)
BR = Polybutadiene (Cis 4)
T   = Polysulfide
EPM = Ethylene propylene rubber

CR = Neoprene (chloroprene)
NBR = Acrylonitrile butadiene
AU = Polyurethane
VHQ = Silicone (polysiloxane)
CSH = Chlorosulfonated polyethylene (Hypalon)
ACH = Acrylics (polyacrylate)
FPH = Fluoroelastomers (fluorinated hydrocarbon)
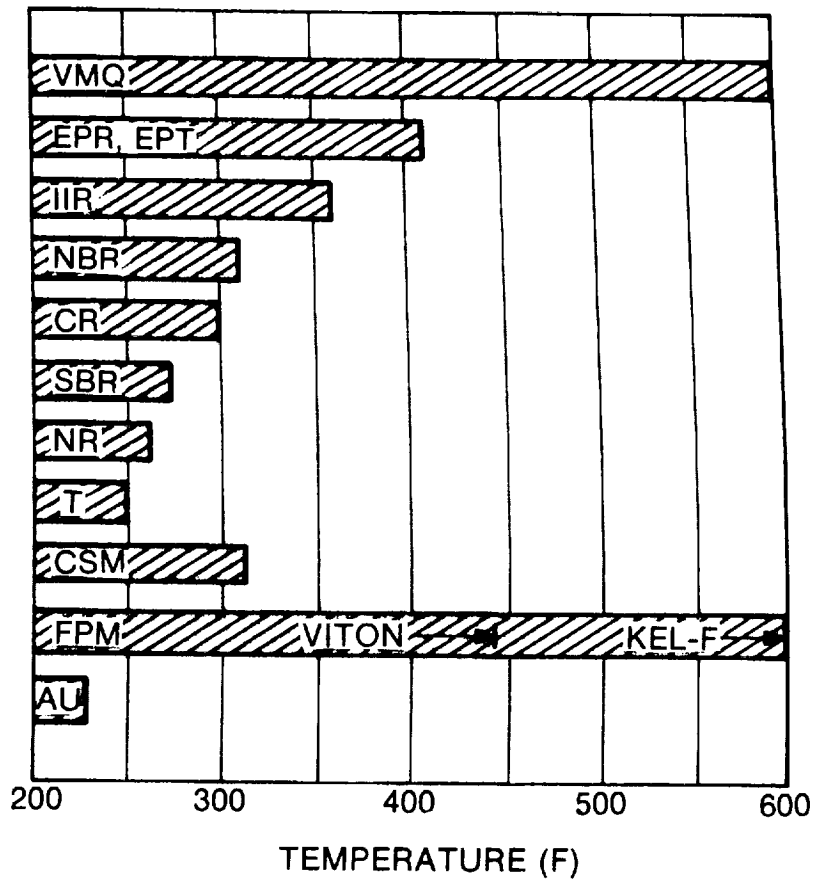
152

* Reference 6.2

Fig. 65 High Temperature Service Limits (Short-Time Exposure) for Various Elastomers (After [6.2])

NR = NATURAL RUBBER
SBR = STYRENE-BUTADIENE
CR = NEOPRENE OR CHLOROPRENE
NBR = BUNA N OR ACRYLONITRILE-BUTADIENE
IIR = BUTYL OR ISOBUTYLENE ISOPRENE
T = POLYSULFIDE
CSM = CHLOROSULFONATED POLYETHYLENE
VMQ = SILICONE   FMQ = FLUOROSILICONE

Table 15

EXPRESSIONS FOR SHAPE FUNCTION

In all formulae h = height, i.e. in direction of compression.

Cross-section	Shape function
Square side = a	$1 + B(a/h)^2$
Circular diameter = d	$1 + B(d/h)^2$
Rectangular long side = l short side = w	$\dfrac{1 \cdot 33 + 0 \cdot 66w/l + C(w/h)^2}{1 + w/l}$
Annulus outer diameter = d_2 inner diameter = d_1 Case 1: d_2 much greater than d_1 Case 2: d_1 almost as large as d_2	$1 + B(d_2 - d_1)^2/h^2$ $1 \cdot 33 + D(d_2 - d_1)^2/h^2$
Hollow Square outer side = a_2 inner side = a_1 Case 1: a_2 much greater than a_1 Case 2: a_1 almost as large as a_2	$1 + B(a_2 - a_1)^2/h^2$ $1 \cdot 33 + D(a_2 - a_1)^2/h^2$

Variation of B, C, and D with shear modulus G

					units
G 69	69–103	103–138	138–207	207	$\times 10^4$ N/m^2
G 100	100–150	150–200	200–300	300	lb/in^2
B 0·120	0·103	0·080	0·063	0·056	
C 0·26	0·225	0·175	0·14	0·12	
D 0·065	0·056	0·044	0·035	0·030	
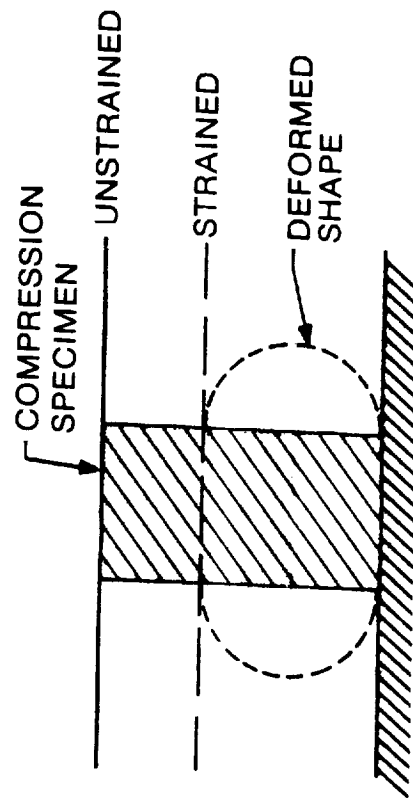
Fig. 66   Deformation of a Bonded (No-Slip) Compression Specimen

155

(usually epoxy) between the already vulcanized elastomer and the structure. In the former case, bonding agents (such as isocyanates or "chemloks" [6.4]) are often used for pretreating the bonding surfaces. In the latter case, good success has been achieved for several types of elastomers (particularly those for which dynamic properties are given below) with Renwald epoxy TWA-1077*. This adhesive has been effective even in an oily environment. In some cases (particularly when extreme environmental conditions are likely), it may be advisable to perform some tests on the compatibility and durability of a particular adhesive, or bonding method, with specific elastomer and structural materials, and a particular set of environmental conditions. When bonding an elastomer to a structure, it is advisable to clean the surfaces with emery paper and a compatible solvent (one which will not degrade the elastomer), to apply the adhesive (usually to both surfaces), to assemble the components, and to place and maintain pressure on the bond until the adhesive is fully cured.

6.2 Dynamic Properties

Empirical dynamic property data have been determined for several elastomer materials by the use of the BERM test method; (see Section 5.0). These materials were polybutadiene, flourocarbon (Viton), nitrile (Buna-N), EPDM (Ethylene-Propylene-Diene) and chloroprene (neoprene). As dynamic properties of elastomers are sensitive to the percent and type of filler used in the material composition, batch-to-batch variation may occur in dynamic properties. For this reason, all elastomer specimens for each material tested were drawn from a single batch of elastomer stock. In each case, additional material was taken from the same batch for measuring some of the relevent general physical properties [6.6 and 6.7] presented in Table 16. Note that, of these materials, Viton has the highest transition temperature (closest to ambient). Consequently, the loss coefficient for Viton is the highest but is also the most sensitive to changes in frequency or temperature; see Section 4.0.

Shear specimen BERM tests were conducted for each of these materials to develop relationships for the shear storage and loss moduli. These tests were conducted for a variety of operating conditions (i.e. frequency, temperature and dynamic strain). Using statistical regression analyses, the measured shear moduli have been quantitatively related to the values of the operating condition parameters. This relationship is described in this section. A set of compression sample tests (Section 5.0) has also been conducted for polybutadiene. Using the shear moduli values from the shear tests, values for the dynamic shape factors (Section 4.0) have been determined; these shape factors have been related to the operating condition parameters as discussed for the shear moduli.

A series of BERM tests was also conducted for O-rings composed of fluorocarbon (Viton - CFM) and nitrile (Buna-N - NBR). Each test for each elastomer involved material from a single batch, although not the same batch from which the corresponding elastomer material for the shear tests was drawn. O-ring geometry is too complex to easily relate engineering parameters (i.e. stiffness and damping) to the shear moduli. Consequently, the test results presented are in terms of the support parameters as functions of the operating conditions.

---

* Ren Plastics, Lansing, Michigan

156

Table 16

SOME PHYSICAL PROPERTIES OF FIVE ELASTOMER MATERIALS USED FOR
DYNAMIC PROPERTY TESTS AT MECHANICAL TECHNOLOGY INCORPORATED, LATHAM, NEW YORK

Elastomer Material	Thermal Conductivity* (W/mK)	Thermal Coefficient of Linear Expansion (per C)	Specific Heat* (J/gk)	Transition Temperature Tg (°K)
Butadiene Polybutadiene (BR)	0.25	2.0×10^{-5}	1.58	218**
Flurocarbon Viton (CFM)	0.29	15.9×10^{-5}	1.22	256
Nitrile Buna-N (NBR)	0.40	27.7×10^{-5}	1.58	243
Chloroprene Neoprene (CR)	0.42	20.4×10^{-5}	1.44	222
Ethylene-Propylene-Diene (EPDM)	0.39	21.3×10^{-5}	1.72	217

* Average value measured over a range of temperatures from about 20 to 100°C.

** Could not be measured due to high filler loading. Estimated from iteratively determined value for characteristic temperature.

The results of shear and compression specimen tests for butadiene (Polybutadiene - BR) are presented in detail; see [6.8]. As the form of the results for the other materials is similar, that data will be presented in somewhat less detail. For butadiene (Polybutadiene - BR), typical plots of stiffness, damping and loss coefficient as functions of frequency (for a single temperature but a variety of dynamic strain values) are presented in Figures 67 and 68. Similarly, typical plots of stiffness, damping and loss coefficient as functions of dynamic strain (for a single temperature but for a variety of frequency values) are presented in Figures 69 and 70. All four plots are for the compression specimen tests at 66°C. However, the results for the shear specimen tests and the remainder of the compression specimen tests are qualitatively very similar. With frequency as an independent variable, a linear least squares fit has been applied to the common logarithms of the data. With strain as an independent variable, a second-order least squares fit has been applied to the common logarithms of the data.

The effects of dynamic strain are summarized in Figures 71 and 72. The curves, with strain as an independent variable, show certain distinct characteristics for butadiene (Polybutadiene - BR):

- Stiffness decreases with increasing strain

- Loss coefficient increases with increasing strain

- Stiffness decreases consistently as the ambient temperature is increased*

- Loss coefficient decreases with increasing temperature*

- Low strain loss coefficient falls by a small amount with increasing temperature*

- Reduction in loss coefficient is more pronounced at high strain*

- A distinct clustering of data points is evident about the fitted curves.

- The plots for the compression test specimen are even more closely clustered about the fitted line than for the shear specimen

- The plots as a function of strain provide, with reasonable scatter, a uniform trend for data at all frequencies.

The plots as a function of frequency do not provide a uniform trend for the data at all strains; the scatter is very broad, indicating that, for this material and in this frequency range, the effects of strain are much more pronounced than the effects of frequency. In the case of stiffness, the data tend to show increasing stiffness with increasing frequency; but, as previously stated, the scatter is considerable. In the case of loss coefficient, the data suggests little dependence on frequency.

---

* Also see Figures 73 and 74.
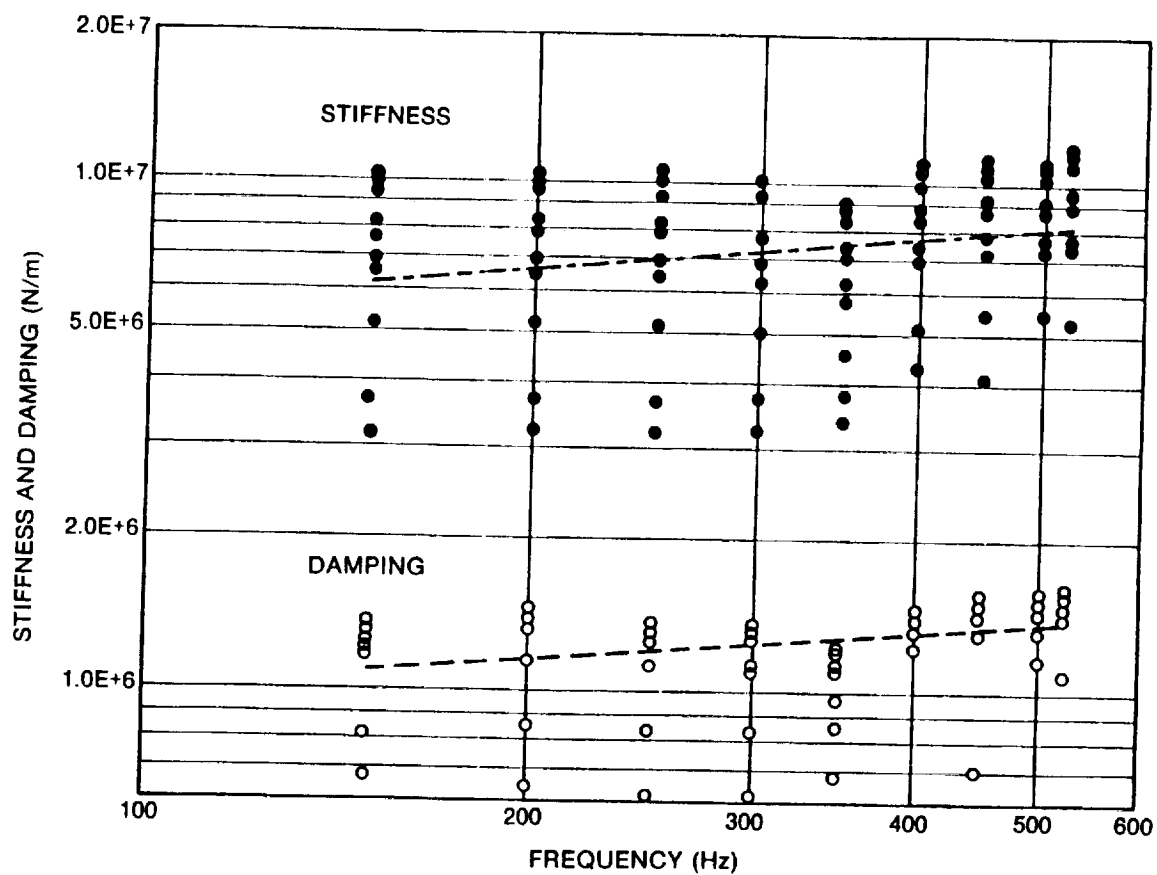
Fig. 67 Stiffness and Damping as a Function of Frequency for the 66°C Butadiene (Polybutadiene) Compression Tests

159
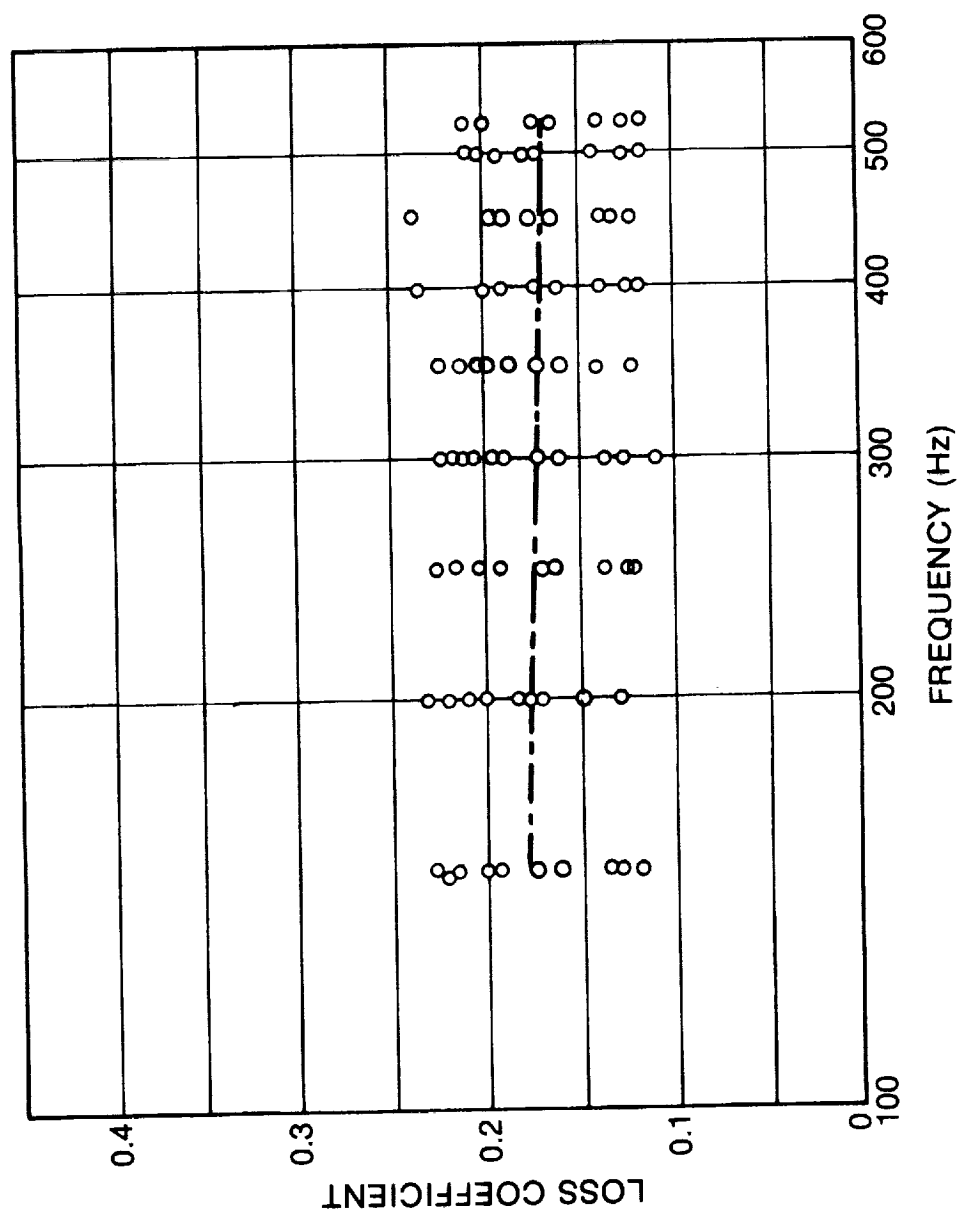
Fig. 68   Loss Coefficient as a Function of Frequency for the 66°C Butadiene (Polybutadiene) Compression Tests

160
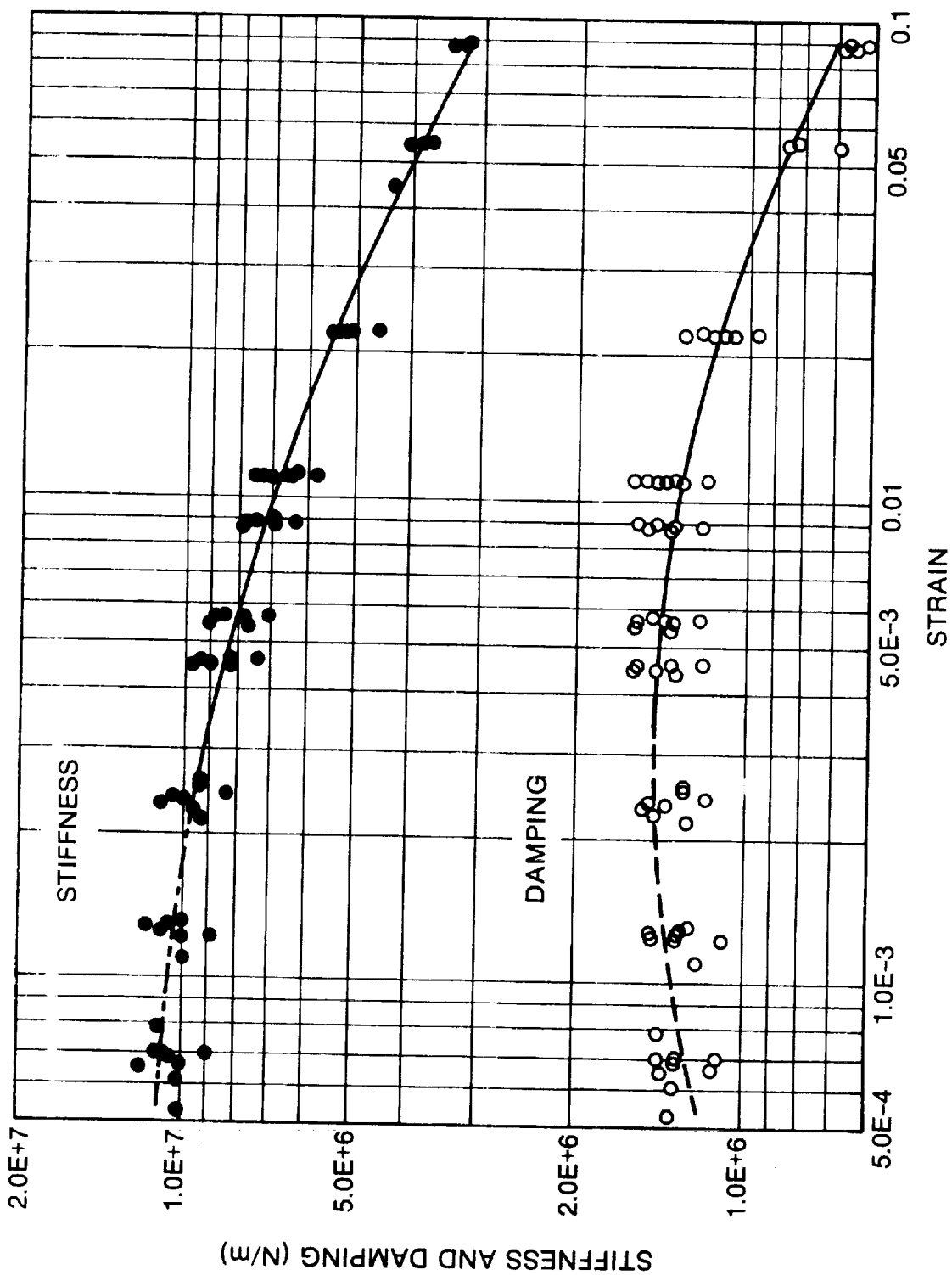
Fig. 69 Stiffness and Damping as a Function of Strain for the
66°C Butadiene (Polybutadiene) Compression Tests

161
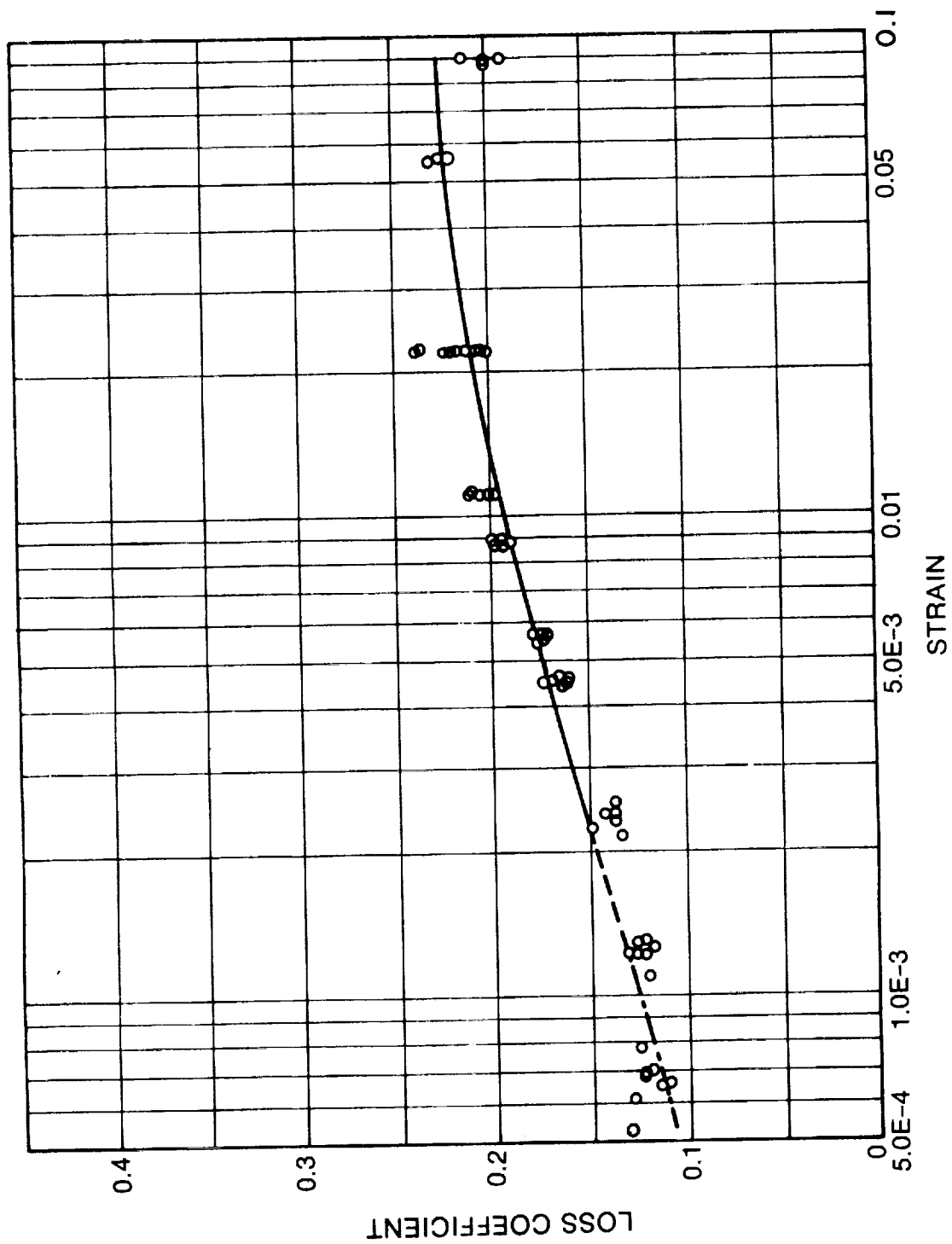
Fig. 70 Loss Coefficient as a Function of Strain for the 66°C Butadiene (Polybutadiene) Compression Tests

162
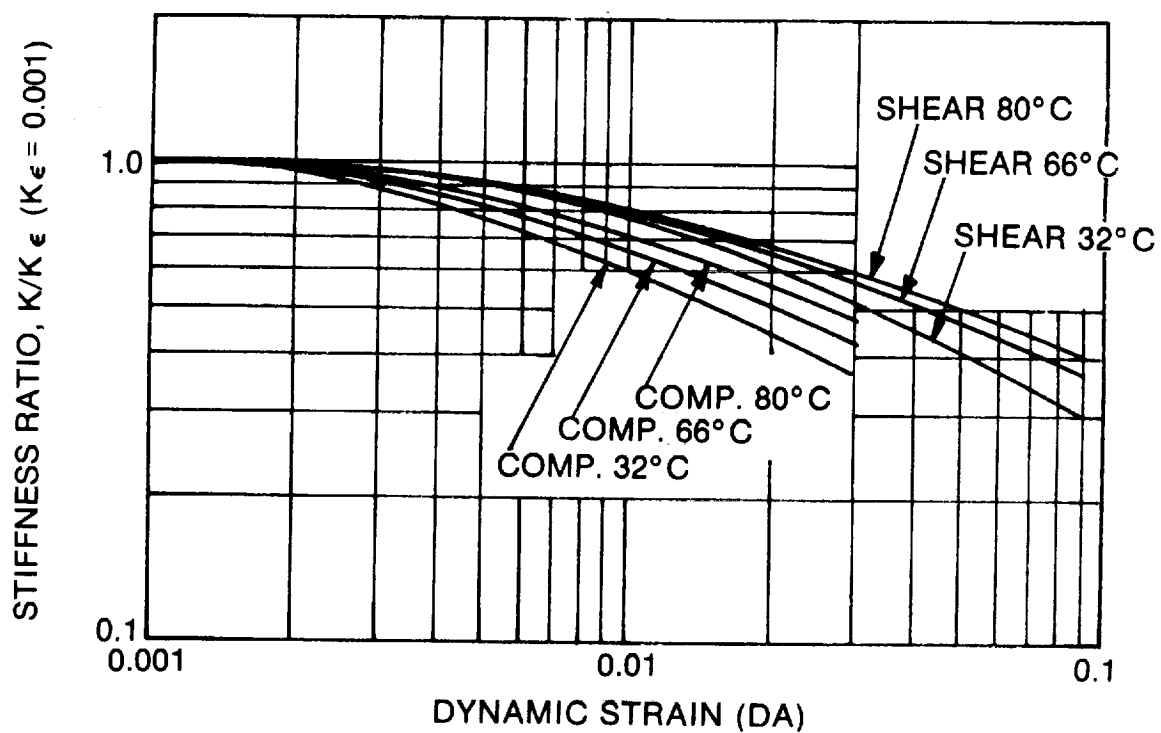
Fig. 71 Ratio of Stiffness at Finite Strain to Stiffness at 0.001 Strain as a Function of Dynamic Strain. Shear and Compression Specimens, Butadiene (Polybutadiene) at 32°C, 66°C, and 80°C.
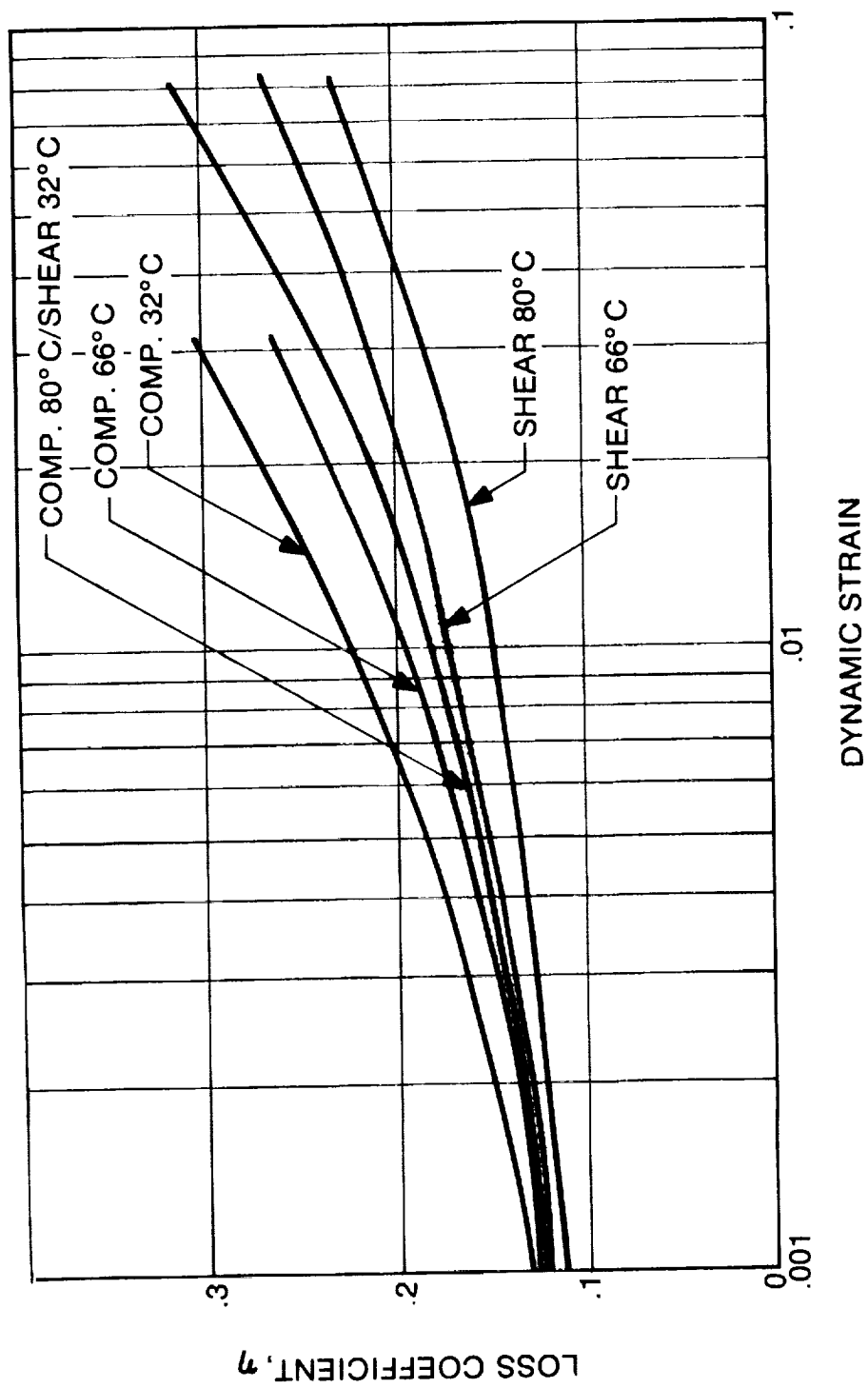
Fig. 72 Loss Coefficient vs Dynamic Strain, Butadiene (Polybutadiene) Shear and Compression Specimens, 32°C, 66°C, and 80°C

164
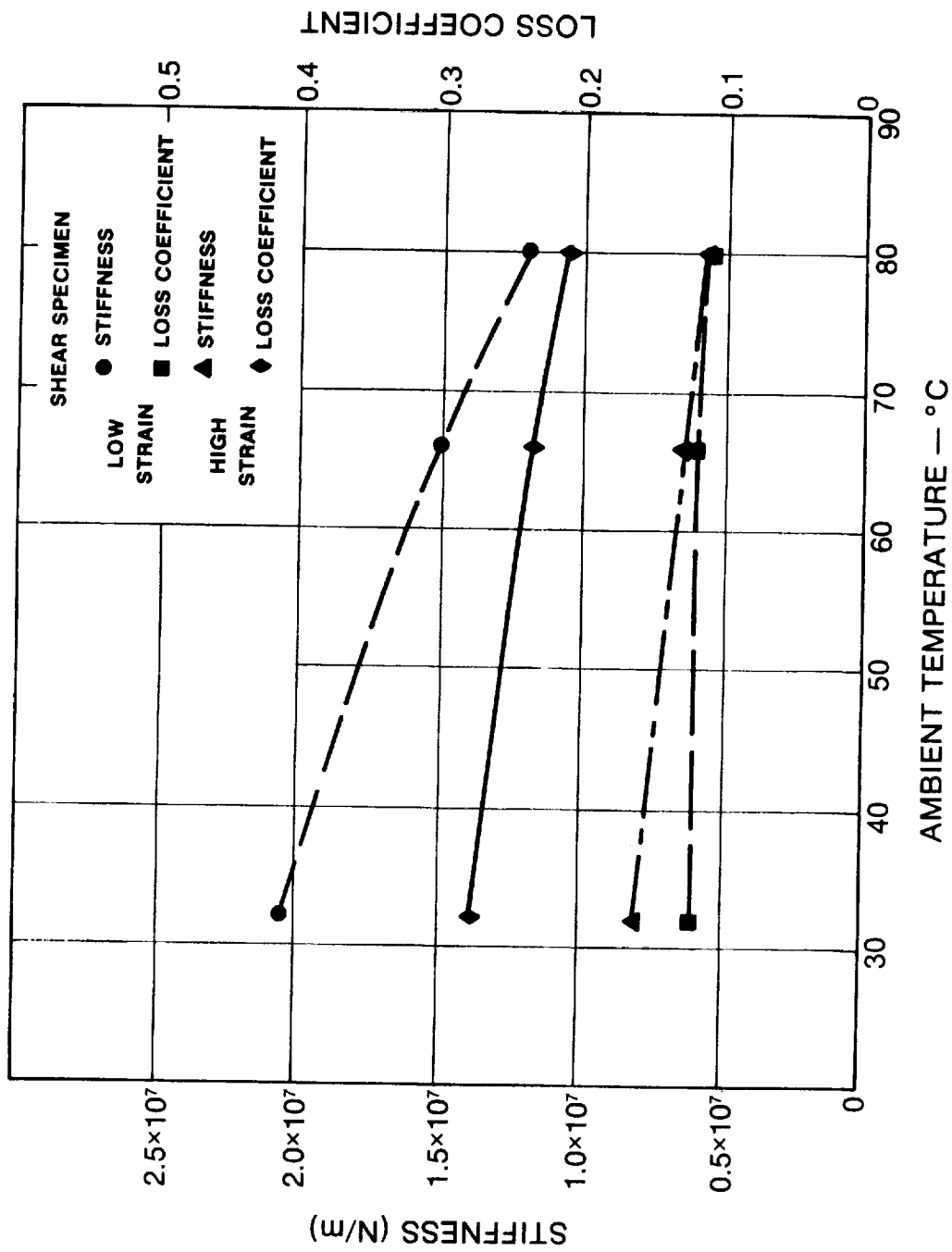
Fig. 73   Effect of Ambient Temperature on Dynamic Properties of Shear Specimen
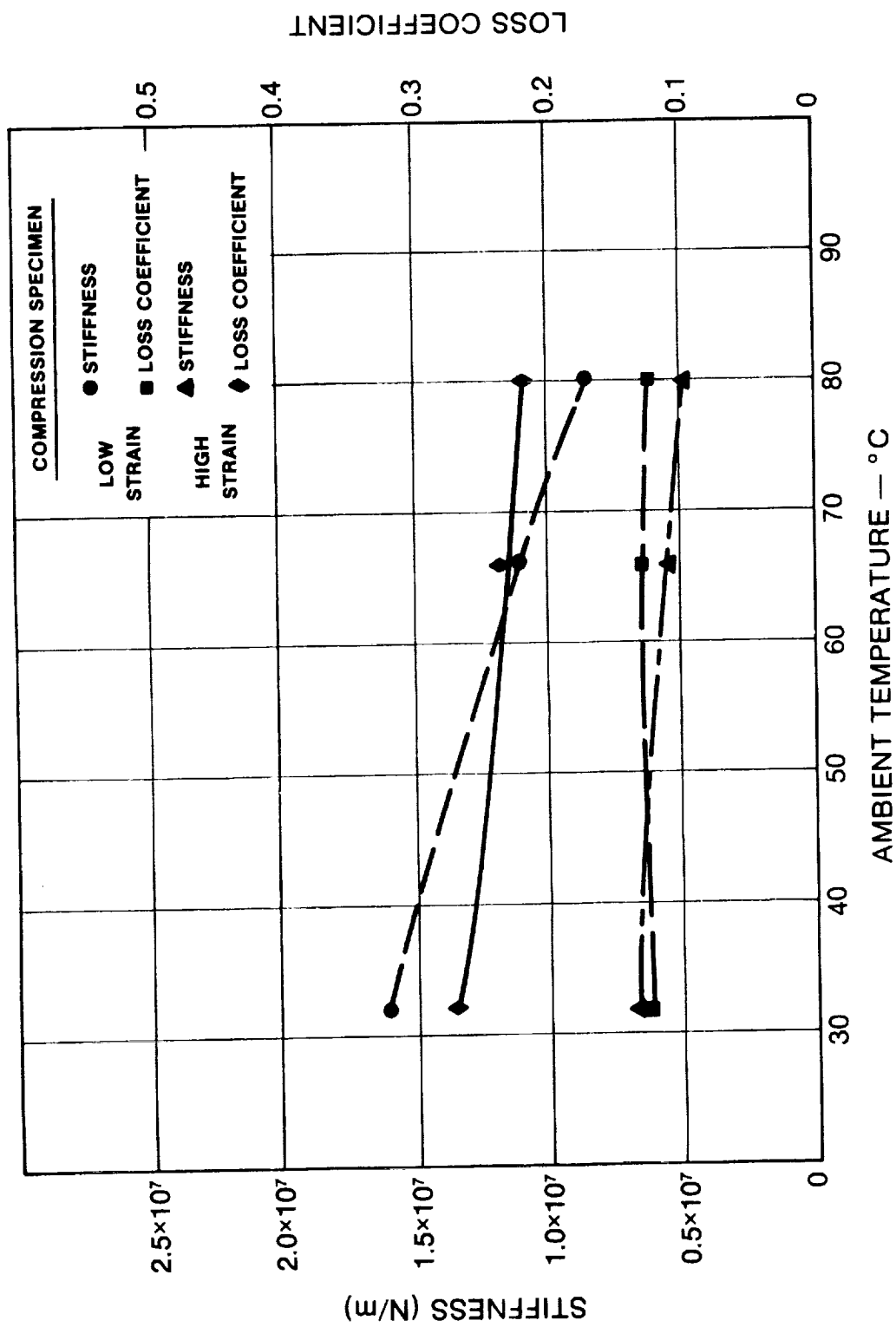
Fig. 74 Effect of Ambient Temperature on Dynamic Properties of Compression Specimen

Based on the two sets of plots, dependence on strain is obviously more pronounced and more consistent for the range of frequencies investigated than the dependence on frequency for the range of strains investigated.

Figure 75 presents plots of stiffness and damping as functions of frequency for a single low value of strain for the butadiene (Polybutadiene - BR) shear test specimen at 66°C. These plots show a more consistent variation with frequency to which an acceptable straight line fit on log paper may be applied.

When compared to the polybutadiene shear specimen results, the test data for the other four materials (fluorocarbon (Viton - CFM), nitrile (Buna-N - NBR), chloroprene (Neoprene - CR), and EPDM) show more sensitivity to frequency and temperature. For example, using loss coefficient as an indicator, the effects of frequency at three different temperatures are compared for the five materials in Figures 76 through 78; similarly, the effect of temperature at a fixed frequency (500 Hz) is illustrated in Figure 79; and each of the five materials is considered individually in Figures 80 through 84. The following observations have been made from the results of these tests:

- Fluorocarbon (Viton - CFM) is extremely sensitive to frequency and temperature (loss coefficient rises with increasing frequency and falls with increasing temperature).

- Unlike the other four materials, loss coefficient for fluorocarbon (Viton - CFM) falls at high strain (may be related to self-heating and temperature sensitivity).

- Unlike the other four materials, the loss coefficient for EPDM falls with increasing frequency.

- In general, butadiene (Polybutadiene - BR) is less sensitive to frequency and temperature, and more sensitive to strain than the other four materials.

- At low temperature, the loss coefficient for fluorocarbon (Viton - CFM) (~0.7) is substantially higher and nitrile (Buna-N - NBR) (~0.15) somewhat lower than for the other materials.

- At high temperature, 80°C, the loss coefficients for all the materials ranges between 0.1 and 0.2 for the entire frequency range.

- Other than butadiene (Polybutadiene - BR), nitrile (Buna-N - NBR) and EPDM are the least affected by temperature.

Treating the distortion in the shear specimens as pure shear (discussed in Section 4.0), the shear storage and loss moduli are directly proportional to the measured stiffness and damping values, respectively, and may be calculated from

167
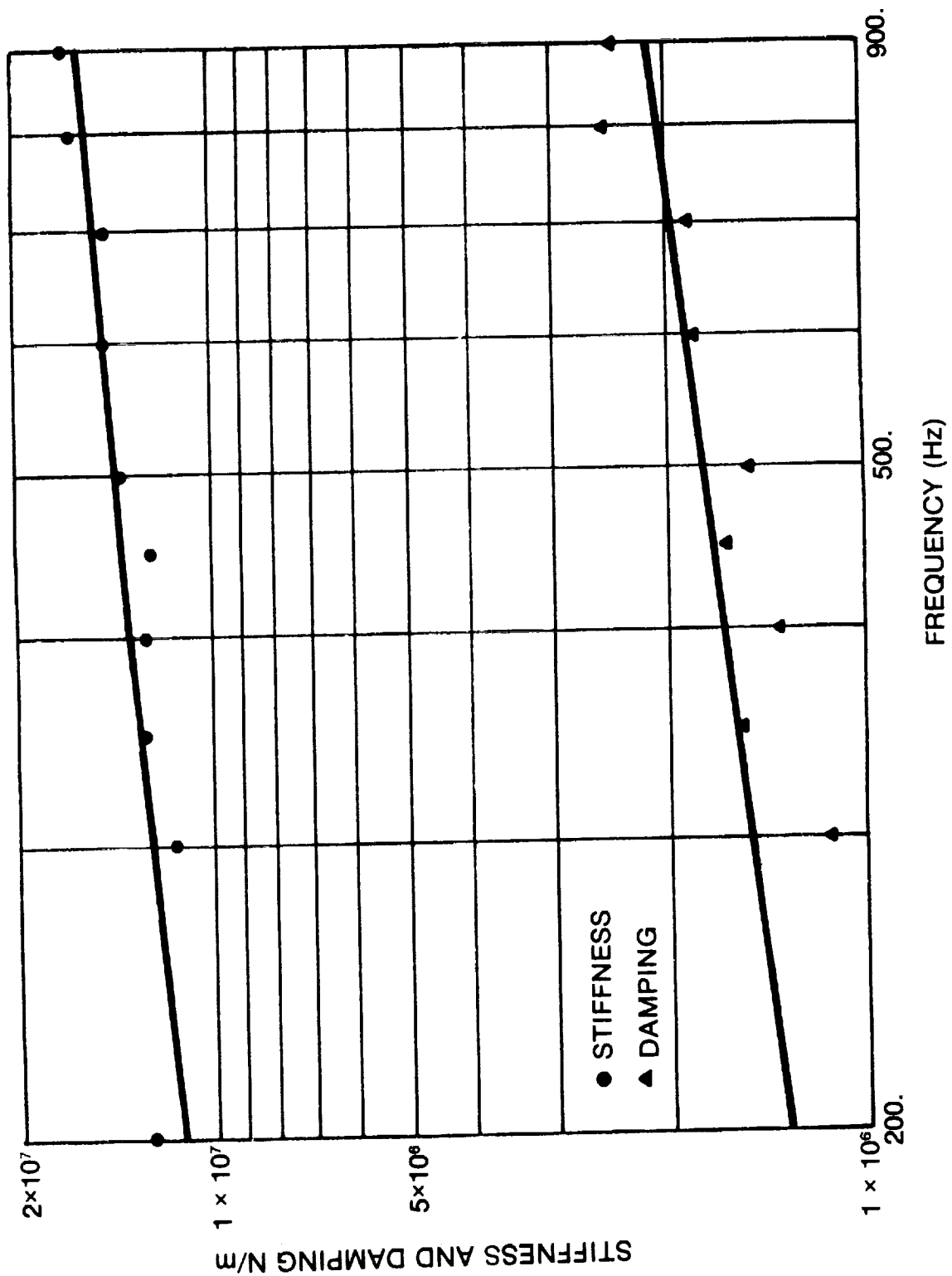
Fig. 75 Stiffness and Damping vs Frequency. Low Strain ($\epsilon \cong 0.0008$),
Shear Specimen, Butadiene (Polybutadiene) at 66°C

168
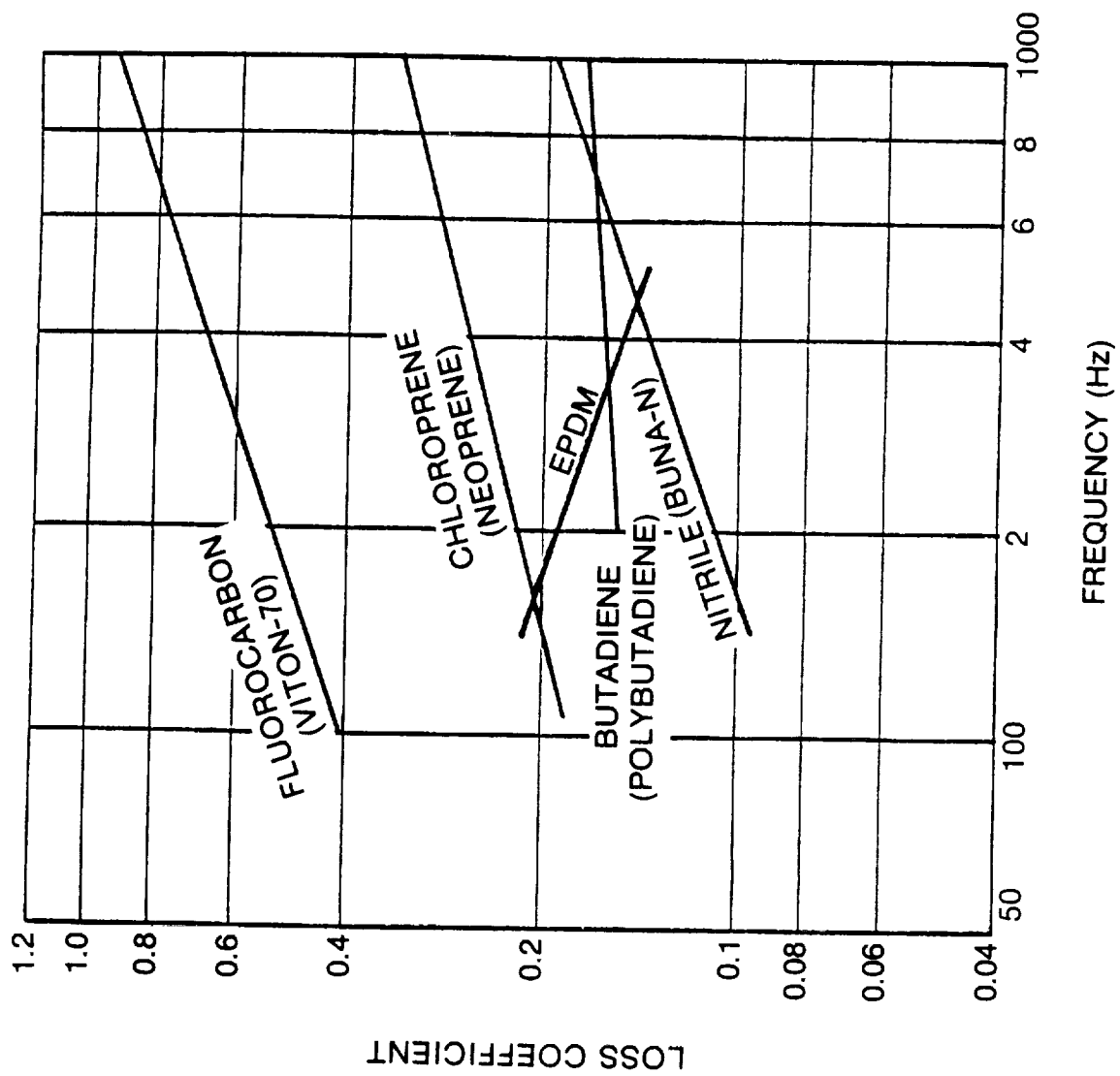
Fig. 76 Shear Specimen Data at 32°C

FREQUENCY (Hz)

LOSS COEFFICIENT

FLUOROCARBON
(VITON-70)

CHLOROPRENE
(NEOPRENE)

EPDM

BUTADIENE
(POLYBUTADIENE)

NITRILE (BUNA-N)

169
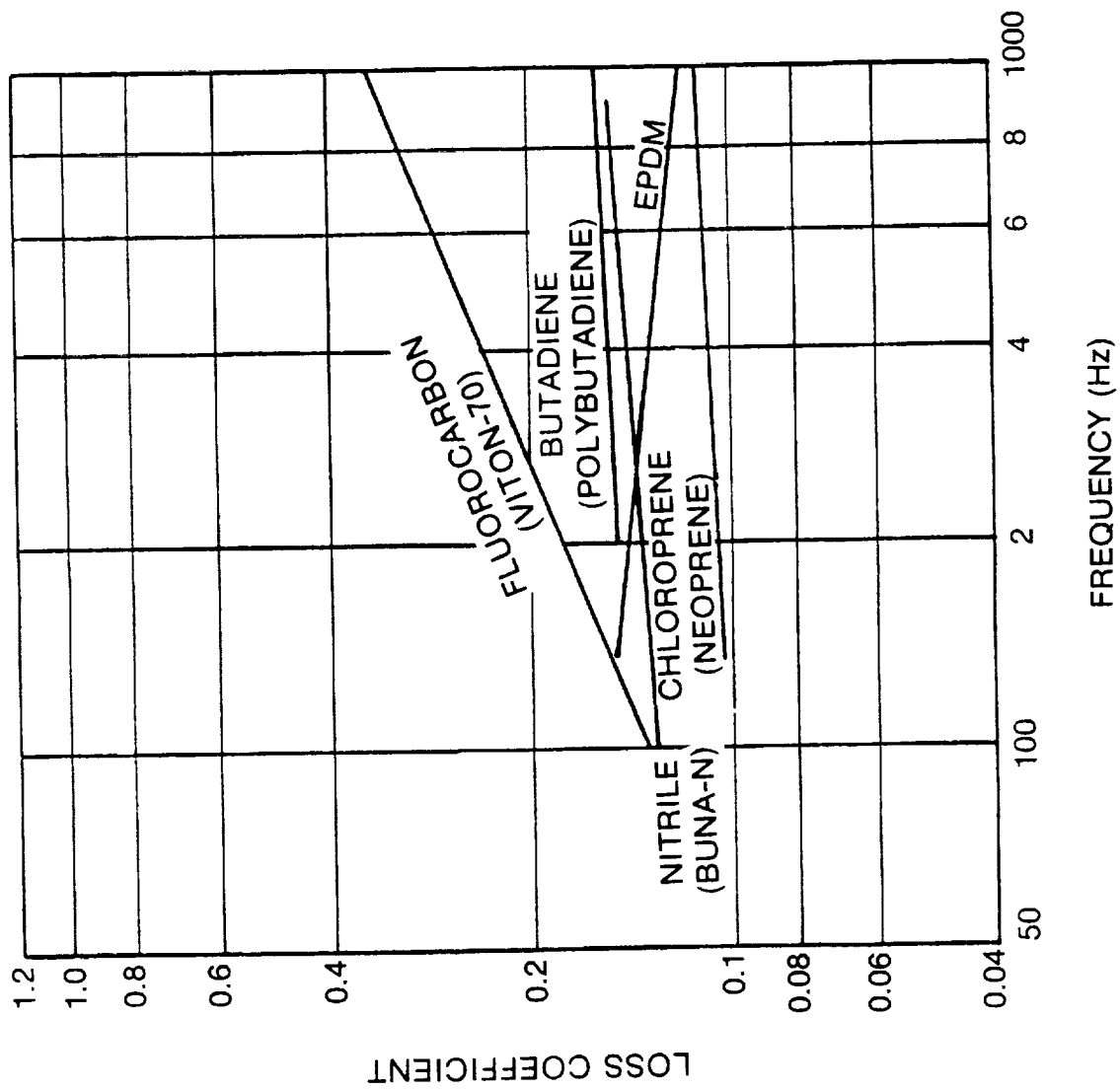
Fig. 77 Shear Specimen Data at 66°C

170
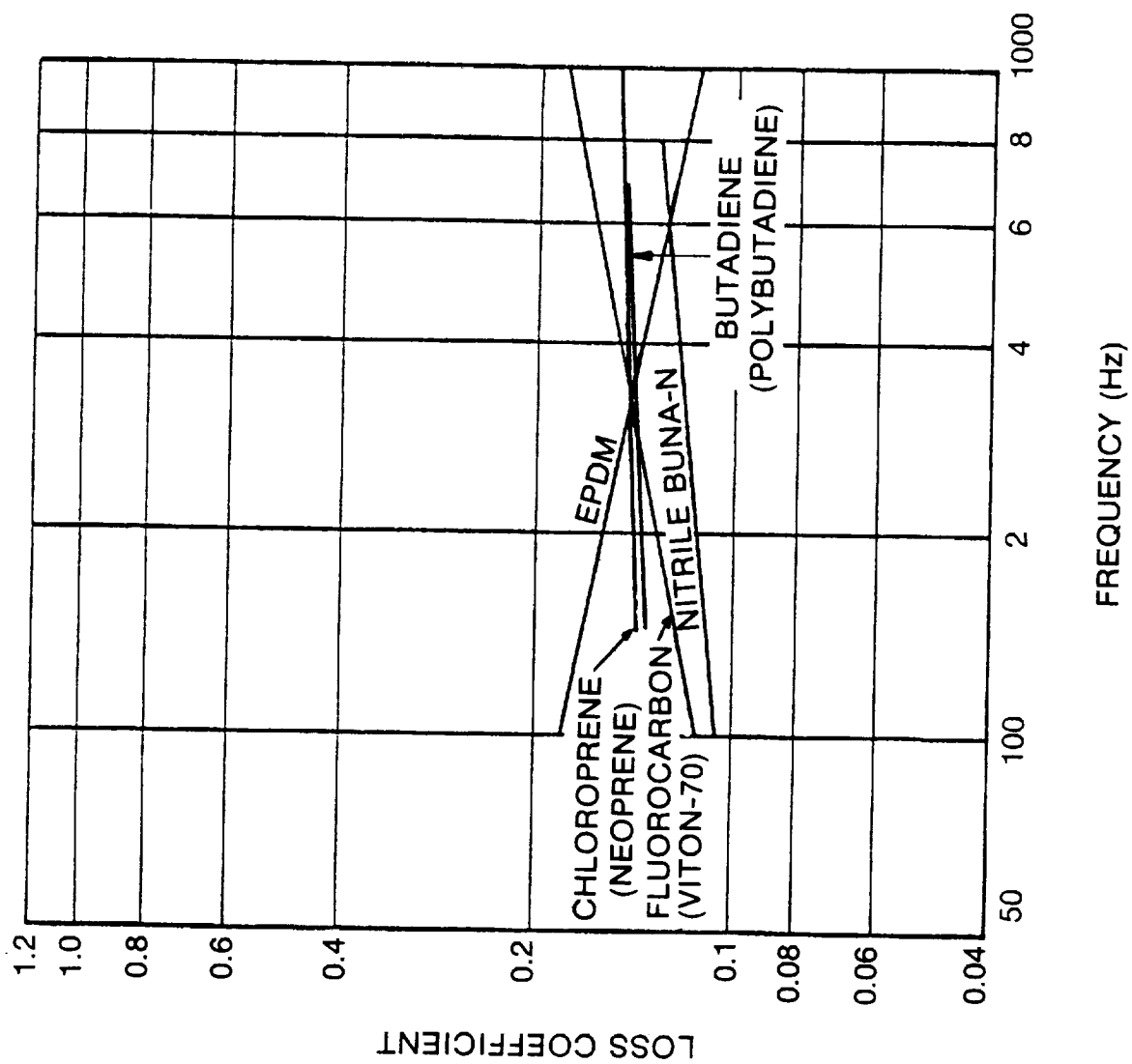
Fig. 78 Shear Specimen Data at 80°C

171
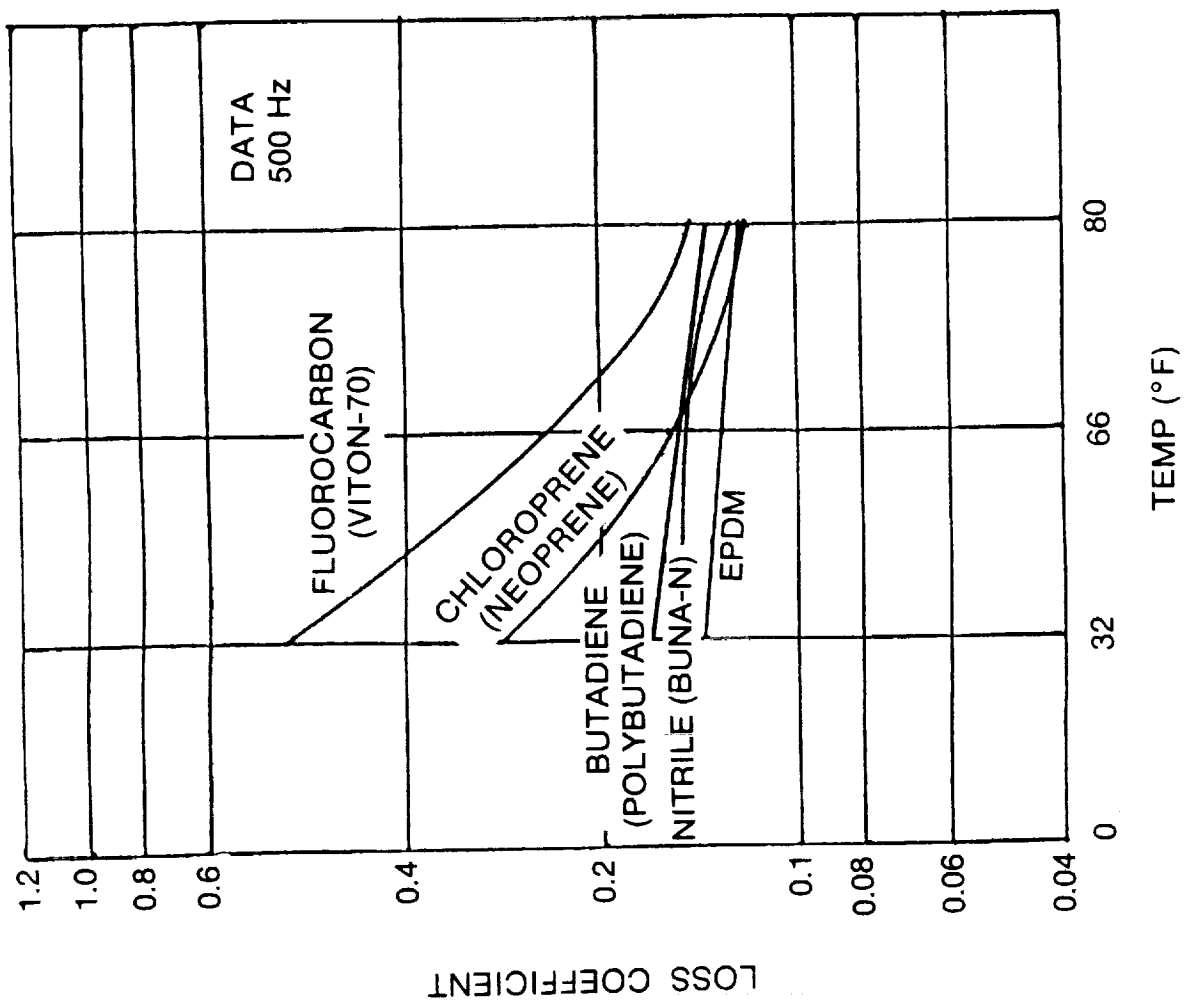
Fig. 79 Temperature Variation of Elastomer Loss Coefficient (at 500 Hz) for Shear Tests

172
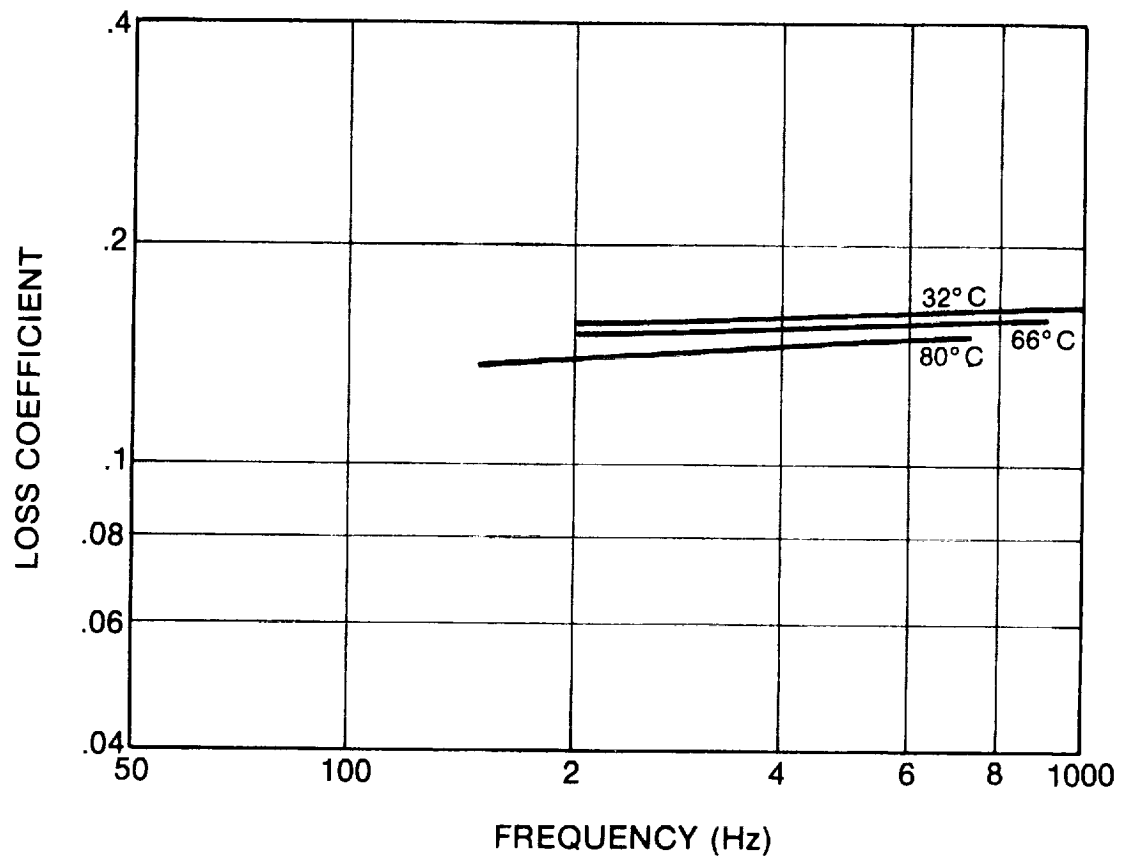
Fig. 80 Butadiene (Polybutadiene) Shear Specimen Data

173
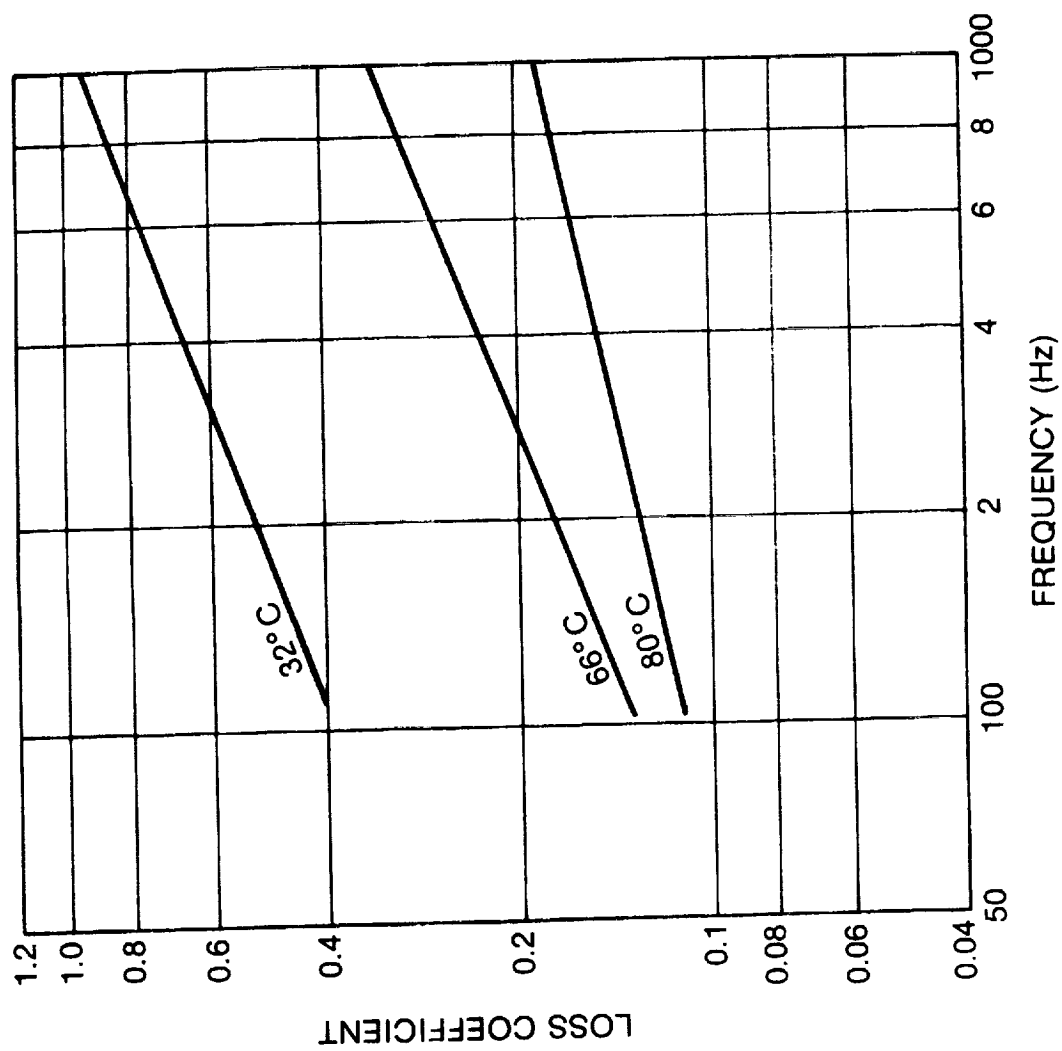
Fig. 81   Fluorocarbon (Viton-70) Shear Specimen Data

174
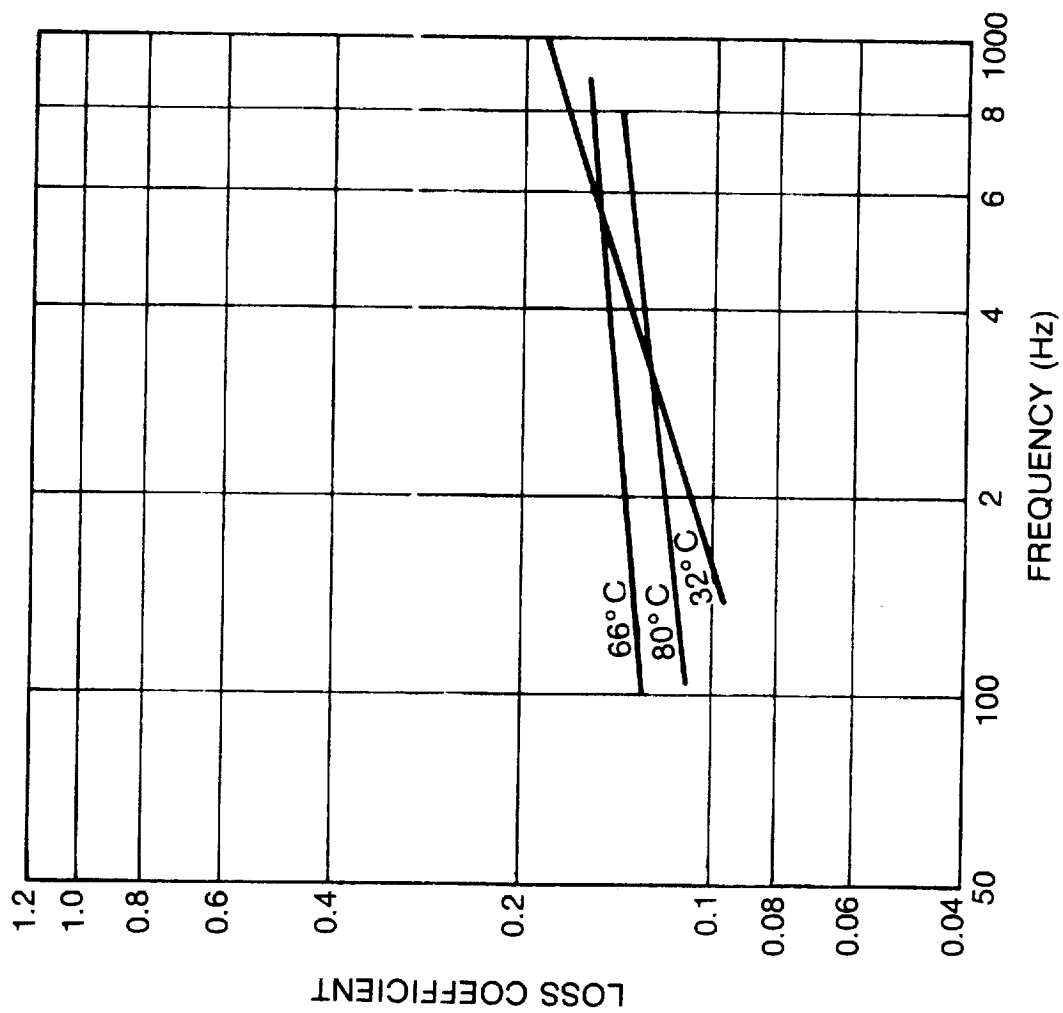
Fig. 82 Nitrile (Buna-N) Shear Specimen Data

175
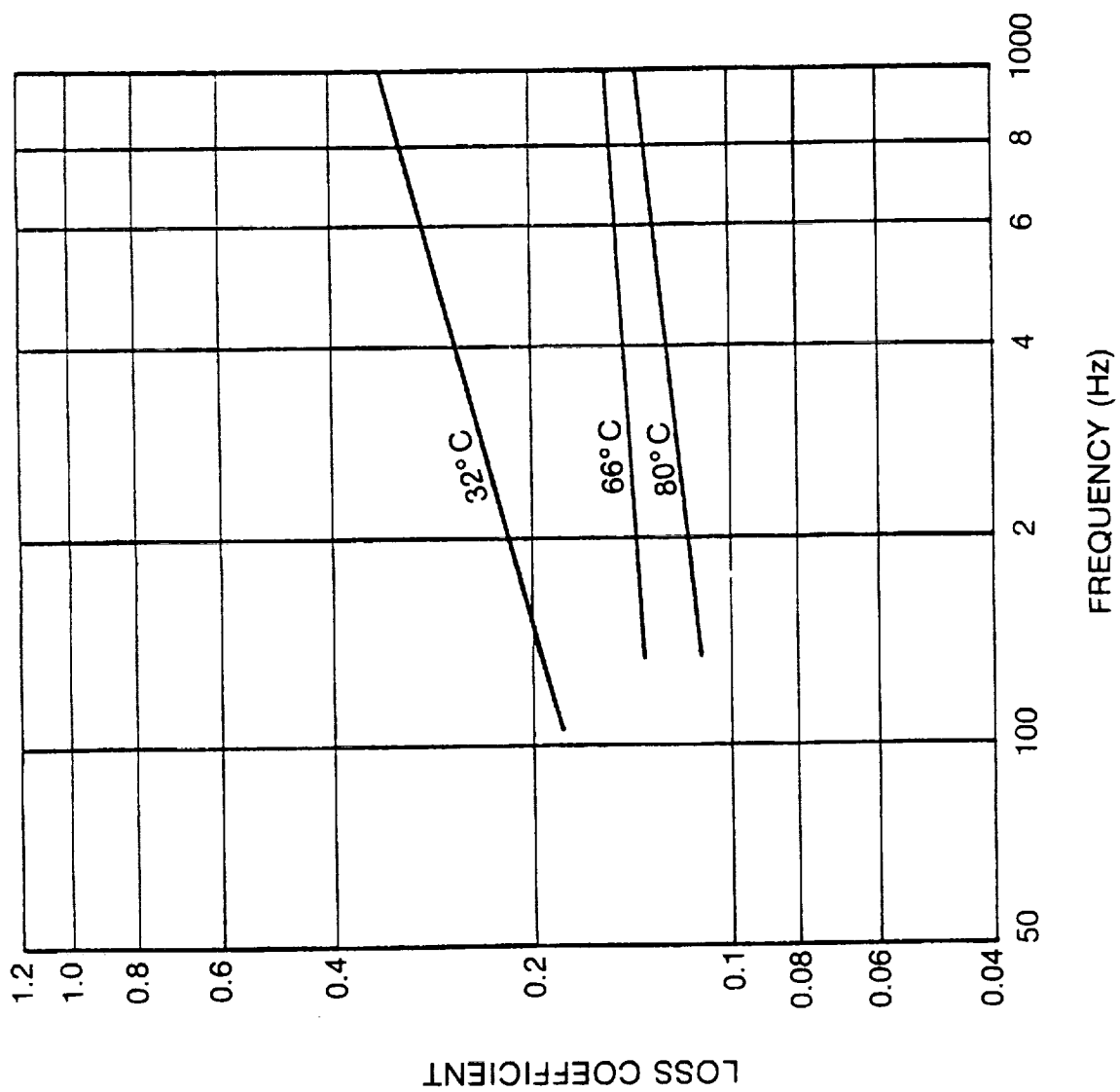
Fig. 83   Chloroprene (Neoprene) Shear Specimen Data

176
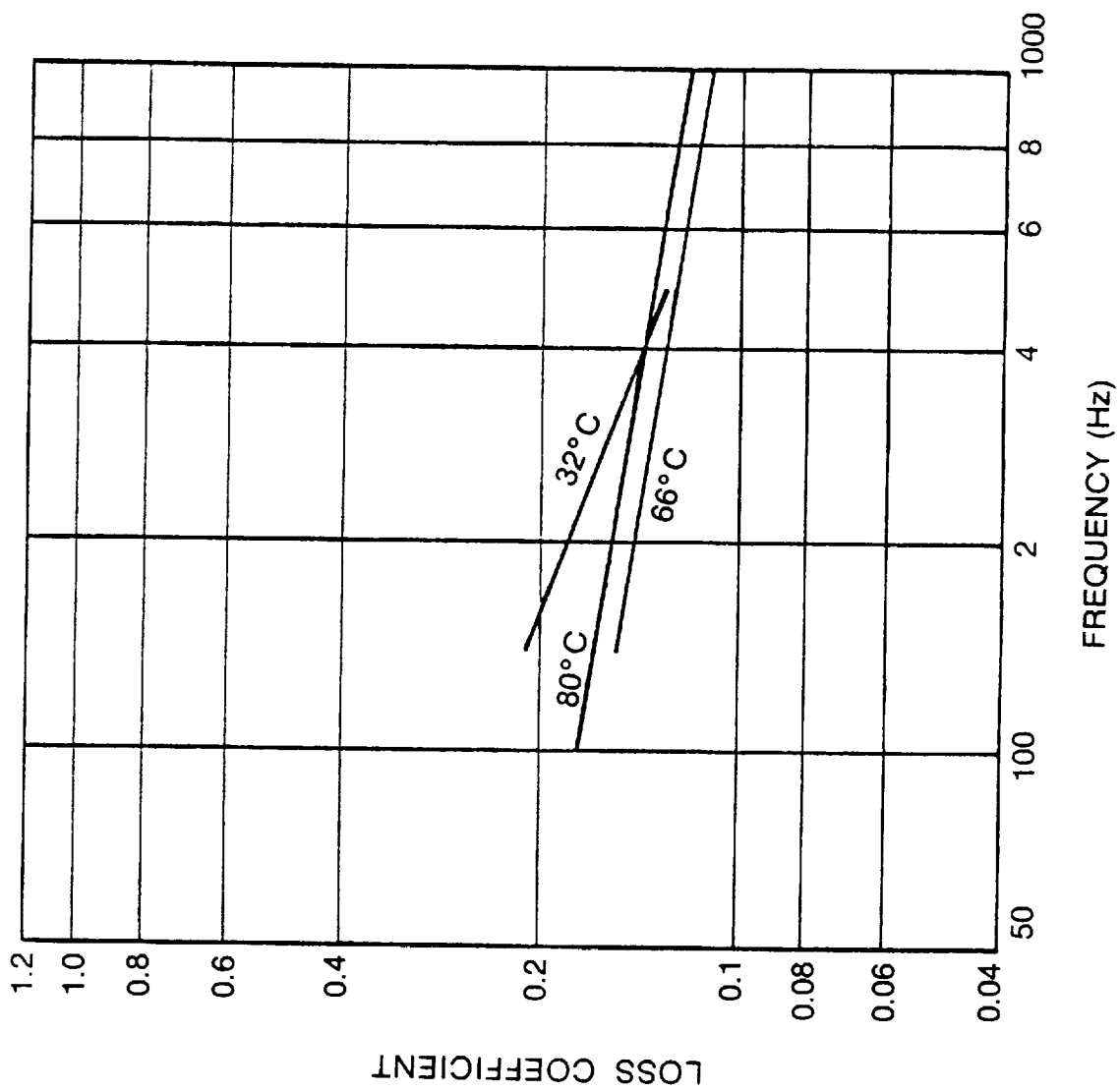
Fig. 84 EPDM Shear Specimen Data

177

$$G' = K_s' \left(\frac{t}{A}\right) \qquad (6-3)$$

$$G'' = K_s'' \left(\frac{t}{A}\right) \qquad (6-4)$$

where

G' = shear storage modulus - N/m^2

G'' = shear loss modulus - N/m^2

K_s' = stiffness of shear specimen (real part) - N/m

K_s'' = damping of shear specimen (imaginary part) - N/m

t = thickness of shear elements - m

A = total bonded area (one side only) of shear elements - m^2

Thus, the shear moduli (like the stiffness and damping) are functions of frequency, temperature and dynamic strain. The relationships between the shear moduli, the stiffness and the damping values of the compression specimen are much more complex.

$$K_c' = \frac{3G'A}{t} \; 1 + \beta' \; \left(\frac{D}{4t}\right)^2 \qquad (6-5)$$

$$K_c'' = \frac{3G''A}{t} \; 1 + \beta'' \; \left(\frac{D}{4t}\right)^2 \qquad (6-6)$$

where β' and β'' are shape factors (Section 4.0). These shape factors are also functions of frequency, temperature and dynamic strain. Thus, the logical procedure is to develop empirical relations for the shear moduli based on the results of the shear specimen tests and then to develop empirical relations for the shape factors, based on the results of the compression specimen tests together with the shear moduli relations.

Section 4.0 also showed that the effects of temperature and frequency on the shear moduli are inversely related and may be represented by a single independent variable. Reduced shear moduli are used, as given by

$$G_r' = G' \frac{T_c}{T} \qquad (6-7)$$

$$G_r'' = G'' \frac{T_c}{T} \qquad (6-8)$$

where G_r' and G_r'' are the reduced shear storage and loss moduli, T is the elastomer temperature and T_c is the characteristic temperature (^oK) for the particular elastomer materials.

Assuming that dynamic strain is the only other important independent variable and that the effects of strain and reduced frequency can be separated, the reduced shear moduli are given by

$$G_r' = f'\ (\alpha_T \omega)\ g'\ (\varepsilon) \tag{6-9}$$

$$G_r'' = f''\ (\alpha_T \omega)\ g''\ (\varepsilon) \tag{6-10}$$

where f and g represent unknown functions, $(\alpha_T \omega)$ is the reduced frequency, and ε is the dynamic strain. The coefficient α_T is determined from:

$$\log_{10} \alpha_T = \frac{C_1 (T - T_c)}{C_2 + (T - T_c)} \tag{6-11}$$

where the constants C_1 and C_2 depend on the elastomer material composition. In cases where high filler loadings are not present, C_1 and C_2 are essentially invariant with elastomer material and equal to -8.86 and 101.6, respectively [6.6].

The logarithms of the shear moduli have been shown to vary approximately linearly with the logarithm of the frequency. Extending this relationship to the reduced frequency, the logarithm of the functions f' and f" are linearly related to the logarithm of the reduced frequency. Thus, the functions themselves are of the form

$$f'(\alpha_T \omega) = a_1 (\alpha_T \omega)^{a_2} \tag{6-12}$$

$$f''(\alpha_T \omega) = b_1 (\alpha_T \omega)^{b_2} \tag{6-13}$$

where a and b are constants which are determined empirically for any particular elastomer material.

The logarithms of the shear moduli also have been shown to possess a quadratic relationship to the logarithm of the dynamic strain. Thus, the logarithms of the functions g' and g" take the form

$$\log_{10} g'(\varepsilon) = a_3 + a_4 \log_{10} \varepsilon + a_5 (\log_{10} \varepsilon)^2 \tag{6-14}$$

$$\log_{10} g''(\varepsilon) = b_3 + b_4 \log_{10} \varepsilon + b_5 (\log_{10} \varepsilon)^2 \tag{6-15}$$

to give

$$g'(\varepsilon) = a_3' \varepsilon^{a_4 + (a_5 \log_{10} \varepsilon)} \tag{6-16}$$

$$g''(\varepsilon) = b_3' \varepsilon^{b_4 + (B_5 \log_{10} \varepsilon)} \tag{6-17}$$

where a_3' and b_3' are the antilogarithms of a_3 and b_3, respectively, i.e.

$$a_3' = 10^{a_3}, \ b_3' = 10^{b_3}$$

Equations (6-12) through (6-15) may be substituted into equations (6-9) and (6-10) to give the reduced shear moduli as

$$G'_r = a_6 (\alpha_T \omega)^{a_2} \epsilon^{a_4} \epsilon^{(a_5 \log_{10} \epsilon)} \quad ; \quad a_6 = a_1 \bullet a'_3 \qquad (6\text{-}18)$$

$$G''_r = b_6 (\alpha_T \omega)^{b_2} \epsilon^{b_4} \epsilon^{(b_5 \log_{10} \epsilon)} \quad ; \quad b_6 = b_1 \bullet b'_3 \qquad (6\text{-}19)$$

The relations for the original shear moduli can be determined from equations (6-7) and (6-8) as

$$G' = a_6 (\frac{T}{T_c}) (\alpha_T \omega)^{a_2} \epsilon^{a_4} \epsilon^{(a_5 \log_{10} \epsilon)} \qquad (6\text{-}20)$$

$$G'' = b_6 (\frac{T}{T_c}) (\alpha_T \omega)^{b_2} \epsilon^{b_4} \epsilon^{(b_5 \log_{10} \epsilon)} \qquad (6\text{-}21)$$

Equations (6-20) and (6-21) can be made linear with respect to the unknown coefficients by taking the logarithm of both sides of these equations to give

$$\log_{10}(G' \frac{T_c}{T}) = a_7 + a_2 (\log_{10} \alpha_T + \log_{10} \omega) +$$

$$a_4 \log_{10} \epsilon + a_5 (\log_{10} \epsilon)^2; \quad a_7 = \log_{10} a_6 \qquad (6\text{-}22)$$

$$\log_{10}(G'' \frac{T_c}{T}) = b_7 + b_2 (\log_{10} \alpha_T + \log_{10} \omega) +$$

$$b_4 \log_{10} \epsilon + b_5 (\log_{10} \epsilon)^2; \quad b_7 = \log_{10} b_6 \qquad (6\text{-}23)$$

Thus, once a quantity of experimental data has been generated for a particular elastomer material, the unknown coefficients of equations (6-22) and (6-23) can be found using a standard statistical regression analysis [6.9]. This has been done using the results of the shear specimen tests for butadiene (Polybutadiene - BR), fluorocarbon (Viton - CFM), nitrile (Buna-N - NBR), EPDM and chloroprene (Neoprene - CR). The values of these coefficients determined for these four materials are presented (with 90% confidence intervals) in Table 17, along with the estimate for the standard deviation of the data. That is, there is a 90% likelihood that the true value of each of the coefficients falls within the corresponding confidence interval. Using these coefficients, the shear moduli log terms can be estimated for any general set of operating conditions (for one of these four materials) using equations (6-22) and (6-23).

A 90% confidence prediction interval can be assigned to each of these moduli as described in Appendix A to this Section. As an alternative to the above

Table 17

REGRESSION COEFFICIENTS FOR DYNAMIC SHEAR STORAGE AND
LOSS MODULI FROM DYNAMIC PROPERTY TESTS

Elastomer Material	a_7	a_2	a_4	a_5	Standard Deviation (for G' data)	b_7	b_2	b_4	b_5	Standard Deviation (for G" data)
butadiene (Polybutadiene - BR)	5.73 ±0.03	0.192 ±0.004	-0.746 ±0.030	-0.129 ±0.007	0.0266	5.48 ±0.06	0.242 ±0.008	-0.387 ±0.061	-0.0872 ±0.0142	0.0544
fluorocarbon (Viton - CFM)	6.31 ±0.04	0.149 ±0.005	-0.115 ±0.031	-0.0159 ±0.0057	0.0527	5.31 ±0.05	0.389 ±0.006	-0.135 ±0.040	-0.179 ±0.0074	0.0676
nitrile (Buna-N - NBR)	6.19 ±0.02	0.124 ±0.002	-0.148 ±0.017	-0.0209 ±0.0035	0.0211	5.53 ±0.07	0.290 ±0.007	0*	0*	0.0680
chloroprene (Neoprene - CR)	6.18 ±0.01	0.0911 ±0041	-0.273 ±0.012	-0.0424 ±0.0026	0.0103	5.58 ±0.04	0.197 ±0.012	-0.132 ±0.037	-0.0289 ±0.0079	0.0314
EPDM	5.65 ±0.04	0.141 ±0.005	-0.838 ±0.034	-0.137 ±0.007	0.0329	5.78 ±0.07	0.154 ±0.009	-0.223 ±0.060	-0.0553 ±0.0128	0.0583

* Not significant at the 0.1 level.

181

equations, the charts in Figures 85 through 94 may be used for predicting
the values of the shear storage and loss moduli for the five materials
tested. For example, using the illustration in Appendix A of butadiene
(Polybutadiene - BR) at 60°C and 400 Hz, with a dynamic strain of 0.01,
gives $\alpha_T \omega$ equal to 1.9×10^{-2}. Then, from Figures 85 and 86, the reduced
moduli are 5.5×10^6 and 9.5×10^5 N/m^2 for G'_r and G''_r, respectively. Multi-
plying by T/T_c (1.242) gives 6.8×10^6 and 1.2×10^6 for G' and G",
respectively. These values compare favorably with the corresponding nominal
values obtained directly from the equations in Appendix A.

For the butadiene (Polybutadiene - BR) samples, the filler loading was found
to be so high that the generally used values for C_1 and C_2 in equation (6-11)
were not adequate and an interactive procedure was used to determine these
values, as well as the value for T_c [6.6]. The filler loading was much
lower for the remainder of the materials tested and the generally used values
for C_1 and C_2 were found to be adequate. The values for T_c for these materials
were estimated from the values for T_g in Table 16. The appropriate values for
C_1, C_2 and T_c are given in Table 18 for each of the elastomer materials tested.

Given the relations for the shear modulus, as specified above, equations (6-5)
and (6-6) can be solved for the shape factors β' and β'' to give

$$\beta' = \left[\frac{K_c' t}{3G'A} - 1 \right] \left(\frac{4t}{D}\right)^2 \qquad (6\text{-}24)$$

$$\beta'' = \left[\frac{K_c'' t}{3G'A} - 1 \right] \left(\frac{4t}{D}\right)^2 \qquad (6\text{-}25)$$

Then, using the results of compression specimen tests (such as those for
butadiene (Polybutadiene - BR)), relations for β' and β'' as functions of
frequency, temperature and strain can be found using statistical regression
analyses in the manner described above for the shear moduli. The relationships
are again logarithmic and are given by

$$\log_{10} \beta' = d_1 + d_2 \log_{10} \omega + d_3 \log_{10} \left(\frac{T}{Tc}\right) + d_4 \log_{10} \varepsilon \qquad (6\text{-}26)$$

$$\log_{10} \beta'' = e_1 + e_2 \log_{10} \omega + e_3 \log_{10} \left(\frac{T}{Tc}\right) + e_4 \log_{10} \varepsilon \qquad (6\text{-}27)$$

The values of the coefficients in equations (6-26) and (6-27) for butadiene
(Polybutadiene - BR) are given in Table 19, along with the values for
standard deviation. Confidence prediction intervals can be calculated for β'
and β'' as described in Appendix A. These equations may also be used to con-
struct design charts, such as those in Figures 95 through 98. For example,
using the conditions in Appendix A for butadiene (Polybutadiene - BR)
(T = 60 C, ω = 400 Hz, ε = 0.01), Figures 95 and 97 gives values of β' and β''
as 3.2 and 3.9, respectively. These values compare very favorably to the
corresponding nominal values from Appendix A.

Fig. 85 Butadiene (Polybutadiene) Design Curves

STRAIN (ϵ)

REDUCED SHEAR STORAGE MODULUS (G', T_c/T) N/m²

$\alpha_T\omega = 10^4$

$\alpha_T\omega = 10^3$

$\alpha_T\omega = 10^2$

$\alpha_T\omega = 10$

$\alpha_T\omega = 1$

$\alpha_T\omega = 10^{-2}$

$\alpha_T\omega = 10^{-3}$

183
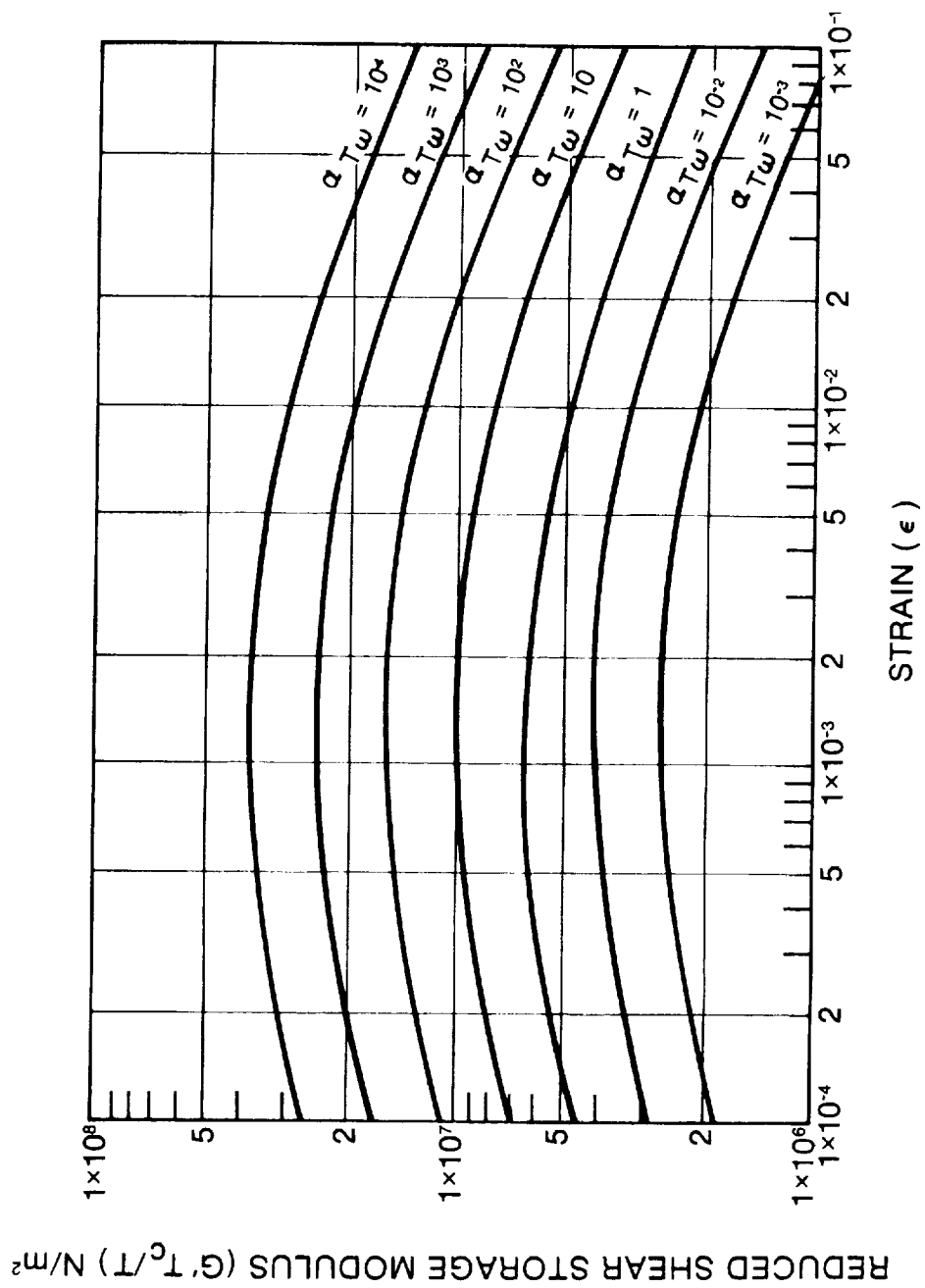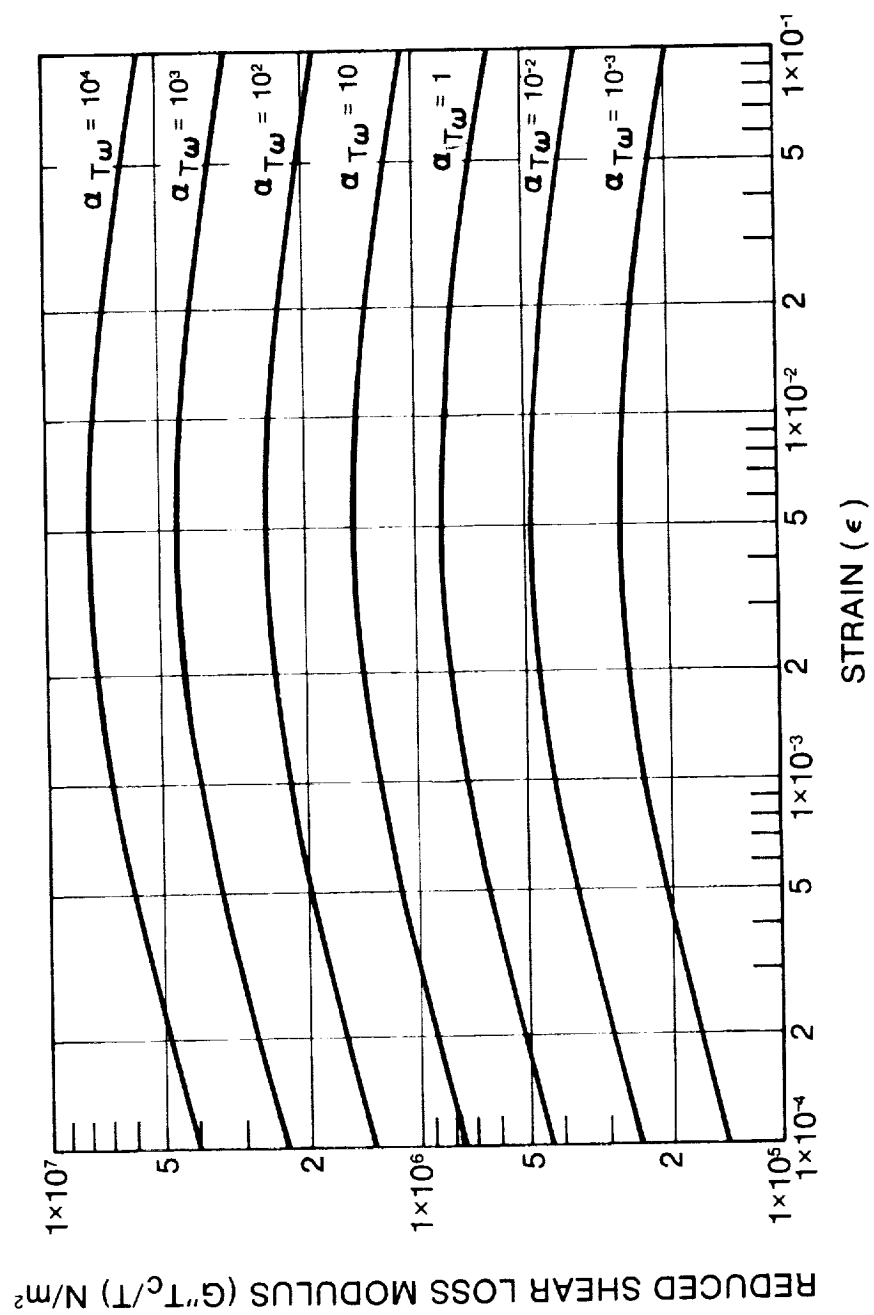
Fig. 86 Butadiene (Polybutadiene) Design Curves

Fig. 87 Fluorocarbon (Viton-70) Design Curves

STRAIN (ϵ)

REDUCED SHEAR STORAGE MODULUS ($G'T_o/T$) N/m²

$\alpha_T \omega = 10^4$

$\alpha_T \omega = 10^3$

$\alpha_T \omega = 10^2$

$\alpha_T \omega = 10$

$\alpha_T \omega = 1$

$\alpha_T \omega = 10^{-2}$

$\alpha_T \omega = 10^{-3}$

185
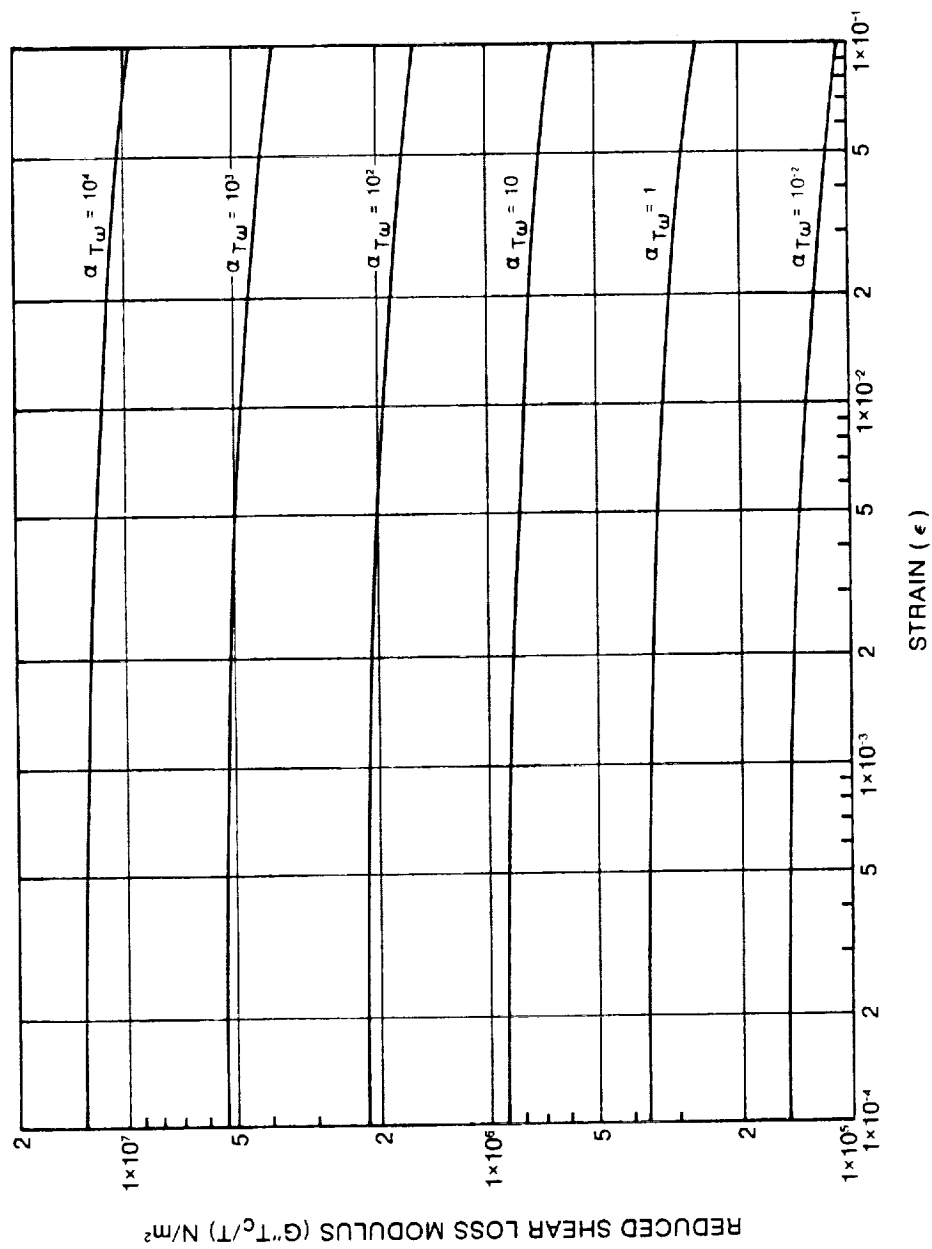
Fig. 88 Fluorocarbon (Viton-70) Design Curves

STRAIN (ϵ)

REDUCED SHEAR LOSS MODULUS ($G''T_c/T$) N/m²

$\alpha_T\omega = 10^4$

$\alpha_T\omega = 10^3$

$\alpha_T\omega = 10^2$

$\alpha_T\omega = 10$

$\alpha_T\omega = 1$

$\alpha_T\omega = 10^{-2}$

Fig. 89 Nitrile (Buna-N) Design Curves

187
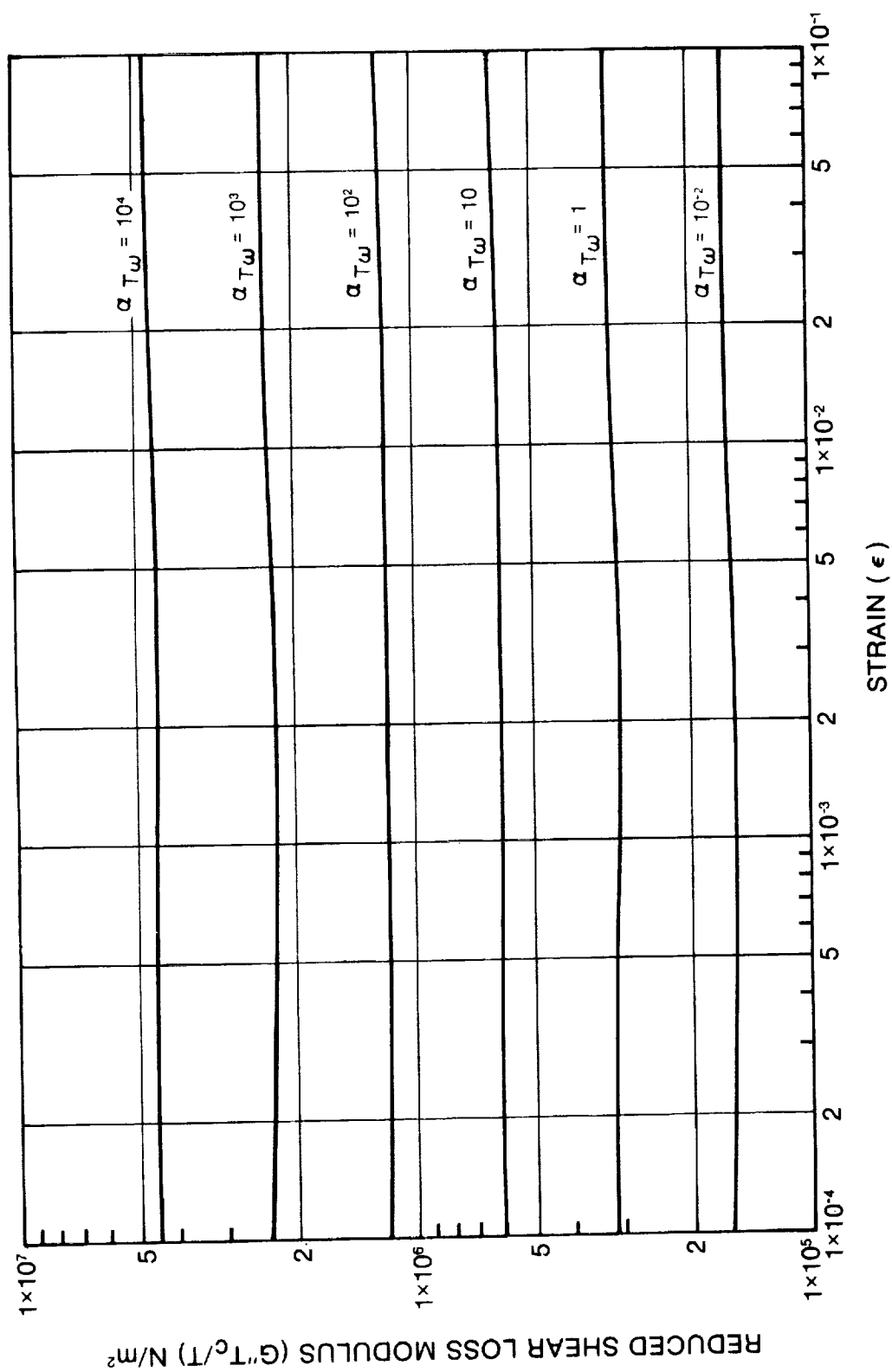
Fig. 90 Nitrile (Buna-90) Design Curves

Fig. 91 EPDM Design Curves

189

STRAIN (ϵ)

REDUCED SHEAR LOSS MODULUS ($G''T_o/T$) N/m^2

$\alpha_T\omega = 10^4$

$\alpha_T\omega = 10^3$

$\alpha_T\omega = 10^2$

$\alpha_T\omega = 10$

$\alpha_T\omega = 1$

$\alpha_T\omega = 10^{-2}$

$\alpha_T\omega = 10^{-3}$
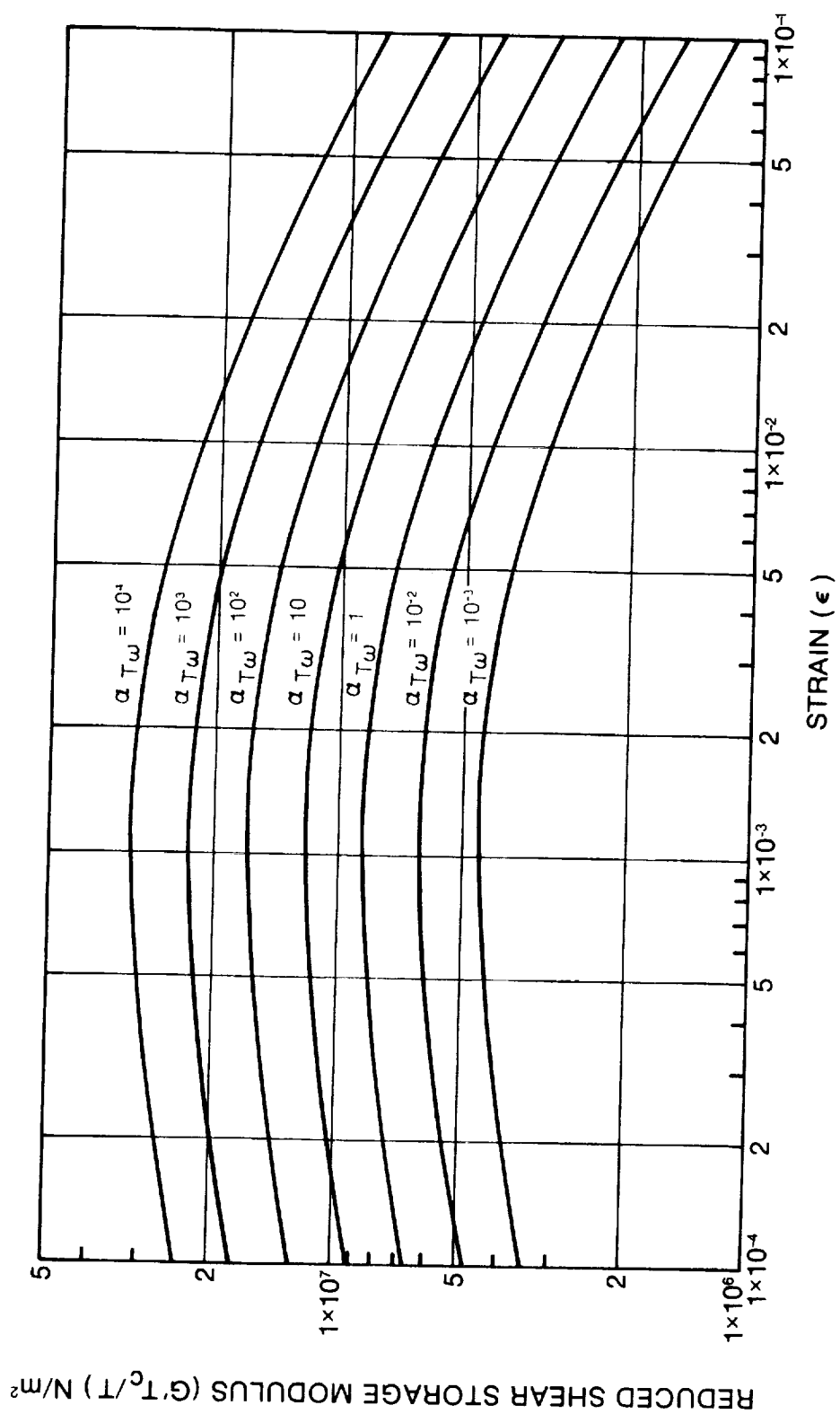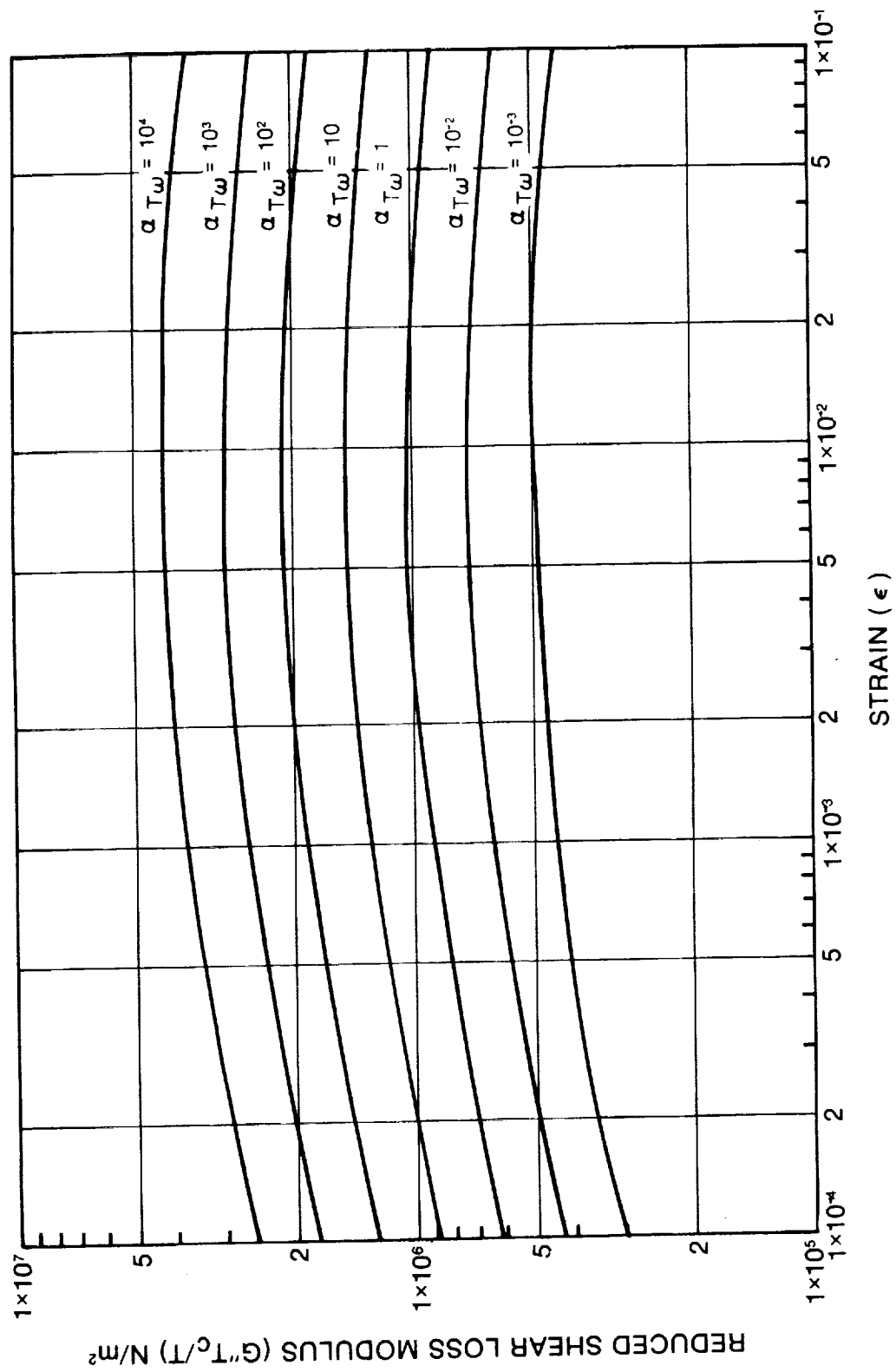
Fig. 92 EPDM Design Curves

190

Fig. 93 Chloroprene (Neoprene) Design Curves

REDUCED SHEAR STORAGE MODULUS $(G'T_c/T)$ N/m²

STRAIN (ϵ)

$a_T\omega = 10^4$
$a_T\omega = 10^3$
$a_T\omega = 10^2$
$a_T\omega = 10$
$a_T\omega = 1$
$a_T\omega = 10^{-2}$
$a_T\omega = 10^{-3}$

191
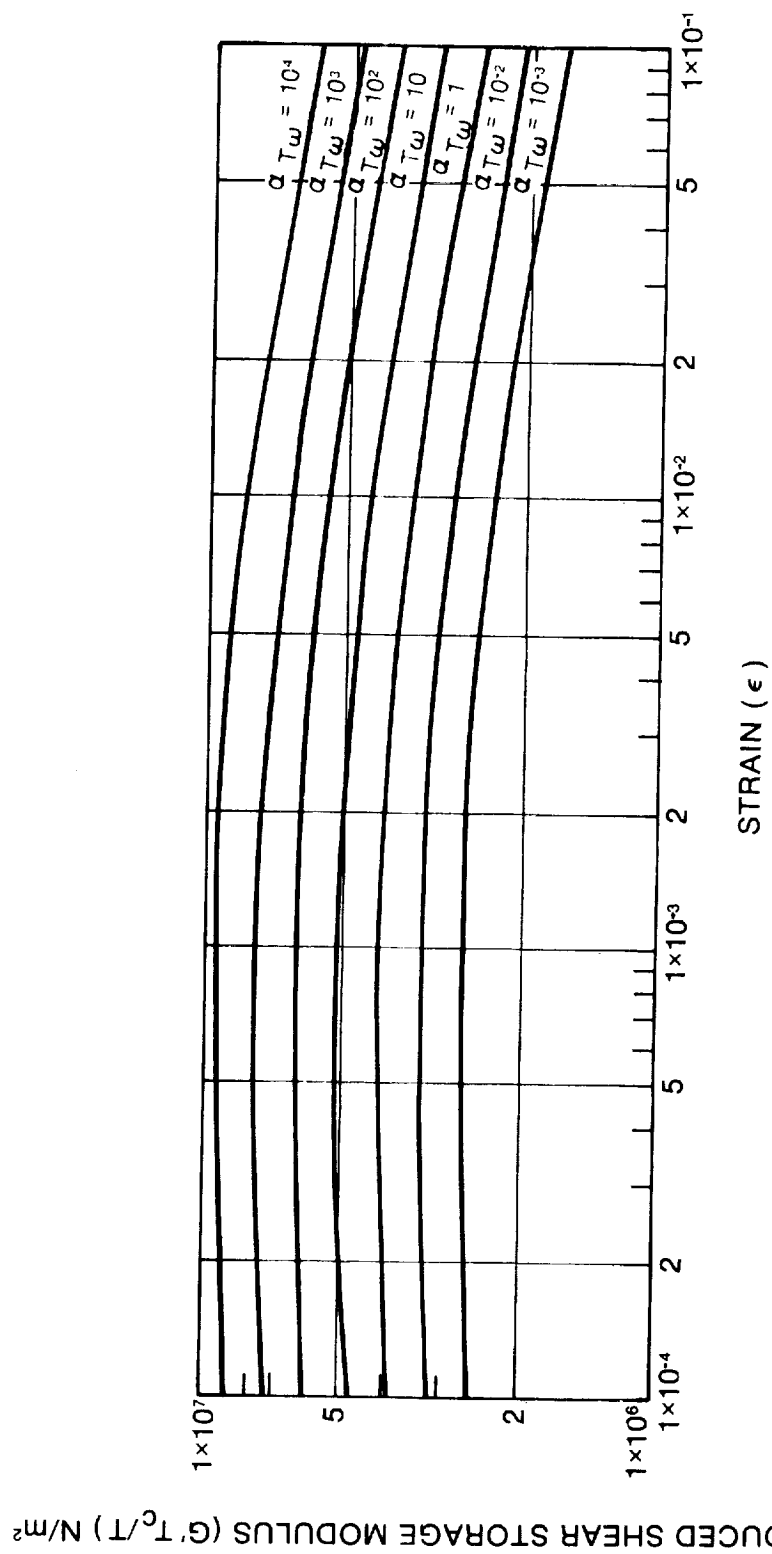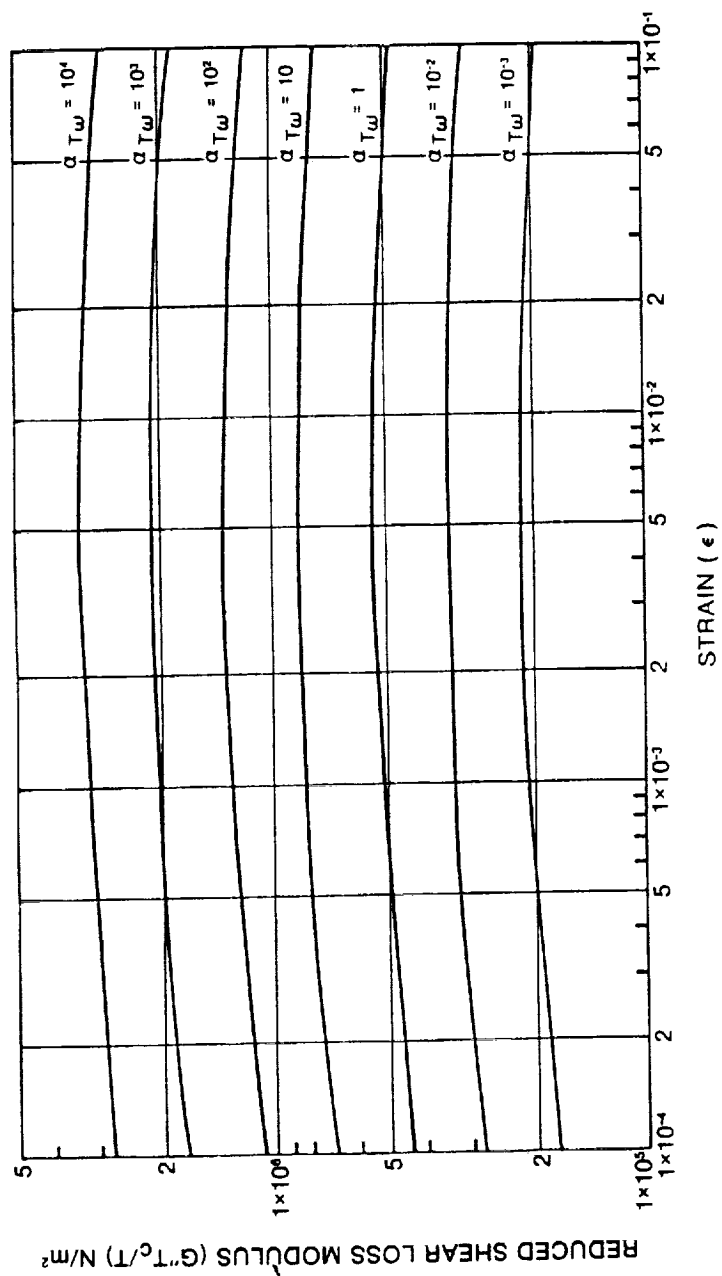
Fig. 94   Chloroprene (Neoprene) Design Curves

192

Table 18

VALUES FOR C_1, C_2 AND CHARACTERISTIC TEMPERATURE (T_c)

FOR THE DYNAMIC TEST MATERIALS $[6.6 \quad 6.7]$

Elastomer Material	C_1	C_2	T_c (°K)
butadiene (Polybutadiene - BR)	-7.48*	90.7*	268.1*
fluorocarbon (Viton - CFM)	-8.86	101.6	306**
nitrile (Buna-N - NBR)	-8.86	101.6	293**
chloroprene (Neoprene - CR)	-8.86	101.6	272**
EPDM	-8.86	101.6	267**

* Determined by iterative approximation

** Estimated from transition temperature $(T_g + 50)$

Table 19

REGRESSION COEFFICIENTS FOR DYNAMIC STORAGE AND LOSS SHAPE FACTOR FROM POLYBUTADIENE COMPRESSION TESTS

Subscript	For Storage Shape Factor (d)	For Loss Shape Factor (e)
1	0.615 ± 0.175	0.884 ± 0.145
2	-0.142 ± 0.049	-0.180 ± 0.041
3	2.13 ± 0.32	1.29 ± 0.27
4	-0.0837 ± 0.0148	-0.101 ± 0.012
Standard Deviation S	0.0799	0.0662
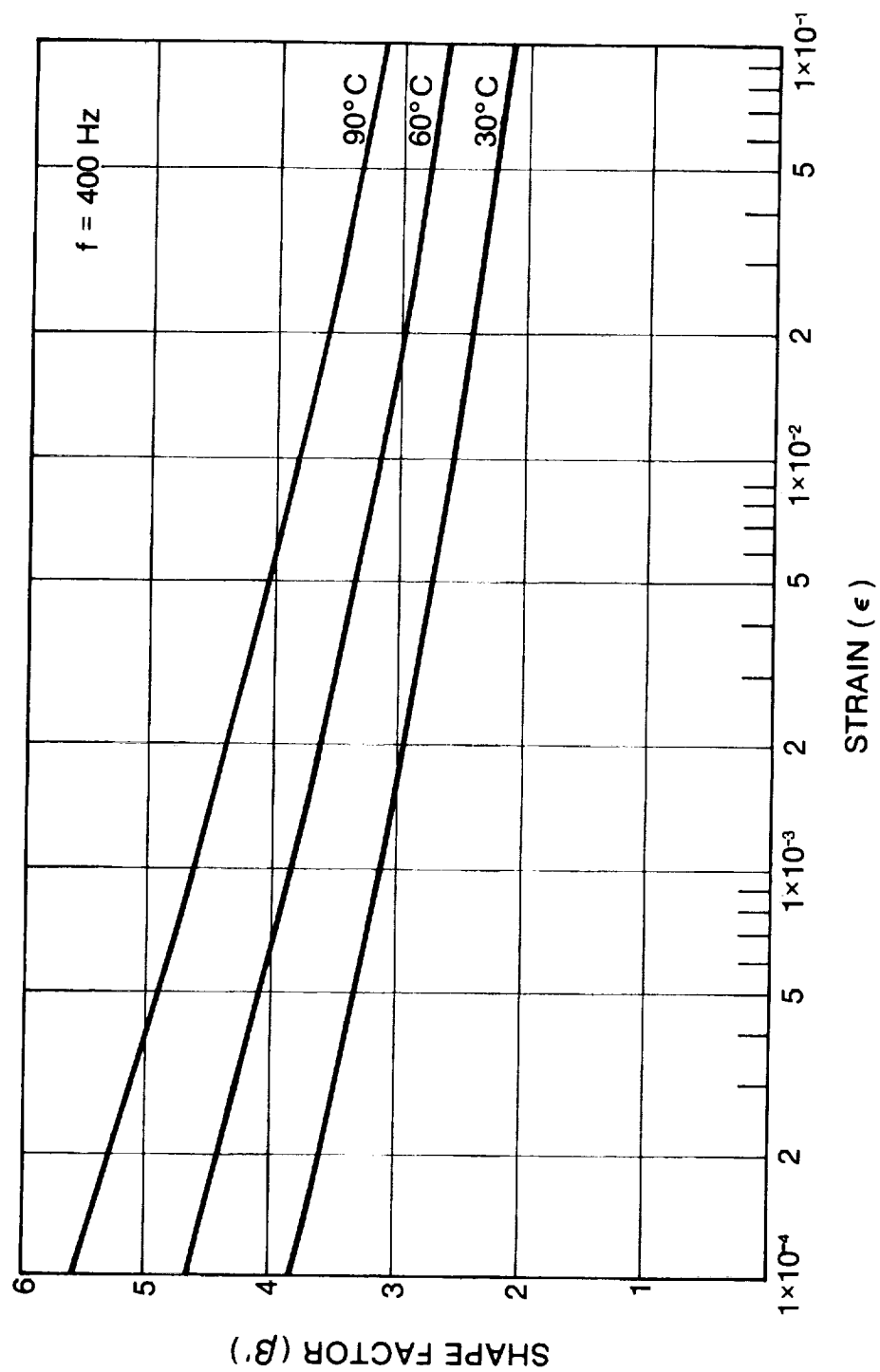
Fig. 95   Shape Factor vs Strain

195
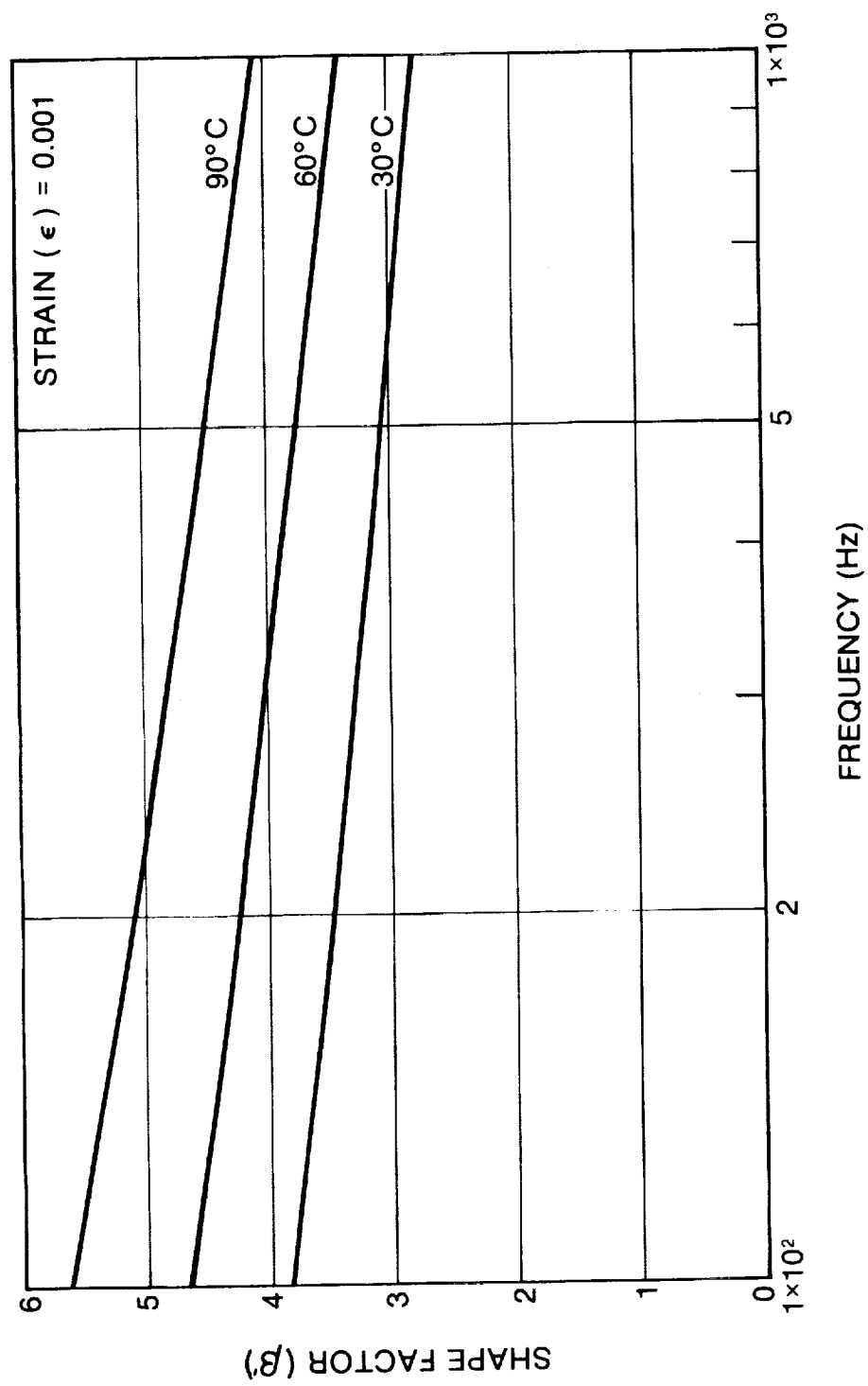
Fig. 96 Shape Factor vs Frequency
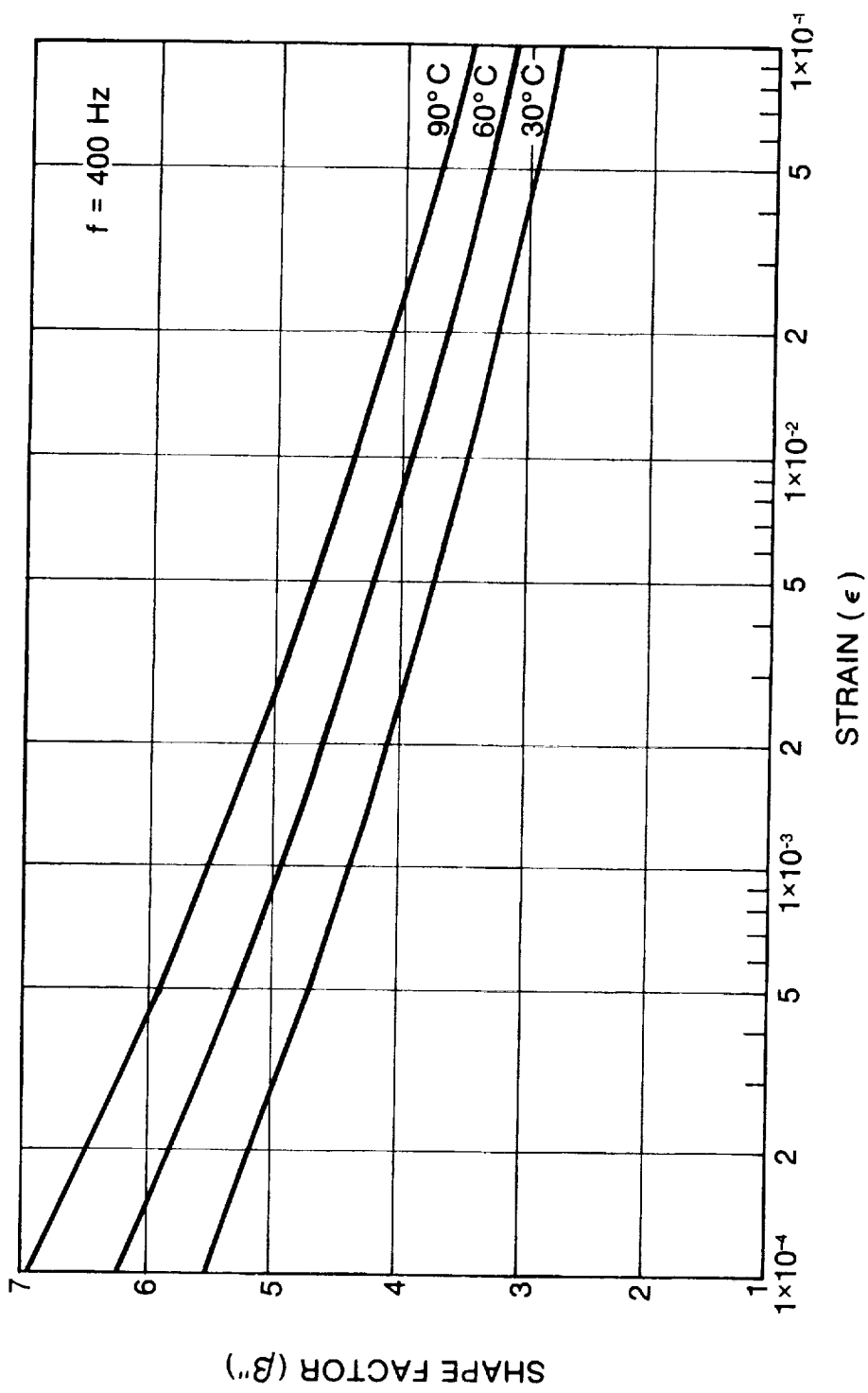
Fig. 97 Shape Factor vs Strain

197
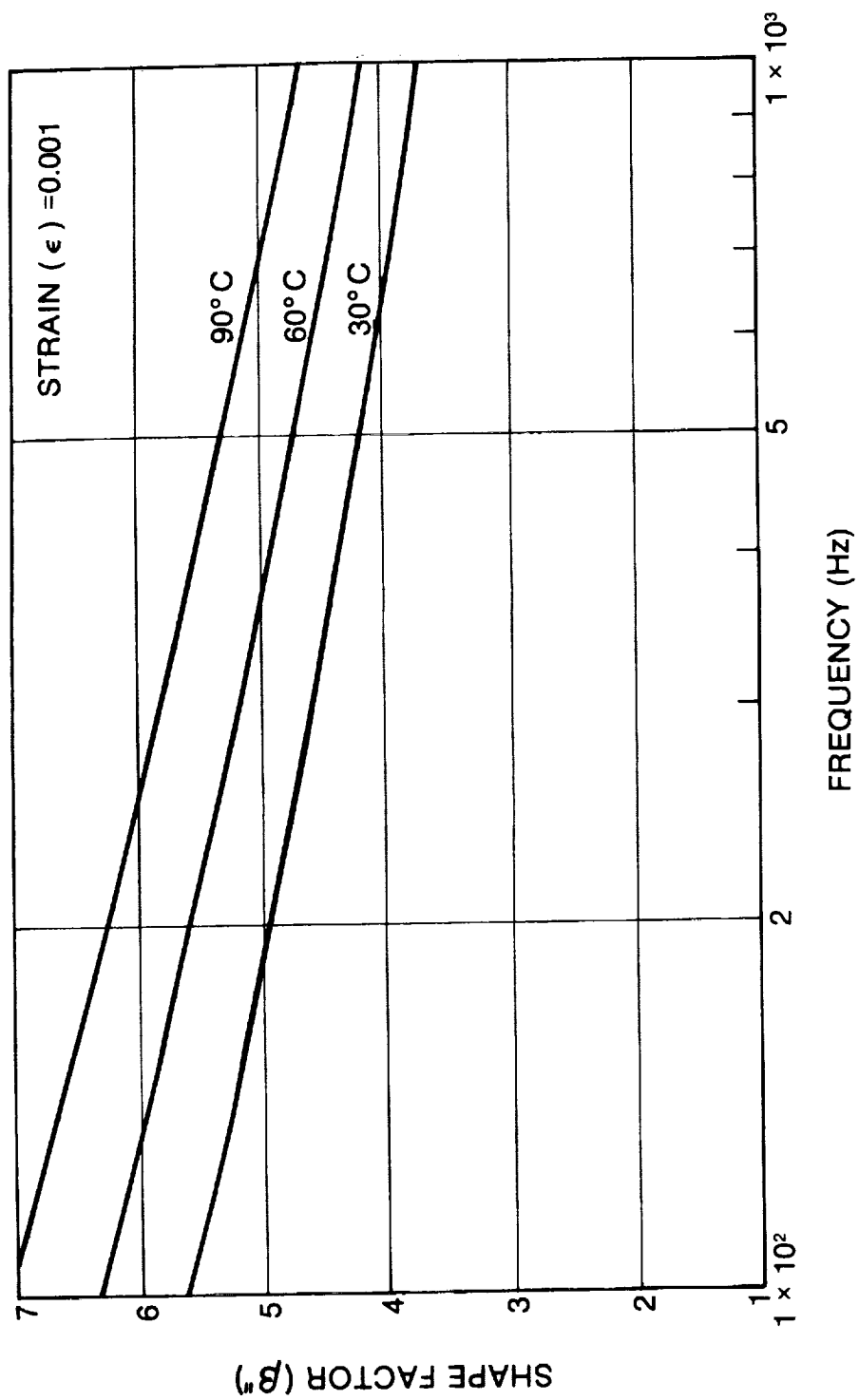
Fig. 98 Shape Factor vs Frequency

The determination of the dynamic characteristics of O-rings requires special consideration. O-rings geometry and resulting loading conditions generally represent a much more complex dynamic support structure than do the simpler shear or compression buttons. Accordingly, O-ring dynamic property testing requires that considerations of O-ring material, assembly pre-distortions (stretch on squeeze), preload, strain, temperature and frequency all of which may greatly influence the dynamic property data. However, as O-rings are often used as low cost dampers and consequently the results of these test are very meaningful. Such data has been provided in detail per Reference 6.10. The results are presented directly in terms of stiffness, damping and loss coefficient.

The test plan for O-rings was designed to provide maximum information for a minimum of test condition changes. With the large number of test parameters (7+ frequency), it was apparent that, unless an effort was made to hold the number of changes to a minimum, a very large test program would be required. To meet these constraints, a "parameter perturbation" approach was undertaken. Under this approach, a reference combination of all test parameters was defined and data for this reference combination was generated as a function of frequency; the reference condition is defined in Table 20. One single parameter was then varied about its reference value and data generated as a function of frequency for each variation. This parameter was then set back to its reference value and a second parameter varied about its reference value.

The variation was repeated for each parameter, in turn, according to the schedule of Table 21, for a total of nineteen tests.

This parameter perturbation test method was advantageous in that it returns a large amount of information from a small number of tests. Its disadvantage was that it does not reveal the interactions which result from varying more than one parameter at a time. Thus, the results of this series of tests should be regarded as baseline data from which major trends and influential parameters can be identified; the less significant parameters can be identified and eliminated from further tests in which interaction effects between parameters are investigated.

The test frequency range generally lies between 70 and 1,000 Hz. A plot of the test data for the nominal test condition is presented in Figure 99. Actual test data points are shown; and a line which gives the minimum RMS deviation between test data and the fitted line is drawn through the full set of data points. All test results are for a pair of O-rings, as tested, since this is the most likely configuration to be encountered in practice.

Significant characteristics of most of the data are a strong increase in stiffness with frequency (typically by a factor of 2.5) and a high value of loss coefficient (in the range of 0.7 to 1.1). Of further interest is the fact that the 1,000-Hz stiffness is over 9 times the static stiffness of a pair of O-rings (static stiffness measurement is discussed in the following paragraphs). These characteristics are indicative of an elastomer in its transition region [6.11] and are consistent with others measured for fluorocarbon (Viton - CFM) [6.12].

Table 20

REFERENCE OR NOMINAL TEST CONDITION

Material. . . .	Viton-70	Stretch	5 percent
Temperature . .	25°C	X-Section Diameter. .	1/8" Nominal (0.353 cm**)
Amplitude . . .	7.62×10^{-6} m	Groove Width*	135 percent
Squeeze	15 percent	O-Ring OD	2 1/2" Nominal (6.35 cm)

*   Based on actual X-Section diameter

**   Measured Average

Table 21

PERTURBATION PARAMETER VALUES

Material	nitrile (Buna-N – NBR)		fluorocarbon (Viton-90 – CFM)	
Temperature	$38^{\circ}C$	$66^{\circ}C$	$149^{\circ}C$	$216^{\circ}C$
Amplitude	2.54×10^{-5} m		1.27×10^{-4} m	
Squeeze	5%	10%	20%	30%
Stretch	0%	10%		
X-Section Diameter	1/16" nominal (1.778×10^{-3} m) 3/16" nominal (5.334×10^{-3} m)			
Groove Width	115%	150% of actual Cross-Section diameter		

CROSS-SECTION
DIAMETER: ⅛ in. (0.353 cm)
STRETCH: 5%
GROOVE WIDTH: 135%

MATERIAL: FLUOROCARBON
                 (VITON-70)
TEMPERATURE: 25°C
AMPLITUDE: 7.62 × 10⁻⁴ m
SQUEEZE: 15%
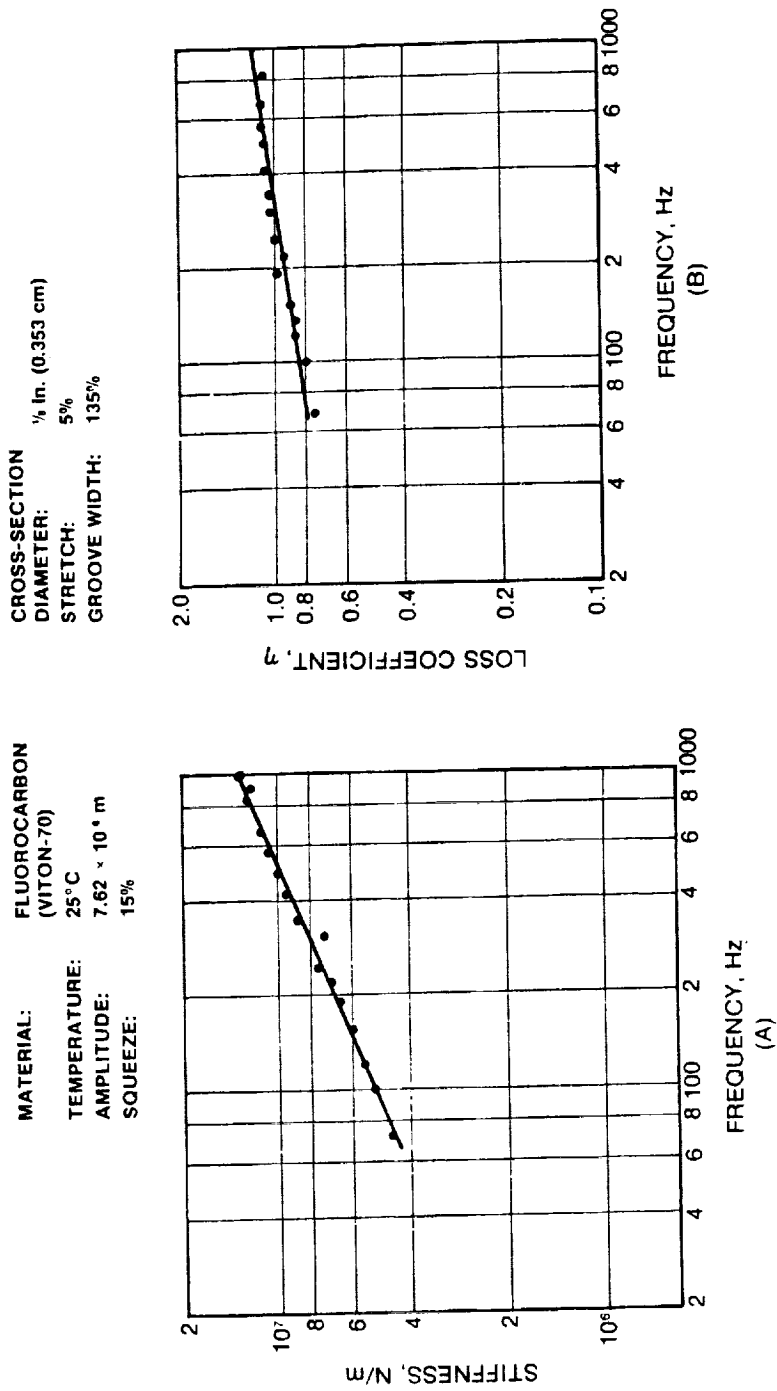
Fig. 99 O-Ring Test Results: Nominal Case

202

In addition to the dynamic stiffness tests described above, the effect of a static load upon O-ring deflection was investigated. Even under a static load the visco-elastic nature of the elastomer leads to time-dependent deflection; see Figure 100 where the deflection resulting from a sudden load application is plotted as a function of time. It is apparent that the deflection continuously increases with time and doubles in the elapsed time between 3 seconds and 300 seconds. Even after 7 minutes, the further deflection which occurs in the period between the 7 minutes and 8 minutes amounts to over 1% of the deflection at that point in time.

In order to obtain some meaningful comparison between the elastomers, the deflection occurring 6 minutes after load application has been plotted against static load, and the results are presented in Figure 101. These curves illustrate some softening of the O-rings as the static load is increased; for example, the 6 minute deflection of a nitrile (Buna-N – NBR) ring under 200 Newtons is five times the 50 Newtons for the same time. It is seen that nitrile (Buna-N – NBR) and fluorocarbon (Viton 70 – CFM), which are both 70 durometer materials, have very similar static stiffness. The curves further show that the 90 durometer fluorocarbon (Viton – CFM) has close to 4 times the stiffness of the 70 durometer materials.

Table 22 provides a summary of effective static stiffness values (load/deflection) for the three materials under loads of 50, 100, and 200 Newtons. As previously discussed, the static stiffnesses are much lower than the dynamic stiffnesses. Table 23 provides the ratios of dynamic stiffness at 100 Hz and 1,000 Hz to the effective static stiffness under 200 Newtons for the three different materials, and it may be seen that these ratios range from over 4 to almost 11. Ratios such as these can be used (when better data is not available) to estimate the dynamic stiffness of an elastomer specimen based on its static stiffness. A good estimate of the static shear modulus of an elastomer material can be made from hardness (durometer or Shore A ®) as shown in Figure 64 [6.4]. The static stiffness of the element can then be calculated from the geometry.

Inspection of the test data plots for individual test conditions revealed that certain parameters had a significant effect upon O-ring dynamic characteristics and that other parameters had a less pronounced effect. To bring these trends more sharply into focus, plots have been prepared in which power law curves for each of the seven parameter perturbation ranges are presented on a single plot. These "trend summary" plots are presented in Figures 102 through 108 and clearly reveal the important effects of the governing parameters. The effect of all seven parameters are discussed in the following section.

6.3 Effects of Specific Parameters

6.3.1 Material

The selection of material and durometer value have a pronounced effect on the dynamic performance achieved from an O-ring flexible support, as shown in Figure 102. Fluorocarbon (Viton 70 – CFM) and nitrile (Buna-N – NBR) have a similar average dynamic stiffness of 6×10^6 N/m (39,000 lb/inch) but that

PRELOAD — 3 lb 7.28 oz (1.57 kg)
LOAD — 39 lb 12 oz (STATIC) (18.05 kg)
⅛" FLUOROCARBON (VITON-90) #44 & #47
TEMPERATURE 74° F (23° C)

50MV

.010" = 1 VOLT

50 sec
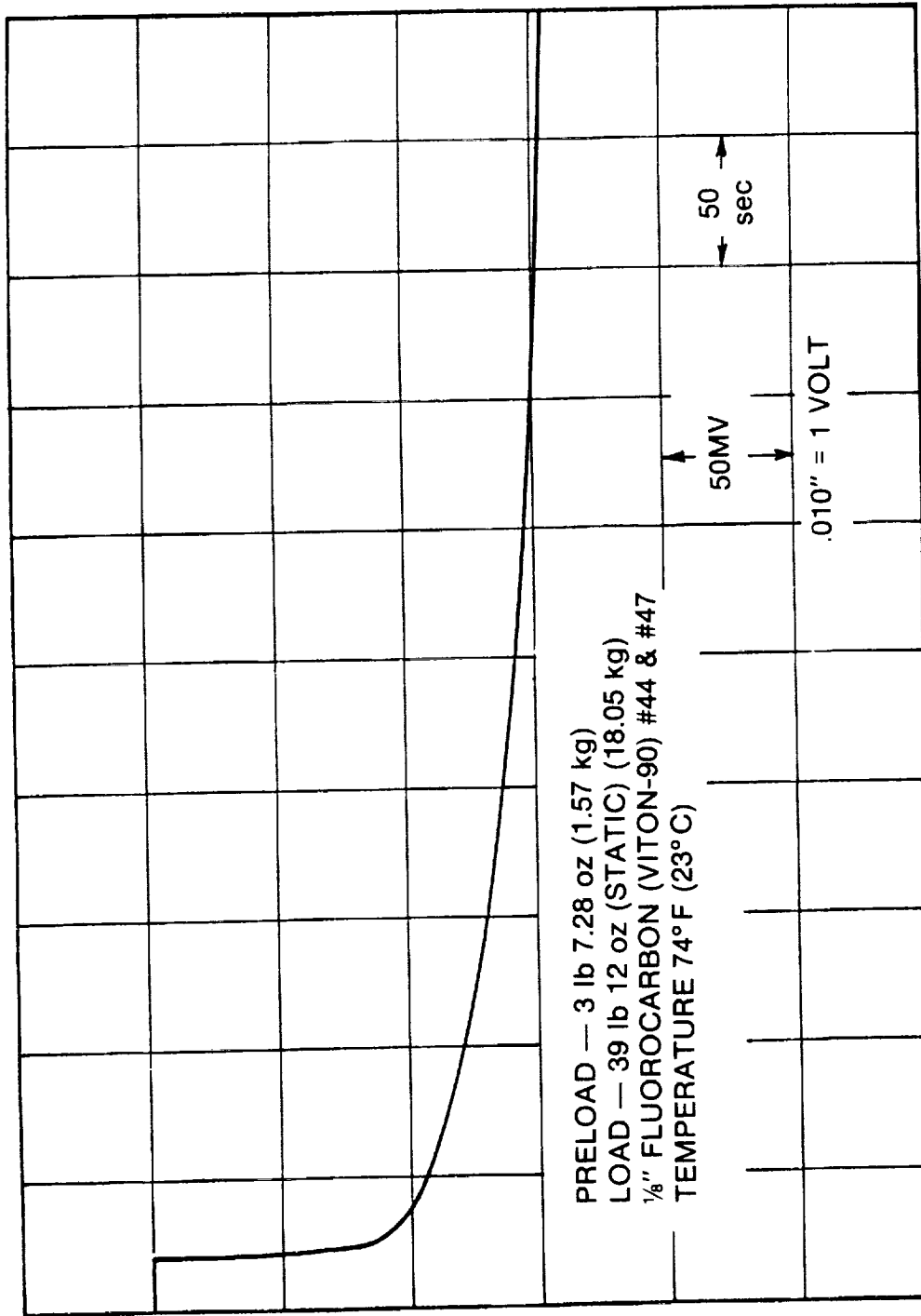
Fig. 100   Typical Trace of Deflection vs Time Under Static Load for O-Ring Tests
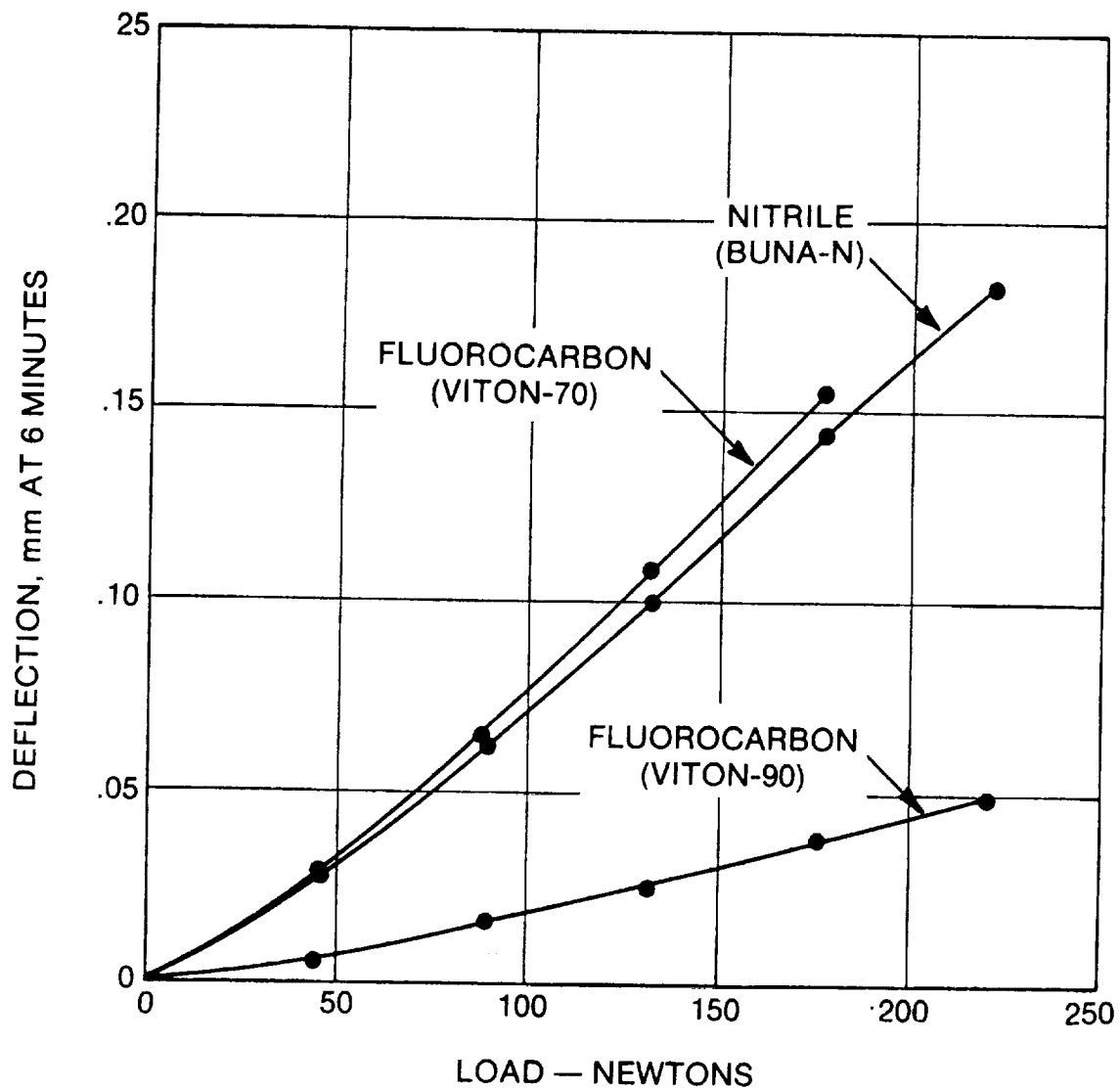
Fig. 101 "Static" Deflection as a Function of Applied Load for O-Ring Tests

Table 22

STATIC STIFFNESS SUMMARY FOR O-RING TESTS

Load, Newtons	fluorocarbon (Viton-70 - CFM)	Effective Stiffness, N/m nitrile (Buna-N - NBR)	fluorocarbon (Viton-90 - CFM)
50	1.52×10^6	1.52×10^6	7.69×10^6
100	1.29×10^6	1.38×10^6	5.71×10^6
200	1.14×10^6	1.21×10^6	4.55×10^6

Table 23

RATIO OF DYNAMIC STIFFNESS TO EFFECTIVE STATIC STIFFNESS UNDER 200 NEWTONS FOR O-RING TESTS

Material	Stiffness Ratio 100 Hz	1000 Hz
fluorocarbon (Viton 70 - CFM)	4.35	10.89
nitrile (Buna-N - NBR)	4.91	6.98
fluorocarbon (Viton-90 - CFM)	4.73	7.69

206
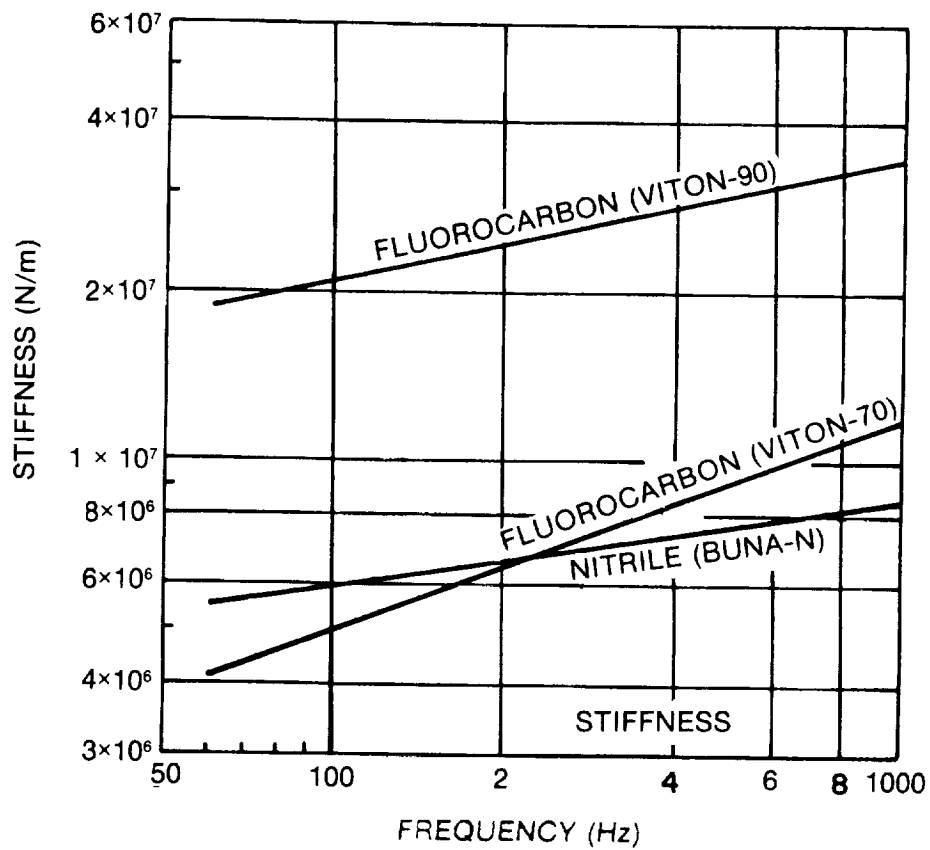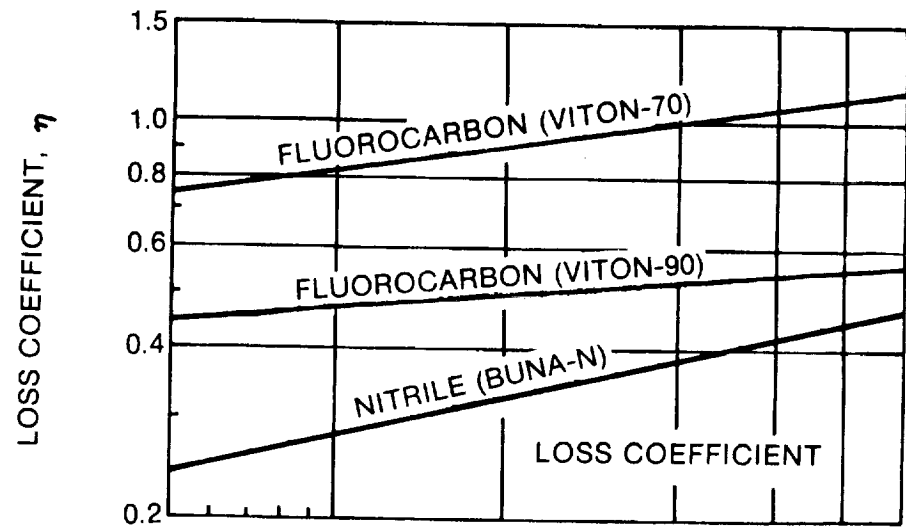
Fig. 102   Trend Summary: The Effect of Material on Stiffness
and Loss Coefficient for O-Ring Dampers

207
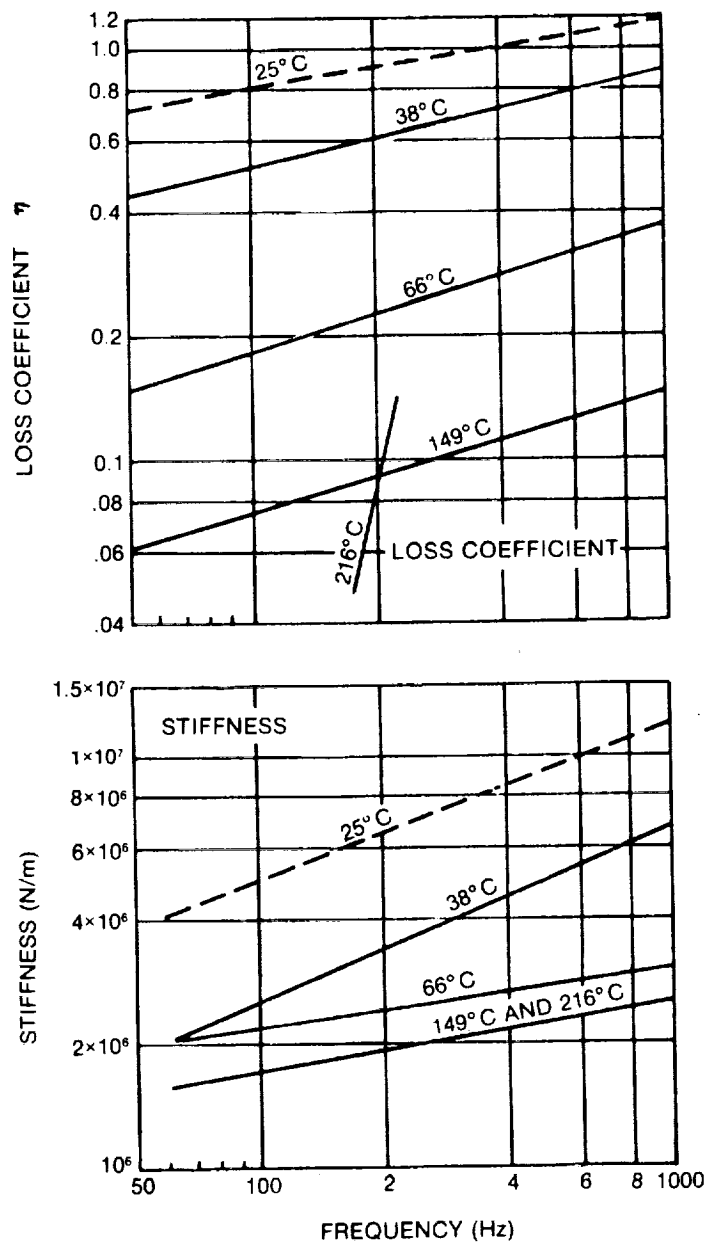
Fig. 103   Trend Summary: The Effect of Temperature on Stiffness and Loss Coefficient for O-Ring Dampers

208
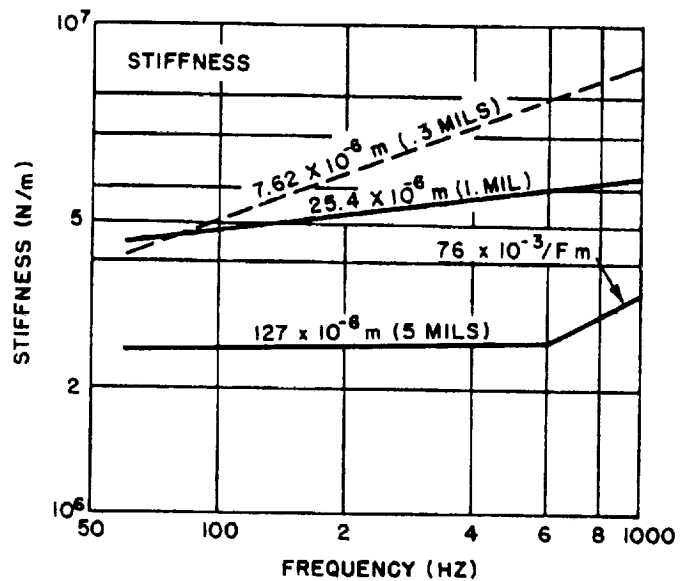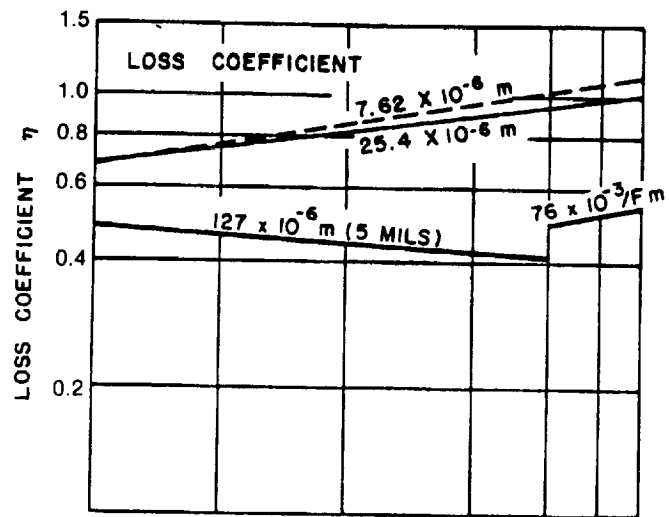
Fig. 104 Trend Summary: The Effect of Amplitude on Stiffness and Loss Coefficient for O-Ring Dampers
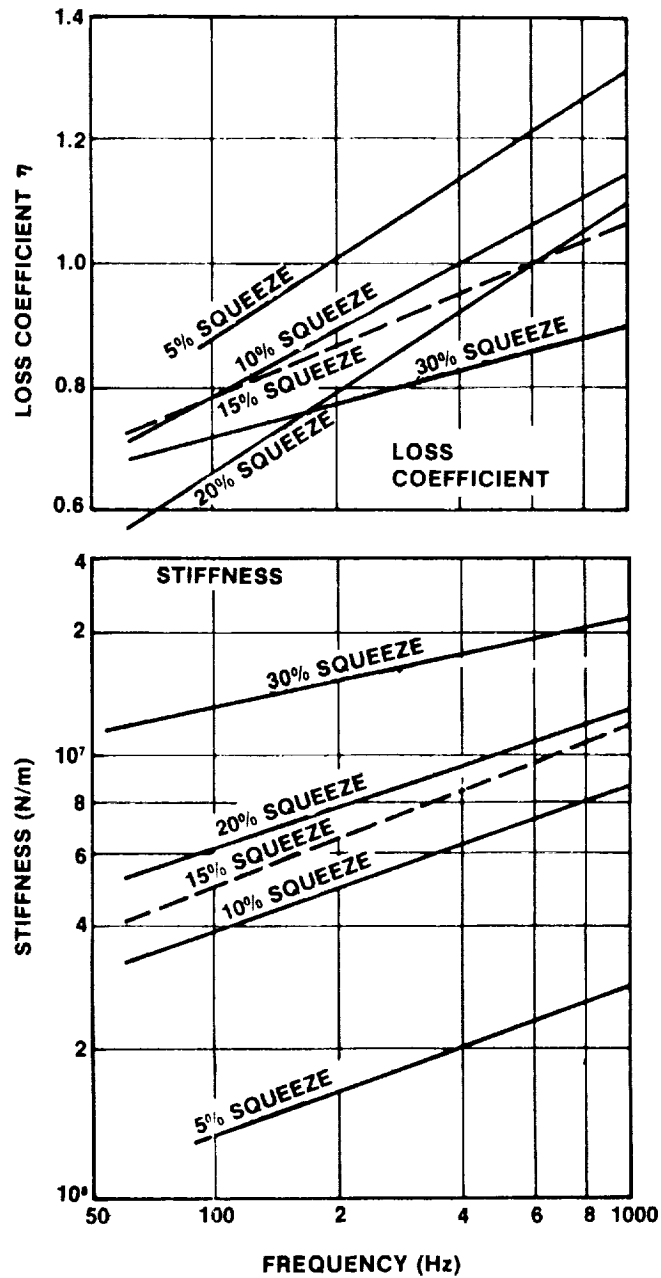
Fig. 105 Trend Summary: The Effect of Squeeze on Stiffness and Loss Coefficient for O-Ring Dampers

210
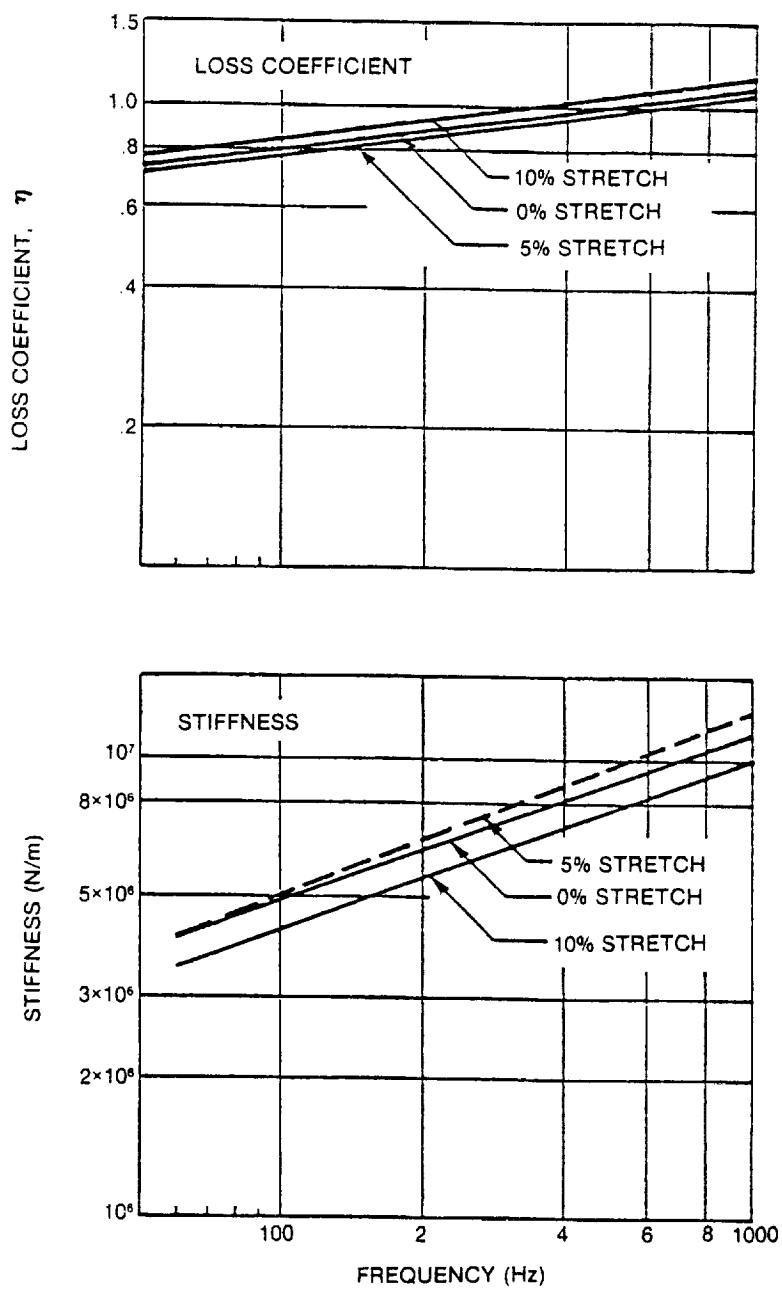
Fig. 106 Trend Summary: The Effect of Stretch on Stiffness and Loss Coefficient for Fluorocarbon (Viton-70)

211
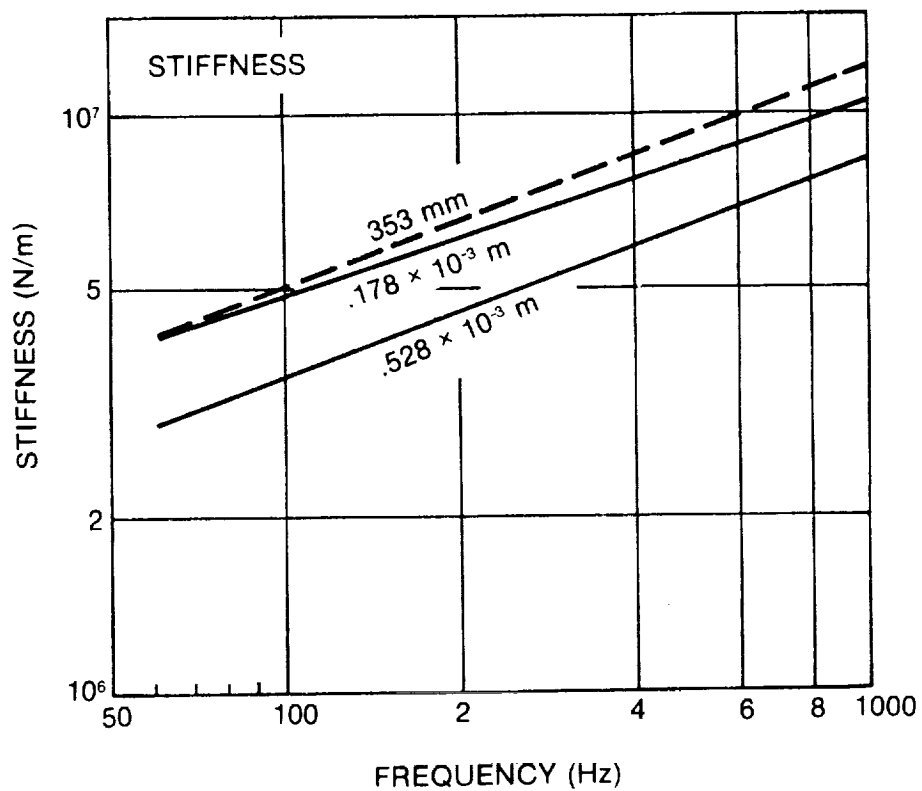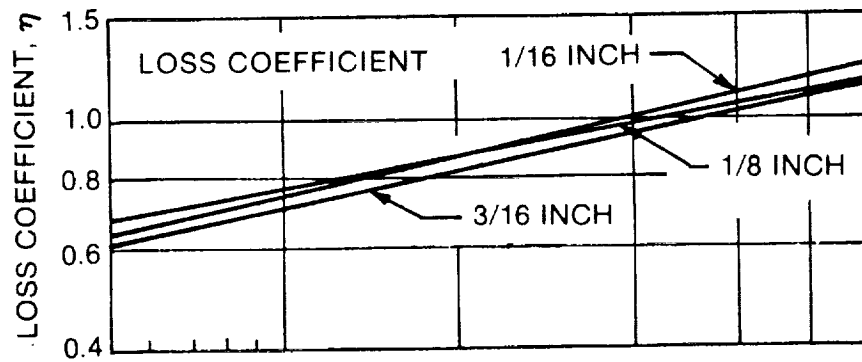
Fig. 107 Trend Summary: The Effect of Cross-Section Diameter on Stiffness and Coefficient for Fluorocarbon (Viton-70)

212
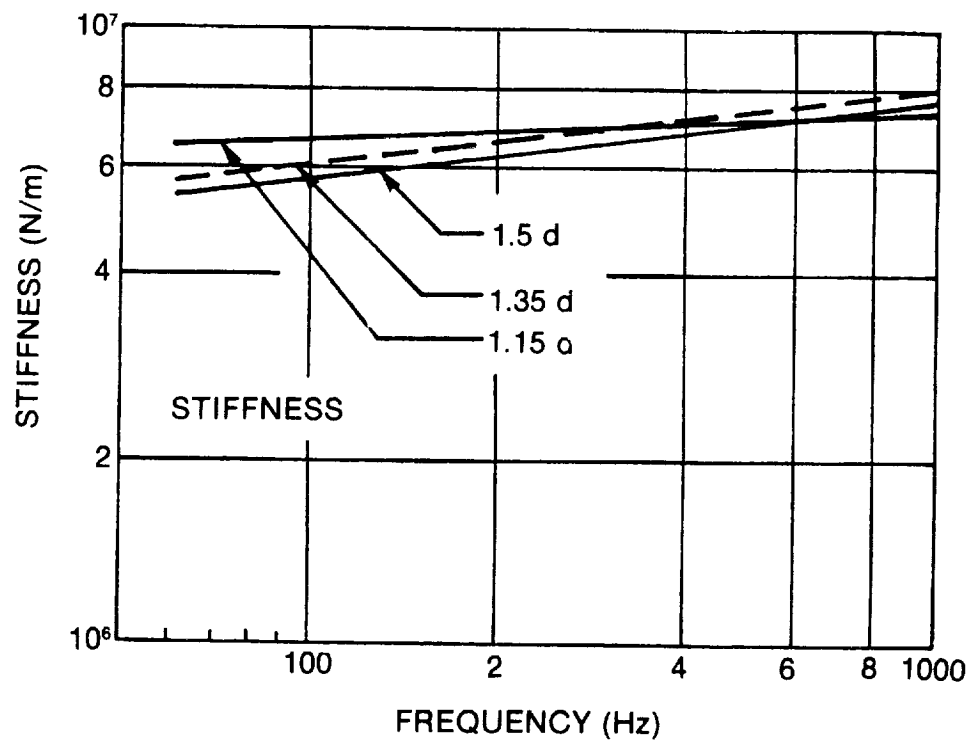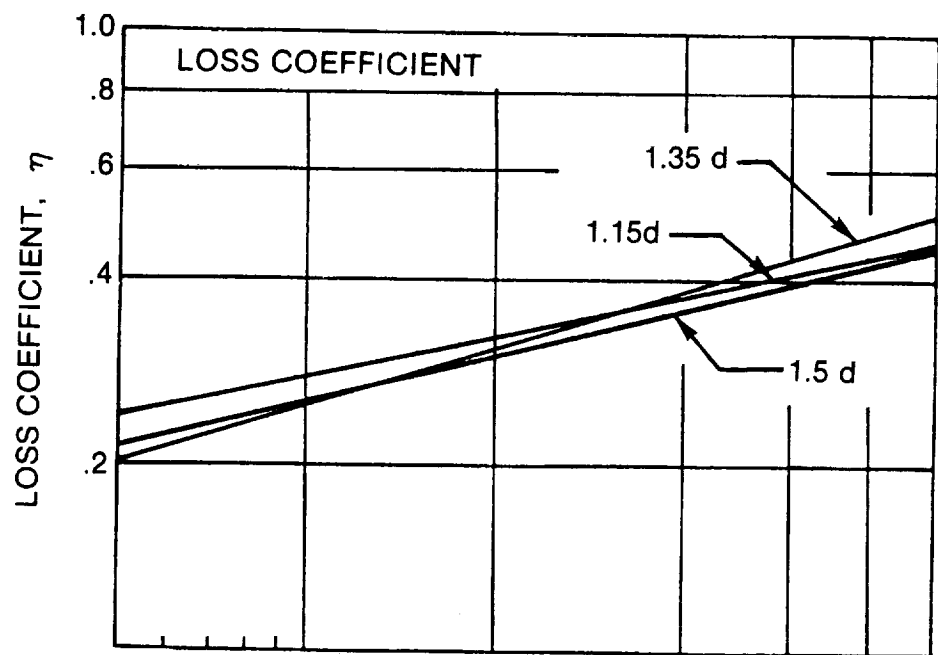
Fig. 108 Trend Summary: The Effect of Groove Width on Stiffness
and Loss Coefficient for Nitrile (Buna-N)

213

fluorocarbon (Viton 70 - CFM) has a stronger frequency dependence over the range covered, and a loss coefficient almost three times that of nitrile (Buna-N - NBR). Provided temperature and amplitude can be controlled, the fluorocarbon (Viton - CFM) appears to be a better damping material. If higher stiffness is required, an increase factor of 3 to 4 can be achieved by a shift to 90 durometer fluorocarbon (Viton - CFM); but the loss coefficient for fluorocarbon (Viton 90 - CFM) is about half that of fluorocarbon (Viton 70 - CFM), and the frequency dependence of the fluorocarbon (Viton 90 - CFM) properties is less pronounced than those of fluorocarbon (Viton 70 - CFM).

6.3.2 Temperature

The effects of temperature on stiffness and loss coefficient for fluorocarbon (Viton 70 - CFM) are very strong, particularly for small increases in temperature above 25°C as shown in Figure 103. Both stiffness and loss coefficient fall sharply with increasing temperature; stiffness by a factor of two or more between 25 and 66°C; and loss coefficient by a factor of four. Above 66°C the effects of temperature are less pronounced, and no change in stiffness was observed above 149°C.

The trends in stiffness and loss coefficient as a function of temperature are emphasized by a cross plot of these quantities versus temperature, at 200 and 800 Hz (Figure 109). Figure 110 compares the loss coefficient results with those from the shear test. These results indicate consistency.

6.3.3 Amplitude

The effect of amplitude on stiffness and loss coefficient is strong, as shown in Figure 104. In the range from 100 Hz to 1000 Hz, increasing amplitude consistently decreases stiffness and damping and decreases their frequency dependence. At 500 Hz, even a modest increase in amplitude from 7.62×10^{-3} mm (0.3 mil) to 25.4×10^{-3} mm (1 mil) cuts the stiffness by over 30%. An increase to 127×10^{-3} mm (5 mils) causes an additional reduction of over 50%. The loss coefficient is less affected; an increase from 7.67×10^{-3} mm to 127×10^{-6} mm reduces the loss coefficient from 1 to 0.43. This effect is also consistent with the results of the fluorocarbon (Viton - CFM) shear specimen tests.

6.3.4 Squeeze

The radial precompression, or squeeze, imposed on the O-ring affects its dynamic behavior, particularly its stiffness; see Figure 105. The Hertzian nature of the contact, in which increasing squeeze increases the area of contact between the ring and metal, thereby enables the force to be developed for a given relative radial displacement. For squeeze values in the region of 15% (Figure 111 defines squeeze), the stiffness is least sensitive to squeeze (which probably makes 15% a good design value of squeeze). As squeeze is reduced to 5%, the stiffness starts to fall off sharply, because, under even light gravity loads, contact between ring and metal is not maintained over 360° when 5% squeeze is coupled with the reference value of 5% stretch. The interaction of squeeze and stretch must be recognized. When the ring is stretched, its effective cross-sectional diameter is reduced and the effective squeeze is less than the squeeze as defined in Figure 111.
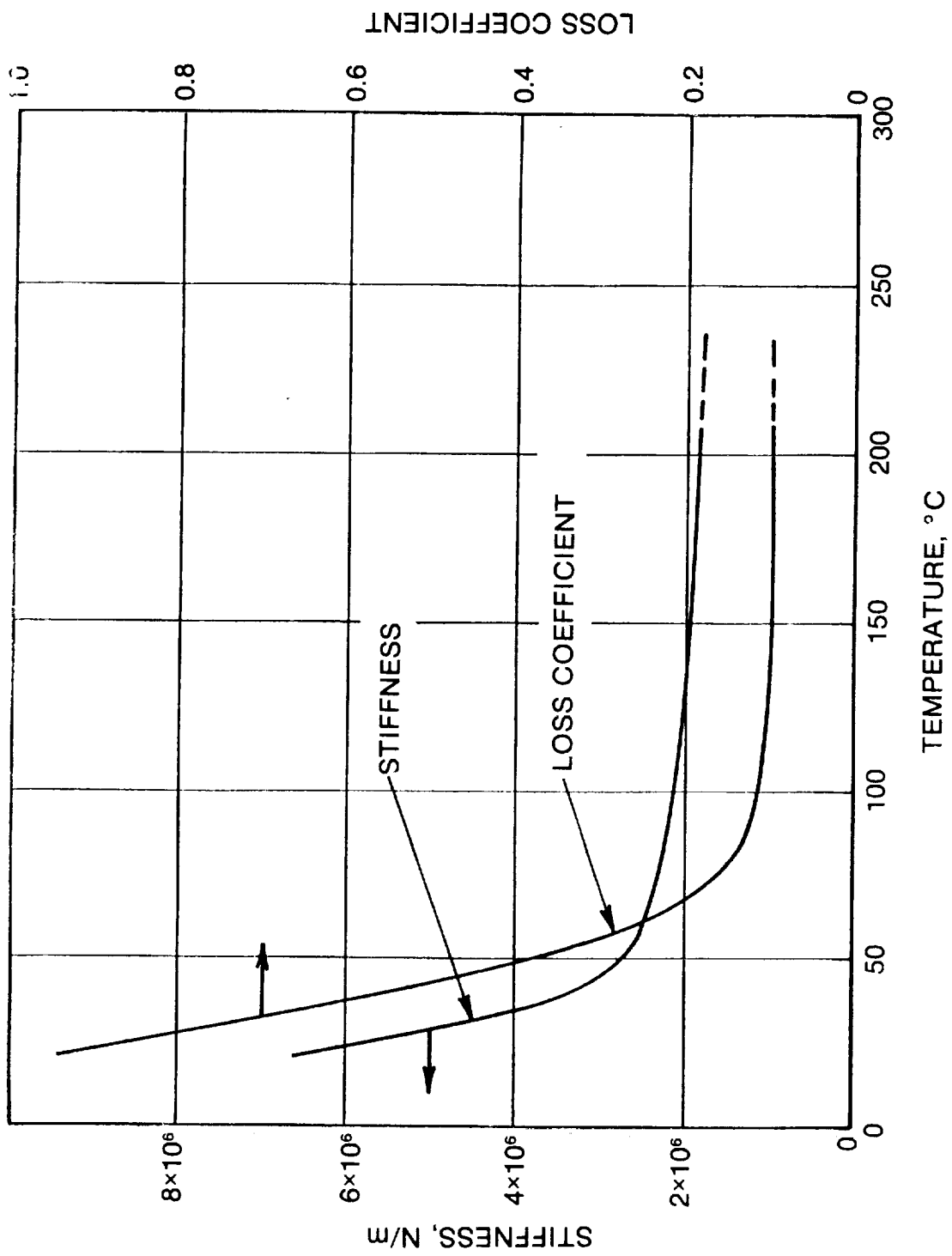
Fig. 109 Stiffness and Loss Coefficient vs Temperature for Fluorocarbon (Viton-70)
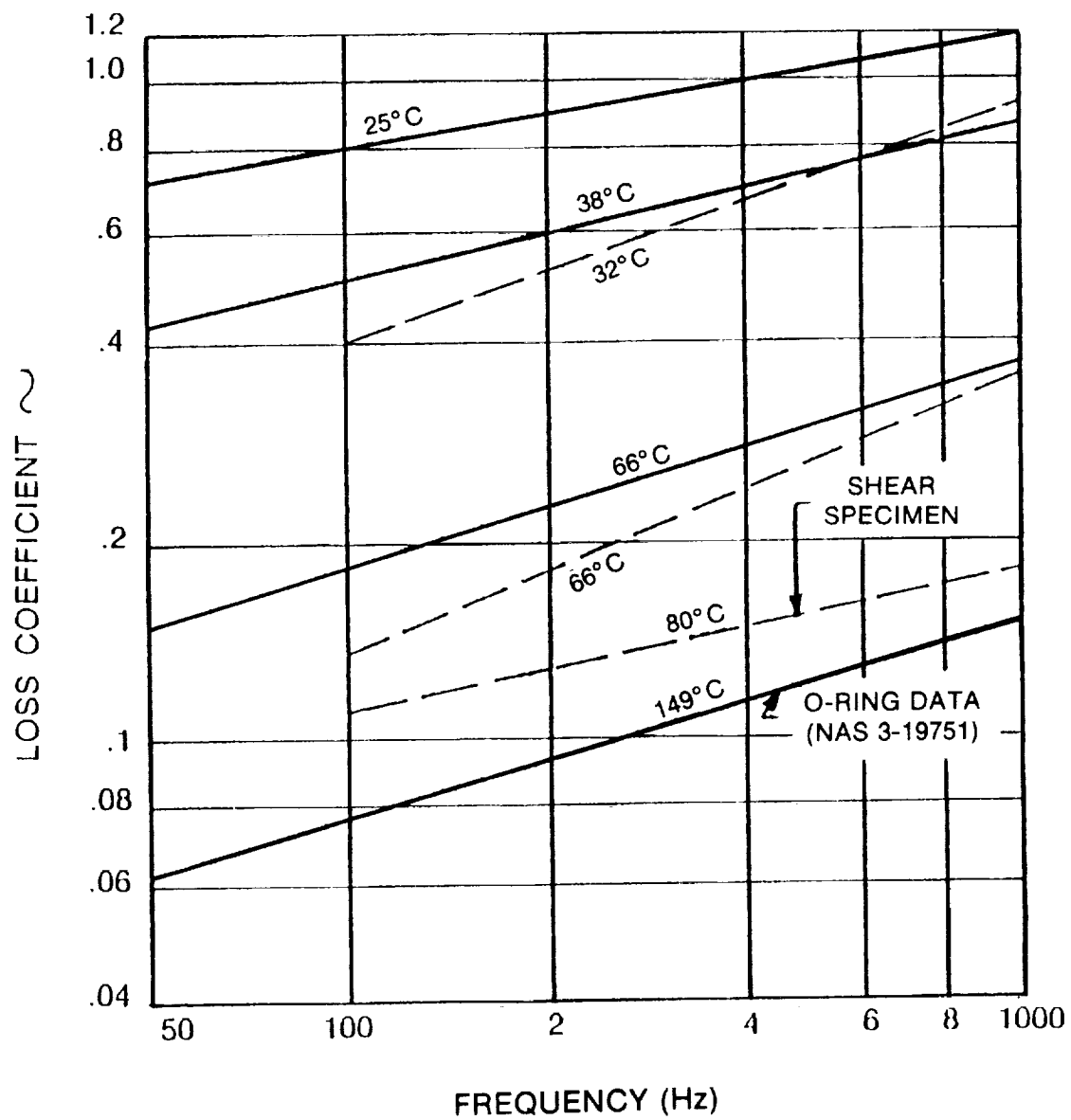
Fig. 110 Comparison of Fluorocarbon (Viton-70) Shear Specimen and O-Ring Test Data

216

O-RING HOUSING

O-RING (CROSS-SECTION DIAMETER d, INNER DIAMETER D_i)

BEARING HOUSING

BEARING

C

D_g

W_g

L

% STRETCH = 100 $(D_g - D_i)$ / D_i

% SQUEEZE = 100 $(d - L)$ / d
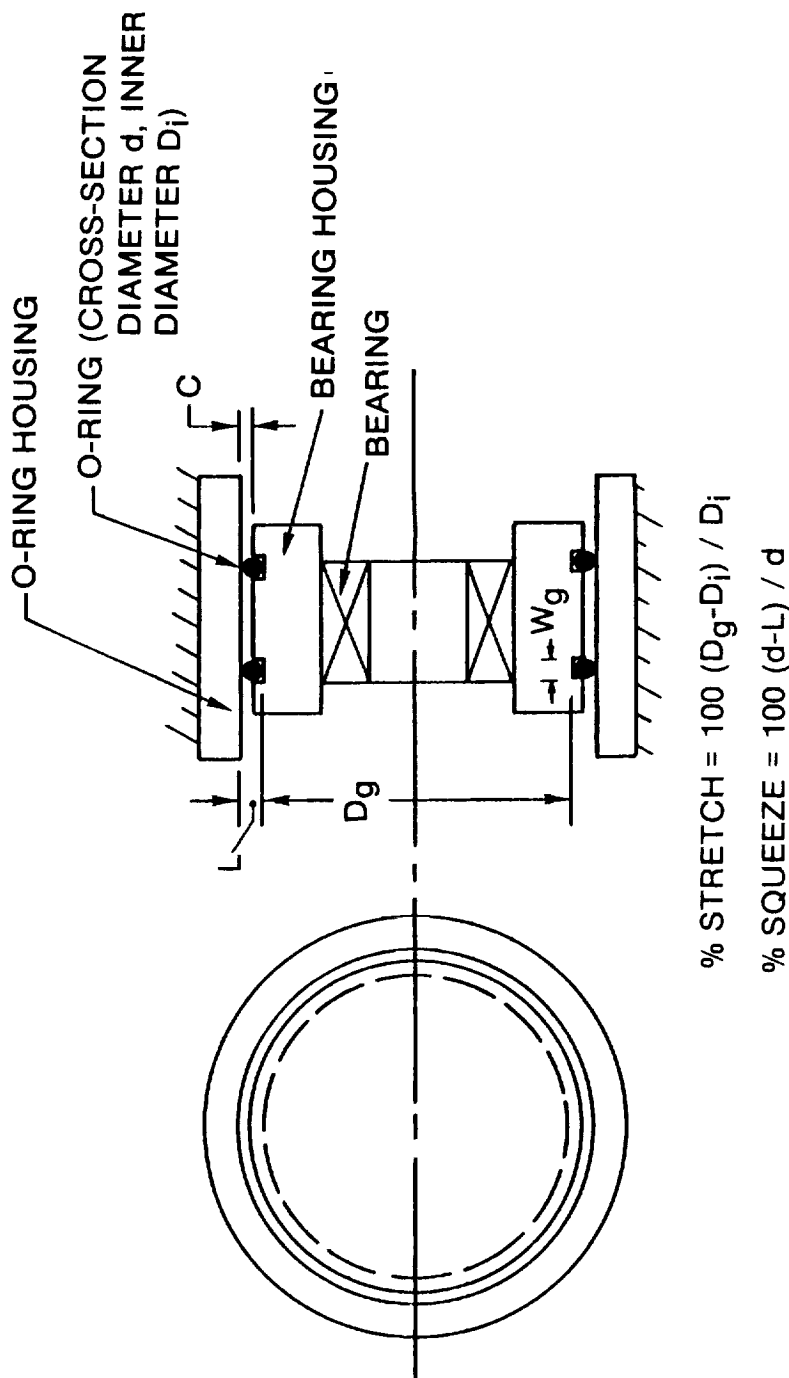
Fig. 111   Definition of Stretch and Squeeze

217

When squeeze is increased to 30%, stiffness increases more rapidly than at 15%. The reason could be contact between groove walls and ring or simply, the increased rectangularity of the squeezed O-ring cross section and an increased influence of elastomer bulk modulus on deflection characteristics. The trends in stiffness as a function of squeeze are emphasized in Figure 112 which is a cross plot of stiffness versus squeeze at 200 Hz. It shows the turning point at around 15% squeeze.

6.3.5 Stretch

The influence of stretch on stiffness and loss coefficient is shown in Figure 106. It is apparent that no clear trend can be defined since 5% stretch causes a higher stiffness and lower loss coefficient than either 0 or 10%. Also, the spread for all stretch values is only 20% in stiffness and 10% in loss coefficient. Stretch is, therefore, shown to be of minimal importance.

6.3.6 Cross Sectional Diameters

As shown in Figure 107, cross sectional diameter is another parameter which develops no clear trend within the available test results. The reference value of 1/8 for cross section diameter develops the highest stiffness, and either a smaller or larger cross section causes a reduced stiffness. For loss coefficient, the spread of values is very small and some intersection of the lines occurs.

Simple analysis would suggest that cross sectional diameter should have little effect provided squeeze remains the same. Both stressed and strained dimensions of the cross section are proportional to cross section diameter, and stiffness should be independent of this diameter. Secondary effects such as stretch-squeeze interaction and the dependence of strain on diameter (for constant amplitude) may cause some secondary trends, which could be clearly identified by more extensive testing.

6.3.7 Groove Width

As would be expected, groove width has a negligible effect on stiffness and loss coefficient. This statement would have to be modified only if interaction of an O-ring with the groove walls occurred. Since the smallest groove width investigated was 1.15 times the cross sectional diameter, this interaction did not occur and, as shown in Figure 108, very similar stiffness and loss coefficient values were obtained for all three groove widths considered.

The most notable feature of Figure 108 is that the stiffness and loss coefficient do not correspond to the reference values for other tests. This is because nitrile (Buna-N - NBR) O-rings were inadvertantly used for these tests instead of fluorocarbon (Viton 70 - CFM) rings. The conclusion of a negligible effect of groove width is expected to be the same for fluorocarbon (Viton 70 - CFM).

The recommended value for groove width (from O-ring design guides) is 1.35d, shown to be an entirely satisfactory value to use. If space is at a premium, 1.15 is also an acceptable value from dynamic performance considerations.
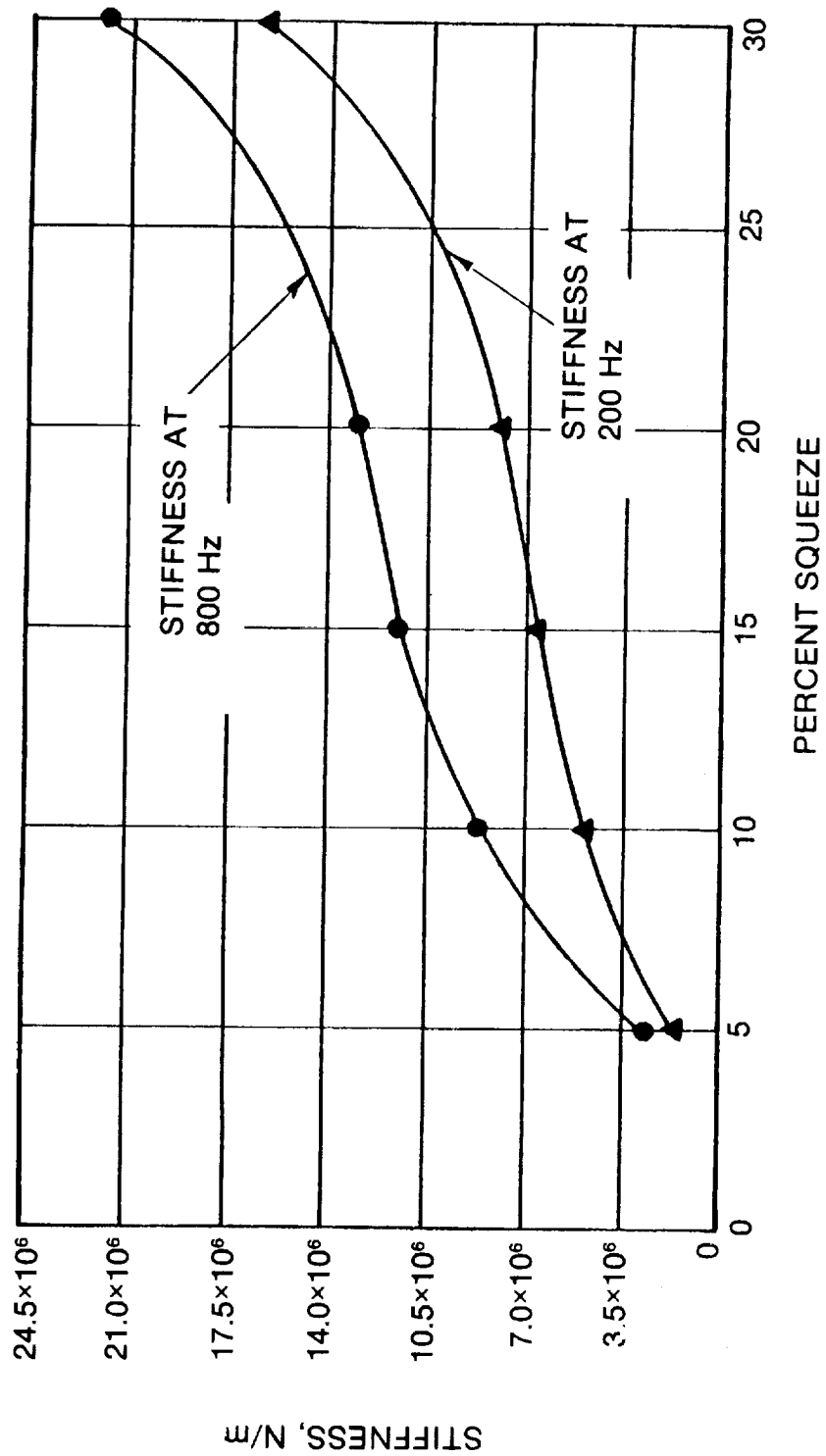
Fig. 112 Stiffness vs Squeeze for Fluorocarbon (Viton-70)

219

6.4 Summary

Accurate elastomer material properties are an essential element in the design of elastomer dampers. These property values are generally obtained from empirical data collected in a reference, such as this chapter, or determined from specific tests. The designer should be certain to use reliable elastomer property data. Reliable data will insure that the damper design is valid. Thus, it may be advisable to conduct some amount of independent experimental verification of the more important material properties.

6.5 References

6.1 <u>Elastomeric Materials</u>, Desk-Top Data Bank, The International Plastics Selector, Inc., San Diego, California, 1977.

6.2 Anwar, I., and Kramberger, F., "Testing of Elastic Mounts for Application in Bearings", Franklin Inst. Research Lab Interim Report I-C2429, Prepared for Office of Naval Research, August 1975.

6.3 Payne, A.R. and Scott, J.R., <u>Engineering Design with Rubber</u>, Maclaren & Sons, London, 1960.

6.4 Gobel, E.F., <u>Rubber Springs Design</u>, John Wiley and Sons, New York, 1974.

6.5 Smalley, A.J., and Tessarzik, J.M., "Development of Procedures for Calculating Stiffness and Damping Properties of Elastomers in Engineering Applications, Part III: The Effects of Temperature, Dissipation Level and Geometry," NASA Report CR-134939, November 1975.

6.6 Howgate, P.G., "Report of Observations Made During the Visit of P.G. Howgate to MTI Latham", Rubber and Plastics Research Association of Great Britain, Technical Report 3558, October 1977.

6.7 Rubber and Plastics Research Association of Great Britain, direct communication, September 1979.

6.8 Tecza, J.A., Darlow, M.S., and Smalley, A.J., "Development of Procedures for Calculating Stiffness and Damping Properties of Elastomers in Engineering Applications, Part V: Elastomer Performance Limits and the Design and Test of an Elastomer", NASA Report CR-159552.

6.9 Seber, G.A.F., <u>Linear Regression Analysis</u>, John Wiley and Sons, 1976.

6.10 Smalley, A.J., Darlow, M.S., and Mehta, R.K., "Stiffness and Damping of Elastomeric O-Ring Bearing Mounts", NASA Report CR-135328, November 1977.

6.11 Snowden, J.C., <u>Vibration and Shock in Damped Mechanical Systems</u>, J. Wiley and Sons, Inc., New York, 1968.

6.12 Harris, C.M., and Crede, C, editors, <u>Shock and Vibration Handbook</u>, Second Edition, McGraw-Hill, New York, 1976.

APPENDIX 6A

CALCULATION OF PREDICTION CONFIDENCE INTERVALS FOR DYNAMIC PROPERTIES OF ELASTOMERS

When calculating the dynamic properties of elastomer materials from the equations in Section 6.0, it is useful to be able to estimate the uncertainty inherent in these calculations (due to the experimental error in the original test data). Thus, a 90% confidence prediction interval can be assigned to each of the modulus and shape factor values by attaching the term:

$$\pm\ 1.645\ s\sqrt{1 + \underline{\ell}^T \underline{Q}\, \underline{\ell}} \qquad (6A-1)$$

to the common logarithm of each of the reduced modulus and shape factor predictions. In equation (6A-1), s is the appropriate standard deviation from Table 17 or 18, $\underline{\ell}$ is a four element column vector given by:

for reduced modulus:

$$\underline{\ell} = \begin{bmatrix} 1 \\ \log_{10}\alpha_T + \log_{10}\omega \\ \log_{10}\varepsilon \\ (\log_{10}\varepsilon)^2 \end{bmatrix} \qquad (6A-2)$$

for shape factor:

$$\underline{\ell} = \begin{bmatrix} 1 \\ \log_{10}\omega \\ \log_{10}\left(\dfrac{T}{Tc}\right) \\ \log_{10}\varepsilon \end{bmatrix} \qquad (6A-3)$$

$\underline{Q}$ is a square matrix of rank four which is given for each of the materials for the modulus calculations in Table 6A-1 and for the shape factor calculations in Table 6A-2.

Note that the term $\underline{\ell}^T \underline{Q}\, \underline{\ell}$, where ℓ^T is the transpose of $\underline{\ell}$, is the same for either the storage or loss modulus of a given material.

The center and extremes of the confidence interval for the actual moduli or shape factors can then be determined by taking the antilogarithm base 10 of each of the corresponding values. For the moduli, the reduced moduli are then converted to actual moduli by multiplying by the ratio of the elastomer temperature to the characteristic temperature. Alternately, the predicted values for the moduli or shape factors can be found directly from the equations in exponential form, and the extremes of the confidence intervals found by multiplying by the antilogarithm of equation (6A-1).

Elements of Q Matrix from Dynamic Property Tests

Elastomer Material	Q Matrix			
butadiene (Polybutadiene - BR)	0.478	0.00260	0.460	0.103
	0.00260	0.00788	0.00445	0.000805
	0.460	0.00445	0.461	0.106
	0.103	0.000805	0.106	0.0252
fluorocarbon (Viton - CFM)	0.225	-0.00314	0.162	0.0273
	-0.00314	0.00336	0.00163	0.000138
	0.162	0.00163	0.129	0.0229
	0.0273	0.000138	0.0229	0.00436
nitrile (Buna-N - NBR)	0.365	-0.00290	0.292	0.0550
	-0.00290	0.00405	0.000988	0.0000368
	0.292	0.000988	0.250	0.0490
	0.0550	0.0000368	0.0490	0.0100
chloroprene (Neoprene - CR)	0.650	0.0500	0.559	0.114
	0.0500	0.0575	0.0243	0.00292
	0.559	0.0243	0.507	0.107
	0.114	0.00292	0.107	0.0235
EPDM	0.505	0.00516	0.438	0.0886
	0.00516	0.00822	0.00496	0.000947
	0.438	0.00496	0.396	0.0826
	0.0886	0.000947	0.0826	0.0177

Table 6A-2

Elements of Q Matrix from butadiene (Polybutadiene – BR)
Compression Tests

1.78	−0.480	−1.60	0.0223
−0.480	0.140	0.280	0.00326
−1.60	0.280	6.07	−0.0406
0.0223	0.00326	−0.0406	0.0128

For example, for butadiene (Polybutadiene - BR) at a temperature of 60 degrees centigrade, a frequency of 400 HZ, and a dynamic strain of 0.01, the logarithms of the reduced moduli become, from equations (6-22) and (6-23)

$$\log_{10}(0.805\ G') = 6.76 \tag{6A-4}$$

$$\log_{10}(0.805\ G'') = 5.97 \tag{6A-5}$$

The vector $\underset{\sim}{\ell}$, for modulus calculations, becomes

$$\underset{\sim}{\ell} = \begin{bmatrix} 1.0 \\ 0.280 \\ -2.0 \\ 4.0 \end{bmatrix} \tag{6A-6}$$

Equation (6A-1) then gives

$$\pm\ 0.044 \text{ for storage modulus} \tag{6A-7}$$

$$\pm\ 0.090 \text{ for loss modulus} \tag{6A-8}$$

Thus, the extremes of the 90% confidence intervals for G' and G" are

$$6.46 \times 10^6 \text{ N/m}^2 < G' < 7.91 \times 10^6 \text{ N/m}^2 \tag{6A-9}$$

$$0.95 \times 10^6 \text{ N/m}^2 < G'' < 1.44 \times 10^6 \text{ N/m}^2 \tag{6A-10}$$

while the nominal values for G' and G" are

$$G' = 7.15 \times 10^6 \text{ N/m}^2 \tag{6A-11}$$

$$G'' = 1.17 \times 10^6 \text{ N/m}^2 \tag{6A-12}$$

Similarly, for the shape factor calculations, for the same specifications

$$\log_{10}\beta' = 0.500 \tag{6A-13}$$

$$\log_{10}\beta'' = 0.595 \tag{6A-14}$$

From equation (6A-3)

$$\underset{\sim}{\ell} = \begin{bmatrix} 1.0 \\ 3.40 \\ 0.094 \\ -2.0 \end{bmatrix} \tag{6A-15}$$

224

Equation (6A-1) then gives

$$\pm 0.131 \text{ for storage shape factor} \qquad\qquad (6A-16)$$

$$\pm 0.109 \text{ for loss shape factor} \qquad\qquad (6A-17)$$

Thus, the extremes of the 90% confidence intervals for β' and β'' are

$$2.34 < \beta' \quad 4.28 \qquad\qquad (6A-18)$$

$$3.07 < \beta'' \quad 5.06 \qquad\qquad (6A-19)$$

while the nominal values for β' and β'' are

$$\beta' = 3.16 \qquad\qquad (6A-20)$$

$$\beta'' = 3.94 \qquad\qquad (6A-21)$$

The nominal values for G', G'', β' and β'' can also be easily extracted from the design charts in Section 6.0.

7.0 PRACTICAL DESIGN CONSIDERATIONS AND PROCEDURES

This section provides a detailed discussion of the steps required for the proper design of elastomer dampers and the practical considerations implicit in such a design. A brief discussion related to applications for control of unidirectional vibrations is presented; however, the major emphasis is placed on rotordynamic applications, the subject of this handbook. The specific procedure required for the design of elastomer dampers for rotating machinery is described in detail, including both machinery dynamics and hardware-related considerations. Several examples of actual designs, including details of the design procedure, designed hardware, and test results, are presented in Section 8.0.

The basic steps involved in elastomer damper design are to:

- Analyze the system dynamics and establish the best or optimal levels of support damping and stiffness to be provided by the elastomer elements under the given design requirements

- Choose the elastomer material and geometry to best approximate this stiffness and damping, based on reasonable ranges of the operating parameters (e.g. frequency, temperature and strain) and any appropriate environmental considerations (e.g., fluid immersion, ozone)

- Predict the system response with the actual expected ranges of elastomer stiffness and damping

- Design the actual damper hardware based on manufacturing, assembly, and other practical considerations.

To assist the engineer, each step is considered in detail in this section.

7.1 Determine Best or Optimal Damping and Stiffness

For unidirectional, as well as rotordynamic applications, it is first necessary to develop an analytical model which approximately represents the dynamic characteristics of the vibratory system. For simplicity, linear models are often used and are generally adequate. For unidirectional applications, elastomer dampers are often used in the form of foot pads on which relatively rigid machines are mounted. In such cases, a single-degree-of-freedom, damped, forced vibration model, as described in Section 2.0, may be sufficient. If the most likely forcing frequencies are known (from previous analysis or machinery experience), it is a straightforward procedure to determine the stiffness and damping levels which minimize the transmissibility of the damper [7.1]*.

More complex unidirectional systems, such as those employing constrained-layer damping [7.2], may require fairly complicated analytical models. In such cases, numerical tools using discretized models (e.g., finite difference or finite element representations) and digital computers are generally used [7.3]. Although these predictive tools are more expensive than those approximations for the single-degree-of-freedom model, the objective of the analysis is the

---

* Numbers in brackets indicate References found in Section 7.6

same: to minimize the system vibration (using some predefined critical
response criteria) through variation of the damping and stiffness of
dampers. Essentially, this optimization procedure involves analyzing the
system model with a number of realistic combinations of damping and stiffness
for dampers. The optimum combination of stiffness and damping can then be
selected. Awareness of the effect on the system response of small changes in
these parameters is essential, since a certain amount of uncertainty exists
in the specification of elastomer properties (as there is in the design of
any damper). Further, elastomer materials tend to be moderately sensitive
to changes in operating conditions and to be somewhat nonlinear. If there
are alternatives available in the choice of damper location, it would be
advisable to locate the damper(s) as near to the antinode(s) of vibration
as is practical, or at any location which would insure that motion of the
damper would maximize the energy dissipated.

The first step in the analysis of rotordynamic systems also involves the
development of an analytical model. The amount of detail required in such
a model is dependent on the complexity of the rotordynamic system. For
systems with rigid rotors, for example, it is often sufficient to lump the
mass and inertia of the rotor and to consider only the one or two degrees-of-
freedom provided by the rotor supports. However, more detailed rotor models
are necessary for flexible rotors. Rigid rotors are those for which no
significant shaft deformation is exhibited for running speeds up to the
maximum operating speed of the rotor. Conversely, flexible rotors are those
which exhibit appreciable shaft deformation. Numerous computer software
packages are available for analyzing rotordynamic systems. The actual system
modelling procedure is dependent on the particular type of analysis used.
The most common of these analytical tools employs transfer matrix [7.4, 7.5,
7.6] or finite element [7.7] representations. These representations are
generally composed of linear elements, although nonlinear analyses may also
be conducted. Several examples involving the use of such linear analytical
tools are presented in Section 8.0.

Selection of the most appropriate analytical tools require that the principal
motivation for the addition of damping to the system be ascertained. For
example, the damping may be necessary to aid in the control of synchronous
vibrations due to rotor mass unbalance or to stabilize otherwise unstable
nonsynchronous, or even transient, vibrations. Some form of acceptable
vibration or stability criteria must then be established as a guide in the
design process.

Part of the modelling procedure necessitates the determination of damper
location(s). Rotor dampers are generally located in the bearing supports and,
accordingly, may also be used to support the superstructure of the rotordynamic
system. Several alternate locations can be available for the dampers, with
the final decision being based on the analytical results and other considera-
tions (temperature, maintainability, etc.).

To begin this analytical procedure, realistic ranges of stiffness and damping
values (and possibly damper locations) are selected. The rotordynamic model
is then analyzed for support parameters spanning these ranges and a pre-
established critical response (based on the criteria mentioned above) is
plotted as a function of these support parameters. The optimum values of

227

stiffness and damping can then be identified. It is also useful to note the effect of small changes in support stiffness or damping on the critical response. A commonly used critical response criterion is system logarithmic decrement, which gives an indication of overall damping effectiveness of each critical speed, as discussed in Section 2.0. Thus, the log decrement is indicative of the sensitivity of the rotor response to unbalance, as well as the system stability. Section 8.0 discusses several examples in which log decrement is used as a design criteria.

7.2 Specify Elastomer Material and Geometry

Proper specification of the elastomer material and geometry is dependent on a number of factors. Material selection is affected by both dynamic and environmental considerations. The desired dynamic properties of the damper, particularly loss coefficient, have a major impact on the choice of elastomer material. The damper operating parameters (frequency, temperature and strain) are also important.

Elastomer dampers are often subjected to severe environmental conditions, such as exposure to fluids or gases, which may be incompatible with the elastomer material. Even in a relatively clean environment, exposure to ozone and ultra-violet light (at normal ambient levels) over an extended period of time can result in aging of the elastomer material. Such aging is generally manifested by an increase in the stiffness of the elastomer. The aging effect may be so significant for some elastomer materials that a limitation must be placed on the shelf life of the elastomer specimens (generally not less than several years).

Data presented in Section 6.0 concerns the resistance of many elastomer materials to degradation from prolonged exposure to a variety of liquids and gases. Using such data, in cases when environmental considerations are expected to be important, elastomer material selection can be narrowed to those best suited to a particular set of environmental conditions. Similarly, the effects of frequency, temperature and dynamic strain on the dynamic properties of an elastomer material can be evaluated using empirical relationships (Section 6.0).

Once the appropriate elastomer material has been selected, a suitable mode of bonding, using an adhesive or bonding agent, must be chosen. A brief discussion on bonding of elastomer materials is also included in Section 6.0. If elevated elastomer temperatures are likely to be a problem, cooling, using either forced air convection or liquid in cooling channels, should be considered.

There are many possible geometric configurations for the elastomer elements in a damper. Four typical examples are: 1) Shear cartridge, 2) Compression button cartridge, 3) Continuous compression cartridge and 4) O-rings. The particular choice of geometric configuration is determined somewhat by the application. However, the shear cartridge and compression button cartridge configuration generally are recommended since they inherently lend themselves to a more straightforward evaluation of dynamic properties and to less complicated damper hardware design, assembly and maintenance.

228

A shear cartridge configuration can be in the form of a continuous cartridge (Figure 113) or a segmented cartridge (Figure 114). In this segmented shear cartridge design, the elastomer elements are subjected to pure shear loading from rotating radial forces. Using a slightly different design (Figure 115), the elastomer elements are subjected to a combination of shear and compressive loading. The pure shear design simplifies the analysis required to predict dynamic properties. Any elastomer element which is subject to an oscillatory compression (and tension) load must be sufficiently preloaded in compression to preclude the possibility of subjecting the element to an absolute tensile load; elastomer materials and bonding interfaces tend to be less reliable in tension than in compression (or shear).

For the pure shear designs (either continuous or segmented), the calculation of the stiffness and damping values for the damper is straightforward. Presumably, the shear storage and loss moduli for the chosen elastomer material are available from test results or from data as presented in Section 6.0. The stiffness and damping of the damper are then given by

$$K'_s = G' \frac{A}{t} \qquad\qquad (7\text{-}1)$$

$$K''_s = G'' \frac{A}{t} \qquad\qquad (7\text{-}2)$$

where

$$K_s = K'_s + iK''_s$$

and

K'_s = damper shear stiffness (real part) - N/m

K''_s = damper shear damping (imaginary part of stiffness) - N/m

G' = shear storage modulus - N/m^2

G'' = shear loss modulus - N/m^2

A = total bonded area (one side only) of shear elements - m^2

t = thickness of shear elements - m

For example, if a segmented pure shear cartridge is constructed with three cylindrical buttons, 10 mm in diameter and 3 mm thick, the total area, A, would be 2.36 x 10^{-4} m^2, and the ratio of stiffness component (K' or K") to shear modulus (G' or G") would be 0.0785 m. The analysis of the combined shear and compression configuration, Figure 115, is somewhat more complicated and is very similar to the analysis for the compression button cartridge discussed in the following paragraphs.

A typical compression button cartridge configuration is illustrated in Figure 116. The application of a rotating force results in the elastomer elements being subjected to a combination of compression and shear loading. Also, as discussed, preloading the elastomer buttons in compression is

Elastomer
Ring

Section A-A

Elastomer Rings

Outer
Damper
Housing

Inner
Damper
Housing

Ball Bearing

Shaft

A

A
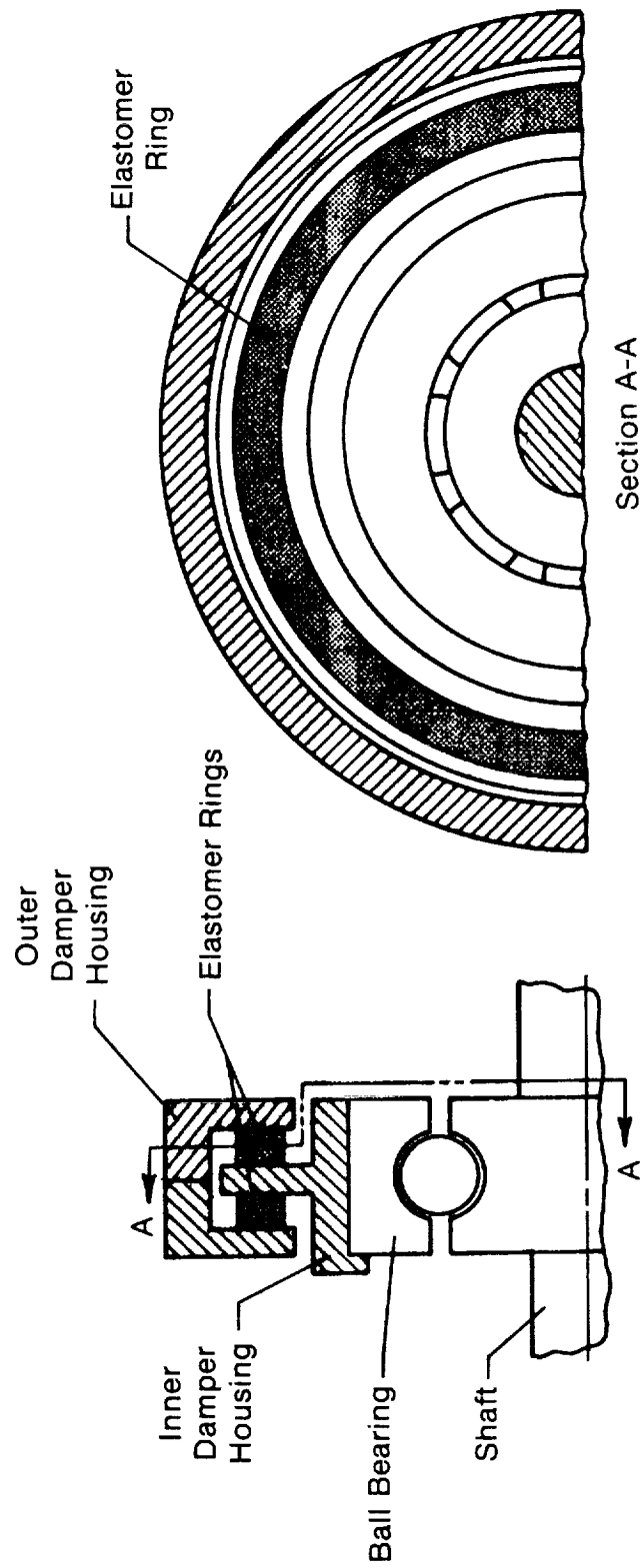
Fig. 113   Example of Continuous Shear Cartridge Elastomer Damper Configuration

230

Outer
Damper
Housing

Elastomer
Buttons

Inner
Damper
Housing

Ball
Bearing

Shaft

Elastomer
Buttons

Section A-A
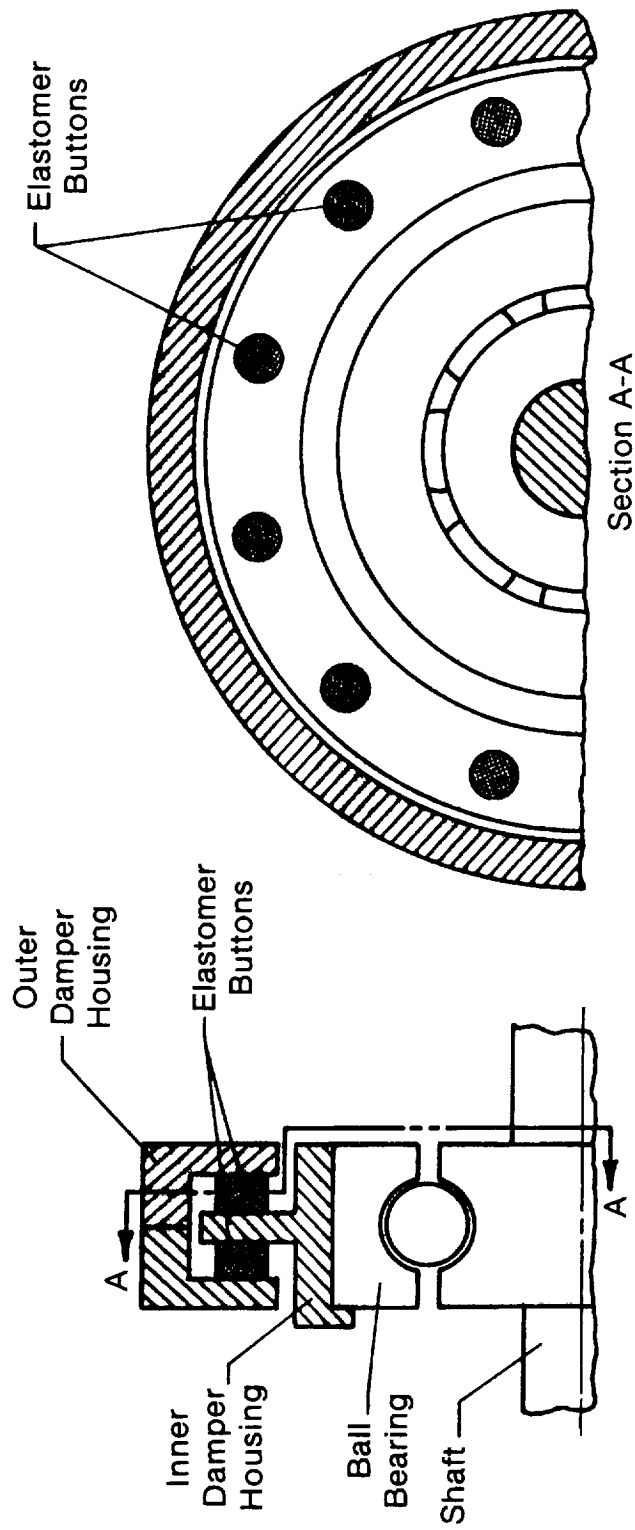
Fig. 114 Example of Segmented Shear Cartridge Elastomer Damper Configuration with Pure Shear Loading of Elastomer Elements

231

Elastomer
Buttons

Section A-A

Outer
Damper
Housing

Elastomer
Button

A

A

Inner
Damper
Housing

Ball
Bearing

Shaft

A

A
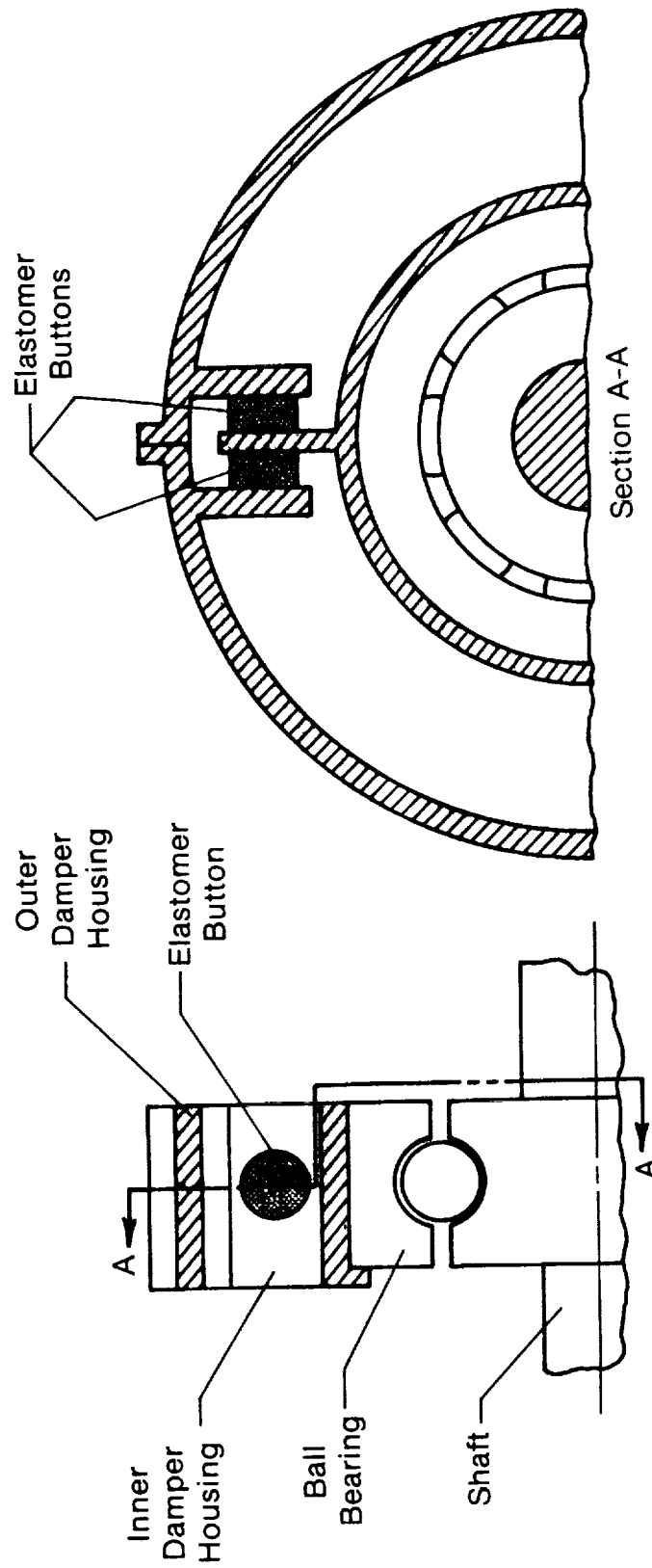
Fig. 115 Example of Segmented Shear Cartridge Elastomer Damper Configuration
with Both Shear and Compressive Loading of Elastomer Elements

232

Elastomer Buttons

Outer Damper Housing

Elastomer Button

Inner Damper Housing

Ball Bearing

Shaft
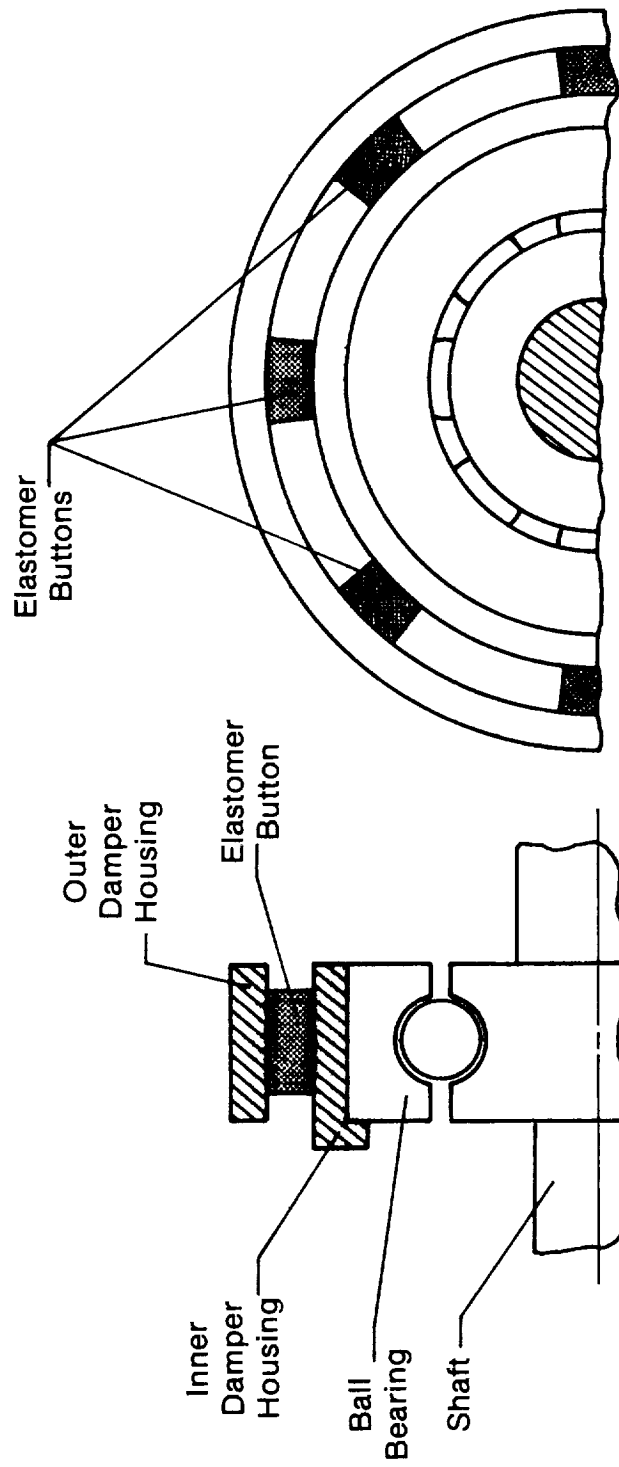
Fig. 116   Example of Compression Button Cartridge Elastomer Damper Configuration

233

necessary to exceed the largest anticipated dynamic tensile load. The principal attraction of this configuration is the simplicity it lends to the damper hardware design; see two examples in Section 8.0.

When calculating the effective stiffness and damping of this elastomer damper configuration, it is convenient to separate the effects of shear and compression loading and to superimpose the separate results. The stiffness and damping of an individual button in shear are calculated directly from equations (7-1) and (7-2). However, the relationships between the shear moduli and the compression stiffness and damping of an elastomer button are considerably more complex; this complexity is due to the resistance to out-of-plane deformation provided by the bonded surfaces (Section 4.0). These relationships are of the form

$$K_c' = \frac{3G'A}{t} (1 + \beta'\delta^2)$$ (7-3)

$$K_c'' = \frac{3G''A}{t} (1 + \beta''\delta^2)$$ (7-4)

where the moduli of elasticity are taken to be three times the shear moduli (Poisson's ratio of about 0.5), the β' and β'' are dynamic shape factors, and δ is a dimensionless geometric factor ($D/4t$ for a short cylinder). Values for the β's (as functions of the operating conditions) may be obtained from empirical data such as that presented in Section 6.0 or directly from experimental results.

Once the stiffness and damping for an individual button have been determined separately for compression and shear loading, the overall stiffness and damping of the elastomer damper may be calculated [7.8]. The expressions K_c and K_s are used to represent the complex stiffness of a single button in compression and shear, respectively, where

$$K_s = K_s' + iK_s''$$ (7-5)

$$K_c = K_c' + iK_c''$$ (7-6)

K_s = the elastomer button stiffness in shear

K_c = the elastomer button stiffness in compression

Consider the support geometry given in Figure 117a which shows three elastomer buttons, spaced at 120° intervals and separating a bearing housing from the surrounding pedestal. When the housing is given a downward displacement of some distance X, the individual buttons are deformed in some combination of compression and shear. This is illustrated in Figure 117b for one of the buttons, where: X is the total downward deflection, X_c is that component of the total deflection taken up by elastomer compression, and X_s is that component accommodated by shearing. If the individual buttons are labeled 1, 2, and 3 starting from the top, the compression and shear deflection of the individual buttons can be described in terms of the imposed bearing housing deflection X. The deflection of the first button is simply as follows:

b. Enlarged Detail of Individual
   Deflected Button — No. 2

a. Overall Support
   Geometry

Fig. 117 Support Geometry and Button Deformation for Stiffness Calculations of Compression Button Cartridge Elastomer Damper Configuration (after [7.8])

235

$$X_{1c} = X \qquad (7\text{-}7)$$

$$X_{1s} = 0 \qquad (7\text{-}8)$$

where X_{1c} is the compressive, or normal, deflection and X_{1s} is the shear deflection. For buttons 2 and 3, the corresponding deflections are

$$X_{2c} = X_{3c} = X\cos 60^\circ = \frac{X}{2} \qquad (7\text{-}9)$$

$$X_{2s} = X_{3s} = X\cos 30^\circ = \frac{\sqrt{3}}{2} X \qquad (7\text{-}10)$$

The forces produced by these displacements are the products of the individual button spring constants (K_c for compression and K_s for shear) with the normal or shear displacements. For the first button, the forces are

$$F_{1c} = K_c X \qquad (7\text{-}11)$$

$$F_{1s} = 0 \qquad (7\text{-}12)$$

where F_{1c} and F_{1s} are the compressive and shear forces, respectively. For buttons 2 and 3, the same procedure is followed:

$$F_{2c} = F_{3c} = K_c \frac{X}{2} \qquad (7\text{-}13)$$

$$F_{2s} = F_{3s} = K_s \frac{\sqrt{3}}{2} X \qquad (7\text{-}14)$$

The total force F_T in the direction of displacement X is the sum of the force through button 1 and the components of force in the X direction from buttons 2 and 3.

$$F_T = F_{1c} + (F_{2c} + F_{3c}) \cos 60^\circ + (F_{2s} + F_{3s}) \cos 30^\circ = K_c X + \frac{X}{2} K_c + \frac{3}{2} X K_s$$

$$(7\text{-}15)$$

The above equation may be simplified to give

$$F_T = 1.5 (K_c + K_s) X \qquad (7\text{-}16)$$

If the elastomer mount consists of cartridges with a number of individual axial elastomer buttons or elements, the total force is, simply, the sum of the individual element forces,

$$F_T = 1.5 N_B (K_c + K_s) X \qquad (7\text{-}17)$$

where N_B is the number of buttons or elements per cartridge at each circumferential location. The radial stiffness of the assembly, K_R, is the resultant force divided by the imposed displacement.

$$K_R = \frac{F_T}{X} = 1.5 N_B (K_c + K_s) \qquad (7\text{-}18)$$

236

If the circumferential arrangement of elastomer buttons is different from
that shown in Figure 117, the above analysis must be modified to account
for the actual configuration. While the final equation will be somewhat
different, the general procedure will be essentially the same.

Some elastomer damper designs utilize continuous compression cartridges
(Figure 118) or O-rings (Figure 119) as the elastomer elements. O-rings
provide certain conveniences as they are often used as seals (and may thus
serve a dual purpose) and may be obtained quickly and cheaply in a large
variety of sizes and materials. However, the mode of dynamic deformation
of continuous compression cartridges and O-rings is very complicated, and
attempts at representing such deformation analytically have not been very
successful. Consequently, instead of using analytical procedures for
predicting stiffness and damping, it has been generally necessary to generate
large quantities of experimental data (as presented in Section 6.0) directly
in terms of stiffness and damping. Because O-rings do not have a constant
cross-sectional dimension (relative to radial position), they are more
sensitive to changes in preload and more nonlinear than for the other
geometric configurations. In fact, the effect of modest preload (10% or less)
on the properties of pure shear and compression specimens has been shown to
be relatively unimportant [7.9], while that for O-rings (in the form of
squeeze) has been shown to be very significant [7.10]. Consequently, the
use of such elastomer elements in a rotor damper design requires the avail-
ability or generation of test data for the specific geometry.

When considering elastomer damper geometry, it is important to keep in mind
the limitations within which the analyses are valid. The elastomer element
must be short enough that beam effects become negligible when considering
shear and that column effects become negligible when considerating compres-
sion (Section 4.0).

7.3   Reanalyze System with Specified Elastomer Damper Configuration

Once the elastomer material and geometric configuration have been specified,
the corresponding support stiffness and damping values can be determined;
these values can then be compared with the optimal stiffness and damping
values. Invariably, there will be some difference, although it may not be
large. Consequently, reanalysis of the system dynamics will generally be
necessary to consider these actual support parameter values. This is true
for both unidirectional and rotordynamic systems. When analyzing rotordynamic
systems with elastomer dampers, consideration of the effects of angular
stiffness and damping in the dampers may be important, particularly when
axial rows of elastomer shear or compression elements are used. (See Section
8.0 for an example.)

7.4   Design of Damper Hardware

Many factors must be considered in the design of actual elastomer damper
hardware. These factors include both the general design considerations
(simplicity, ease of assembly, durability and cost) and considerations peculiar
to elastomer dampers, such as the choice of geometric configuration for the
elastomer elements, and whether those elements should be permanent or replace-
able. Elastomer dampers for control of unidirectional vibrations usually

237

Outer
Damper
Housing

Elastomer
Ring

Inner
Damper
Housing

Ball
Bearing

Shaft
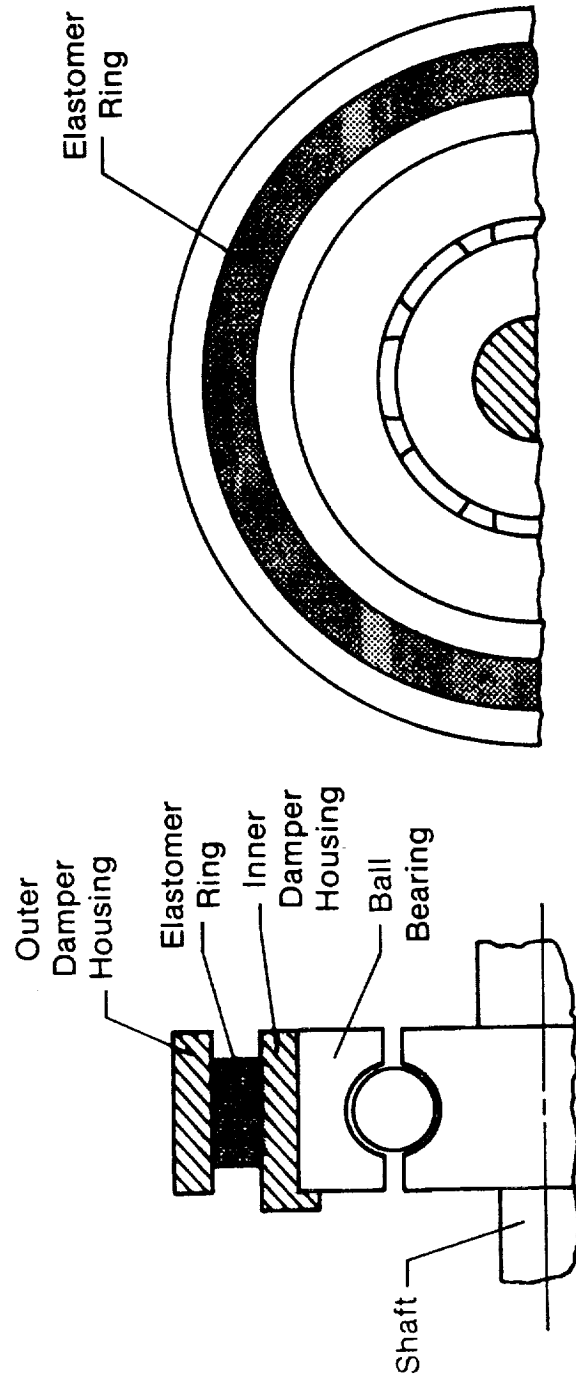
Elastomer
Ring

Fig. 118   Example of Continuous Compression Cartridge Elastomer Damper Configuration
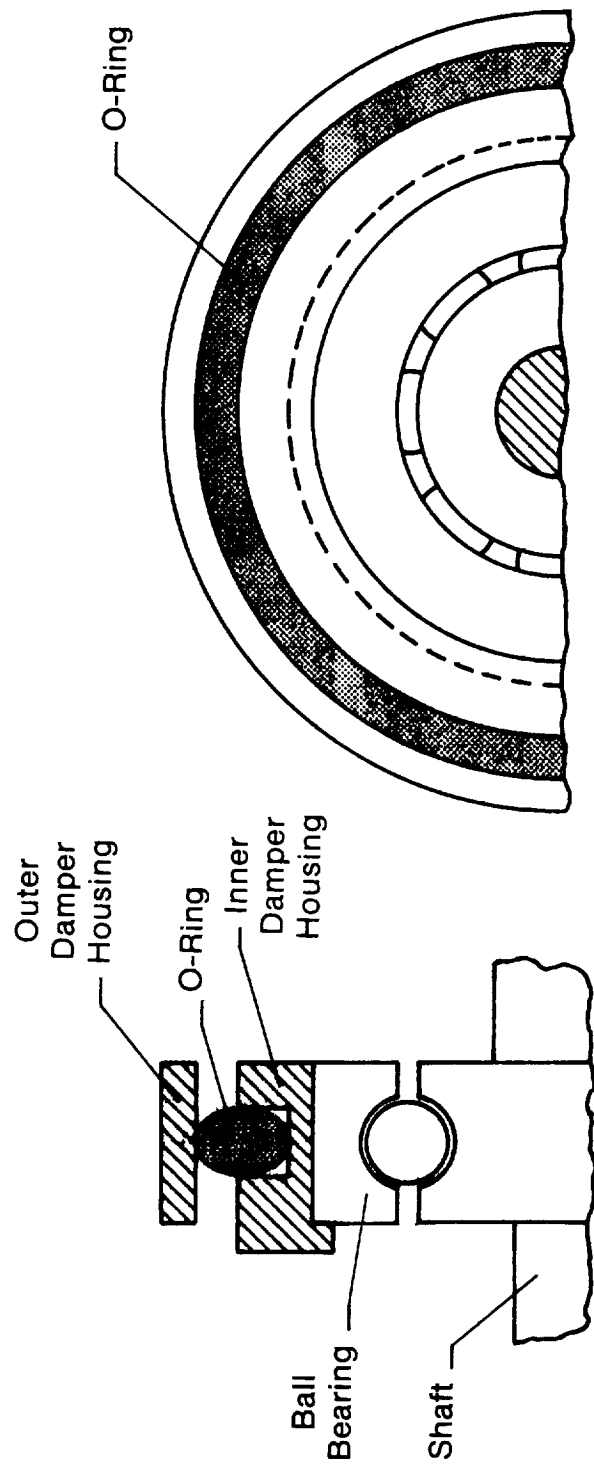
Fig. 119 Example of O-Ring Elastomer Damper Configuration

Outer Damper Housing

O-Ring

Inner Damper Housing

O-Ring

Ball Bearing

Shaft

239

involve simple foot mounting of machines and thus require rather straightforward designs. Occasionally, constrained layer damping (e.g. surface coatings) may be appropriate [7.2].

The required damper designs are generally more complex for rotordynamic systems; space limitations and maintenance requirements tend to be stricter for rotordynamic dampers. For most applications, a segmented elastomer cartridge configuration (with either shear or compression buttons) is recommended. The segmented cartridge is well suited for the design of compact dampers with replaceable elastomer elements. While the use of replaceable elastomer elements results in a small increase in the number of components in the damper, this factor is more than offset by the resulting simplification of the assembly and alignment procedures and the improved maintainability of the damper. The testing of alternative elastomer element materials and dimensions is also possible with replaceable elements, permitting in-service optimization of the damper. The elastomer elements may also be easily replaced after a specified length of running or calendar time during scheduled maintenance operations, thus minimizing the effects of elastomer aging, work hardening, and fatigue.

O-rings may also be utilized as replaceable elastomer elements. However, O-rings are not as convenient to use since they generally require splicing when being replaced. Also, splicing of O-rings results in some variation in circumference which can, in turn, produce some variation in the dynamic properties of the damper.

Several examples of actual elastomer damper designs with replaceable compression or shear button elastomer elements are presented in Section 8.0. Test results and operating experience with these dampers are also discussed.

7.5 Summary

Several steps are involved in the proper design of elastomer dampers for rotating machinery. A recommended set of steps is summarized in the flowchart in Figure 120, corresponding to the steps listed below:

1. Review elastomer materials available for the required parameters and operating environment (temperatures, lubricant compatibility, etc.).

2. Construct a rotordynamics model of the shaft system in its bearings.

3. Compute the damped natural frequencies and logarithmic decrements of the shaft system for a range of support coefficients within the elastomer material limits.

4. Choose optimum support properties in terms of elastomer stiffness and loss coefficient.

5. Confirm this choice of parameters by performing an unbalance response analysis to obtain bearing loads, steady-state orbits, etc.
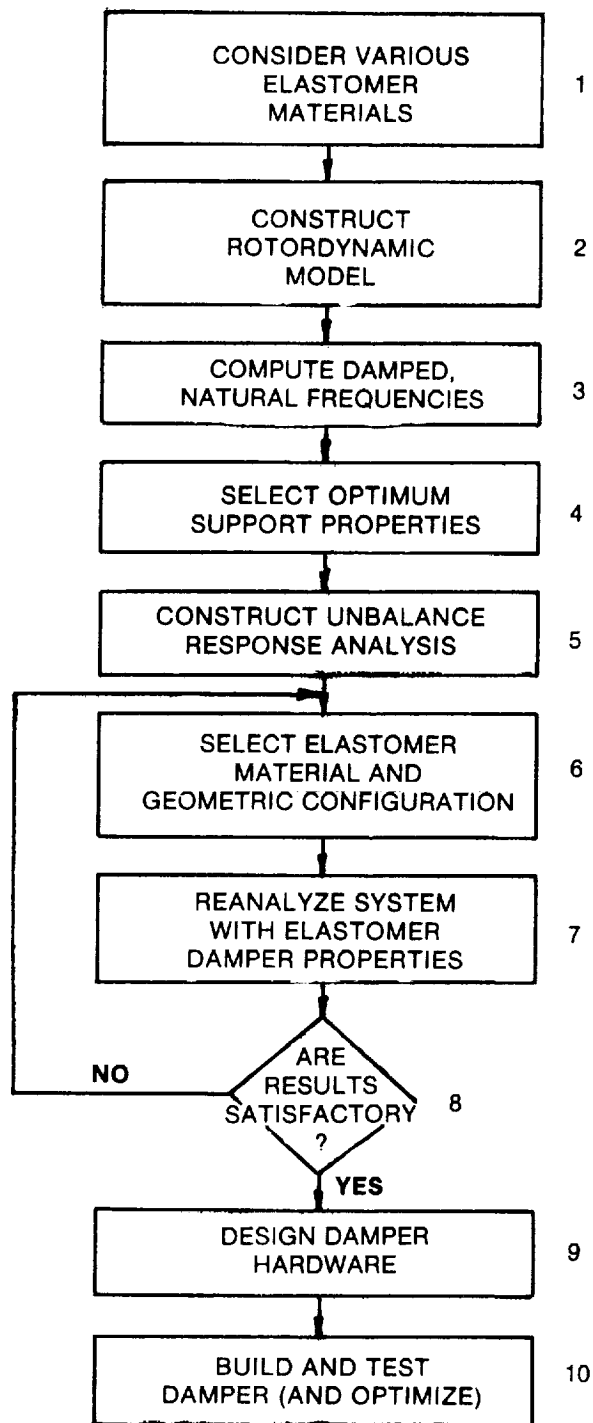
Fig. 120   Flow Chart Showing Steps of Elastomer Damper Design
(Numbers Refer to Number Steps In Text)

6. Select candidate materials and configurations for the damper; perform tests to confirm properties and suitability for the expected operating environment (if such data are not available).

7. Lay out possible configurations for the most promising elastomer; select dimensions to give stiffness and damping properties as close as possible to optimum values for each material; and evaluate the performance of the chosen configurations (using, for example, unbalance response analysis).

8. If the results of step 7 are satisfactory, choose one or more configurations and design the damper in detail; if the results of step 7 are not satisfactory, repeat steps 6 and/or 7 until acceptable combinations are found.

9. Build and test the dampers to experimentally verify their predicted performance, and make final selections.

Several specific examples of this design procedure and of the resulting damper hardware and test results are presented in Section 8.0.

7.6 References

7.1 Harris, C.M. and Crede, C., editors, Shock and Vibration Handbook, Second Edition, McGraw-Hill, New York, 1976.

7.2 Zorzi, E.S., and Frohrib, D., "Stability and Response of a Viscoelastic Shear Damped Kineto-Elastodynamic Mechanism," World Congress on Theory of Machines and Mechanisms, 1973.

7.3 Wang, Ping-Chen, Numerical and Matrix Methods in Structural Mechanics, John Wiley and Sons, Inc., New York, 1966.

7.4 Prohl, M.A., "A General Method for Calculating Critical Speeds of Flexible Rotors", Journal of Applied Mechanics, Vol. 12, Trans. ASME, Vol. 67, 1945, pp. A-142-A-148.

7.5 Lund, J.W., and Orcott, F.K., "Calculations and Experiments on the Unbalance Response of a Flexible Rotor", Journal of Engineering for Industry, Trans. ASME, Series B, Vol. 80, No. 4, Nov. 1967, pp. 785-796.

7.6 Lund, J.W., "Stability and Damped Critical Speeds of a Flexible Rotor in Fluid-Film Bearings", Trans. ASME, Journal of Engineering for Industry, May 1974, pp. 509-517.

7.7 Zorzi, E.S., and Nelson, H.D., "Finite Element Simulation of Rotor-Bearing Systems with Internal Damping", ASME Transactions, Journal of Engineering for Power, ASME paper no. 76-GT-89, April 1976.

7.8   Tecza, J.A., Darlow, M.S., and Smalley, A.J., "Development of Pro-
cedures for Calculating Stiffness and Damping Properties of Elastomers
in Engineering Applications, Part V: Elastomer Performance Limits and
the Design and Test of an Elastomer", NASA Report CR-159552, February
1979.

7.9   Smalley, A.J. and Tessarzik, J.M., "Development of Procedures for
Calculating Stiffness and Damping Properties of Elastomers in Engineer-
ing Applications, Part III: The Effects of Temperature, Dissipation
Level and Geometry", NASA Report CR-134939, November 1975.

7.10   Smalley, A.J., Darlow, M.S., and Mehta, R.K., "Stiffness and Damping
of Elastomeric O-Ring Bearing Mounts", NASA Report CR-135328, November
1977.

8.0 EXAMPLES OF ELASTOMER DAMPER DESIGNS

The step-by-step procedure for the design of elastomer dampers for rotating machinery was discussed in detail in Section 7.0. Three such dampers, which were designed using this procedure, are described in this section. These dampers were built, tested, and operated satisfactorily. The three dampers described were used on a gas turbine simulator [8.1]*, a power transmission shaft [8.2], and an actual power turbine shaft from a gas turbine engine [8.3].

8.1 Gas Turbine Simulator [8.1]

An elastomer damper was applied to a gas turbine simulation rig adapted from an earlier test rig as described in Reference 8.4. The rotor was designed to represent the power turbine of an advanced gas turbine engine and consisted of a 2.22 cm (7/8 in.) x 58.4 cm (23 in.) shaft with a 26 cm (10.25 in.) diameter disc mounted at one end. A small air turbine at the opposite end was used to drive the rotor to a maximum speed of 30,000 rpm. Figure 121 shows this rotor during assembly. The rotor was supported by a pair of angular contact ball bearings at either end, originally mounted in pedestals with metallic flexures and damped with squeeze-film dampers. These pedestals were put aside, and a new set was designed to substitute elastomeric mounts for the original flexure-squeeze-film arrangement.

The new mounts were designed by creating a mathematical model of the rotor. This model, shown schematically in Figure 122, consisted of 31 stations defining 30 discrete sections. Each section was defined by length, outer diameters, inner diameter, elastic modulus, density and shear modulus. Additionally, discs described by concentrated mass and inertia values were located at appropriate stations. The mathematical model of this rotor is shown in Table 24. Elastomeric pedestals were represented by radial stiffness and equivalent viscous damping coefficients. The ball bearings were represented by a radial elastic stiffness and a small viscous damping coefficient. The bearings and pedestals were assumed to have had zero angular stiffness and damping.

The mathematical analysis of the elastomer damper test rig was composed of three phases. The first phase consisted of a damped critical speed analysis [8.5] which allowed the optimum support properties to be determined, along with the selection of elastomers to be tested. The second phase consisted of performing a response analysis to compute expected unbalance response of the test rig [8.6], and the third phase involved the actual design of the elastomer supports.

A damped natural frequency analysis was performed to assess the values required for elastomer stiffness and damping. The pedestals were assumed to have stiffnesses of 1.75×10^6, 5.25×10^6 and 1.75×10^7 N/m (10^4, 3×10^4 and 10^5 lb/in.) at both ends. Damped natural frequencies were computed for pedestal damping coefficients of 1750, 3500 and 8750 Ns/m (10, 20, and 50 lb-sec/in.). Table 25 shows the results of these calculations. Damped

---

* Numbers in brackets indicate references found in Section 8.5.
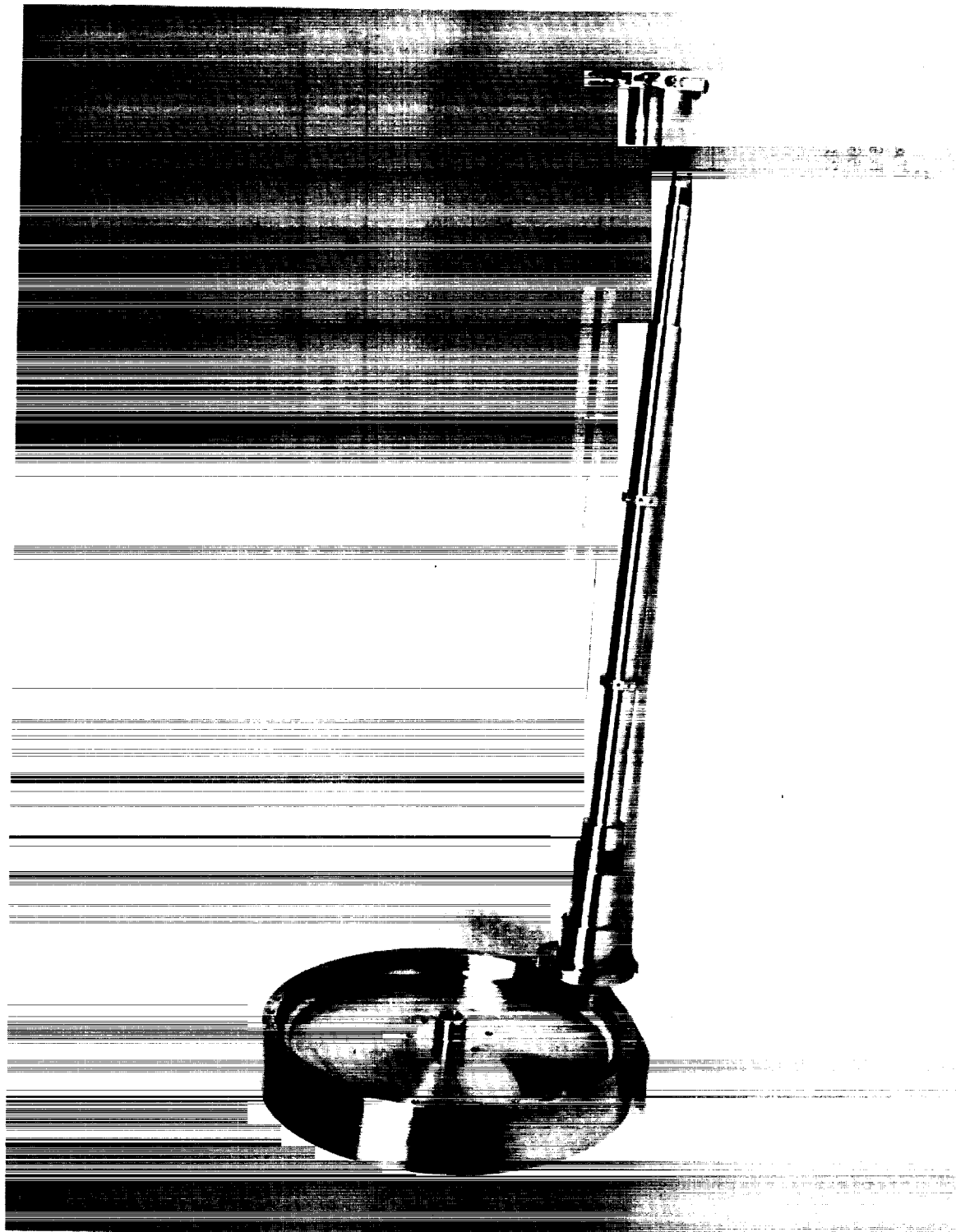
Fig. 121   Test Rotor During Assembly
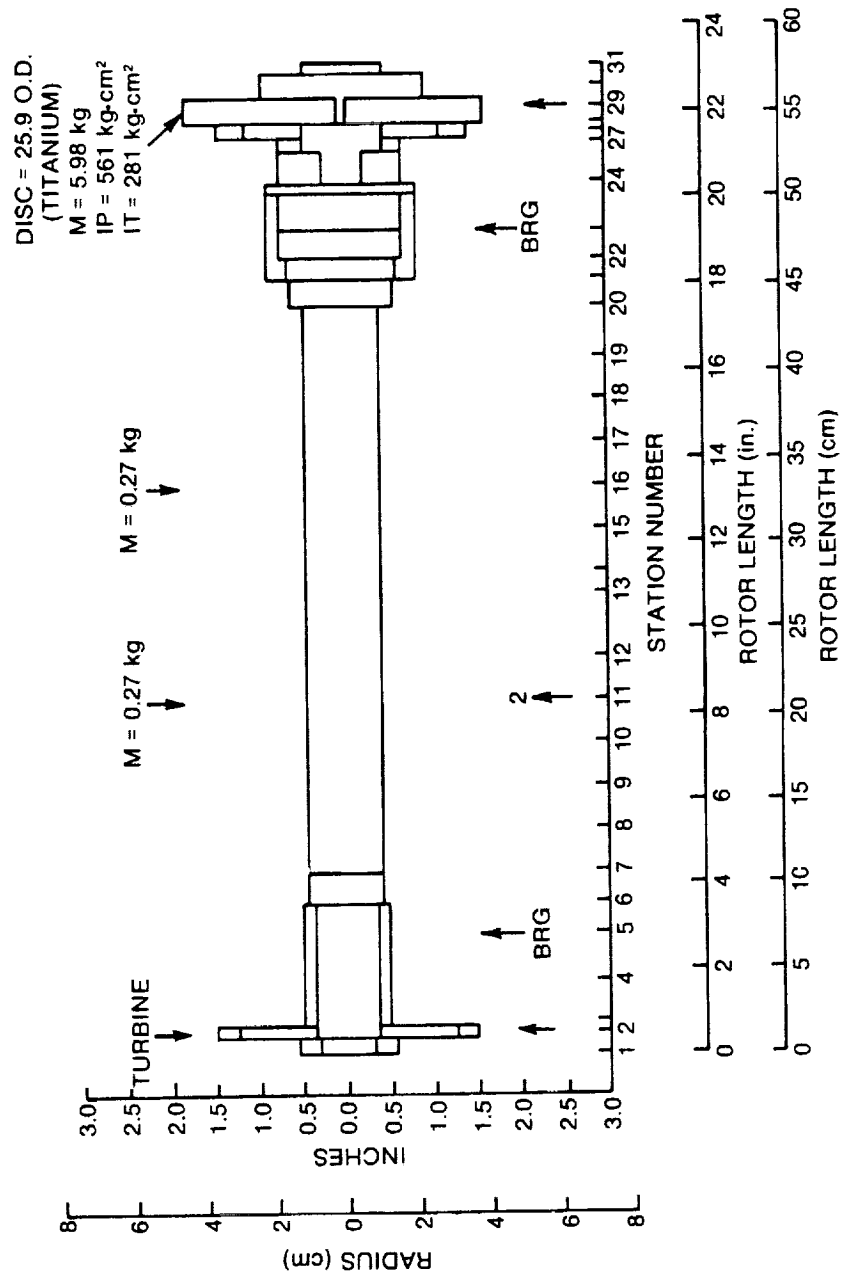
Fig. 122   Test Rotor Schematic Diagram

DISC = 25.9 O.D.
(TITANIUM)
M = 5.98 kg
IP = 561 kg·cm²
IT = 281 kg·cm²

M = 0.27 kg

M = 0.27 kg

TURBINE

BRG

BRG

INCHES

RADIUS (cm)

STATION NUMBER

ROTOR LENGTH (in.)

ROTOR LENGTH (cm)

Table 24

TEST ROTOR MATHEMATICAL MODEL

ROTOR DATA

STATION	MASS-LBS	POLAR M.IN	TRNSV.M.IN	LENGTH	DIA(STIFF)	DIA(MASS)	INNER DIA.	YOUNGS MOD	(SHEAR)*G	DENSITY
1	-0.	-0.	-0.	.4300E+00	.6250E+00	.1125E+01	0.	.3000E+08	.8650E+07	.2830E+00
2	-0.	-0.	-0.	.2500E+00	.7000E+00	.3000E+01	0.	.3000E+08	.8650E+07	.2830E+00
3	-0.	-0.	-0.	.1000E+01	.7000E+00	.1000E+01	0.	.3000E+08	.8650E+07	.2830E+00
4	-0.	-0.	-0.	.1062E+01	.7000E+00	.1000E+01	0.	.3000E+08	.8650E+07	.2830E+00
5	-0.	-0.	-0.	.7800E+00	.7000E+00	.1000E+01	0.	.3000E+08	.8650E+07	.2830E+00
6	-0.	-0.	-0.	.6950E+00	.8750E+00	.8750E+00	0.	.3000E+08	.8650E+07	.2830E+00
7	-0.	-0.	-0.	.1000E+01	.8750E+00	.8750E+00	0.	.3000E+08	.8650E+07	.2830E+00
8	-0.	-0.	-0.	.1000E+01	.8750E+00	.8750E+00	0.	.3000E+08	.8650E+07	.2830E+00
9	-0.	-0.	-0.	.1000E+01	.8750E+00	.8750E+00	0.	.3000E+08	.8650E+07	.2830E+00
10	-0.	-0.	-0.	.1000E+01	.8750E+00	.8750E+00	0.	.3000E+08	.8650E+07	.2830E+00
11	.6000E-01	-0.	-0.	.1000E+01	.8750E+00	.8750E+00	0.	.3000E+08	.8650E+07	.2830E+00
12	-0.	-0.	-0.	.1500E+01	.8750E+00	.8750E+00	0.	.3000E+08	.8650E+07	.2830E+00
13	-0.	-0.	-0.	.5000E+00	.8750E+00	.8750E+00	0.	.3000E+08	.8650E+07	.2830E+00
14	-0.	-0.	-0.	.1000E+01	.8750E+00	.8750E+00	0.	.3000E+08	.8650E+07	.2830E+00
15	-0.	-0.	-0.	.1000E+01	.8750E+00	.8750E+00	0.	.3000E+08	.8650E+07	.2830E+00
16	.6000E-01	-0.	-0.	.1000E+01	.8750E+00	.8750E+00	0.	.3000E+08	.8650E+07	.2830E+00
17	-0.	-0.	-0.	.1000E+01	.8750E+00	.8750E+00	0.	.3000E+08	.8650E+07	.2830E+00
18	-0.	-0.	-0.	.1000E+01	.8750E+00	.8750E+00	0.	.3000E+08	.8650E+07	.2830E+00
19	-0.	-0.	-0.	.1150E+01	.8750E+00	.8750E+00	0.	.3000E+08	.8650E+07	.2830E+00
20	-0.	-0.	-0.	.6500E+00	.1700E+01	.1200E+01	0.	.3000E+08	.8650E+07	.2830E+00
21	-0.	-0.	-0.	.4000E+00	.1250E+01	.1700E+01	0.	.3000E+08	.8650E+07	.2830E+00
22	-0.	-0.	-0.	.6750E+00	.1400E+01	.1700E+01	0.	.3000E+08	.8650E+07	.2830E+00
23	-0.	-0.	-0.	.9400E+00	.1400E+01	.1700E+01	0.	.3000E+08	.8650E+07	.2830E+00
24	-0.	-0.	-0.	.2000E+00	.1700E+01	.1700E+01	0.	.3000E+08	.8650E+07	.2830E+00
25	-0.	-0.	-0.	.2500E+00	.1400E+01	.1400E+01	.4375E+00	.3000E+08	.8650E+07	.2830E+00
26	-0.	-0.	-0.	.7000E+00	.1400E+01	.1400E+01	.8750E+00	.3000E+08	.8650E+07	.2830E+00
27	-0.	-0.	-0.	.3000E+00	.2200E+01	.2900E+01	.8750E+00	.3000E+08	.8650E+07	.2830E+00
28	-0.	-0.	-0.	.5000E+00	.3600E+01	.1000E-02	0.	.1550E+08	.4310E+07	.1630E+00
29	.1310E+02	.1914E+07	.9579E+07	.5000E+00	.1900E+01	.1000E-02	0.	.1550E+08	.4310E+07	.1630E+00
30	-0.	-0.	-0.	.5000E+00	.8750E+00	.1000E-02	0.	.1550E+08	.4310E+07	.1630E+00
31	-0.	-0.	-0.	0.	0.	0.	0.	.1550E+08	.4310E+07	.1630E+00

ROTOR WEIGHT	TRANS.MOM.IN	POLAR MOM.IN	STATION 1-CG	ROTOR LENGTH
.19357461+02	.83286636+03	.19351246+03	.19878956+02	.22990006+02

247

Table 25

DAMPED NATURAL FREQUENCY AND LOG DECREMENT AS A
FUNCTION OF BEARING SUPPORT STIFFNESS AND DAMPING

Bearing Support Stiffness $\left(\dfrac{N}{m} \middle/ \dfrac{lb}{in.}\right)$	Bearing Support Damping $\left(\dfrac{Ns}{m} \middle/ \dfrac{lb\text{-}sec}{in.}\right)$	Damped Natural Frequency (cpm)		System Log Decrement	
$1.75 \times 10^6/10^4$	1750/10	4,425	17,278	1.311	.077
	3500/20	4,144	17,241	2.791	.152
	8750/50	-	16,997	-	.371
$5.25 \times 10^6/ 3 \times 10^4$	1750/10	7,373	17,521	.767	.086
	3500/20	7,217	17,478	1.574	.168
	8750/50	-	17,301	-	.186
$1.75 \times 10^7/10^5$	1750/10	12,988	18,380	.100	.081
	3500/20	12,948	18,382	.200	.156
	8750/50	12,609	18,282	.460	.392

natural frequencies were calculated by assuming a rotor speed and calculating the natural frequencies corresponding to that speed. Damped natural frequencies are complex quantities and of the form $\sigma \pm i\omega$, where σ denotes system stability (negative σ implies stability) and ω denotes the frequency as the solution form, is $\exp(\sigma \pm i\omega)^\tau$.

The stiffness range of 1.75×10^6 to 1.75×10^7 N/m (10^4 to 10^5 lb/in.) was established as the practical elastomer stiffness range for this size and type of rig.

For a particular elastomer material, the loss coefficient (ratio of damping, ωB, to stiffness, K) is relatively fixed. The equivalent viscous damping, B, generally falls off rapidly with increasing frequency. Consequently, the decision was made to target the elastomer damper design for the higher stiffness of 1.75×10^7 N/m, which maximizes the available damping.

If the log decrement is plotted against pedestal damping for an elastomer stiffness of 1.75×10^7 N/m (100,000 lb/in.), the curves in Figure 123 are the result. From this figure, it is apparent that an optimum value of damping exists, approximately 1.75×10^4 N-sec/m (100 lb-sec/in.), and that the corresponding log decrement is 0.965. Figure 124 shows how damping, B, varies with the loss coefficient, η. For a loss coefficient of 0.8, which is typical for fluorocarbon (Viton 70 - CFM) at 70°F, the equivalent viscous damping at 20,000 rpm is 6655 N-sec/m (38 lb-sec/in.), and, for a loss coefficient of 0.15, which is typical for butadiene (Polybutadiene - BR) at 70°F, the damping is 1261 N-sec/m (7.2 lb-sec/in.)*.

For this series of tests, two elastomer materials, fluorocarbon (Viton - CFM) and butadiene (Polybutadiene - BR), were considered since they represent the practical extremes of elastomer capability in terms of internal damping. Both elastomers incur a penalty with respect to the damping, as compared to the optimum log decrement. Table 26 presents this penalty by comparing the expected log decrement of an elastomer damper with the optimum value of log decrement. The table shows a larger penalty with butadiene (Polybutadiene - BR) than with fluorocarbon (Viton - CFM).

A series of unbalance response calculations were performed to estimate the unbalance sensitivity of the elastomer-mounted rotor. Unbalance may be added in the form of threaded masses screwed into tapped holes at several locations along the rotor (Figure 120). Mass addition locations are at the large disc, two discrete locations along the shaft and at the drive turbine. Figures 125 through 128 illustrate the results of unbalance response calculations using an unbalance of 2.54 gram centimeters (1 gram-inch) in either the disc or the shaft (Stations 29 or 11, respectively, in Figure 122). These figures show the response of the disc (Station 31 of Figure 125) for a mass added to the disc or the response of the center of the shaft (Station 13) for a mass added to the shaft.

---

* The use of equivalent viscous damping to represent hysteretic damping for a single frequency is discussed in Section 2.0.

249
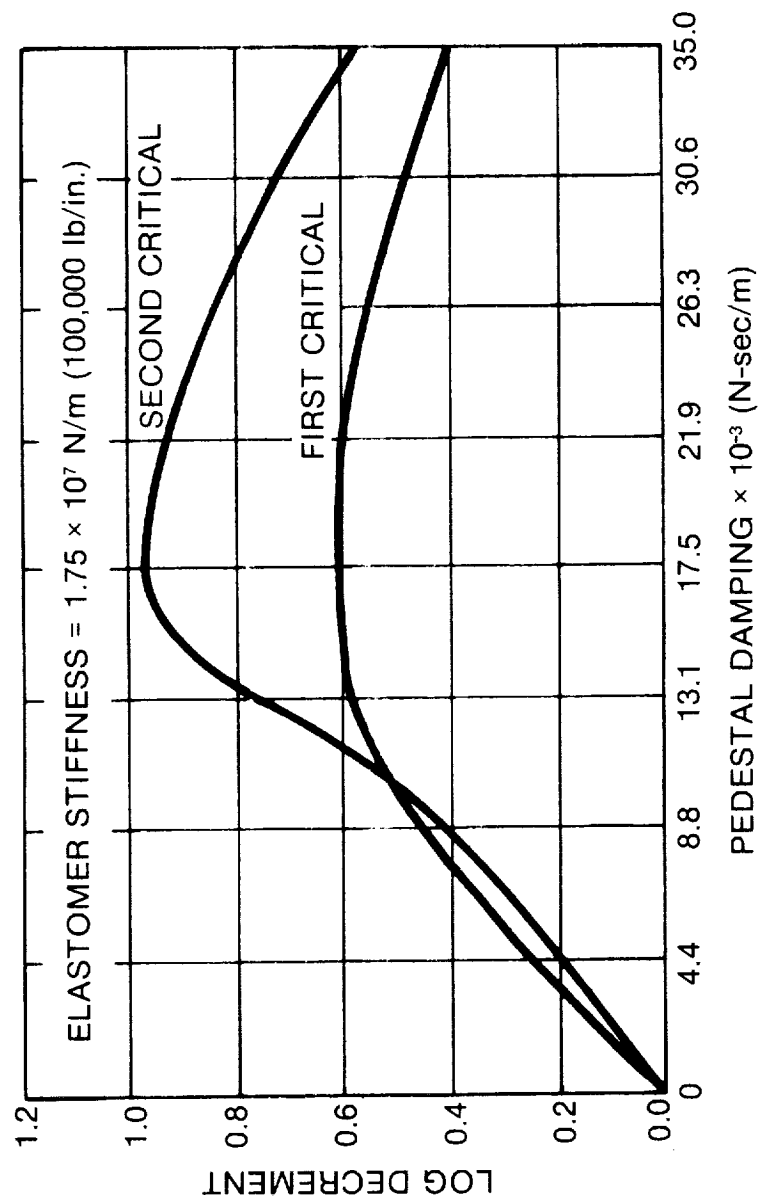
Fig. 123 Elastomeric Damper Test Rig, Log Decrement as a Function of Elastomer Damping

250
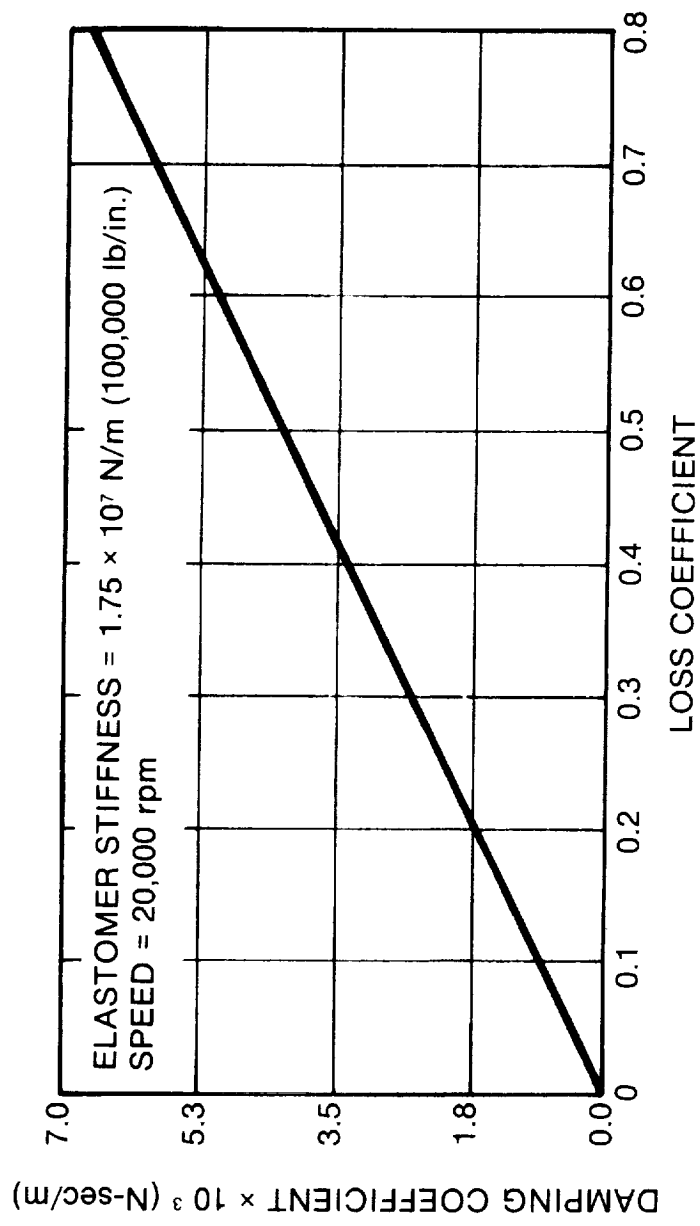
Fig. 124 Damping Coefficient as a Function of Loss Coefficient

251

Table 26

COMPARISON OF MODE-2 LOG DECREMENT FOR BUTADIENE (POLYBUTADIENE - BR)
AND FLUOROCARBON (VITON 70 - CFM) WITH OPTIMUM DAMPING

		$B \left(\dfrac{\text{N-sec}}{\text{m}} \right) \Big/ \left(\dfrac{\text{lb-sec}}{\text{in.}} \right)$	δ
(1)	Optimum	17513/100	.965
(2)	butadiene (Polybutadiene - BR)	1261/7.2	.075
(3)	fluorocarbon (Viton 70 - CFM)	6655/38	.31
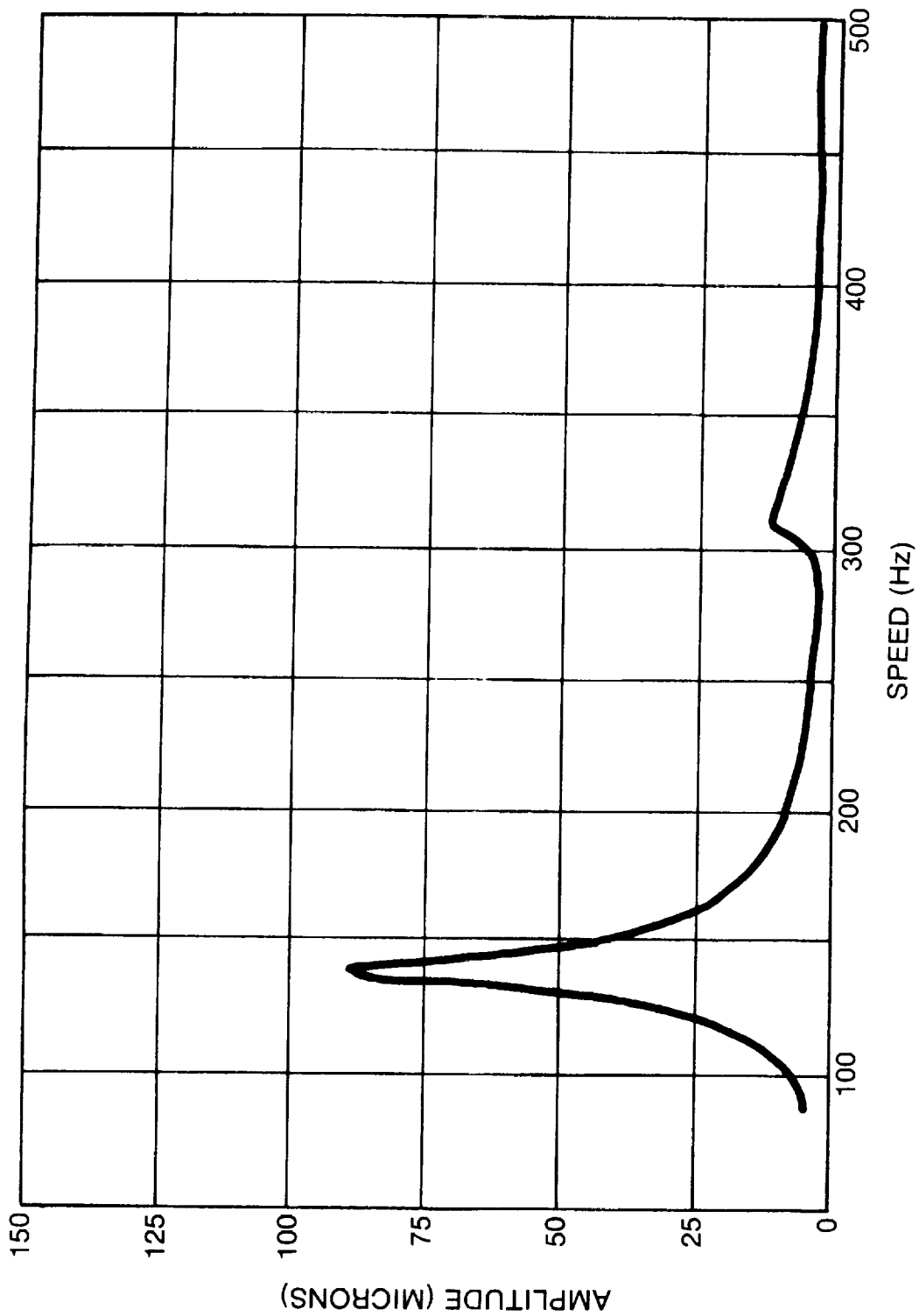
Fig. 125   Disc Unbalance, Sensitivity to Weight at Disc for Butadiene (Polybutadiene) Mounts

253
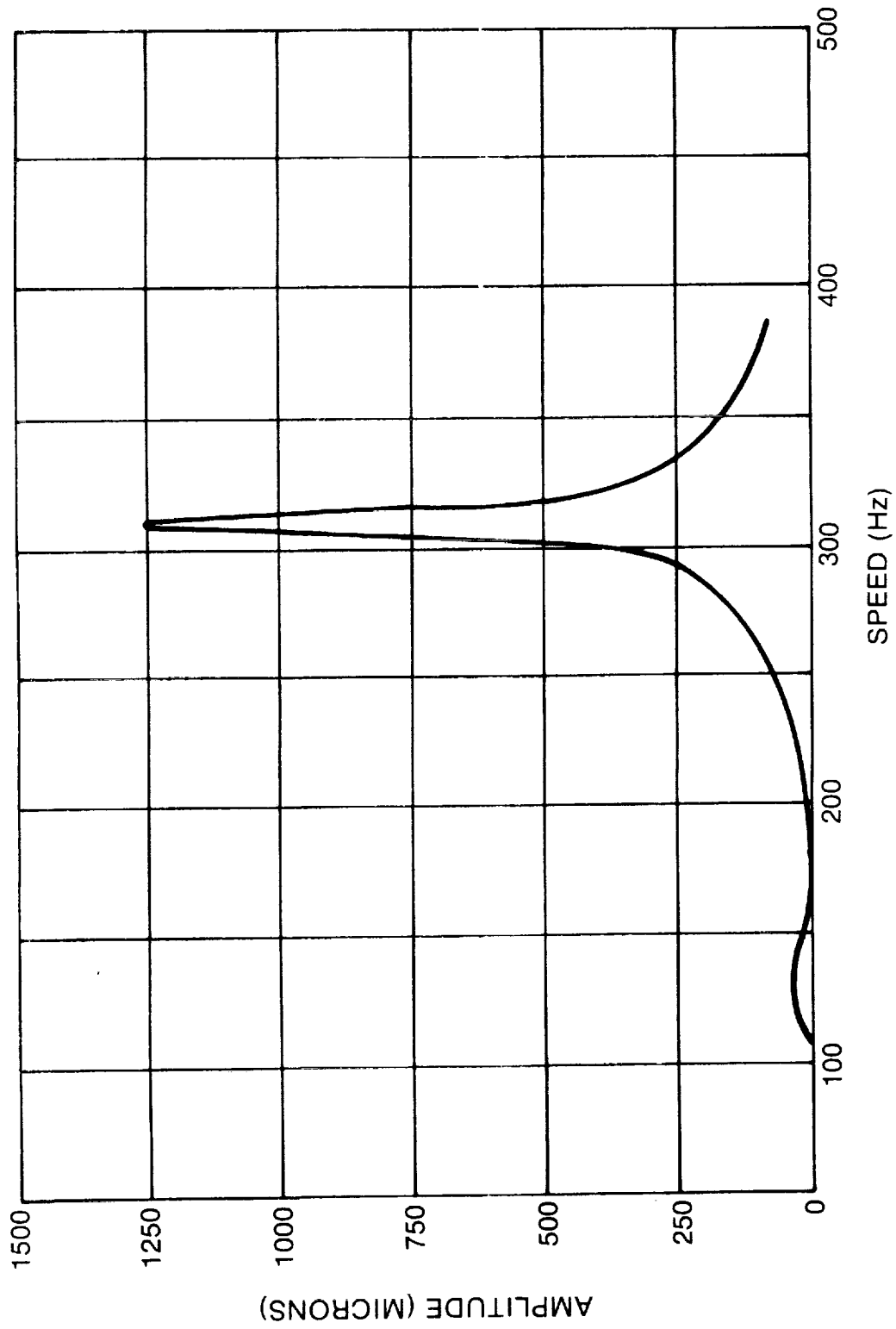
Fig. 126   Shaft Unbalance, Sensitivity to Weight at Shaft for Butadiene (Polybutadiene) Mounts

254
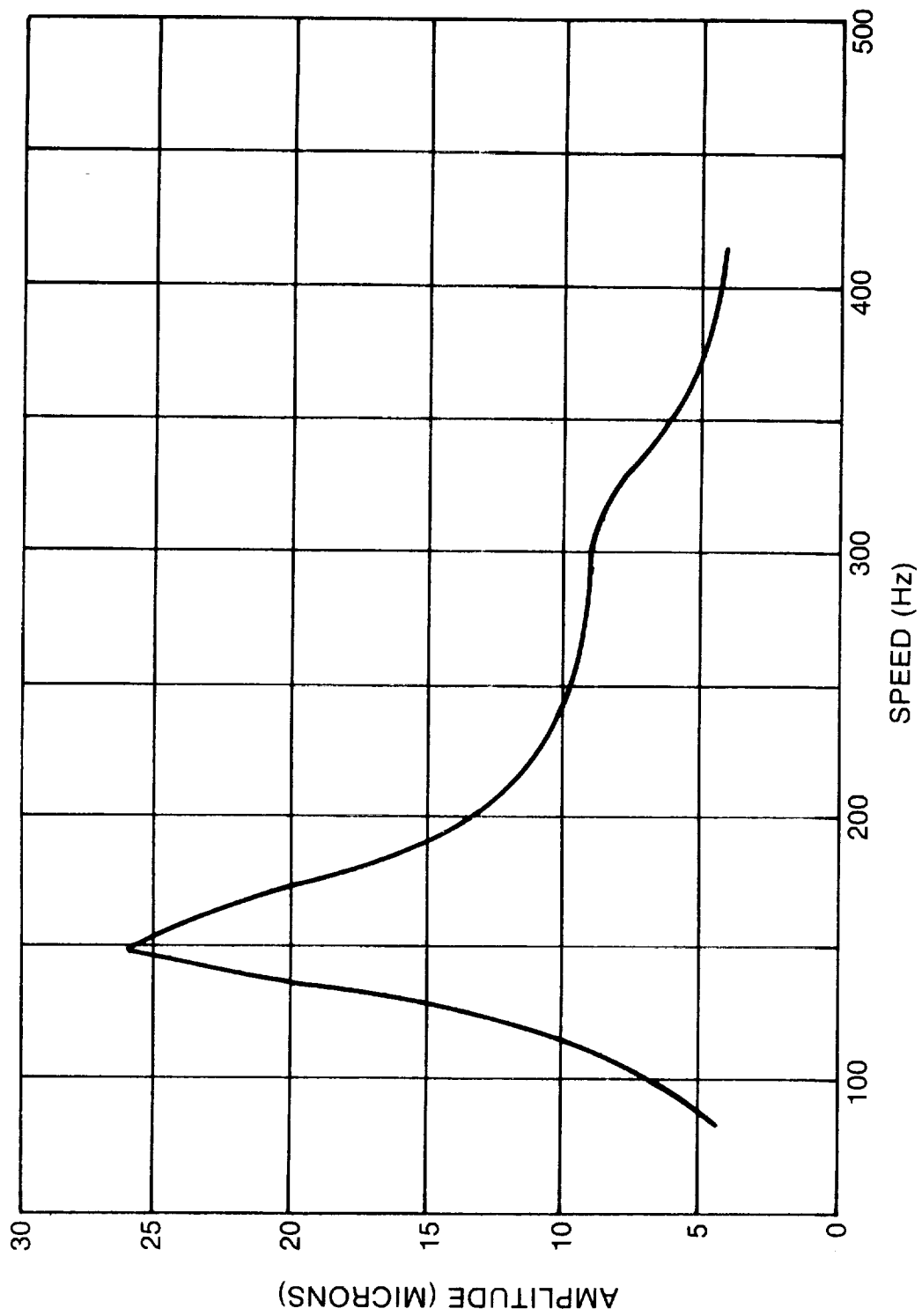
Fig. 127   Disc Unbalance, Sensitivity to Weight on Disc for Fluorocarbon (Viton-70) Mounts

255
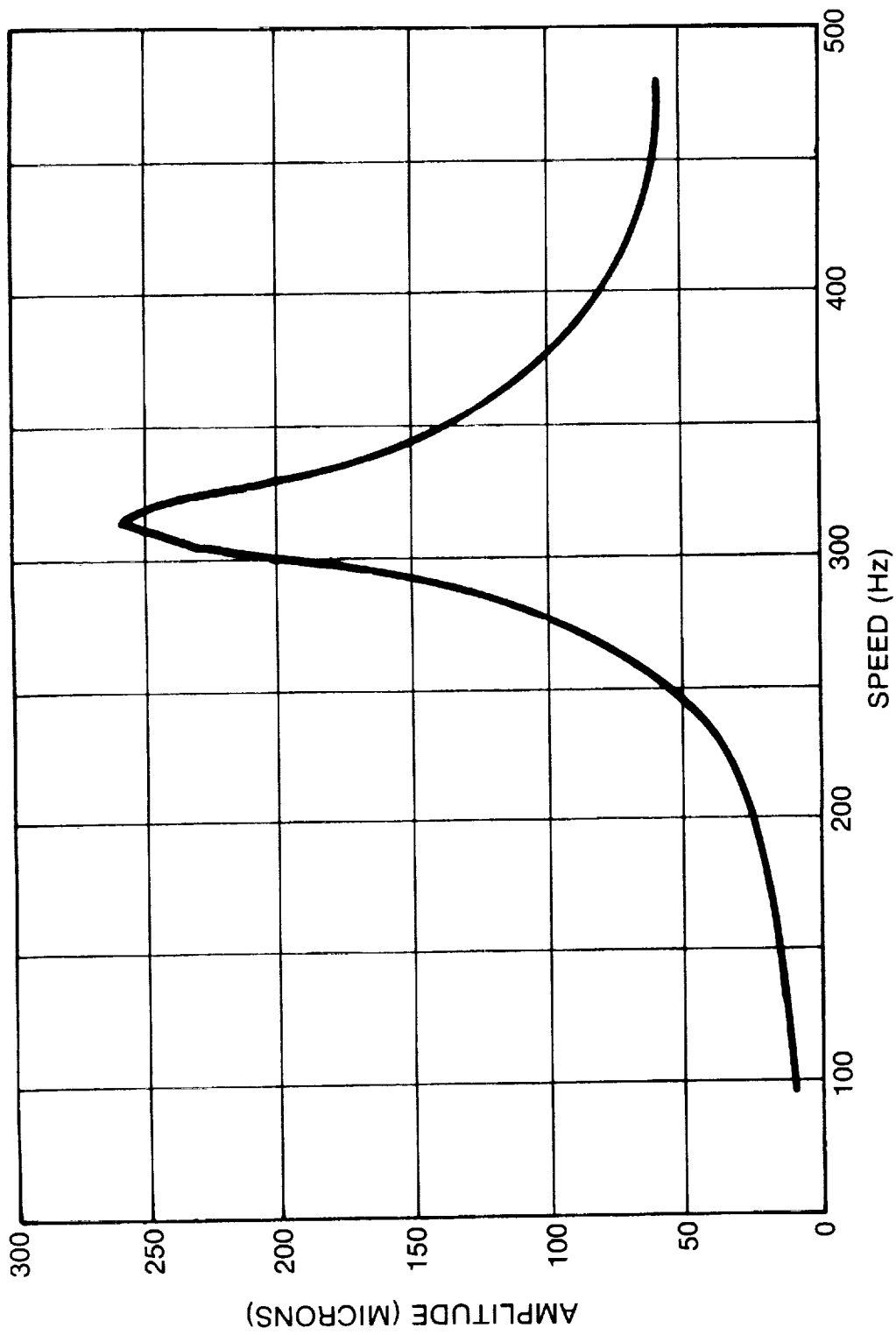
Fig. 128 Shaft Unbalance, Sensitivity to Weight on Shaft for Fluorocarbon (Viton-70) Mounts

256

Figures 125 and 126 show the calculated response plots of amplitude against rotor speed for the test rig on butadiene (Polybutadiene - BR) mounts (loss coefficient $\eta \simeq .15$). Figures 127 and 128 show the response to these same unbalances, but with fluorocarbon (Viton 70 - CFM) supports ($\eta \simeq .8$). These sets of curves indicate that the second critical should be the most troublesome and that the rig should be much more sensitive to unbalance when mounted on the butadiene (Polybutadiene - BR) supports. Table 27 gives the computed values of the rig critical speeds and the expected sensitivity to unbalance in units of microns (peak-to-peak) per gram of unbalance at the balance hole radius.

The elastomer supports were designed by mounting each bearing housing on three elastomer cartridges spaced 120° apart, as shown in Figure 129a. The elastomers' elements were composed of one or more buttons, glued to upper and lower platens to form easily replaceable cartridges as shown in Figure 129b. The number, diameter, and thickness of the buttons in each cartridge were chosen to satisfy the requirement of a 1.75×10^7 N/m (100,000 lb/in.) overall stiffness at 20,000 rpm under specified ambient conditions. The elastomers were preloaded about 10% by a pair of preload screws on each cartridge so the elastomer buttons would always remain in compression.

For the elastomer mounting configuration shown in Figure 129, the overall stiffness was calculated by using the relationship defined in equation (7-18).

In considering the design for individual buttons with the required support stiffness of 1.75×10^7 N/m (100,000 lb/in.), equation (7-18) gives

$$N_B (K_c + K_s) = 11.7 \times 10^6 \text{ N/m (66,666 lb/in.)} \tag{8-1}$$

The empirical correlations for the compressive and shear stiffness of butadiene (Polybutadiene - BR) buttons presented in Section 6.0 were not available at the time that this damper was designed. Consequently, less complete correlations for the shear storage modulus and shape factor developed in Reference 8.7 were used and are given below:

$$K_c = 3G' \frac{\pi D^2}{4h} \left[1 + 12.33\omega^{-0.29} \left(\frac{D}{4h}\right)^2 \right] \tag{8-2}$$

$$K_s = G' \frac{\pi D^2}{4h} \tag{8-3}$$

butadiene (Polybutadiene - BR) at 32°C;

$$G' = 3.686 \times 10^6 \ \omega^{0.2037} \ \text{Pa}(\text{N/m}^2) \tag{8-4}$$

butadiene (Polybutadiene - BR) at 50°C;

$$G' = 1.902 \times 10^6 \ \omega^{0.2727} \ \text{Pa}(\text{N/m}^2) \tag{8-5}$$

257

Table 27

COMPUTED VALUES OF CRITICAL SPEED AND SENSITIVITY TO UNBALANCE

Support Material	Loss Coefficient	Critical Speed Number	Value (rpm)	Sensitivity to Unbalance $\left(\dfrac{\text{microns P-P}}{\text{gram}}\right) / \left(\dfrac{\text{mils P-P}}{\text{gram}}\right)$
butadiene (Polybutadiene – BR)	0.15 0.15	1 2	9,030 18,894	917/36.1 (Disc on Disc) 1478/58.2 (Shaft on Shaft)
fluorocarbon (Viton 70 – CFM)	0.8 0.8	1 2	8,184 18,570	254/10.0 (Disc on Disc) 297/11.7 (Shaft on Shaft)

258

Bearing
Pedestal

Preload
Screw

Elastomer Cartridge

Bearing
Housing

Shaft

Upper
Platen

Elastomer
Button

Lower
Platen
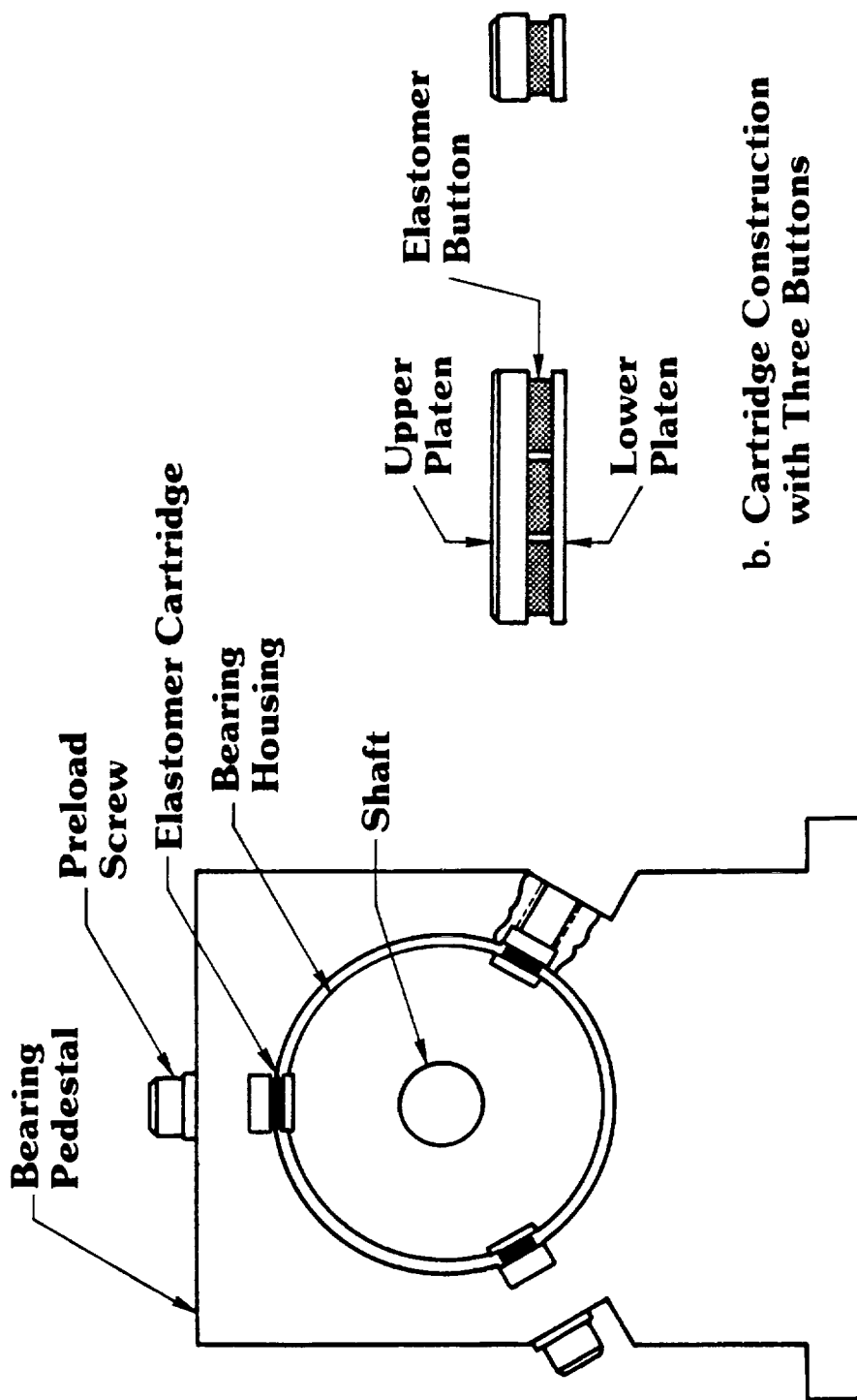
b. Cartridge Construction
with Three Buttons

a. Arrangement of
Elastomer Cartridges

Fig. 129   Elastomer Damper Construction

259

where D is the diameter and h the height of a cylindrical elastomer button (meters); where G' is the shear storage modulus (N/m^2) and ω is the frequency (rad/sec). While the shear modulus is frequency-, temperature-, and dynamic-strain-dependent, the temperature and strain levels encountered in this test rig were similar to those used in Reference 8.7. Thus, the correlations from Reference 8.7, which were not complete in terms of temperature and strain, were shown to be adequate for this application.

Equations (7-18), (8-2), and (8-3) were combined to find the radial stiffness for butadiene (Polybutadiene - BR) buttons as

$$K_R = 4.5 N_B G' \frac{D^2}{4h} \left[1.33 + 12.33^{-0.29} (\frac{D}{4h})^2 \right] \tag{8-6}$$

Similar test data was not available for fluorocarbon (Viton 70 - CFM); however, the radial stiffness correlation for butadiene (Polybutadiene - BR) given in Equation (8-6) was assumed to apply to fluorocarbon (Viton 70 - CFM). Only a value for the shear modulus at the frequency of interest had to be found. The static shear modulus for 70-durometer elastomers (from Reference 8.8) is 1.861 MPa (270 lb/in.^{2}); (see also Figure 64). As the squeeze film is supported on fluorocarbon (Viton - CFM) O-rings, a dynamic multiplier of 6.084 is necessary to correct the static shear modulus to the operating condition of 2,000 rad/sec at 32°C, Reference 8.9. An additional factor of 0.614 is also required to correct for an operating temperature of 50°C at that frequency. Table 28 lists the assumed values of shear modulus for both elastomer types at 2,000 rad/sec.

Equation (8-6) was applied for the appropriate elastomer buttons design. Figures 130 through 133 plot radial stiffness against button diameter for the case of a single button per cartridge (N_B = 1). Each figure consists of three curves corresponding to elastomer thicknesses of 2.38, 3.18 and 4.76 mm (3/32, 1/8 and 3/16 inch). Figure 130 corresponds to fluorocarbon (Viton 70 - CFM) at 32°C, Figure 131 to fluorocarbon (Viton 70 - CFM) at 50°C; Figure 132 to butadiene (Polybutadiene - BR) at 32°C; and Figure 133 to butadiene (Polybutadiene - BR) at 50°C. The required button diameter for any given stiffness is readily found from these curves. Table 29 gives the necessary stiffness per button to achieve the 100,000 lb/in. that was desired for the overall stiffness value.

Table 30 gives the necessary button diameters, based on Table 29 and Figures 130 through 133, to achieve the 1.75 x 10^7 N/m (100,000 lb/in.) stiffness.

Preliminary layout work indicated that a 3-button-per-cartridge arrangement using 1/8-inch thick elastomer stock would be dimensionally convenient. This combination was selected, and, for simplicity, the decision was made to use a single diameter for fluorocarbon (Viton - CFM) and butadiene (Polybutadiene-BR) buttons. A diameter of 15 mm (0.59 in.) was selected (see Table 30) to insure that a minimum stiffness of 1.75 x 10^7 N/m (100,000 lb/in.) existed at all times.

Figure 134 shows the elastomer cartridges being assembled. On the right are two platens and three individual buttons, while the assembled cartridge can be seen on the left. Figure 135 shows the two pedestals and bearings: the

Table 28

VALUES OF SHEAR MODULUS G' AT 2000 RADIANS/SECOND

Elastomer	Temperature ($^{\circ}$C)	Shear Modulus $MPa/\dfrac{lb}{in.^2}$
fluorocarbon (Viton 70 - CFM)	32	11.33/1,643
fluorocarbon (Viton 70 - CFM)	50	6.96/1,009
butadiene (Polybutadiene - BR)	32	17.31/2,511
butadiene (Polybutadiene - BR)	50	14.00/2,031

Table 29

STIFFNESS VALUES TO BE USED IN FINDING BUTTON DIAMETERS

Number of Elastomer Buttons Per Cartridge	Stiffness Value to be Used in Figures 140 through 143 $(\dfrac{N}{m}/\dfrac{lb}{in.})$
1	1.75×10^7/100,000
2	8.76×10^6/50,000
3	5.84×10^6/33,333
4	4.38×10^6/25,000
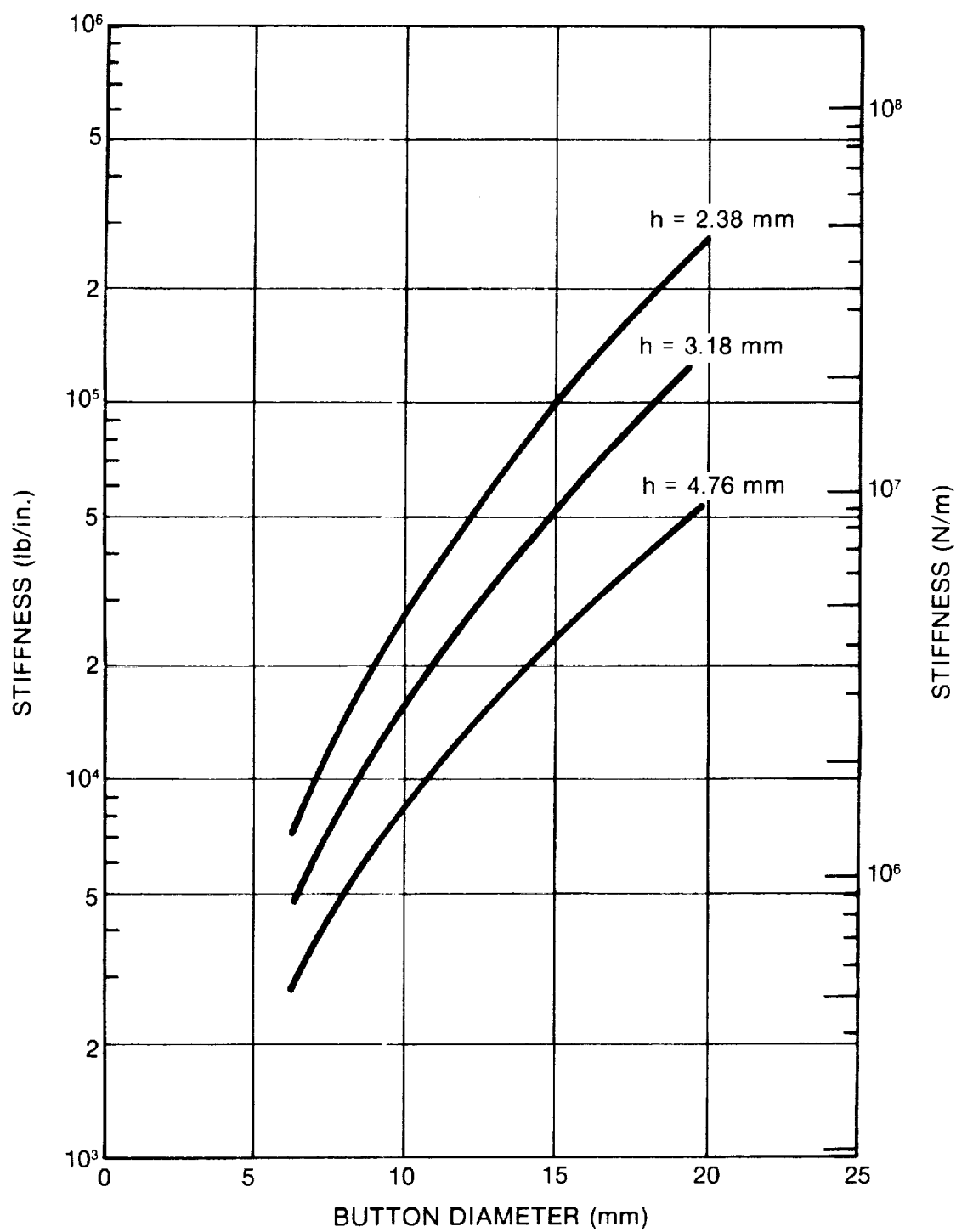
Fig. 130   Plot of Support Stiffness versus Button Diameter for Fluorocarbon (Viton-70) at 32°C
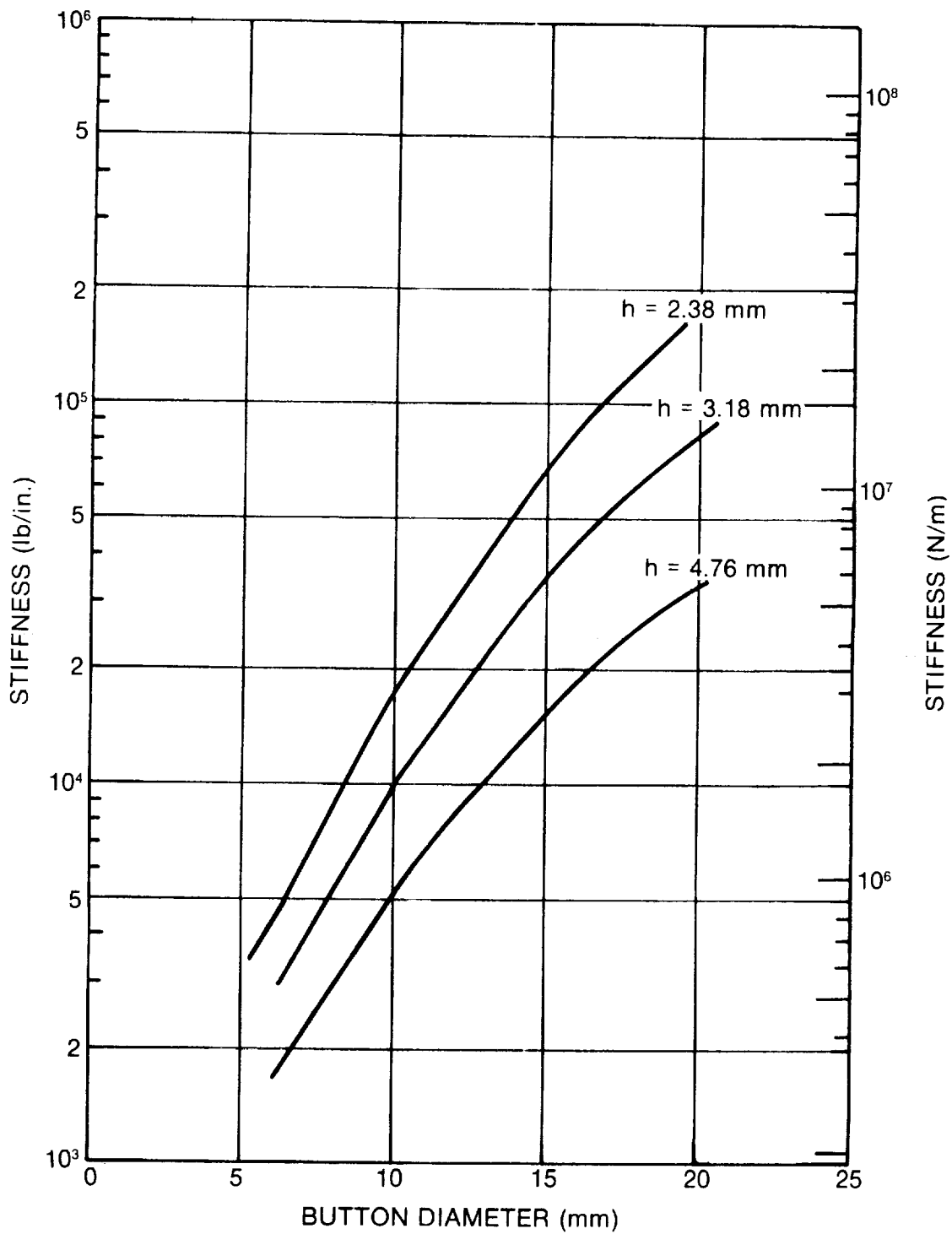
Fig. 131   Plot of Support Stiffness versus Button Diameter for Fluorocarbon (Viton-70) at 50°C
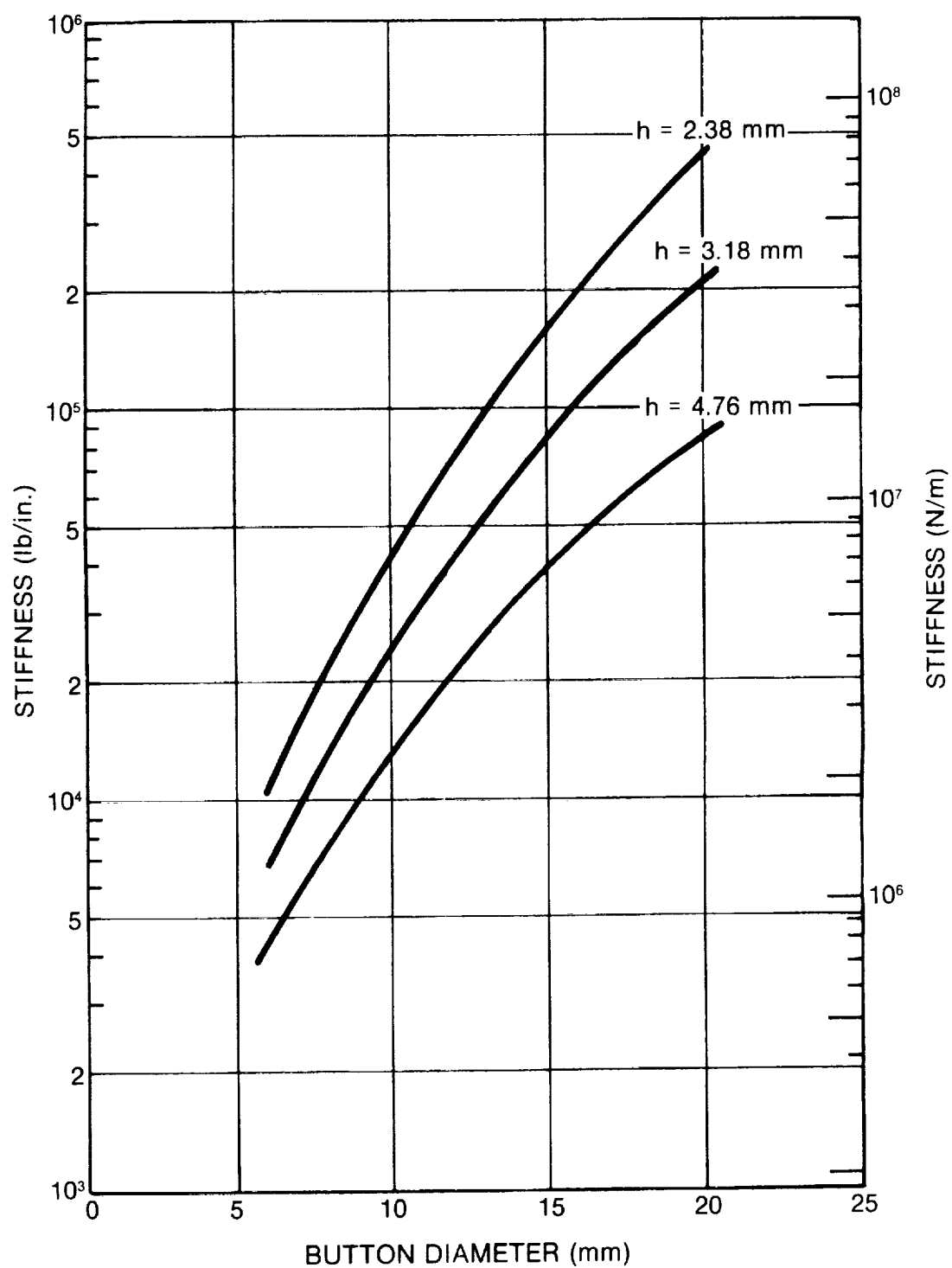
Fig. 132   Plot of Support Stiffness versus Button Diameter for Butadiene (Polybutadiene) at 32°C
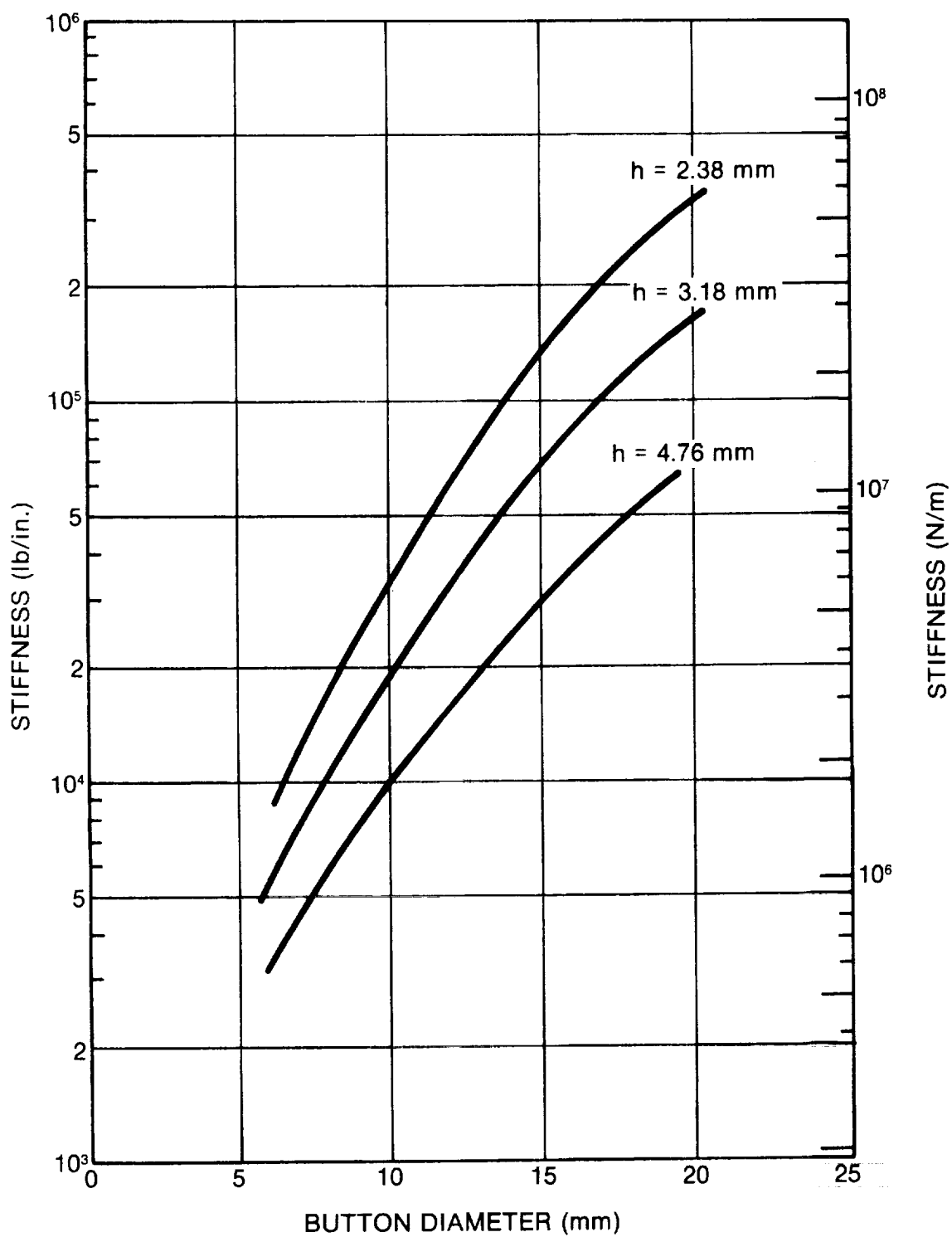
Fig. 133   Plot of Support Stiffness versus Button Diameter for Butadiene (Polybutadiene) at 50°C

265
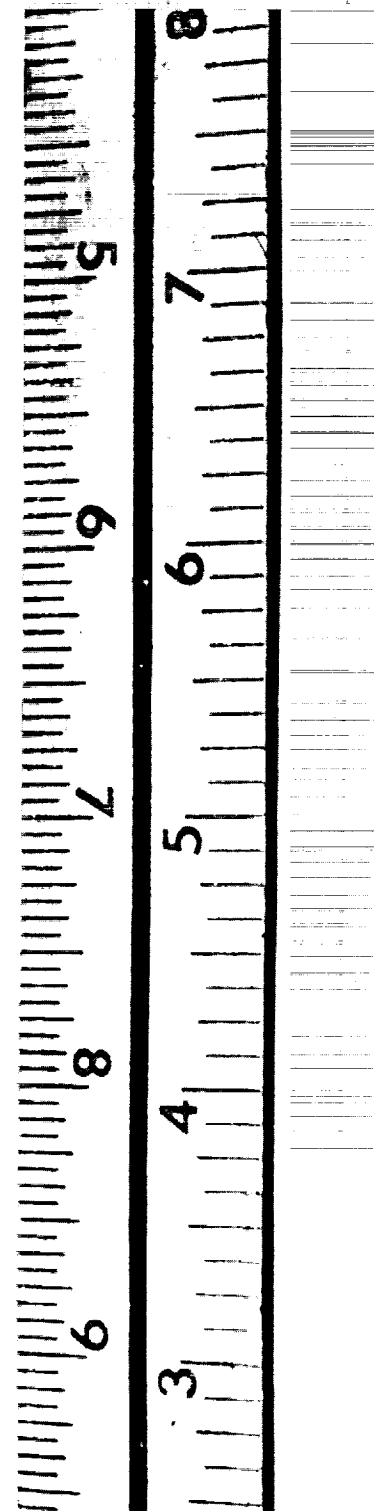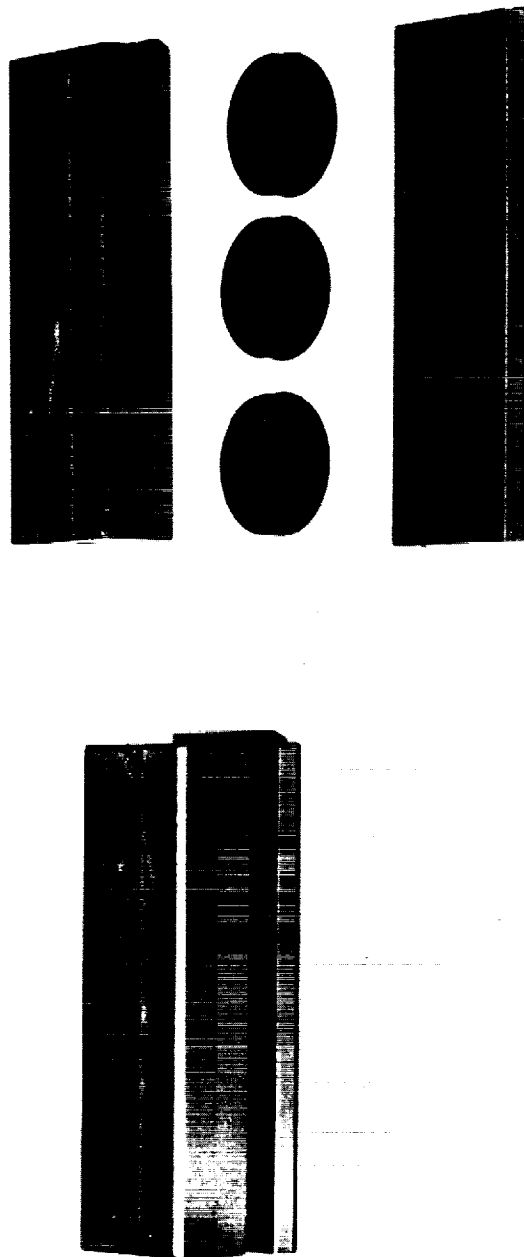
Fig. 134 Detail View of Elastomer Cartridge During Assembly

266

Table 30

BUTTON DIAMETERS TO ACHIEVE A 100,000 LB/IN. RADIAL STIFFNESS

Button Thickness (mm/in.)	Number of Buttons Per Cartridge	flourocarbon (Viton) at 32°C	flourocarbon (Viton) at 50°C	butadiene (Polybutadiene) at 32°C	butadiene (Polybutadiene) at 50°C
$2.38/\frac{3}{32}$	1	14.7/.58	17.0/.67	13.2/.52	14.0/.55
	2	12.2/.48	14.0/.55	10.7/.42	11.4/.45
	3	10.7/.42	12.4/.49	9.4/.37	9.9/.39
	4	9.9/.39	11.4/.45	8.6/.34	9.1/.36
$3.18/\frac{1}{8}$	1	18.0/.71	21.6/.85	16.0/.63	17.0/.67
	2	14.7/.58	17.0/.67	13.0/.51	13.7/.54
	3	13.0/.51	15.0/.59	11.2/.44	12.2/.48
	4	11.7/.46	13.7/.54	10.2/.40	10.9/.43
$4.76/\frac{3}{16}$	1	24.4/.96	28.2/1.11	21.3/.84	22.6/.89
	2	10.6/.77	22.9/.90	16.5/.65	18.0/.71
	3	16.8/.66	20.1/.79	14.5/.57	15.5/.61
	4	15.2/.60	18.0/.71	13.0/.51	14.2/.56
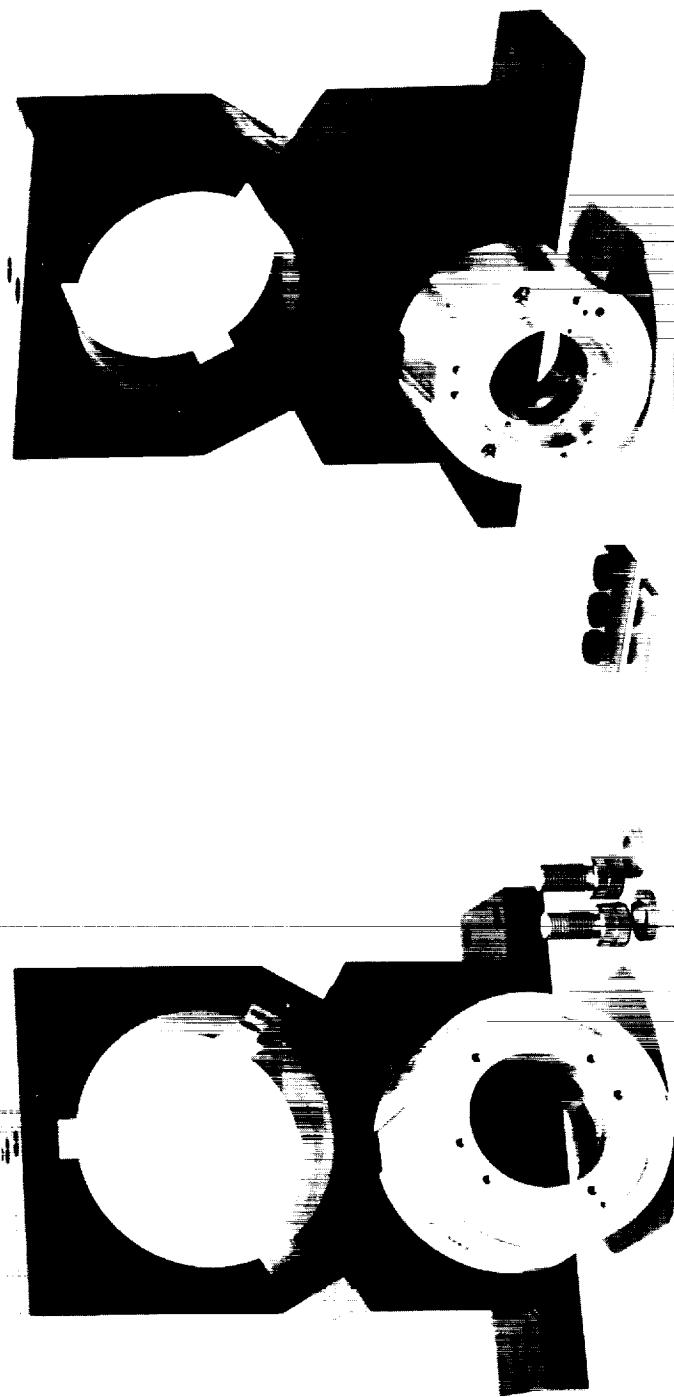
Fig. 135 Elastomer Damper Rig, Pedestals, and Bearing Housings

disc end on the left and the turbine end on the right. Additionally, the figure shows two preload screws with their calibrated washers (the washers were trimmed on assembly to get the correct preload) as well as a partially assembled elastomer cartridge. Figure 136 shows the disc end bearing housing assembled within its pedestal. Note that solid steel blocks have been inserted instead of the elastomer cartridges. These blocks allowed comparisons in unbalance response to be made between hard-mounted and elastomer-mounted rotors.

Figure 137 shows a side view of the test rig as finally mounted and instrumented in the test cell. The disc is inside a vacuum box on the left, and the drive turbine is on the right. Figure 138 shows the rig from the front, with the vacuum hoses in the foreground. Figure 139 shows a detailed view of the turbine-end bearing housing and pedestal. Two elastomer cartridges are visible in the 12 o'clock and 4 o'clock positions. The two noncontacting probes were used to measure the motion of the housing relative to the pedestal, and the two visible flexible tubes are the bearing oil feed and drain lines.

A series of tests were conducted with this test rig to evaluate the effectiveness of the elastomer dampers. The test procedure was as follows:

1. Install butadiene (Polybutadiene - BR) damper cartridges at both locations (turbine end and disk end).

2. Balance the rotor.

3. Create an unbalanced condition in the disk in four discrete steps.

4. Create an unbalanced condition in the shaft in four separate steps after the unbalance has been removed from the disc.

5. Remove shaft unbalance and install fluorocarbon (Viton 70 - CFM) damper cartridges in place of the butadiene (Polybutadiene - BR) cartridges.

6. Rerun with disc unbalances.

7. Repeat shaft unbalance runs.

8. Replace fluorocarbon (Viton - CFM) dampers with solid steel blocks and run with disc unbalance.

9. Replace turbine end steel block with fluorocarbon (Viton - CFM) damper and run with a limited number of unbalances.

10. Record data from selected runs on magnetic tape.

11. Plot displacement amplitude against rotor speed for test runs.

12. Photograph disc and shaft orbits for selected runs.
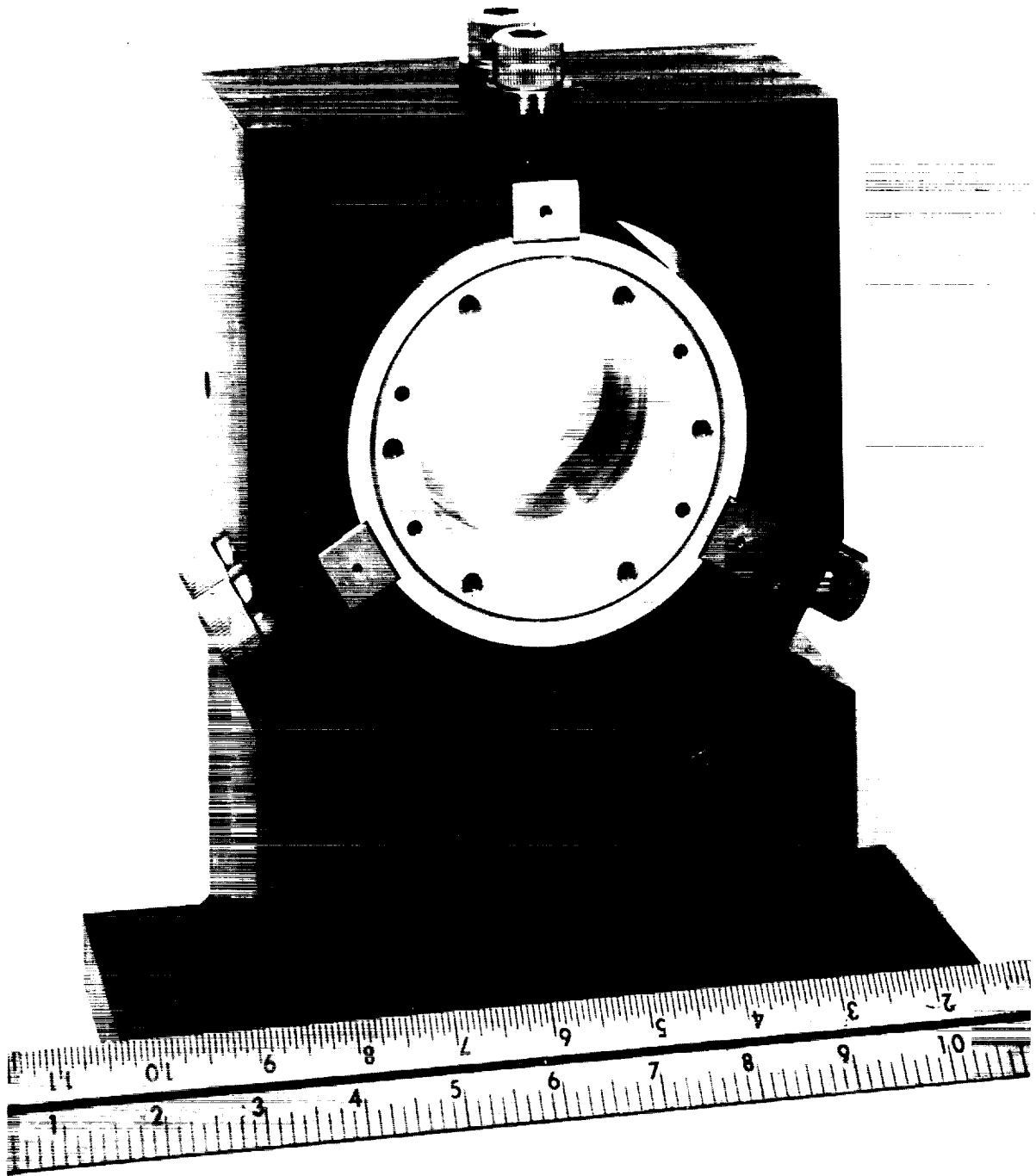
Fig. 136 Partially Assembled Disc, Bearing Housing and Pedestal
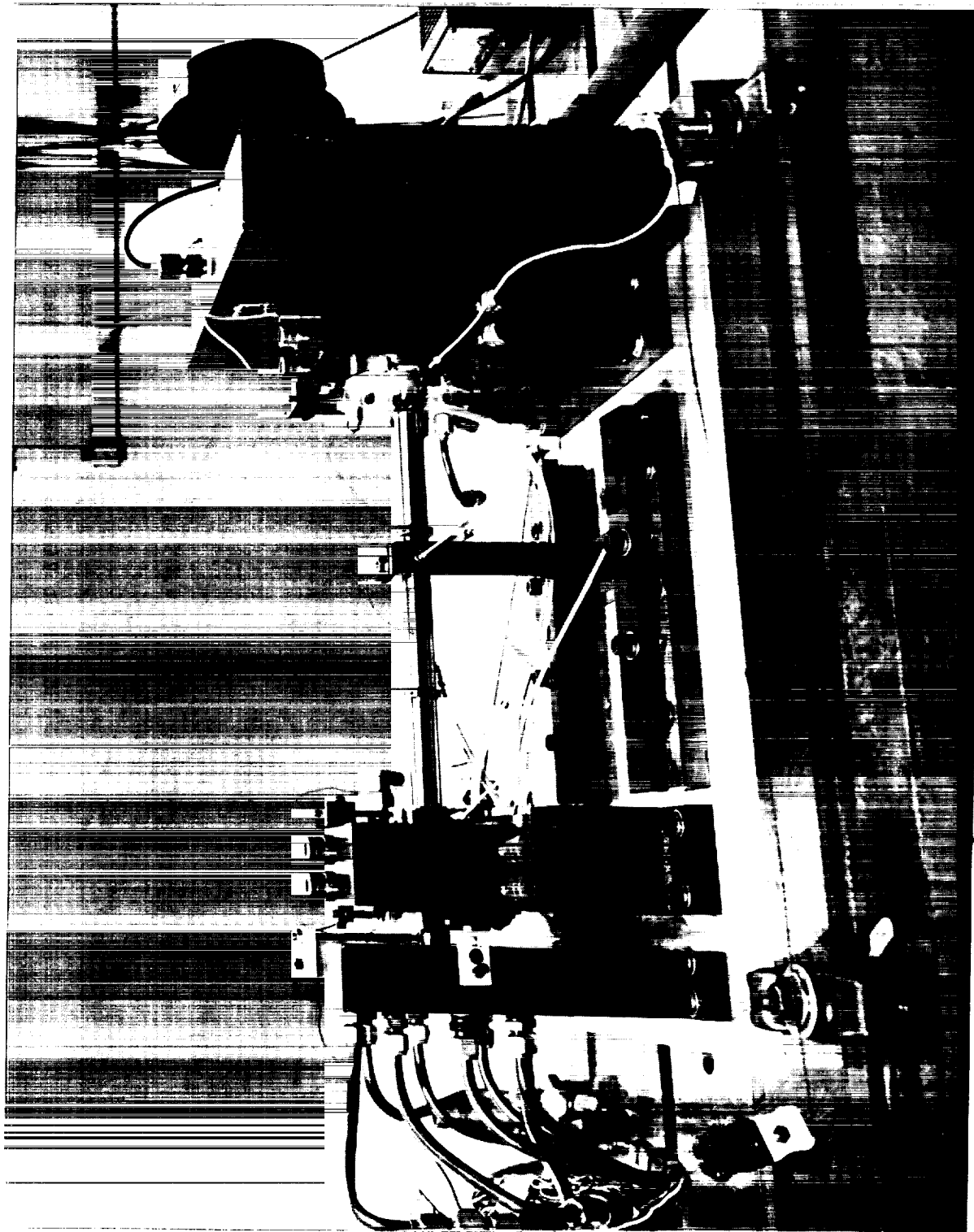
Fig. 137 Side View of Assembled Test Rig
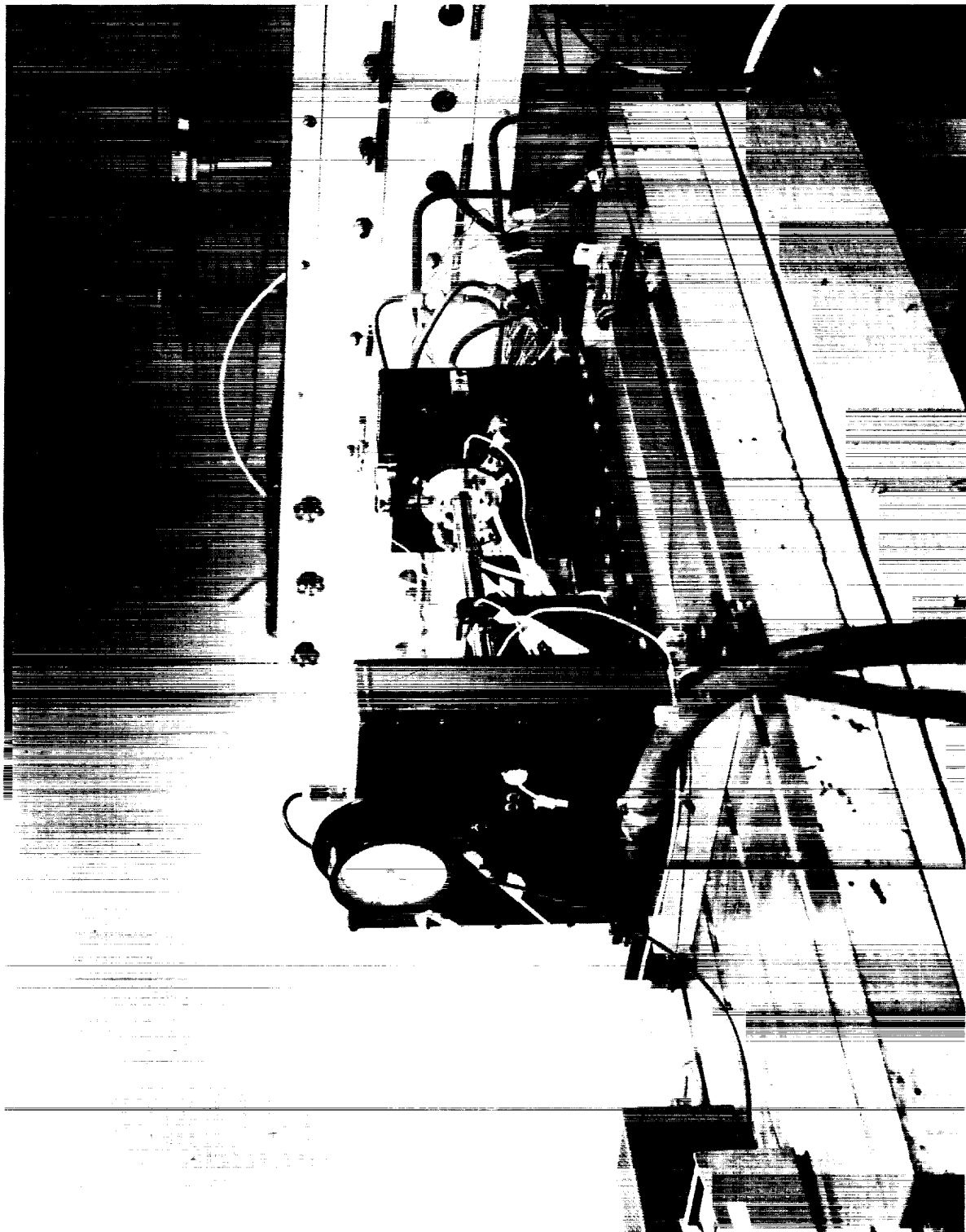
Fig. 138 Front View of Assembled Test Rig

The plan for reducing elastomer damper test rig data involved calculation of sensitivity to unbalance masses, calculation of modal damping values, and comparing these values with predictions. The sensitivity, S_u, to unbalance masses is defined as:

$$S_u = \frac{\text{Modal Response}}{\text{Unbalance Magnitude}} \left[\frac{\text{Mils P-P}}{\text{gram}} \right] \qquad (8-7)$$

The sensitivity for a particular mode depends on the locations of both the unbalance mass and the measurement probe. This sensitivity is valuable in that it is an indication of the difficulty to be expected in balancing a particular mode (at that location).

Damping information was extracted from the test runs by making use of the width of the resonance curve at the half-power points and also by using the rate of change of the phase angle through the resonant speed. With the half-power point method, the resonant speed, f_n (for a particular critical speed), is located by finding the peak of the resonance curve for that mode and noting the frequency at which it occurs. The half-power points are the two locations on the resonance curve where the amplitude is equal to the peak amplitude divided by the square root of two. Then Δf is defined as the difference in frequency between the two half-power points. With this information, the system log decrement, δ, may be found with the equation:

$$\delta \simeq \pi \frac{\Delta f}{f_n} \qquad (8-8)$$

An alternate method takes advantage of the fact that the logarithmic decrement is inversely proportional to the rate of change of the phase angle through the resonant speed. Equation (8-9) expresses the relationship between the log decrement, the resonant frequency, and the rate of change of phase through the resonant speed.

$$\delta \simeq \frac{360}{\left| \frac{d\theta}{df} \right| f_n} \qquad (8-9)$$

Using either equation (8-8) or (8-9), the quality or amplification factor, Q, may be calculated from

$$Q \simeq \frac{\pi}{\delta} \qquad (8-10)$$

The initial or baseline balancing was done with butadiene (Polybutadiene – BR) dampers using an influence coefficient balancing program. Because the first critical speed could not be initially negotiated, influence coefficients were calculated at 7,000 rpm for the first three correction mass runs. Correction masses were only placed in the disc plane.
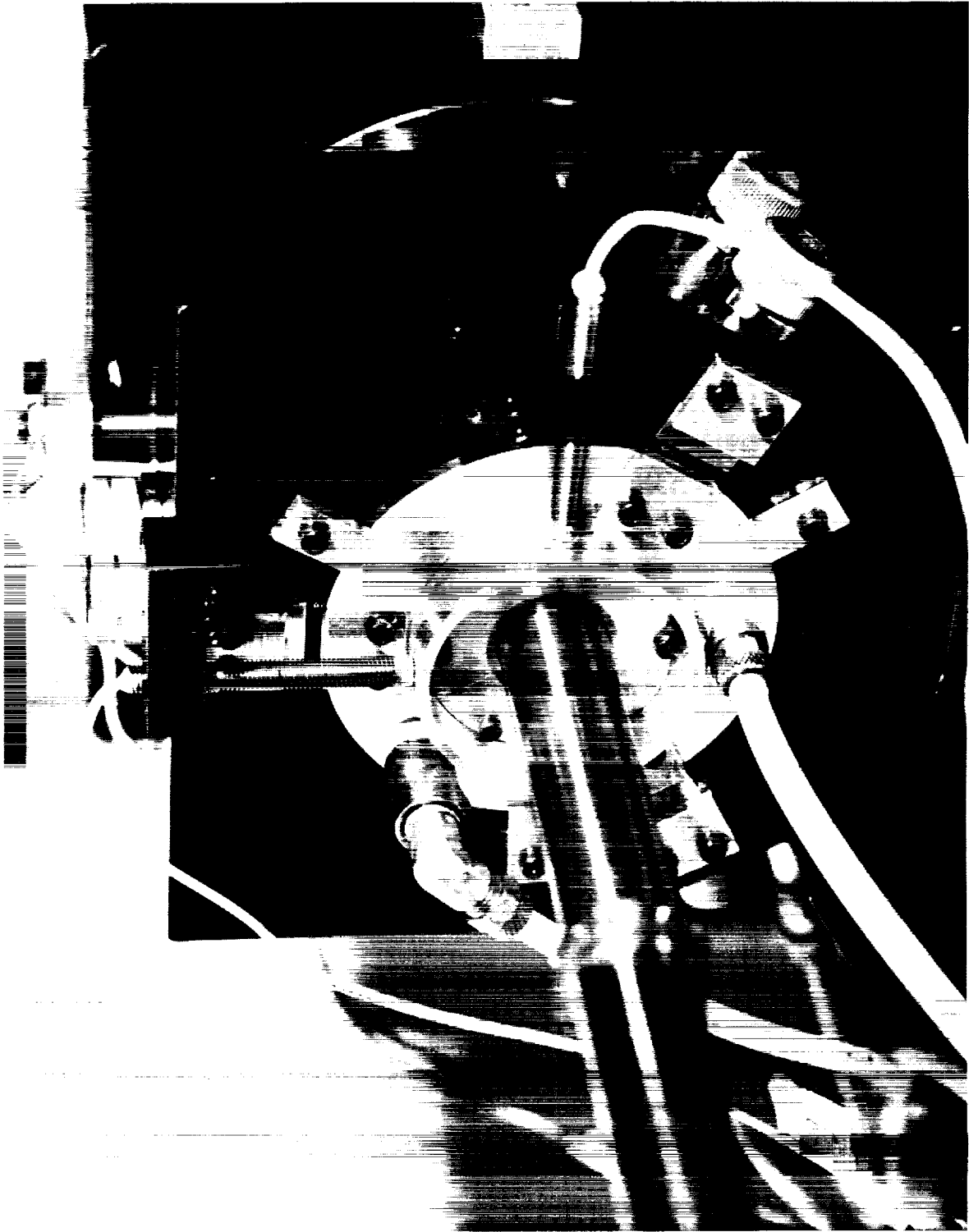
Fig. 139 Close-up of Turbine in Bearing Housing Showing Elastomer Cartridges at 12 o'clock and 4 o'clock Positions

274

Influence coefficients were then calculated at 11,500 rpm and one additional correction mass was installed. The next correction mass run calculated a mass of 0.058 grams which was too small to install. The vibration level was low throughout the speed range (less than 20 microns (.001 inch or 1 mil) peak to peak). Test runs were made with unbalance masses in either the disc (plane 1 of Figure 140) or in the shaft (plane 3 of Figure 140).

Table 31 shows the magnitudes of the unbalance masses used. In the disc, four separate and distinct masses were used alternately in the same holes, but the small hole size on the shaft required simultaneous use of from one to four masses in adjacent holes to obtain the necessary unbalance. The corresponding shaft unbalance mass shown in Table 31 is the equivalent mass (if only one hole were used, i.e., the vector sum of the unbalance masses).

Table 31

SUMMARY OF MASSES USED TO UNBALANCE THE TEST RIG DISC AND SHAFT

Unbalance in Disc (grams)	Unbalance in Shaft (grams)
0.2	0.183
0.3	0.353
0.4	0.583
0.5	0.621

Figure 141 shows the installation of one of the shaft unbalance masses.

Table 32 shows the location of the first two critical speeds of the test rig with the two different damper materials. The critical speeds were higher with the fluorocarbon (Viton - CFM) dampers than with the butadiene (Polybutadiene - BR) dampers. This indicates the fluorocarbon (Viton - CFM) dampers were stiffer than the butadiene (Polybutadiene - BR). The butadiene (Polybutadiene - BR) shear moduli used in the design (Equation 8-4) were based on tests of a previous material batch although while changes in carbon black had been made between batches by the manufacturer. Moduli for the pertinent batch, given in Section 6.0, were only 60% of the values in Equation (8-4).

Table 32

LOCATIONS OF CRITICAL SPEEDS FOR DIFFERENT ELASTOMER SUPPORTS

Elastomer	First Critical Speed	Second Critical Speed
butadiene (Polybutadiene - BR)	10,200	20,500
fluorocarbon (Viton 70 - CFM)	12,050	24,000

275
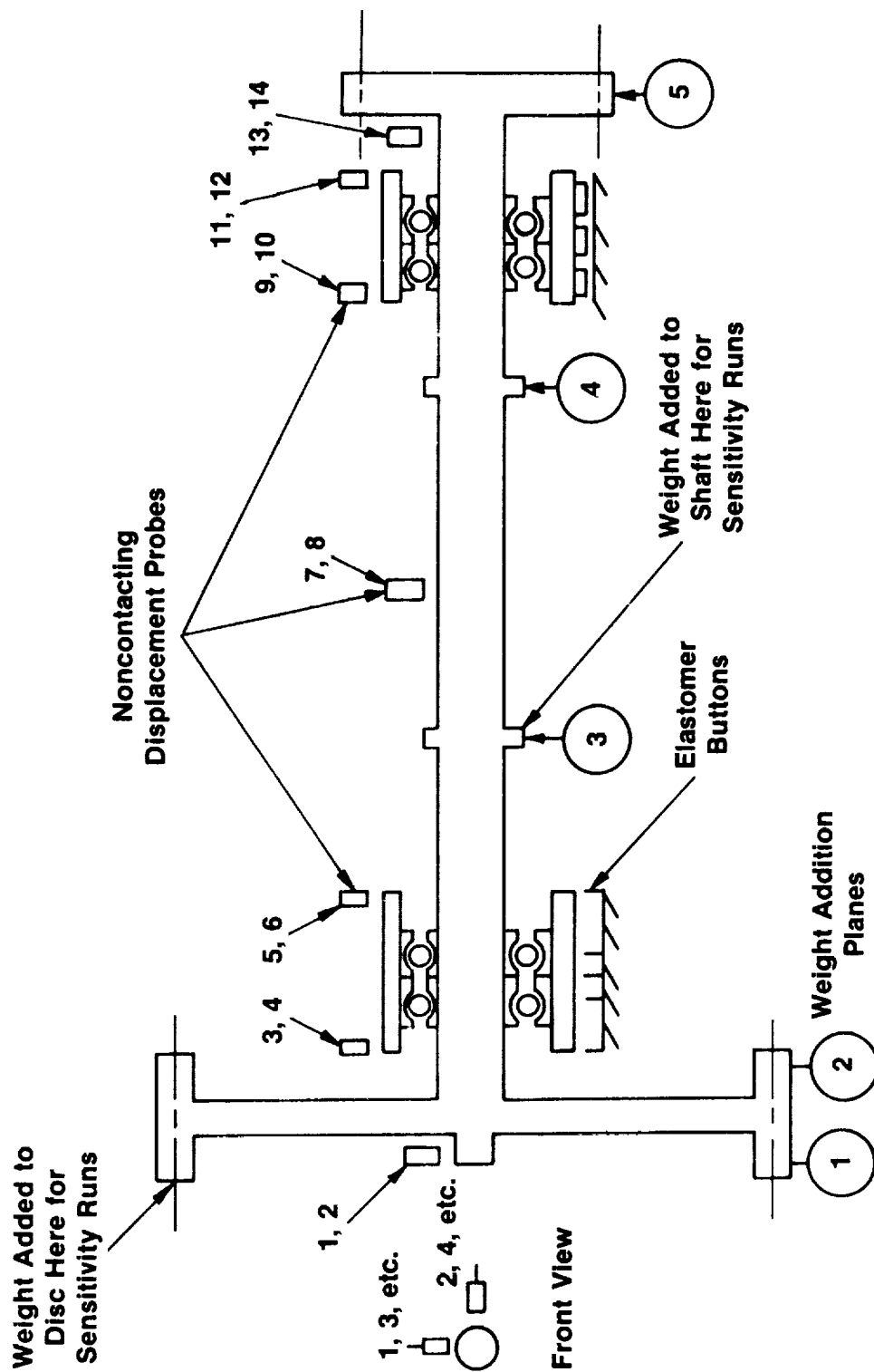
Fig. 140 Schematic of Rotor System Showing Weight Addition Planes and Displacement Probe Locations

276
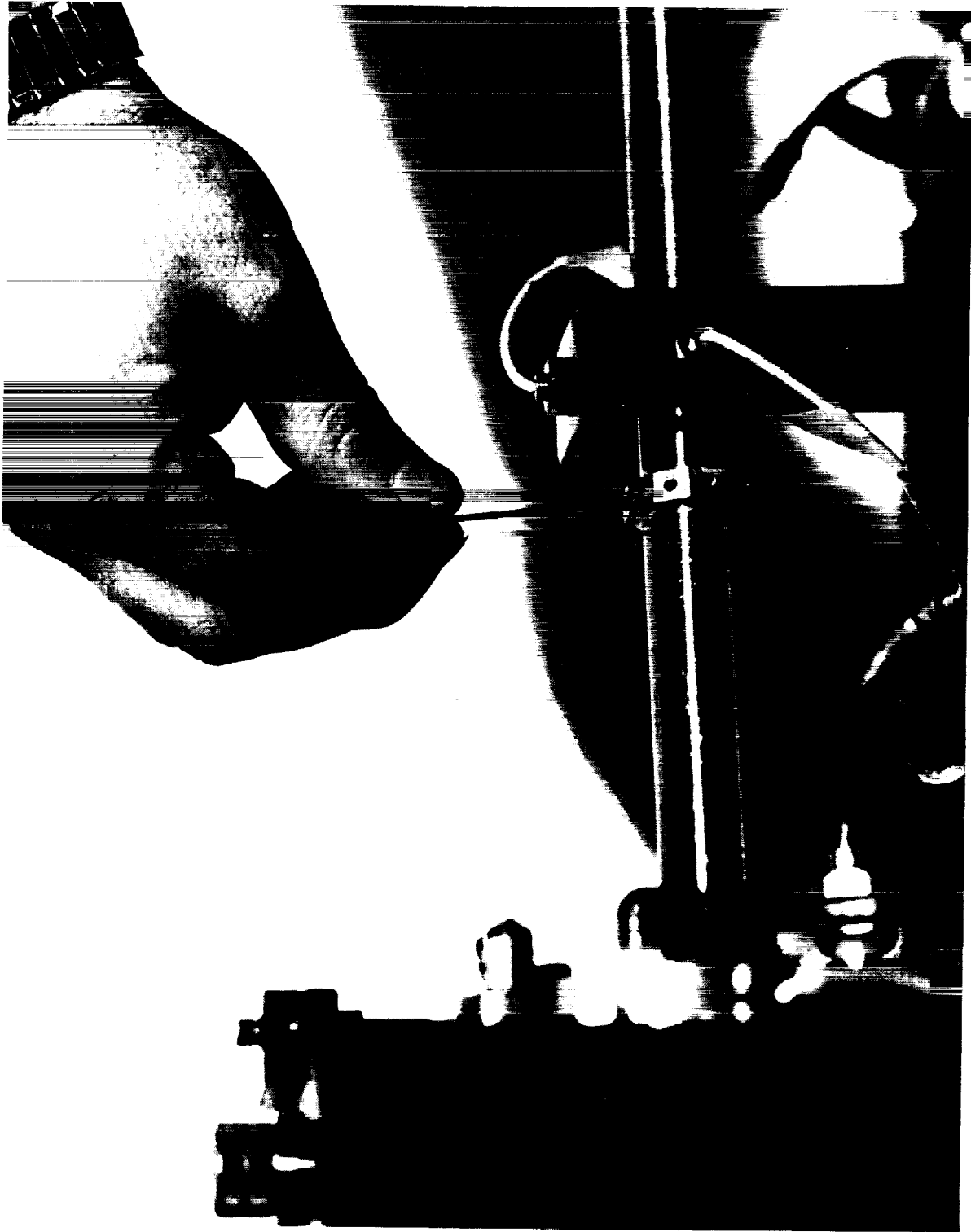
Fig. 141   Installation of Unbalance Weight on the Test Rig Shaft

277

Figures 141 through 145 show the rig's response to the unbalances introduced in the different planes with the two different damper materials. Note that the locations of the critical speeds drop in frequency with increasing unbalance, indicating a small strain-softening effect in the elastomer mounts as described in Section 4.0. At highest strain, the drop in resonant frequency is approximately 8%, indicating at least 16% loss in stiffness (and probably more). Peak amplitudes at the damper were approximately 10 to 20 microns (0.4 to 0.8 mils), which is a dynamic strain of 0.003 to 0.007 in a 3.2-mm button. Previous test results [8.1] indicate that such a strain could result in a 9 to 32 percent loss in stiffness in a compression specimen. Thus, the test results for vibration control testing of an elastomer damper were consistent with the earlier component test results for strain effects.

The influence of unbalance mass on peak amplitude is shown in Figure 146. The slopes, which are equal to the unbalance sensitivities, are approximately the same for fluorocarbon (Viton - CFM) and for butadiene (Polybutadiene - BR) in this application; this is a discrepancy from the predicted behavior with these materials discussed previously. There is some reduction in sensitivity with increasing amplitude; this reduction is consistent with the increase in log decrement with increasing strain observed in earlier tests. Table 33 compares the observed and predicted sensitivity to unbalance. In all cases the rotor is less sensitive than predicted. This lesser sensitivity indicates that the system damping achieved by the elastomer dampers exceeded expectations of the original system dynamic model. Two reasons are hypothesized. First, the computer model assumed purely radial stiffness and damping, with no moment restraint. In fact, the elastomer cartridges and double-row ball bearings probably provided some finite amount of moment stiffness and damping in addition to the radial values. Second, the elastomers ran at average temperatures of 27°C and 16°C at the disc and turbine end, respectively (as opposed to the design temperature of 50°C), contributing to both greater stiffness and damping than was originally expected.

Table 34 shows the calculated values of the log decrement for butadiene (Polybutadiene - BR) and fluorocarbon (Viton - CFM), using both the half-power point and the rate of change of phase angle methods, and the discrepancies between the two methods used. The agreement was generally good.

The average log decrements and Q values are shown in Table 35. The predicted values for the logarithmic decrement δ in mode two are: $\delta_{poly} = 0.057$ and $\delta_{Viton} = 0.298$.

The repeatability of the test rig during acceleration and deceleration is shown in Figure 147. This figure was obtained with the damper material (butadiene (Polybutadiene - BR)) at approximately equilibrium temperature with a 0.4-gram unbalance in the disc. This plot is a good representation of the rig's repeatability. The only significant deviations observed occurred when there were large temperature differences in the elastomers between the initial run up-to-speed and the coast-down, which were avoided during testing by running the rotor to speed at least once before a test sequence began.

278
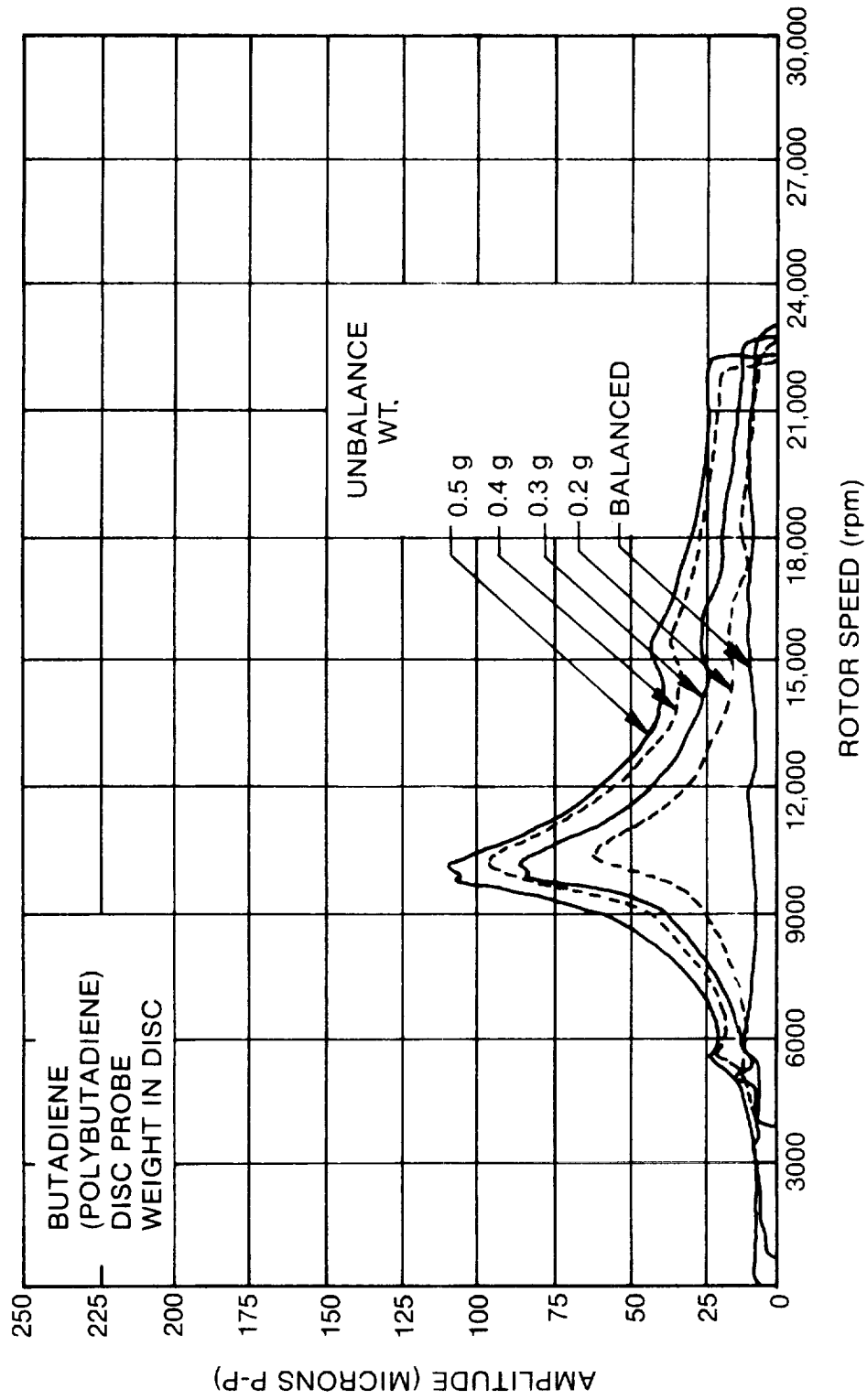
Fig. 142 Effect of Disc Unbalance With Butadiene (Polybutadiene) Dampers
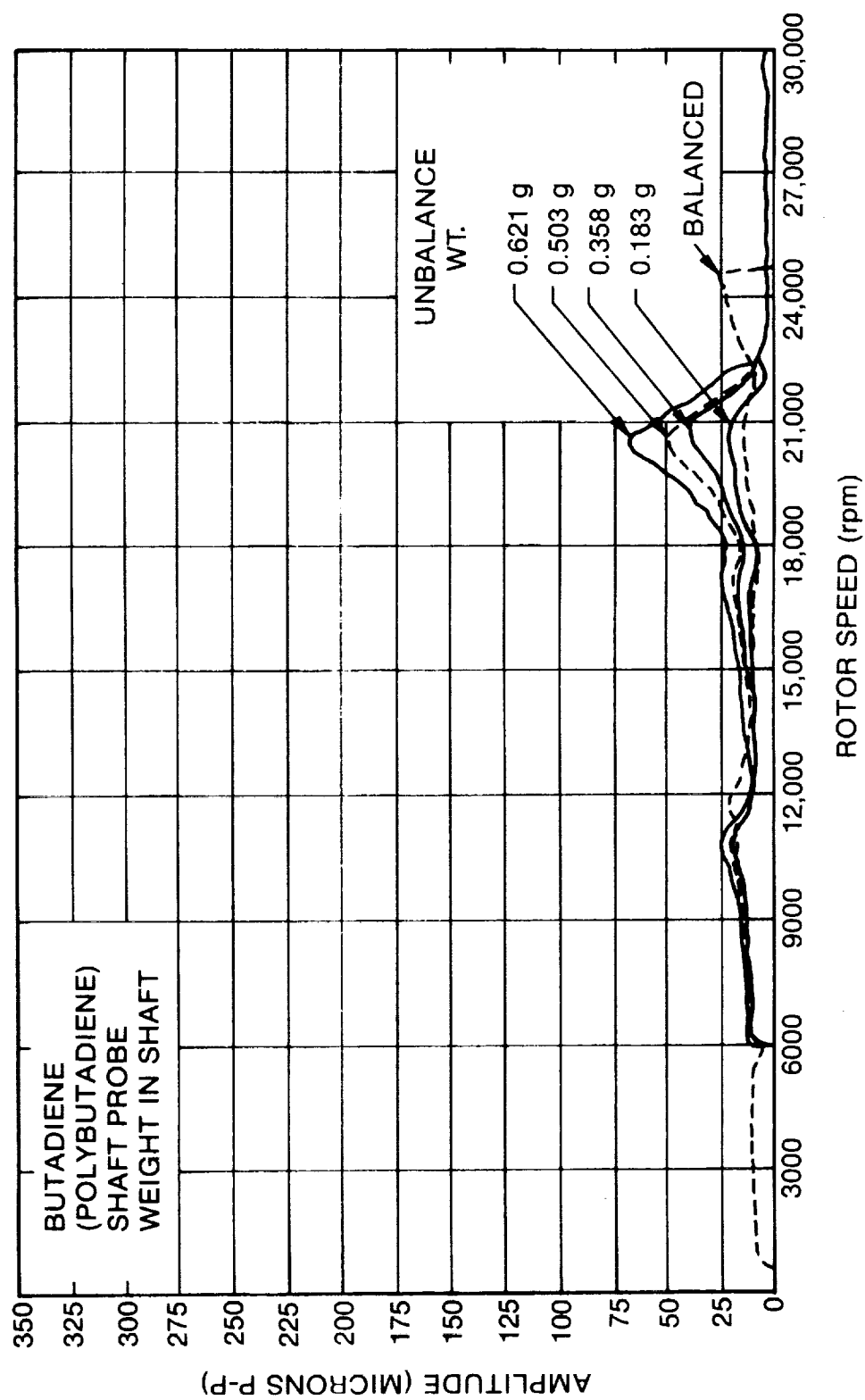
Fig. 143 Effect of Shaft Unbalance With Butadiene (Polybutadiene) Dampers
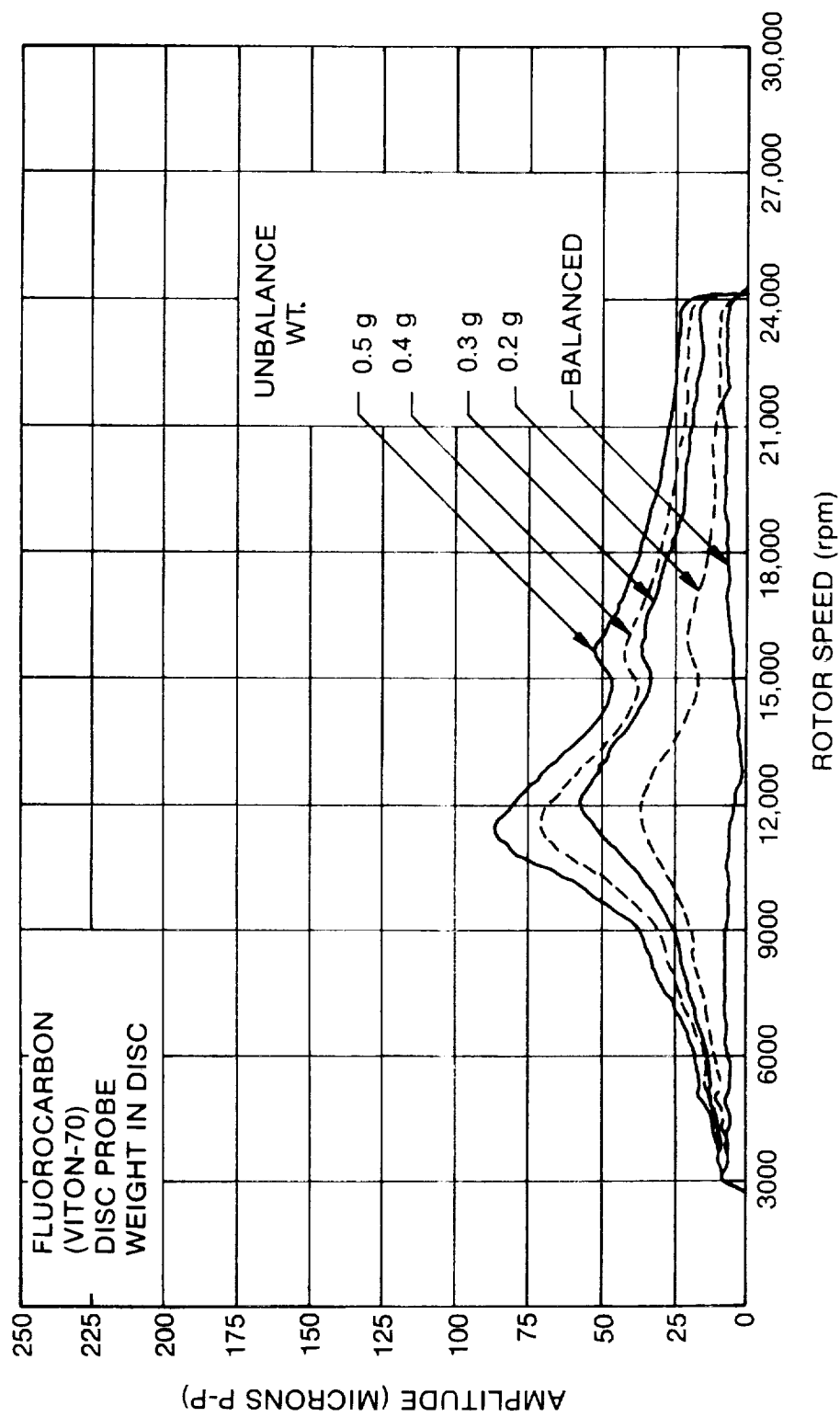
Fig. 144   Effect of Disc Unbalance With Fluorocarbon (Viton-70) Dampers

281
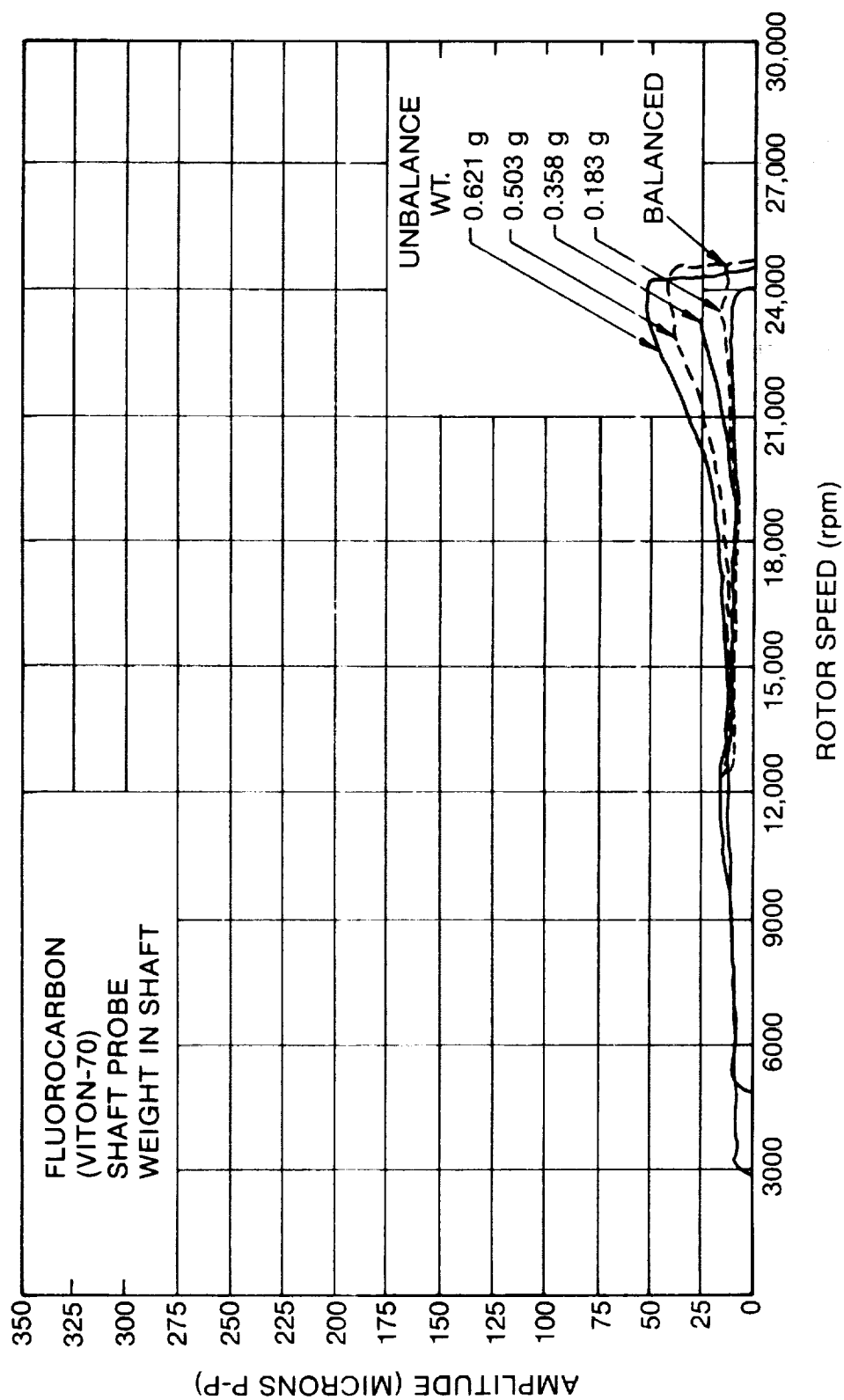
Fig. 145 Effect of Shaft Unbalance With Fluorocarbon (Viton-70) Dampers

282
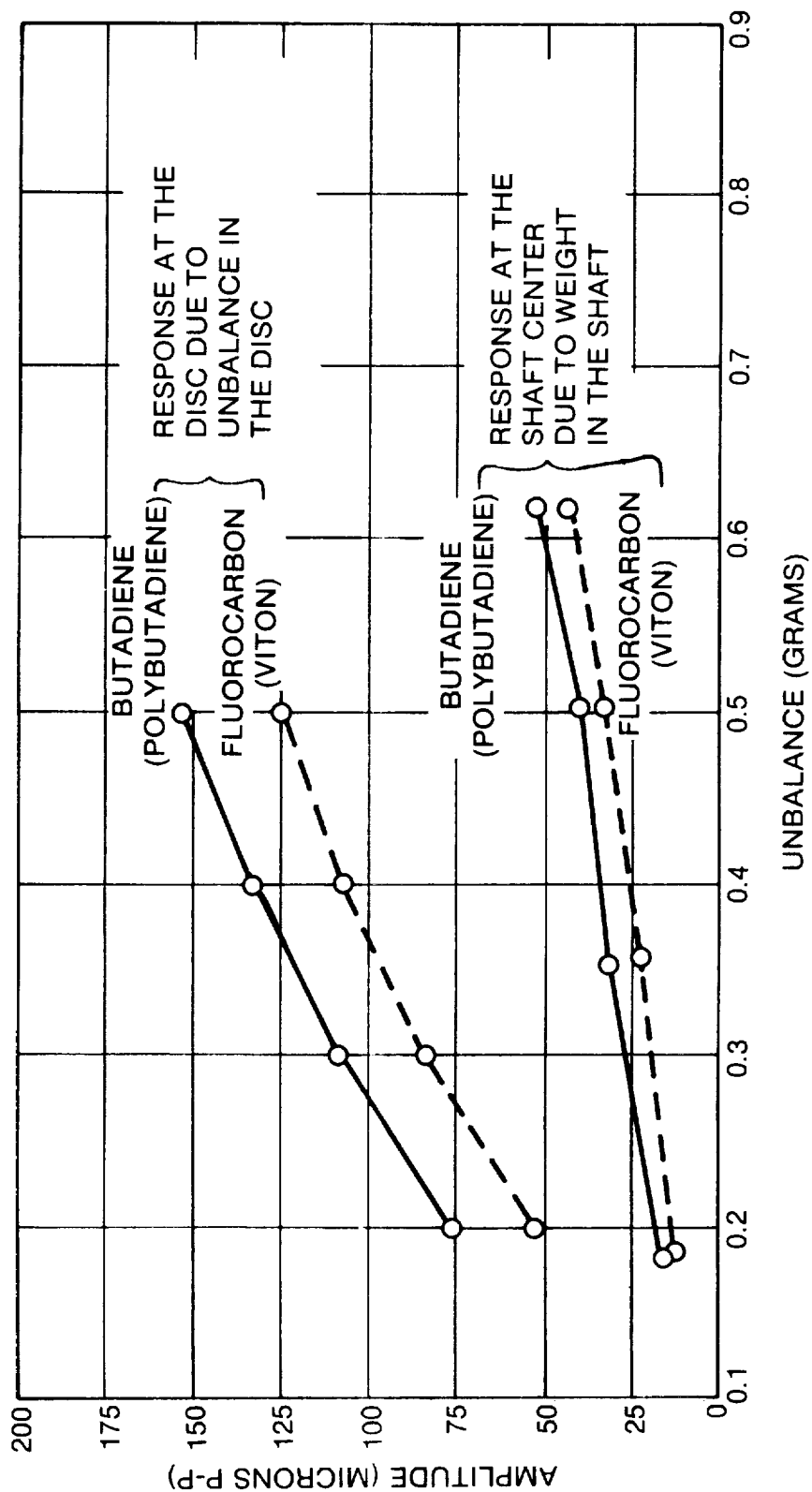
Fig. 146   Sensitivity of Test Rig to Unbalance
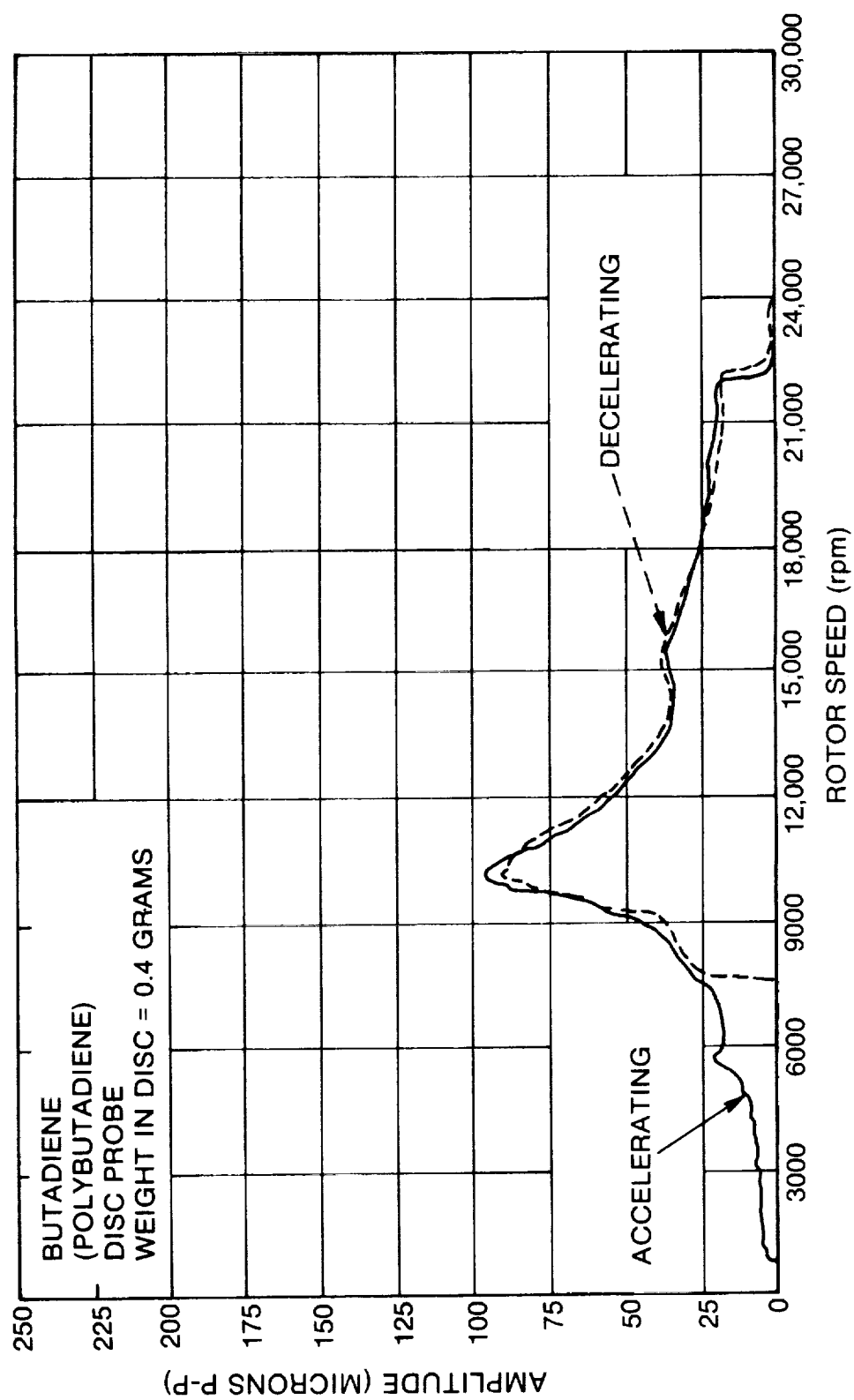
Fig. 147   Repeatability of Elastomer-Mounted Rotor Running To and From Speed

284

Table 33

SENSITIVITY OF TEST RIG TO UNBALANCE

Elastomer	Location of Unbalance Mass and Probe	Observed Sensitivity to Unbalance microns P-P / mils P-P gram / gram	Predicted Sensitivity to Unbalance microns P-P / mils P-P gram / gram
butadiene (Polybutadiene - BR)	Disc	259/10.2	917/36.1
butadiene (Polybutadiene - BR)	Shaft	84/3.3	1478/58.2
fluorocarbon (Viton 70 - CFM)	Disc	246/9.7	254/10.0
fluorocarbon (Viton 70 - CFM)	Shaft	69/2.7	297/11.7

Table 34

MEASURED VALUES OF LOG DECREMENT FOR BUTADIENE (POLYBUTADIENE – BR) AND FLUOROCARBON (VITON – CFM)

Material	Unbalance Magnitude (grams)	Mass Location	Critical	δ_{hp} Log Dec (half-power)	δ_s Log Dec (phase)	$\dfrac{\delta_s}{\delta_{hp}}$
butadiene (Polybutadiene – BR)	.2	Disc	1	.426	.442	1.038
	.3	Disc	1	.485	.512	1.055
	.4	Disc	1	.496	.507	1.023
	.5	Disc	1	.531	.540	1.017
	.183	Shaft	2	*	*	–
	.353	Shaft	2	.272	.282	1.037
	.583	Shaft	2	.241	.246	1.022
	.621	Shaft	2	.230	.277	1.203
fluorocarbon (Viton – CFM)	.2	Disc	1	.935	.857	.917
	.3	Disc	1	.859	.894	1.041
	.4	Disc	1	.831	.852	1.026
	.5	Disc	1	.842	.814	.967
	.183	Shaft	2	.852**	.526	.618
	.353	Shaft	2	.715	.814	1.138
	.583	Shaft	2	.605	.688	1.104
	.621	Shaft	2	.571	***	–
Steel	None	–	1	.171	–	–
	.2	Disc	1	.124	–	–

* Signal level too low
** Approximate values, could not reach second half-power points
***Difficulty with taped data

Table 35

AVERAGE VALUES FOR LOG DECREMENT AND AMPLIFICATION FACTOR

Material	Critical	Log Decrement by Half-Power Point		Log Decrement by Slope of Phase		Amplification Factor	
		Mean	Std. Dev.	Mean	Std. Dev.	Q Half-Pwr.	Q Phase
butadiene (Polybutadiene – BR)	1	.485	.044	.500	.042	6.48	6.28
	2	.248	.022	.268	.020	12.7	11.7
fluorocarbon (Viton – CFM)	1	.867	.047	.854	.033	3.62	3.68
	2	.686	.127	.669	.144	4.58	4.70
Steel	1	.148	–	–	–	21.3	–

After the elastomer damper data were taken, solid steel blocks were substituted in place of the elastomers. See Figure 136 for the pedestal with steel blocks in place of the elastomer cartridges. With the steel blocks installed, the rig had only one resonance in the speed range, at approximately 19,000 rpm, and greatly increased response amplitude.

Figures 148 and 149 show the response at the disc and shaft, respectively, when an unbalance mass was added to the disc. The data were not taped or digitally acquired so the phase change is unknown, but the response appeared to be nonlinear. The log decrement values are included in Tables 34 and 35, but confidence in these numbers is limited because of the support nonlinearity. It was noticed during these runs that the shaft was not as free to rotate with the steel blocks installed as it was with the elastomer dampers. The increased resistance was the result of a small amount of binding in the bearing caused by misalignment of the pedestals and shaft. The relatively soft elastomer mounts were able to tolerate this misalignment, but the stiff steel blocks could not.

Figure 150 shows the rig response with fluorocarbon (Viton - CFM) dampers in the turbine end and steel blocks at the disc end. This arrangement simulated the use of elastomeric supports at only the cold end of a gas turbine power shaft. The response amplitude is between the values observed with both elastomers' steel blocks at both ends. Thus, damping benefits can be gained with elastomers at the cold end only.

The amplitude data for the response plots were handled in two distinct ways. In some cases the probe output was not taped, and the plots were made "on-line", directly from the probe output after conditioning by a tracking filter to extract the synchronous component. In other cases, the signals were tape-recorded, and the tape-recorded signals were analyzed by feeding them into a spectrum analyzer and using the analyzer to create a "peakhold" average spectrum for each run, which was plotted using a digital plotter. The tape-recording method is valid when the synchronous component of the signal is larger than any other signal components at all speeds so the analyzer is effectively acting as a tracking filter. This was the case for the elastomer rig, and two sample instantaneous spectra are shown in Figure 151. The upper spectrum shows the frequency content of the disc probe and the lower spectrum, the content of a probe at the turbine. For both cases, the rotor speed is 6,000 rpm, well away from the first critical speed where the synchronous component is greatly amplified. The disc probe shows a large signal at running speed and very little elsewhere. The turbine probe shows very low vibration and, indeed, was not considered in the data analysis because of its low amplitude for both modes. However, the output of this probe is interesting because it shows very small peaks at multiples of running speed. These peaks are the result of forced vibration due to the impact of the compressed air jets on the machined "buckets" of this impulse air turbine. Traces of these spikes can be seen in the disc spectrum as well but, at all frequencies, were exceeded by the amplitude of the synchronous component.

Figure 152 shows the orbit of the disc at three different speeds: below, at, and above the first critical speed of the rig when a 0.5-gram unbalance mass was installed in the disc (Plane 1 of Figure 140). Figure 153 shows the orbit of the shaft center at three speeds which are below, at, and above the
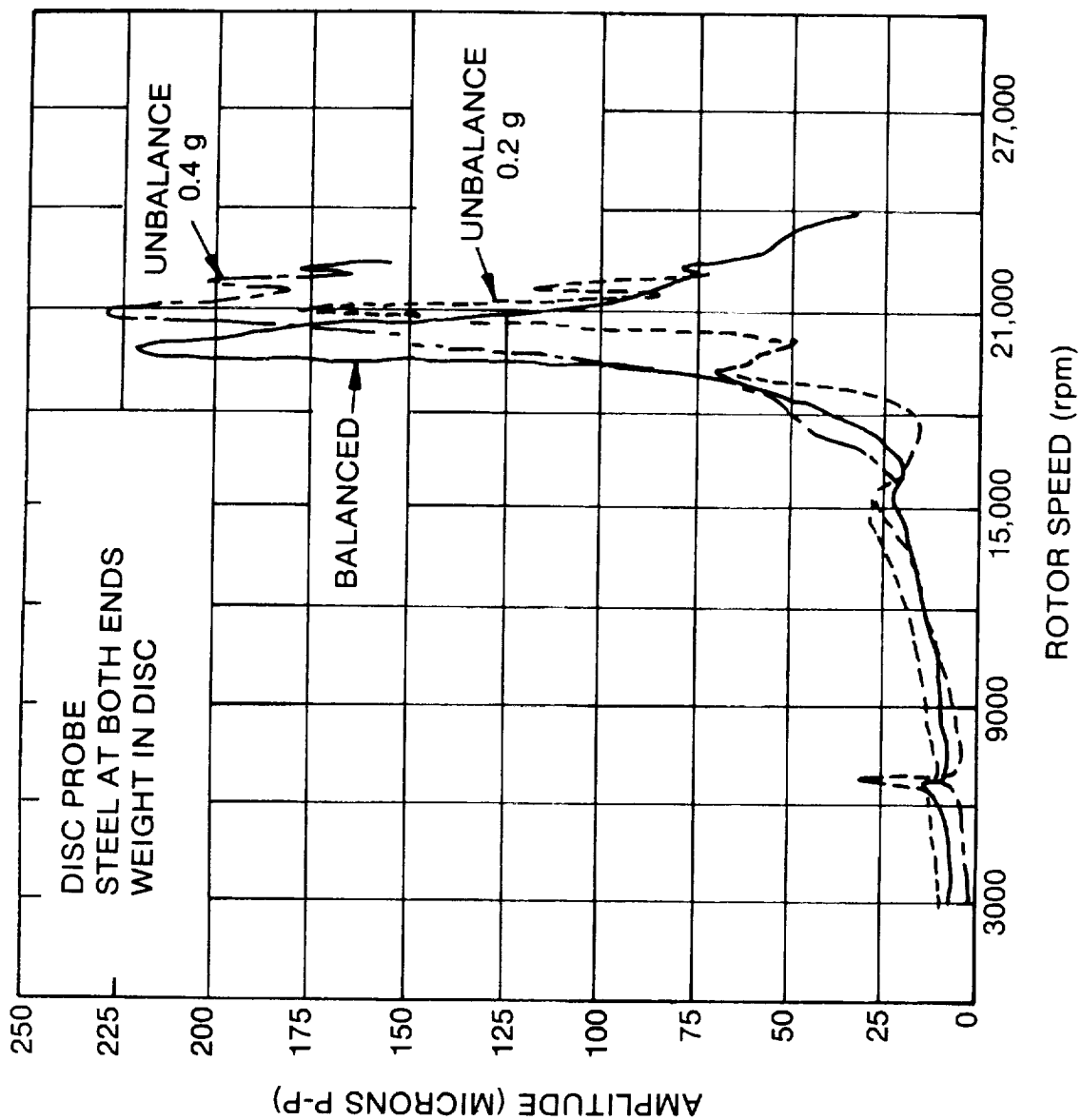
Fig. 148   Response at the Disc-to-Disc Unbalance for the Hard-Mounted Rotor

289
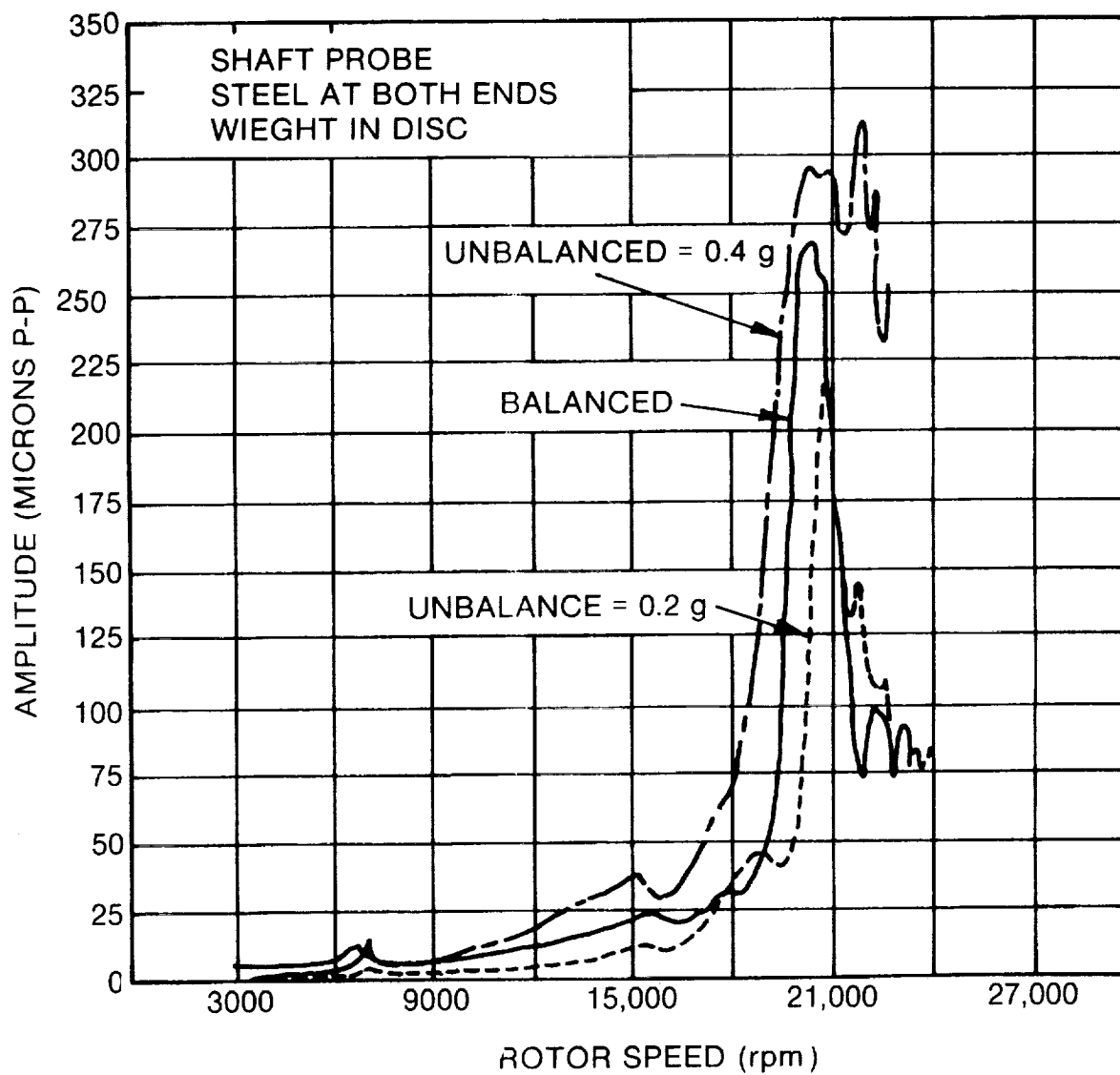
Fig. 149 Response at the Shaft to Disc Unbalance for the Hard-Mounted Rotor

290
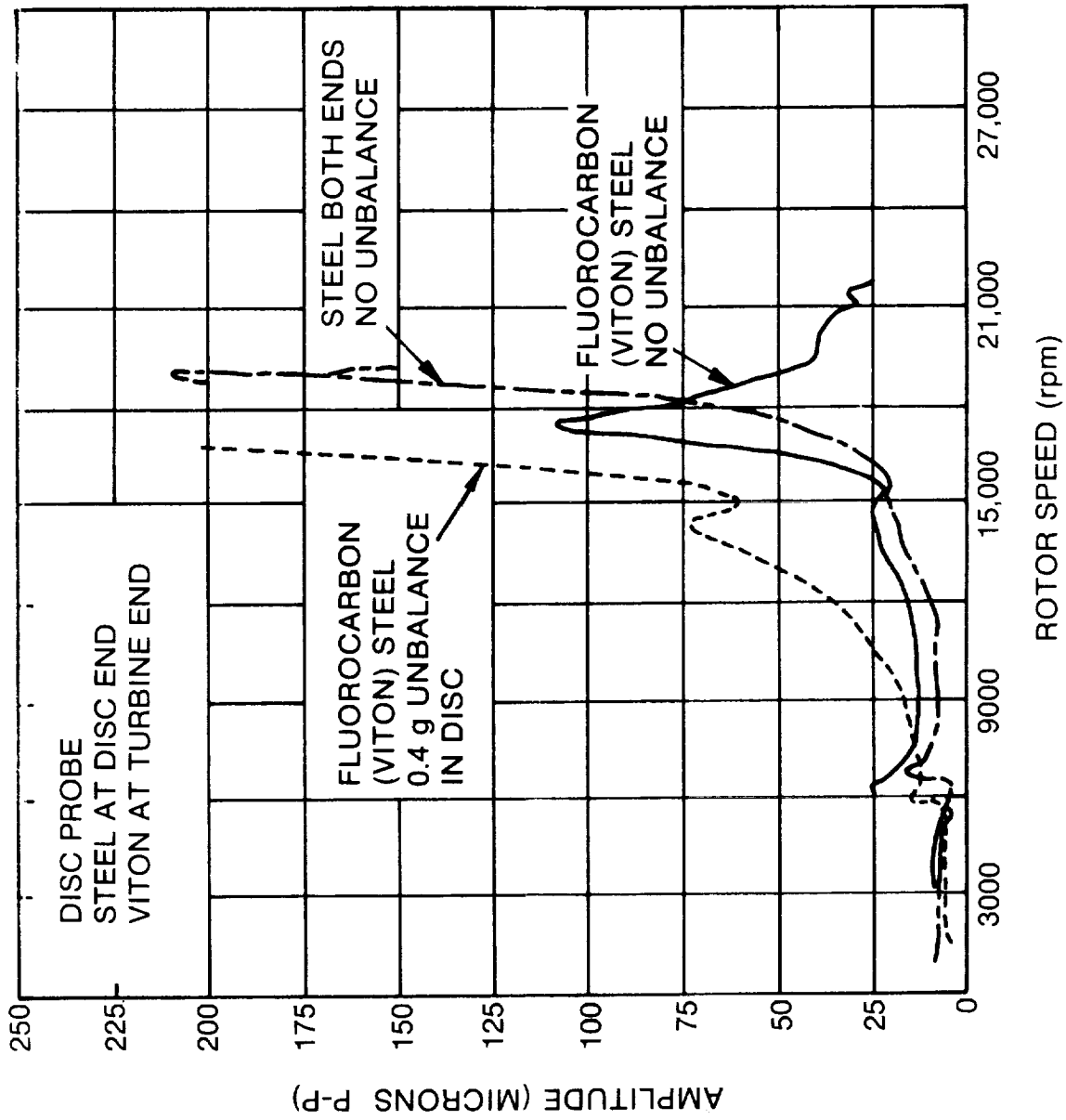
Fig. 150   Effect of Using Viton Damper Cartridges at the Turbine End Only

291
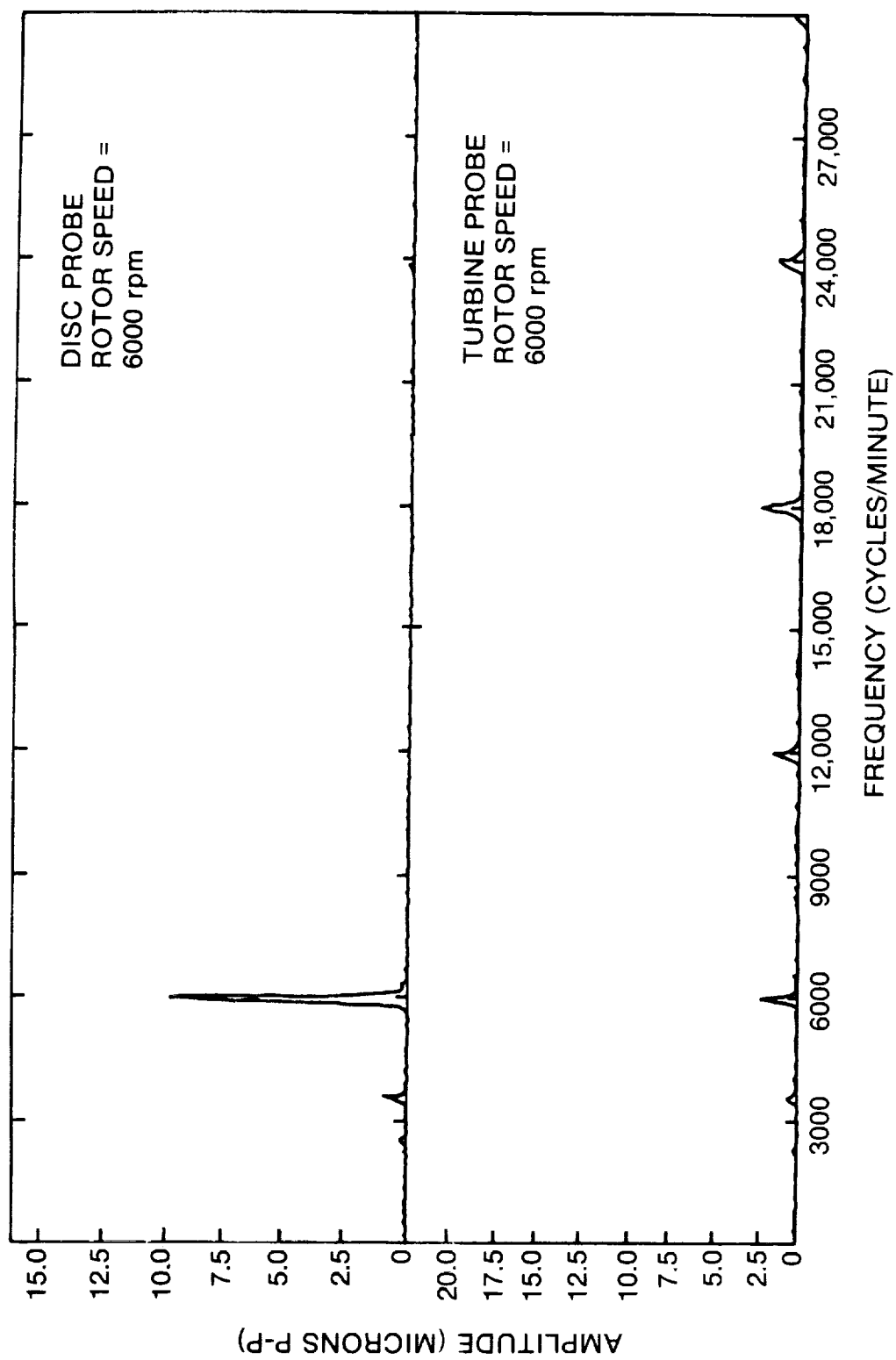
Fig. 151   Spectrum Analyses of Output from Disc and Turbine Probes

c) Above First Critical
   (12,000)

Probe 1

Probe 2

Shaft

a) Below First Critical
   (9000 rpm)
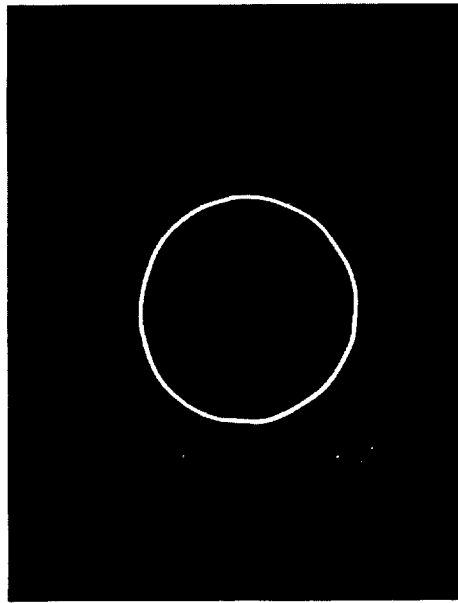
b) At First Critical (10,950 rpm)
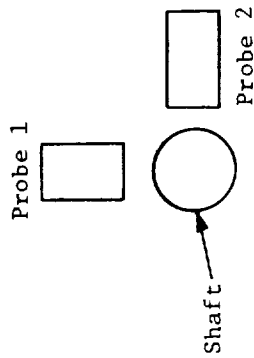
Fig. 152 Disc Orbit Through First Critical With Unbalance in Disc

293

c) Above Second Critical
(26,500 rpm)
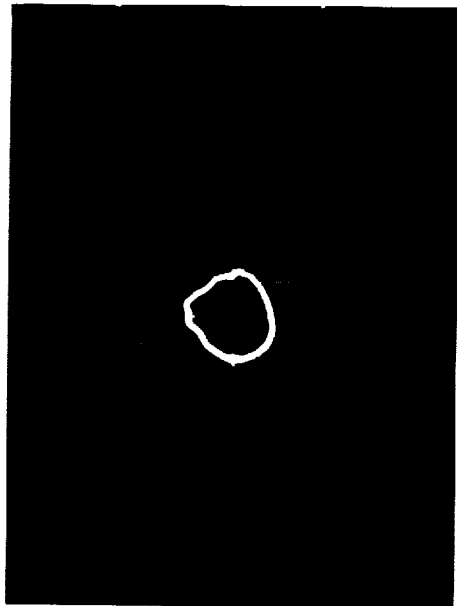
a) Below Second Critical
(21,000 rpm)
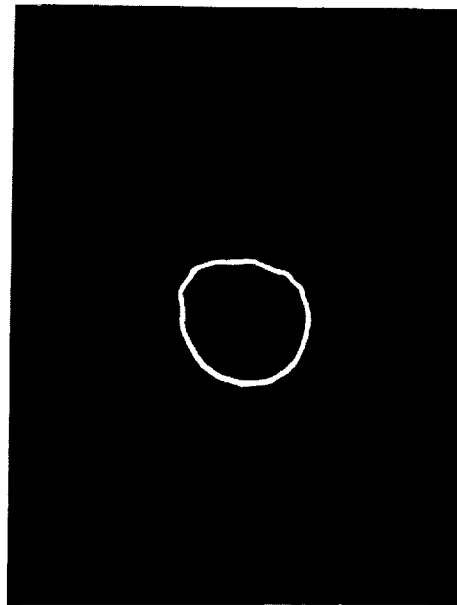
b) At Second Critical
(23,000 rpm)
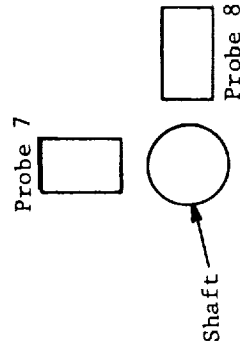
Fig. 153 Shaft Orbit Through Second Critical With Unbalance in Shaft

second critical speed. The unbalance for this case was 0.621 grams in the shaft (Plane 3 of Figure 140). These photographs are presented to illustrate the fact that the orbits are essentially circular; therefore, the elastomer support can be considered isotropic. The maximum amplitudes of the orbits for both figures are given in Table 36.

Table 36

SPEEDS AND MAXIMUM AMPLITUDE OF SHAFT ORBITS

Probe Location	Shaft Speed (rpm)	Maximum Amplitude (microns/mils p-p)
Disc	9,000	56/2.2
Disc	10,950	94/3.7
Disc	12,000	33/1.3
Shaft	21,000	51/2.0
Shaft	23,000	79/3.1
Shaft	26,500	46/1.8

The small irregularities in the orbits are due to a phenomenon called "electrical runout", in which small irregularities in surface finish or variations in electrical conductivity of the rotor are seen by the eddy-current-type displacement pickup as if they were vibration signals. Since they are fixed to the rotor surface, these small "ripples" in the orbit make phase changes easily visible. This is seen in Figure 153a where a small bump appears at the top of the orbit. In Figure 153b, the bump appears at some midway point (apparently smaller since the orbit has enlarged but the "electrical runout" signal has not). This bump appears at the bottom in Figure 153a. These correspond to speeds below, at, and above the second critical speed, respectively. Note also that a total phase change of about 180° has occurred while traversing the resonance.

8.2 Supercritical Power Transmission Shaft [8.2]

A test rig was designed and built for demonstrating the use of supercritical power transmission shafting. During the operation of this test rig, nonsynchronous vibrations from a variety of sources were observed. The test rig was first run with a minimum amount of external damping and then with a larger amount of external damping. In this way, the effect of external damping on nonsynchronous vibration and rotordynamic stability was observed. The external damping was provided by a self-contained, oil squeeze-film damper and an elastomer damper, both designed to permit operation through the fourth bending mode. The elastomer damper is of principal interest here, but the oil damper was used as the basis of comparison of damping effectiveness.

Tests were performed to identify any problems, needed technology, or limitations inherent in the use of supercritical shafting. One of the principal areas of interest involved demonstrating the balancing of supercritical shafts. The tests included balancing of a very flexible shaft with both damped and undamped supports.

A sketch of the test rig is presented in Figure 154. A 224-kW (300 hp) electric motor is the prime mover for this test rig. The motor drives a variable-speed magnetic coupling, whose output speed is continuously variable from 50 to 3,600 rpm. A gearbox with a ratio of approximately 5.7 to 1 produces a drive-shaft speed of up to 20,000 rpm. The drive shaft is formed from a section of aluminum tubing, 7.62 cm (3 in.) in diameter and 3.66 m (12 ft.) in length with a wall thickness of 3.175 mm (0.125 in.).

Early testing without a damper did not permit rig operation above 1,200 rpm due to the instability of the subsynchronous excitation of the 16-Hz first critical speed. Stability problems which occurred during this stage of testing clearly established that some form of external damping, coupled with balancing, would be required for control of vibrations. Several methods for applying external damping were investigated, and an oil-squeeze-film-type damper was chosen first based upon its flexibility and predictability in the level of damping achieved [8.10 through 8.13]. This damper was subsequently replaced with an elastomer damper which proved to be equally effective.

For this particular application, some special considerations arose beyond the normal considerations discussed in earlier sections. These considerations were that the damper should have the following capabilities:

- Easily added to the existing test rig.

- Compact and self-contained to be practical in helicopter drive shaft applications.

- Providing support stiffness as well as damping.

The approach selected was to flexibly couple an extension shaft with a damper to the existing test shaft and perform undamped critical speed analysis of the new shaft geometry. Figure 155 shows the predicted mode shapes and critical speeds for the first five modes. It should be noted that, for all of these modes, some significant amplitude exists at the location of the damper as represented by bearing number 2. This is important to achieve the necessary dissipation of vibration energy at the damper.

The initial model of the test rig included a support of 1.75×10^5 N/m (1,000 lb/in.). A damped natural frequency analysis was conducted using a series of damping values from 875 to 10,500 N-s/m (5 to 60 lb-sec/in.) with this stiffness. The second critical speed was found to be critically damped. The log decrement is plotted as a function of damping for the remainder of the first five critical speeds in Figure 156. The optimum value of damping appears to be about 8,750 N-s/m (50 lb-sec/in.).

The damped natural frequency analysis was then conducted for a series of values of support stiffness from 1.75×10^5 to 2.625 to 10^6 N/m (1,000 to

TORQUING GEARBOX (2500 hp)

LOW SPEED SHAFT

FLOOR LEVEL

DRIVE GEARBOX

LUBE RESERVOIR

MAGNETIC COUPLING SPEED CONTROL

300 hp 1800/3600 rpm DRIVE MOTOR

TRANSMISSION SHAFT TEST SECTION (SECTIONS UP TO 30-FT LONG CAN BE TESTED AT SPEEDS TO 20,000 RPM)

38'-6"

11'-10"
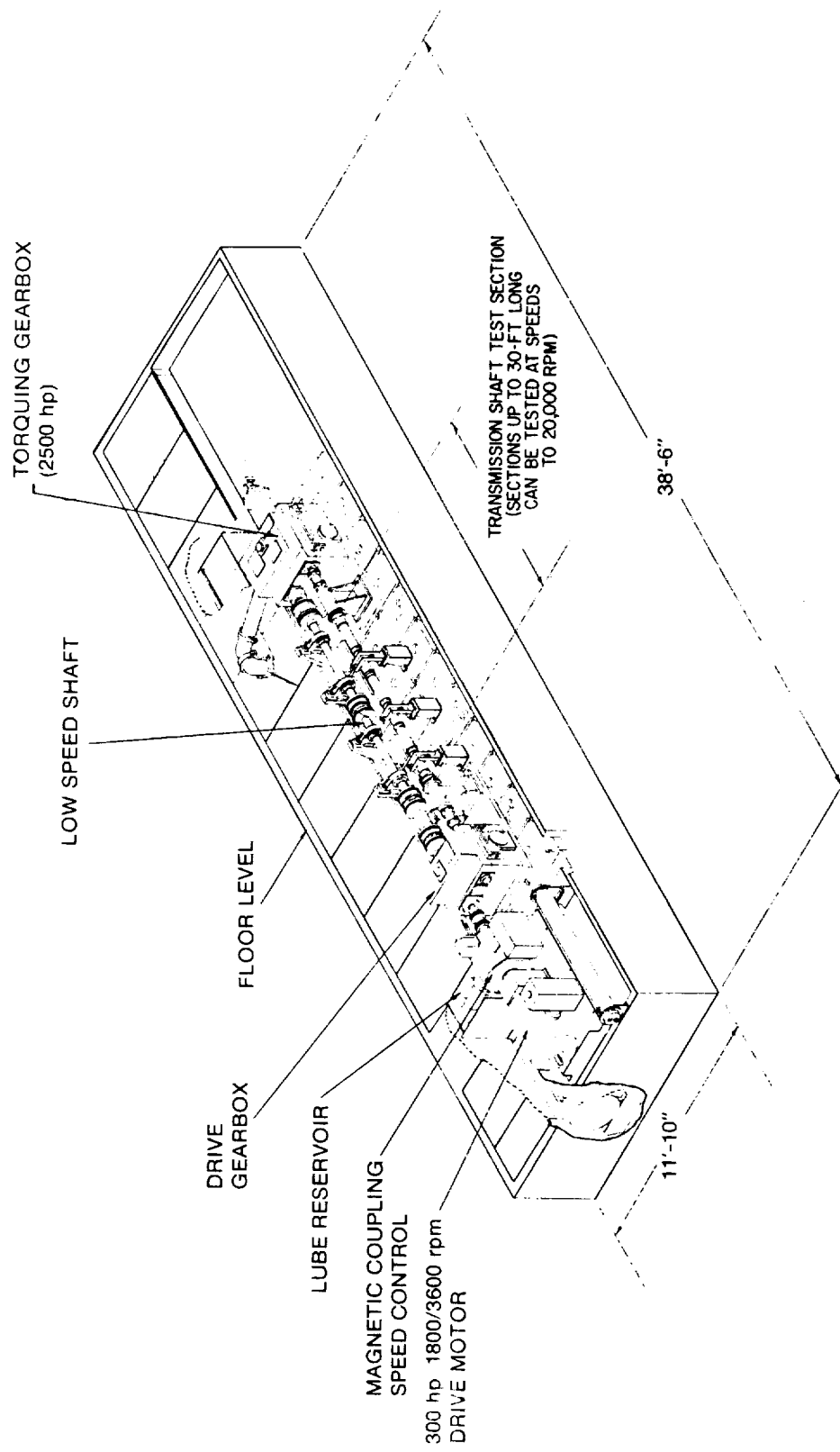
Fig. 154 Drive Train Technology Test Rig Configuration for High-Speed Shaft Balancing
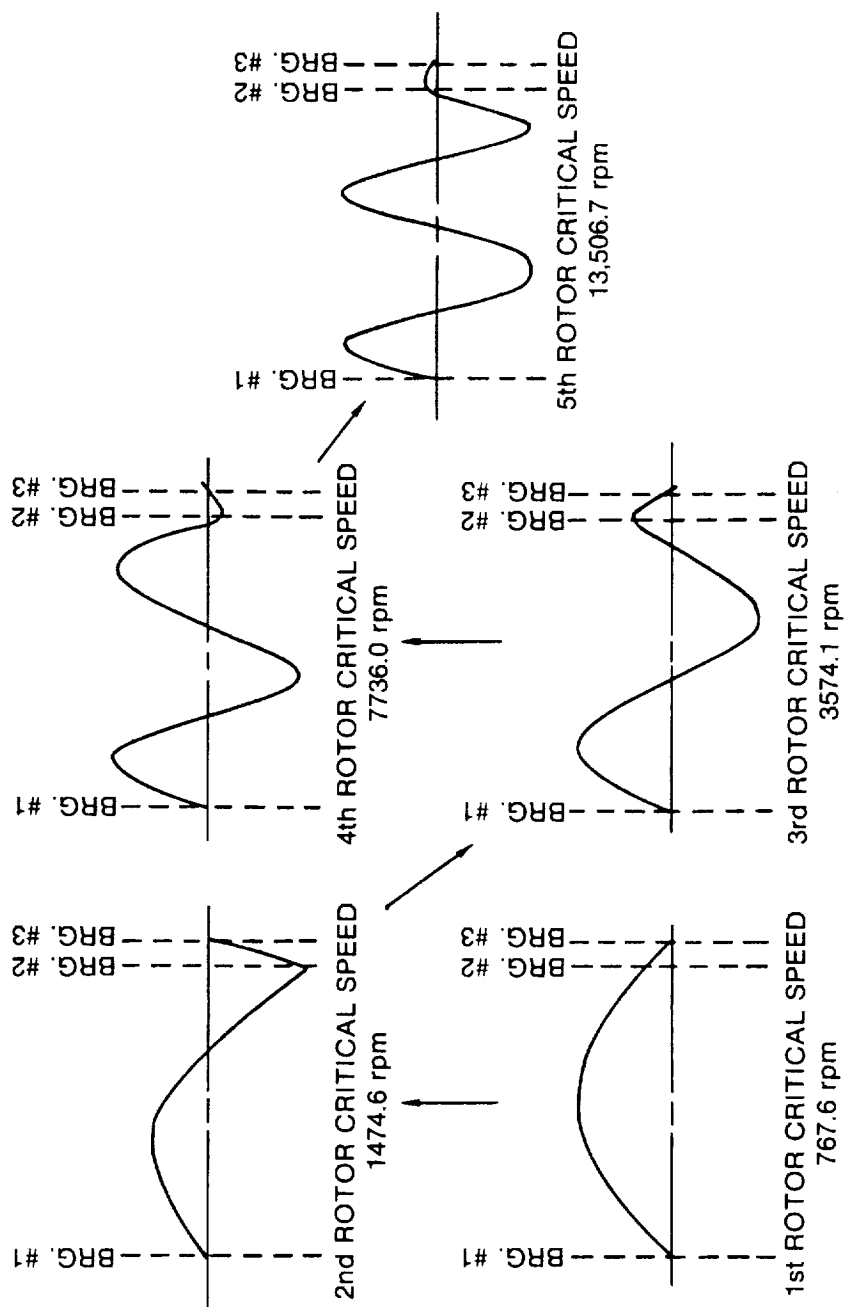
Fig. 155 Mode Shapes of the First Five Critical Speeds, Original
Shaft with Extension to Carry Squeeze-Film Dampers

298
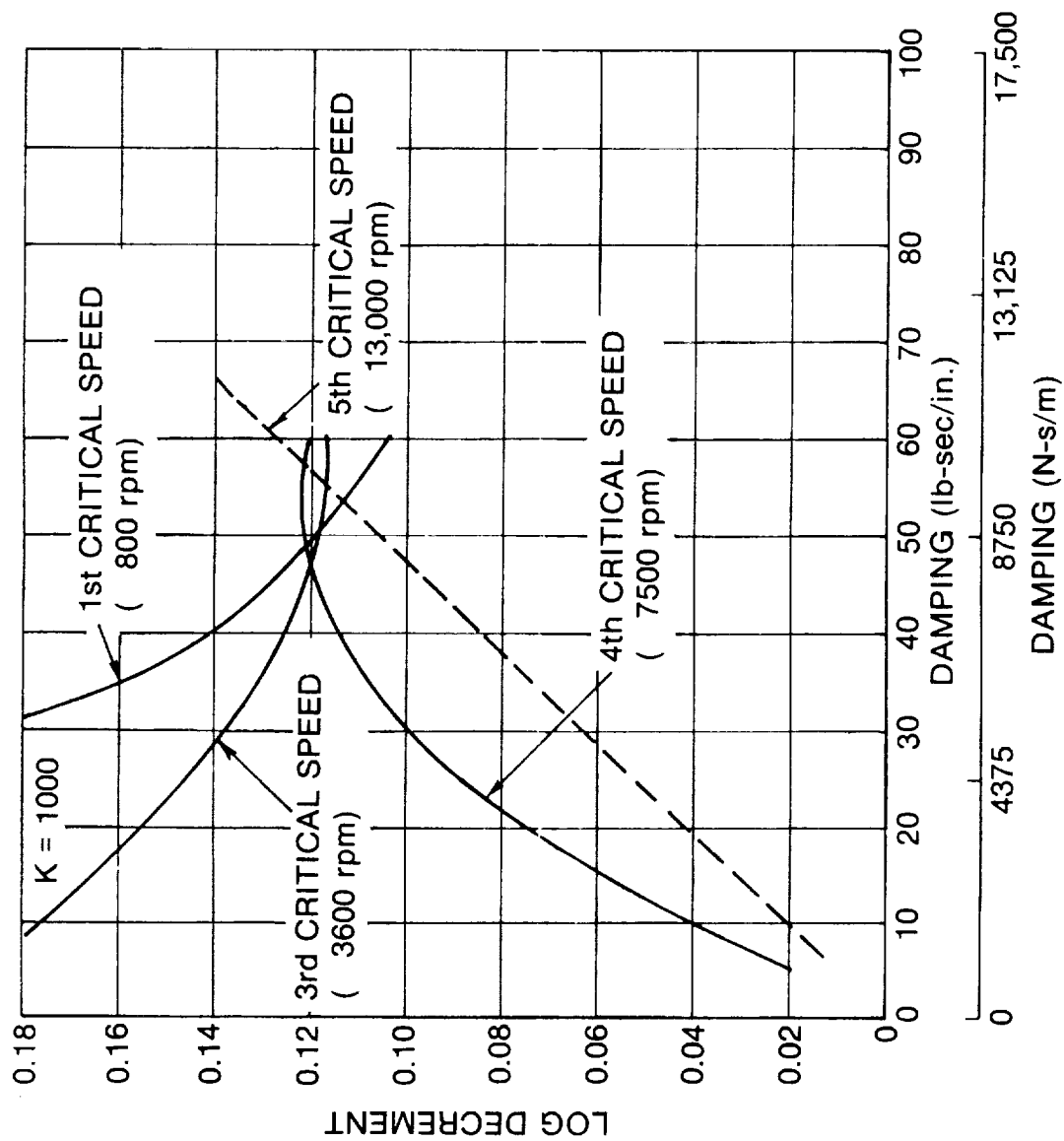
Fig. 156   Log Decrement as a Function of Damping
(Stiffness = 1.75 × 10⁵ N/m [1000 lb/in.])

15,000 lb/in.) with a constant damping value of 8,750 N-s/m (50 lb-sec/in.). Again, the second critical speed was critically damped. Log decrement is plotted as a function of stiffness for the remainder of the first five critical speeds in Figure 157. The only critical speed for which there was a substantial detrimental effect from increasing support stiffness was the first critical speed. However, this effect was serious enough to require that the support stiffness be kept below 8.175×10^5 N/m (5,000 lb/in.).

Based on the rotordynamic analysis, the decision was made to first design a squeeze film for a stiffness of 7×10^5 N/m (4,000 lb/in.) using an O-ring as the spring member. Studies recently performed by Smalley, Darlow and Mehta [8.14] indicate that this is about as low as can be practically achieved for a continuously supported O-ring in this configuration.

The squeeze-film damper was designed to be a sealed damper with no circulation of oil. In this way, the damper would require no support hardware (such as oil supply pumps) which would prohibit its use in helicopter or other space- and weight-limited applications.

A sketch of the test rig damper is shown in Figure 158. The squeeze-film damper was evacuated, filled and sealed, and pressurized by the use of a bladder. The damper was predicted to generate less heat than the bearings, so the dissipation of heat was not expected to be a serious problem. The O-ring retainers are radially adjustable, so that the squeeze film damper may be centered manually to compensate for static deflection of the O-rings. The damper was designed to achieve a level of damping in the range of 8,750 N-s/m (50 lb-sec/in.) for silicone oil with a viscosity of about 80 centistokes, using the short bearing theory and assuming no cavitation. The radial clearance is 0.635 mm (25 mils) and the length and diameter are 7.62 cm (3 in.) and 10.16 cm (4 in.), respectively. Although the squeeze film damper was designed to allow for the two O-rings, it was used initially with just one O-ring to obtain a low parallel support stiffness of 7×10^5 N/m (4,000 lb/in.) for a continuously supported O-ring.

Testing showed that the squeeze-film damper improved the dynamic stability of the test rig. However, the addition of external damping alone could not provide complete control of all test shaft vibrations. The test shaft also had to be balanced to achieve safe operation throughout its speed range.

Through the combined use of external squeeze-film damping and balancing, the rig was safely run to over 12,000 rpm while negotiating the first four flexural critical speeds of the test shaft. This speed was over 10 times that which could be achieved without any external damping.

Substantial synchronous growth of the response of the fifth critical speed occurred at 12,000 rpm. A very large subsynchronous response of the first and fourth critical speeds also occurred. In fact, the subsynchronous response of the first critical speed, while running at 12,000 rpm, was such that the test rig could not be run higher in speed. The subsynchronous response of the first critical speed possibly was due to internal damping similar to that observed with the undamped test rig. If this is the case, then the effect of the added damping was to raise the threshold of this instability from just over one time the first critical speed to almost 13
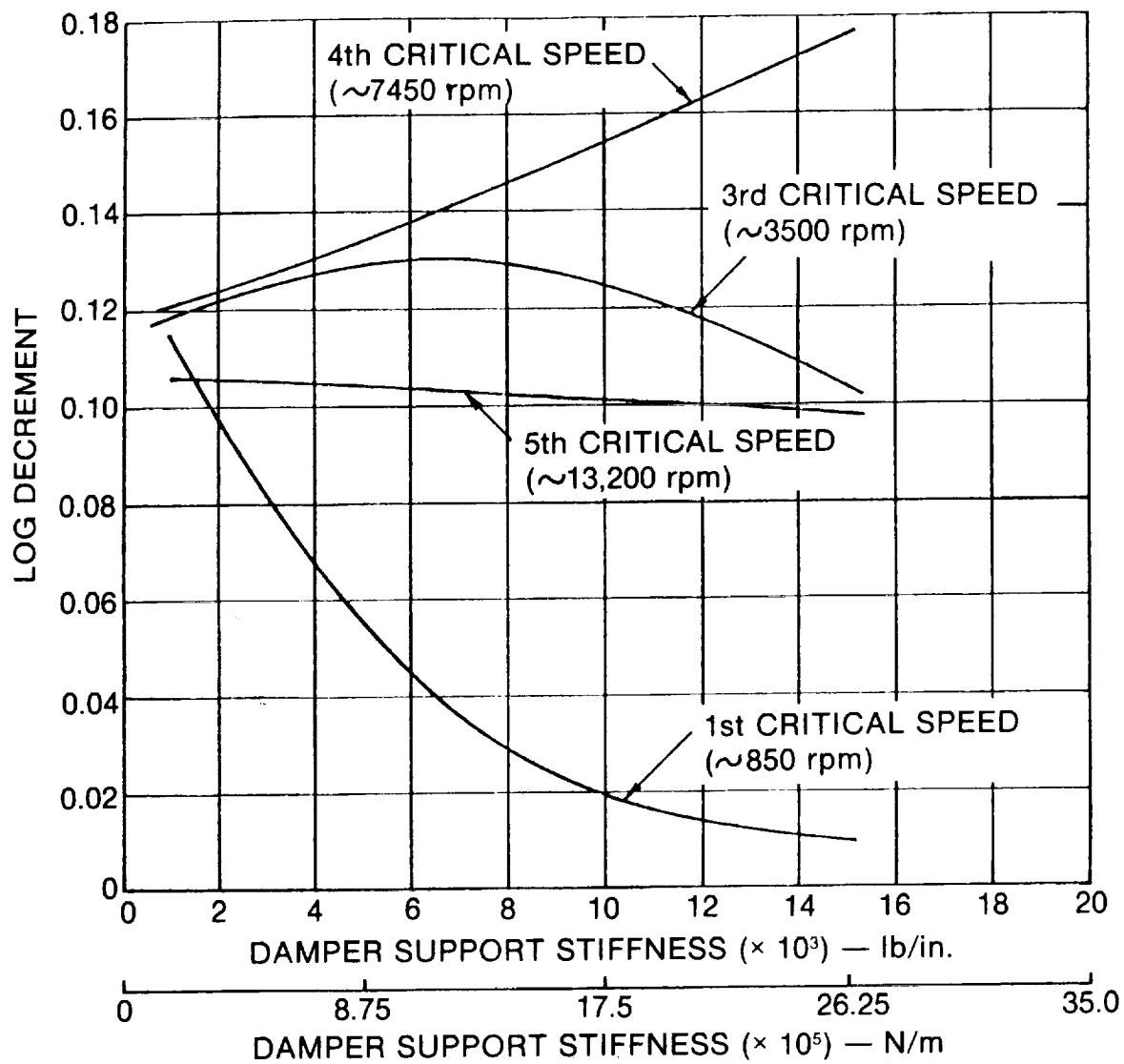
Fig. 157   Log Decrement as a Function of Support Stiffness
(Damping = 8760 N-s/m [50 lb-sec/in.])
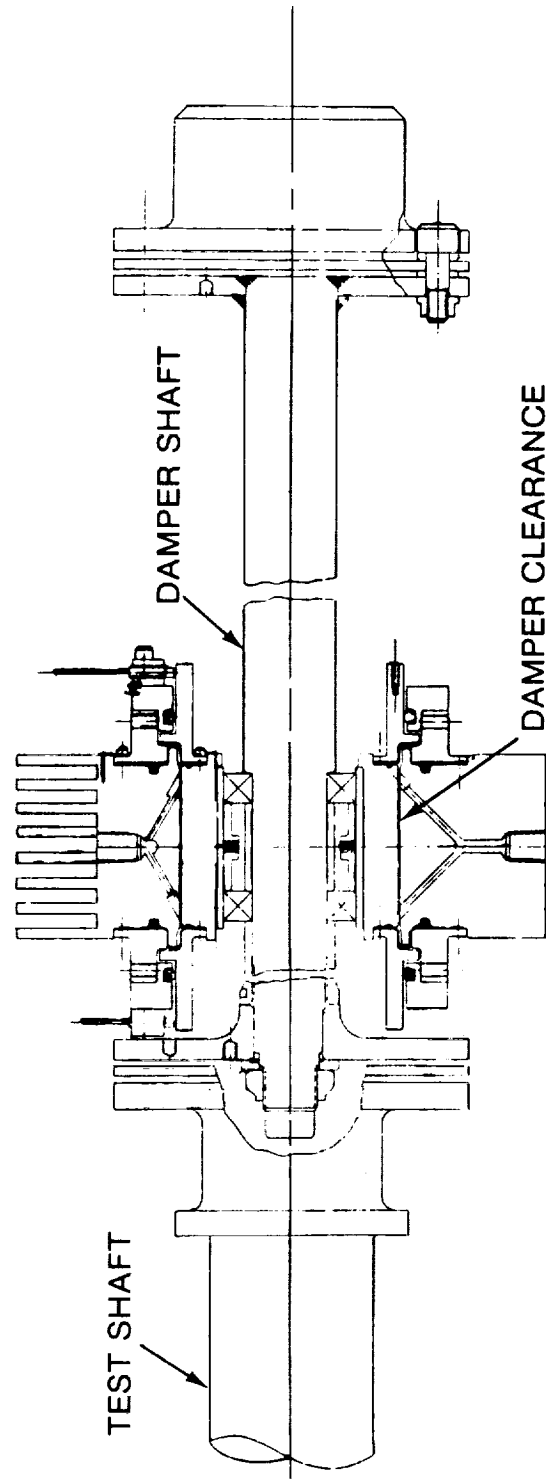
Fig. 158 Squeeze-Film Damper Designed to Suppress Vibrations in Supercritical Power Transmission Shaft

302

times the first critical speed, which was a substantial improvement. The subsynchronous response of the fourth critical speed was most significant at a rotational speed of about 11,800 rpm, as illustrated by the frequency spectrum plot at the top of Figure 159. However, at a rotational speed of 12,000 rpm, the subsynchronous response of the first critical speed became predominant; that of the fourth critical speed had become much less significant, as illustrated by the frequency spectrum plot presented at the bottom of Figure 159. In any case, it was demonstrated that the test rig could be run to more than 11,000 rpm with no large synchronous or nonsynchronous response of the test shaft. Additional details of the observed nonsynchronous effects noted with the power transmission shaft were provided by Darlow and Zorzi [8.15].

The design of the fluorocarbon (Viton 70 - CFM) elastomers utilized in the supercritical shaft was based upon extrapolated data obtained from 0-ring testing during previous elastomer testing [8.14], and the stability analysis performed is shown in Figure 156. The supercritical shaft squeeze-film damper (Figure 160) was modified to accept replacement elastomer dampers. The design requirements included consideration of shaft disassembly and reassembly unbalance changes. The elastomer dampers were required to replace the squeeze-film damper without the necessity of shaft/damper disassembly. This permitted a direct comparison of elastomer and squeeze-film performance. The six fluorocarbon (Viton 70 - CFM) buttons shown in Figure 161 were 0.635 cm (0.25 in.) in diameter and 0.635 cm thick. Six buttons provided a stiffness of approximately 7×10^5 N/m (4,000 lb/in.) with a loss coefficient of 0.75 used for design purposes. Figure 162 shows an elastomer button as assembled in the squeeze-film damper housing, Figure 160.

The elastomer consistently permitted higher operational speeds than the squeeze-film mount. Figure 163 illustrates the synchronous response measured when the power transmission shaft was balanced through the third critical speed with an elastomer damper. A change to the squeeze-film mount did not permit operation through the third mode. With the squeeze film operable, trim balancing of the first and third modes was continued, and the elastomer was again installed. Figure 164 illustrates the fact that the elastomer once again outperformed the squeeze-film mount, although for this run, the elastomer did not reduce vibration through the first mode as well as the squeeze film.

Later balancing with the elastomer permitted operation to 13,000 rpm (Figure 165), which is 1,000 rpm higher than that achieved with the squeeze-film Figure 159. However, as was the case with the squeeze film, the unstable subsynchronous excitation of the 16-Hz first critical was again the factor which limited higher speed operation of the power transmission shaft (Figure 166).

These results clearly demonstrate that elastomer dampers can control nonsynchronous, as well as synchronous, vibration of high-speed rotating machinery. Further, the elastomer damper used in this application continually outperformed the squeeze film and permitted higher speed operation of the supercritical shaft.
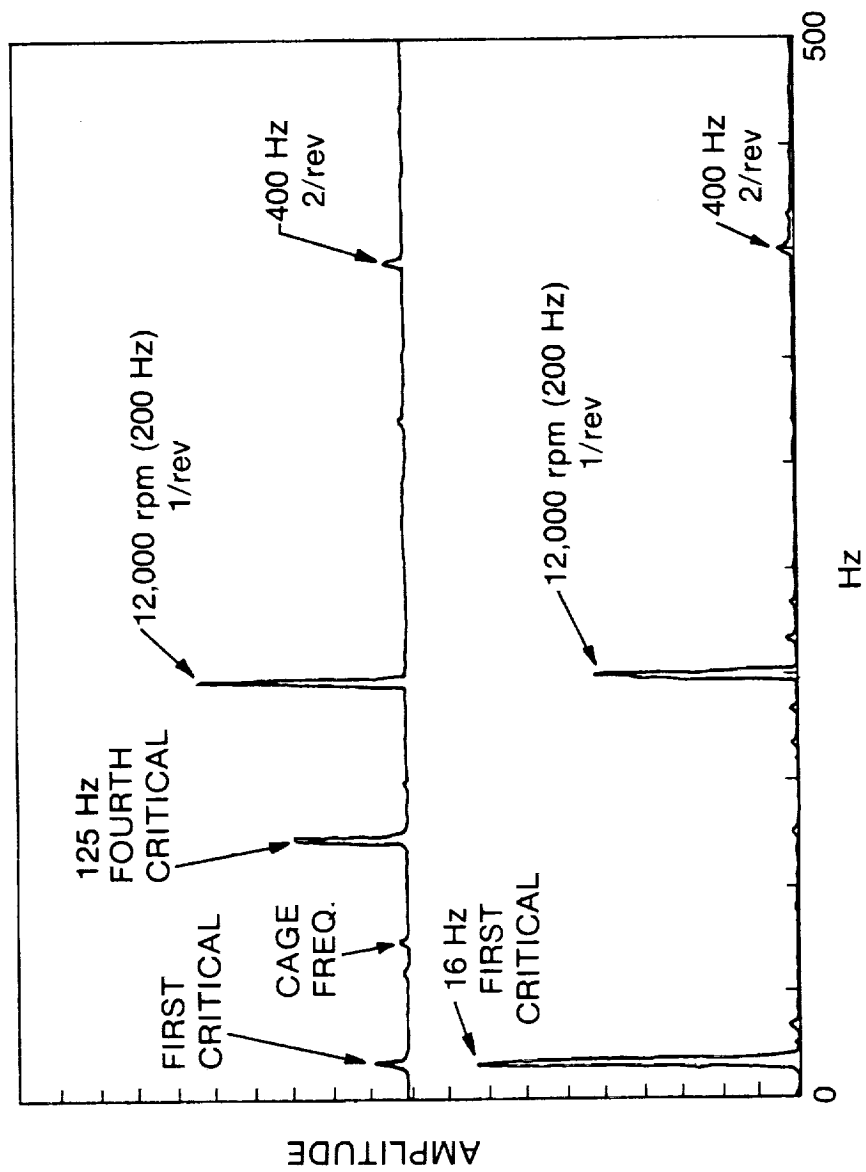
Fig. 159 Frequency Spectrum Plots of Test Shaft Vibrations With a Damper Running Near 12,000 rpm

BUMPER SCREWS

PROBE LOCATION

ELASTOMER
(6 CIRCUMFERENTIAL
LOCATIONS, DOUBLE-
ROW PERMITTED)

ELASTOMER

EXISTING

DAMPER
SHAFT

SQUEEZE-
FILM
CLEARANCE

O-RING
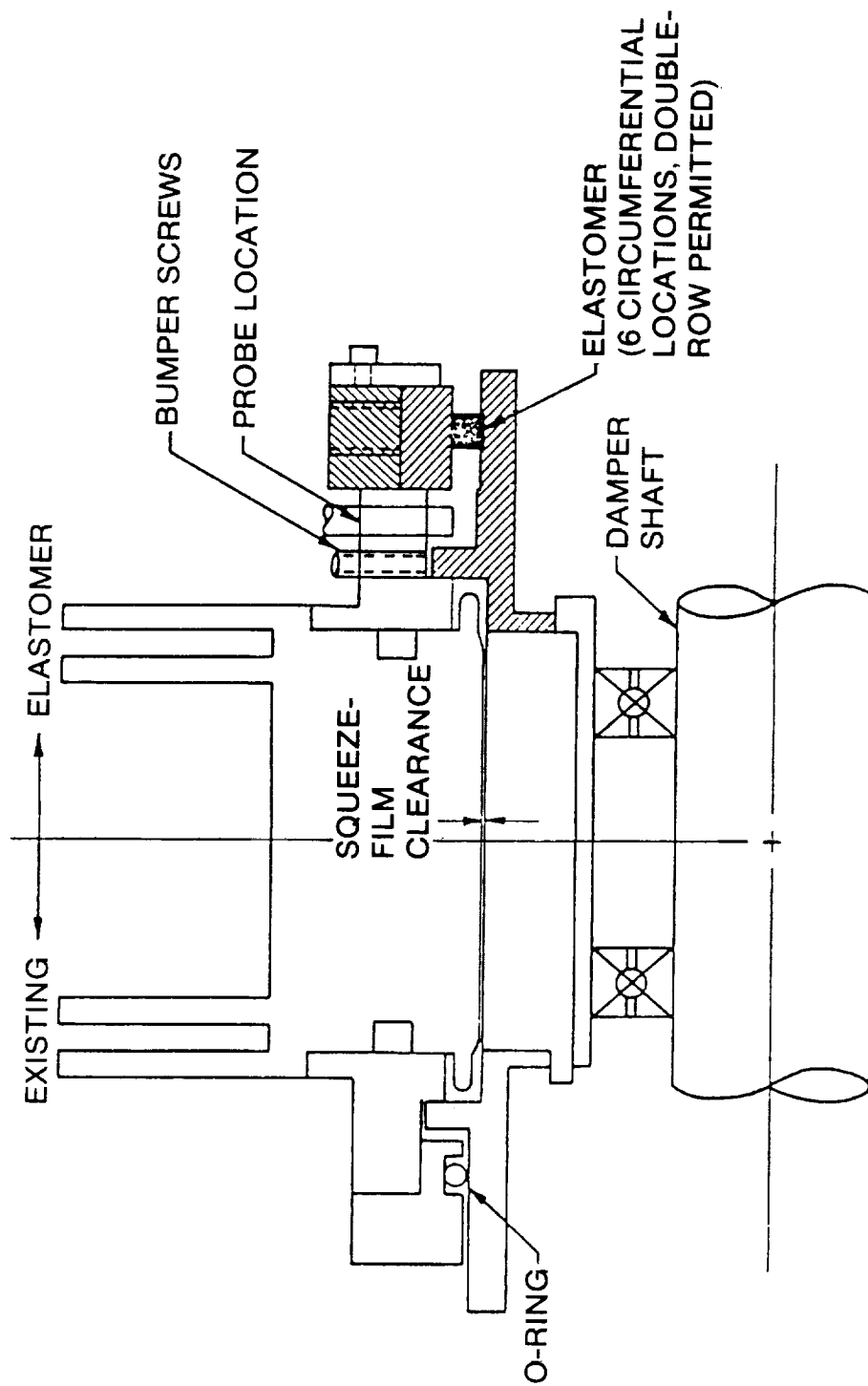
Fig. 160   Elastomer Damper/Squeeze-Film Damper Schematic

305

RING ASSEMBLY

ELASTOMER

PLATEN

PRELOAD SCREW
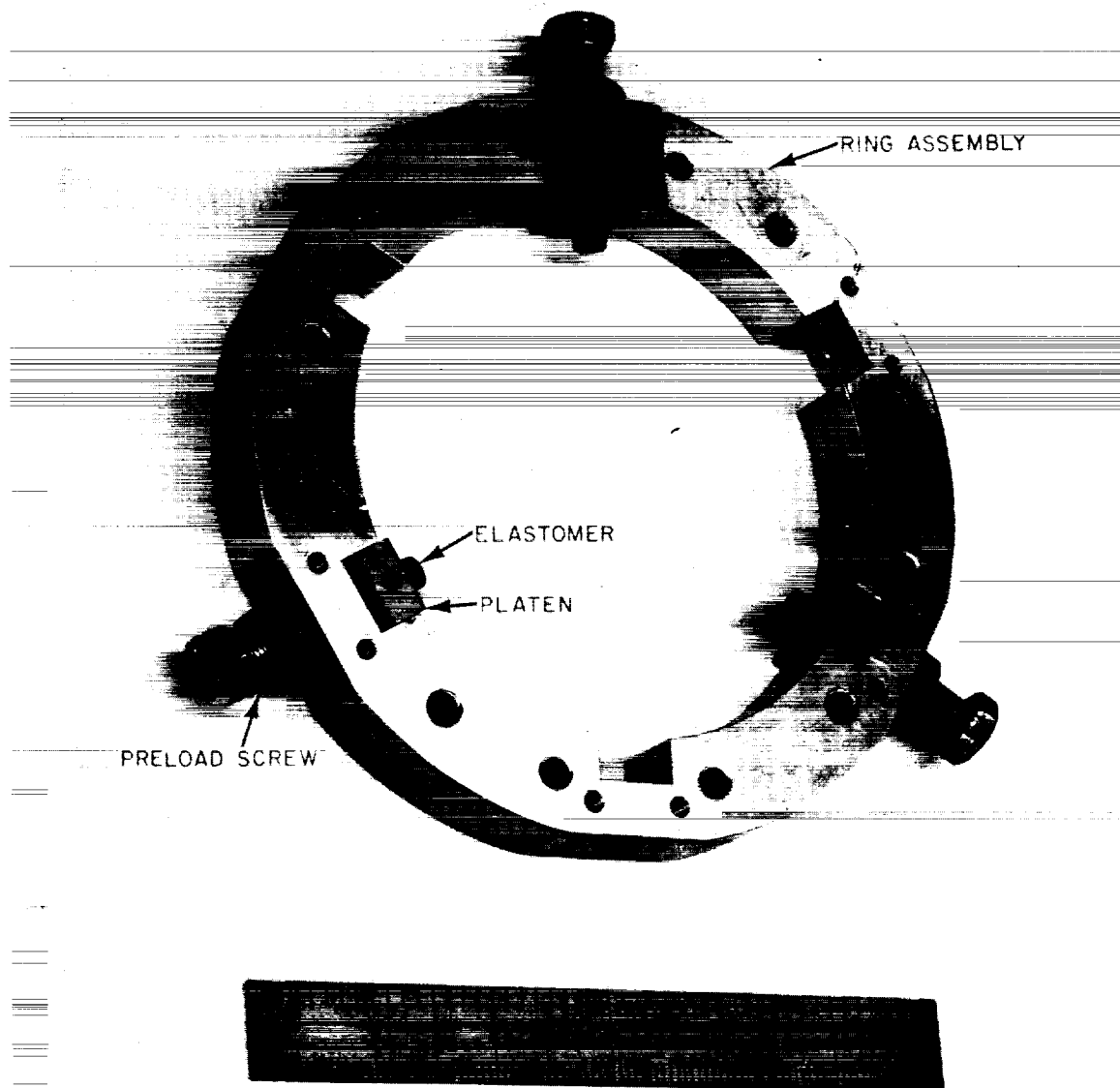
Fig. 161   Elastomer Damper Assembly
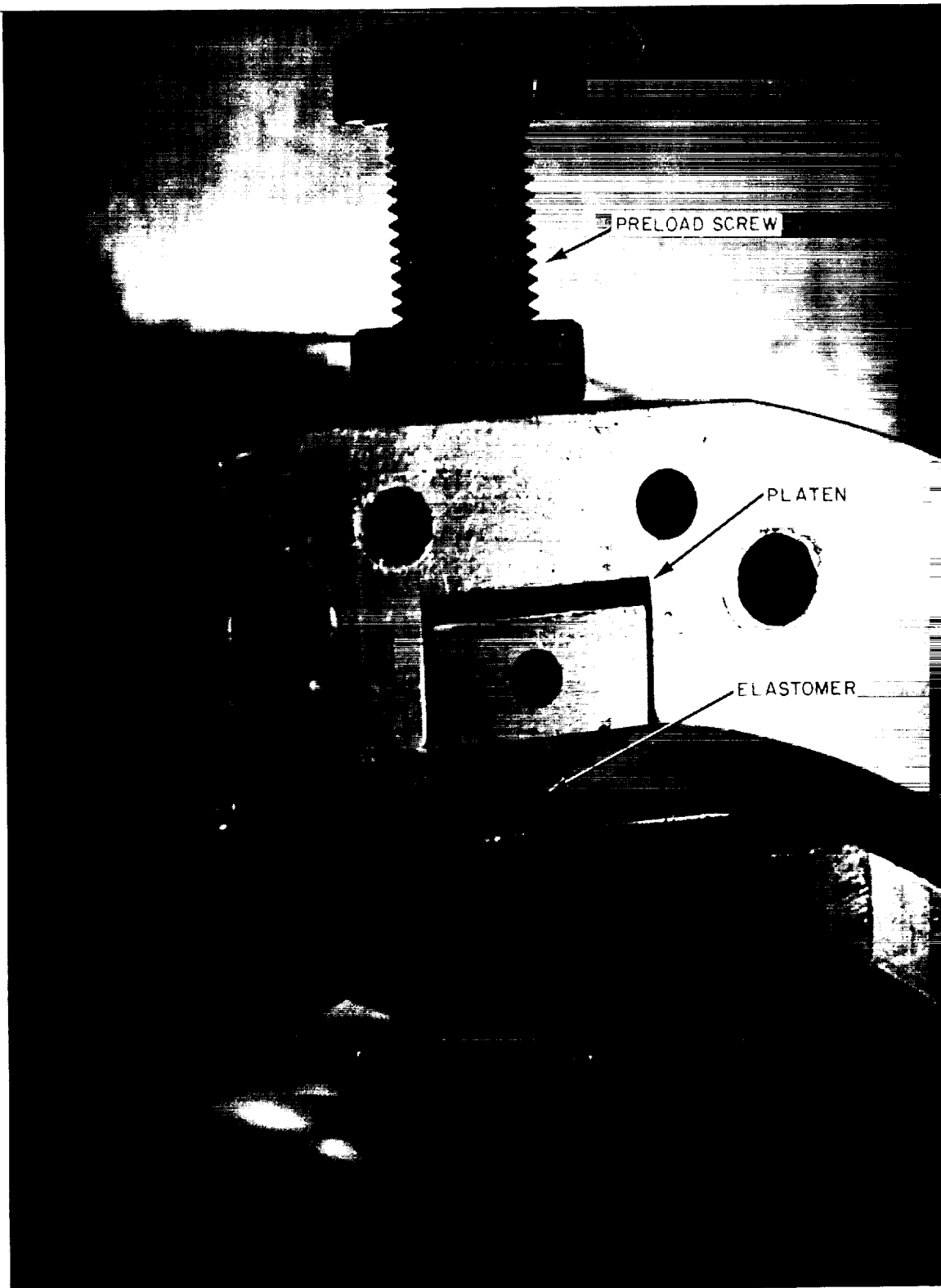
Fig. 162 Elastomer Damper Installed in Rig

307

SQUEEZE FILM

ELASTOMER

AMPLITUDE

50 MILS

Hz

0

500
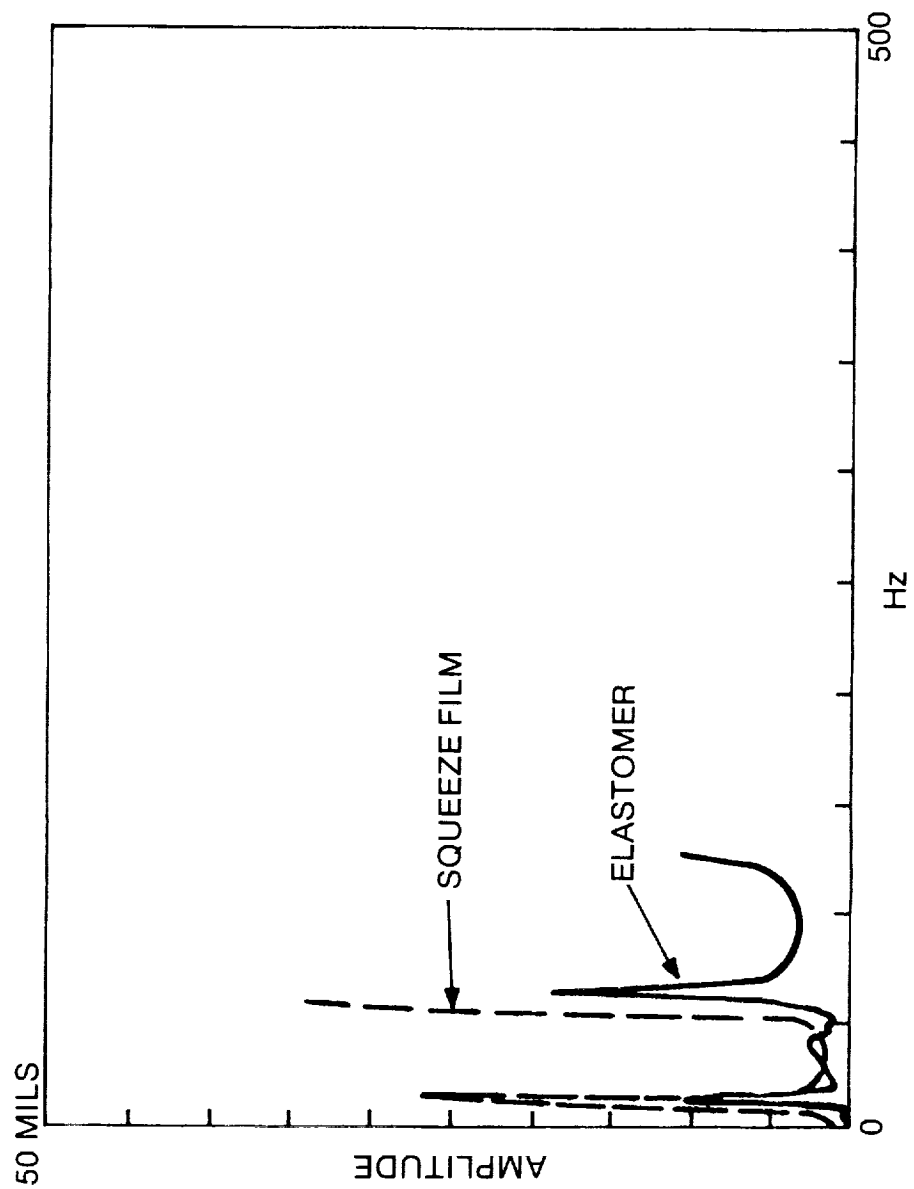
Fig. 163 Synchronous Response
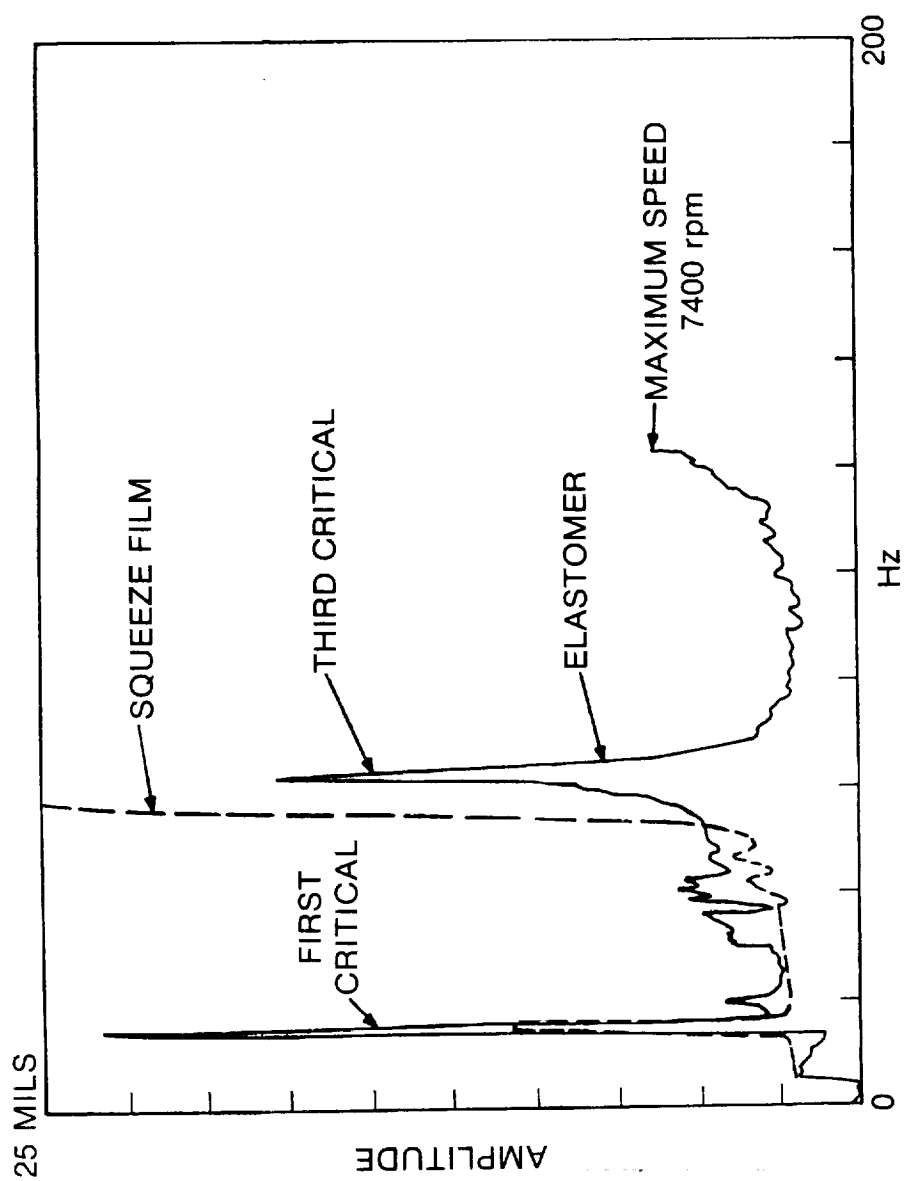
Fig. 164 Synchronous Response

309
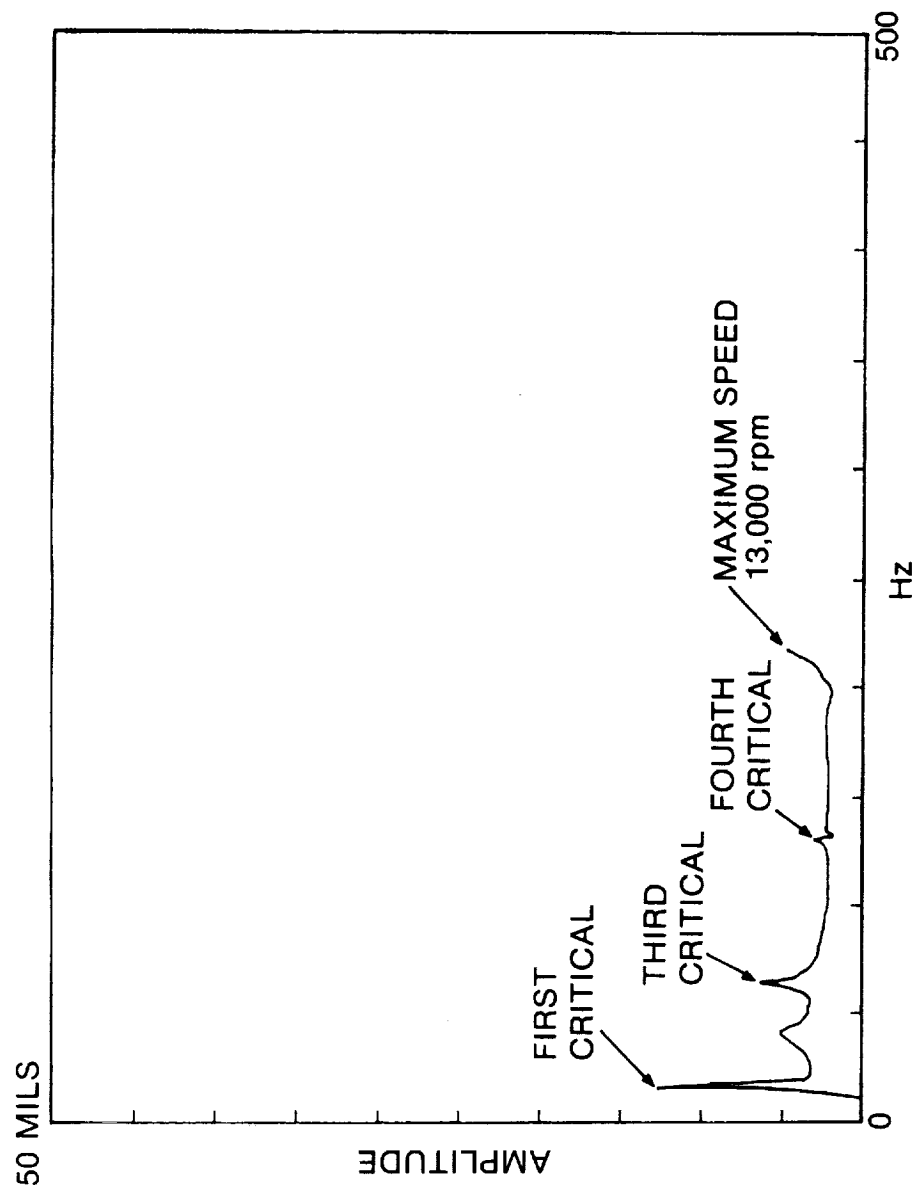
Fig. 165 Synchronous Response on Elastomer Damper
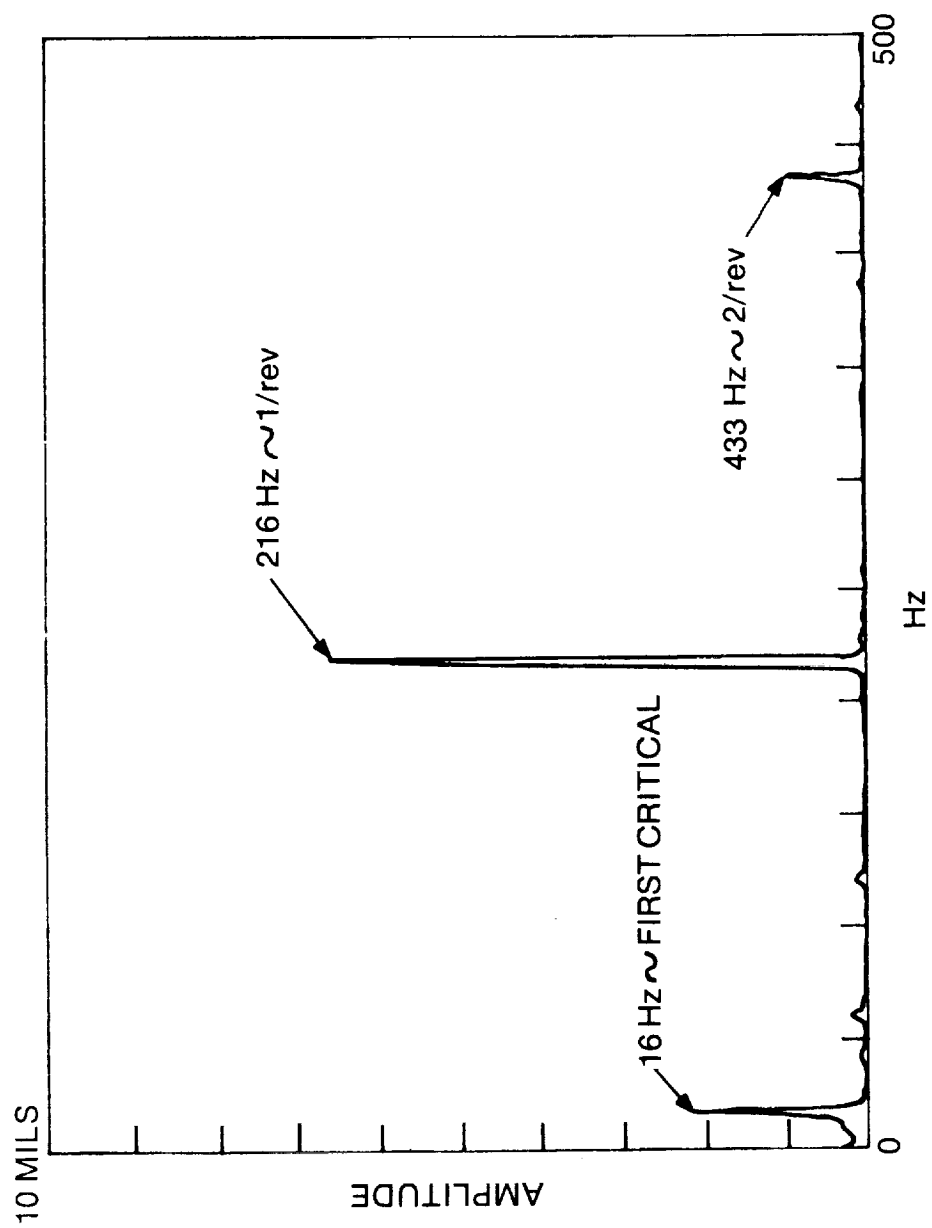
Fig. 166   Frequency Spectrum at 13,000 rpm With Elastomer Damper Operational

Computer/Control Console

Auxiliary Control Panel

CRT Display/Terminal

Test Rotor (T53)

Gearbox

Vacuum Chamber

Hydraulic Pump-
Vac. Chamber Cover

Lube Oil
Scavenge Pump
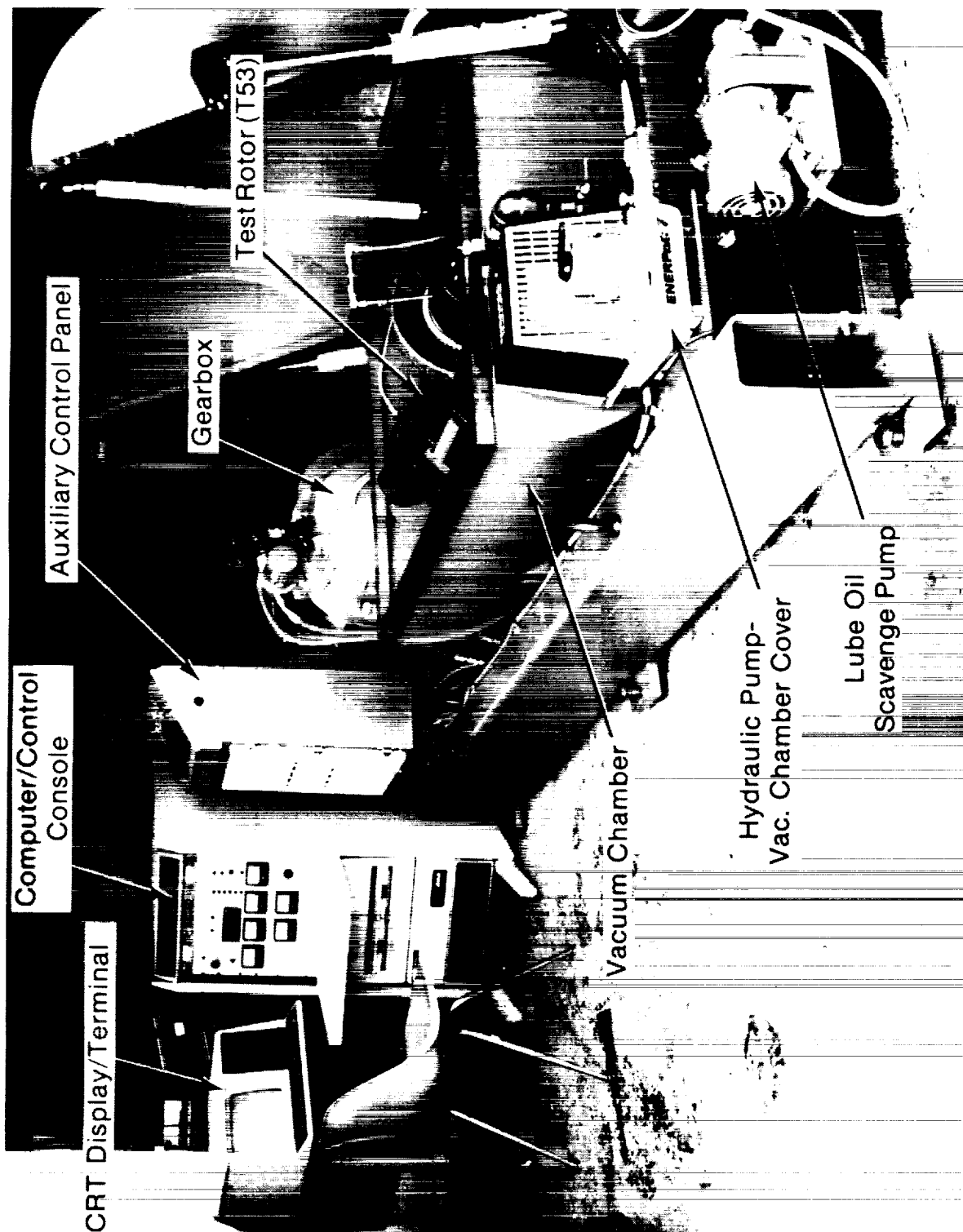
Fig. 167 CCAD Balancing Rig

312

8.3 T55 Helicopter Power Turbine Shaft 8.3

A turbine engine balancing rig was used as a test facility for this elastomer testing. The major hardware components of the test facility consist of a drive motor gearbox/belt drive speed increaser, vacuum chamber and computerized data acquisition and balancing system; see Figures 167, 168, and 169.

The drive motor is a 45-kW (60 hp) variable-speed motor. Motor speed is varied from zero to 1700 rpm by a solid-state silicon-controlled rectifier circuit. The speed increaser provides approximately a 12:1 increase in speed via two components: a standard belt drive and a high-speed gearbox. The belt drive provides a 2:1 step-up in speed from the motor output to the input to the gearbox. The gearbox (Sunstrand Model LMV311) provides an additional 6:1 increase to the power turbine. The vacuum chamber reduces windage and permits operation with the low-power drive system. The automated data acquisition and balancing system is configured about a PDP 11/03 mini-computer with 32K words of memory and a RXV11 dual floppy disk drive for mass storage.

The rig had successfully operated the T55 power turbine to the speed of 16,000 rpm on its production hardware supports. Typical response data is as shown in Figure 170. Figure 170 is a trace of the synchronous response of an acceleration pattern for a 90° pair (vertical and horizontal probes) at approximately midshaft location. The two dominant features are the peaks at approximately midshaft location. The two dominant features are the peaks at approximately 4,000 and 6,000 rpm. It is significant that the horizontal peak at 4,000 rpm occurs when the vertical probe response is minimum. The vertical peak at 6,000 rpm shows similarity in the lack of response of the horizontal probe. This highly elliptical horizontal orbit rapidly changing to a dominant vertical ellipse is typical of rotor characteristics encouraged by asymmetric support characteristics. The response of the turbine end at these two speeds is dominant, whereas the roller bearing end (cold end) shows little activity indicating a strong precession of the turbine such as a rigid body conical mode shape. A subsequent set of peak occurs in the 8,000 to 9,000 rpm speed range, with all probe sets along the shaft indicating motion. The activity at this speed has not been predicted analytically, but is generally subordinate to the two main peaks at 4,000 and 6,000 rpm; see Figure 170.

To assess possible rotor modes and the acceptability of the proposed rotor dynamic model, a shaker was attached to the CCAD rig to excite a nonrotating T55 power turbine. Swept sine-wave excitation, Figure 171, indicated three possible structural modes:

- 115-Hz bounce mode of turbine

- 210-Hz bending mode of shaft

- 600-Hz bending mode of shaft

Figure 172 indicates the location of these structural frequencies when compared to a tuned analytical model of the T55 (whirl speed marked by "X" at zero spin speed axis). This model, also predicted a first retrogarde

313

Fig. 168   CCAD Balancing Rig - Vacuum Chamber

314

Fig. 169 CCAD Balancing Rig - Data Acquisition and Balancing System
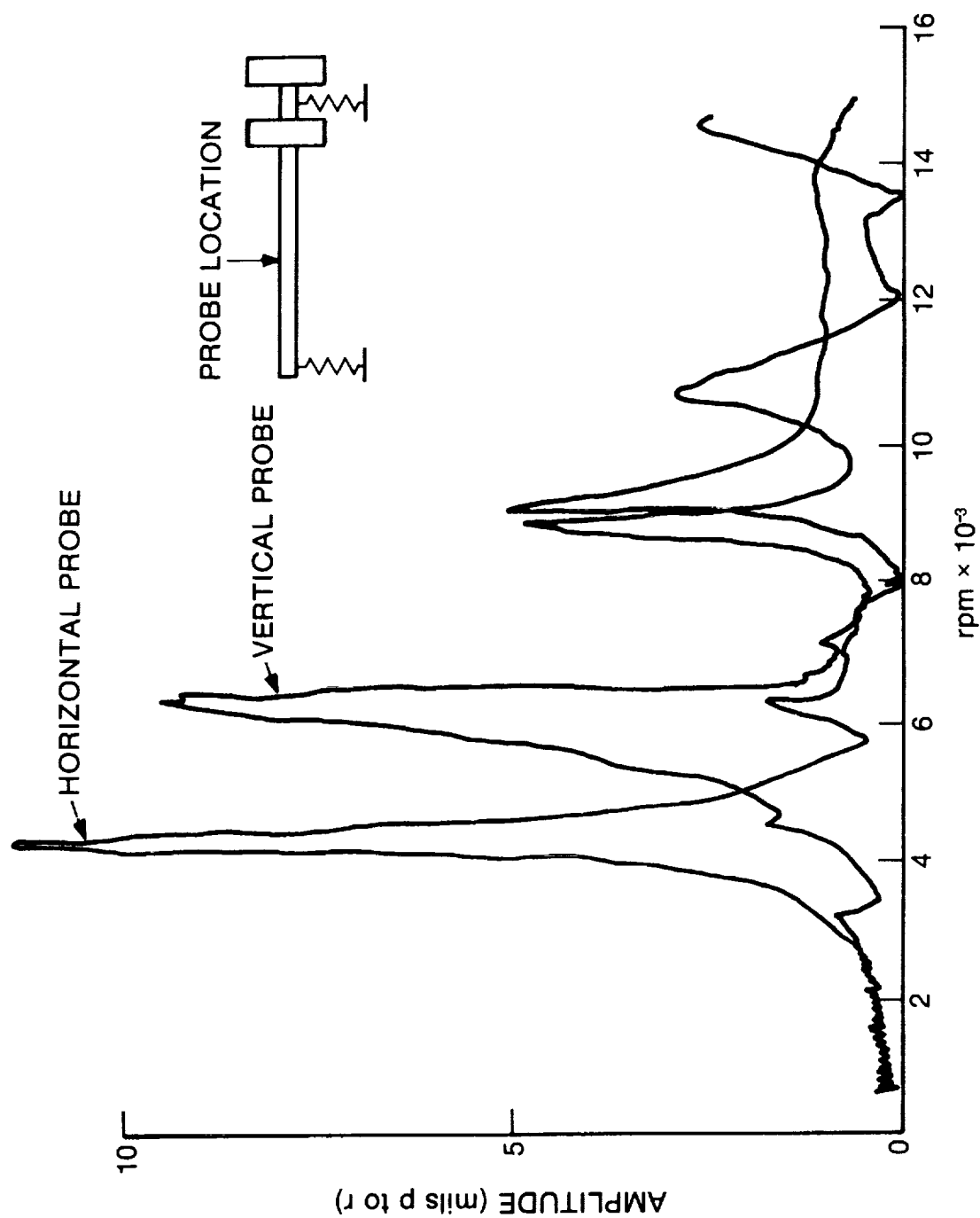
Fig. 170 Synchronous Response T55 on CCAD Rig

316
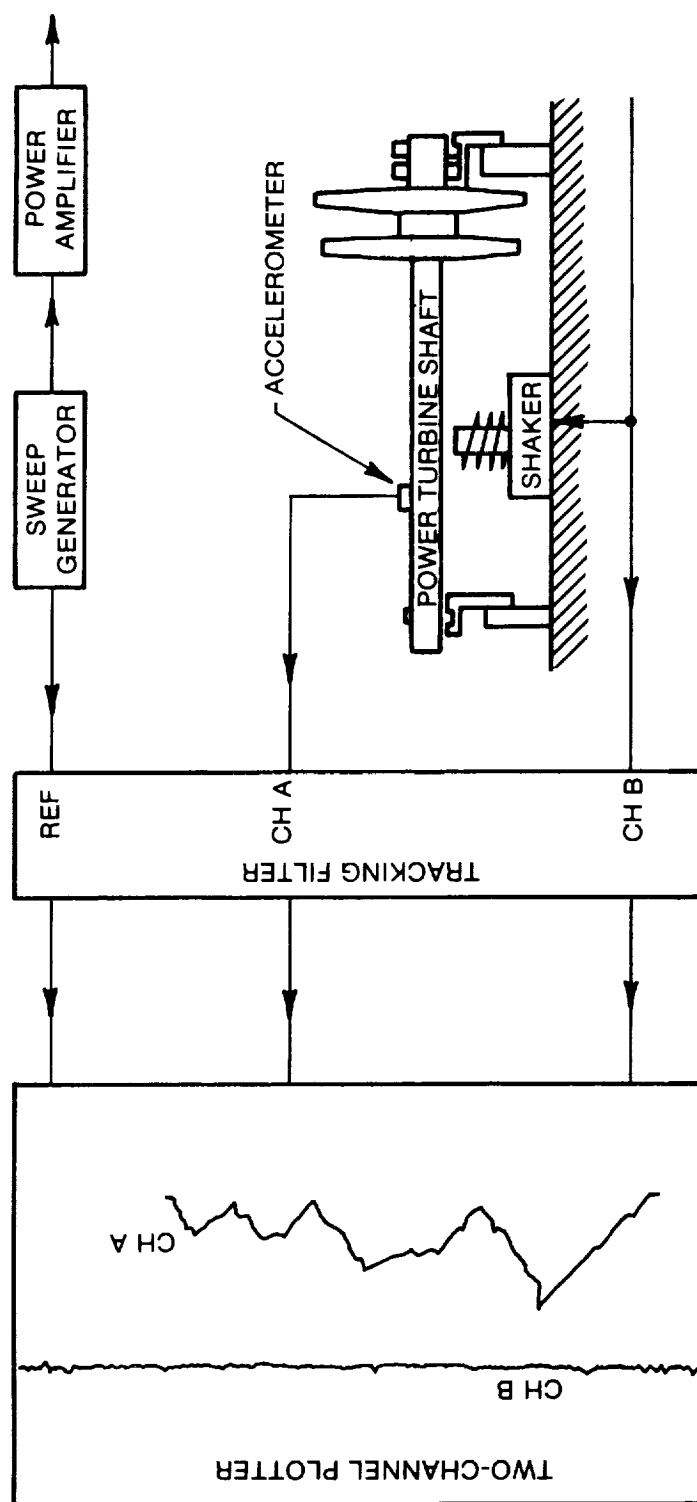
Fig. 171 Sine Swept Shaker Test Setup

317
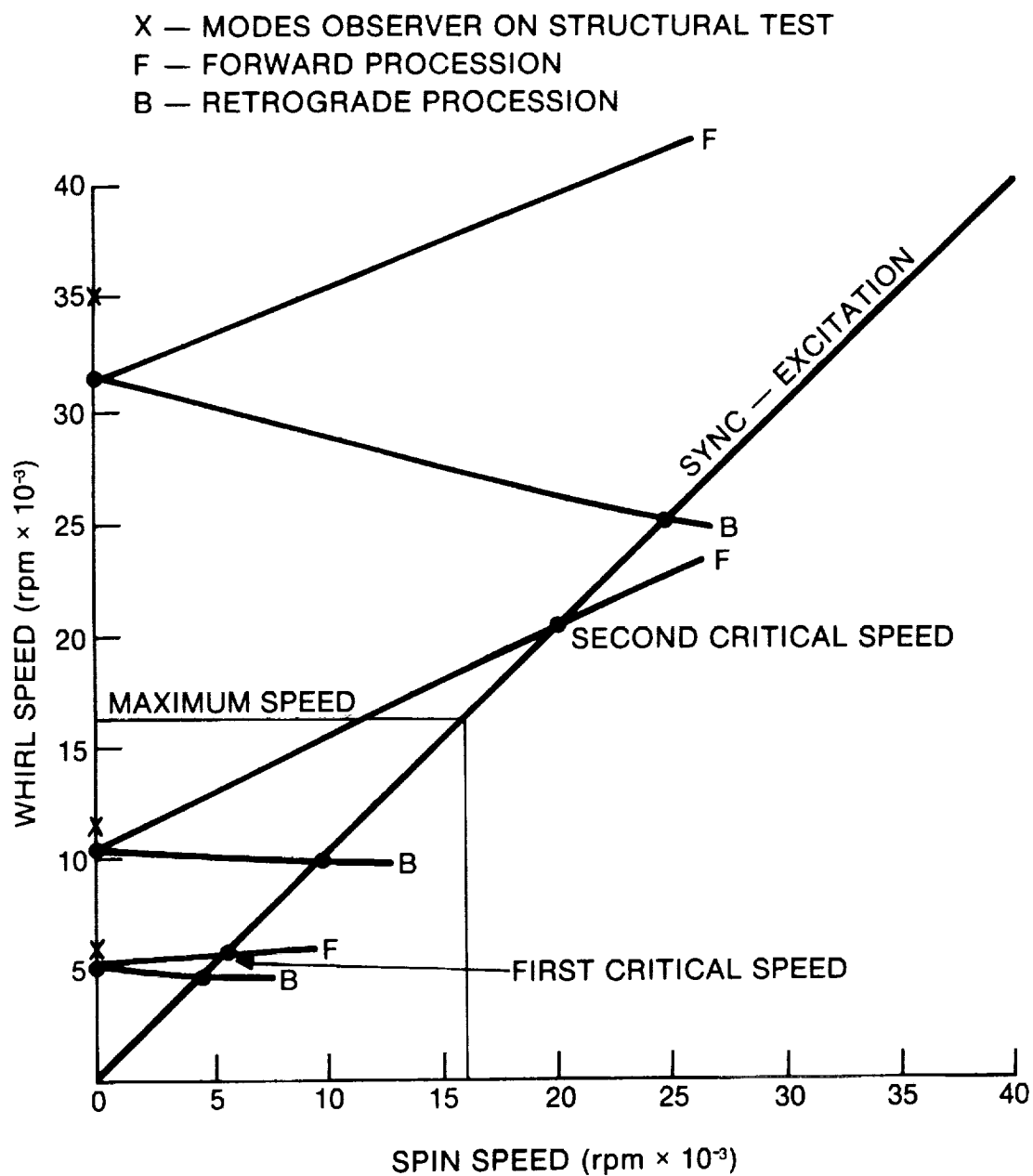
Fig. 172   Whirl Speed vs Spin Speed

80829

(backward) precision turbine conical mode at 4500 rpm, a first forward mode at 6000 rpm and a first bending (2nd critical) at 21,000 rpm. The production engine support rigidity needed to provide this model was reasonable, with a roller bearing stiffness of 8.75 x 10^7 N/m (500,000 lb/in.) and a ball bearing (turbine) pedestal stiffness of 1.4 x 10^7 N/m (80,000 lb/in.).

Thus, it is reasonable to predict the modes at 4000 to 6000 rpm yet not encounter the bending mode with operation to 16,000 rpm. Gyroscopic forces affect the speed of the first backward and forward so that a minimum of asymmetry is necessary to induce excitation of both the 4500 rpm and 6000 rpm peak.

Further evidence that the location of the second mode for the baseline T55 configuration was above the operating speed of 16,000 rpm was obtained from observing the supersynchronous excitation of the small 2/rev component of motion throughout a normal acceleration pattern to maximum speed. The 2/rev peaked while operating at 7100 rpm indicating the presence of a mode. This is shown as a circled dot located on the dashed line extending from the lower left to the upper middle of Figure 122. The dashed line represents a whirl speed of twice the corresponding spin speed (2/rev excitation).

Therefore, from observation of rotor synchronous response, static shaker excitation data and observation of the 2/rev vibration, the rotordynamics model, Figure 173, was considered as acceptable for analytic examination of possible elastomeric-damper designs.

Previous elastomer material testing of shear specimen using the Ling Shaker* was reviewed for candidate elastomer material selection. From Figures 76 through 78 the fluorocarbon (Viton 70 - CFM) data for 32°C showed that it had the largest measured value of loss coefficient for the entire range of frequencies. As temperature increased, the selection of material for damping became somewhat arbitrary as the loss coefficient for all materials nitrile (Buna-N - NBR), butadiene (Polybutadiene - BR), EPDM, chloroprene (Neoprene - CR) and fluorocarbon (Viton - CFM) ranges between 0.1 and 0.2 (Figure 76) for the entire frequency range. Therefore, the selection to use fluorocarbon (Viton - CFM) as the damping material was based upon the following:

- Superior damping properties than the other materials tested for 32°C or 66°C operation (Figures 76 and 77).

- Dissipation characteristics as good as any of the other materials tested for operation at 88°C (Figure 78).

- Previous use as a damper in successful testing of high-speed rotor dampers.

_____

* Mechanical Technology Incorporated, Latham, N.Y.

Fig. 173   Rotordynamics Model Details of T55 Power Turbine

320

The range of loss coefficient from data obtained from shear specimen shaker testing of fluorocarbon (Viton 70 - CFM) indicated that a range of loss coefficients from 0.15 to 0.75 was reasonable for the 0-16,000 rpm operation of the CCAD balancing rig. Accordingly, the T55 power turbine rotordynamics model was modified to determine the "optimal" damper design, Figures 174 and 175. All system damping was assumed to be due to the elastomer damper; consequently no structural damping was modelled for the turbine or gearbox bearing. The two disc pack couplings were included as elastic elements which offered a minimum of bending rigidity but offered full shear restraints. Figure 173 indicates these couplings at stations 8 and 19 of the rotor model.

From the rotor damper optimization studies, Figures 174 and 175, a number of facts surfaced regarding the design of the elastomeric damper:

- The first mode is a conical precession of the turbine. The nodal point is extremely close to the elastomer-damper test bearing location. Accordingly, the first critical speed offers little damping and is insensitive to the elastomer-damper stiffness or damping characteristics.

- The second and third mode shapes offer significant activity of the elastomeric damper. Consequently, the critical speed location and log decrement of those modes are sensitive to damper selection.

- A "best" or "optimal" tradeoff between the second and third mode is obtained by a fluorocarbon (Viton 70 - CFM) elastomeric damper of between $5.25 \times 10^6 - 7.0 \times 10^6$ N/m (30,000-40,000 lb/in.).

- With this value of stiffness, the T55 rotor mounted on the elastomeric damper is expected to traverse the second critical, which is not within the operational range of the roller-bearing-mounted production T55 configuration, Figure 170.

- The range of log decrement expected for the second critical speed is between 0.2 to 1.1 depending upon the loss coefficient (temperature of operation) for the elastomer damper.

The T55 elastomer-damper design offered uniquely challenging problems. This damper configuration was to be more compatible with actual gas turbine design technology and constraints. Buttons require added radial envelope and are not necessarily a desirable geometry for a bearing which may also be required to tolerate thrust. Most gas turbines do not have large amounts of radial envelope available, particularly if they are multishaft, turbofan, or turboshaft engines, such as the T55. Design maneuverability and flexibility are generally less restricted in the axial direction. The design must also accommodate possible thrust loading (although the T55 cold-end mount does not take thrust) in combination with radial loads and must be a design capable of controlled preload. These requirements were satisfied by a shear damper configuration.
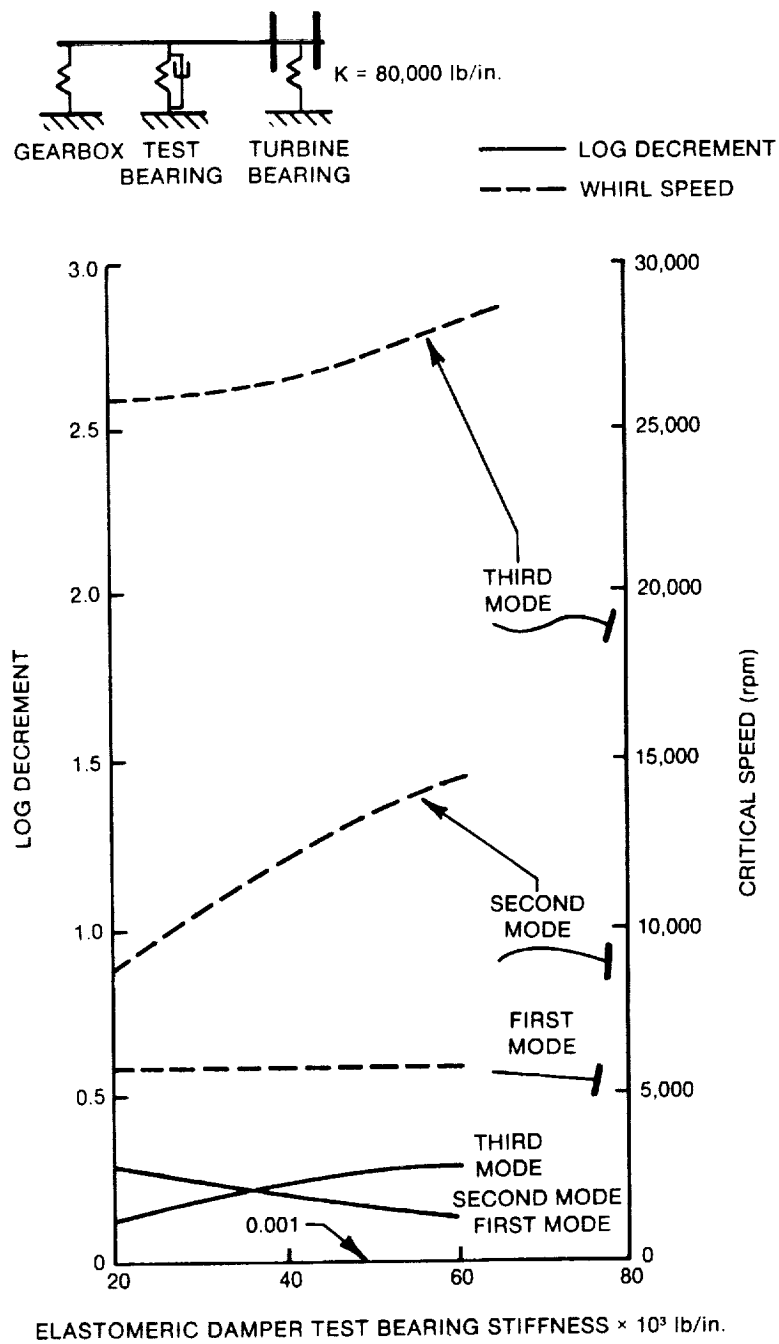
321

Fig. 174   T55 Power Turbine — Critical Speeds and Log
Decrement vs Bearing Stiffness for Fluorocarbon
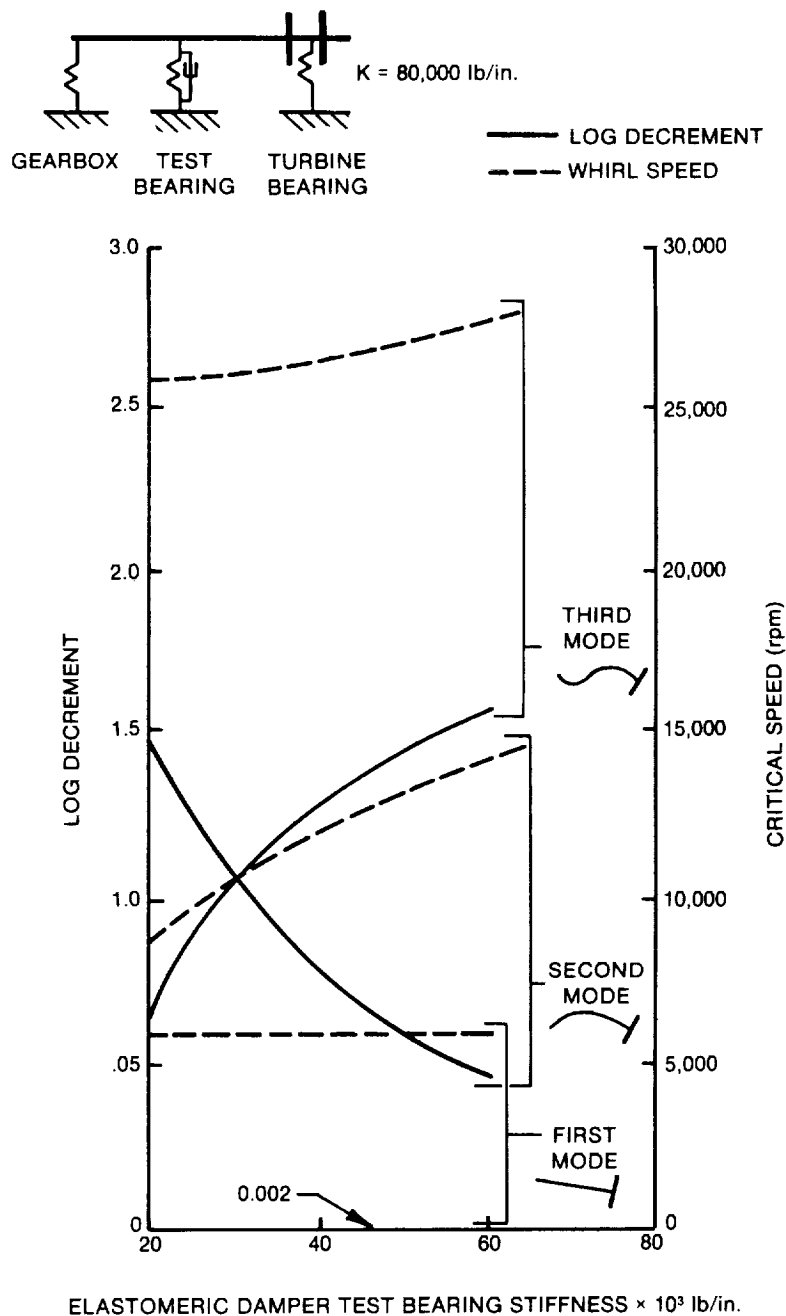(Viton-70) Elastomeric Damper (η= 0.15)

K = 80,000 lb/in.

——— LOG DECREMENT
— — — WHIRL SPEED

GEARBOX   TEST   TURBINE
           BEARING   BEARING

ELASTOMERIC DAMPER TEST BEARING STIFFNESS × 10³ lb/in.

Fig. 175   T55 Power Turbine — Critical Speeds and Log Decrement vs Bearing Stiffness for Fluorocarbon (Viton-70) Elastomeric Damper (η= 0.75)

Figure 176 illustrates the concept used for the elastomer-damper mount on the roller bearing support for the T55. Two fluorocarbon (Viton 70 - CFM) shear rings mounted along the entire circumference satisfied all require-ments. Axial preload was accommodated by controlled machining of the outer flanges which attached to the housing by 12 equally spaced socket head cap screws. An overload protector was installed by using an O-ring with a prescribed clearance 0.254 mm (0.010 in.) that would not interfere with normal operation of the damper but which would be available as a back-up protection if the shear damper failed. (As all testing proved successful, the O-ring was never required to dampen rotor vibrations.)

To obtain fluorocarbon (Viton 70 - CFM) shear damper with the required stiffness, the results of previous shear specimen data were used. Using the values for material properties and characteristic temperature for fluorocarbon (Viton 70 - CFM) and the unified design curves in Figures 87 and 88, the analysis showed that an I.D. of 6.98 cm (2-3/4 in.) and an O.D. of 9.52 cm (3-3/4 in.) for 3.175 mm (1/8 in.) thick fluorocarbon (Viton - CFM) specimen would produce a stiffness in shear of approximately $6.12 \times 10^6 - 7.0 \times 10^6$ N/m (35,000 to 40,000 lb/in.) depending upon strain amplitude experienced in operation.

Construction of the elastomeric damper, Figure 177, consisted of machining the aluminum bearing supports and shear restraining plates, bonding the fluorocarbon (Viton - CFM) using REN H998* hardner with a RP-138 resin adhesive, and inserting four thermocouples and two capacitance probes into the assembly. The overload O-ring was also attached using the REN adhesive, Figure 178. As shown, the damper was split radially into two halves for ease of assembly and replacement with the production T55 support (shown on the left of Figure 179). Prior to installation of the damper on the CCAD rig, the elastomer was subjected to static loading for calibration purposes. Figure 180 presents the static data for shear loading on the damper. The static values of stiffness determined were between 6.12×10^6 and 6.47×10^6 N/m (35,000 and 37,000 lb/in.). Static loads were applied and held for up to 5 minutes. No reduction in load was observed on the pressure load gauge, Figure 181. For the purpose of shear loading, a mandrel was machined to support the inner block on a "V"-block setup, Figure 182. In addition to shear loading, a static compression load was applied to the two 3.175 mm (1/8") elastomer pads. An axial compression stiffness of 1.26×10^7 N/m (72,000 lb/in.) was determined, Figure 183. Again, holding load for a period of up to 5 minutes did not produce measurable load relaxation.

With fabrication of the elastomer damper complete, the CCAD balancing rig with a balanced T55 power turbine was made available for this test, Figure 184. Figure 185 illustrates the location and designation of the proximity probes which were active throughout this testing. After establishing a baseline condition for the T55 production configuration operating in the CCAD rig, the elastomer damper was installed, and the power turbine generated to 16,000 rpm. Imbalance was introduced at balance planes #1, #2 and #3 at various stages in testing [8.3], as shown in Figure 185.
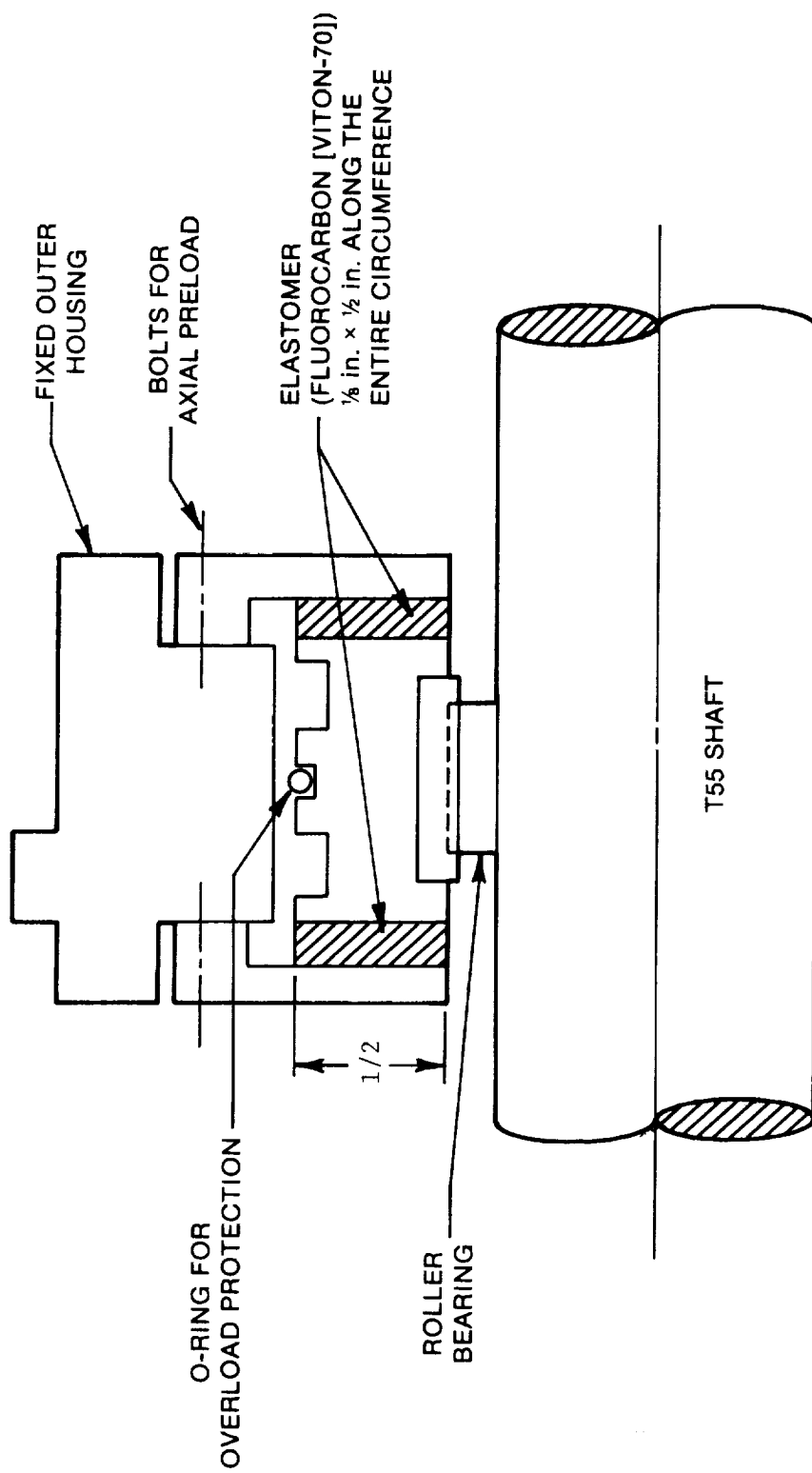
FIXED OUTER HOUSING

BOLTS FOR AXIAL PRELOAD

ELASTOMER (FLUOROCARBON [VITON-70]) ⅛ in. × ½ in. ALONG THE ENTIRE CIRCUMFERENCE

O-RING FOR OVERLOAD PROTECTION

ROLLER BEARING

T55 SHAFT

1/2

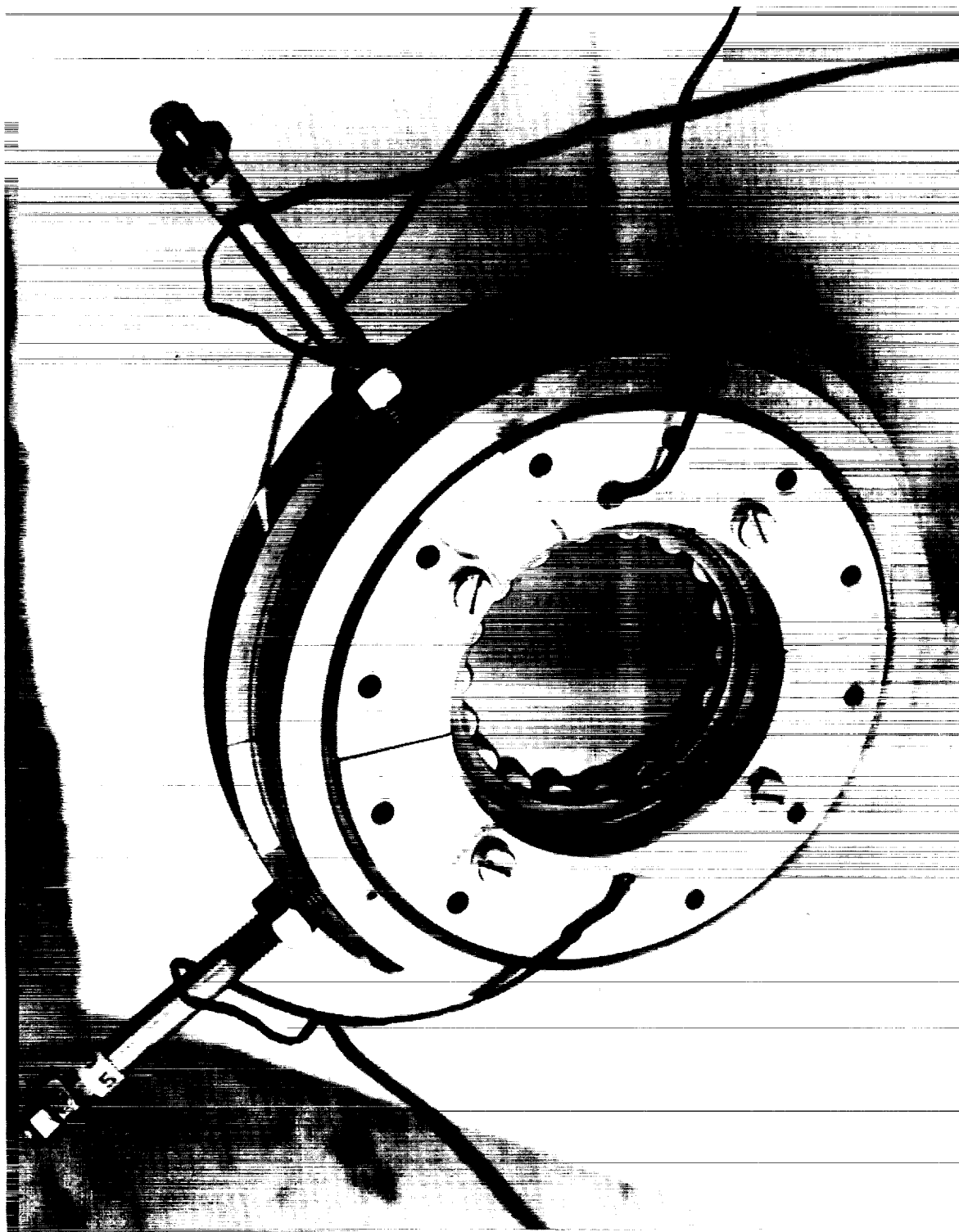Fig. 176 T55 Elastomer-Supported Roller Bearing Cartridge
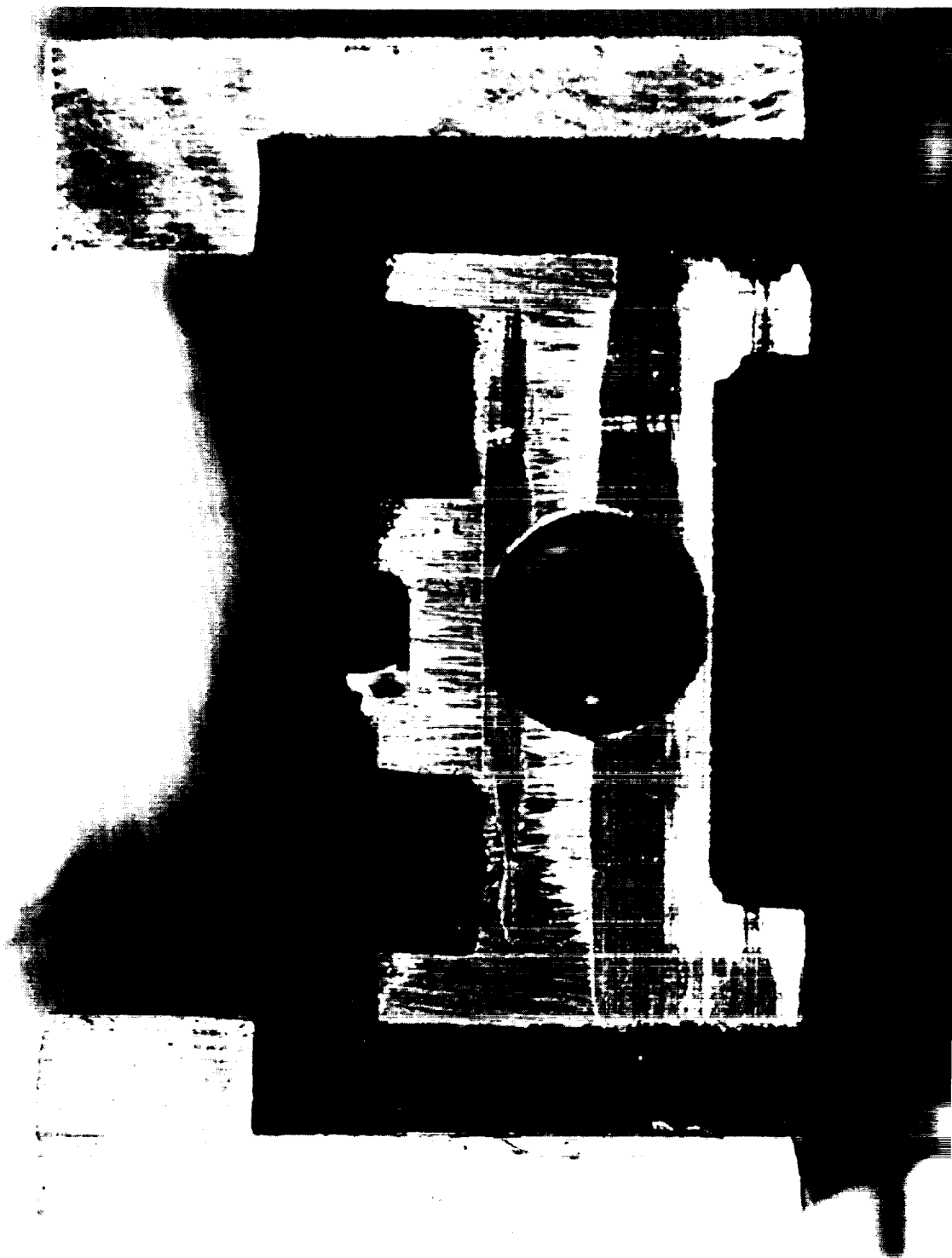
Fig. 177 Assembled T55 Power Turbine Elastomeric Damper

326

Fig. 178 Cross Section of the T55 Elastomer Damper

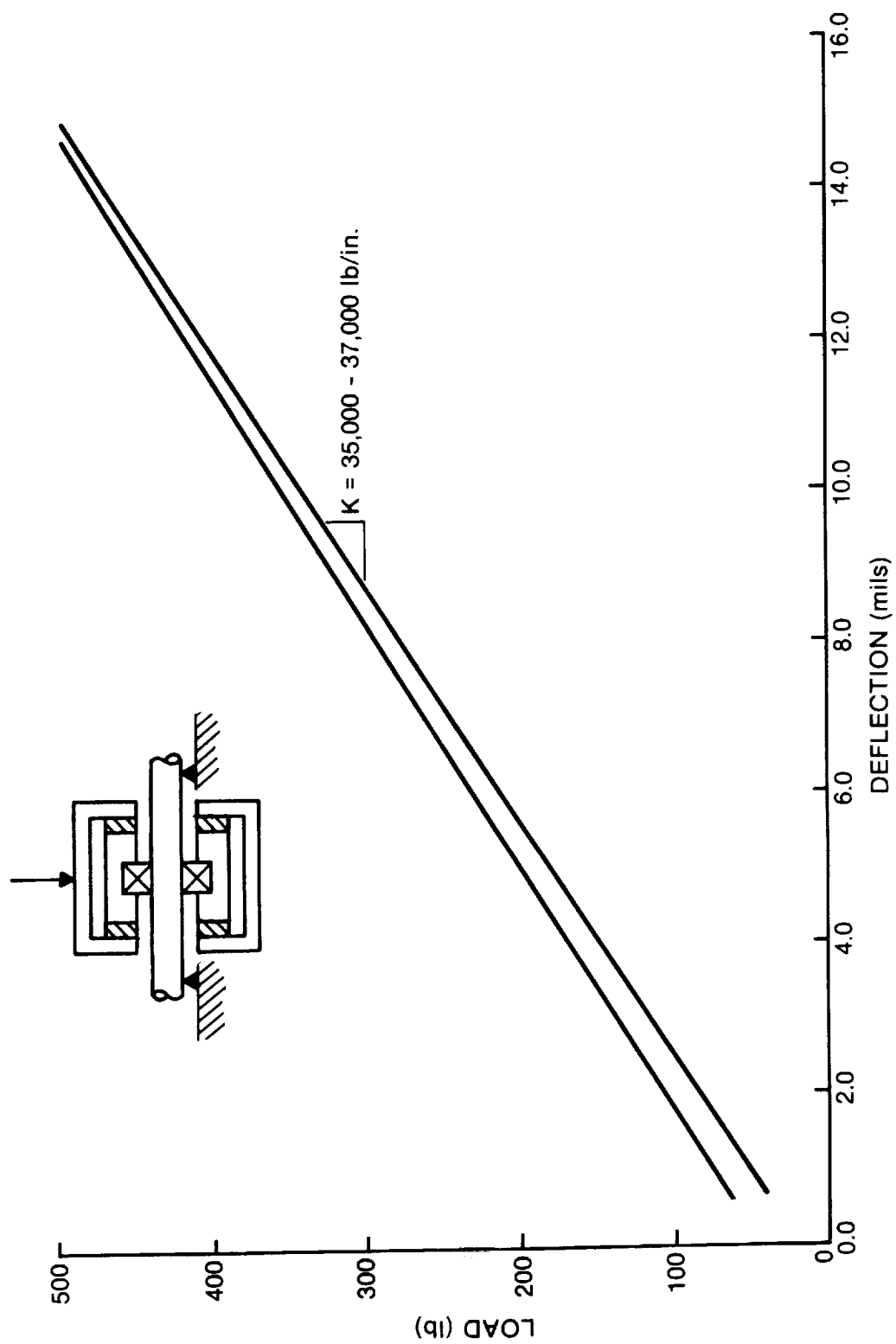Fig. 179 Production T55 Roller Bearing Support and the Replacement Elastomer Damper

328

K = 35,000 - 37,000 lb/in.

LOAD (lb)

DEFLECTION (mils)

Fig. 180   Static Shear Loading of Fluorocarbon (Viton-70) T55 Elastomer Mount

329
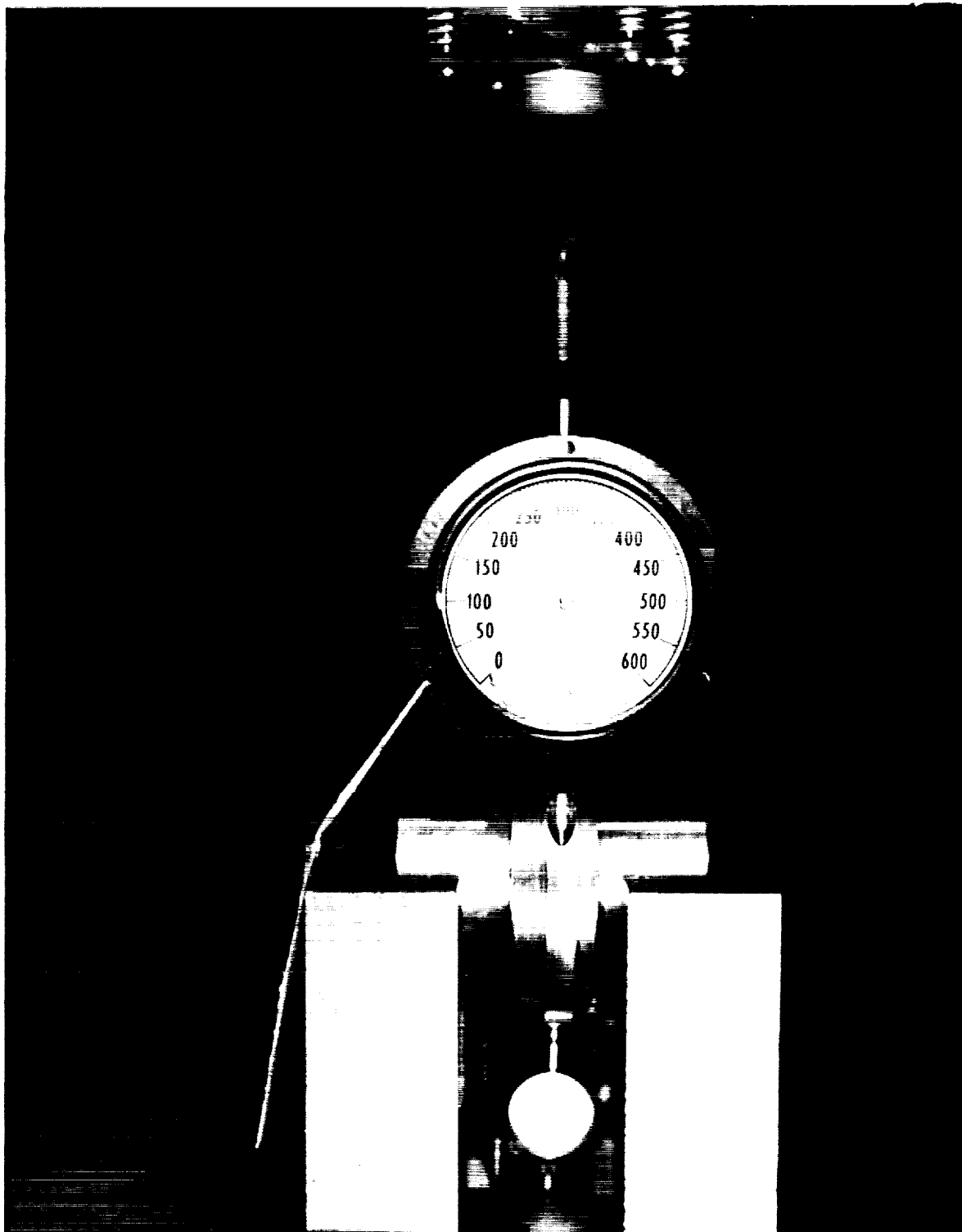
Fig. 181 Static Shear Load Test Setup for T55 Elastomer Damper

330
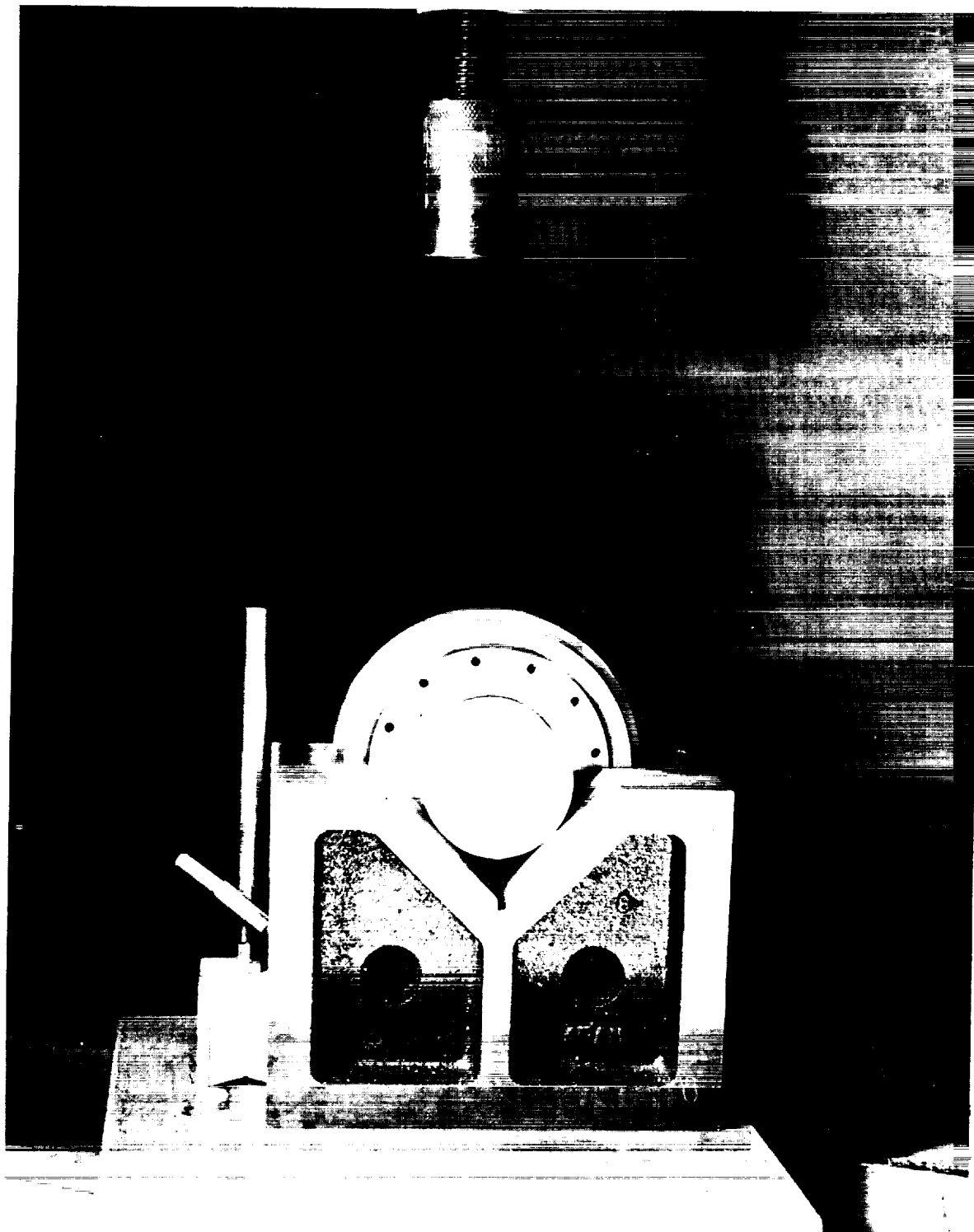
Fig. 182 "V-Block" Setup for Static Shear Testing
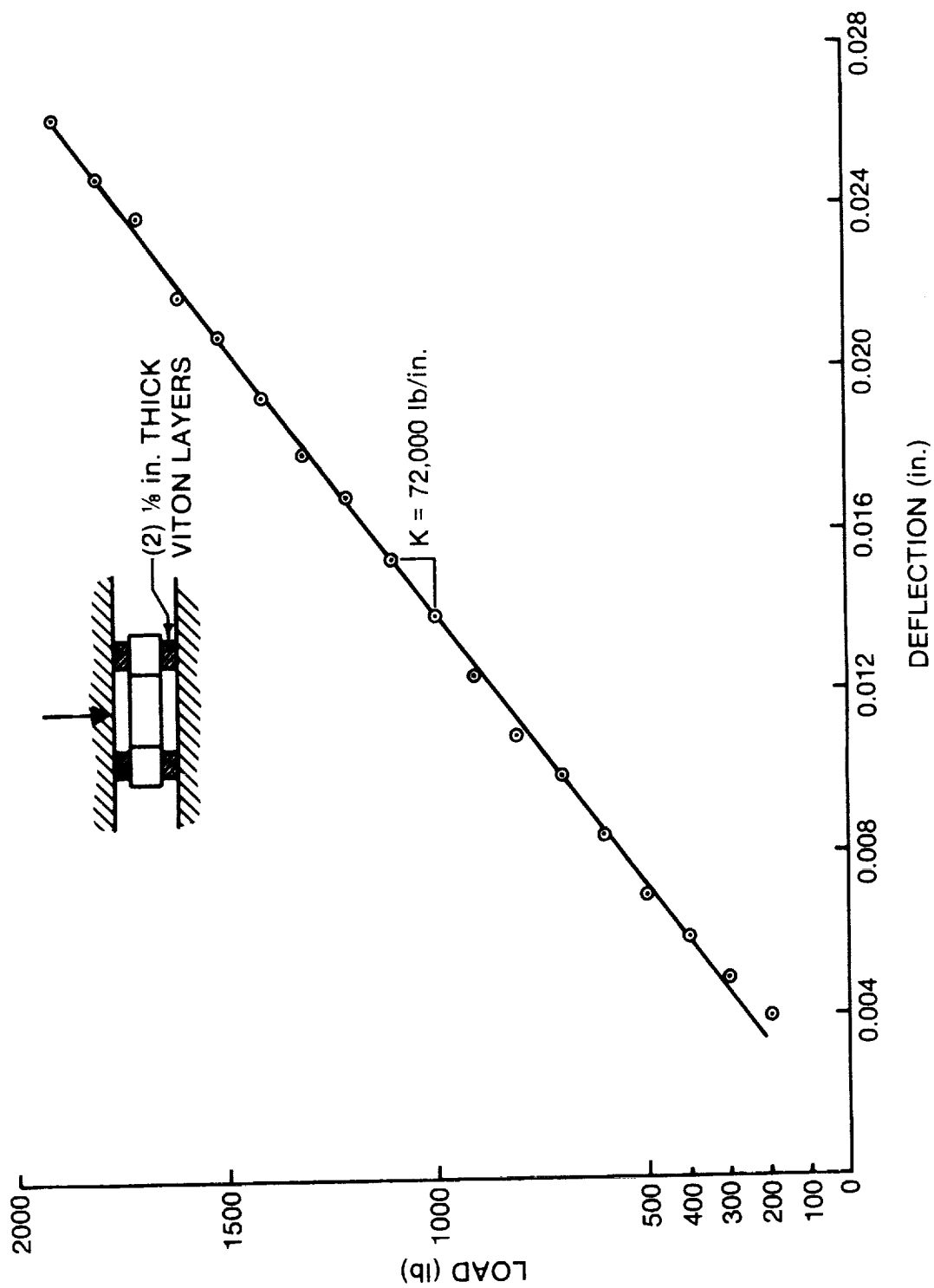
Fig. 183   Axial Static Loading of Fluorocarbon (Viton-70) T55 Elastomer Mount
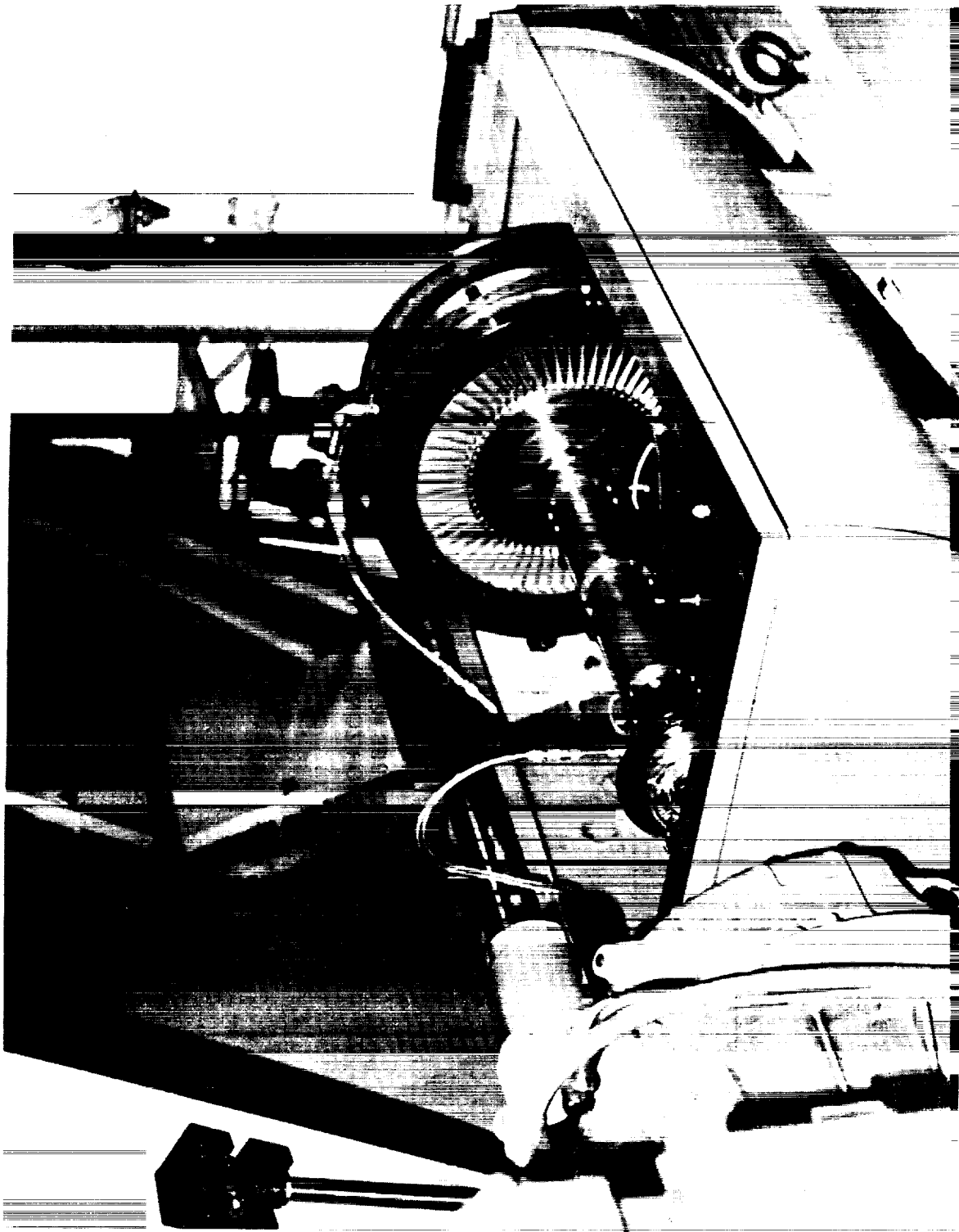
Fig. 184 CCAD Test Rig with Installed T55 Power Turbine and Elastomer Damper
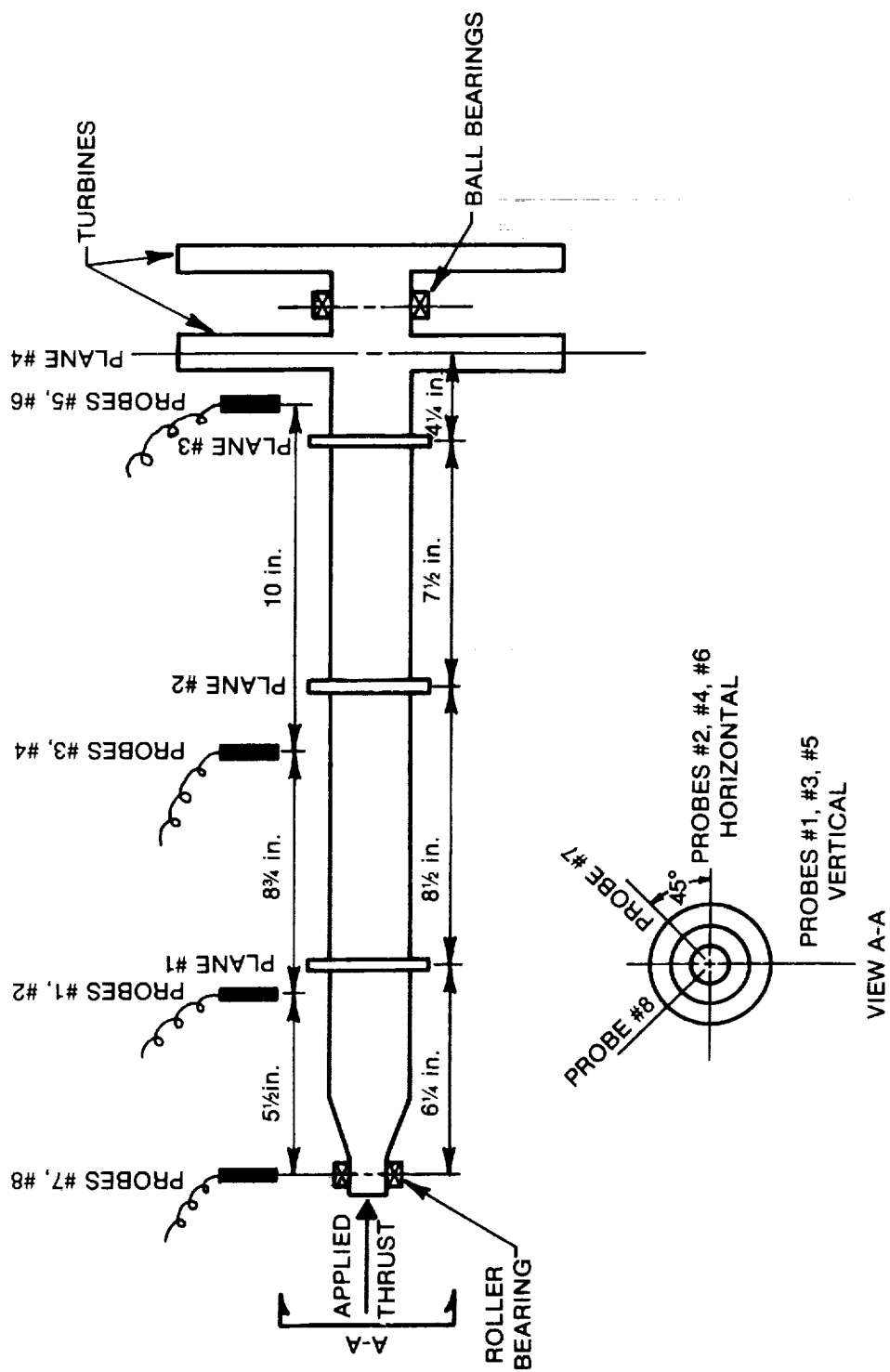
Fig. 185 T55 Power Turbine Rotor in CCAD Rig

334

The baseline run of the T55 power turbine supported on the production roller bearing housing showed the characteristics noted in Figure 170. Figures 186 through 188 show the runout-compensated synchronous response for probes #1 through #6. The data from Figure 186 for probes #1 and #2 indicates that the 4,000 and 6,000 rpm peaks are very small. These occur in Figure 188 for probes #5 and #6 and are larger amplitudes, indicating strong precessing of the turbine end. The intermediate peaks occur for all probes in the 8,000-9,000 rpm range. For the production T55 engine power turbine operating in the CCAD rig, no critical speeds have ever been observed above the peaks recorded in the 8,000-9,000 rpm range, regardless of the imbalance conditions.

The T55 roller bearing housing was removed and the elastomer damper housing was installed. Two of the four thermocouples monitored elastomer temperatures, whereas the other two thermocouples monitored outer race bearing metal temperatures. The two additional probes (probe #7 and #8 of Figure 185) were installed with output recorded on the Sanagamo Sabre VI tape recorder. The T55 power turbine was then operated to 16,000 rpm. The filtered synchronous vibration response obtained is documented in Figures 189 through 191. Comparative results from the baseline T55 run (Figures 186 through 188) and the elastomer-damper test results (Figures 189 through 191) are provided for probes #1 and #5 in Figures 192 and 193. From these results a number of facts emerged:

- A substantial reduction in synchronous response occurs for the 6,000 and 8,000 rpm peaks with the elastomer operation (Figures 192 and 193).

- That a reduction in vibration occurs for the entire 16,000 rpm operational range for probe #5 (Figure 193).

- A definite peak occurs (Probe #1) in the 13,500-14,000 rpm range which has provided an increase in rotor vibration with the elastomer damper operational (Figure 192).

By adding weight imbalance, confirmation of a second bending mode was obtained. In particular, the response of probes #7 and #8 of Figure 194 clearly indicates the presence of a mode critical speed at 13,500 rpm.

Thermocouple readings on the elastomer indicated a temperature of approximately $65^\circ \pm 5.5^\circ C$ ($150^\circ \pm 10^\circ F$) was typical for operation of this damper. This temperature was consistently within $3^\circ C$ of the bearing metal temperature. Further, changes in axial thrust load of the thrust bearing did not alter significantly the response characteristic of the rotor.

A comparison of the analysis performed for the elastomer-damper supported system with the measured data provides good correlation for mode shapes, Figure 195. Table 37 provides a comparison of critical speeds and logarithmic decrements for the two criticals observed.
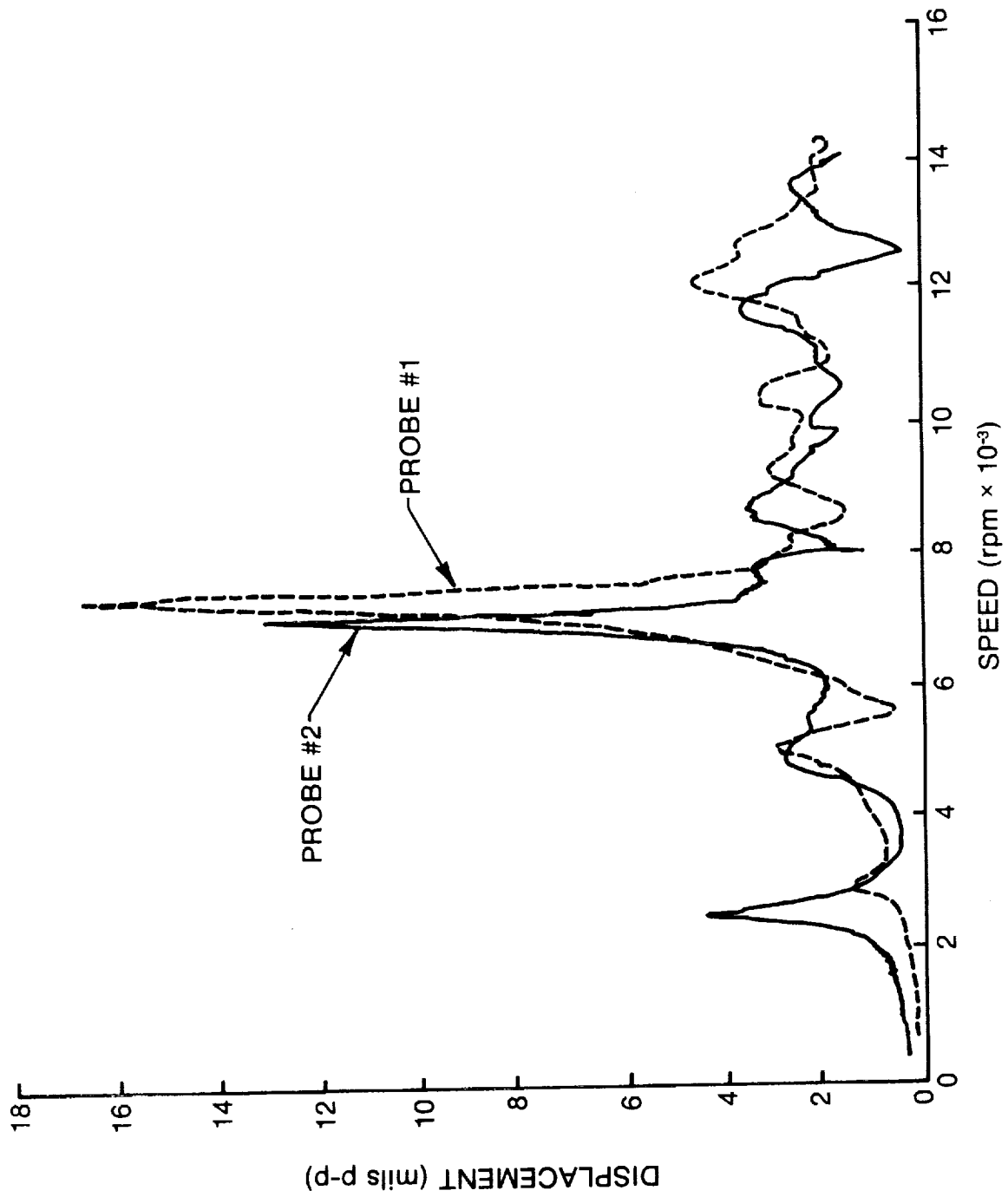
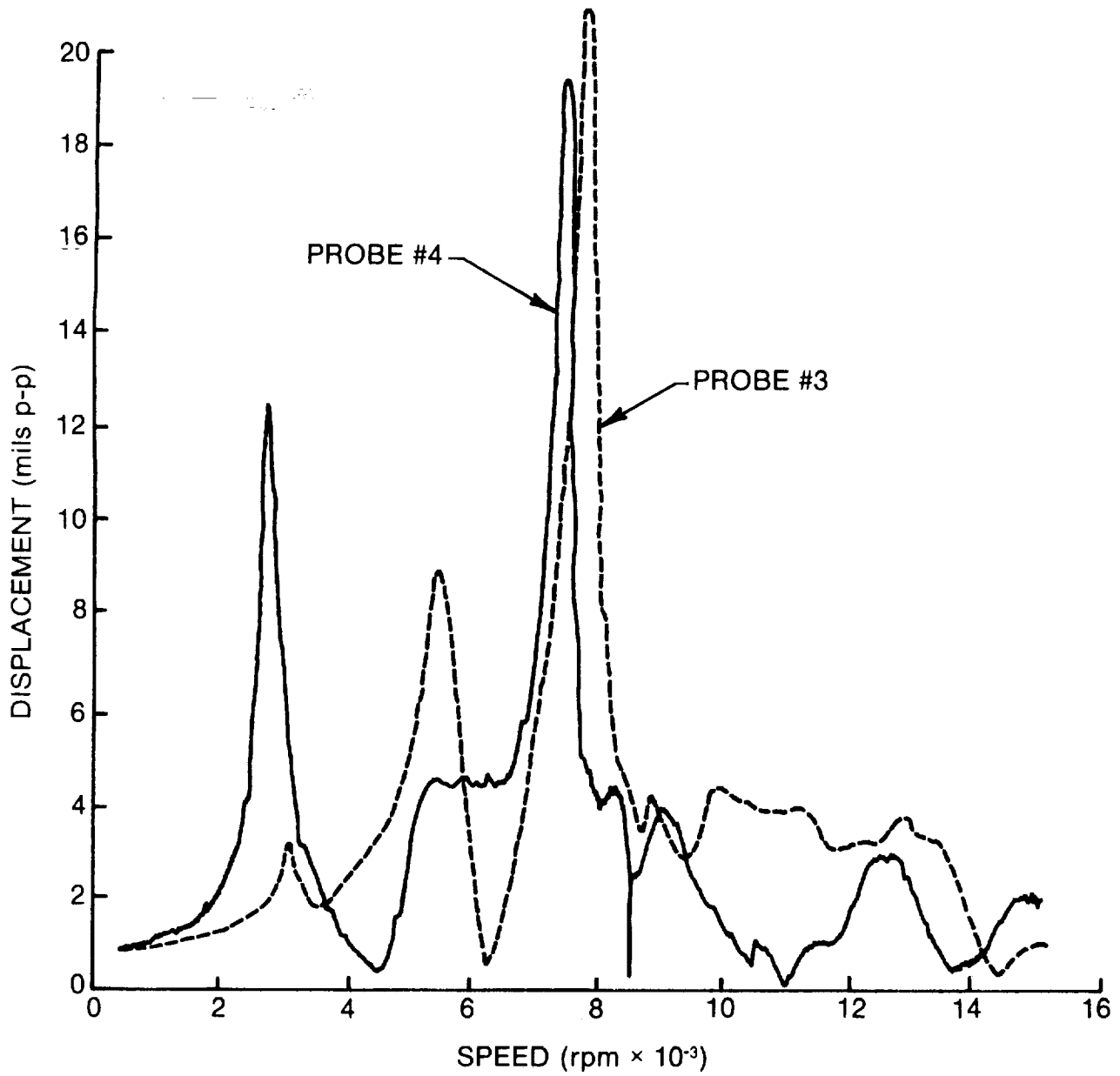Fig. 186 T55 Production Power Turbine Baseline Data — Probes #1 and #2

Fig. 187   T55 Power Turbine Baseline Data — Probes #3 and #4
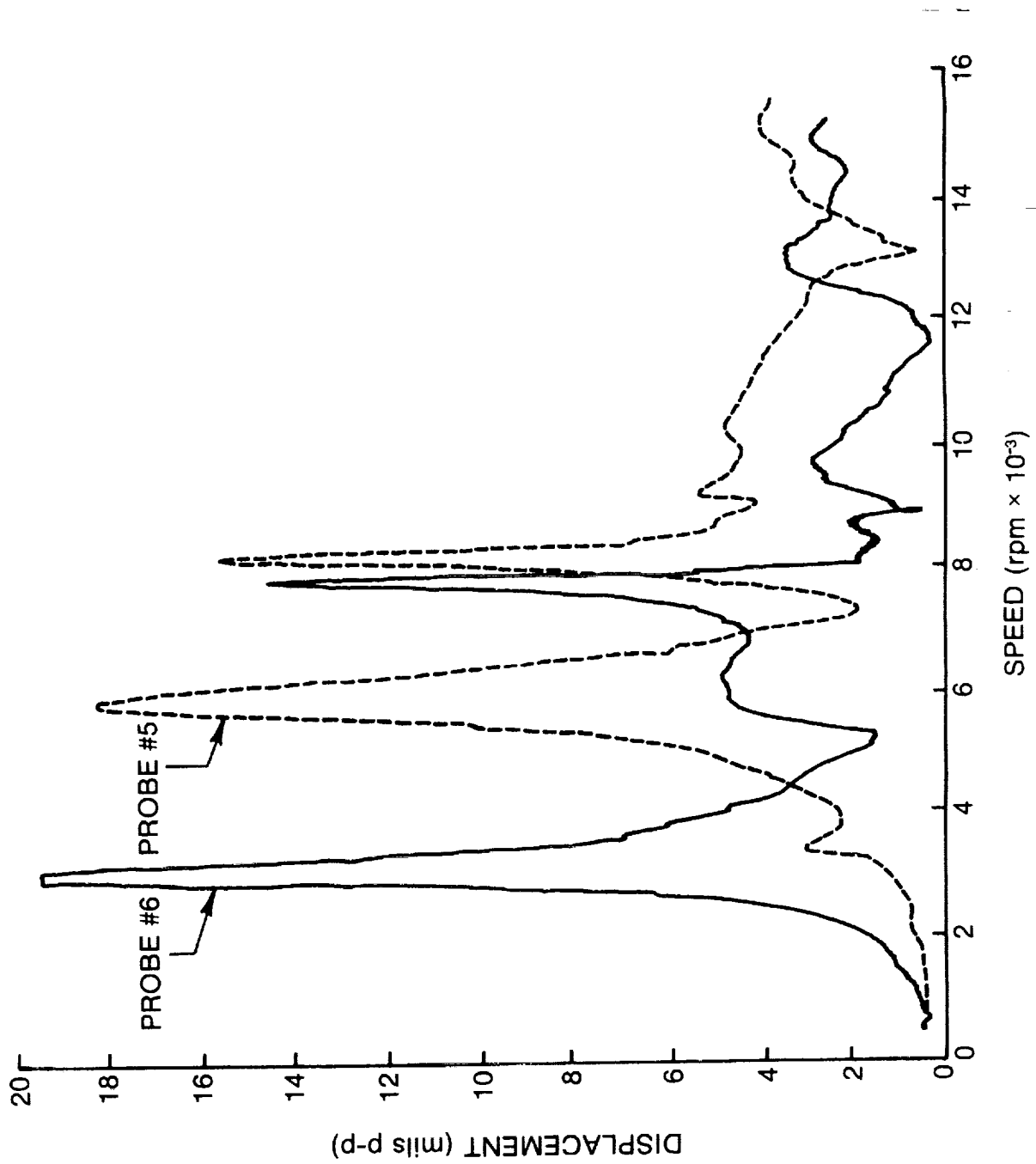
337

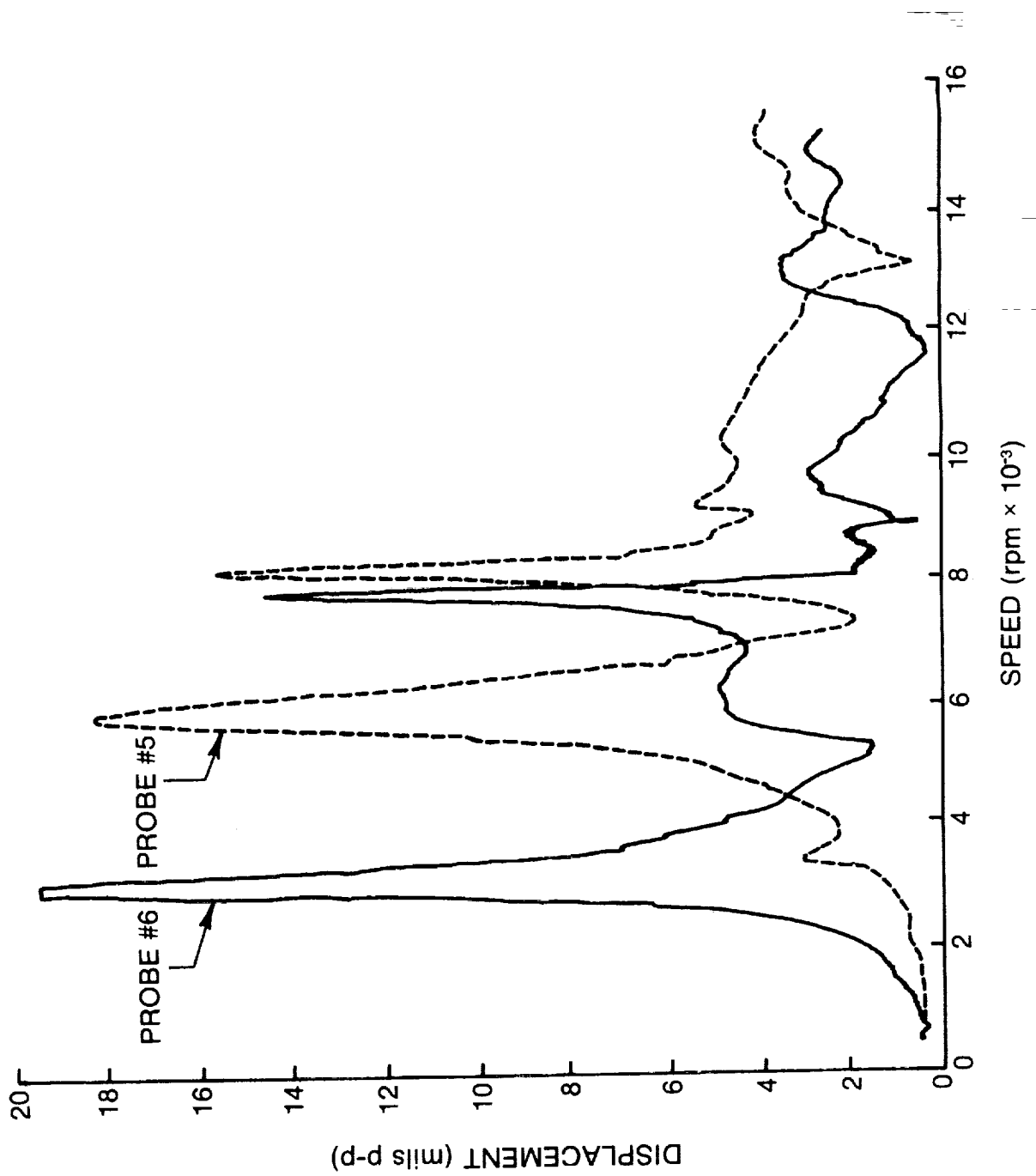Fig. 188 T55 Power Turbine Baseline Data — Probes #5 and #6

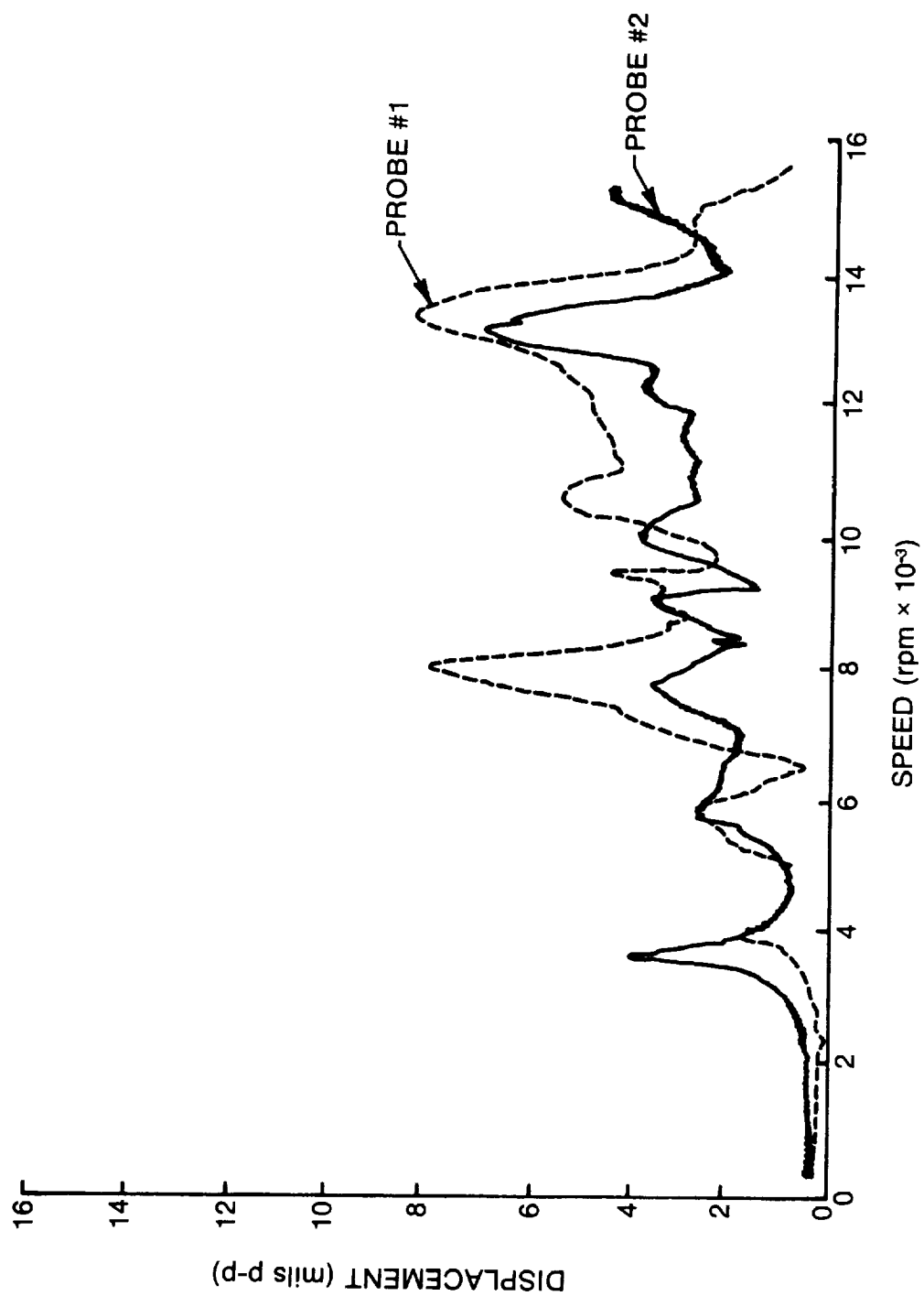Fig. 188 T55 Power Turbine Baseline Data — Probes #5 and #6

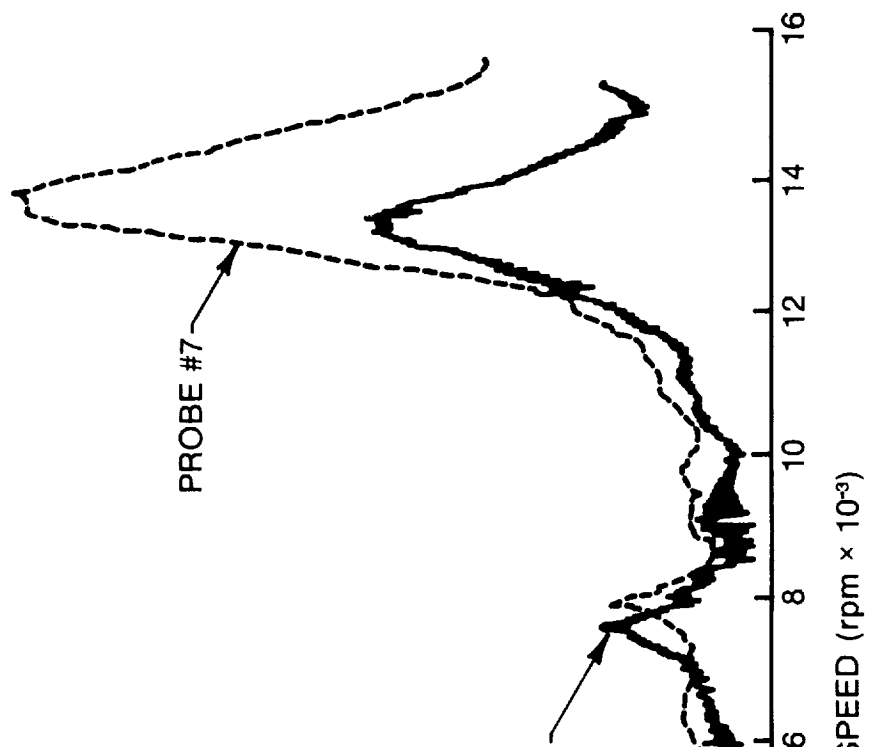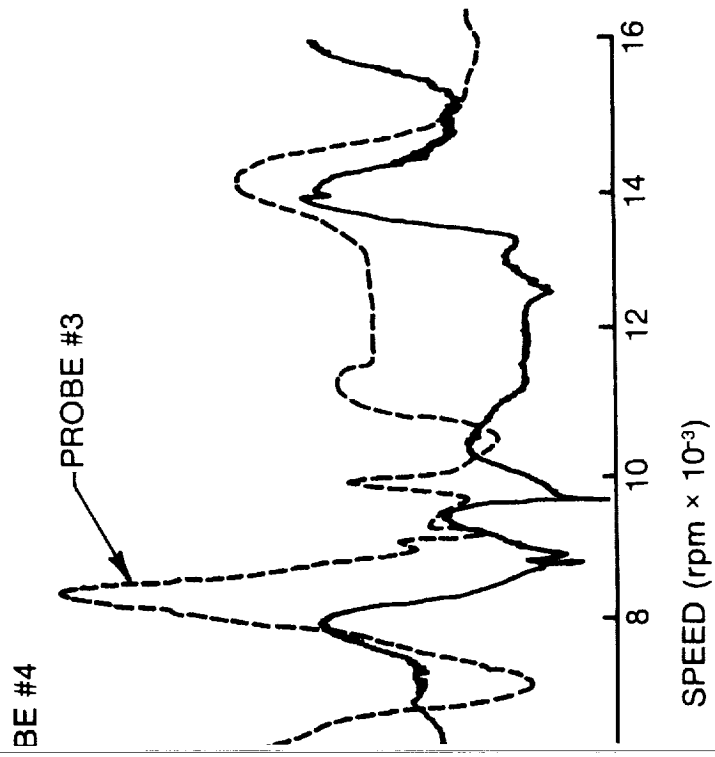Fig. 189 T55 Elastomeric Damper Baseline Data — Probes #1 and #2

PROBE #3

BE #4

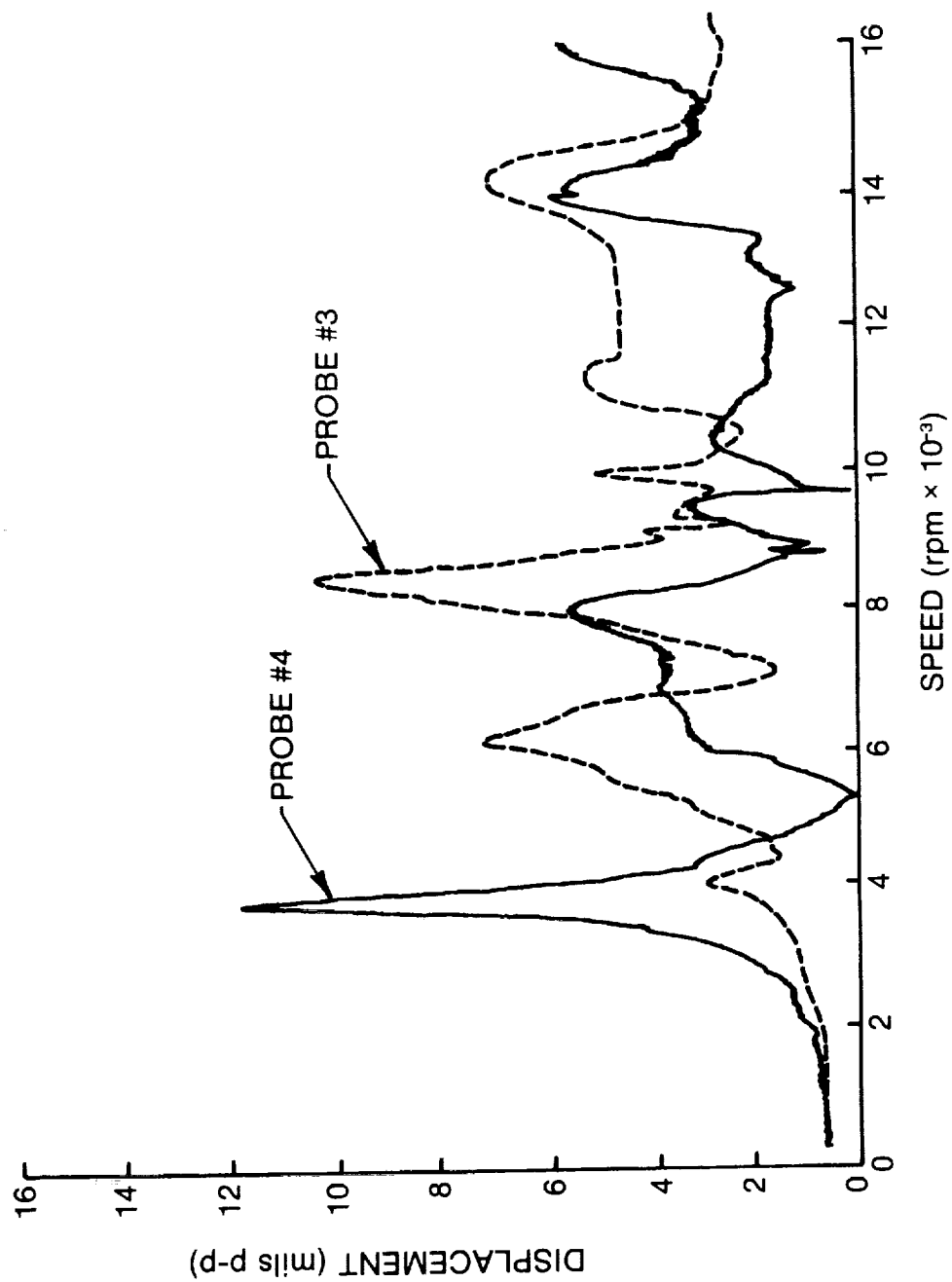SPEED (rpm × 10⁻³)

ric Damper Baseline Data — Probes #3 and #4

PROBE #7

SPEED (rpm × 10⁻³)

of T55 Elastomer-Damped Power Turbine

ric Damper Baseline Data — Probes #3 and #4

of T55 Elastomer-Damped Power Turbine

Fig. 189 T55 Elastomeric Damper Baseline Data — Probes #1 and #2

339
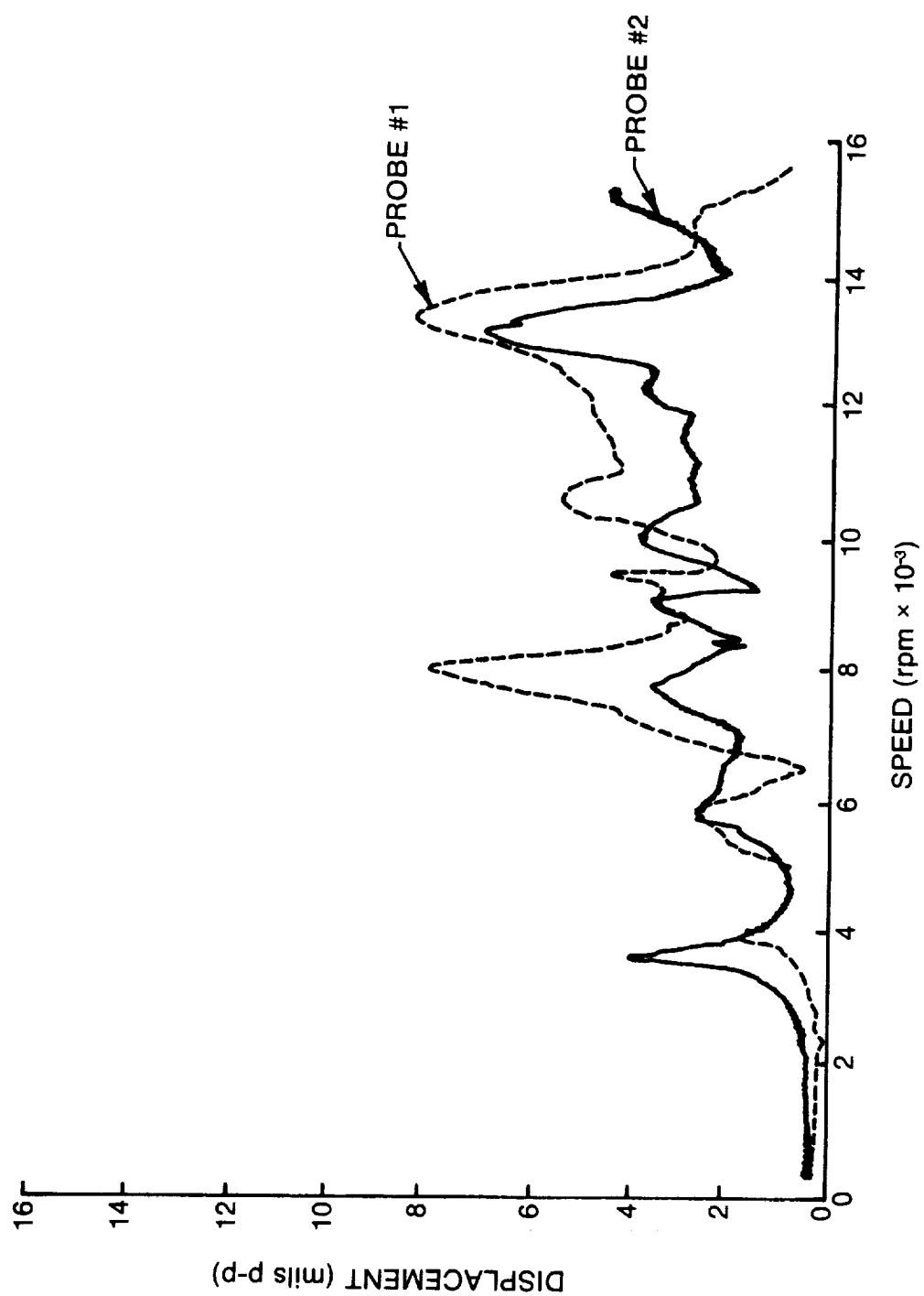
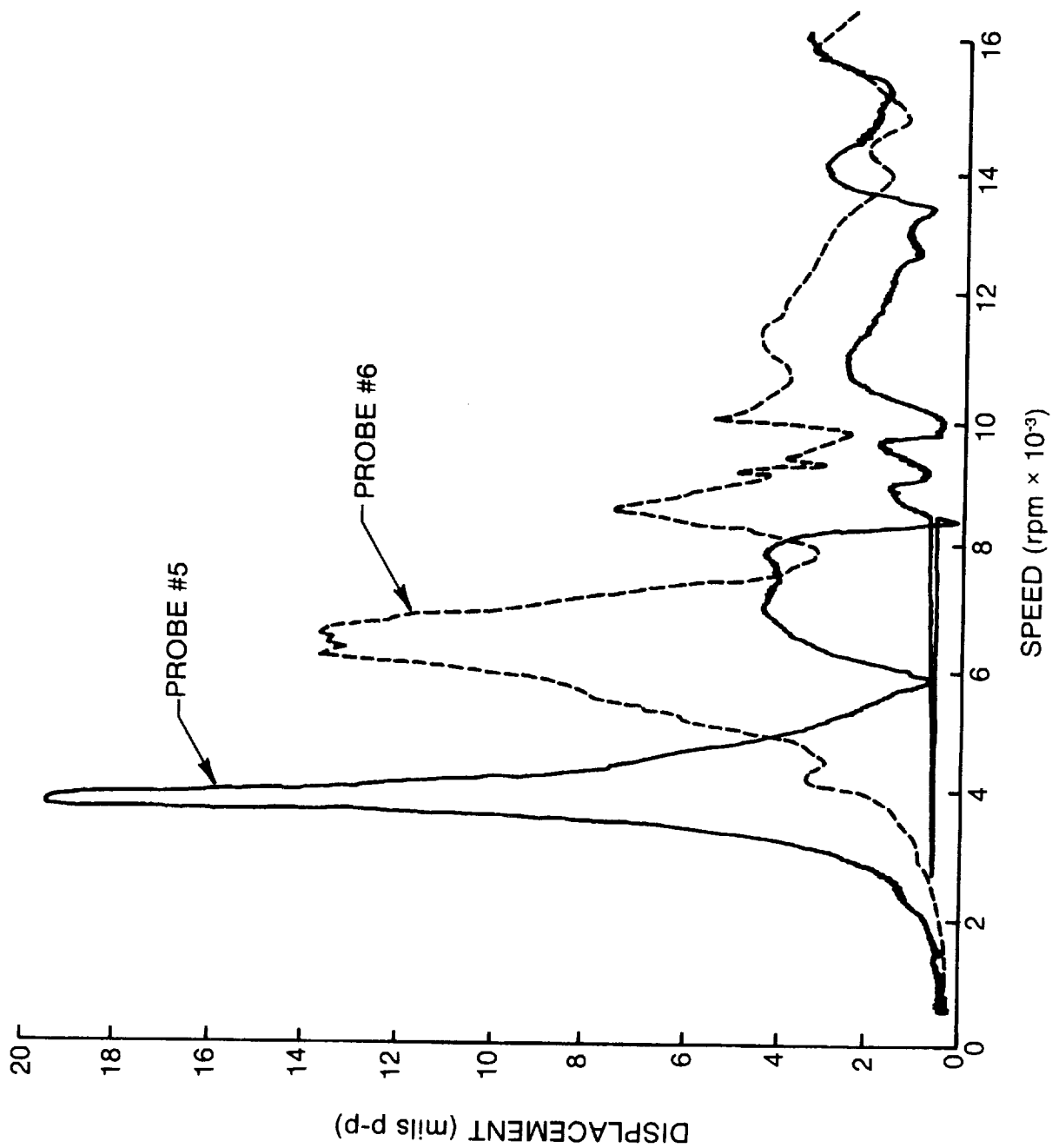Fig. 190 T55 Elastomeric Damper Baseline Data — Probes #3 and #4

340

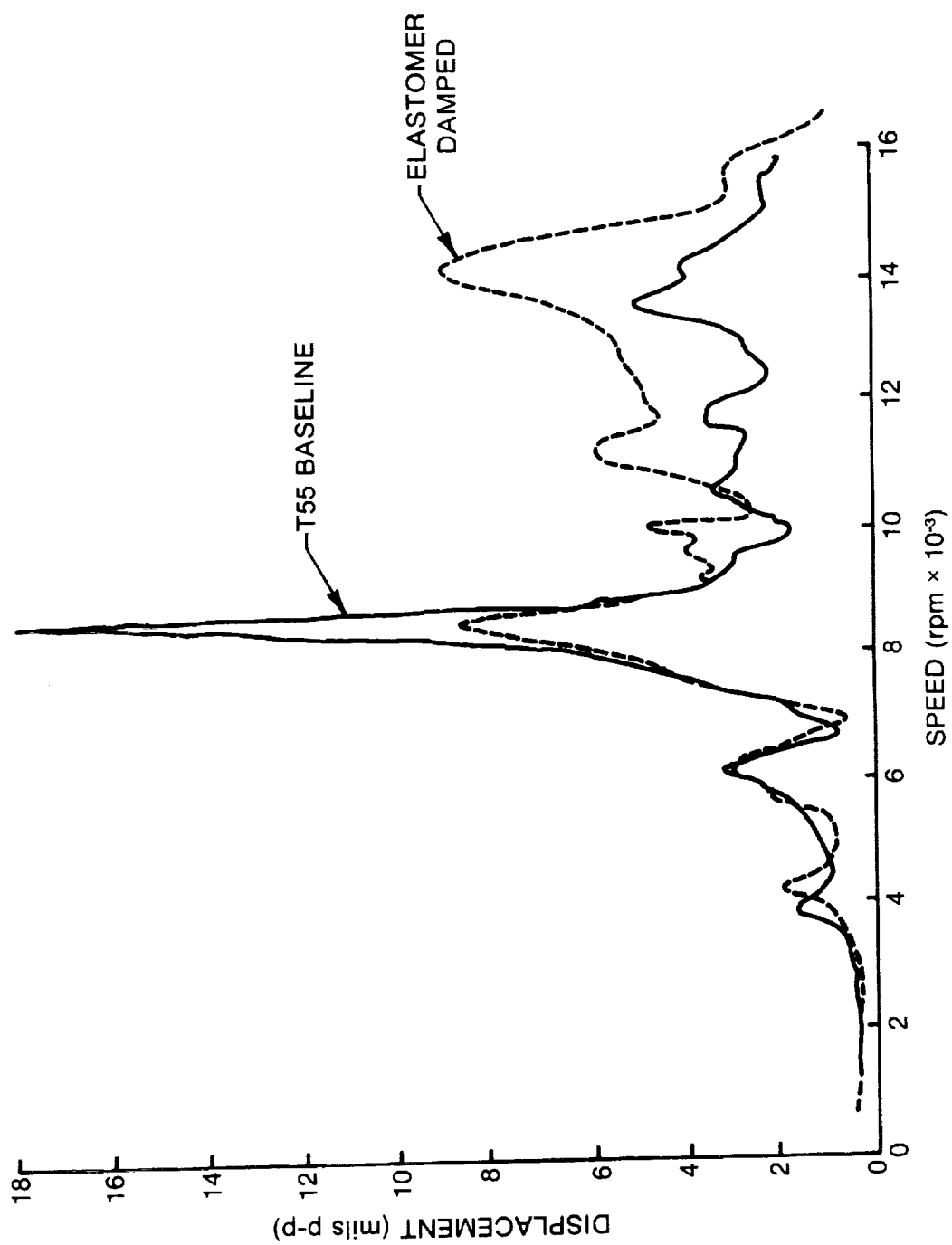Fig. 191 T55 Elastomeric Damper Baseline Data — Probes #5 and #6

341

Fig. 192 Vibration Plot Comparing Baseline and Elastomer-Mounted Rotor Response at Probe #1
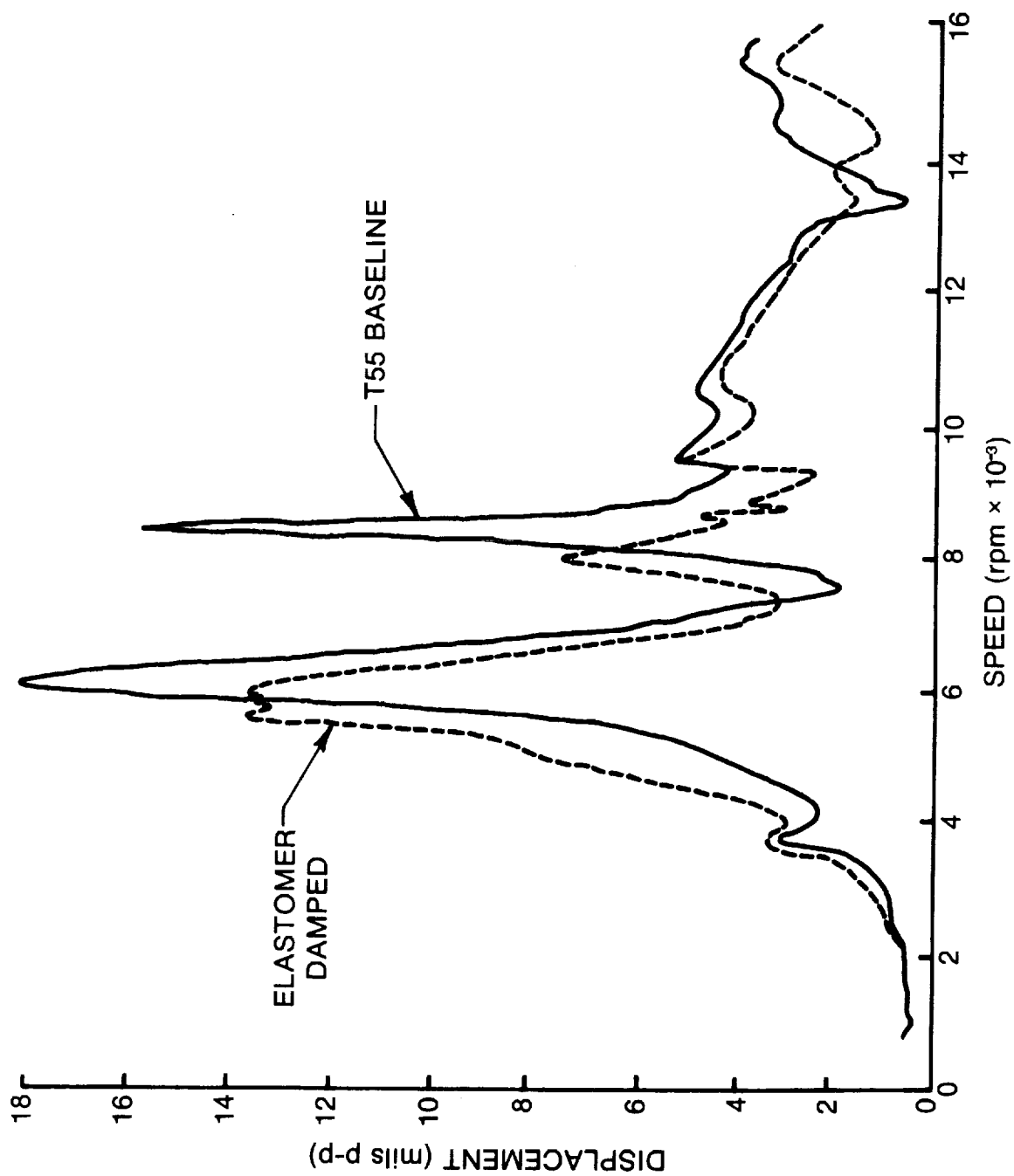
Fig. 193 Vibration Plot Comparing Baseline and Elastomer-Mounted Rotor Response at Probe #5
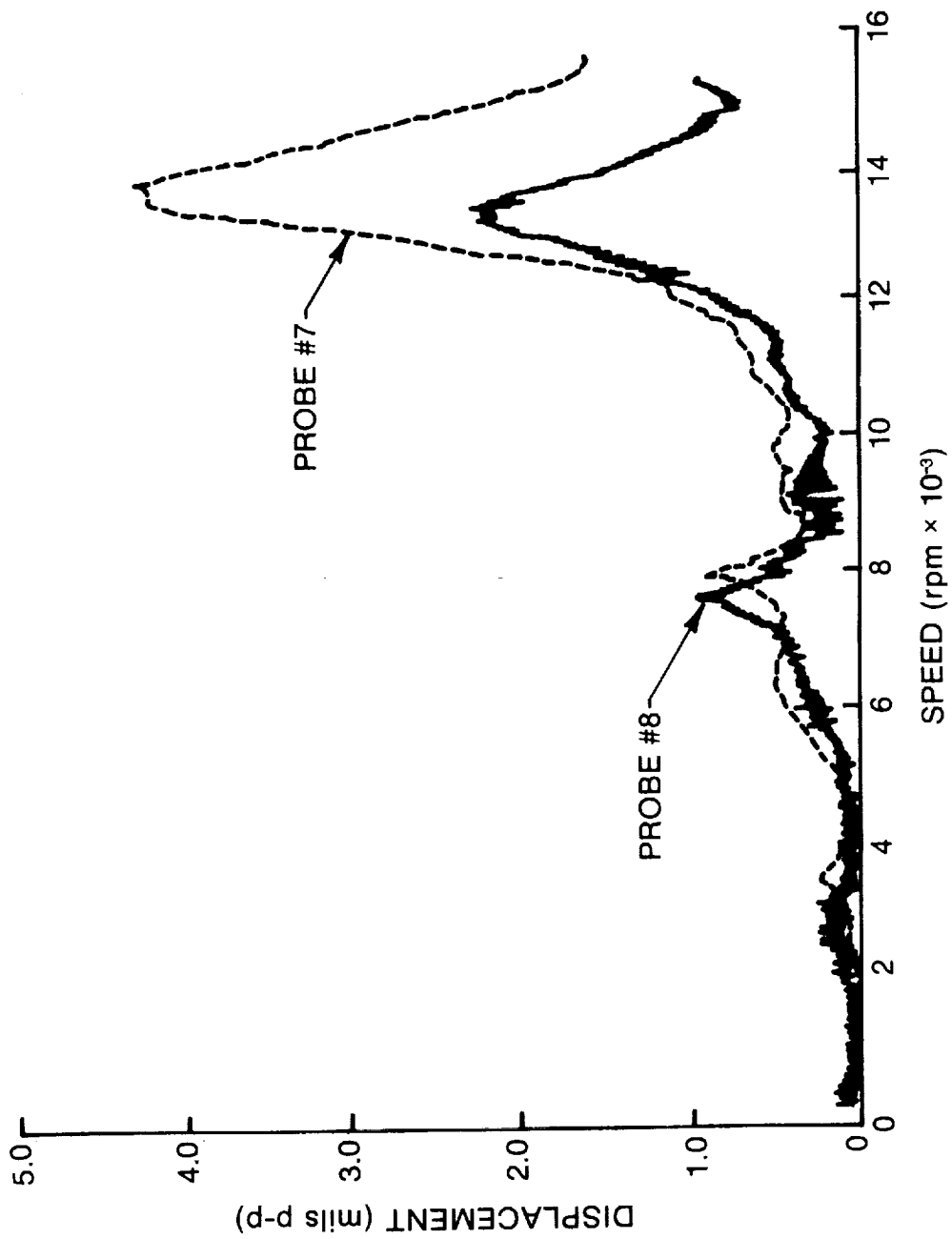
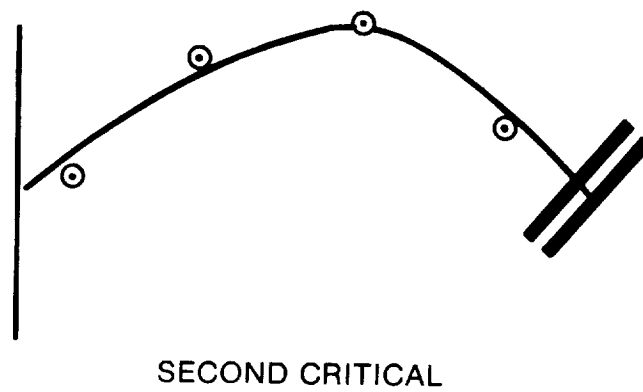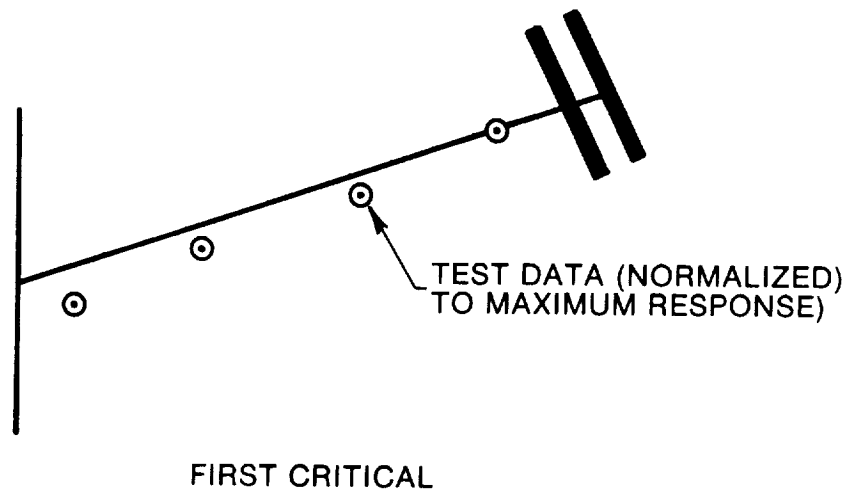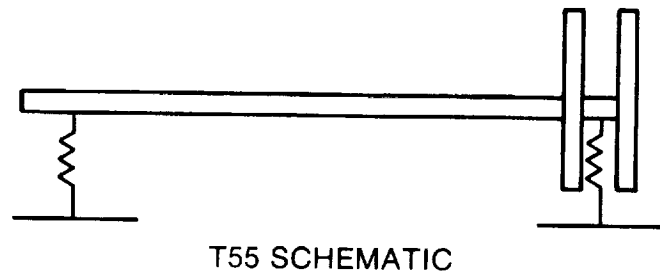Fig. 194   Response of T55 Elastomer-Damped Power Turbine

T55 SCHEMATIC

FIRST CRITICAL

TEST DATA (NORMALIZED)
TO MAXIMUM RESPONSE)

SECOND CRITICAL

Fig. 195 Comparison of Test Data with Analytic Predicted Modes

345

Table 37

	Analysis		Measured	
	Speed (rpm)	Log Decrement	Speed (rpm)	Log Decrement
First Critical	6,022	0.001	6,007	0.090*
Second Critical	13,535	0.201	13,666	0.206*

* Average value for all data obtained

There is excellent correlation in whirl speed, but the first critical's log decrement is significantly different in value between measured and analysis. This is due to the fact that analysis has indicated a node at the damper for the first critical. Slight changes in rigidity of the shaft or location of roller bearing support would alter appreciably the analytically predicted value of log decrement for the first critical. Consideration of structural damping which occurs at the turbine-end bearing (which is heavily participating in the first critical (Figure 195)) was not included in the analysis. Therefore, the analysis does not reflect this form of damping which can significantly effect the log decrement of the first critical speed.

Typical measured response indicated dominant 1/rev excitation of the rotor through the testing with the elastomer damper active. Figure 196 presents a typical frequency spectrum from probe #5 at 13,000 rpm. As shown, relatively minor subsynchronous and supersynchronous excitations were experienced, and the operation of the T55 power turbine was as predicted throughout the entire test phase.

8.4 Summary

Three different elastomer dampers were designed and tested for three different test rigs. The three test rigs were a gas turbine simulator, a supercritical power transmission shaft, and a T55 power turbine shaft. The results of these tests clearly demonstrated the simplicity, convenience, flexibility and effectiveness of elastomer dampers. The detailed descriptions of the design procedures and actual hardware for these elastomer dampers can also serve as a valuable guide in the design of other elastomer dampers.

8.5 References

8.1 Tecza, J.A., Darlow, M.S., and Smalley, A.J., "Development of Procedures for Calculating Stiffness and Damping Properties of Elastomers in Engineering Applications, Part V: Elastomer Performance Limits and the Design and Test of an Elastomer", NASA Report CR-159552, February 1979.
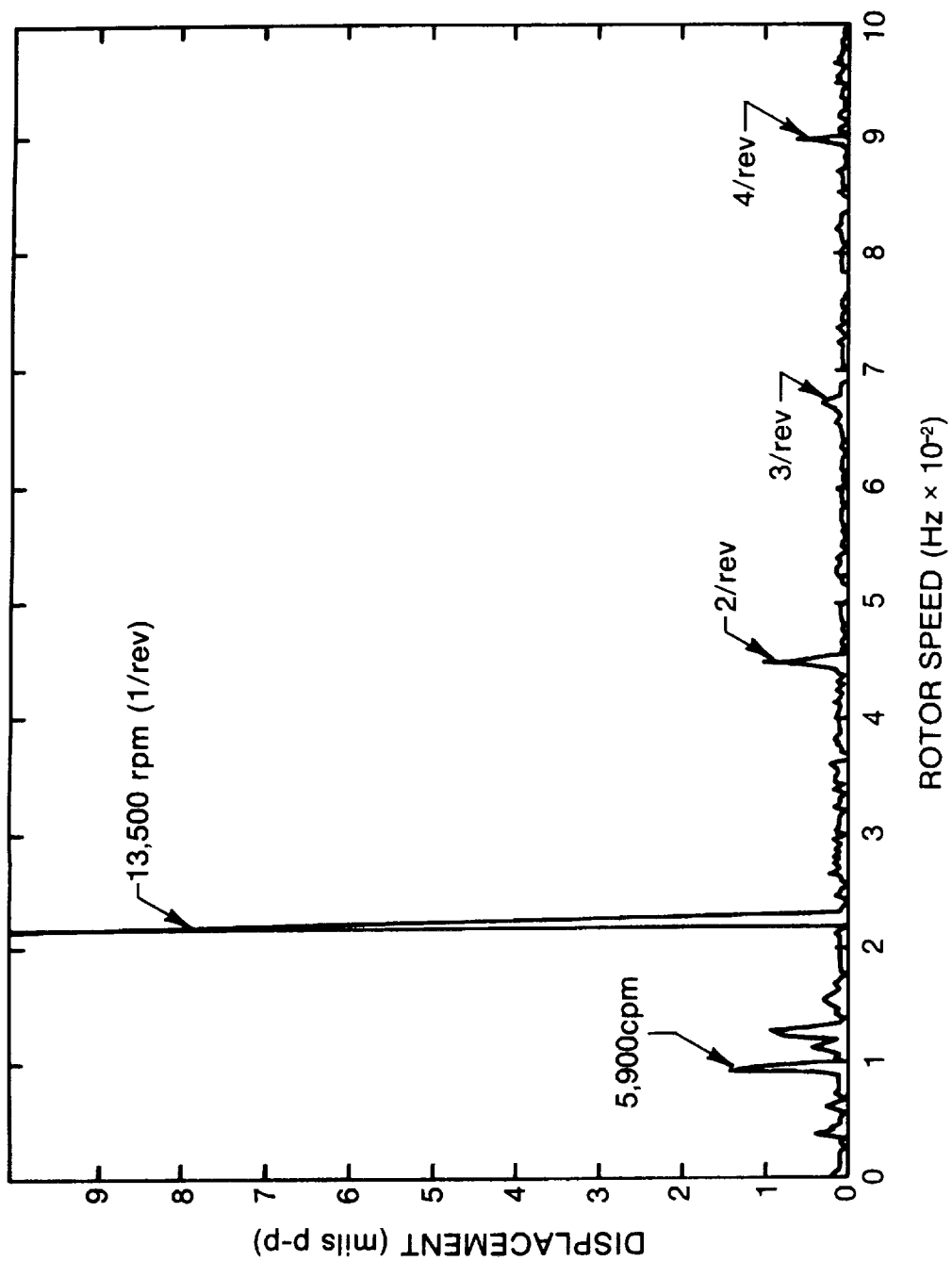
Fig. 196 Spectrum Plot on Elastomer Probe #5; 3 g at 300° Plane 1

8.2   Zorzi, E.S., Burgess, G., and Cunningham, R., "Elastomer Damper Performance - A Comparison with a Squeeze Film for a Supercritical Power Transmission Shaft", ASME Paper, presented at the ASME 1980 Gas Turbine Conference, March 1980.

8.3   Rieger, A., and Zorzi, E., "Development of Procedures for Calculating Stiffness and Damping Properties of Elastomers in Engineering Applications, Part VII, NASA Report CR-165138.

8.4   Cundiff, R.A. and Badgley, R.H., "Pneumomechanical Critical Speed Control for Gas Turbine Engine Shafts", USAF Report AFAPL-TR-101, AD 772805.

8.5   Dynamic Stability of a Flexible Rotor: Cadense Program CAD-25, Computer Program User Manual, Mechanical Technology Incorporated.

8.6   Unbalance Response of a Flexible Rotor: Cadense Program CAD-21, Computer Program User Manual, Mechanical Technology Incorporated.

8.7   Smalley, A.J., and Tessarzik, J.M., "Development of Procedures for Calculating Stiffness and Damping Properties of Elastomers in Engineering Applications, Part III: The Effects of Temperature, Dissipation Level and Geometry", NASA Report CR-134939, November 1975.

8.8   Payne, A.R., and Scott, J.R., "Engineering Design with Rubber", London: MacLaren & Sons, Ltd., 1960.

8.9   Smalley, A.J., Darlow, M.S., and Mehta, R.K., "Stiffness and Damping of Elastomeric O-Ring Bearing Mounts", NASA Report CR-135328, November 1977.

8.10   Thomsen, K.K., and Anderson, H., "Experimental Investigation of a Simple Squeeze-Film Damper". ASME Paper No. 73-DET-101.

8.11   Vance, J.M., and Kirton, A.J., "Experimental Measurement of the Dynamic Force Response of a Squeeze-Film Bearing Damper", Journal of Engineering for Industry, Trans. ASME, Series B, Vol. 97, No. 4.

8.12   Sharma, R.K., and Botman, M., "An Experimental Study of the Steady-State Response of Oil-Film Dampers", ASME Paper No. 77-DET-33.

8.13   Marmol, R.A., and Vance, J.M., "Squeeze-Film Damper Characteristics for Gas Turbine Engines", ASME Paper No. 77-DET-18.

8.14   Smalley, A.J., Darlow, M.S., and Mehta, R.K., "The Dynamic Characteristics of O-Rings", ASME Trans., Journal of Mechanical Design, Vol. 100, No. 1, January 1978, pp. 132-138.

8.15   Darlow, M.S., and Zorzi, E.S., "Nonsynchronous Vibrations Observed in a Supercritical Power Transmission Shaft", ASME 79-GT-146.

1. Report No. NASA CR-3423	2. Government Accession No.	3. Recipient's Catalog No.

4. Title and Subtitle MECHANICAL DESIGN HANDBOOK FOR ELASTOMERS		5. Report Date June 1981
		6. Performing Organization Code

7. Author(s) M. Darlow and E. Zorzi	8. Performing Organization Report No. MTI 81TR5
	10. Work Unit No.

9. Performing Organization Name and Address Mechanical Technology Incorporated 968 Albany-Shaker Road Latham, New York 12210	11. Contract or Grant No. NAS3-21623
	13. Type of Report and Period Covered Contractor Report

12. Sponsoring Agency Name and Address National Aeronautics and Space Administration Washington, D.C. 20546	14. Sponsoring Agency Code 505-04-42

15. Supplementary Notes

Final report. Project Manager, Robert E. Cunningham, Structures and Mechanical Technologies Division, NASA Lewis Research Center, Cleveland, Ohio 44135.

16. Abstract

This handbook provides design engineers with a comprehensive guide for the design of elastomer dampers for application in rotating machinery. Design data was collected from an extensive group of references and, together with recent information, was assembled into a single volume. This handbook is a self-contained reference but does include some theoretical discussion to assure the reader's understanding how and why dampers are used for rotating machines. This handbook pre-sents a step-by-step procedure for the design of elastomer dampers and detailed examples of actual elastomer damper applications.

17. Key Words (Suggested by Author(s)) Viscoelasticity; Elastomers; Dynamic prop-erties; Damping; Critical speeds; Vibrations; Resonance testing; Gas turbine; Strain effects	18. Distribution Statement Unclassified - Unlimited STAR Category 37

19. Security Classif. (of this report) Unclassified	20. Security Classif. (of this page) Unclassified	21. No. of Pages 353	22. Price* A16